BEHAVIOUR OF UNDERGROUND EXCAVATIONS IN SQUEEZING GROUND CONDITIONS

Ph.D. THESIS

by

RAMA DHAR DWIVEDI

DEPARTMENT OF CIVIL ENGINEERING
INDIAN INSTITUTE OF TECHNOLOGY ROORKEE
ROORKEE – 247 667 (INDIA)
JUNE, 2014

BEHAVIOUR OF UNDERGROUND EXCAVATIONS IN SQUEEZING GROUND CONDITIONS

A THESIS

Submitted in partial fulfilment of the requirements for the award of the degree

of

DOCTOR OF PHILOSOPHY

in

CIVIL ENGINEERING

by

RAMA DHAR DWIVEDI

DEPARTMENT OF CIVIL ENGINEERING
INDIAN INSTITUTE OF TECHNOLOGY ROORKEE
ROORKEE – 247 667 (INDIA)
JUNE, 2014

INDIAN INSTITUTE OF TECHNOLOGY ROORKEE
ROORKEE

CANDIDATE'S DECLARATION

I hereby certify that the work presented in the thesis entitled "**BEHAVIOUR OF UNDERGROUND EXCAVATIONS IN SQUEEZING GROUND CONDITIONS"** in partial fulfilment of the requirements for the award of the degree of Doctor of Philosophy and submitted in the Department of Civil Engineering, Indian institute of Technology Roorkee, Roorkee is an authentic record of my own work carried out during a period from August, 2007 to June, 2014 under the guidance and supervision of **Dr. Mahendra Singh**, Professor, Department of Civil Engineering, **Dr. M. N. Viladkar**, Professor, Department of Civil Engineering and **Dr. R. K. Goel**, Scientist-G, Central Institute of Mining & Fuel Research (CIMFR), Regional Centre, Roorkee.

The matter presented herein has not been submitted by me for the award of any other Degree or Diploma of this or any other Institute or University.

(**RAMA DHAR DWIVEDI**)

This is to certify that the above statement made by the candidate is correct to the best of our knowledge.

(**R. K. GOEL**)	(**M. N. VILADKAR**)	(**MAHENDRA SINGH**)
Supervisor	Supervisor	Supervisor

Date: June 30, 2014

The Ph. D. Viva-Voce Examination of **Mr. RAMA DHAR DWIVEDI**, Research Scholar, has been held on …….

Signature of Supervisors **Chairman, SRC** **Signature of External Examiner**

Head of the Dept. / Centre & Chairman, ODC

ABSTRACT

Increase in population has broadened the supply-demand gap for energy. It has forced mankind to construct more number of hydro-electric power projects. On the other hand, large traffic has increased load on the roads and hence the effective travel time, especially in the hilly regions, has increased. Construction of hydro projects and shortening the routes in hilly regions involve tunnelling. In addition to this, other facilities like underground repositories for burial of high level nuclear waste (HLNW), safe storage of warplanes, missiles and explosives for defense purposes, storage of petroleum products and underground research laboratories etc. involve large underground excavations. Therefore, a silent tunnelling revolution is presently going on in India. Most of the underground excavations are carried out in the Himalayan region, which is extremely fragile and exhibits complex rock mass behaviour. High in-situ stresses, which are very common in the Himalayan region due to continuing tectonic activity, affect tunnelling in the form of time dependent tunnel deformation resulting in to large convergence of rock mass in to the tunnels. These time dependent large deformations associated with tunnelling is known as squeezing. Such deformations may terminate during construction or continue over a long time period, if adequate supports are not installed in time. Currently no methods are available which could be used with confidence in the field to assess the squeezing potential.

The earlier research work relevant to the area of present study has been reviewed and discussed in detail in Chapter 2. Important outcome of some of these studies are:

Wood (1972) suggested that grounds undergo squeezing, if the ratio of unconfined compressive strength of rock mass to overburden stress assumes a value less than 2.

Daemen (1975) reported that deformations in tunnels are due to relaxation of broken zone and progressive reduction in residual strength of the rock has a significant influence on support pressures. It was further suggested that flexible supports are preferable in squeezing ground condition as these mobilize lesser rock pressure.

Dube (1979) reported that radius of the broken zone varies in the range of 2.5 - 4 times the radius of tunnel in squeezing ground conditions. In-situ stresses are the critical parameters

affecting the geometry of the broken zone, support pressure and the tunnel deformation. It was also suggested that Barton's approach for predicting the support pressure needs a new parameter, viz the tunnel size, especially in squeezing conditions.

Jethwa (1981) modified Daemen's (1975) approach for predicting the support pressure after incorporating the effect of advance of tunnel face and commented that Q-system provides reliable estimates of rock pressure for tunnels in non-squeezing ground only. None of the classification systems is as such reliable in squeezing ground conditions.

Verman (1993) developed empirical correlations for assessment of support pressure and tunnel deformation in squeezing ground condition involving ten parameters.

Goel (1994) proposed empirical correlation after introducing Rock Mass Number, N for assessment of the squeezing ground condition. Correlations were also proposed for support pressure and tunnel closure for both non-squeezing and squeezing ground conditions. It was pointed out that the effect of tunnel size on support pressure is insignificant in case of non-squeezing ground conditions but it becomes quite significant in squeezing ground conditions.

Choudhari (2007) proposed an elasto-plastic closed form solution for predicting the tunnel deformation using critical internal pressure as a parameter for circular tunnels and concluded that rock mass behaves anisotropically when in-situ stress ratio, $k \neq 1$ and closed form solutions are no more applicable.

Singh et al. (2007) suggested a critical strain parameter as an indicator to quantify the squeezing ground potential of the rock mass around tunnels.

Lian-Chong et al. (2008) suggested that initiation of creep failure is governed by the ratio, k of the far field stresses and the creep failure initiates always in the direction of the minimum far field stress component since in that direction, the octahedral shear stress reaches the highest value.

Barla et al. (2011) optimized the yield-control support system in squeezing grounds to enhance the rate of tunnel advance.

Cantieni et al. (2011) suggested that if the ground exhibits a moderate time-dependent behaviour and the effect of the support measures is taken into account, the prediction of

deformation by core extrusion measurements is feasible. On the other hand, if the ground behaviour is pronouncedly time-dependent, tunnel deformation prediction becomes very difficult, because core extrusion is governed by the short-term characteristics of the ground, which may be different from the long-term properties which control the final convergence.

Scussel and Chandra (2013) developed expressions based on elastic-plastic theory for the prediction of tunnel support pressure for both non-squeezing and squeezing grounds under conditions of hydrostatic in-situ stresses.

Keeping in view the above discussion, following major objectives of the present study were set forth:

- Study of existing tunnel case histories for understanding state-of-art of knowledge,
- Collection of required data, viz., diameter and depth of tunnel, in-situ stress, rock mass quality parameters (joint properties, uniaxial compressive strength and rock mass number) and details of supports installed in tunnels from case histories,
- Collection of data acquired on the basis of in-situ instrumentation and monitoring like deformations, support pressures etc.,
- Development of empirical correlations for prediction of ground conditions,
- Development of empirical correlations to predict tunnel deformation and support pressure for non-squeezing and squeezing ground conditions.

In the present study, geo-mechanical data of 366 tunnel sections from 24 case projects located in India and other countries was collected and analyzed. Out of these, fourteen projects are located in the Himalayan region. These projects lie in India (states of Uttarakhand, Himachal Pradesh, Jammu & Kashmir, Arunanchal Pradesh and Manipur), Nepal and Bhutan. A few projects considered for study are located in the states of Madhya Pradesh, Maharashtra, Karnataka and Kerala. Four case study projects, namely from France-Italy (border), Turkey, Norway and United Kingdom were also included in the study. These data were used to develop empirical correlations for predicting the ground behaviour (squeezing, degree of squeezing, non-squeezing, self-supporting, and rock burst). Correlations have also been developed for predicting – a) tunnel deformation in squeezing and non-squeezing conditions and b) tunnel support pressure in both squeezing and non-squeezing conditions. If the behaviour of the ground is known prior to excavation

of the tunnel-face, necessary preparations in form of excavation strategy and support installing strategy can be worked out.

These correlations have been developed using joint factor (J_f), rock mass quality (Q) and rock mass number (N) separately. Other influencing parameters like tunnel radius, a; horizontal and vertical in-situ stresses; uniaxial compressive strength, σ_{ci} of intact rock; and support stiffness, K have also been considered for the study.

Correlations developed using J_f for prediction of tunnel deformation and support pressure have been found to fit best with the observed values in the field and have been recommended for use in the field and also in the design office.

Correlations developed for prediction of ground conditions (squeezing and non-squeezing) and prediction of tunnel deformation have been validated by comparing with the respective conditions and values observed in two Himalayan highway tunnels (Escape tunnel and Main tunnel) located between Chenani and Nashri villages on national highway (NH)-1A in Jammu & Kashmir in India. Some sections of escape and main tunnels have been numerically modelled using Phase^2 code and the deformation values obtained from modelling have also been compared with the predicted and observed values of tunnel deformation at respective tunnel sections. The observed values were found in good agreement with the values predicted by recommended correlations.

Parametric study was also carried out for the correlations recommended for prediction of tunnel deformation and support pressure. It was observed that there is no influence of tunnel radius on the tunnel strain and the support pressure in non-squeezing ground and also on the support pressure in the squeezing ground. Further, a significant influence of uniaxial compressive strength of intact rock, σ_{ci} has been observed for weaker rocks (σ_{ci} < 20 MPa) at higher tunnel depth in squeezing ground condition.

The correlations recommended in the present study are valid for tunnels excavated by drill and blast method. The correlations recommended for prediction of tunnel deformation in squeezing grounds, are valid for the cases where radial tunnel strain exceeds value of 1%. On the other hand, correlations recommended for prediction of tunnel deformation in non-squeezing grounds are valid where radial tunnel deformation is below 1%.

ACKNOWLEDGEMENTS

I feel immense pleasure to express my deep sense of gratitude to Prof. Mahendra Singh, Prof M. N. Viladkar and Dr. R. K. Goel, the supervisors, for their guidance, encouragement, fruitful technical discussions, critical reviews of my work and other technical helps during the research work.

The author extends his deep gratitude to Prof (Retd.) Bhawani Singh for his encouragement and moral boosting attitudes which has energised me from time to time during the research work.

Author's sincere thanks are due to Prof N. K. Samadhiya for his encouragement and sharing a thesis work of Dr. Naresh Kumar to collect some data of Nathpa Jhakri hydroelectric project for the present study.

I thank to Student's research committee members, Prof. Akhil Upadhyay and Prof. R. Anbalagan for their presence and suggestions during the meeting despite of their busy schedules.

The author is grateful to Dr. Amalendu Sinha, Director, CSIR-CIMFR, Dhanbad for permitting to pursue the research work for Ph. D. degree.

The author is thankful to the Scientist-in-charge, CSIR-CIMFR, Regional Centre, Roorkee for extending the peripheral facilities for the work.

The author also acknowledges the cooperation extended to him by his colleagues – Dr. V. V. R. Prasad (Retd.), Dr. J. K. Mohnot, Mr. Anil Swarup, Er. Harsh Verma and Mr. V. K. Garg at CSIR-CIMFR Regional Centre, Roorkee for their help.

At the end, I wish to express my deep gratitude to my parents and wife for their moral support and encouragement during the periods of hard work and to my son, Anany, who co-operated me by sacrificing his father's company and necessary guidance for his study especially at the time of his exams, when he really needed it.

(RAMA DHAR DWIVEDI)

TABLE OF CONTENTS

LIST OF FIGURES

LIST OF TABLES

ABBREVIATIONS, NOTATIONS AND SYMBOLS

ABBREVIATIONS

ESR	Excavation support ratio
GRC	Ground response curve
GSI	Geological strength index
HRT	Head race tunnel
NATM	New Austrian tunnelling method
RF	Reduction factor
RMi	Rock mass index
RMR	Rock mass rating
RQD	Rock quality designation
RSR	Rock structure rating
SRF	Stress reduction factor for Q
UCS	Uniaxial compressive strength

NOTATIONS

A	Cross sectional area of tunnel
A_s	Cross sectional area of steel rib
a	Radius of tunnel
b	Radius of elastic broken zone
b_f	Radius of plastic or fractured broken zone
B	Tunnel width or span or diameter
B_s	Self-supporting tunnel span
c	Cohesion
C_v	Coefficient of volumetric expansion
c_r	Residual cohesion of rock after failure
d	Tunnel strain (%)
d_b	Diameter of rock bolt
D	Diameter of opening or tunnel
E	Modulus of elasticity of rock

E_s	Modulus of elasticity of steel
E_i	Tangent modulus of intact rock
E_{tj}	Tangent modulus of rock mass
E_d	Deformation modulus of rock mass
E_{min}	Smaller of two moduli of deformation of rock mass in vertical and horizontal directions
f	Correction factor for tunnel depth; Correction factor for closure
f'	Correction factor for tunnel closure
f''	Correction factor for time after excavtaion
$F(n)$	Function of porosity (n) of material
$\boldsymbol{F}$	Fracture tensor
H	Tunnel depth or overburden height
H_p	Rock load factor
H_t	Height of loosened rock mass above tunnel crown
J_f	Joint factor
J_n	Joint set number for Q and number of joint per meter depth for J_f
J_r	Joint roughness number
J_a	Joint alteration number
J_c	Joint condition
J_w	Joint water reduction factor
k	Coefficient of volumetric expansion of failed rock mass and ratio of horizontal to vertical in-situ stress
K	Support stiffness
K_b	Stiffness of rock bolt
K_ϕ	Coefficient of internal friction
K_c	Stiffness of shotcrete or concrete
l	Length of rock bolt
m	Material constant of Hoek-Brown failure criterion
m_i , m_b	Value of m for intact and broken rock respectively
n	Joint inclination parameter
N	Rock mass number; Stability number
p	Estimated support pressure
p_o	Hydrostatic far-field (in-situ) stress
p_H	Horizontal far-field (in-situ) stress

p_i	Radial internal pressure on opening; Support pressure
p_v	Vertical far-field (in-situ) stress
P	Overburden pressure
p_{el}	Predicted support pressure in non-squeezing ground condition
P_{if}	Estimated short-term support pressure
Q	Rock quality index; Load deformation constant
q_c	Uniaxial compressive strength of rock material
r	Joint strength parameter
r_e	Radius of elasto-plastic interface
r_i	Internal radius of opening
p_{obs}	observed tunnel support pressure
P_b, P_s, P_N, P_u	Predicted support pressure
p_α	Vertical in-situ stress
p_a	Stress on lining
P_i^{cr}	Transformed critical internal pressure
R^2	Correlation coefficient
R_{pl}	Radius of plastic zone
S	Spacing of joints; Spacing of steel ribs from centre to centre
S_o	Transferred far-field stress
S_c & S_l	Circumferential and longitudinal spacing of rock bolt
S_u	Undrained shear strength of clay
t_b	Thickness of backfill
u_{ao}	Initial radial tunnel deformation
u_a	Radial tunnel deformation
u_b	Radial displacement of elastic plastic boundary
u_p	Predicted radial tunnel deformation
u_{asq}	Radial tunnel deformation in squeezing ground condition
u_{ael}	Radial tunnel deformation in non-squeezing ground condition
V_b	Rock block volume
V_p	P-wave velocity

SYMBOLS

ρ	Radius of plastic zone; Average number of joints per unit volume
α	Angle between joint strike and tunnel alignment
β	Orientation of joint with loading direction
γ	Unit weight of rock mass
ν	Poisson's ratio
ϕ	Angle of internal friction
ϕ_p	Peak angle of internal friction of rock mass in elastic zone
ϕ_r	Residual angle of internal friction after rock failure
θ	Dip of joint
θ_A	Apparent dip of joint
ε	Critical tunnel strain in percent
σ	Hydrostatic rock pressure
σ_h & σ_v	Horizontal and vertical in situ-stress
σ_v`	Effective vertical in-situ stress
σ_c, σ_{ci}	Uniaxial compressive strength of intact rock
σ_{cm}	Uniaxial compressive strength of rock mass
σ_θ	Tangential stress at point of interest
η_p, η_s , η_f	Normalised strain levels
ψ^2	Coefficient of accordance

Chapter 1

INTRODUCTION

1.1 GENERAL

The trend of utilizing underground space is increasing in India day by day in the form of traffic rail and road tunnels in Himalayan region, hydro tunnels/caverns in hill states of Jammu and Kashmir, Himachal Pradesh, Uttarakhand and north-eastern states of Arunachal Pradesh, Assam, Sikkim and the neighboring countries like Nepal, Bhutan etc., underground repositories for burial of high level nuclear waste (HLNW), safe storage of warplanes, missiles and explosives for strategic defense purposes, storage of petroleum products and some underground research laboratories. A silent tunnelling revolution is presently going on in India. Most of the underground excavations are carried out in Himalayan region. The geology of this region is extremely fragile and exhibits complex rock mass behaviour. Some of the regions are highly tectonically active leading to high horizontal in-situ stresses, which affects the underground excavation work and gives rise to squeezing in weak rock masses and rock bursts even at a shallow depth in competent & strong rock masses. The phenomenon of squeezing may be defined as - "*Squeezing of rock is the time-dependent large deformation, which occurs around a tunnel and other underground openings, and is essentially associated with creep caused by (stress) exceeding the shear strength (limiting shear stress). Deformation may terminate during construction or continue over a long time period*" (Barla, 1995). Currently no method is available which could be used with confidence in the field to assess the squeezing potential (Singh et al., 2007).

On excavation of rock mass, the equilibrium of in situ stresses is disturbed around the excavation and redistribution of stresses takes place. If the induced stresses exceed the strength of the rock mass around the periphery of an underground opening, failure of rock mass takes place leading to development of a broken zone around it (Dwivedi et al., 2012). The radius of the broken zone depends upon the magnitude of in-situ stresses and the rock mass quality, whereas its shape varies with the shape of the tunnel and in-situ stress anisotropy. The failed rock mass around the tunnel periphery starts advancing in to the tunnel. The resulting excessive tunnel closure has to be arrested by installing

the supports in time. In very poor quality rock masses under the influence of high in-situ stresses, this closure is very high and leads to squeezing ground conditions.

The squeezing conditions are common in the Lower Himalaya in India, the Alps and other young mountains of the world where the rock masses are weak, highly jointed, faulted, folded and tectonically disturbed and where the overburden is high.

1.2 STATE-OF-THE-ART AT A GLANCE

The outcome of the research work of various research workers has been presented here in brief in the form of Table 1.1.

Table 1.1 Brief Review of Literature

Authors	Outcome
Wood (1972)	• Grounds undergo squeezing, if ratio of unconfined compressive strength of rock mass to overburden pressure falls below 2.
Daemen (1975)	• Deformations in tunnels are due to relaxation of broken zone. • Progressive reduction in the residual strength of rock has a significant influence on the support pressures. • Flexible/softer supports are successful in squeezing condition. • Stiffer rock mass mobilizes less rock pressure.
Jaeger and Cook (1976)	• An expression (Eq. 2.31 in Chapter 2) to predict tangential stress on the boundary of a circular tunnel.
Dube (1979)	• Radius of the broken zone varies in the range of 2.5 - 4 times the radius of tunnel. • In-situ stresses are the critical parameters affecting the geometry of broken zone, support pressure and the tunnel deformation. • Barton's (1974) approach for support pressure needs a new parameter, namely the tunnel size, especially for squeezing conditions.
Jethwa (1981)	• Modified the approach given by Daemen (1975) for support pressure to include the effect of the face advance. • Q-system provides reliable estimates of rock pressure for tunnels in non-squeezing ground only. • None of the classification systems is reliable for the squeezing ground conditions.

Saari (1982)	• Ground undergoes squeezing behaviour when the tangential strain exceeds 1 %.
Verman (1993)	• Presented empirical correlations for assessment of support pressure and tunnel deformation in squeezing ground condition involving ten parameters.
Goel (1994)	• Presented empirical correlation introducing rock mass number (*N*) for assessment of squeezing ground condition. • Empirical correlation for support pressure, closure for non-squeezing and squeezing conditions using rock mass number (*N*) incorporating *H* and *a*. • Effect of tunnel size on support pressure is insignificant in the case of non-squeezing ground condition but it becomes significant in squeezing rock conditions.
Singh (1997)	• With increase in confinement, failure mode may converge towards shearing. The convergence of splitting and sliding to shearing is expected near the brittle-ductile transition. • For sliding, the geometry does not affect the behaviour of the rock mass.
Bhasin et al. (2006)	• Support pressure increases significantly with tunnel size for an elastic-plastic rock mass. • Maximum axial force on shotcrete lining doubles when the diameter of tunnel is increased from 5 m to 20 m. • The effect of tunnel size on support pressure is very small in the case of elastic rock.
Kumar (2002)	• Correlation suggested by Barton et al. (1974) for prediction of support pressure is not reliable for squeezing ground conditions. • Empirical approach suggested by Singh et al. (1992, 1995) for support pressure may not be applicable beyond a support pressure of 0.25 MPa. • Predicted values of support pressure using the empirical correlation based on RMR and given by Unal (1983) are unsafe for squeezing conditions. • Rock Structure Rating (RSR) overestimates the support requirement in non-squeezing ground conditions.
Shrestha (2005)	• Squeezing is significantly high in weaker rocks like schists than that in stronger rocks like gneiss. • The available criterion for prediction of squeezing condition could not predict squeezing behaviour in Khimti-1 hydro tunnels. • Existing correlations gave a good agreement for support pressure and closure in non-squeezing conditions but not in squeezing conditions.

Choudhari (2007)	• Rock mass behaves anisotropically when in-situ stress ratio (k) ≠ 1 and closed form solutions are no more applicable. • Presented an elasto-plastic closed form solution for closure using critical internal pressure as a parameter for circular tunnels.
Lian-chong et al. (2008)	• Initiation of creep failure is governed by the ratio of the far field stresses (k). Further suggested that creep failure always initiates in the direction of the minimum far field stress component since the octahedral shear stress reaches the highest value in that direction.
Barla et al. (2011)	• Optimization of yield-control support system in squeezing grounds increases the rate of tunnel advance.
Cantieni et al. (2011)	• Demonstrated that if the ground exhibits a moderate time-dependent behaviour and the effects of the support measures are taken into account, the prediction of deformation by core extrusion measurements is feasible. On the other hand, if the ground behaviour is pronouncedly time-dependent, tunnel deformation predictions become very difficult, because core extrusion is governed by the short-term characteristics of the ground, which may be different from the long-term properties that govern the final convergence.
Scussel and Chandra (2013)	• Expressions based on elastic-plastic theory for prediction of tunnel support pressure for non-squeezing and squeezing grounds in hydrostatic conditions of in-situ stresses.

1.3 CRITICAL COMMENTS

Although many studies have been carried out in India and abroad to tackle the squeezing ground condition, however, the existing knowledge still needs refinement for reliable prediction of support pressures and deformations in such rock masses. Barla (2001) reviewed the existing approaches for design of tunnels under squeezing ground conditions and concluded that even today, with significant advances in Geotechnical Engineering; the fundamental mechanisms of squeezing are yet not fully understood. Some of the facts responsible for inadequate understanding in analyzing squeezing ground conditions are: i) the effect of the size of opening is not well understood, ii) rock mass strength under the prevailing stress conditions at the periphery of the opening is still a difficult problem due to presence of discontinuities, iii) effect of in-situ stresses and the deformational behaviour of the openings is complex, especially due to anisotropic nature of rock masses.

Deformational behaviour of tunnels in squeezing ground condition is essentially a problem involving strength and deformational behaviour of jointed rock masses under a given stress environment. Squeezing behaviour of tunnels of Khimti hydro-electric project (location) could not be predicted by the existing approaches (Shrestha, 2005). Predicted values of support pressure and tunnel deformation were found to be in good agreement with the respective values observed in the field for non-squeezing grounds but not for squeezing grounds (Shrestha, 2005).

1.4 IDENTIFICATION OF THE PROBLEM

In view of the above discussion, it is found that there is still a need of some easier solution with regard to prediction of the ground condition, deformations, and support pressures in and around tunnels, especially when excavated in squeezing conditions. The squeezing ground conditions are frequently met in Himalaya. The extent of squeezing may vary from place to place, even in the same tunnel, depending upon relative magnitudes of parameters which are responsible for squeezing to occur. In the present work, an attempt has been made to collect data from various hydro power projects which have already been executed in the lower Himalaya and this data has been analyzed to understand the squeezing phenomenon in a better manner.

1.5 OBJECTIVES OF THE STUDY

Keeping the aforementioned problems in view, the following objectives were set forth in the present study:

- Study of large no. of tunnel case histories,
- Collection of required data, viz., diameter and depth of tunnel, in situ stresses, rock mass quality parameters (joint properties, uniaxial compressive strength and rock mass number, etc.), observed radial tunnel deformation (closure), support pressure and details of supports installed in tunnels,
- Development of empirical correlations for prediction of ground condition,
- Development of empirical correlations for prediction of tunnel deformation and support pressure for non-squeezing and squeezing ground conditions.

1.6 ORGANISATION OF THESIS

The thesis contains following chapters:

Chapter 2: Review of Literature

This chapter is devoted to presentation of the state-of-art with regard to the studies carried out for prediction of ground condition, estimation of support pressures and tunnel deformations in squeezing and non-squeezing tunnels. Self-supporting, non-squeezing and squeezing ground conditions have been explained with the help of ground and support reaction curves. Various design approaches like empirical, analytical, observational, numerical and physical modelling have been discussed and compared.

Chapter 3: Geology of the Case Study Projects

The chapter describes geology, tunnelling problems and details of installed supports in tunnels/galleries of 24 tunnelling/ mining projects located in India, France, Italy, Turkey, Norway and United Kingdom, which have been taken up for the study.

Chapter 4: Prediction of Ground Condition

An attempt has been made in this chapter to develop empirical correlations for prediction of self-supporting, non-squeezing, squeezing and rock burst ground behaviour separately using Joint Factor (J_f), rock mass quality (Q), and rock mass number (N) as a measure of rock mass quality and tunnel diameter (D) as a measure of tunnel size. The approaches have been developed using 181 sets of data of various tunnel sections of different case studies. In addition to this, a correlation between joint factor and rock mass number has also been established.

Chapter 5: Prediction of Tunnel Deformation

In this chapter, dimensionally correct (same dimension of units in both sides of equations) correlations have been developed for prediction of tunnel deformations for non-squeezing and squeezing ground conditions. The correlations involving parameters, viz., Joint factor (J_f), Q and rock mass number (N) have been developed. Data has been collected from 63 sections of tunnels / adits / mine galleries for development of

correlations for squeezing ground conditions, whereas data from 35 tunnel sections have been utilised for development of correlations for non-squeezing ground conditions. In addition to this, parametric analysis of the recommended correlations has also been carried out.

Chapter 6: Prediction of Support Pressure

In this chapter, dimensionally correct correlations have been developed for prediction of support pressure in non-squeezing and squeezing ground conditions using data of 35 and 53 tunnel sections respectively. Accordingly parametric analysis has also been done for the correlations developed for both the ground conditions.

Chapter 7: Validation of Proposed Correlations

In this chapter, correlations developed in chapters 4 & 5 for ground prediction and tunnel deformation respectively have been validated with the data observed in the field through instrumentation and monitoring (Chenani-Nashri project, J & K, India) and also with the results obtained via numerical modelling using Phase^2 software. The correlations developed for prediction of support pressure could not be validated due to non-availability of field data.

Chapter 8: Summary and Conclusion

This chapter concludes the present study and suggests ideas for further research.

Chapter 2

REVIEW OF LITERATURE

2.1 GENERAL

Due to continuous growth of population (especially in the developing countries), increasing trend of industrialization and infrastructural development, utilization of underground space has been sought as a solution. Numerous hydro, highway and railway and metro underground tunnels are being constructed to help the need of the mankind. On the other hand, underground space is also utilized as rock caverns for petroleum storage, military bunkers, explosives & ammunition storage, research laboratories etc. Creation of underground space involves excavation and supporting of rock mass at various depths from the ground surface. Rock mass when excavated may exhibit self-supporting, non-squeezing or squeezing behaviour depending upon its quality, strength, size of tunnel/cavern, depth of over burden and the in-situ stresses.

The author has carried out study of numerous tunnel case histories for refinement of the existing knowledge in order to predict reliable support pressures and deformations in underground excavations for squeezing ground conditions. The chapter summarizes the state-of-the-art with regard to prediction of ground condition, tunnel deformation and the support pressure.

2.2 GROUND BEHAVIOUR AND SUPPORT INTERACTION

In rock mass-tunnel support interaction analysis, first half of the curve determines ground response and the other half can be described as the load-deflection curve of the support system. The point where the two characteristics intersect defines the equilibrium state. In general, a ground response curve can have descending and ascending sections. Ideally the support stiffness and the time of support erection should be selected in such a way that equilibrium is attained at the lowest minimum of the ground characteristic (Daemen, 1975).

Self-supporting, non-squeezing, and squeezing conditions of ground can be understood with the help of Figs. 2.1a and 2.1b (Hoek and Brown, 1982). Stronger rock masses may exhibit self-supporting and non-squeezing conditions depending upon the size of tunnels. Ground response curves for a typical rock mass with uniaxial compressive strength of plutonic intact rock material as 300 MPa are shown in Fig. 2.1a. The Figure illustrates how increase in tunnel depth or overburden affects the rock mass behaviour and support requirements in an 8 m diameter tunnel. At an overburden / cover pressure of 27 MPa, represented by curve 'A' in Fig. 2.1a, the opening would attain stability without any support and the condition is known as self-supporting. When the cover pressure (P) increases to 54 MPa, curve 'B' shows that the opening would stabilize, if p/P > FG (where p is support pressure). However, a support capacity less than FG can be used if some spalling and fracturing can be tolerated. At an in-situ stress of 81 MPa, curve 'C' shows that the support capacity has to be raised to HG if rock fracturing around the opening is to be prevented. The required support in this case may be a concrete lining which is difficult to provide near the face. It is advisable in this situation to allow the opening to deform and cross the critical line MM which signifies the beginning of rock fracturing and spalling. Although it is possible to stabilize the opening without support if one can tolerate significant roof falls, it was suggested to use un-tensioned rock bolts with wire-mesh and shotcrete to allow rock fracturing and tunnel closure upto GV without allowing roof falls.

The rock-mass and tunnel support interaction for squeezing ground condition can be explained by ground response and the support reaction curves shown schematically in Fig. 2.1b, which is a relation between the required support pressure (p) and the normalized tunnel closure (u/a). If no radial deformation is allowed, it gives rise to very high pressure requiring a very stiff support system at the tunnel face itself. This would be prohibitively expensive. The support pressure can be brought down by allowing the tunnel to deform. As the tunnel deforms, a broken zone is formed. The advantage of a broken zone can be maintained till the failed rock mass retains some cohesion. If the tunnel is allowed to deform beyond an optimum limit, given by point 'A' in Fig. 2.1b, the failed rock mass loses its cohesion and the ground arch is destroyed.

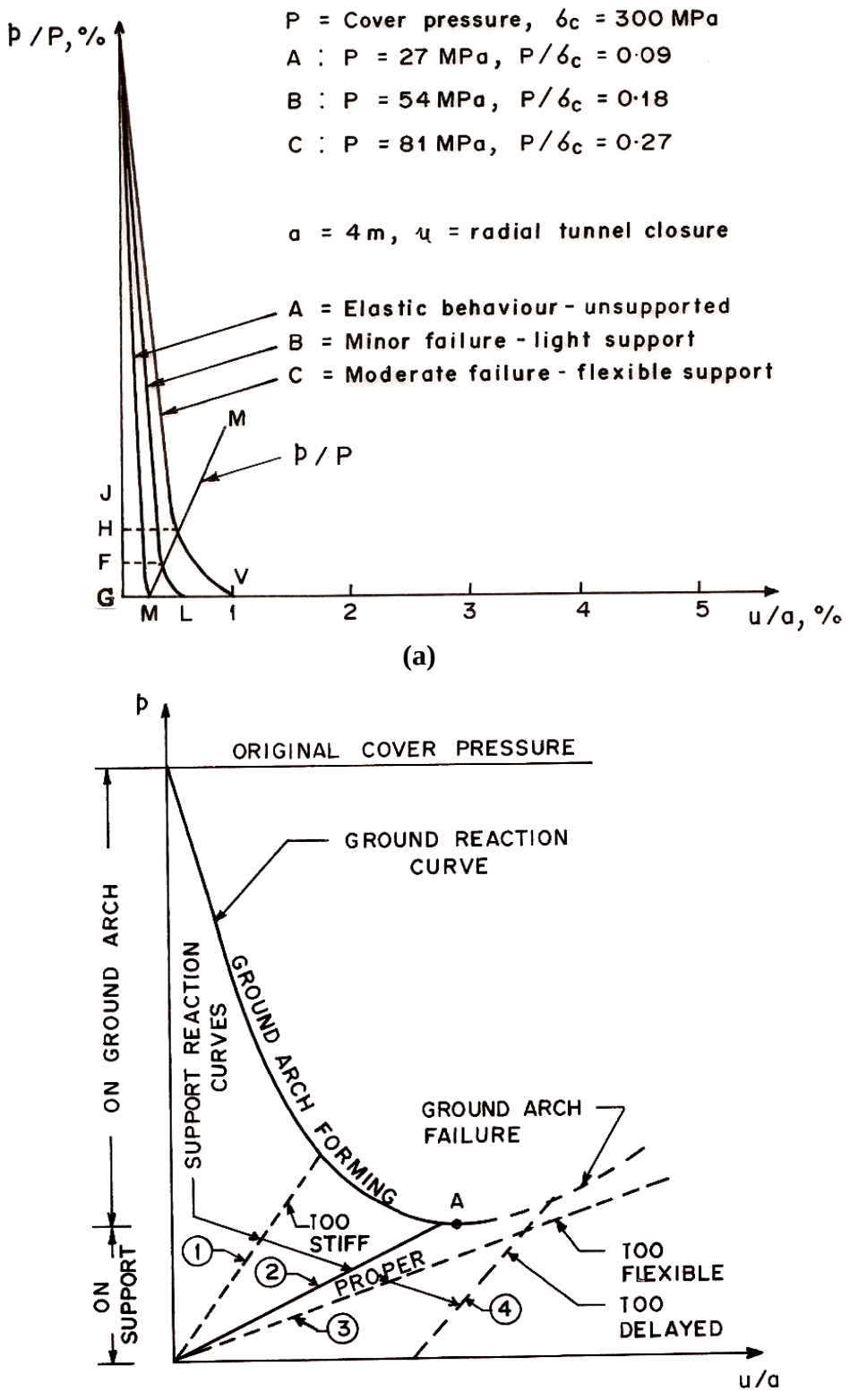

Fig. 2.1 Schematic Presentation of Ground Response and Support Reaction Curves

(a) Self-supporting and non-squeezing ground conditions and

(b) Squeezing ground condition (after Hoek and Brown, 1982)

The Figure 2.1b also shows four possible types of support reaction curves i.e. the relation between the measured support pressure (p) and the normalized tunnel closure (u/a). A very stiff support system would not allow desired level of radial tunnel closure and therefore, the support pressure would be very high (curve 1). A very flexible support (curve 3), on the other hand, would permit excessive deformation leading to failure of the ground arch. Even if a support having stiffness equivalent to curve 1 is used but its installation is delayed (curve 4), the ground arch may still be destroyed. A support of appropriate stiffness must be installed soon after excavation (curve 2) in order to obtain the maximum benefits of the ground arch formed due to the broken zone. In other words, the tunnel must be allowed to deform to an optimum level under controlled conditions in order to reduce the support pressure to an optimum value.

From the above discussion, it is clear that reliable prediction of ground condition, support pressure and deformation are important for the design of any support system. The scope of this chapter is limited to review of methods for the prediction of ground condition, the support pressure and the deformation in tunnels under non-squeezing and squeezing ground conditions.

Daemen (1977) has also explained the basic concept of the rock mass-tunnel support interaction with the help of Fig. 2.2. The explanation is as follows:

Differential steps of tunnel excavation and support installation have been shown in Fig. 2.2. Hydrostatic stress state (p_o) has been assumed. In Fig 2.2, a tunnel is being excavated by full face using drill and blast method and after each mucking cycle, steel rib supports are installed. All the steps are pertaining to the tunnel section X-X. In Fig. 2.2, ground response and the support reaction curves are depicted for the tunnel section under consideration and points corresponding to different steps are marked on these curves.

Step-1 explains the situation when the tunnel face has not yet reached the section X-X and the rock mass there is still in a state of pre-excavation equilibrium. This situation is denoted by point A on the ground reaction curve where the pressure required to be supported by the support system is equal to value of in-situ stress (p_0).

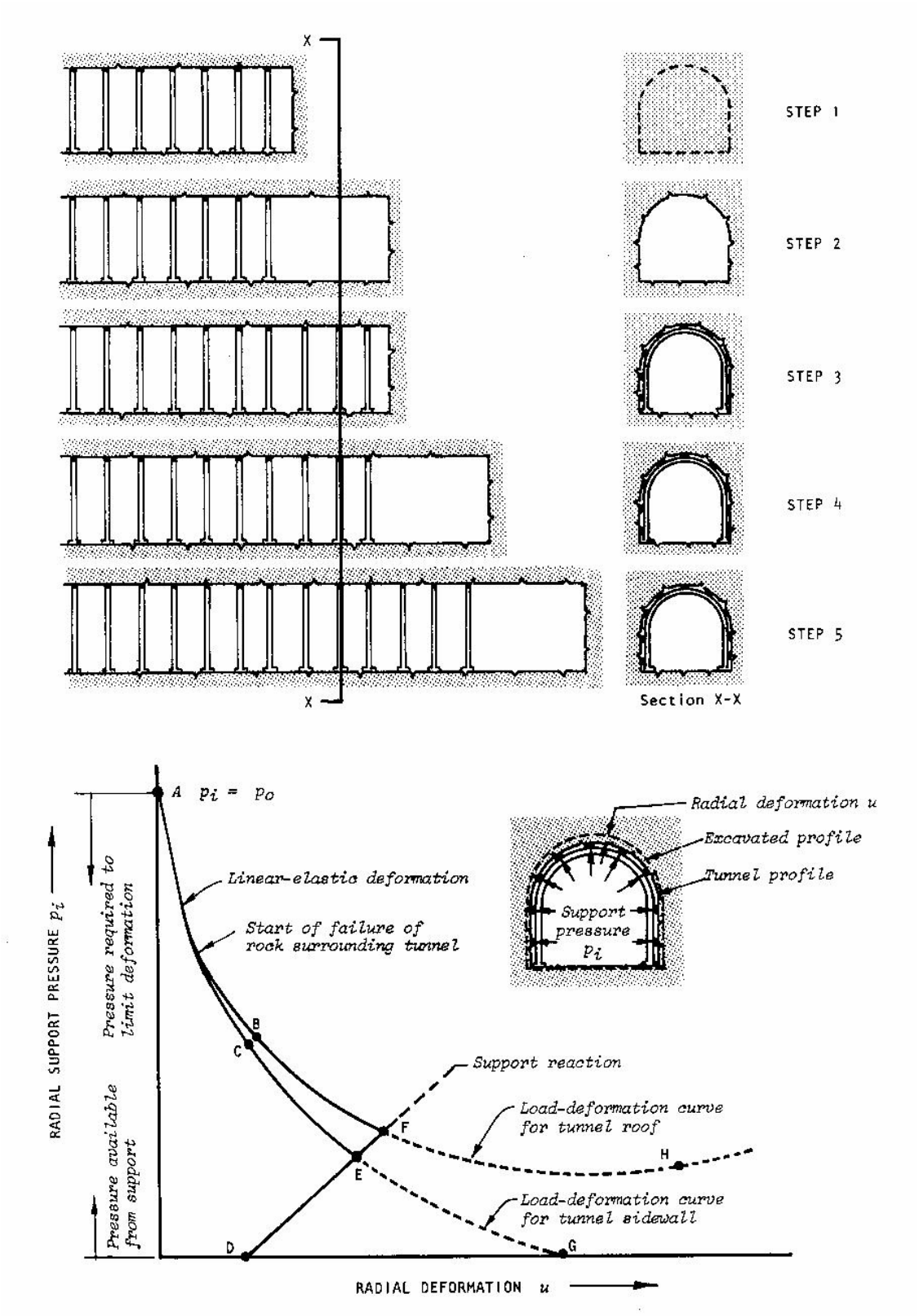

Fig. 2.2 Concept of Rock Mass-Tunnel Support Interaction (after Daemen, 1977)

In fact, at this stage, the support is being provided by the rock mass inside the dotted line shown in the cross-section in step-1.

In step-2, the rock mass from within the dotted line is excavated as the tunnel face advances beyond section X-X. Removal of the rock mass which was acting as a support means that the available support pressure has now become equal to zero. However, this will not result in a collapse of the tunnel as the support is now being provided by the restraint available due to the proximity of the tunnel face to the section X-X.

The support pressure now available due to this restraint, denoted by points B and C (on ground response curves for tunnel roof and side walls respectively) limits the deformation to a value on X-axis corresponding to these points. The support pressure required to limit the tunnel roof deformation is higher than that required to limit the sidewall deformations because the weight of the loosened rock mass above the tunnel roof is added to the support pressure required to limit the tunnel roof deformation.

In step-3, the steel ribs have been installed at section X-X. However, since the tunnel face has not advanced further, no further deformation has taken place (assuming the there is no time dependent deformation). The support at section X-X, therefore, carries no load and this situation is denoted by point D which is the starting point for the support-reaction curve.

In step-4, the tunnel face has moved about 1.5 times the tunnel diameter beyond section X-X and the restraint provided by the proximity of the tunnel face is thereby considerably reduced. This results in an additional radial deformation of the tunnel (indicated by curves BFH and CEG) which, in turn, induces load on the support system. The support system, acting as a stiff spring, provides more and more support pressure with increasing tunnel deformation and the support-reaction curve follows the path DEF.

In step-5 the restraint provided by the face at section X-X has totally disappeared as the face has moved much beyond the section. If no supports were installed, the radial tunnel deformation would have continued to increase as indicated by the curves EG and FH. In the case of sidewalls, the support pressure required to restrict further deformation, drops to zero at point G and, in this case, the sidewalls become stable.

For the roof, however, the required support pressure drops to a minimum (denoted by point H) and then begins to rise again. This is because the downward movement of the loosened rock mass above the roof causes more rock mass to become loose. The weight of this additional loosened rock mass is added to the required support pressure. The continuously rising trend of the ground response curve for the roof shows that the roof would have collapsed if no support had been installed.

The most important feature of Fig. 2.2 is the point of intersection of the ground response and the support reaction curves (denoted by E and F for sidewall and roof respectively). At this point, the support pressure required to limit further deformation is balanced by the pressure available from the support system. Thus, at this point, the supported tunnel attains a state of equilibrium.

The example of Fig. 2.2 adequately brings out the importance of considering the interactive nature of the rock mass and the support system for the rational design of the latter. For this, the load-deflection behaviour of both rock mass and support system must be clearly understood and lot of literature has appeared in this respect.

The design approaches on tunnelling in squeezing ground have been classified into six broad categories; i) empirical, ii) semi-empirical, iii) analytical, iv) observational v) numerical, and vi) physical modeling. These are discussed as follows:

2.3 EMPIRICAL APPROACHES

Empirical approaches are based purely on experience and comparison of the effects of parameters in the field. Various research workers have proposed empirical approaches for the assessment of the potential squeezing phenomenon, which are as follows:

2.3.1 Prediction of Ground Condition

Various ground conditions, which may be encountered during tunnelling, are elastic self-supporting, elastic supporting or non-squeezing, raveling, squeezing, swelling, running, flowing and rock burst.

The scope of the present work is limited to only the prediction of following ground conditions:

i) Self-supporting elastic ground condition,
ii) Elastic ground conditions requiring supports, here-after called non- squeezing ground condition, and
iii) Squeezing ground condition requiring flexible supports.

Wood (1972) initially proposed the concept of Competence Factor to assess the stress induced instability in tunnel. The factor is defined as the ratio of the unconfined compressive strength of the rock mass (σ_{cm}) to the overburden stress. When this factor is less than 2, the ground will undergo squeezing. This parameter has been used by many authors in many cases to recognize the squeezing potential of tunnels. However, σ_{cm} needs to be estimated using empirical correlations expressed in terms of either uniaxial compressive strength of intact rock (σ_{ci}) or the rock mass quality.

Jethwa et al. (1979) conducted study in tunnels of Loktak hydro-power project in India and suggested following criteria for the squeezing ground condition on the basis of the ratio of cover pressure, σ_v and uniaxial compressive strength, σ_{ci} of rock material as shown below in Table 2.1.

Table 2.1 Criteria for Degree of Squeezing (after Jethwa et al., 1979)

Value of $2\sigma_v / \sigma_{ci}$	**Ground Condition**
<1	Non-squeezing
1-3	Mild to moderate squeezing
>3	High squeezing

Saari (1982) suggested the use of the tangential strain in tunnels as a parameter to assess the degree of squeezing of rock, and a threshold value of 1% was also suggested for the recognition of squeezing (Shrestha, 2005).

Singh et al. (1992) developed an approach to predict squeezing behaviour of rock mass on the basis of rock mass quality Q (Barton et al., 1974) and overburden depth, *H* (m). The approach was developed after analyzing the data of 41 tunnel section (17 from case histories given in Barton et al., 1974 and 24 were obtained from the tunnels

of Himalayan region). This approach has given a demarcation line (Eq. 2.1) to differentiate squeezing condition from non-squeezing condition (Fig. 2.3).

$$H = 350\ Q^{1/3} \text{ m} \tag{2.1}$$

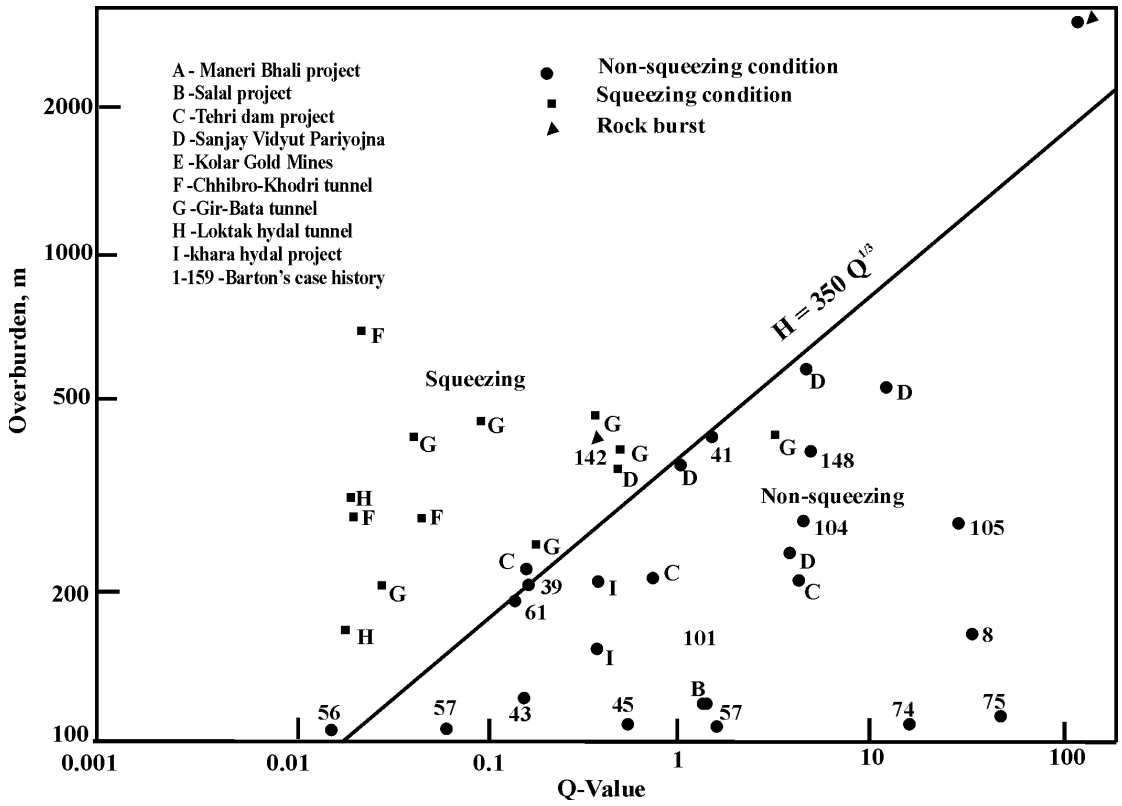

Fig. 2.3 Prediction of Squeezing Ground Condition (after Singh et al., 1992)

The data points lying above the demarcation line represent squeezing conditions, whereas those below this line represent non-squeezing conditions. This can be summarized as follows:

For squeezing condition, $H > 350\ Q^{1/3}$ m (2.2)

For non-squeezing condition, $H < 350\ Q^{1/3}$ m (2.3)

Verman (1993), included the tunnel diameter in addition to the tunnel depth H and rock mass quality Q, and suggested the following empirical inequalities to predict ground condition:

For squeezing ground condition, $H\ (B\text{-}B_s)^{0.1} > 483\ Q^{1/3}$ m (2.4)

For non-squeezing ground condition, $H\ (B\text{-}B_s)^{0.1} < 483\ Q^{1/3}$ m (2.5)

where

B is tunnel span in m; B_s is self-supporting tunnel span in m and is computed as -

$B_s = 2\ ESR\ Q^{0.4}$ (Barton et al., 1974) (2.5a)

where *ESR* is Excavation Support Ratio.

Goel (1994) developed an empirical approach based on the rock mass number *N*, defined as rock mass quality, Q with stress reduction factor, *SRF* = 1. *N* was used to avoid the problems and uncertainties in obtaining the correct rating of parameter *SRF* in the *Q* system. Considering the overburden depth *H*, the tunnel span or diameter *B*, a log-log plot between rock mass number (*N)* and $HB^{0.1}$ was made. Line AB in the plot (Fig. 2.4) distinguishes the squeezing and non-squeezing cases. The data points lying above the line represent squeezing conditions, whereas points lying below the line represent the non-squeezing conditions. Empirical approaches using *N* were also developed to estimate support pressure and closure in tunnels under squeezing conditions.

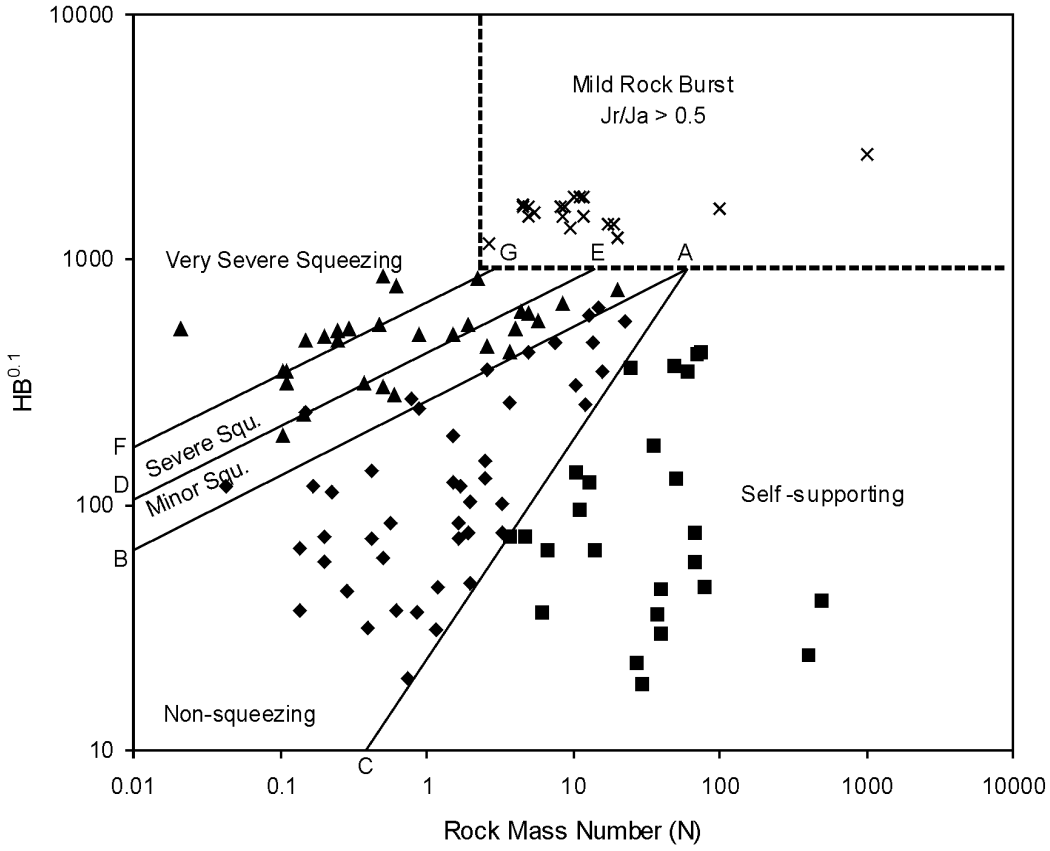

Fig. 2.4 Prediction of Squeezing Ground Condition (after Goel, 1994)

As shown in the Fig. 2.4, a line AB separates the squeezing and non-squeezing cases. The equation of this line is given as follows:

$$H = (275\, N^{0.33})\, B^{-0.1} \quad (2.6)$$

$$H > (275\, N^{0.33})\, B^{-0.1} \quad \text{(for squeezing condition)} \quad (2.6a)$$

$$H < (275\, N^{0.33})\, B^{-0.1} \quad \text{(for non-squeezing condition)} \quad (2.6b)$$

where

H = height of overburden above tunnel or tunnel depth, m,

N = rock mass number (rock mass quality Q with SRF=1) and

B = width of tunnel, m.

The data points lying above the line represents the squeezing conditions, whereas points below the line represent the non-squeezing conditions.

Russo (2008) suggested a multi-graph to predict ground behaviour using intact rock strength (uniaxial compressive strength, σ_c), joint conditions (J_c), rock block volume, (V_b), geological strength index (GSI), rock mass rating (RMR), rock mass strength (σ_{cm}) and vertical in-situ stress ($\sigma_v = \gamma H$). The graph has four quadrants, i.e. I-quadrant (lower right quadrant) to IV-quadrant (upper right quadrant) in Fig. 2.5. Quadrant-wise steps for assessment of ground behaviour by the graph have been described as follows:

Quadrant-I: Lower right segment of the graph is Quadrant-I. In this segment, graph of GSI versus joint condition (J_c) for various values of block volume (V_b) has been plotted. With the help of known values of J_c and V_b, corresponding GSI value is obtained by projecting the coordinate (J_c, V_b) on the GSI-axis of the graph.

Quadrant-II: Lower left segment of the graph is Quadrant-II. In this segment, graph of GSI versus σ_{cm} for various values of σ_c has been plotted. With the help of known values of GSI and σ_c, value of σ_{cm} is obtained on projecting the coordinate (σ_c , GSI) on σ_{cm} – axis (upper horizontal line of the segment).

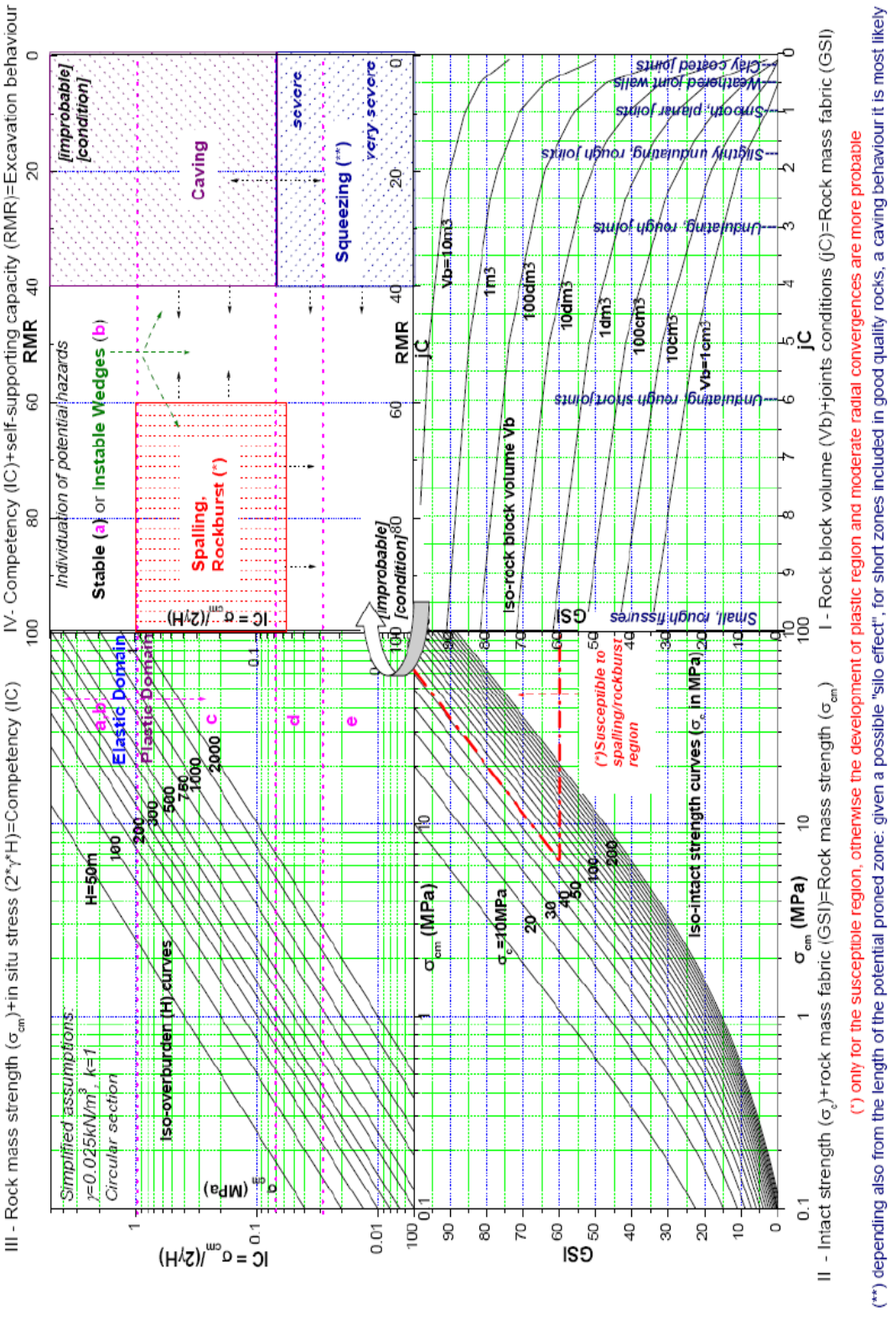

Fig. 2.5 Proposed Multiple Graph for Prediction of Ground Behaviour
(after Russo, 2008)

Quadrant-III: The upper left segment of the graph is Quadrant-III. In this segment, the graph of competency index ($IC = \sigma_{cm} / 2\gamma H$) and σ_{cm} for various values of tunnel depth (overburden height, H) has been plotted. With the help of σ_{cm} and H, value of IC is obtained by projecting the coordinate (σ_{cm} , H) on IC-axis.

Quadrant-IV: Upper right segment is Quadrant IV of the multi-graph. In this segment, areas have been marked at various places with respect to the IC and RMR-axes. Area marked as (a) is stable as it is near coordinate (IC=10, RMR=100). On moving in a straight line towards upper right corner in this segment, value of RMR increases but value of IC remains constant. The area marked as (b) in the graph, exhibits unstable block conditions. Area located at lower right corner of the segment shows squeezing behaviour of the ground as this area represents low IC and RMR values.

2.3.2 Prediction of Support Pressure

Terzaghi (1946) was the first to make a successful attempt in classifying rock masses for the engineering purposes who proposed a rock load factor, H_p which is the height of loosening zone over the tunnel roof and likely to load the steel arches. These rock load factors were estimated by Terzaghi (1946) from his observations on several 5.5 m wide steel arch supported rail road tunnels in the Alps ranges during the early part of twentieth century. Terzaghi (1946) considered various structural discontinuities of rock masses and classified them qualitatively into nine categories, viz., i) hard and intact, ii) hard, stratified and schistose, iii) massive to moderately jointed, iv) moderately blocky and seamy, v) very blocky and seamy, vi) completely crushed but chemically intact, vii) squeezing rock at moderate depth, viii) squeezing rock at great depth and ix) swelling rock. The results of his 'Trap-door' experiments were combined and rock loads estimated from Alpine tunnels to compute rock load factor, H_p in terms of tunnel width, B and tunnel height, H_t of the loosened rock mass above the tunnel crown. A certain height of the loosened rock mass (called 'rock load factor') assigned to each of the aforesaid nine qualitative categories of rock masses, was considered to load the steel sets. This height of the loosened rock mass was treated as a function of the width and height of the opening. Thus, Terzaghi's method

is strictly applicable to the loosening pressures which are assumed to increase directly with the tunnel width. The rock load values presented in Table 2.2 apply, if a tunnel is located under the water table. However, if the tunnel is located above the groundwater table, the rock loads for classes 4-6 can be reduced by 50% (Rose, 1982).

Table 2.2 Terzaghi's (1946) Rock Load Classification

Rock Class	Rock Condition	Rock Load Factor, H_p (m)	Remarks
I	Hard and intact	Zero	Light lining required only if spalling or popping occurs
II	Hard stratified or schistose	0 - 0.5B	Light support mainly for protection against spalling. Load may change erratically from point to point
III	Massive moderately jointed	0 - 0.25B	No side pressure
IV	Moderately blocky and seamy	0.25B - 0.35(B+ H_t)	No side pressure
V	Very blocky and seamy	(0.35 - 1.10)(B+ H_t)	Little or no side pressure
VI	Completely crushed	1.10(B+ H_t)	Considerable side pressure. Softening effects of seepage toward bottom of tunnel require either continuous support for lower ends of ribs or circular ribs
VII	Squeezing rock at moderate depth	(1.10 - 2.10)(B+ H_t)	Heavy side pressure, invert struts required. Circular ribs are recommended
VIII	Squeezing rock at great depth	(2.10 - 4.50)(B+ H_t)	-do-
IX	Swelling rock	Up to 80m, irrespective of the value of (B + H_t)	Circular ribs are required. In extreme cases, use of yielding support recommended

Notation: ***B- tunnel span, m; H_t = height of the tunnel, m; H_p = height of the loosened rock mass above tunnel crown developing load.***

Despite the fact that Terzaghi's (1946) classification provided only qualitative information regarding the rock mass properties, the approach cannot be underestimated because the method still finds application under conditions similar to those for which it was developed (Singh et al., 1995).

Wickham et al. (1972, 1974) introduced 'Rock Structure Rating' (RSR) and proposed a quantitative classification system called 'Ground Support Prediction Model'.

The RSR concept primarily considers the geological and constructional parameters, which influence the rock mass behaviour around a tunnel periphery. The geological parameters comprised the rock type, joint spacing, joint orientation (dip and strike), type of discontinuities, major faults, shears and folds, rock material properties, and status of weathering or alteration. The constructional parameters included the size of tunnel, direction of the drive and the method of excavation. All the above factors were grouped into three basic parameters A, B and C. The sum of these three basic parameters gives the RSR value, which reflects the quality of rock mass with respect to its need for support. Wickham et al. (1974) proposed the following correlation to estimate the support pressure:

$$p = \frac{B}{302}\left[\frac{8800}{RSR + 30} - 80\right] \tag{2.7}$$

where p is the estimated support pressure (klbs/ft^2); and B is the width of the tunnel in ft.

In the above correlation, the effect of in-situ stresses and permissible tunnel closure has not been considered, whereas these parameters play key roles in development of support pressure, especially in squeezing ground conditions.

Bieniawski (1976) developed 'Rock Mass Rating' (RMR) or Geo-mechanical Classification System which was subsequently revised. This classification system includes six parameters, viz., recommended excavation methods and support systems for a 10 m diameter tunnel, but did not suggest any value of support pressure. The rock mass rating, RMR is the sum of the following rated parameters: i) uniaxial compressive strength of intact rock material, ii) rock quality designation RQD, iii) joint or discontinuity spacing, iv) joint condition, v) ground water condition, and vi)

joint orientation with respect to the tunnelling direction. Bieniawski (1989) suggested various support systems using RMR for 10 m diameter tunnels (Table 2.3), but it was not generalized for all cases.

Table 2.3 Geo-mechanical Classification Guide for Excavation and Support in Rock Tunnels (after Bieniawski, 1989)

Rock Mass Class	Excavation	Supports		
		Rock Bolts (20 mm diameter fully grouted)	**Shotcrete**	**Steel ribs**
Very good RMR= 81- 100	Full face. 3 m advance	Generally, no support required except for occasional spot bolting		
Good RMR = 61- 80	Full face. 1.0-1.5m advance. Complete support 20 m from face	Locally, bolts in crown 3 m long, spaced 2.5 m, with occasional wire mesh	50 mm in crown where required	None
Fair RMR = 41- 60	Heading and bench. 1.5 – 3 m advance in heading. Commence support after each blast. Complete support 10m from face	Systematic bolts 4 m long spaced 1.5 - 2 m in crown and walls with wire mesh in crown	50-100 mm in crown and 30 mm in sides	None
Poor rock RMR = 21- 40	Top heading and bench. 1.0-1.5 m advance in top heading. Install support concurrently with excavation 10m from face	Systematic bolts 4-5 m long, spaced 1-1.5 m in crown and wall with wire mesh	100-150 mm in crown and 100 mm in sides	Light to medium ribs spaced 1.5 m where required
Very poor rock RMR< 20	Multiple drifts 0.5 - 1.5 m advance in top heading. Install support concurrently with excavation. Shotcrete as soon as possible after blasting	Systematic bolts 5 -6 m long spaced 1-1.5 m in crown and walls with wire mesh. Bolt invert.	150-200 mm in crown 150 mm in sides and 50 mm on face	Medium to heavy ribs spaced 0.75 m with steel lagging and fore-poling, if required. Close invert

Note: ***The tabulated support systems were developed for 10 m diameter, horse-shoe shaped tunnels excavated by drill and blast method at overburden pressure below 25MPa.***

Unal (1983) studied the case histories of coal mines and proposed the following correlation for prediction of the support pressure using RMR:

$$p = \frac{100 - RMR}{100}.\gamma B \tag{2.8}$$

where p is the estimated support pressure in kg/cm^2, γ, the rock density in kg/cm^3, and B, the tunnel width in cm.

Jethwa and Goel (1992) evaluated Eq. 2.8 for its application to Indian tunnels by comparing the measured support pressures with estimates from Eq. 2.8. The comparison showed that Eq.2.8 is not applicable for rock tunnels. It was found that the estimated support pressures were unsafe for all tunnels under squeezing ground conditions irrespective their sizes. Further, the estimates for non-squeezing ground conditions were unsafe for small tunnels and over-safe for large tunnels (diameter > 9m), which implies that the size effect was over emphasized by Unal (1983) in Eq.2.8.

Barton et al. (1974) suggested following generalized correlation (Eq. 2.9) to estimate the ultimate support pressure in a tunnel:

$$p = \frac{0.2}{J_r} Q^{-1/3} \text{ MPa} \tag{2.9}$$

where p is the estimated ultimate support pressure, J_r, the joint roughness number, and Q, the rock mass quality. Further Barton et al. (1974) suggested following correlation (Eq. 2.10) for the case where number of joint sets is less than 3:

$$p = \frac{0.2}{J_r}\left(\frac{\sqrt{J_n}}{3}\right) Q^{-1/3} \text{ MPa} \tag{2.10}$$

where J_n is the joint set number.

Equations 2.9 and 2.10 do not involve tunnel size, in-situ stresses, permissible tunnel deformation and any intact rock parameters, which play a very important role in squeezing ground condition and hence cannot give reliable predictions, especially in squeezing ground conditions.

In addition to the above, Singh et al. (1992) proposed the following approach for prediction of support pressure using Barton's Q-value.

$$p = \frac{0.2}{J_r} Q_i^{-1/3} f . f' f'' \quad \text{MPa} \tag{2.11}$$

where

Q_i = $5Q$ for short-term support pressure,

= Q for ultimate support pressure,

f = $1 + (H - 320) / 800$ for overburden, $H > 320$m,

f' = correction factor for tunnel closure (from Fig. 2.6),

f'' = correction factor for time after excavation,

= $\log (9.5\, t^{0.25})$, (2.11a)

t = time (in months) after excavation, and

Q = actual post construction rock mass quality.

The above approach is general in nature and not specifically for squeezing or non-squeezing conditions. It does not include the size of tunnel which also plays a very important role as it influences the degree of anisotropy, especially in poor rock mass. In addition to this, the approach is not valid for overburden depth less than 320 m (as value of f is valid for H > 320 m in Eq. 2.11), whereas, squeezing behaviour has been observed even for rock cover of less than 300 m. For instance, railway tunnel No. 1 between Udhampur and Katra (Jammu-Udhampur rail line project, Jammu & Kashmir, India) exhibited squeezing ground condition when excavated through claystone at about 270 m of rock cover above it.

Verman (1993) determined the ground and support reaction curves from the data of instrumented tunnels of Himalayan region and proposed a correlation using RMR for estimation of deformation modulus of rock mass. Correlations were also proposed for estimation of short-term support pressures in tunnels (Eq. 2.12).

$$P_{if} = \frac{1 - \left[(1-e) - (b_f/a)^2 e - 2(b/a)u_b + (u_b/a)^2\right]^{1/2} - (u_{ao}/a)}{(S.A/A_s.E_s) + (0.86a^{1.05}/t_b.E_{bf})} \tag{2.12}$$

where

$$u_b = \frac{(1+\nu)}{RF.E_{\min}} \left[p_o \sin\phi_p + \cos\phi_p\right] \tag{2.12a}$$

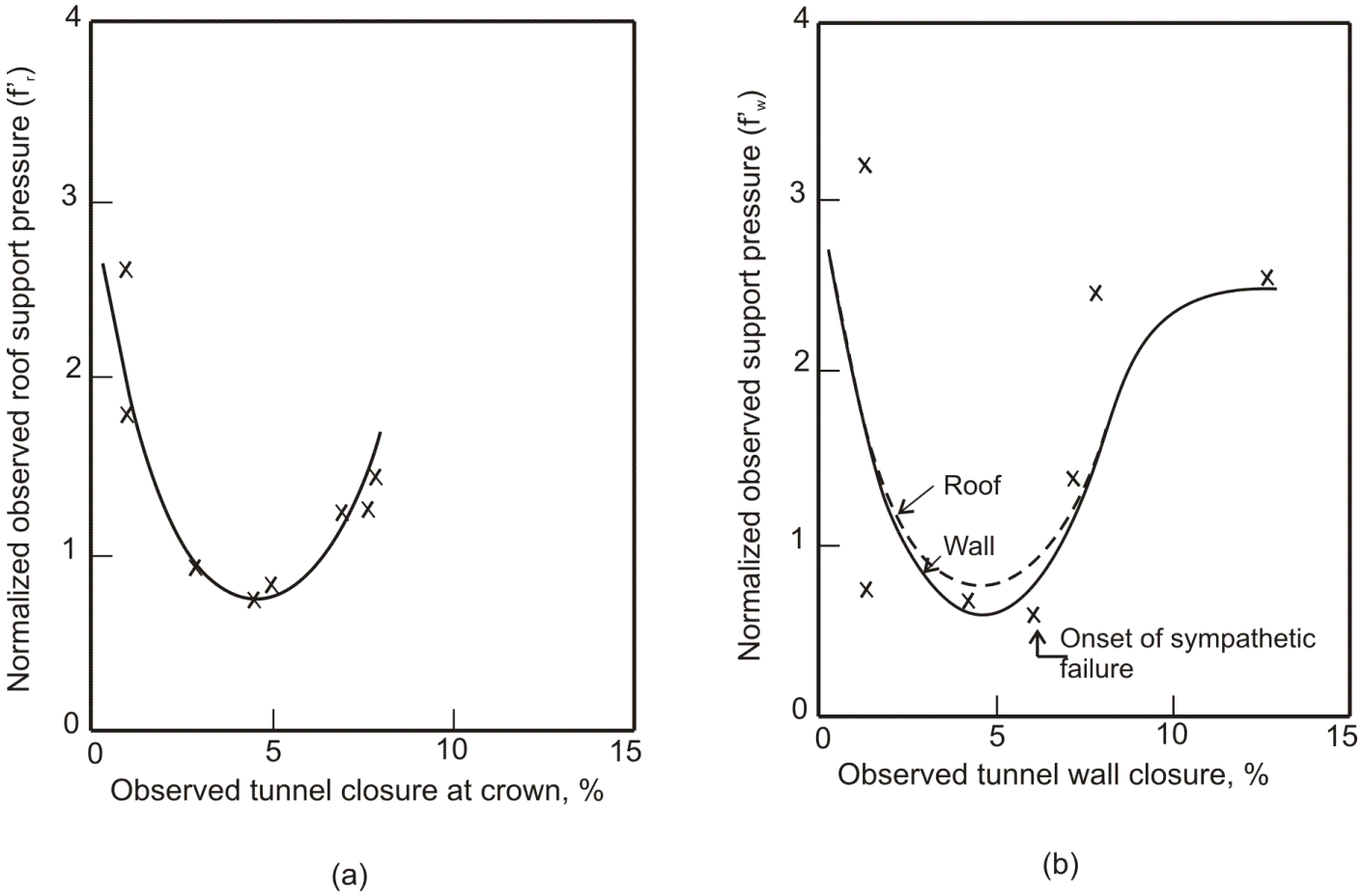

Fig. 2.6 Correction Factor for (a) Roof Closure and (b) Wall Closure, under Squeezing Ground Condition

(after Singh et al., 1992)

P_{if} defines the estimated short-term support pressure; E_{bf}, the modulus of elasticity of backfill at support pressure of P_{if}; E_s, the modulus of elasticity of steel; A, the cross sectional area of tunnel; S, the spacing of steel ribs from centre to centre; A_s; the cross sectional area of steel rib; u_{ao}, the initial radial tunnel deformation before installation of support; u_b, the radial displacement of elastic-plastic boundary; e, the coefficient of volumetric expansion of the failed rock mass; a, the radius of tunnel; b, the radius of elastic broken zone; b_f, the radius of fractured broken zone; t_b, the thickness of backfill; v, the Poisson's ratio of rock material; p_o, the hydro-static in-situ stress; RF, the reduction factor; ϕ_p, the peak angle of internal friction of rock mass in elastic zone; and E_{min} is the smaller of two moduli of deformation of rock mass in horizontal and vertical directions.

Goel (1994) concluded from the analysis of sixty three case studies (36 from India, 4 from Kielder experimental tunnel reported in Hoek & Brown (1982), and 23 NGI cases reported by Bieniawski (1984)) that the effect of tunnel size and depth of overburden is less in non-squeezing conditions, but, it is significant in squeezing conditions. Based on this study, following empirical correlations (Eqs. 2.13 and 2.14) were suggested for prediction of ultimate support pressure for squeezing and non-squeezing ground conditions:

$$p = \left(\frac{f}{30}\right) 10^{\frac{H^{0.6} a^{0.1}}{50 N^{0.33}}} \tag{2.13}$$

$$p_{el} = \frac{0.12 H^{0.1} a^{0.1}}{N^{0.33}} - 0.038 \tag{2.14}$$

where p is the estimated ultimate support pressure in squeezing ground conditions, MPa; and p_{el}, the estimated ultimate support pressure in non-squeezing ground condition, MPa; f, the correction factor for closure (Fig. 2.7); H, the depth of tunnel, m; a, the radius of tunnel, m; and N is the rock mass number.

Horizontal in-situ stress (σ_h) plays key role in development of support pressure and tunnel deformation in squeezing ground conditions, especially in Himalayan region where the rock mass is under the influence of tectonic activity giving rise to directly increased horizontal stresses. In addition to this, intact rock property (σ_{ci}) is also

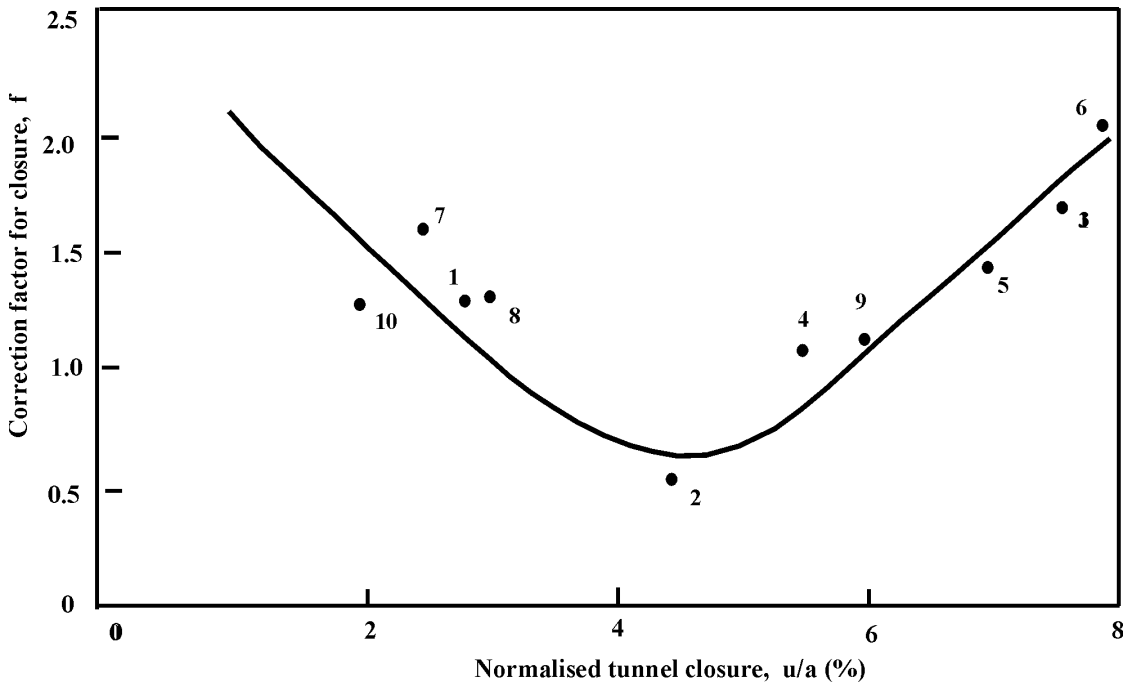

Fig. 2.7 Correction Factor for Tunnel Closure (after Goel, 1994)

important in this regard. Therefore, values of support pressure predicted in squeezing ground conditions using Eq. 2.13 would have been more close to the observed values, if the aforementioned both parameters (σ_h and σ_{ci}) were involved.

Bhasin and Grimstad (1996) proposed following equation to estimate the support pressure (p).

$$p = \frac{0.4}{J_r} B.Q^{-1/3} \tag{2.15}$$

where, B is span or diameter of the tunnel in metre and other symbols are already defined in Eq. 2.11.

Grimstad and Bhasin (1999) discussed the stability problems caused by high stresses in hard rock tunnels. Observational and empirical methods were used for analyzing the rock stress problems.

Kumar (2002) studied various existing rock mass classification systems and concluded that - i) parameter, Q was not reliable for squeezing ground conditions, ii) Support pressures prediction by Unal (1983) were unsafe for squeezing conditions, iii) RSR over estimates the support requirement in non-squeezing conditions, v)

RMR was unsafe for both non-squeezing and squeezing conditions, and vi) RMi highly over-estimated the rock pressure. It was also suggested that in over stressed conditions, if $J_r/J_a \geq 0.5$, rock burst was observed.

Shrestha (2005) evaluated the required supports using various empirical approaches for Khimti-I and Melamchi tunnels in Nepal. Empirical approaches suggested by Singh et al. (1992) and Goel (1994) were found to be valid in prediction of non-squeezing conditions in these tunnels, but the approaches were found to be conservative for squeezing condition. For instance, the aforementioned approaches predicted non-squeezing conditions at the sections Adit-1, 475m downstream and Adit-1 500m downstream, whereas severe squeezing was observed at both the sections. Further, tunnel deformations at these sections were observed to be considerably very large as compared to the values predicted by the empirical correlation given by Goel (1994). In the analysis of squeezing behaviour of the Khimti tunnel, valley-side effect of the topography was observed. The valley side slope was 22°. This effect was not considered in any of the available squeezing prediction criteria. It was recommended for further study to correlate the valley side slope and maximum topographical height with stress increase in the tunnel. Moreover, on observation of the strong effect of rock mass strength on squeezing behaviour, it was suggested to include rock mass strength as a parameter in the approaches for prediction of squeezing behaviour of the ground.

Viladkar et al. (2008a, b) suggested an approach for determination of ground and support response curve for non-squeezing and squeezing ground conditions on the basis of analysis of field instrumentation data of nine different tunnelling projects in India and observed the dependency of deformation modulus of poor rock on support pressure and reduction in support pressure by intermediate in-situ stress along the tunnel length. An approach was also suggested to determine stiffness of backfill between rib support and rock.

2.3.3 Prediction of Tunnel Deformation

Goel (1994) suggested following correlation to estimate tunnel deformation in squeezing and non-squeezing ground conditions:

$$u_{asq} = \frac{1}{10.5} \frac{a^{1.12} H^{0.81}}{N^{0.27} K^{0.62}} \tag{2.16}$$

$$u_{ael} = \frac{1}{28} \frac{aH^{0.61}}{N^{0.406} K^{0.35}} \tag{2.17}$$

where

H = depth of tunnel, m

a = radius of tunnel, m

N = rock mass number,

u_{asq} = estimated radial tunnel deformation in squeezing ground, cm,

u_{ael} = estimated radial tunnel deformation in non-squeezing ground, cm, and

K = effective support stiffness, MPa.

Sakurai (1997) and Chern et al. (1998) showed that for tunnels constructed in Taiwan, problems with tunnel stability occurred when the 'strain' exceeded about 1% (in Shrestha, 2005).

Singh et al. (2007) suggested a critical strain parameter as an indicator to quantify the squeezing potential of the tunnelling ground. The parameter is defined as the strain level on the tunnel periphery beyond which squeezing problems are likely to occur. In general, the value of critical strain is taken as 1%. Further, the authors have explained in the study that critical strain is an anisotropic property and depends on the properties of the intact rock and the joints in the rock mass. A correlation of critical strain with the uniaxial compressive strength, tangent modulus of intact rock and the field modulus of the jointed mass have been suggested in their study. It is also suggested that the modulus of deformation being anisotropic in nature should be obtained from field tests. In absence of field tests, expressions for critical strain have also been suggested in terms of rock mass quality, *Q*. A rational classification based on Squeezing Index (SI) is proposed to identify and quantify the squeezing potential in tunnels. Applicability of the approach has been demonstrated through its application to 30 case histories from the field.

2.4 SEMI-EMPIRICAL APPROACHES

Following semi-empirical approaches have been proposed for ground condition prediction, support pressure and tunnel deformation.

2.4.1 Prediction of Ground Condition

Singh et al. (2007), based on the tests conducted on rock mass specimens, came out with following approach for prediction of squeezing ground condition:

$$\varepsilon_{cr} = \frac{\sigma_{ci}}{\left(E_{tj}\right)^{0.37}\left(E_i\right)^{0.63}} x100 \qquad (2.18)$$

where ε_{cr}, σ_{ci}, E_{tj}, and E_i are critical strain in percent, uniaxial compressive strength of intact rock, tangent modulus of rock mass and tangent modulus of intact rock respectively. It was suggested that E_{tj} be determined in the field. If the observed or predicted tunnel strain, $\varepsilon_\theta{}^a \left(= u_a/a\right)$ exceeds value of critical strain, squeezing condition is likely to occur according to the squeezing index ($\varepsilon_\theta{}^a/\varepsilon_{cr}$) as suggested in the Table 2.4.

Table 2.4 Proposed Classification for Squeezing Potential in Tunnels
(after Singh et al., 2007)

Class Number	Squeezing Level	Squeezing Index (SI)
1	No squeezing (NS)	SI < 1.0
2	Light squeezing (LS)	1.0 < SI ≤ 2.0
3	Fair squeezing (FS)	2.0 < SI ≤ 3.0
4	Heavy squeezing (HS)	3.0 < SI ≤ 5.0
5	Very heavy squeezing (VHS)	5.0 < SI

Gutierrez and Xia (2009) conducted studies on shales and clay and proposed correlations for prediction of ground condition. Tunnels will have high potential of squeezing, if one of the following conditions exists:

$$\sigma_v' > \left(\frac{F(n)}{aN}\right)^{(-1/b)} \left(5.4\sigma_{ci}^{\ 0.73}\right) \tag{2.19}$$

$$\sigma_v' > \left(\frac{F(n)}{aN}\right)^{(-1/b)} \left(1.08.10^{-8} V_p^{\ 2.5}\right) \tag{2.20}$$

where $N = \frac{\sigma_v}{S_u}$,

in which N is the stability number; σ_v , the vertical in-situ stress (MPa); S_u , the un-drained shear strength of clay (MPa); $F(n)$, the function of porosity (n) of material; σ_v' , the effective vertical in-situ stress (MPa); σ_{ci} , the uniaxial compressive strength of intact rock (MPa); V_p , the P-wave velocity (m/s); and *a, b* are the empirical constants.

2.4.2 Prediction of Tunnel Deformation

Detourney and Fairhurst (1987) proposed a semi-empirical elasto-plastic model for a long cylindrical tunnel like cavity to obtain an explicit solution for stresses and deformations under a non-hydrostatic stress field. According to this model, the tunnel deformation at any point on the tunnel periphery is taken in perpendicular direction to the maximum in-situ compressive stress, if the rock failed is large enough. This provides the possible explanation of large deformation in tunnels driven through squeezing ground condition and having high in-situ vertical stress.

Aydan et al. (1993) developed correlations amongst strains (elastic, plastic, squeezing, and rupture) and uniaxial compressive strength. This approach is based on analogy between the axial stress-strain response of rocks in laboratory tests and tangential stress-strain response of rocks surrounding the tunnels.

On the basis of experience gained with tunnels in Japan, Aydan et al. (1993) proposed the following correlations between uniaxial compressive strength of the intact rock, σ_{ci} in MPa and the strain levels:

$$\eta_p = \frac{\varepsilon_p}{\varepsilon_\theta} = 2\sigma_{ci}^{-0.17}, \quad \eta_s = \frac{\varepsilon_s}{\varepsilon_\theta} = 2\sigma_{ci}^{-0.25}, \quad \eta_f = \frac{\varepsilon_f}{\varepsilon_\theta} = 2\sigma_{ci}^{-0.32} \tag{2.21 a,b,c}$$

where η_p, η_s and η_f are normalized strain levels and other strain levels are defined in Fig. 2.8. Values of the strain for different conditions are calculated using the following relations:

$$\varepsilon_\theta = \frac{1+\nu}{E}(p_o - p_i) \tag{2.22}$$

$$\varepsilon_p = \frac{1+\nu}{E}(p_o - p_i)\frac{R_{pp}^{f+1}}{a} \tag{2.23}$$

$$\varepsilon_{sf} = \frac{1+\nu}{E}(p_o - p_i)\eta_{sf}\frac{R_{pb}^{f^*+1}}{a} \tag{2.24}$$

$$\frac{\varepsilon_p}{\varepsilon_\theta} = f(q, \beta, \alpha, f) \tag{2.25}$$

$$\frac{\varepsilon_{sf}}{\varepsilon_\theta} = f(\eta_{sf}, q, \beta, \alpha, f, q^*, \alpha^*, f^*) \tag{2.26}$$

where

p_o = overburden pressure (hydrostatic condition),

p_i = support pressure,

R_{pp} = radius of perfect plastic region (the region after residual plastic region till elasto-plastic boundary),

R_{pb} = radius of residual plastic region (up to some distance from tunnel boundary),

a = radius of opening,

$\eta_{sf} = (\eta_s+\eta_f)/2$, $\varepsilon_{sf} = (\varepsilon_s+\varepsilon_f)/2$, (2.26 a,b)

f = ratio of radial to axial strain with ν for perfect plastic part,

$\beta = p_i/p_o$, $\alpha = \sigma_{ci}/p_o$, and (2.26 c,d)

$q^* = (1+\sin\phi^*)/(1-\sin\phi^*)$, (2.26e)

* = relates the respective values for plastic condition or failed rock mass.

Equations 2.25 & 2.26 are used to estimate the strain ratio and then degree of squeezing is found by comparing them with the values calculated from Eq. 2.18. If squeezing is predicted, then support (p_i) will be provided. In addition to σ_{ci}, this method requires laboratory tests to find out Poisson's ratio for perfect plastic and residual plastic conditions and friction angle for intact and failed rock masses.

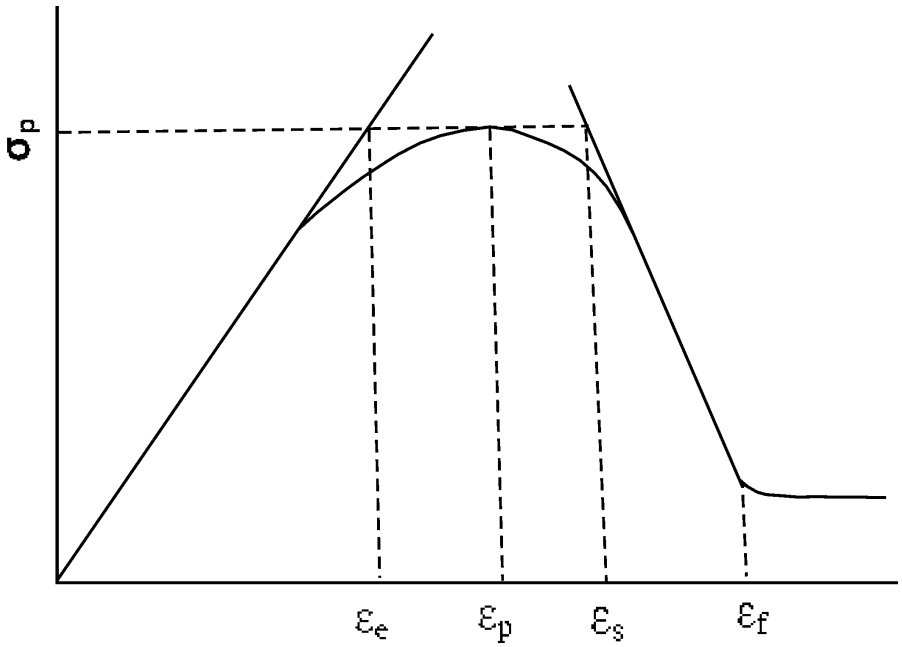

Fig. 2.8 Idealized Stress-Strain Curves (after Aydan et al., 1993)

The fundamental concept of the Aydan et al. (1993) approach is based on the analogy between the axial stress-strain response of rocks obtained in laboratory tests and tangential stress-strain response of rocks surrounding the tunnels. It considers $\sigma_1 = \sigma_\theta$ and $\sigma_3 = \sigma_r = \sigma_{pi}$. Figure 2.9 shows the boundary rock conditions in squeezing tunnels.

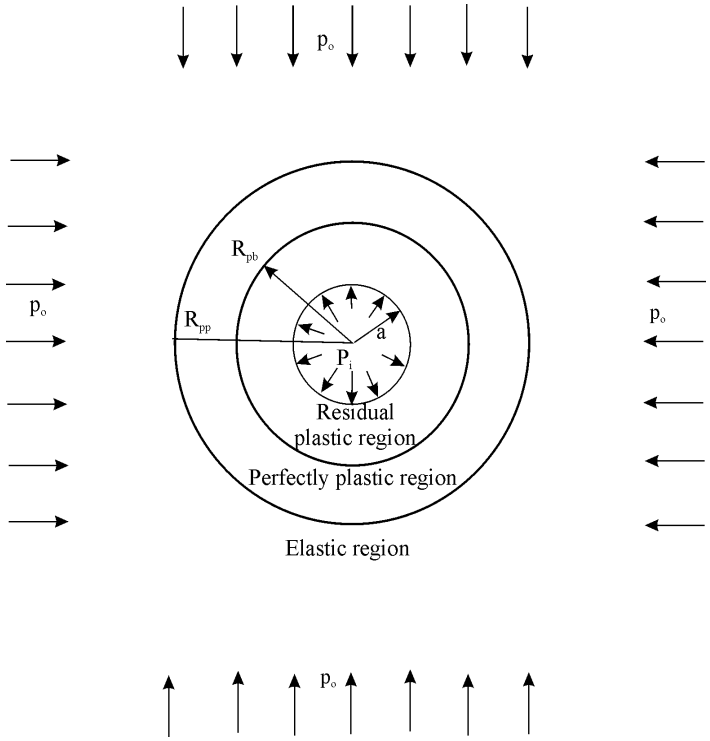

Fig. 2.9 Boundary Rock Conditions in Squeezing Tunnels (after Aydan et al., 1993)

Kovari (1998) developed an approach for circular openings and assuming isotropic, homogenous and elasto-plastic material behaviour. An approach was developed for displacement at the boundary of the excavated opening, for a given displacement at the boundary of the plastic zone.

A few semi-analytical approaches have been proposed for estimation of deformation due to squeezing and for estimation of required support pressure for tunnels excavated in squeezing ground. These are discussed in the following paragraphs:

Kovari (1998) suggested following expression for radial displacement, u_a at the boundary of the opening corresponding to a given radial displacement, u_ρ at the boundary of the plastic zone (broken zone):

$$u_a = u_\rho \left(\frac{\rho}{a} \right)^k \tag{2.27}$$

where ρ and a are radii of plastic zone and the excavated opening respectively. Volume change is taken into account using the parameter *k*. Its value varies between 1 and [(1+sinϕ)/ (1-sinϕ)]. Value of '*k*' is evaluated as referred to ρ/a ratio. Following equations were given to calculate radius of the plastic zone, ρ and various stresses:

$$\frac{\rho}{a} = \left[(1 - \sin\phi) \frac{p_\alpha'}{p_a'} \right]^{\frac{1-\sin\phi}{2\sin\phi}} \tag{2.28}$$

$$p_\alpha' = p_\alpha + c\cot\phi \tag{2.28a}$$

$$p_a' = p_a + c\cot\phi \tag{2.28b}$$

Above equation shows that –

$$u_a = f(p_a, p_\alpha, c, \phi, a, k)$$

where p_α is vertical in-situ stress, p_a, the stress on the lining, *c, the* cohesion, and ϕ is the angle of internal function.

Hoek and Marinos (2000) suggested that a plot of strain in the tunnel (ε) versus the ratio of uniaxial compressive strength to hydrostatic in-situ stress could be used effectively to assess the tunneling problems under squeezing conditions (Eq. 2.29). Hoek and Brown criterion for estimating the strength and deformation characteristics of rock masses assume that rock mass behaves isotropically. Highly fractured rock mass also behaves isotropically and therefore, this criterion can also be applied to weak heterogeneous rock masses too (Eq. 2.29).

$$\varepsilon = \left[0.002 - 0.0025 \frac{p_i}{p_o} \right] \left(\frac{\sigma_{cm}}{p_o} \right)^{\left(24\frac{p_i}{p_o} - 2 \right)} \tag{2.29}$$

in which, $\sigma_{cm} = \left(0.0034 m_i^{\,0.8}\right) \sigma_{ci} \left\{ 1.029 + 0.025 e^{(-0.1 m_i)} \right\}^{GSI}$ (2.29a)

where ε is the closure strain, p_i, the internal support pressure (MPa), p_o, the overburden pressure (γH), σ_{cm}, the uniaxial compressive strength (MPa), m_i, is a constant depending on the frictional characteristics of rock material, and *GSI* is the geological strength index.

For unsupported condition, the support pressure, p_i is zero. The value of p_i is increased up to an acceptable value of strain so as to obtain an appropriate value of support pressure, p_i from Eq. 2.29.

This analysis is a simple closed-form solution which assumes circular shape of tunnel with hydrostatic stress field and proper contact of support throughout the periphery. These assumed conditions are seldom met in the field, particularly in tunnels which are excavated by drill & blast method. So, the predictions made by the approach may not be reliable.

Barla et al. (2010a) suggested a correlation (Eq. 2.30) for estimation of the radial visco-plastic strain rate at the distance r from the tunnel centre at time, t under following assumptions:

- The tunnel is of circular section, is not lined and is at depth;
- Plane strain conditions are applicable;
- The initial stress state is isotropic;
- The ground is homogeneous, isotropic, and incompressible (v=0.5)

$$\frac{\partial}{\partial \tau}\left(\frac{\varepsilon_r^{vp}}{\varepsilon_R^{e}}\right)^{1/\alpha} = \left\{ u\left[1+(\beta-1)u^{\beta-1}\tau^{\alpha}\right]^{\frac{1}{1-\beta}} + u^{1/\beta}\frac{1}{\beta}\left\{1-\left[1+(\beta-1)u^{\frac{\beta-1}{\beta}}\tau^{\alpha}\right]^{\frac{1}{1-\beta}}\right\}\right\}^{\frac{\beta}{\alpha}} \tag{2.30}$$

where $\alpha = \frac{1}{1-m}$; $\beta = \frac{n}{1-m}$; $a = \left(\frac{\gamma}{\alpha}\right)^{\alpha}$; (2.30 a,b,c)

$$\tau = t \Big/ \left(\frac{\varepsilon_R^{e}}{a_{cyl}(2\sigma_o)^{\beta}}\right)^{1/\alpha}; \qquad \varepsilon_R^{e} = \frac{3\sigma_o}{2E}; \tag{2.30 d,e}$$

$$a_{cyl} = a\left(\frac{\sqrt{3}}{2}\right)^{\beta+1}; \text{ and} \qquad u = \left(\frac{R}{r}\right)^{2}; \tag{2.30 f,g}$$

in which, R is the tunnel radius, σ_o, the isotropic stress state, ε_R^{e}, the elastic radial strain at the tunnel contour, E, the elastic modulus, γ, the fluidity parameter, m, the shape factor and n represents the load dependency.

All the above mentioned three semi-empirical approaches consider a circular opening in homogeneous rock material with a hydrostatic stress state to estimate squeezing deformation. Hoek and Marinos (2000) and Aydan et al. (1993) approaches also consider the same condition for the estimation of supports, whereas Kovari (1998) approach can also accommodate anisotropic stress conditions. The approaches consider instantaneous squeezing deformation.

2.5 ANALYTICAL APPROACHES

The behaviour of rock mass encountered during tunnelling may be elastic, elasto-plastic, visco-elastic, visco-plastic or a combination of these. Analytical solutions are usually based on certain simplified assumptions as the rock masses are very complex in nature. One of the often made assumptions is that the rock mass acts as a continuum and some average physical and engineering properties are assigned to it. This assumption can be well considered either for the case of massive rocks or for very poor rocks, which are not common. For rocks having intermediate strength and with definite discontinuities, which are very common, the assumption of continuum may not be valid and therefore, the approaches are not reliable and have not been much popular. However, attempts have been made by some research workers in recent years to provide analytical solutions for prediction of support pressure and tunnel deformation. Their work has been summarized in following paragraphs:

2.5.1 Prediction of Ground Condition

Squeezing ground condition takes place when the tangential stress (σ_θ) exceeds the uniaxial compressive strength (σ_{cm}) of rock mass and the rock mass fails at the periphery of an opening. On the other hand, non-squeezing ground condition is encountered, if a strong rock mass around the opening is not over-stressed.

Jaeger & Cook (1976) suggested following expression for tangential stress on the boundary of a circular opening:

$$\sigma_\vartheta = \sigma_v\left[(1+k)-2(1-k)\cos 2\theta\right] \tag{2.31}$$

where θ is the angle from the vertical, *k* defines the ratio of horizontal in-situ stress to vertical in-situ stress, and σ_v is the cover pressure.

2.5.2 Prediction of Support Pressure

Fenner (1938) made the first major attempt to present elasto-plastic stress analysis for predicting tunnel support pressure by using the Mohr-Coulomb yield criterion. It was proved theoretically that any cylindrical opening can stand on its own without supports, provided that the plastic zone is allowed for unhindered expansion. It was also demonstrated through numerical examples that the extent of plastic zone required to ensure tunnel stability without supports was several times larger than the tunnel radius and concluded that it was desirable to install flexible supports rather than removing large volume of crushed zone. The short-term support pressure, p_i suggested by Fenner (1938) is as following:

$$p_i = \left[P(1-\sin\phi) + c.\cot\phi\right]\left(\frac{a}{b}\right)^{\alpha} - c.\cot\phi \tag{2.32}$$

where p_i is the short term support pressure, *P*, the overburden pressure, ϕ, the angle of internal friction, *c*, the cohesion of rock mass, $\alpha = 2\sin\phi/(1-\sin\phi)$, *a*, the tunnel radius, and *b* is the radius of broken zone.

Goguel (1947) was the first to recognize the fact that failed rock mass has low cohesion and friction as compared to an intact rock mass and therefore concluded that supports were necessary for tunnel stability. It was also further suggested that radial displacements may continue even after the broken zone has stabilized.

Labasse (1949) neglected loss in cohesion and friction in the broken rock mass zone and derived the following approximate solution for the short-term tunnel support pressure (p_s):

$$p_s = \sigma_b.\left(\frac{a}{b}\right)^{J-1} - \frac{3.\gamma.\beta}{2(J-2)}[1-\left(\frac{a}{b}\right)^{J-2} \tag{2.33}$$

where β is the angle made by any point under consideration from horizontal, σ_b, the radial stress at the broken zone boundary corresponding to the point under consideration,

$$J = (1 + sin\phi) / (1 - sin\phi), \qquad (2.33\ a)$$

and γ is the unit weight of rock mass.

Winkel et al. (1972) analyzed the time-dependent deformation of underground openings in salt media by deriving three dimensional constitutive equations for a Carlsbad potash material by means of laboratory tests and developing a method of analysis capable of handling the constitutive equations. It was concluded that elastic-visco-plastic material response is a reasonable model for potash ore exhibiting high values of uniaxial compressive strength of rock mass.

Daemen and Fairhurst (1969) gave rational design of support pressure whereas, Daemen and Fairhurst (1970) discussed the strength reduction in the broken rock mass zone and the resulting change in support pressure requirements in terms of the complete stress-strain curve. Daemen (1975) commented that the concept of constant volume increase throughout the broken zone (as assumed by Labasse, 1949) was an over simplification. Instead, Daemen suggested that these displacements were due to elastic relaxation of the broken zone which has a lower modulus as compared to that of the rock mass in the elastic zone. Further, it was suggested that the volumetric expansion ratio (k_v) ranges between 0.01 and 0.05 which is one order of magnitude lower than that proposed by Labasse (1949). Daemen (1975) developed a closed form solution and a numerical method for estimation of support pressure in circular tunnels under squeezing ground conditions. This closed form solution is comprised of material properties like peak cohesion and peak angle of internal friction of intact rock applicable to the elastic zone and residual cohesion and residual angle of internal friction of failing rock mass applicable to the broken zone. The closed form expression (Eq. 2.34) is based on the assumption that the in-situ stresses are hydrostatic and gravity acts towards the centre of the tunnel so that the problem becomes axisymmetric. The positive and the negative signs correspond to support pressures at the roof and the floor respectively.

$$p_i = \left[P(1-\sin\phi_p) - c_p\cos\phi_p + c_r\cot\phi_r\right]M_\phi - c_r\cot\phi_r \pm \gamma.(b-a)M_\gamma \qquad (2.34)$$

where

ϕ_p = peak angle of internal friction of intact rock applicable to the elastic zone,

ϕr = residual angle of internal friction of failing rock mass of the broken zone,

c_p = peak cohesion of intact rock mass applicable to the elastic zone,

c_r = residual cohesion of failing rock of the broken zone,

$M_\phi = (a/b)^\alpha$, (2.34 a)

$\alpha = (2\sin\phi_r) / (1-\sin\phi_r)$, (2.34 b)

$$M_\lambda = \left(\frac{a}{a-b}\right)\left(\frac{1-\sin\phi_r}{1-3\sin\phi_r}\right)\left[\left(\frac{a}{b}\right)^{\alpha-1} - 1\right] \qquad (2.34\ c)$$

In another study, Daemen (1975) used a strain-softening dilatant continuum model to include the effect of face advance on support pressure and concluded that the stiffer support mobilizes higher support pressure. Moreover, supports installed close to the face always attract higher pressure.

Panet (1975) assumed that the rock mass remains initially elastic but suffers lot of strength failure and undergoes volume increase on account of failure when an opening is made. Panet concluded that a tunnel may remain stable if the residual strength of rock mass in the close proximity of tunnel periphery is not destroyed fully, say by using rock bolts.

Fairhurst (1976) emphasized that it would be more rational to design underground structures in squeezing ground conditions on basis of the concept of mechanics tunnel stability. Thus, a support system may be allowed to underground plastic deformations so long as the post failure capacity of the support system is greater than the support pressure acting on it. Similarly, Lee and Lo (1976) suggested that ground squeezes due to long-term recovery of strain energy.

Dube (1979) and Dube et al. (1986a) modified the closed form solution proposed by Daemen (1975) to obtain short-term vertical and horizontal support pressures in a non-hydrostatic primitive stress field. Jethwa (1981) also modified the closed form solution of Daemen (1975) by including the three dimensional effect and hence

considering the influence of the face advance and shear stresses across the tunnel axis so as to obtain the short-term tunnel support pressure. Further, on the basis of field observations, it was suggested that k-value varies between 0.003 and 0.01 for commonly occurring soft rock masses.

Kaiser (1980, 1981) recognized the need for consideration of the effect of loading history on the rock mass response in stress analysis around underground openings. Kaiser emphasized the use of different elastic constants for the elastic and broken zones and suggested that the modulus reduction associated with progressive failure of rock mass can alone account for observed tunnel closures.

Kovari (1982) studied the behaviour of rock mass, which is largely determined by orientation and nature of the discontinuities present in it and properties of the intact rock. Mathematical modelling of the observed phenomena was carried out considering the elasticity, internal friction, cracking and viscosity. The author opined that in tunnelling, classification of rock mechanics problem in loosening type of rock pressure and swelling pressure provides a useful guide to choose adequate computational models.

Panet and Guenot (1982) studied the effect of face advance on tunnel closure and suggested that 90% of the tunnel closure occurs when the face is 1.8 to 3.7 times the tunnel radius away from the location where the closure has to be estimated. This is applicable when the radius of broken zone is 1 to 2 times the radius of an opening. Kaiser (1981) further added that the time dependent deformation can be evaluated by monitoring the tunnel deformation at a distance of more than 1 to 2 times the diameter from the tunnel face.

Fritz (1984) presented elasto-plastic analysis of a circular tunnel assuming that behaviour of plastic zone developed around the periphery of tunnel is governed primarily by the properties of plastic St. Venant element. The initial deformation was characterized by the residual strength. Modified Mohr-Coulomb criterion, characterizing both the peak and the residual strengths, was used to represent the rock mass behaviour.

Sharma (1985) developed an approach for estimation of tunnel closure in good rock masses with high overburden and considering five parameters viz., yield strength of

rock mass, support pressure, cover pressure, joint frequency (number of joints per metre), modulus of elasticity of intact rock and average joint stiffness.

Dube et al. (1986b) verified the analytical solutions for prediction of tunnel support pressure for squeezing grounds suggested by Dube (1979, 1986) using observed data of Giri Bata hydro-electric tunnel in lower Himalaya in India and opined that flexible support were more useful for the tunnels driven in squeezing grounds.

Lu (1986) used modified Mohr-Coulomb yield criterion to point out that consideration of strain hardening behaviour results in a higher tangential stress at the tunnel periphery and hence higher support pressure.

Sulem et al. (1987a) suggested a convergence law and differentiated between the effect of face advance and time dependent behaviour of rock mass on the tunnel convergence. The authors used two case histories of Frejus tunnel between France and Italy and the Las-Planas tunnel in the south of France for analysis of convergence.

Sulem et al. (1987b) analyzed ground–support interaction in a tunnel during excavation and proposed a closed form solution for radial tunnel deformation and the support pressure acting on the lining assuming circular shape of tunnel excavated through homogeneous and isotropic rock mass. The expressions for support pressure (P_s) and tunnel deformation are as follows:

$$P_s = \frac{K_s}{K_s + 2G_\infty}\left(1 - \frac{2G_\infty}{\sigma_o}\left(\frac{u_o}{r}\right)\right)\sigma_o \tag{2.35}$$

$$\frac{u_r}{r} = \frac{\lambda(x(t))\sigma_o}{2G_o}\left(1 + \frac{2G_o}{G_f} f(t)\right) \tag{2.36}$$

where K_s defines the support stiffness; G_∞, the long term shear modulus; G_o, shear modulus; G_f, the creep modulus; u_o, the radial displacement at intrados when the support is installed; r, the radial distance; σ_o, the initial stress; λ, the fictitious support pressure coefficient; $x(t)$, the distance of the face from the support; and $f(t)$ is the creep function such that $f(0) = 0$ at $t = 0$, and lim $f(t) = 1$ when t tends to ∞.

Stille et al. (1989) and Indraratna and Kaiser (1990) proposed closed form elasto-plastic solutions for underground openings supported with rock bolts. Using modified Mohr-Coulomb failure criterion and non-associated flow rule, ground reaction curves were obtained for the rock mass after installation of the grouted rock bolts.

Pan and Dong (1991a) proposed a time-dependent model of tunnel convergence for tunnelling in a viscoelastic rock mass to model the excavation-construction process during tunnelling in a rock mass with rheological properties. The expression for radial deformation of a circular tunnel in visco-elastic rock mass is given by the following equation:

$$\frac{u_r(t)}{r} = g_{ve}\left[h_c(t)F_c(t)\right] - K_s H(t-t_s)\left[D(t)F_c(t)\right] \tag{2.37}$$

where

$u_r(t)$ = radial tunnel deformation in time '*t*',

g_{ve} = compliance function relating to the deformability properties of the visco-elastic medium,

$F_c(t)$ = reduction factor of the radial deformation due to existence of support,

K_s = support stiffness,

t_s = time of support installation,

$H(t\text{-}t_s)$ = unit step function such that –

$H(t - t_s) = 1$ for $t \geq t_s$,

$H(t - t_s) = 0$ for $t < t_s$, and

$$D(t) = \frac{d\left[u_r(t) - u_r(t_s)\right]}{dt}. \tag{2.37a}$$

Pan and Dong (1991b) conducted a parametric study based on the time-dependent model proposed by Pan and Dong (1991a) to investigate the effect of the advance of the tunnel and support installation respectively on tunnel deformation and on the support-pressure. The authors also suggested a non-linear optimization procedure to calibrate the required model parameters from the observed data of tunnel deformation.

Corbetta et al. (1991) developed a method to investigate the effect of distance of tunnel support from tunnel face on the convergence of tunnel to use convergence-confinement for elastic-perfectly plastic ground. The support pressure and convergence were evaluated with due considering to the plasticity of the ground.

Wang (1996) proposed closed form solutions for the support pressure and radial deformation of circular tunnels excavated through poor rock masses under hydrostatic stress conditions. The author proposed the use of bisection method to compute the plastic radius and the Gauss-Legendre method to obtain the general solution for the radial deformation of tunnel. The proposed expressions are :

$$\sigma_r = \frac{m\sigma_c}{4}\left[\ln\frac{r}{a}\right]^2 + \left[\ln\frac{r}{a}\right]\left(m\sigma_c p_w + s\sigma_c{}^2\right)^{1/2} + p_w \tag{2.38}$$

$$\begin{aligned}\frac{u}{r} = {} & \frac{\left(1-\nu^2\right)m\sigma_c}{E\left(N_d+1\right)}\left\{\left(\frac{R}{r}\right)^{(N_d+1)}\ln\frac{R}{a} - \ln\frac{r}{a} + \left(\frac{1}{N_d+1}-\frac{1}{2}\right)\left[1-\left(\frac{R}{r}\right)^{(N_d+1)}\right]\right\} \\ & + \frac{\left(1-\nu^2\right)m\sigma_c}{2E}\ln\frac{r}{a}\left[\frac{(1-2\nu)}{2(1-\nu)}\ln\frac{r}{a}+1\right]\end{aligned} \tag{2.39}$$

where σ_r is the radial stress; m & s, the Hoek-Brown rock constants; σ_c, the uniaxial compressive strength of intact rock; r, the radial distance; a, radius of tunnel; p_w, the internal support pressure; u, the radial tunnel deformation; ν, the Poisson's ratio; R, the radius of plastic zone; N_d, the constant related to dilatancy angle; and E defines the Young's modulus.

Kovari and Staus (1996) have suggested to follow sequential method of excavation (side drift method and heading & benching method) during tunnelling through a squeezing ground in order to avoid attraction of large support pressure. Further, the authors have suggested to install steel rib supports with provision of yielding joints in such ground conditions. The yielding joints, if provided, will allow controlled deformation resulting in reduced support pressure.

Oreste and Peila (1996) suggested an analytical approach for radial passive rock bolting for tunnels using Convergence-Confinement Method (CCM) and later, Oreste (2009) applied the C-C method and concluded that the method is very useful in tunnel

design, especially in designing the rock bolts as a support system. This was possible because the method suggests the expression of the radius of plastic zone around the tunnel, which determines the length of the rock bolts.

Hoek (2000) studied the tunnels with a span of 10 m to 16 m which were excavated through squeezing grounds and concluded that squeezing of the rock mass becomes a great problem, when the ratio of rock mass strength to in-situ stress falls below 0.2. It can cause instability of both the tunnel and the face. The author suggested the following correlations to assess the strain of tunnel (ε_t) and face (ε_f):

$$\varepsilon_t(\%) = 0.15(1-(p_i/p_o))\left[\frac{\sigma_{cm}}{p_o}\right]^{-((3p_i/p_o)+1)/((3.8p_i/p_o)+0.54)} \tag{2.40a}$$

$$\varepsilon_f(\%) = 0.1(1-(p_i/p_o))\left[\frac{\sigma_{cm}}{p_o}\right]^{-((3p_i/p_o)+1)/((3.8p_i/p_o)+0.54)} \tag{2.40b}$$

where p_o is the hydrostatic stress, p_i , the internal support pressure, and σ_{cm} , the uniaxial compressive strength of rock mass.

Carranza-Torres and Fairhurst (2000) presented a solution based on the 'general' form of the Hoek-Brown criterion proposed by Londe (1988). If a circular tunnel of radius, R is subjected to a uniform far-field stress σ_o, internal pressure p_i, the rock mass is assumed to satisfy the Hoek-Brown failure criterion defined by Eq. 2.41 as-

$$\sigma_1 = \sigma_3 + \sigma_{ci}\left(m_b\frac{\sigma_3}{\sigma_{ci}} + s\right)^a \tag{2.41}$$

The variables characterizing the strength of rock mass are the unconfined compressive strength of intact rock, σ_{ci}; intact rock parameter, m_i and the rock mass parameters, m_b and s. Value of the parameter a is assumed to be 0.5.

The uniform internal pressure p_i and far-field stress, σ_o can be scaled to give the scaled internal pressure, P_i and far-field stress, S_o respectively.

$$P_i = \frac{p_i}{m_b\sigma_{ci}} + \frac{s}{m_b^{\,2}} \tag{2.42}$$

$$S_o = \frac{\sigma_o}{m_b \sigma_{ci}} + \frac{s}{m_b^{\,2}} \tag{2.43}$$

The pressure P_i^{cr}, defined by point E in the GRC of Fig. 2.8, marks the transition from elastic to plastic behaviour of the rock mass, i.e. for an internal pressure $p_i \geq P_i^{cr}$, the rock remains elastic, and for $p_i < P_i^{cr}$, plastic region of radius R_{pl} develops around the tunnel. The scaled critical (internal) pressure P_i^{cr} for which the elastic limit is achieved is given by the following expression:

$$P_i^{cr} = \frac{1}{16}\left(1 - \sqrt{1+16S_o}\right)^2 \tag{2.44}$$

The actual (i.e., non-scaled) critical pressure is found from the inverse of Eq. 2.42.

$$p_i^{\,cr} = \left[P_i^{cr} - \frac{s}{m_b^{\,2}} \right] m_b \sigma_{ci} \tag{2.45}$$

Provided $p_i \geq p_i^{cr}$, the relationship between the radial displacements, $u_r^{\,el}$ and internal pressure, p_i in the elastic part of the GRC (i.e., segment OE in Fig. 2.8) is given by following equation:

$$u_r^{\,el} = \frac{\sigma_o - p_i}{2G_{rm}} R \tag{2.46}$$

where R is the radius of tunnel and G_{rm} is the shear modulus of the rock mass. For values of internal pressure, $p_i < p_i^{cr}$, the extent of the plastic region R_{pl} that develops around the tunnel is

$$R_{pl} = R.\exp\left[2\left(\sqrt{P_i^{cr}} - \sqrt{P_i} \right) \right] \tag{2.47}$$

To define the plastic part of the GRC (EM part in the Fig. 2.8), a flow rule for the material is needed. A flow rule defines the relationship between the strains that produce distortion and those that produce volumetric changes, as plastic deformation occurs in the material. In underground excavation practice, the flow rule is usually assumed to be linear, with the magnitude of volumetric change characterized by a dilation angle ψ, such that, if $\psi = 0^o$, the material undergoes no change in volume during plastic deformation; if $\psi > 0^o$, the volume increases during plastic deformation.

In the solution described here, plastic flow rule will be characterized by a dilation coefficient, K_ψ, which is computed from the dilation angle, ψ, according to the expression $K_\psi = (1 + sin\ \psi) / (1 - sin\ \psi)$. Note, for example, that for $\psi = 0^o$, the dilation coefficient is $K_\psi = 1$ and for $\psi = 30^o$, the dilation coefficient is $K_\psi = 3$. With

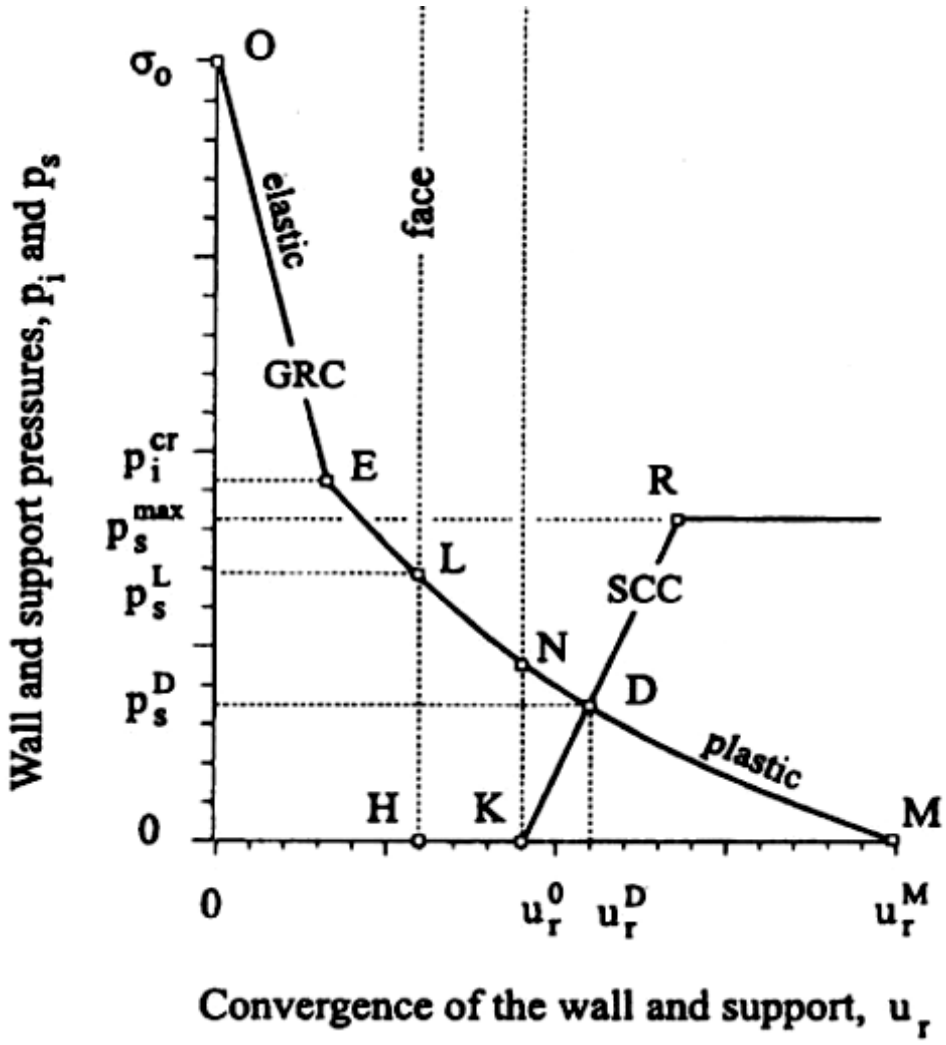

Fig. 2.10 Schematic Representation of Ground Reaction Curve (GRC) and Support Characteristic Curve (SCC) (after Carranza-Torres and Fairhurst, 2000)

the flow rule characterized by the dilation coefficient K_ψ, plastic part of the GRC, i.e. the segment EM in Fig. 2.10 is given by following expression:

$$\frac{u_r{}^{pl}}{R}\left(\frac{2G}{\sigma_o - p_i{}^{cr}}\right) = \frac{K_\psi - 1}{K_\psi + 1} + \frac{2}{K_\psi - 1}\left(\frac{R_{pl}}{R}\right)^{K_\psi + 1} + \frac{1-2\nu}{4\left(S_o - P_i^{cr}\right)}\left[\ln\left(\frac{R_{pl}}{R}\right)\right]^2$$

$$-\left[\frac{(1-2\nu)\sqrt{P_i^{cr}}}{\left(K_\psi + 1\right)\left(S_o - P_i^{cr}\right)}\right] x \left[\left(K_\psi + 1\right)\ln\left(\frac{R_{pl}}{R}\right) - \left(\frac{R_{pl}}{R}\right)^{K_\psi - 1} + 1\right] \tag{2.48}$$

where v is the Poisson's ratio of the rock mass. For non-dilating rock masses, the expression given in Eq. 2.46 can be obtained by substituting $K_\psi = 1$.

Carranza Torres (2003) suggests to compute the transformed variables S_o, P_i and P_i^{cr} from the variables σ_o, p_i and p_i^{cr} respectively as follows:

$$S_o = \sigma_o + \frac{\sigma_{ci}}{\left(K_\phi - 1\right)} \tag{2.49}$$

$$P_i = p_i + \frac{\sigma_{ci}}{\left(K_\phi - 1\right)} \tag{2.50}$$

$$P_i^{cr} = p_i{}^{cr} + \frac{\sigma_{ci}}{\left(K_\phi - 1\right)} \tag{2.51}$$

Value of σ_{ci} is to be replaced with σ_{cm} for jointed rock masses. The transformed critical internal pressure, P_i^{cr}, below which the plastic zone develops, depends upon the value of transformed far-field stress S_o and the parameter (coefficient of internal friction) K_ϕ as follows:

$$\frac{P_i^{cr}}{S_o} = \frac{2}{K_\phi + 1} \tag{2.52}$$

If the given value of transformed internal pressure, P_i is below the critical value P_i^{cr}, then the radius, R_{pl} of the plastic zone is -

$$\frac{R_{pl}}{a} = \left[\frac{P_i^{cr}}{P_i}\right]^{\frac{1}{K_\phi - 1}} \tag{2.53}$$

The radial convergence at the tunnel wall is given by Eq. 2.54 as-

$$\frac{u_r{}^a}{a}\left(\frac{2G}{S_o - P_i^{cr}}\right) = \frac{(K_\psi - 1)(K_\phi - 1) - 2C}{(K_\psi + 1)(K_\phi - 1)} + \frac{2(K_\psi + K_\phi) + 2C}{(K_\psi + 1)(K_\psi + K_\phi)}\left(\frac{R_{pl}}{a}\right)^{K_\psi + 1}$$

$$+ \frac{2C}{(K_\psi + K_\phi)(K_\phi - 1)}\left(\frac{a}{R_{pl}}\right)^{K_\phi - 1} \qquad (2.54)$$

where the constant, $C = (1\text{-}v)\,(K_\phi K_\psi + 1) - v\,(K_\phi + K_\psi)$ (2.54a)

Jiang et al. (2001) studied the development of broken zone around the periphery of tunnel excavated through soft rocks and suggested an expression for the loosening pressure on supports. The authors explained that with increasing tunnel deformation, ground pressure (p_g) decreases and loosening pressure (p_l) increases due to the development of plastic flow zone. The ground characteristic curve can be modified by the following expression:

$$p_i = max(p_g, p_l); \qquad and \ \epsilon\ (0, u_a/a) \qquad (2.55)$$

where p_i is internal support pressure, u_a stands for the final radial tunnel deformation corresponding to non-internal support pressure and ground pressure (p_g). Because of the loosening pressure, there is always a minimum point on the newly modified ground characteristics curves. The support pressure and tunnel strain corresponding to the minimum point are defined as the optimum support pressure and the controlled tunnel strain. These optimum parameters depend upon mechanical properties of rock mass and size of the tunnel cross-section.

Sharan (2003) conducted elastic-brittle-plastic analysis of circular tunnels under hydrostatic stress state and derived following expression for assessing radial tunnel deformation:

$$u_a = r^{-K_d}\int_R^r r^{K_d} f(r)dr + u_R\left(\frac{R_p}{r}\right)^{K_d} \qquad (2.56)$$

where u_a defines the radial tunnel deformation, r , the radial distance, ψ, the dilation angle, R_p , the radius of plastic zone, u_r , the radial deformation of elastic-plastic interface, and

K_d = (1+sinψ) / (1-sinψ) (2.56a)

Park and Kim (2006) suggested analytical solutions for the prediction of deformation around a circular opening in an elastic-brittle-plastic rock mass compatible with a linear Mohr-Coulomb or a non-linear Hoek-Brown yield criterion. The analytical solutions for the deformation in plastic region were derived on a theoretically consistent way by using a non-associated flow rule. The solutions predict comparable value of deformation for zero dilation angle, whereas differ considerably for non-zero values of dilation angle. Considering the existence of plastic region between radial distance, $r = a$ (radius of tunnel) and $r = c$ around the tunnel periphery, the tunnel deformation can be predicted with the expression as follows:

$$u = \frac{1}{r^{\beta}} \int_{c}^{r} r^{\beta} f(r) dr + u_c \left(\frac{c}{r} \right)^{\beta} \tag{2.57}$$

where u is the radial tunnel deformation, r, the radial distance,

β = (1+sinψ) / (1-sinψ), (2.57a)

ψ = dilation angle of the rock,

$f(r)$ = $\varepsilon_r^e + \varepsilon_\theta^e$, (2.57b)

$$\varepsilon_r^e = \frac{1}{2G} \left[(1-2\nu) C + \frac{D}{r^2} \right], \tag{2.57c}$$

$$\varepsilon_\theta^e = \frac{1}{2G} \left[(1-2\nu) C - \frac{D}{r^2} \right] \tag{2.57d}$$

$$C = \frac{(p_{iy} - p_o) c^2 - (p_i - p_o) a^2}{c^2 - a^2}, \tag{2.57e}$$

$$D = \frac{(p_i - p_{iy}) c^2 a^2}{c^2 - a^2}, \tag{2.57f}$$

$$u_c = \frac{(p_o - p_{iy}) c}{2G}, \tag{2.57g}$$

$$p_{iy} = p_o - \sigma_c \left\{ \frac{1}{2} \sqrt{\left(\frac{m}{4} \right)^2 + \frac{m p_o}{\sigma_c}} + s - \frac{m}{8} \right\}, \tag{2.57h}$$

p_o is the hydrostatic stress; m & s are the Hoek-Brown rock constants; G, the shear modulus; σ_c, the uniaxial compressive strength of intact rock; and ν defines the Poisson's ratio.

Park et al. (2008) suggested stepwise procedure to obtain the ground response curve for a circular tunnel excavated in elastic-strain softening rock mass compatible with linear M-C and non-linear H-B yield criteria by modifying the procedure proposed by Brown et al. (1983). In the modified procedure, the effect of elastic strain increments and variable dilatancy within the plastic region has been considered.

Lee and Pietruszczak (2008) proposed a numerical procedure for calculating the distribution of stresses and deformations around a circular tunnel excavated in a strain-softening Mohr-Coulomb or generalized Hoek-Brown rock mass. The problem was assumed to be axisymmetric (hydrostatic initial state of stress and the isotropic rock mass). By invoking the finite difference approximation of the equilibrium and compatibility equations, the authors calculated the increments of stresses and strains for each ring in a successive manner. In the proposed approach, the potential plastic zone is divided into a finite number of concentric rings whose thicknesses are determined internally to satisfy the equilibrium equation. For the strain-softening behaviour, it was assumed that all the strength parameters are a linear function of deviatoric plastic strain. It was observed that the results show a good agreement with the closed-form solution for the both cases (brittle-plastic and strain-softening).

González-Nicieza et al. (2008) proposed a modification in the C- C method so as to introduce directly the effect of depth and shape of the tunnel cross-section in determination of the radial displacement of the tunnel. For this, the authors determined a series of functions to approximate the radial deformation at different points around the periphery of the tunnel and at several cross-sections located at different distances from the working face. The authors proposed to use the calculated shape functions in order to get good results of C- C method in the design of the support systems.

Ahmad and Masoud (2009) suggested a procedure to obtain the ground reaction curves for a tunnel reinforced with active grouted rock bolts assuming that grouted rock bolts increase internal pressure within a broken rock mass. The authors also

considered the effect of distance of supported section from the tunnel face. The study is based on the assumption that the shape of tunnel is circular and the in-situ stress conditions are hydrostatic.

Federica and Vincent (2010) carried out a study on a Swiss road tunnel and using C-C method and suggested an approach for tunnel support design, considering its long term stability. However, the authors have assumed simplified conditions regarding the tunnel shape as circular and in-situ stress conditions as hydrostatic.

Sterpi and Gioda (2009) developed a rheological constitutive model to analyze the visco-plastic behaviour around advancing tunnels in squeezing ground conditions because the visco-plastic behaviour of rocks plays an important role in tunnelling, especially for deep tunnels subjected to high in-situ stresses and making the tunnel prone to squeezing behaviour. The rheological model accounts for visco-elastic (primary) and visco-plastic (secondary) contributions to rock creep. The effects of tertiary creep are included in the model by a gradual mechanical damage governed by the cumulative visco-plastic strains. The parameters of intact rock were determined in the laboratory. The laboratory results are then suitably scaled down for the rock mass. The rheological expressions for stress and strain are as follows:

$$s_1^{vp} = \frac{2}{3-\sin\phi_{\lim}}\left\{\sigma_1\left(1-\sin\phi_{\lim}\right)-\sigma_2\left(1+\sin\phi_{\lim}\right)-2c_{\lim}\cos\phi_{\lim}\right\} \tag{2.58}$$

$$s_2^{vp} = -\frac{1}{3-\sin\phi_{\lim}}\left\{\sigma_1\left(1-\sin\phi_{\lim}\right)-\sigma_2\left(1+\sin\phi_{\lim}\right)-2c_{\lim}\cos\phi_{\lim}\right\} \tag{2.59}$$

$$\varepsilon_1^{vp} = \frac{2}{\eta^{vp}\left(3-\sin\phi_{\lim}\right)}\left\{\sigma_1\left(1-\sin\phi_{\lim}\right)-\sigma_2\left(1+\sin\phi_{\lim}\right)-2c_{\lim}\cos\phi_{\lim}\right\} \tag{2.60}$$

$$\varepsilon_2^{vp} = -\frac{1}{\eta^{vp}\left(3-\sin\phi_{\lim}\right)}\left\{\sigma_1\left(1-\sin\phi_{\lim}\right)-\sigma_2\left(1+\sin\phi_{\lim}\right)-2c_{\lim}\cos\phi_{\lim}\right\} \tag{2.61}$$

where s_1^{vp}, s_2^{vp} are the deviatoric stress vectors; ε_1^{vp}, ε_2^{vp} are the deviatoric strain vectors; σ_1 , σ_2, the stress vectors; c_{lim} , the cohesion associated with the visco-plastic envelope; ϕ_{lim},, the friction angle associated with the visco-plastic envelope; and η^{vp} is the viscosity coefficient for visco-plasticity.

Scussel and Chandra (2013) used elasto-plastic theory given by Singh and Goel (2006) for estimation of tunnel support pressure in radial and tangential directions for elastic or non-squeezing ground condition (Eqs. 2.62 and 2.63) and plastic or squeezing ground condition (Eqs. 2.64 and 2.65).

$$\sigma_{re} = \frac{\sigma_v(1+k)+2(1-k)\cos 2\theta - \sigma_{cm} - \sigma_2(A/2)}{(2+A/2)} \tag{2.62}$$

where $$A = \frac{2\sin\phi_p}{1-\sin\phi_p} \tag{2.62a}$$

$$\sigma_{\theta e} = \sigma_v[(1+k)+2(1-k)\cos 2\theta] - \sigma_{re} \tag{2.63}$$

$$\sigma_{rb} = [\sigma_{re} + c_r \cot\phi_r](r/r_p)^{\alpha} - c_r \cot\phi_r \tag{2.64}$$

where $$\alpha = \frac{2\sin\phi_r}{1-\sin\phi_r} \tag{2.64a}$$

and $$\sigma_{\theta b} = N_{\phi,r}\sigma_{rb} + \sigma_{cr} \tag{2.65}$$

where $$N_{\phi,r} = \frac{1+\sin\phi_r}{1-\sin\phi_r} \tag{2.65a}$$

in which σ_{re} and σ_{rb} are the radial support pressure in elastic and broken zones respectively; σ_{rb}, $\sigma_{\theta b}$ are the tangential support pressure in elastic and broken zones respectively; σ_2 is the intermediate principal stress in the direction of the tunnel axis; *k*, the ratio of horizontal to vertical in-situ stress; σ_{cr}, c_r, ϕ_r are the residual compressive strength, cohesive strength and angle of internal friction respectively; and *r* and r_p are the radii of tunnel and plastic zone respectively. In this analysis, Scussel and Chandra (2013) assumed circular shape of tunnel and hydrostatic in-situ stress condition for the Eqs. 2.64 and 2.65 proposed for squeezing ground conditions. Further, parameters used in the approach are difficult to assess and need time consuming laboratory and field tests. In addition to this, the approaches (Eqs. 2.64 and 2.65) are not applicable for tunnels excavated at depths less than 1000 m as the authors have assumed hydrostatic in-situ stress conditions.

2.5.3 Prediction of Tunnel Deformation

Labasse (1949) proposed an expression to predict tunnel deformation in squeezing ground conditions (Eq. 2.66) and emphasized the necessity to consider the volume increase associated with rock failure.

$$u_a = a - \left[a^2 - C_v\left(b^2 - a^2\right)\right]^{\frac{1}{2}} \tag{2.66}$$

where u_a represents the radial tunnel closure, a, the tunnel radius, b, the radius of the broken zone, and C_v, the coefficient of volumetric expansion for failed rock mass and is defined as a ratio of increase in the volume of the failed rock mass to its original volume.

Hoek and Brown (1982) also suggested an expression to estimate the deformation of unsupported tunnel in non-squeezing (elastic) ground conditions:

$$u_a = \frac{\sigma(1+\nu)a}{E_d} \tag{2.67}$$

where u_a defines the radial tunnel deformation; σ, the hydrostatic rock pressure (σ_v = σ_h = σ); a, the radius of tunnel; v, the Poisson's ratio; and E_d, the deformation modulus of rock mass.

Daemen (1983) suggested an approach to assess the extent of slip zone for discontinuities parallel to circular tunnels or shafts.

Sharma (1985) proposed following correlation for estimation of tunnel deformation for low values of the ration of support pressure to rock cover pressure (p / σ_v) i.e. for good rock masses with high overburden.

$$\frac{u_a}{a} = 1 + \frac{0.052nE_iB'}{K_n\left(p/\sigma_v\right)^C} \tag{2.68}$$

where n represents the joint frequency (number of joints per metre), and E_i, the modulus of elasticity of intact rock, and

$$B' = \left[\frac{1}{\ln\left\{\left(\sigma_1 - \sigma_3\right)/\sigma_v\right\}}\right]^{0.5} \tag{2.68a}$$

$$C = \left[1 \Big/ \ln\{(\sigma_1 - \sigma_3)/\sigma_v\} \right]^{0.15} \qquad (2.68b)$$

Equation 2.68 can be used to plot the ground response curve by varying the value of (p / σ_v) in Eq. 2.68.

2.6 NUMERICAL APPROACHES

Design problems in rock mechanics practices can also be dealt with by numerical modelling. Reliability of this method is purely based on input parameters. Many research workers carried out numerical modeling to solve design problems of tunnels and arrived at some significant outcomes, which have been discussed in following paragraphs.

Kobayashi et al. (1981) studied the behaviour of an advancing face of Seikan Undersea tunnel (Japan) excavated in soft rock. Mechanical properties like stress-strain relationship, creep characteristics and failure condition of Kuromatsunai mudstone present in Seikan tunnel were analyzed and mathematical modelling was carried out for numerical analysis. The authors analyzed the problem by FEM and concluded that the boundary integral equation method is a powerful tool for three dimensional elasto-plastic analysis of stress and deformation for generalized in-situ initial stress state.

Sharma et al. (1985a) carried out numerical modelling for rock slopes using FEM code and Sharma et al. (1985b) performed elasto-visco-plastic finite element analysis of underground openings assuming plane strain condition and using Hoek and Brown (1982) failure criterion. The effect of sequential excavation in the elasto-visco-plastic analysis had also been considered. Using FEM, Sharma and Sharma (1986) analysed anisotropic rock medium of rock mass for tunnels.

Gioda and Cividini (1996) resorted to numerical modeling using finite element method to study time dependent behaviour of rock mass in squeezing and swelling conditions. The authors suggested that laws based on linear and non-linear rheological models are particularly suitable for analyses carried out through finite element method and concluded that rock salt also exhibits the time dependent behaviour.

Bhasin et al. (1996) carried out detailed investigation and also performance monitoring studies at the site of an underground powerhouse cavern in the Himalayan Region of India. Updated empirical (Q-system) and numerical (UDEC-BB) approaches were used for predicting the behaviour of the rock mass prior to the construction of an underground cavern (20 m wide × 49 m high × 216 m long). The behavior thus obtained has been compared with the instrumentation data from multi point borehole extensometers (MPBX). It was observed that maximum deformation of 18 mm predicted by numerical method was very close to the observed value of 24 mm for 20 m arched span.

Sridevi and Sitharam (2000) did finite element modeling of jointed rock mass as an equivalent continuum in which jointed rock properties were represented by a set of empirical relationships expressed as a function of joint factor and the properties of intact rock. These relationships have been derived from a large set of experimental data of tangent elastic modulus. It was concluded that equivalent continuum analysis gives the best results for jointed rock having both single and multiple sets of joints. The reliability of analysis depends on the estimation of joint factor, which is a function of joint orientation, joint frequency and joint strength.

Sitharam et al. (2001) also used the concept of equivalent continuum modeling using FEM code. The model developed was also applied to calculate deformation around a large power station cavern excavated in rhyolite rock at a depth of 200 m.

Sitharam and Latha (2002) verified the results obtained from numerical continuum modeling with three case studies, namely two large power station caverns out of which one is in Japan and the other in the lower Himalaya and the third one is Kirunavara mine cavities in Sweden. Attempt was made to simulate stepwise excavation by assigning null model available in FLAC to the excavated rock mass in each stage. Wall deformation observed in the field for the three caverns was compared with the numerically predicted observations and were found to be in good agreement.

Zhu et al. (2003) studied the mechanics of construction process for analyzing the stability of tunnels in squeezing grounds and performed numerical simulation based on FEM for deformation and failure of rock mass around the tunnel periphery. The authors came to the conclusion that time elapsed between heading excavation and

application of lining is very important from the stability point of view. Longer duration usually leads to large deformations in tunnel under squeezing ground conditions. The authors further suggested that single-benching is a better scheme as compared to multi-benching because the former takes comparatively shorter time to complete the section, so lining can be applied. High tunnel depth and high in-situ stresses usually cause large heaves in the invert of tunnels due to geometrical design and stress concentration.

Barla et al. (2004) performed numerical analyses using finite difference method and an axi-symmetric coupled model reproducing the full excavation sequence. The computed values in terms of axial tunnel deformation were compared with the corresponding data observed in a tunnel excavated through clay shales and suggested that the values obtained in laboratory experiments need to be scaled up significantly to represent the respective in-situ values.

Shalabi (2005) investigated the movement and pressure on lining of still-water tunnel (Utah, USA). Axisymmetric finite element analysis was carried out using power law and hyperbolic creep models for modelling of squeezing ground to show the difference between the results obtained from each model. The conclusion of the study was that lining pressure and deformation could be predicted using power law creep model, if the delay time before lining-erection is considered.

For non-circular tunnels, numerical modelling helps in stability analysis for selection of optimum supports. In addition to this, the results obtained from numerical modeling enhance the confidence of practicing engineers, particularly during application of the empirical approaches, if the predicted results are in close agreement. On the other hand, non-agreement of the results obtained from numerical modelling with the values predicted by the empirical approaches provide a direction for improvement either in the values of input parameters of numerical modelling or in values of geo-engineering parameters involved in empirical approaches. Shrestha (2005) carried out numerical modelling of non-circular Khimti-1 and Melamchi hydro tunnels of Nepal and recommended numerical modelling to supplement analytical calculations for recognizing critical stress situation and tunnel deformation.

Sitharam et al. (2005) developed a FISH program to account for the joint factor which is the integration of the properties of joints, namely the joint frequency, orientation

and strength of joints which are required for modeling of jointed rocks. The modeling was done by using Duncan and Chang (1970) hyperbolic model in FLAC-3D. The settlement observations reported from field studies undertaken in Nathpa-Jhakri power house cavern in the state of Himachal Pradesh in India were compared with the observations predicted from 3-D numerical analysis and found that the model was suitable for analysis of jointed rocks with both single and multiple joints sets in non-squeezing condition.

Bhasin et al. (2006) conducted numerical modelling using 2-D elasto-plastic finite element program and concluded that support pressure increases significantly with tunnel size in an elastic-plastic rock mass. The study showed that maximum axial force on shotcrete lining doubles with increase in tunnel diameter from 5 m to 20 m. However, the effect of tunnel size on support pressure is very small in case of elastic rocks. Further, Bhasin et al. (2006) also modified the empirical approach of Barton et al. (1974) by introducing diameter of tunnel as a new parameter.

Lian-chong et al. (2008) analyzed the closure and failure behaviour of tunnels using Rock Failure Process Analysis (RFPA2D) for numerical modelling and concluded that initiation of creep failure is governed by the ratio of the far field stresses (k). Creep failure always initiates in the direction of minimum far field stress component since the octahedral shear stress in that direction reaches the highest value. In case when $k \neq 1$, the rock is more unstable as compared to the case when $k=1$, where k is the ratio of horizontal to vertical in-situ stress.

Verma and Singh (2010) studied the effect of orientation of joints on the failure mode and strength of the rock mass by analyzing stress-strain models and by recording various stress–strain histories at constant strain loading rate. Velocity of compression at the top surface of the specimen was controlled to avoid unbalanced force to exceed the minimum limit at any moment of time. This was numerically simulated using $FLAC^{3D}$ code. The simulated rock results are compared with the analytically calculated results of the jointed rock mass and found in good agreement.

Barla et al. (2008, 2010, 2011, 2012) conducted numerical experiments of Saint Martin access adit excavated in a Carboniferous formation along the base tunnel of

the Lyon-Turin rail line and suggested optimized yield-control support system to increase the rate of tunnel advance in severely squeezing ground.

Scussel and Chandra (2014) proposed a methodology to implement a polyaxial constitutive model, which is characterized by the direct influence of all the three principal stresses in the mobilization of the resistance of rock mass. The proposed methodology makes use of Mohr-Coulomb model expressed in terms of equivalent angle of friction and cohesion of the rock mass surrounding the tunnel. The equivalent parameters of rock mass, which are directly derived from the common Mohr-Coulomb parameters, are also influenced by the intermediate principal stress, σ_2, as suggested in the poly-axial strength criterion, and by the approach chosen for quantifying the uniaxial compressive strength, σ_{ci} of the rock mass. To verify the constitutive model, it was used to predict the squeezing ground condition at three different instrumented tunnel sections.

2.7 OBSERVATIONAL APPROACHES

Observational approach based on instrumentation and monitoring, before; during and after construction of underground excavations, provides a qualitative solution to a problem. It is derived from the experience gained while working. Some of these approaches pertaining to the squeezing ground conditions have been considered here for discussion.

The conventional tunnelling method i.e., NATM (New Austrian Tunnelling Method), a technique for supporting a tunnel developed by Rabcewicz (1964) is the best example of this approach. This technique is based on observation of the performance of installed supports and modification of the same at every stage, if required. The philosophy of this technique is “Observe and support as you go”. Further, Muller (1978) listed five important principles of this technique: i) mobilization of the strength of the surrounding rock mass, ii) prevention of rock mass from loosening and excessive deformation, iii) instrumentation to assess the influence of time on behaviour of rock mass and support system, iv) permanent support and lining must be thin walled to the minimize bending moment, and v) statically, the tunnel is considered as a thick-walled tube, comprised of rock and the support and/or lining.

Selmer-Olsen and Broch (1977) described an old rule of thumb in Norway: if the valley side height above the tunnel is 500 m or more with a slope of 25° or steeper, there is a possibility of stress induced instability. This rule of thumb was developed on basis of the repeated experiences that in tunnels running parallel to fjords (a long narrow inlet of the sea between steep cliffs; common in Norway) with steep hill sides, rock-burst problems occurred in the tunnel-wall and in the part of the roof that was closest to the fjord.

Ward (1978) felt that tunnelling through squeezing ground is an art and observed that a support installed close to the face attracts higher load.

Dube (1979) carried out field instrumentation in Giri hydel power tunnel in lower Himalaya excavated in squeezing ground condition and developed a graphical method to assess the radius of the broken zone which was observed to be 2-10 times the radius of the tunnel. It was also inferred that in-situ stresses are the critical parameters that affect the geometry of the broken zone, support pressure and displacement at the periphery of the openings.

Lunardi (1980) suggested that ongoing time-dependent deformations in tunnels at large distances behind the face are due to viscous phenomena that increase with depth and decrease with time at a logarithmic scale. The logarithmic nature of deformations means that these have not ceased even at the moment of placing the final concrete lining.

Jethwa (1981) observed support pressures and tunnel closures by instrumentation in Chhibro-Khodri tunnel in the Yamuna valley of the lower Himalayan region under squeezing conditions and discovered the existence of compact zone adjacent to the tunnel periphery within the broken zone in a supported tunnel. In the compact zone, volume of failed rock mass reduced with time because of the support reaction. It was concluded that the ultimate support pressures would be 2 to 3 times the short-term support pressures in squeezing ground conditions.

Myer et al. (1981) conducted a study for developing a fundamental understanding of the relationship between the size of an advancing tunnel face, the rate of excavation, and the stand-up time in squeezing ground. The authors analyzed the nature, causes, and solutions of several cases of stand-up time problems observed in various tunnels

and performed a series of physical model tests in the laboratory in which tunnel size, face advance rate, material properties, and pressure (representing overburden pressure) were varied. Stand-up time was observed to increase with increase in advance rate or reduction in the tunnel size.

Takano et al. (1981) analyzed the case history of Nabetachiyama tunnel in Japan which traversed through soft mudstone (σ_{ci} = 1- 4 MPa) under an overburden of 150-300 m. It was observed that supports had to be installed at a faster rate and longer rock bolts were required to support the deforming ground.

Whittaker et al. (1983) carried out instrumentation in three mine roadways in Britain and concluded that yield zone developed in competent rock masses after a relatively shorter period of time (3 days) and tunnel advances (9m), whereas complete development of yield zone in the weaker rock masses was found to be time-dependent.

Kimura et al. (1987) studied Enasan tunnels-I & II on Chuo expressway connecting Iida city with Nakatsugawa city in Gifu (Japan) and traversing through two fault zones, namely 400 m long Chobeizawa fault and 450 m long Fuzimidai Higashi fault. Chobeizawa fault consists of grey layers of clay containing blue-grey fractured rock of hornfels under an overburden of more than 400 m. On the other hand, Fuzimidai Higashi fault consists of sandy and clay-like granite. The overburden in this zone exceeds 850 m. Uniaxial compressive strength of the rock present in the fault zones was in the range of 1.7 to 4.0 MPa leading to a competence factor (ratio of uniaxial compressive strength to overburden pressure) of 0.1 to 0.3. The authors compared the performance of flexible supports as compared to that of stiff supports so as to deal with the squeezing ground conditions encountered in fault zones. The authors opined that there exists a limit on the use of flexible support systems such as shotcrete with slots or sliding steel sets when the strength of rock mass is fairly low and overburden pressure is much higher. The authors observed that in case of excessively large deformations in the tunnel, the loosened zone around the periphery of tunnel increases in size. As a result, rock bolts installed initially do not work effectively, and the propagation of the loosening zone causes reduction in the effectiveness as compared to the initial state of the rock mass. On the contrary, when a stiff support system is installed, very high support pressure has to be resisted by the supports. Therefore,

there is a possibility of local failures of the support system, which will repeatedly require repair work. The authors further suggested that theoretically there exists a support system with adequate stiffness in relation to the ground pressure and the mechanical properties of the ground in faulted and fractured zone.

Saini and Dube (1989) studied the squeezing behaviour of two Indian hydroelectric tunnels (Chhibro-Khodri in Yamuna valley and Maneri Bhali stage II on River Bhagirathi, both in lower Himalaya) and concluded that the empirical correlations, developed on basis of data of observed deformations and support pressures during monitoring of the tunnels, may not be perfect but provide very good guidelines for construction of tunnels in squeezing ground conditions.

Saini and Dube (1990) studied squeezing ground behaviour of Maneri Bhali stage II hydroelectric tunnel, and concluded that Himalayan tunnels require systematic and detailed ground investigations before the commencement of construction. However, this is not always possible on account of topography, inaccessibility and depth. But, problematic zones must be identified, which can be tackled with best alternative methods of construction, planned well before the actual problems are met during tunnelling.

Eisenstein and Branco (1991) applied the Convergence-Confinement Method (C-C method) to design two tunnels excavated in stiff clay in Edmonton, Canada. The authors compared the results obtained by C-C method with actual data obtained via field measurements of the tunnels. Both tunnels were excavated under similar conditions except the depth of overburden. It was observed that due to difference in the depth-to-diameter ratio, the two tunnels exhibited different response as compared to analyses by the C-C method. The deep tunnel showed a good agreement between predicted and the field data, whereas the shallow tunnel did not. The authors attribute the discrepancy to the non-axi-symmetric mode of deformation developed around the shallow tunnel.

Aydan et al. (1996) studied squeezing phenomenon in Japanese tunnels and observed that factors responsible for squeezing are- i) geology, initial stress state, overburden and tunnel geometry, ii) physico-mechanical properties of surrounding rock mass, iii)

seepage rate, tunneling advance rate, and the type of support systems, and iv) time elapsed in loosening of ground and yielding of the support system.

Panet (1996) studied Frejus road tunnel (France-Italy) excavated through calc-schists under a maximum overburden of 1800m and Sidi Mezghiche railway tunnel excavated through laminated argilites excavated with a maximum overburden of 65 m. The author observed that heavy steel-rib supports buckled and failed to sustain the squeezing load in Frejus tunnel, whereas yielding anchored rock bolts with wire-mesh proved to be the most effective supports. It may be due to the fact that large amount of tunnel deformation was allowed in the form of buckling of ribs resulting in the reduced support pressure, and hence the lighter supports which were installed later were sufficient to take the reduced support pressure. On the other hand, in Sidi Mezghiche tunnel, large tunnel deformations were measured due to very poor shear strength of rock mass and rigid supports were successful in resisting the deformations.

Schubert (1996) studied the ways of tackling squeezing behaviour of various tunnels and suggested a low cast element, which can be used between the segments of shotcrete lining to allow certain deformations and avoid cracking of shotcrete. The element is a steel pipe of 100 mm diameter provided with multiple holes on the periphery at its one end. During excessive support pressure, the pipe deforms at perforated end allowing the controlled deformation.

Steiner (1996) analysed case histories of – i) Simplon tunnels (Italian-Swiss border) excavated through crystalline nappes under an overburden ranging from 1500 m to 2000 m, ii) Mofat tunnel (USA) excavated through pegmatite under a maximum overburden of 730 m, iii) Tauren and Arlberg road tunnels (Austria) excavated through phyllites with an overburden of more than 200 m, iv) Furka base tunnel (Switzerland) traversing through schistose gneiss at a depth of about 3000 m, v) Stillwater tunnel (USA) traversing through shales and siltstone and with a overburden of 2400 m, vi) access tunnel (Germany) excavated through sedimentary rock formations at a depth of 1500 m, and vii) Verena tunnel (Switzerland) traversing through a fault zone at a depth of 700 m. These tunnels experienced squeezing ground conditions. The author observed that squeezing ground conditions are influenced by-i) rock type, ii) strength and degree of fracturing of rock mass, iii) orientation of the

rock structure, iv) in-situ stress state, v) water pressure, vi) excavation method, and vii) the type of support systems.

Singh et al. (1997) analyzed the empirical correlations developed by Goel (1994) and Singh et al. (1992) for ground prediction and tunnel support pressure and observed that support pressures were independent of the size of arched excavations (for tunnel diameter ranging from 2 to 22 m) in the non-squeezing grounds. However, the authors opined that support pressure may increase with tunnel size in squeezing grounds.

Malan and Basson (1998) studied the rock mass behaviour around the underground openings of a deep South African gold mine and concluded that the possibility of squeezing behaviour becomes more pronounced with increase in depth of the opening and reduction in the quality of rock mass.

Singh and Singh (1999) studied the behaviour of rock mass by conducting uniaxial and triaxial compressive strength tests on Chunar sandstone for different joint orientations, viz., 30^o, 45^o, 60^o and 90^o. Strength of specimens having joint orientation of 90^o was observed to be highest at the same level of confinement.

Egger (2000) studied design and construction aspects of deep tunnels with an emphasis on strain softening behaviour of rocks and concluded that if a tunnel has attained a value of deformation necessary for disintegration of rock mass, no state of equilibrium is possible without support, even after large deformations have occurred. Further, the author explains that for a given case, there exists a critical value of softening rate which separates the above described unstable condition from that where the rock mass is partially loosened. In the latter case, tunnel is theoretically stable without support, but it remains sensitive to disturbances such as blasting vibrations and seepage forces.

Kontogianni et al. (2006) analyzed the closure data obtained from two Greek and two French tunnels and concluded that even though the time dependent deformation is ignored many times, it is observed to contribute more than 50% of the total deformation that is contributed by time-dependent or creep effect and face advance effect.

Sunuwar (2007) studied tunnel squeezing phenomenon in the Nepal Himalaya while tunnelling through low strength rock, fault and shear/weak zone and observed that the squeezing phenomenon results in reduction of the cross-section of a tunnel. The phenomenon takes place when in-situ stresses exceed the rock mass strength around the tunnel periphery. Time of deformation and degree of squeezing generally depends on overburden pressure and non-swelling clay content. Higher the overburden pressure and clay content, higher is the degree of squeezing.

2.8 PHYSICAL MODELLING

Analysis of deformational behaviour of tunnels essentially involves analysis of strength and deformational behaviour of jointed rock masses under a given stress environment. A good understanding of jointed rocks under uniaxial, bi-axial, tri-axial and poly-axial conditions before and after failure is therefore very much essential.

Physical modelling has been used as one of the most effective ways to study the engineering problem of jointed rocks and rock masses. Some notable studies carried out in the past have been taken for discussion below.

Brown (1970a & b) and Brown and Trollope (1970) tested specimens of jointed block mass under unconfined and confined states. The specimens were formed out of cubical elemental blocks (2.5 cm side), parallelepiped (height: 2.03 cm, length: 3.18 cm) and hexagonal (1.59 cm side) shapes. Various combinations of failure modes, including splitting, shearing and sliding were observed during the failure of rock specimens.

Walker (1971) and Lama (1974) observed an asymptotic variation in strength of rock mass and found that asymptotic value reached for rock mass with 5 to 6 joints when these joints are horizontal. The reduction in strength was observed to be 50% and 30% respectively. Walker (1971) reported that asymptotic value of strength was reached only for rock mass with 2-3 joints when these joints were vertical. Further, Lama (1974) showed that σ_{cj} and deformation modulus of rock mass (E_j) reach their minima values, if the blocky mass contains at least 150 elements.

Ladanyi and Archambalut (1972) simulated behaviour of rock mass with two sets of orthogonal joint sets by conducting bi-axial tests on large sized specimens of blocky mass. The elemental square sized blocks were cut from commercial concrete bricks. The modes of failure were found to be dependent on orientation of principal discontinuities and the value of confining pressure.

Einstein and Hirschfield (1973) conducted tests on jointed block mass to study the effect of joint orientation, joint spacing and number of joint sets, on the strength response of jointed mass. For higher values of confining pressure, shearing was observed along several roughly parallel surfaces associated with increase in plastic flow. The transition between sliding and fracturing was found to coincide with brittle to ductile transition.

Yaji (1984) studied the effect of roughness and inclination of joints on the response of jonted cylindrical specimens of plaster of Paris, sandstone and granite. The experiments led to the conclusions that - i) mode of failure changes with orientation angle, β of the joint plane, ii) UCS of jointed rocks was minimum when angle β was between 30^o to 45^o, iii) at higher confining pressures, the mode of failure changes from splitting and slabbing to shearing along a shear plane, ignoring the presence of joints, and iv) cohesion of jointed rocks follows the trend of σ_{cj}.

Arora (1987) conducted UCS tests on jointed specimens of plaster of Paris (POP), Jamrani sandstone and Agra sandstone, with different orientation of joints and the number of joint per metre (J_n) and reported that reduction in strength of different rocks was of the same order for the same number of joints. Modulus was also observed to give the same trend. Anisotropy in the strength behaviour due to a single joint was also observed in the specimens tested. The minimum strength was found to be 30^o, 40^o and 30^o respectively for the rock types tested.

Indraratna (1990) suggested a similitude criterion for linear discontinuity modelling, which is as follows:

i) Joint friction: ϕ_m / ϕ_p,

ii) Joint spacing: $l_p / l_m = t_p / t_m$,

iii) Joint orientation: $\theta_m = \theta_p$

Subscripts *m* and *p* represent the model and prototype respectively. If all three similitude requirements are fully satisfied, the geo-mechanical model can be representative of the real prototype behaviour. However, all similitude parameters cannot be simultaneously established for any particular rock, especially the material properties. Moreover, the in-situ boundary conditions are rarely simulated perfectly in the laboratory models. Thus, a perfect model replica of any particular prototype behaviour is nearly impossible to achieve. However, realistic prediction of the rock mass behaviour can certainly be made for an acceptable range of material properties (Indraratna, 1990).

Roy (1993) reported strength anisotropy for cylindrical specimens having one close joint or single joint filled with two types of gauge materials. The minimum strength was obtained at $\beta = 34^o$.

Ramamurthy and Arora (1994) conducted about 250 uniaxial compressive strength tests and 1300 tri-axial compression tests on jointed and intact specimens Jamrani sandstone and Agra sandstone and also those made in the laboratory out of plaster of Paris. Based on this extensive experimentation, a joint factor (J_f) has been evolved to account for the number of joints per meter length (J_n), inclination parameter for the sliding joint (n) and the shear strength along this joint (r).The joint factor takes into account anisotropy of rock mass strength realistically.

Vutukuri et al. (1995) conducted study on smooth (sandstone) and rough (coal) joints and observed that minimum strength occurred between $\beta = 30^o$ to 45^o for smooth joints, whereas for rough joints, the minimum strength occurred at 30^o. Joint factor takes into account anisotropy of rock mass strength realistically.

Singh (1997) conducted laboratory testing of block models made of sand-lime bricks having 6 elemental blocks in each direction (total about 260 elemental blocks) to overcome the scale effect. Following conclusions were drawn: i) specimens failed due to shearing, splitting or combination of both for horizontal or vertical continuous joints, ii) up to dip of 30^o, the mode of failure depends on interlocking introduced by stepping and for low/no stepping and the mode of failure shifts towards shearing and splitting, and iv) for dip ranging from 50^o - 60^o, there is no effect of stepping and specimen fails in sliding only.

Singh and Rao (2005) conducted large number of uniaxial compression strength tests on jointed rock specimens, modeled in the laboratory with various combinations of orientations and different levels of interlocking of joints and suggested some correlations to assess the ultimate strength of jointed rock mass.

Tiwari and Rao (2004), on basis of various experimental studies concluded that intermediate principal stress significantly enhances the strength of rock mass. Thus, there is a need for considering the effect of intermediate principal stress along the tunnel axis in the elasto-plastic-brittle-failure analysis around openings under non-hydrostatic in-situ stress conditions.

Choudhary (2007) developed a physical model of a D-shaped tunnel of size 150 mm (width) x 215 mm (height) excavated in a block of jointed rock mass (750 mm x 750 mm x 150 mm) with two sets of continuous and orthogonal joints using plaster of Paris mixed with medium sand. The joints of each set had an equal spacing of 25 mm. The aim was to study the deformational behaviour of the tunnel by varying the *k*-value (= σ_h/σ_v) of in-situ stresses. Horizontal and vertical stresses were applied to the model using hydraulic jacks of 500 kN capacity to simulate the in-situ stresses. It was observed that the deformation increased considerably with time till 24 hrs. However, the rate of deformation lowered subsequently and the rate came to a halt after almost 15-20 days. It gave total deformation of unsupported tunnel.

The empirical approaches developed by various research workers for various rock engineering purposes use measure of rock mass quality in terms of either - Rock Mass Quality (*Q)*, Rock Mass rating (*RMR*), Rock Mass Index (*RMi*), Geological Strength Index (*GSI*) and Rock Mass Number (*N*) as a basic parameter. The afore mentioned rock mass qualities involve sub-parameters which are assigned empirically. Further, values of the rock mass quality parameters increase with increase in the quality of rock mass observed in the field. Apart from the afore mentioned rock mass quality indicators (*Q*, *RMR*, *RMi*, *GSI*, *N*), there are two more indicators, namely

i) Joint factor (J_f), and
ii) Fracture tensor (F_{ij}) introduced by Oda (1982) in Kulatilake et al. (1993).

The concept of *joint factor* (J_f) was developed by Ramamurthy and his co-workers (Arora, 1987; Ramamurthy and Arora, 1994; Roy, 1993; Singh, 1997; Singh et al., 2002;

Singh et al., 2004). It represents the weakness of rock; the larger the joint factor, the greater is the weakness in rock mass. On the other hand, fracture tensor (F_{ij}) represents quality of joints. Articles 2.9 and 2.10 are devoted to joint factor and fracture tensor respectively.

2.9 JOINT FACTOR (J_f)

Rock masses are heterogeneous and discontinuous, containing cracks, fissures, joints, faults and bedding planes with varying degrees of strength along these planes of weakness. The planes of weakness usually present in a rock mass, control its strength and deformational behaviour, i.e. they make a rock mass weaker and more problematic. In addition to the frequency of joints, the orientation of joints with respect to the loading direction shows greater significance from stability point of view. The strength along these joints is another important parameter which controls the stability.

The following three aspects concerning the joints are primarily responsible for the reduction in the strength and are measurable in the field:

i) Joint frequency or number of joints per metre length in the direction of loading (J_n),
ii) orientation of critical joint set with respect to loading direction (β), and
iii) strength along the critical joint set (r).

These three aspects were suitably combined to form a simple parameter called the joint factor (J_f). This joint factor in a way represents the quantitative measure of the quality/ weakness of jointed rock in comparison to the intact rock.

For development of joint factor concept, Ramamurthy and his co-workers (Arora, 1987; Ramamurthy and Arora, 1994; Roy, 1993; Singh, 1997; Singh et al., 2002; Singh et al., 2004) carried our laboratory tests on specimens of plaster of Paris (46% mica, 30% calcite, 18% quartz, and 6% cementing material) representing soft rock and two natural isotropic rocks, namely Jamrani sandstone (96% quartz, and 4% ferruginous cementing material) and Agra sandstone (65% quartz, 29% mica, and 6% siliceous and carbonaceous material). These three materials were selected to provide a wide range of strength of intact specimens. Intact specimens of plaster of Paris,

Jamrani sandstone and Agra sandstone have uniaxial compressive strengths of 11.30, 55.10 and 110.00 MPa respectively.

Anisotropy was induced into the rock specimens by developing a number of clean and rough broken joints at various inclinations (angle between the joint orientation and vertical axis through the specimen, β^0 = 0, 30, 40, 50, 60, 70, 80, 90) by adopting a special technique of notching and then breaking the specimen in the direction of notching. The maximum number of joints developed in 76 mm high specimens at various inclinations is given in Table 2.5.

Table 2.5 Details of Anisotropy Created in Specimens
(after Ramamurthy and Arora, 1994)

β (deg.)	Maximum Number of joints in 76 mm Long Specimen	Equivalent Number of Joints / m, (J_n)
30	1	13
40	2	26
50	3	39
60	5	66
70	6	79
80	7	92
90	7	92

Tests were also conducted on specimens with a vertical joint, β = 0. In all, about 250 uniaxial compressive strength (UCS) tests and 1300 tri-axial tests were conducted on jointed and intact rock specimens of these materials. Minimum strength of specimens of all three rock types was observed for $\beta = 30^o$.

The most significant factors namely, the joint frequency (J_n), joint orientation parameter (n) based on value of β and joint strength (r) influencing the strength of jointed rocks have been suitably clubbed together to evolve a single factor called the *Joint Factor,* and designated as J_f . The joint factor has been defined by the following correlation:

$$J_f = \frac{J_n}{n.r} \tag{2.69}$$

where J_n defines the joint frequency, i.e. number of joints per metre in the direction of loading, n, the orientation or inclination parameter, which depends upon the orientation (β) of the joint plane with respect to loading direction, and r = joint strength parameter, which depends upon the joint condition (whether clean and rough or filled-up joints), thickness of the joint and joint alterations due to weathering. The joint factor reflects the quality reduction /weakness in the intact rock; the lower the joint factor, the higher the strength, i.e. less weakness.

2.9.1 Joint Frequency (J_n)

Joint frequency is defined as the number of joints in the direction of loading. Computation of J_n for rock mass element taken at boundary of a circular tunnel is presented below:

Figure 2.11a shows a circular tunnel excavated through inclined bedding planes. Loading direction on a rock mass element 'A' near springing level has been shown by vertical arrows. Enlarged view of the element 'A' is shown in Fig. 2.11b. Joints with constant spacing, PR (mm) are dipping at $\theta°$. Let the apparent dip of the joints be $\theta_A°$. If the tunnel axis makes an angle of α^o with the strike of joints, the apparent dip is given by Eq. 2.70.

$$\theta_A^{\circ} = \tan^{-1}(\tan\theta°.\cos\alpha°) \tag{2.70}$$

In ΔPQR given in Fig. 2.11b, ∠ PRQ = 90°, ∠ PQR = 90° - θ_A° = β, then

$$\sin(90-\theta_A) = \sin\beta = \cos\theta_A = \frac{PR}{S} \qquad \text{or} \qquad S = \frac{PR}{\cos\theta_A} \text{ mm} \tag{2.71}$$

where S is joint spacing in the direction of loading.

$$J_n = \frac{1000}{S} = \frac{1000}{PR/\cos\theta_A} \qquad \text{or} \qquad J_n = \frac{1000\cos\theta_A}{PR} \tag{2.72}$$

2.9.2 Inclination or Orientation Parameter (n)

The strength of jointed rock is governed by the orientation of joint planes with respect to the direction of the major principal stress (loading direction). A minimum value of

strength was observed when the joints are oriented at β = 30 - 40^o (Ramamurthy and Arora, 1994). Similar behaviour was also observed by Mclamore and Gray (1967), Attewell and Sandford (1974) and others. Values of *n* have been presented in Table 2.6. Depending upon the tunnel position of concern, the value of the inclination parameter *n* varies a lot on a same tunnel. The actual value of *n* at a particular section should be used for computation of joint factor at that section only.

Table 2.6 Joint Inclination Parameter, *n* as a Function of Joint Orientation Angle (after Ramamurthy and Arora, 1994)

β (degrees)	0	10	20	30	40	50	60	70	80	90
n	0.82	0.46	0.11	0.05	0.09	0.30	0.46	0.64	0.82	0.95

Notation: β *- angle of joint with loading direction.*

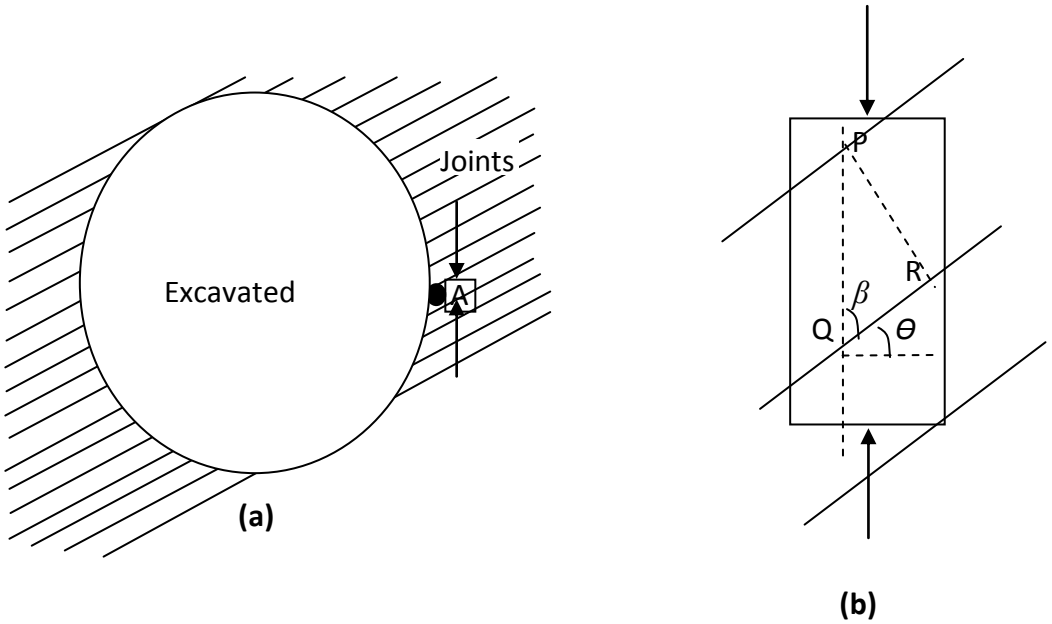

Fig. 2.11 a) Loading on a Rock Mass Element 'A' Near Springing Level in a Circular Tunnel, b) Enlarged Element 'A'

Figure 2.12 shows a correlation established between n-values and β-values using data presented in Table 2.6 and having a correlation coefficient of 0.99. Equation 2.73 can therefore be used to obtain an accurate value of n.

$$n = -6 \times 10^{-6}\beta^3 + 0.0012\beta^2 - 0.057\beta + 0.845 \qquad (R^2 = 0.99) \qquad (2.73)$$

where $\beta = (90 - \theta_A)$

2.9.3 Joint Strength Parameter (r)

The joint strength parameter, r was evolved to depict the roughness condition of the joint and is expressed as $r = \tan\phi_j$ where ϕ_j is friction angle of joints at very low normal stress level (when σ_n tends to zero). For clean joints, joints can be subjected to direct shear test at low stress levels and the value of ϕ_j can be obtained as the secant value of the friction angle. In the absence of actual test data, this parameter may be obtained from uniaxial compressive strength of intact rock material (σ_{ci}). The suggested values of r for various values of σ_{ci} are presented in Table 2.7.

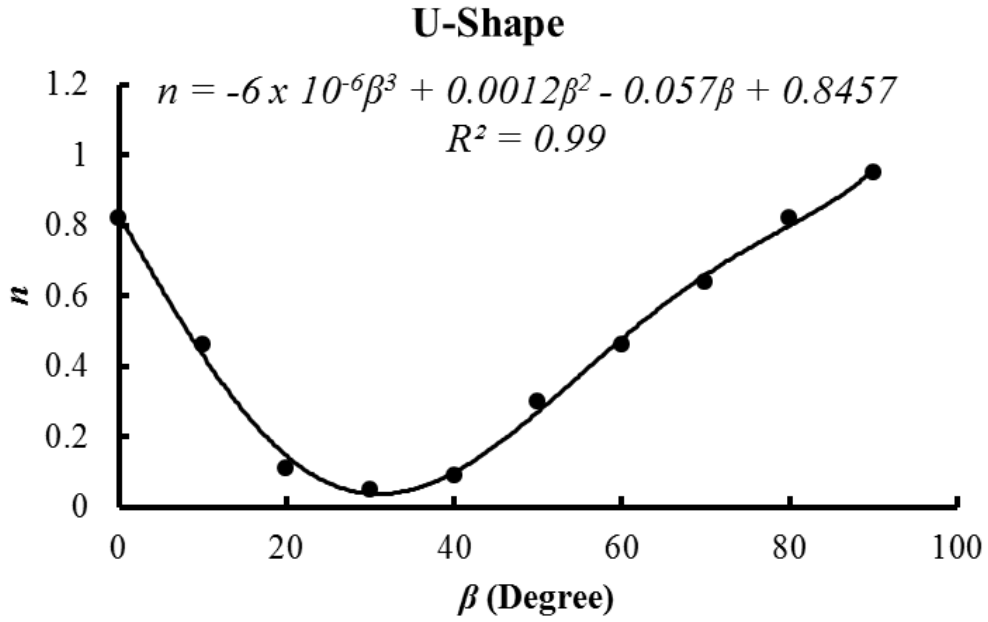

Fig. 2.12 Correlation Between n and Angle β

When a joint has gouge material of sufficient thickness to submerge the joint roughness, frictional parameter of gouge controls the joint strength during shear. Values of friction angles for various gouge materials present in a dense state or near the residual state and corresponding joint strength parameter are presented in Table 2.8.

Table 2.7 Joint Strength Parameter, *r* for Different Range of Values of σ_{ci} (after Ramamurthy and Arora,1994)

σ_{ci} **(MPa)**	***r***	**Remarks**
2.5	0.30	Fine-grained micaceous to coarse-grained
5.0	0.45	
15.0	0.60	
25.0	0.70	
45.0	0.80	
65.0	0.90	
100.0	1.00	

Table 2.8 Joint Strength Parameter, *r* for Gouge Material in Joint near Residual State (after Ramamurthy and Arora, 1994)

Gouge Material	**Friction Angle, ϕ (^{o})**	***r* = tan(ϕ)**
Gravelly sand	45	1.0
Coarse sand	40	0.84
Fine sand	35	0.70
Silty sand	32	0.62
Clayey sand	30	0.58
Clay-silt		
Clay-25%	25	0.47
Clay-50%	15	0.27
Clay-75%	10	0.18

In the Fig. 2.13, angle of internal friction (ϕ) has been plotted against percentage of clay using the values of Table 2.8 for better interpolation of the values. It is suggested in this approach that joint shear strength parameter be obtained by conducting direct shear tests on the joint surface under its natural environmental condition. Further, the joint factor characterizes the jointed rock in unconfined state. The effect of confining stress is required to be considered separately.

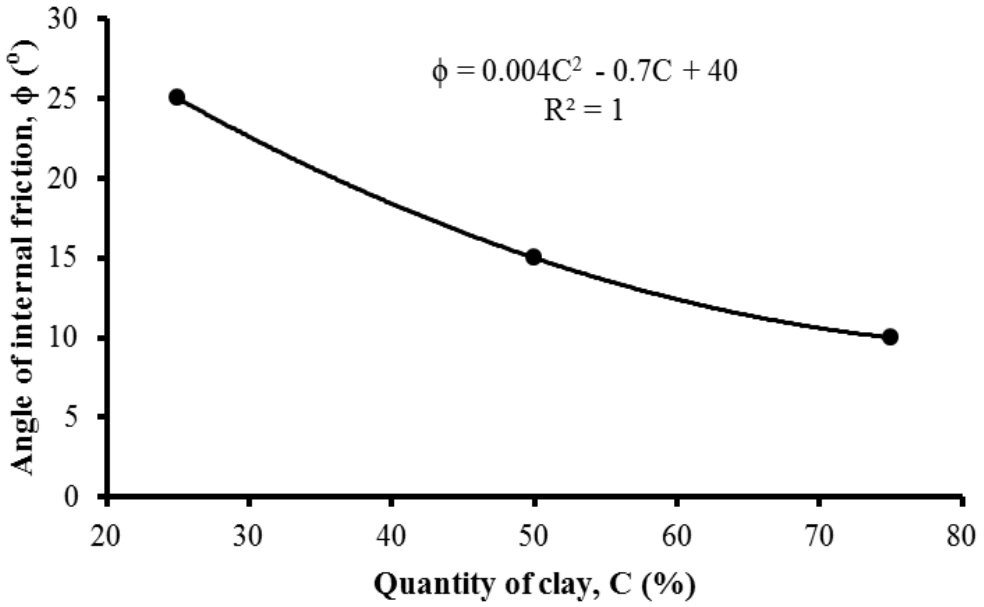

Fig. 2.13 Variation in Angle of Internal Friction with Clay in Gouge Material

Example for Computation of J_f: A tunnel aligned along 5° N traverses through siltstone having a critical joint set with spacing of 100 mm dipping at 65° / N 255°. If angle of internal friction of joints is 18° or 40% clay is present with silt in gouge material, joint factor is computed as shown in the following steps:

i) Dip direction of joints = 255° N and tunnel direction = 5° N, hence angle between tunnel axis and strike of the joints (α) = 360° - (255° + 90°) + 5° = 20°.

ii) Substituting values of dip, θ (65°) and α (20°) in Eq. 2.70, we get apparent dip (θ_A) = 64°.

iii) Substituting the values of spacing (PR) = 100 mm, and θ_A = 64° in Eq.2.71, we get S = 228 mm. It gives J_n = 1000/228 = 4.4 joints /m (from Eq. 2.60).

iv) β = 90- θ_A = 90 ^{o}– 64^o = 36^o, now, substituting the value of β in Eq. 2.73, we get n = 0.07.

v) Value of ϕ = 18^o for given C = 40% (from plot of ϕ versus C in Fig. 2.13), r = tanϕ = tan18^o = 0.32.

vi) Now joint factor, $J_f = J_n / (n.r)$ = 4.4 / (0.07 x 0.32) = 196.

2.10 FRACTURE TENSOR (*F*)

It is necessary to specify the number of joint sets, and for each joint set, statistical distribution for joint density, orientation, size and location to describe the fracture pattern. To evaluate the influence of a joint geometry network on the mechanical properties of a given rock mass, it would require estimation of the effect of each joint geometry parameter belonging to a desired mechanical property and then combined effect of all joints can be evaluated. This is an extremely difficult task. However, it may be simplified by using the concept of fracture tensor.

The fracture tensor is an overall measure of the joint geometry parameters, viz., joint density, orientation, and the number of joint sets. Assuming joints to be thin circular discs, the general form of the fracture tensor at 3-D level for the k^{th} joint set can be expressed as:

$$F_{ij}^{\ k} = 2\pi\rho\int_0^\infty \int\int_{\Omega/2} r^3 n_i n_j f(n,r) d\Omega dr \tag{2.74}$$

where ρ is the average number of joints per unit volume (joint density), r is the radius of the circular joint (joint size), $\boldsymbol{n}$ is the unit vector normal to the joint plane, $f(\boldsymbol{n}, r)$ is the joint probability density function of $\boldsymbol{n}$ and r, $\Omega/2$ is a solid angle corresponding to the surface of a unit hemisphere, and $\boldsymbol{n_i}$ and $\boldsymbol{n_j}$ ($i, j = x, y, z$) are the components of vector $\boldsymbol{n}$ in the rectangular coordinate system. If the distribution of the size and the orientation of the joints are independent of each other, then the fracture tensor formulation at the 3-D level can be given by:

$$F_{ij}^{\ k} = 2\pi\rho\int_0^\infty r^3 f(r) dr \int\int_{\Omega/2} n_i n_j f(n) d\Omega \tag{2.75}$$

where $f(n)$ and $f(r)$ are the probability density functions for unit normal vector $\boldsymbol{n}$ and size r respectively. The directional fracture tensor component for the k^{th} joint set can

be obtained by replacing *ij* with *l* in the Eq. 2.75. The directional fracture tensor (F_l) is given by:

$$F_l^k = 2\pi\rho\int_0^\infty r^3 f(r)dr\int\int_{\Omega/2} n_i n_j f(n)d\Omega \tag{2.76}$$

If there is more than one joint set in the rock mass, the fracture tensor for the rock mass can be expressed as:

$$F_{ij} = \sum_{k=1}^{N} F_{ij}^k \tag{2.77}$$

where N is the number of joint sets in the rock mass. The directional fracture tensor component for the rock mass can be expressed as:

$$F_l = \sum_{k=1}^{N} F_l^k \tag{2.78}$$

Fracture tensor F_{ij} can be written in matrix as following:

$$F\left(F_{ij}\right) = \begin{bmatrix} F_{xx} & F_{xy} & F_{xz} \\ F_{yx} & F_{yy} & F_{yz} \\ F_{zx} & F_{zy} & F_{zz} \end{bmatrix} \tag{2.79}$$

where $F_{xx}, \ldots\ldots F_{zz}$ are the components of fracture tensor $\boldsymbol{F}$. From the formulation of Eqs. (2.74) and (2.75), it is clear that the fracture tensor is symmetric, i.e. $F_{ij} = F_{ji}$. Therefore, F has three principal values F_1, F_2, and F_3, in three mutually perpendicular directions 1, 2 and 3. Three principal values are calculated by solving the following Eq. 2.80:

$$\left|F_{ij} - F\delta_{ij}\right| = 0 \tag{2.80}$$

where δ_{ij} is Kronecker delta, which is defined as $\delta_{ij} = 0$ (if $i \neq j$) and $\delta_{ij} = 1 (i = j)$. The corresponding principal directions $\boldsymbol{P^m}$ are computed by:

$$\left(F_{ij} - F\delta_{ij}\right)P_j^m = 0 \sim \mathrm{I} = 0 \tag{2.81}$$

and

$$P^m P^l = \delta_{kl} \tag{2.82}$$

where *i, j, l, m* values are between 1 and 3. Invariants, I_1^F, I_2^F and I_3^F of the fracture tensor are defined by:

$$I_1^F = F_1 + F_2 + F_3 \tag{2.83a}$$

$$I_2^F = -\left(F_1F_2 + F_2F_3 + F_3F_1\right) \tag{2.83b}$$

$$I_3^F = F_1F_2F_3 \tag{2.83c}$$

A space of principal values F_1, F_2, F_3 of fracture tensor $\boldsymbol{F}$ is shown in Fig. 2.14. In this principal space, the fracture character can be represented by a vector **OP**, with components F_1, F_2, and F_3, respectively. Since the straight line of $F_1 = F_2 = F_3$ passing through the origin represents an isotropic fracture system, it can be called the isotropic axis.

The vector **OP** in the space is resolved into two vectors: **OP** = **OA** + **OB**. The length of **OA** is proportional to the first invariant, I_1^F of the fracture tensor through-

$$|OA| = \frac{1}{\sqrt{3}} I_1^F \tag{2.84}$$

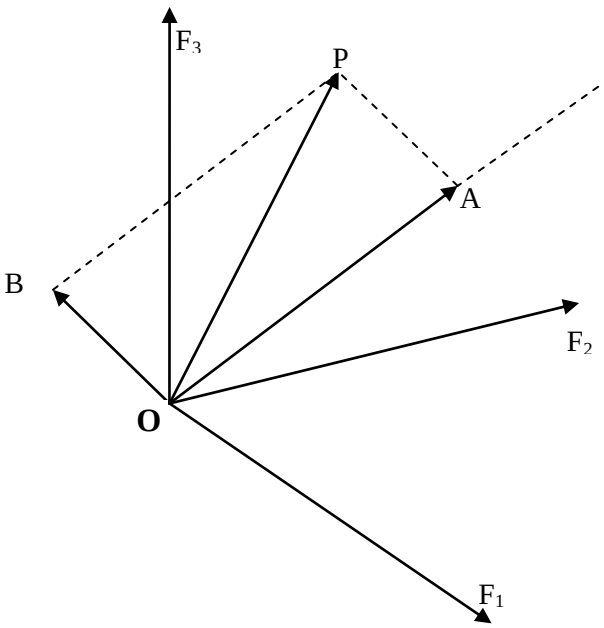

Fig. 2.14 Principal Space for Fracture Tensor (after Kulatilake et al., 1993)

The other vector **OB** which is on the plane of $F_1 + F_2 + F_3 = 0$ characterizes the deviatoric part of fracture tensor, F_{ij}, which is given by:

$$D_{ij} = F_{ij} - \frac{I_1^F}{\sqrt{3}}\delta_{ij} \tag{2.85}$$

It is known that the length, Γ of the vector OB is related to the second invariant, I_2^D of D_{ij} as:

$$\Gamma = \sqrt{2I_1^D} = \sqrt{\frac{1}{3}\left[(F_1 - F_2)^2 + (F_2 - F_3)^2 + (F_3 - F_1)^2\right]} \tag{2.86}$$

The above discussion reflects that the fracture tensor carries the following joint geometrical information:

i) The diagonal components of the fracture tensor F_{xx}, F_{yy} *and* F_{zz}, (directional fracture tensor components) define the combined effect of joint density and joint size in the *x*, *y* and *z* directions respectively.

ii) The first invariant of the fracture tensor, $F_{ij}\left(I_1^F\right)$ can be used as an index to evaluate the porosity of the rock mass resulting from joint density and joint size.

iii) Γ (as given in Eq. 2.72) expresses the distance by which the vector **OP** deviates from its isotropic portion **OA** in the principal space (as shown in Fig. 2.14). So, the value of Γ can be used as an index to evaluate the degree of anisotropy of the fracture system.

2.11 ROCK MASS QUALITY (*Q*)

The *Q*-system was developed as a rock mass quality index by Barton et al. (1974). The system is based on the evaluation of a large number of case histories of underground excavation stability, and is an index for the assessment of the rock mass quality. The numerical value of this index, *Q* is defined by:

$$Q = \left(\frac{RQD}{J_n}\right)\left(\frac{J_r}{J_a}\right)\left(\frac{J_w}{SRF}\right) \tag{2.87}$$

where *RQD* is the rock quality designation, J_n, the joint set number, J_r , the joint roughness number, J_a , *the* joint alteration number, J_w , the joint water reduction factor, and *SRF*, defines the stress reduction factor.

2.12 ROCK MASS NUMBER (*N*)

As suggested by Barton et al. (1974), assessment of SRF values in Eq. 2.87 requires high level of experience, and therefore, to make the rock mass quality assessment easier, Goel (1994) proposed Rock Mass Number (*N*) by eliminating *SRF*-values from the Eq. 2.87. Hence, expression for *N*-values is obtained by substituting *SRF* = 1 in Eq. 2.88 as follows:

$$N = \left(\frac{RQD}{J_n}\right)\left(\frac{J_r}{J_a}\right)\left(J_w\right) \tag{2.88}$$

2.13 ROCK MASS RATING (*RMR*)

Bieniawski (1976) published the details of a rock mass classification system called the Geomechanics Classification or the Rock Mass Rating (*RMR*) system. Over the years, this system has been successively refined as more case records have been examined and Bieniawski has made significant changes in the ratings assigned to different parameters. The following six parameters are used to classify a rock mass using the RMR system of Bieniawski (1989) version:

i) Uniaxial compressive strength of rock material,
ii) Rock quality designation,
iii) Spacing of discontinuities,
iv) Condition of discontinuities,
v) Groundwater conditions, and
vi) Orientation of discontinuities.

The ratings of the above parameters are assigned and sum of the ratings of all parameters is taken as RMR of a particular rock mass.

2.14 ROCK MASS INDEX (*RMi*)

Palmstrom (1995) developed *RMi* system to determine rock mass strength. *RMi* is given by the expression-

$$RMi = \sigma_{ci} \, . \, JP \tag{2.89}$$

where σ_{ci} is the uniaxial compressive strength of intact rock, and *JP* is the jointing parameter (a reduction coefficient representing the block volume and joint condition). The value of *JP* is almost zero for crushed rocks and 1 for intact rock. Its value is obtained by combining the block size and the joint conditions.

2.15 CRITICAL COMMENTS

An empirical approach based on RMR proposed by Unal (1983) predicts entirely unsafe support pressure for tunnels in squeezing conditions (Goel and Jethwa, 1991). Moreover, similar approach based on Bartons' Q-value suggested by Bhasin and Grimstad (1996) gives higher value of support pressure for tunnels greater than 5 m in diameter (Goel et al., 1995 and Singh et al., 1992).

On basis of the above review of literature, it can be concluded that the existing empirical and analytical approaches /correlations for prediction of support pressure and deformation /deformation in tunnels involve number of assumptions. In addition to this, these correlations involve a large number of parameters, determination of which is sometimes a difficult task. For instance, empirical correlation developed by Verman (1993) for prediction of short-term support pressure involves 18 parameters.

Analytical models (closed form solutions) have many limitations and assumed parameters like hydrostatic in-situ stresses, shape of the opening etc. Hence, these are unable to provide realistic solutions for tunnels of different shapes in the field.

The results of numerical modeling are case specific and cannot be generalized for all the cases. Furthermore, there is no simple method available for modelling the rock masses as these contain natural discontinuities of varying size, strength and orientation. In practice, it is almost impossible to – i) explore all the joint systems or

to investigate all their mechanical properties and ii) implement them explicitly in a theoretical model. Further, getting undisturbed samples from the field for experimental study is also very difficult.

Observational approaches enhance the experience and provide a direction for research but cannot give an optimal solution. Semi-empirical approaches still contain some assumed parameters and therefore do not take real inputs leading to inappropriate solutions.

The results obtained by physical modelling approach are based on the laboratory experiments conducted on small scale physical models. The laboratory experiments are normally conducted with many limitations and real field simulations are not possible. However, qualitative response of the physical models is very useful to predict the deformational behaviour of tunnel in the field but the numerical values of deformation obtained from testing of scaled physical models cannot be reliably extrapolated to get the field values.

For quite some time, many research workers have been trying to characterize the rock mass and giving solution to the rock pressure problems in tunnels and other underground openings. The research workers of the above studies agreed upon a common point that none of the existing rock mass classification approaches has been able to reliably predict the support pressure in tunnels under squeezing ground conditions. Q-system of Barton et al. (1974) predicts the support pressures reliably for tunnels under non-squeezing ground conditions but not for squeezing ground conditions. On the other hand, analytical approaches need values of strength parameters and in-situ stresses as input, which are very difficult to assess and are time consuming also. In-situ stresses are very important parameters but these are either assumed as hydrostatic or only vertical stress is considered. Further, size of tunnel matters a lot with regard to support pressure and deformation in case of squeezing rock conditions (Goel et al., 1996; Bhasin et al., 2006) whereas according to Barton et al. (1974) and Jethwa (1981), there is no effect of tunnel size on support pressure.

Deformational behaviour of tunnels in squeezing ground is essentially a problem involving strength and deformational behaviour of jointed rock masses under a given stress environment.

A reliable empirical approach having less number of parameters which can be easily assessed in the field can become a handy tool to solve the support pressure and deformation problems.

Concept of joint factor is based on the results of intensive experiments carried out on numerous intact and jointed rock specimens in the laboratory and involves only three parameters. The concept is easy to understand and parameters can be easily assessed in the field. Therefore, in the present study, joint factor (J_f) has been used as a measure of rock mass quality for development of empirical correlations for prediction of ground conditions (self-supporting, non-squeezing, and squeezing), tunnel deformation and support pressure for non-squeezing and squeezing ground conditions.

2.16 CONCLUSIONS

In view of the above discussion, it is felt that there is still a need to develop a user friendly approach to predict the support pressure and deformation in tunnels under squeezing ground conditions. Involvement of easily assessable geo-mechanical parameters would make the approach user friendly. Development of empirical approaches involving easily assessable geo-mechanical parameters for prediction of support pressure and deformation in underground openings under squeezing condition is urgently required, especially for tunneling in the fragile Himalayan region which is highly tectonically active and squeezing problem has been frequently faced by geologists and construction engineers engaged in tunnelling in the region.

The concept of joint factor (J_f) developed by Ramamurthy and co-workers (Arora, 1987; Ramamurthy, 1993 & 2004; Ramamurthy and Arora, 1994) has been derived through extensive experimental studies in the laboratory. Moreover, this concept involves few parameters (only three) which can be easily assessed in the field and hence may be used for development of new approach to assess ground condition, support pressure and tunnel deformation as it accounts for anisotropy of rock mass strength. In addition to this, strength of rock material also plays an important role, especially when rock mass is very poor like. Therefore, there is a need of inclusion of the intact rock strength while formulation of correlations for estimation of support pressure.

Chapter 3

GEOLOGY OF CASE STUDY PROJECTS

3.1 GENERAL

The success of a tunnelling project primarily depends upon the knowledge of Geology of the project site. This plays a key role in governing the stability of a tunnel and hence also decides the cost factor for the project. Data of 24 tunnelling/ mining projects have been collected in the present study (Table 3.1, Figs. 3.1 and 3.2). Out of these, fourteen projects are located in the Himalayan region. Many times, the desired sites are inaccessible for proper geological exploration and hence the proper prediction of geology at the tunnel grade is not possible, which also costs much for a tunnelling project in the terms of money and time. On the other hand, Himalayan region is highly tectonically active which give rise to the surprises in the form of frequently changing geology. In addition to this, the tectonic activity leads to an increase in in-situ stresses, thereby causing the stability problems to the tunnels.

Major tunnelling problems in India are encountered in the young Himalayan regions, particularly in the lesser Himalayas, where the geology is highly complex and fragile. The rock masses undergo intense tectonic activity giving rise to major faults, folds and other discontinuities (Fig. 3.3). Such problems are rarely encountered in the peninsular (southern part) India, where rocks are hard, rigid, strong and less disturbed.

A number of hydroelectric projects in India are located in the lower Himalayas. These projects lie in India (states of Jammu & Kashmir, Himachal Pradesh Uttarakhand, Sikkim, Arunachal Pradesh and Manipur), Nepal and Bhutan. A few projects considered for the present study are located in the states of Madhya Pradesh, Maharashtra, Karnataka and Kerala (Table 3.1). Four case projects from France-Italy (tunnel bordering France and Italy), Turkey, Norway and United Kingdom have been taken up for the study (Fig. 3.2).

Table 3.1 Worldwide Tunnelling Projects at a Glance Considered for Data Collection

Sl. No.	Name of Project	Type of Project	Place
*1.	Chenani-Nashri	Highway (NH) project	NH-1A, J&K, India
2.	Udhampur Tunnels	USBRL project	Udhampur, J&K, India
3.	Salal	Hydroelectric project	Reasi, J&K, India
4.	Dulhasti	Hydroelectric project	Himachal Pradesh, India
5.	Giri-Bata	Hydroelectric project	Himachal Pradesh, India
6.	Maneri Stage - 1 & II	Hydroelectric project	Uttarakhand, India
7.	Chhibro-Khodri	Hydroelectric project	Uttarakhand, India
8.	Tala	Hydroelectric project	Chukha Dzongkhag, Bhutan
9.	Kaligandaki'A'	Hydroelectric project	Syangi, Nepal
10.	Khimti	Hydroelectric project	Janakpur Zone, Nepal
11.	Noonidih Colliery	Coal mine	Jharia Coal Fields, Jharkhand
12.	Nathpa Jhakri	Hydroelectric project	Shimla, Himachal Pradesh, India
13.	Tehri	Hydroelectric project	Uttarakhand, India
14.	Lower Periyar	Hydroelectric project	Idukki, Kerala, India
15.	Koyna	Hydroelectric project	Satara, Maharashtra, India
16.	Tandsi	Coal mines	Chhindwara, Madhya Pradesh, India
17.	Mansar	Manganese mines	Nagpur, Maharashtra, India
18.	Lakhwar	Hydroelectric project	Uttarakhand, India
19.	Upper Krishna	Irrigation project	Karnataka, India
20.	Loktak	Hydroelectric project	Imphal, Manipur, India
21.	Frejus tunnel	Highway project	France-Italy
22.	Kaletepe tunnel	Highway project	Turkey
23.	Kielder tunnel	Experimental tunnel	United Kingdom
24.	Laerdral tunnel	Highway project	Norway

Note: ****-Geology of this project has been discussed in Chapter 7 as its data has been used for validation of the developed empirical correlations in the present study.***

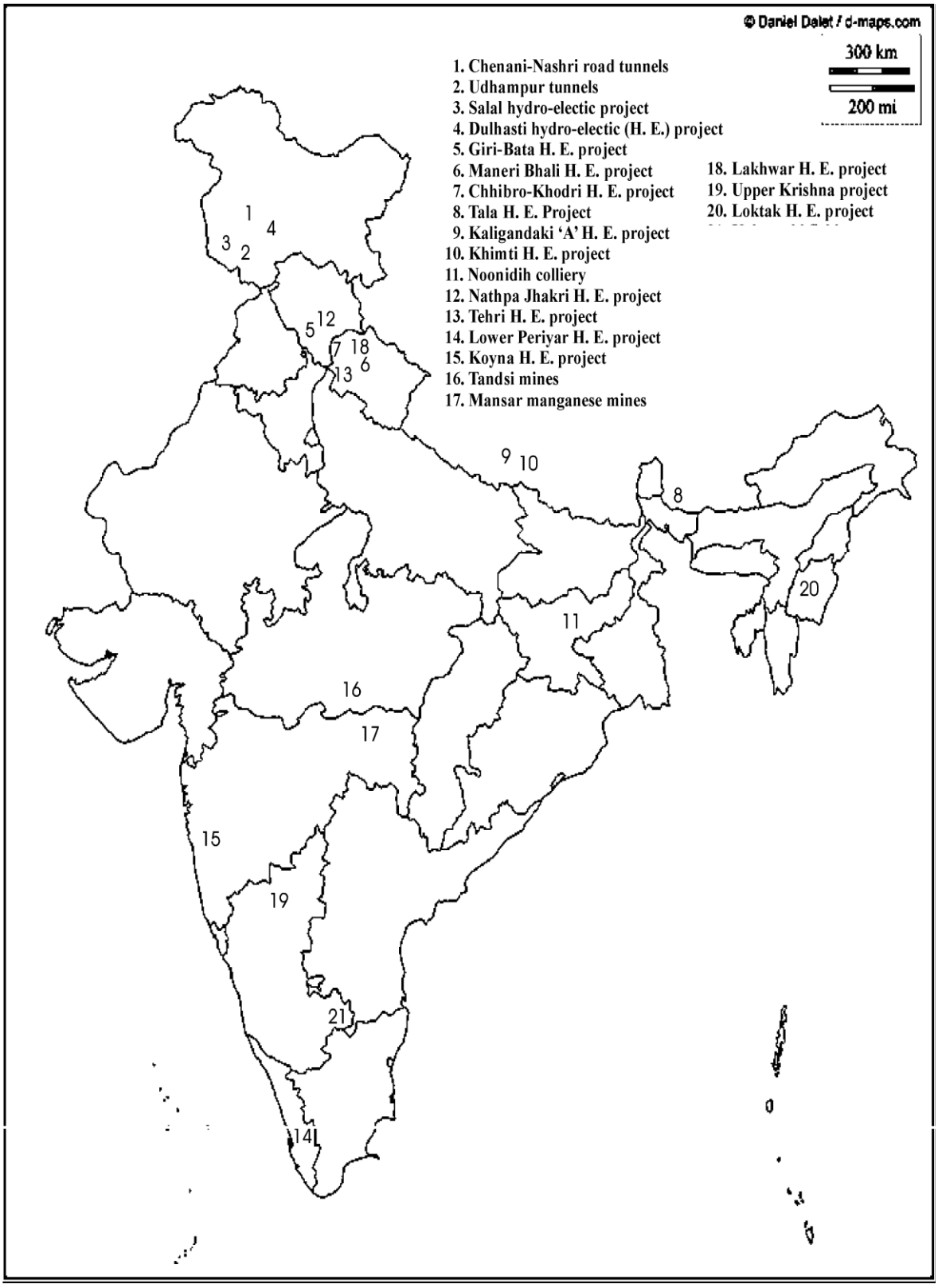

Fig. 3.1 Location of Various Case Histories Considered for Analysis in Present Study

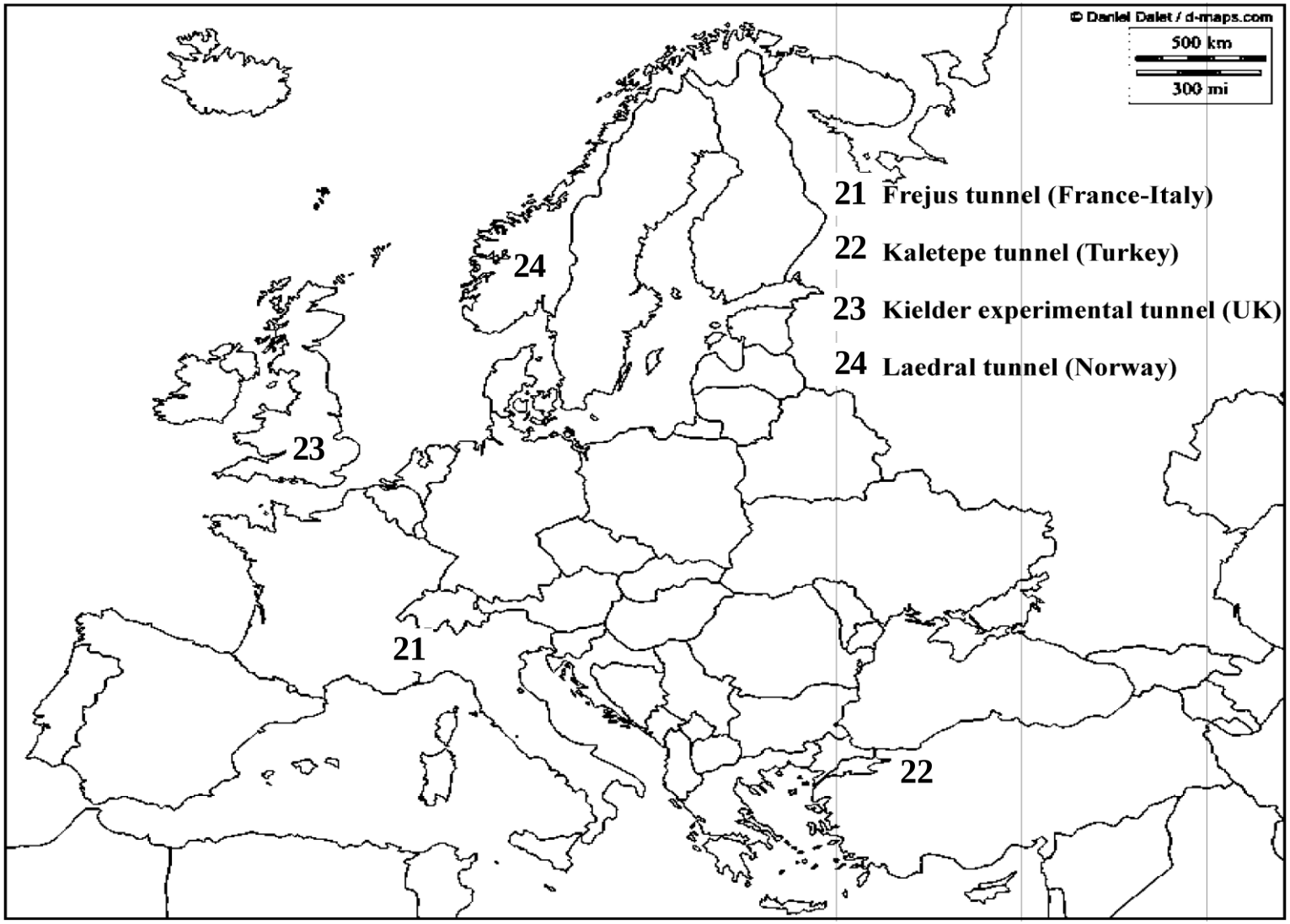

Fig. 3.2 Locations of Various Case Histories in Europe Considered for Analysis in Present Study

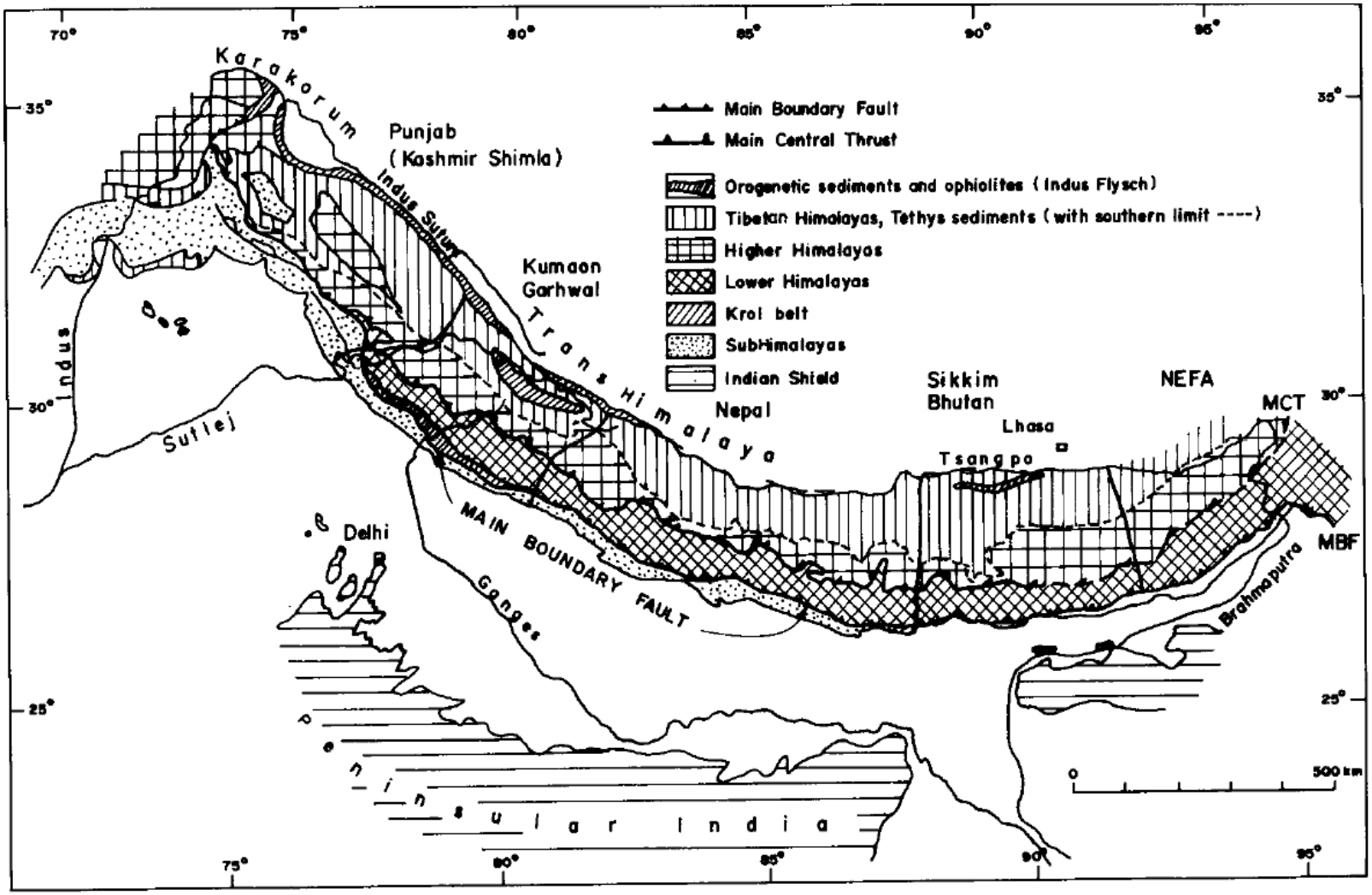

Fig. 3.3 Longitudinal and Transverse Sub-divisions of the Himalayas (after Gansser, 1964)

Central Institute of Mining and Fuel Research (CIMFR) formerly known as Central Mining Research Institute (CMRI), Regional Centre, Roorkee has been carrying out instrumentation and support design for tunnels for the last 40 years. This author had a chance to be a member of a team involved in the instrumentation and monitoring of the data at many tunnelling and mining project sites and all these data have been included in the present analysis.

Since most of the case histories belong to the Himalayan region, brief geology of the region has been presented in the following paragraphs:

The collision, which began with the first contact about 40 million years ago, caused the sediments of the intervening Tethys Sea and the Indian Shield to be folded and faulted into the lofty peaks and outliers visible in the Lesser Himalayas. Continuous northward shifting of the Indian plate is responsible for the continuous mountain building process in this region. Therefore, the zone is still seismically active. Geographically, the Himalayas are divided from West to East, as follows:

WEST : Punjab Himalaya, Kumaon Garhwal Himalaya, Nepal Himalaya, Sikkim Bhutan Himalaya,

EAST : North eastern states of Sikkim, Assam, Arunachal Pradesh, Nagaland, Tripura, Manipur and Meghalaya.

On the basis of the average height of the Himalaya's from Mean Sea Level (MSL), the rock formations from the South to the North are categorised as follows:

Rock Formations	Average Height from Mean Sea Level (MSL)	Popular Name
SOUTH		
Indo-Gangetic Planes ----------**MAIN FRONTAL THRUST**----------		
Soft, loose and easily erodible rocks i.e., sandstone, siltstone, mudstones, claystones, conglomerates	up to 1000m	Sub-Himalays or Shiwaliks
----------**MAIN BOUNDARY FAULT**----------		
Sedimentary formations i.e., slate, dolomites, quartzites, shales, claystones etc. Metamorphic formations, i.e., phyllites, quartzites, schists, gneisses etc.	1000 m - 4000 m	Lesser or Lower Himalayas
----------**MAIN CENTRAL THRUST**----------		
Weak sedimentary formations i.e., shales, sandstones, siltstones, conglomerates and strong metamorphic formations i.e., gneisses, megmatites, schists, marble etc.	> 4000m	Greater or Higher Himalayas
NORTH		

3.2 GEOLOGY OF THE HIMALAYA

3.2.1 Shiwaliks

Main Frontal Thrust (MFT) separates the Shiwaliks from the Gangetic planes (Fig. 3.3). The Shiwalik rocks constitute the southern foothills of the Himalayas. With an average height of about 1000m, the Shiwaliks are generally covered with thick forests and are comprised of the youngest rocks in the Himalayan range. The soft, loose, and easily erodible rocks are represented by sandstones, siltstones, claystones, mudstones and conglomerates. Water penetrates into these rock masses along the fractures and joints and sometimes creates flowing ground conditions (Goel, 1994).

3.2.2 The Lower Himalaya

The lower Himalayas are separated from the Shiwaliks by the Main Boundary Thrust (MBT) (Fig. 3.3). The MBT is still an active fault. The lower Himalayas are a rugged mountain region having an average height of about 4000m. Like Shiwaliks, these are also covered with thick forests. The lesser Himalaya is made of sedimentary and metamorphic rocks. The sedimentary formations vary from weak slates to massive and thickly bedded dolomites. Limestones, quartzites, shales and claystones are also present. These are intensely folded and faulted. The low grade metamorphic rocks in the lesser Himalayas are phyllites, quartzites, schists and gneisses. The metamorphic formations are also folded and faulted (e.g. Chhibro-Khodri tunnel, Giri-Bata tunnel, Loktak tunnel, Maneri Stage I & II tunnels, Salal tunnel and Tehri tunnels) (Zurick, 2006).

3.2.3 The Higher Himalaya

The higher Himalayas are separated from the Lesser Himalayas by the Main Central Thrust (MCT) (Fig. 3.3). The topography is rugged and the average height above mean sea level is about 8000m. These Himalayan ranges remain covered with snow. The formations are divided into two units: a) The Central Crystallines, comprising of the competent and massive high grade metamorphic rocks such as gneisses, megmatites, schists and marbles, and b) The Tibetan-Tethys Zone, composed of incompetent rocks such as shales, sandstones, siltstones and conglomerates. The rocks of higher Himalaya are also intensely folded and faulted.

The above geological description clearly indicates that the Himalayan rocks are tectonically disturbed, weak and the terrain is inaccessible. Tunnels in the Himalayas have, in general, a high overburden because of its great heights from MSL. Because of these features, various tunnelling problems were encountered while excavating tunnels through the Himalayas (Goel, 1994).

In the following paragraphs, case histories of seventeen tunnelling projects have been presented in brief. These projects are the source of the major part of the data used in this study. Geo-mechanical properties of rock mass and critical joints have been tabulated and presented at the end of this chapter. Various details and the geology of Chenani-Nashri

highway tunnels in the state of Jammu and Kashmir, listed at S. No. 1 in the Table 3.1, are presented in Chapter 7.

3.3 UDHAMPUR RAILWAY TUNNEL

Indian Railways are linking the State of Jammu & Kashmir through the Kashmir valley in Himalayas, with a broad gauge railway line which is below the snow line making it an all-weather route. The total route length is 342 km, out of which about 100 km is passing through the tunnels. The ruling gradient of these tunnels / railway tracks is 1 in 100 and the maximum degree of curvature is restricted to 2.75º. Udhampur - Katra section is the 1st phase of Udhampur-Srinagar - Baramula Rail (USBR) Link Project which is 25 km long and involves construction of 7 tunnels aggregating to 10 km. Tunnel No. 1 is D-shaped and having 6.5 m diameter and a height of 8.25 m. It is the longest tunnel of this section with a length of 3.1 km (Goel et al., 2004).

The tunnel falls in Shiwalik Group and Pleistocene Formation and traverses through unconsolidated or poorly consolidated sediments with rocks of upper/middle/lower Shiwaliks and Murree formations. It passes through thickly bedded, moderately soft, sparsely jointed sandstones, sheared clay stones, siltstones and the overburden comprising of boulders / pebbles in sandy /silty matrix. Claystone/siltstone beds have 3 sets of closely spaced joints with random joints dipping at 60-70^{o}. Strike of the joints makes an angle of 30^{o} with the tunnel axis. In the stretch from 270 m to 313 m, which is comprised of weak rock formation (claystone and siltstone), the tunnel experiences squeezing condition. Rock Mass Quality, Q-values of claystone and siltstone vary between 0.041 and 0.2 and the stand-up time is approximately 1 day (CIMFR, 2007). In-situ stresses were measured using flat jack technique and the ratio of horizontal to vertical in-situ stresses (k) was found out as equal to 1.2 at a depth of 300 m (Dwivedi et al., 2014a).

The tunnel was excavated by drill & blast method. Squeezing behaviour of rock mass was experienced during tunnelling. Steel rib supports (ISHB 200) were installed at a spacing of 0.75 m centre to centre. Load cells and closure studs were installed up to 3 m behind the tunnel face. Support pressure was observed to be 0.30-0.52 MPa, whereas the radial deformation was recorded to be 1.5 - 3% (CIMFR, 2007).

3.4 SALAL HEP TUNNEL

The Salal Hydro Electric Project (HEP) is located on river Chenab near Reasi in Udhampur district of Jammu and Kashmir state of India. The total installed capacity of the project is 690 MW with 6 units of 115 MW each. Two tail race tunnels, each of 2.5 km in length, were constructed with a finished horse-shoe section having a width of 11.0m. The excavation was carried out with the conventional method and supported by steel ribs with concrete backfill.

The tunnel alignment crosses the hill under a maximum cover of about 630 m. The longitudinal geological cross-section along the tunnel alignment is presented in Fig 3.4. The tunnel is excavated through dolomites of the great limestone series of Precambrian age. The dolomites are moderately jointed and the joint walls are weathered. At some places, dolomites are highly jointed and sheared. Three regularly spaced prominent joint sets are present. The bedding joints dip at 40^{o}-55^{o} due North. The transverse joints dip at 70^{o}-80^{o} due West and the cross joints dip at 30^{o}-40^{o} due South. The strike of these joints makes an angle of 65^{o} with the tunnel axis at the outlet end and 20^{o} at the inlet end.

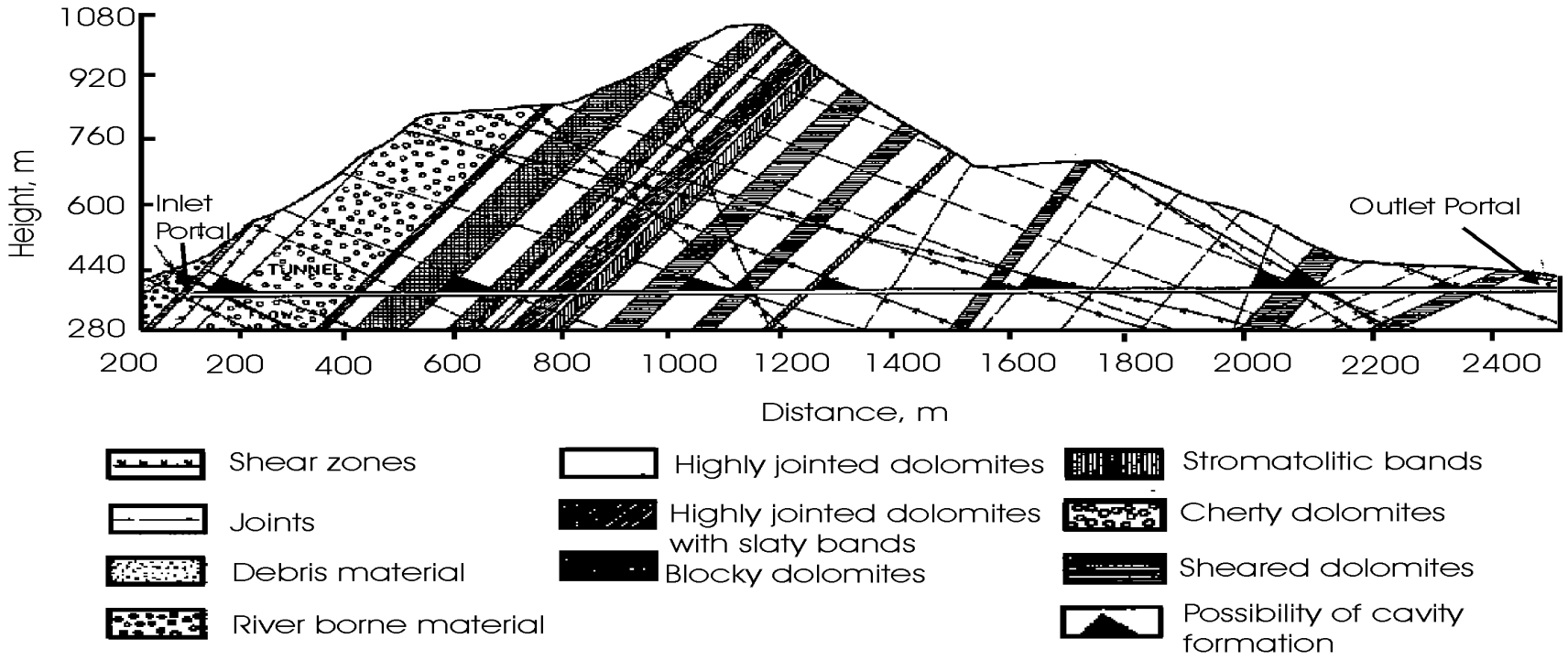

Fig. 3.4 Geological Cross-Section along Salal Hydro Power Project Tunnel (after Jethwa, 1981)

Table 3.2 Classification of Dolomites of Salal Hydro Power Project
(after Goel, 1994)

Sl. No.	Joint Spacing (cm)	Type of Dolomites	Length of Tunnel (%)
1.	30-100	Cherty and blocky	5-10
2.	5-30	Highly jointed	80
3.	<5	Crumbly and sheared	10-15

A number of shear zones were also encountered. These shear zones vary in thickness from a few centimetres to a couple of meters and are filled with crushed calcareous matter, a product of crushing of dolomites due to shearing. The *Q* and *RMR* (Rock Mass Rating) values of jointed dolomites encountered in the tunnel are 1.2-1.7 and 41 respectively.

The dolomites are classified into three categories depending upon the joint spacing and the degree of disintegration and their possible extent into the tunnel is given in Table 3.2 (Goel, 1994).

Presence of three joint sets and shear zones at the tunnel grade has created many wedges above the tunnel crown (Fig. 3.4). These wedges have become unstable and have given rise to the instability problems when installation of the supports was delayed. Squeezing problem was encountered between chainage 660 m and 1300 m, where the overburden is up to 300 m.

3.5 GIRI-BATA HEP TUNNELS

This project with an installed capacity of 120 MW, was constructed on Giri river, a tributary of Himalayan river Yamuna. It is located near Girinagar in Sirmour district of the state of Himachal Pradesh in India. A 7.1 km long head race tunnel with a finished diameter of 3.60 m was driven through a ridge separating the valleys of Giri and Bata rivers (Dube, 1979). The tunnel was excavated by drill & blast method and was supported by steel ribs. Plain cement concrete lining of 300 mm average thickness was applied as final support.

The tunnel traverses through Blaini series rock formations of carboniferous age for a length of about 1500 m and through highly jointed clay stones, highly crushed phyllites and siltstones for the remaining length. The Blainis are dark grey to black quartzitic slates containing angular to rounded pebbles and boulders firmly embedded in a clay-silt matrix (Fig. 3.5). The

rock formations showed extensive jointing and shearing at places and the strike generally remained parallel to the tunnel alignment. Blaini's slates, near the fault at a chainage 1350 m also posed serious problems during construction because of high tunnel closures, which were of the order of 10%. Joints were spaced at 45-50 mm and dipping at 60^{o}-70^{o}. These formations were highly crushed exhibiting a low angle of internal friction lying between 20° and 26^{o} (Dube, 1979). In-situ stresses were measured using flat jack technique and the ratio of horizontal to vertical in-situ stresses (k) was determined to be equal to 2 (Dwivedi et al., 2014a).

Most of the tunnelling problems were faced in zones of phyllites and slates. Load cells and closure studs were installed up to 3 m behind the face. Support pressure was observed in the range of 0.2-0.5 MPa. Plain cement concrete lining of 300 mm average thickness was applied as final support.

3.6 MANERI STAGE-I HEP TUNNELS

This project is constructed on river Bhagirathi, a tributary of river Ganges located in the Uttarkashi district, in the northern state of Uttarakhand in India to generate 84 MW of power. A circular head race tunnel of 4.75 m finished diameter and 8.56 km length was constructed in Stage-I of Maneri-Bhali Hydel Scheme.

The rock masses exposed in the area are quartzites, quartzites interbedded with thin bands of slates, chlorite schists, phyllites, meta-basics and basic intrusives belonging to the Garhwal group (Jain et al., 1976). The general strike directions in Maneri, Heena and Tiloth areas are: N 10°-80^{o}, N 250°-280^{o}, N 290°-350^{o} respectively whereas dip (directions) are 25°-45^{o} (N 100°-170^{o}), 25°-35^{o} (N 160°-190^{o}) and 35°-49^{o} (N 20°-80^{o}) respectively. These lithological units are intensely folded and faulted due to tectonic disturbances (Dwivedi et al., 2013). The tectonic activity in the area has developed closely spaced jointing, brecciation and shearing even in the quartzites. The tunnel passes initially through meta-basics and basic chlorite - schists and then enters into folded quartzites (Fig. 3.6).

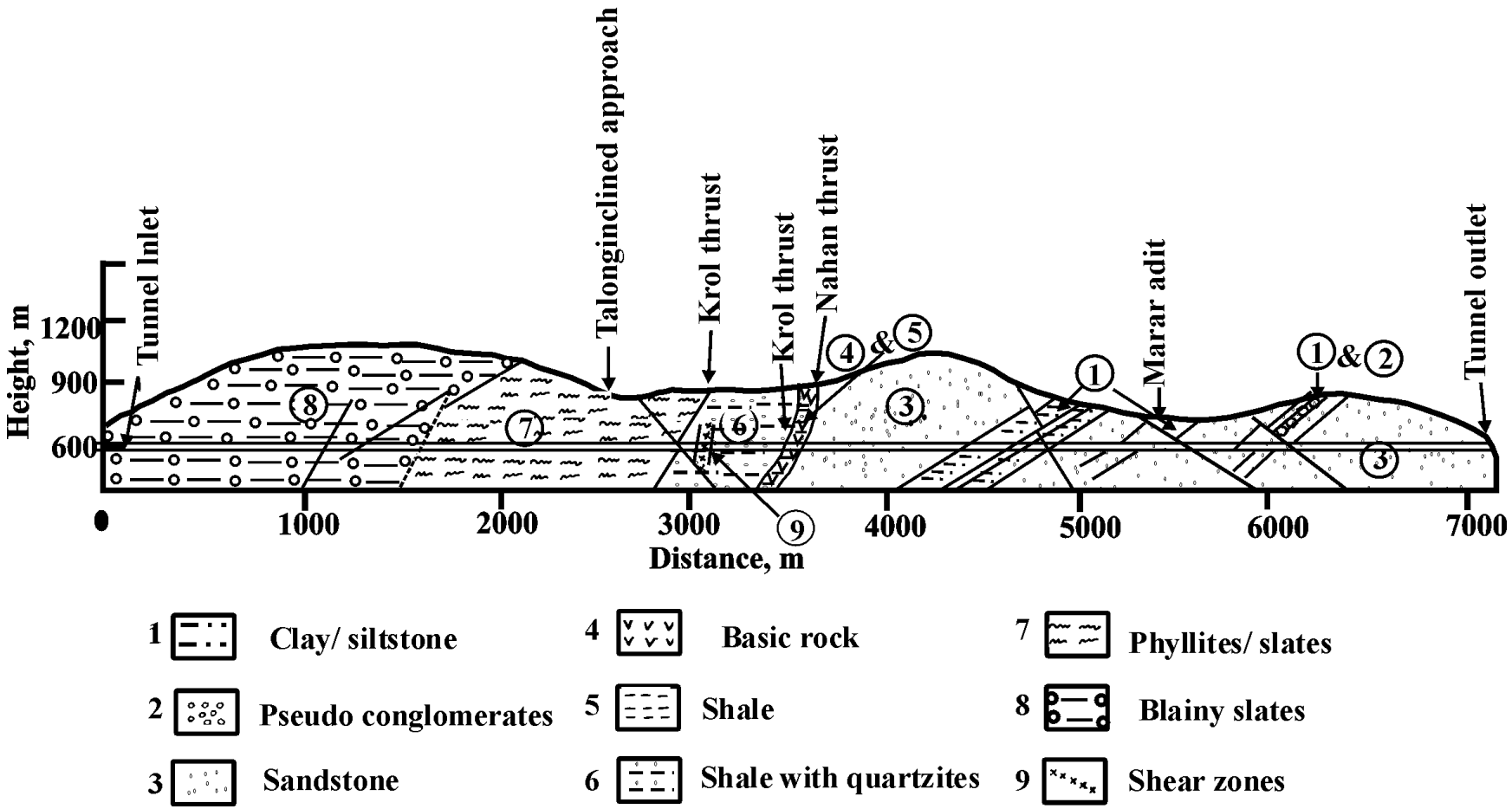

Fig. 3.5 Geological Cross Section along Giri-Bata Tunnel (after Dube, 1979)

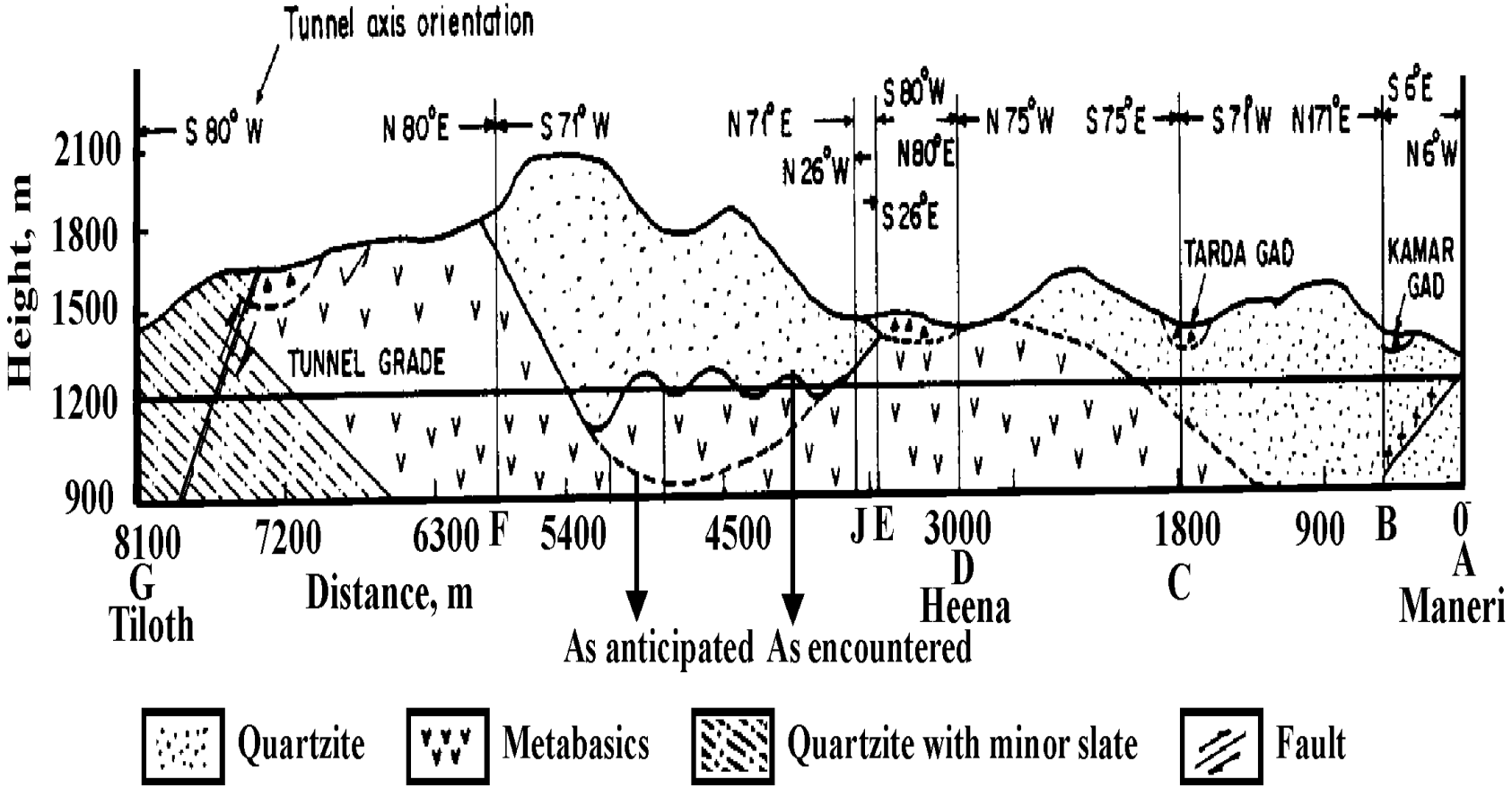

Fig. 3.6 Geological Section along Maneri Stage-I Tunnel (after Goel, 1994)

Two cross shear zones, 0.40 m wide, intersect above the tunnel crown (Goel et al., 1988). In-situ stresses were measured using flat jack technique and the ratio of horizontal to vertical in-situ stresses (*k*) was determined to be equal to 0.33 (Dwivedi et al., 2014a).

Tunnelling activities at depths varying from 700 m to 900 m through moist and thinly foliated meta-basics were beset with severe squeezing problems.

The tunnel was supported by Indian Standard Medium-weight Beam (ISMB) 150 mm x 150 mm steel ribs spaced at 0.60 m. Load cells and closure studs were installed up to 3 m behind the face. Data analysis shows that the maximum deformation was observed to be 7.3% at the contact of meta-basics and quartzites (Goel, 1994).

3.7 MANERI STAGE-II HEP TUNNEL

The project with an installed capacity of 304 MW is constructed across the river Bhagirathi, a tributary of the river Ganga and is located in the lower Himalaya about 150 km north-west of the holy town, Rishikesh, India. The project area lies between the tail works of Maneri Stage-I project and the reservoir of the downstream Tehri hydro project. It comprises of a 16 km long head race tunnel (HRT) having a finished diameter of 6.0 m.

The head race tunnel passes through quartzites, meta-volcanics (also called meta-basics), limestones and epidiorites of the Garhwal group and phyllites, slates and greywackes of Tehri Formation. The Garhwal group thrusts over the Tehri formations. Rock masses, in general, are moderately jointed and a majority of these joints are open. Several cross shear zones are also encountered in the area. The general dip of foliations as well as that of the bedding planes varies from 40^{o} to 80^{o} in N-E direction. The tunnel encountered moderately foliated, jointed and sheared meta-basics (also called meta-volcanics) and quartzites in a length of more than 3000 m. The sheared and jointed meta-basics, massive to moderately jointed quartzites, pyrite-ferrous slates with thin intercalations of quartzites and jointed limestone, massive phyllites and greywackes with calcareous lenses, and thinly bedded greywackes were encountered during tunnelling (Fig. 3.7). The lithological contacts and the contacts between the formations were mostly sheared. In-situ stresses were measured using flat jack technique and ratio of horizontal to vertical in-situ stresses (*k*) was determined to be equal to 0.33 (Dwivedi et al. 2014a).

Tectonically active and young rock masses of the lower Himalayas are highly shattered and weak leading frequently to squeezing ground conditions. The Maneri stage-II tunnel was not an exception. The tunnel was excavated by drill & blast method. Severe squeezing ground conditions were encountered during tunnelling in the zones of meta-basics, sheared meta-basics, greywackes and phyllites.

ISMB 150 mm x 150 mm steel ribs were installed at a spacing of 0.5m centre to centre. Load cells and closure studs were installed up to 3 m behind the face. Support pressures of 0.17 MPa and 0.29 MPa were observed in meta-volcanics and sheared meta-basics respectively, whereas tunnel deformation was observed to be between 2.5% to 3%.

3.8 CHHIBRO-KHODRI HEP TUNNELS

The project was constructed on river Tons, a tributary of Yamuna river located about 45 km North of Dehradun in the state of Uttarakhand, India. Tunnel with a finished diameter of 7.5 m was constructed between Chhibro and Khodri to utilise discharge of the Chhibro powerhouse for generating 120 MW of power through a surface powerhouse at Khodri.

The Chhibro-Khodri tunnel passes through three geological formations namely, Mandhali series (Paleozoic), Subathu-Dagshai (Lower Miocene) and Nahan series (Upper Tertiary). Mandhali series consists of boulder slates, graphitic & quartzitic slates and Bhadraj quartzite unit with 5-10 m thick crushed quartzite along Krol thrust (Fig. 3.8). Subathu-Dagshai series is comprised of : i) 1-3 m thick plastic black clays, ii) red & purple coloured crushed, brecciated & sheared shales and siltstones, iii) minor grey and green coloured crushed quartzites, iv) 20-22 m thick black clays with thin bands of quartzites, and v) 5-10 m thick soft and plastic black clays along the Nahan thrust (Jain et al., 1975). Nahan series is comprised of greenish grey to grey micaceous (Upper Tertiary) sandstones, purple siltstones, red, purple, grey and occasional mottled blue concretionary clays. General strike of these litho units is nearly perpendicular to the tunnel axis and the dip ranges from 20^{o} to 60^{o} in NNW to NNE direction (Shome et al., 1973). There are two main boundary faults running from the state of Punjab in the North to the state of Assam in the East along the foothills of the Himalayas. The faults are known locally as the Nahan and the Krol thrusts. The dip of the Nahan and the Krol thrusts varies from 27^{o} to 30^{o} due $N10^{o}E$ to $N10^{o}W$ and 26^{o} due $N26^{o}$ W respectively. The strike of joints makes an angle of 40^{o}-50^{o} from the tunnel alignment.

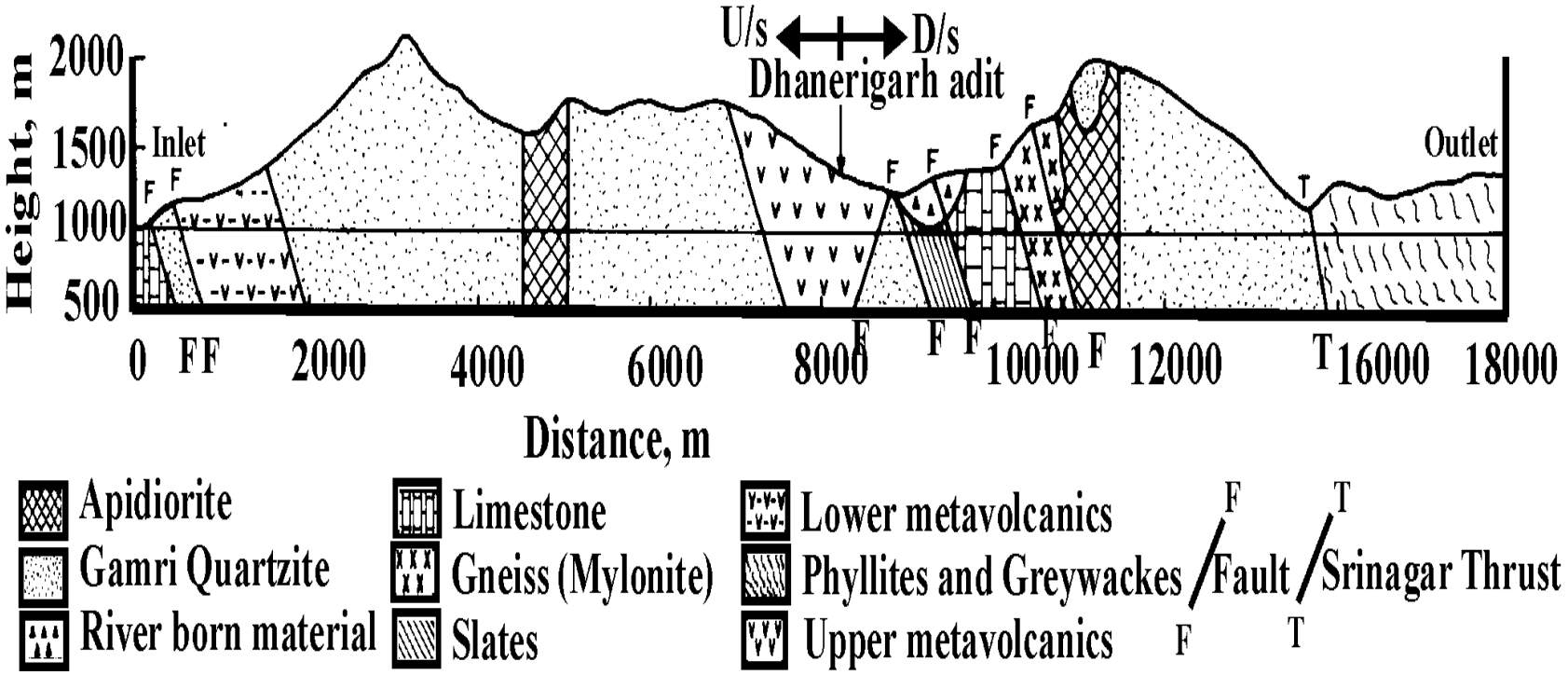

Fig. 3.7 Geological Section along Maneri Stage-II Tunnel (after Varshneya, 1988)

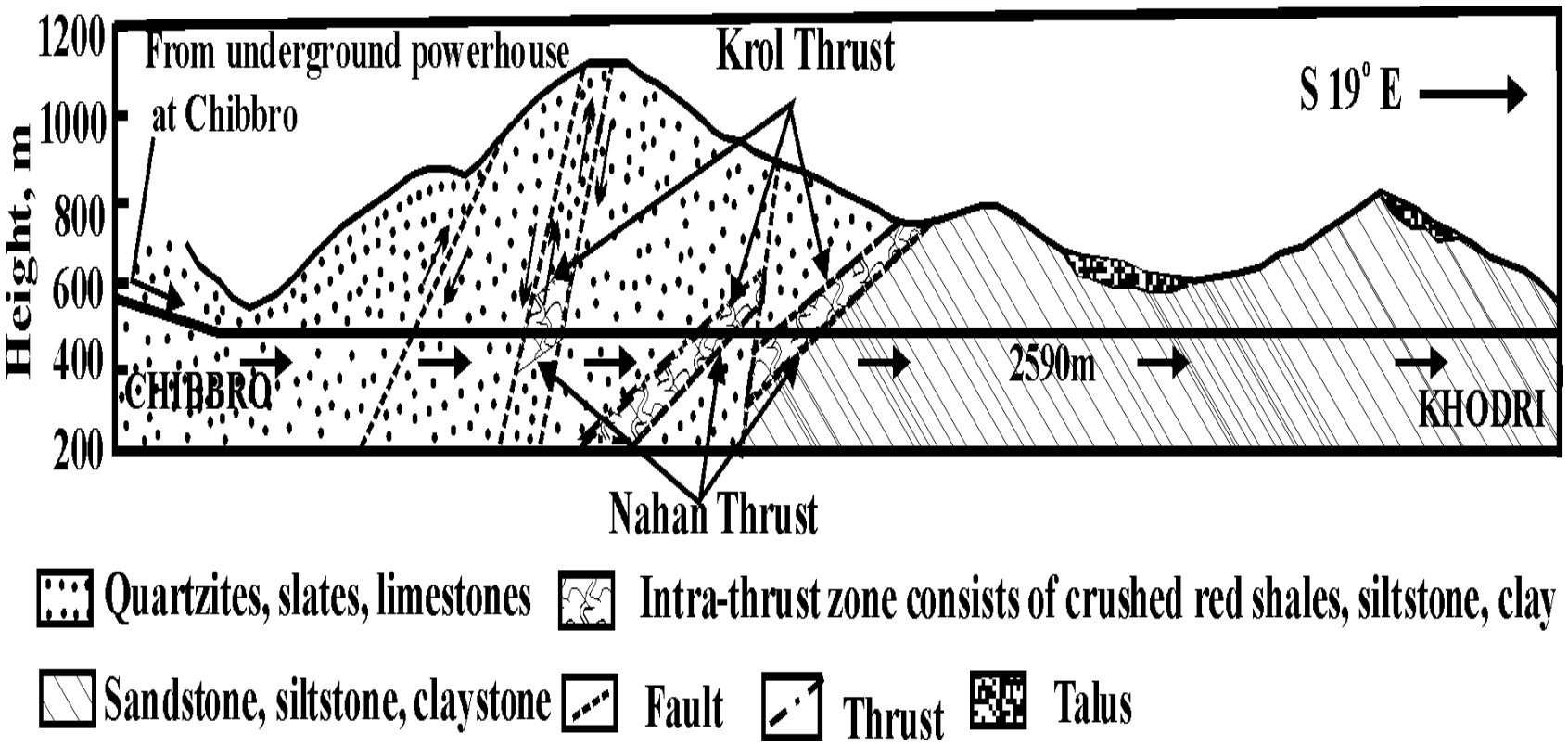

Fig. 3.8 Geological Cross Section along Chhibro-Khodri Tunnel (after Jain et al., 1975)

In-situ stresses were measured using flat jack technique and ratio of horizontal to vertical in-situ stresses (*k*) was found to be equal to 1 except in the thrust regions (Dwivedi et al., 2014a).

Major tunnelling problems were faced within the intra-thrust zones due to squeezing ground conditions. In order to minimise the frequent rock falls, multi-drift method was employed for construction at faces. The tunnel was excavated by drill & blast method.

Heavy steel ribs of 300 mm x 140 mm and 150 mm x 150 mm sections, with 20-25 mm thick plates welded on both flanges were erected at 0.25 - 0.50 m spacing to cope up with high squeezing pressures. The progress rate was tremendously slowed down to 5 - 6 m per month. Load cells and closure studs were installed up to 3.5 m behind the face of advance. The observed support pressure varied from 0.65 to 1.3 MPa giving an average support pressure of 0.975 MPa in the vertical direction (Jethwa et al., 1980). Tunnel deformation observed in the tunnel was in the range from 2% to 18%.

3.9 TALA HEP HEAD RACE TUNNEL

The Tala hydro electric project is situated in South-West Bhutan in the Eastern Himalaya. The project is located in the district of Tala 3 km downstream of the existing 336 MW Chukha Hydroelectric project on river Wangchu (Sripad et al., 2007). The Tala Hydroelectric Project area falls within the central crystalline belt of Thimphu Formation and meta-sediments of Paro Formation. The Thimphu Formation comprises of a variety of granitoid rocks, such as megmatite, augen-gneiss, banded-gneiss, granitic-gneiss, and schistose rocks with subordinate quartizite and marble bands. The Paro Formation consists of high grade calcareous rock and meta-sedimentaries such as marble, calc-silicate rock, quartzite, quartz-garnet-staurolite-kyanite-silmenite schist, graphite schist etc. with subordinate felspathic schist and gneiss bands (Khushlani, 2013). It has a 22 km long head race tunnel (HRT) of 6.8 m excavated diameter.

The head race tunnel traverses through highly weathered biotite schist associated with banded gneiss amphibolites and quartzites. In-situ stresses were measured using flat jack technique and ratio of horizontal to vertical in-situ stresses (*k*) was found to be equal to 0.6 (Dwivedi et al., 2014a).

The tunnel was excavated by drill & blast method. During tunnelling, excessive deformation was encountered at many tunnel sections due to squeezing behaviour of the poor rock mass) (completely sheared & highly weathered biotite schist associated with banded gneiss, amphibolites and quartzites in thin bands) present around the tunnel periphery.

The support system provided to the tunnel is in the form of 5-6 m long rock bolts of 25 mm diameter at 2.0 m c/c spacing in combination with 175 mm steel fibre reinforced shotcrete (SFRC) as a temporary lining and steel ribs (ISMB 200 or SMB 250 at 0.5m centre to centre), along with concrete lining as a permanent support system (Tripathy et al., 2000). Load cells and closure studs were installed up to a distance of 3.5 m behind the face of advance. On measurement, tunnel deformation was observed as 2 - 3.8 %, and the support pressure was in the range of 0.61 - 0.94 MPa.

3.10 KALIGANDAKI 'A' HEP HEAD RACE TUNNEL

The Kaligandaki "A" hydroelectric project is located in the Lesser Himalaya about 200 km West of Kathmandu in Nepal. The project is owned by Nepal Electricity Authority (NEA), an undertaking of the Government of Nepal. The project has an installed capacity of 144 MW and to generate this energy, water of Kaligandaki river is diverted through a head race tunnel with an excavated cross sectional area of about 60 m^2.

The project area is located in a highly deformed rock formation of Lesser Himalaya. The rocks of this area are mainly comprised of Precambrian to lower Palaeozoic shallow marine sediments. The head race tunnel passes through highly deformed siliceous and graphitic phyllites that vary in mineral composition and degree of metamorphism. As a result of tectonic movement, the rock mass in the area has been subjected to shearing, folding and faulting. The phyllites are of poor quality, thinly foliated and highly weathered (NEA, 2002). The orientation and dips of joints are highly scattered due to extreme folding and shearing, giving no distinct joint system except for foliation joints. In general, the foliation joints are oriented in South East-North West direction and dip of about 50^o-60^o towards South West. The alteration and weathering of joints are considerable. The joints are filled with highly sheared clay, quartz and calcite veins. The maximum rock cover above the tunnel is about 600 m and more than 80% of the tunnel alignment has an overburden exceeding 200m (Panthi and Nilsen, 2007) (Fig. 3.9). The ratio of horizontal to vertical in-situ stresses (k) was determined to be equal to 0.5 (Dwivedi et al., 2014a).

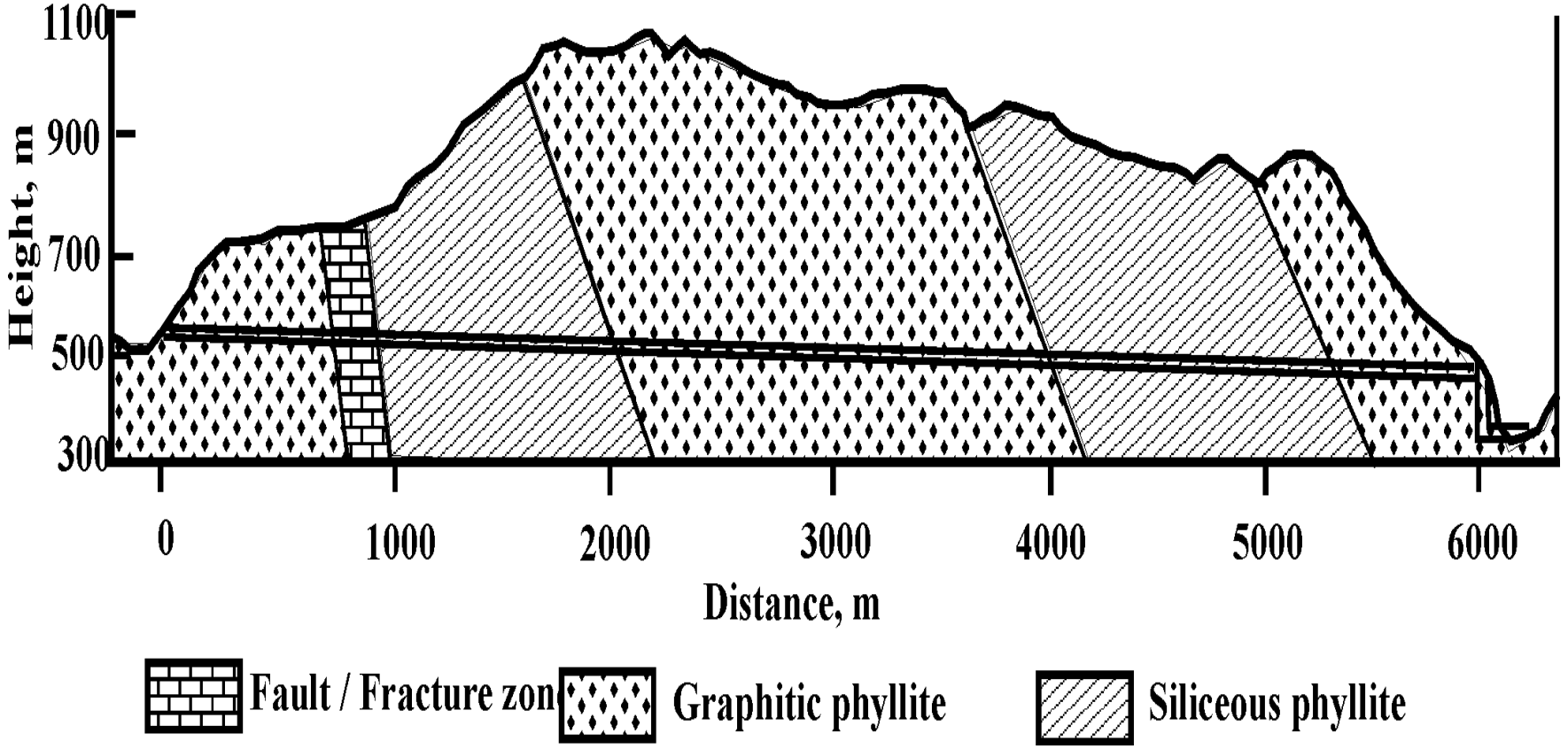

Fig. 3.9 Geological Section along Kaligandaki 'A' Head Race Tunnel (after Panthi and Nilsen, 2007)

The head race tunnel was excavated by drill & blast method and faced severe squeezing problems due to above mentioned geological conditions. The head race tunnel was supported with 25 mm diameter and 4 m long radial rock bolts at a spacing of 1.5 m c/c and steel ribs at 1 m c/c. Load cells and closure studs were installed up to 3 m behind the tunnel face. Tunnel deformation and support pressure were measured and were found to be 1.4 - 8.5% and 0.90 - 1.27 MPa respectively.

3.11 KHIMTI HEP TUNNELS

The Khimti-1 hydropower project is located in Janakpur zone, Central Development Region of Nepal at about 100 km East of Kathmandu. The river Khimti-Khola forms the boundary between Ramechhap and Dolakha districts. It is a run-off the river type of hydroelectric project with an installed generating capacity of 60 MW, utilising a drop from 1272 m to 586 m above the average mean sea level in the Khimti-Khola. The project area lies in the Midland Schuppen zones of the Melung augen gneiss containing mainly grey, coarse-to very coarse-grained, porphyro-blastic augen gneiss (63%), occasionally banded gneiss (12%), and granitic gneiss (7%) with bands of very weak, green chlorite and bright grey talcose schist (18%) parallel to the foliation at intervals of 5 to 15 m. The zone is bounded by two major faults namely Midland thrust to the South and Jiri thrust to the North. The area is also influenced by several minor thrust faults characterised by very weak sheared schist with clay gouge running parallel to the foliation plane. The foliation at the tailrace to the Adit 4 (the saddle of Pipal Danda) has steep dips (45^o to 60^o), whereas it is gently dipping (15^o to 35^o) in the area between Pipal Danda and the head works (Fig. 3.10).

Tunnels/adits of the project faced squeezing problems at various locations, especially in the sections where schist or decomposed gneiss was present with 80 to 420 m overburden depth. Large deformations were recorded after two weeks at different sections of tunnels at about 20m behind the face of advance. The maximum deformation recorded was 6.4% in Adit-1 at downstream Chainage of 500 m (Shrestha, 2005).

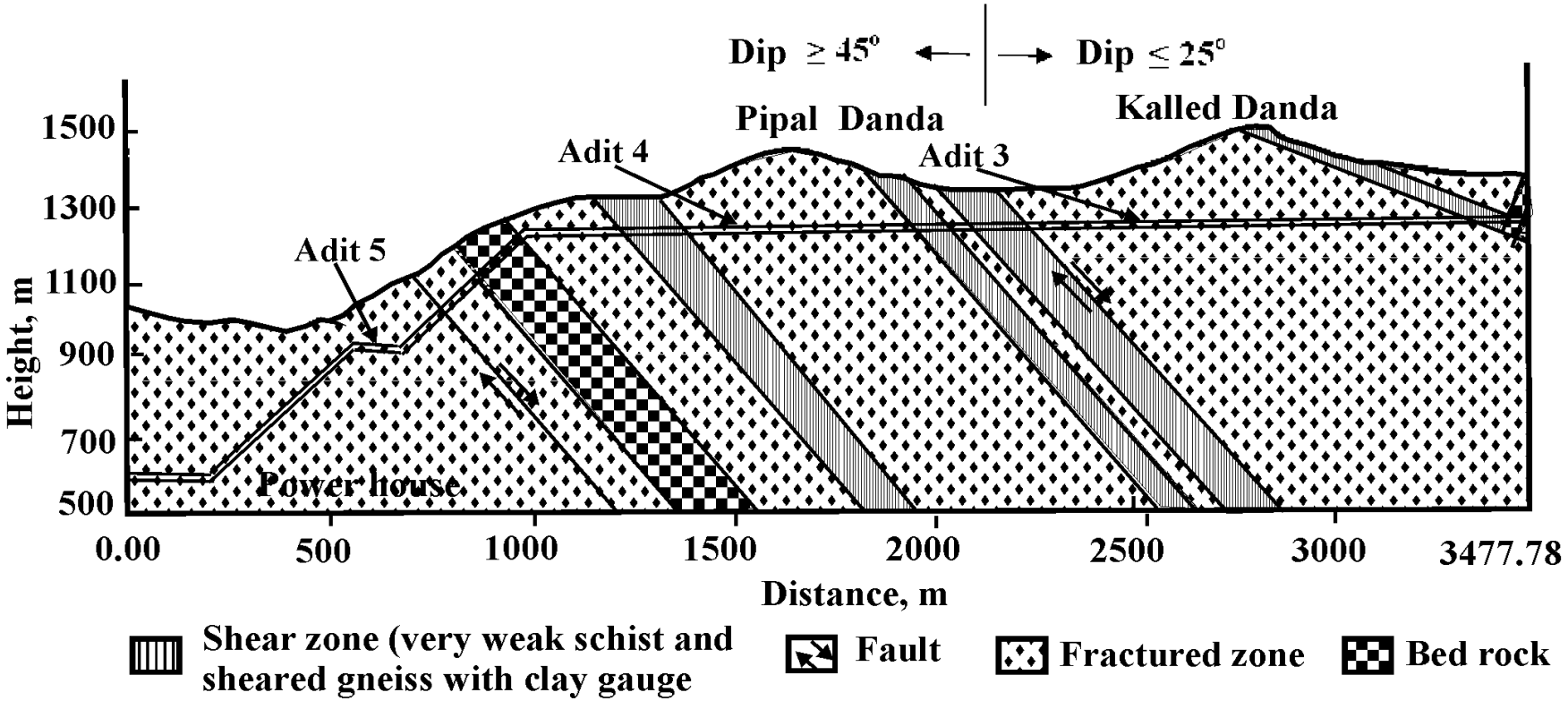

Fig.3.10 Geological Section along Khimti-1 Adit (after Sunuwar et al., 1999)

3.12 NOONIDIH JITPUR COLLIERY

The Noonidih-Jitpur Colliery (a captive coal mine of M/S Indian Iron and steel Company Limited, Jamshedpur, India) is located in Jharia Coal-fields near Dhanbad in the state of Jharkhand in India. Underground working of this colliery consisted of partially or fully developed areas in two seams with thickness of 3.5 m and 2.44 m and at a depth of 134 m and 73 m respectively. These seams dipped at about 8.7^{o} (Dwivedi et al., 2013). Two other seams with thicknesses of 2.44 m and 4.57 m were located at depths of 233 m and 268 m respectively. These seams were worked through two shafts. A main roadway of 3.5 m width was excavated through weak coal at a depth of 450 m to excavate a 9 m thick coal seam. In-situ stresses were measured using hydraulic fracturing technique and ratio of horizontal to vertical in-situ stresses (k) was found to be equal to 0.86 (Dwivedi, 2014a).

Drill & blast method of excavation was adopted to drive the main road. Problem of excessive deformation was observed in the main roadway due to high stresses.

The roadway was supported with steel ribs and monitoring was done for support pressure and tunnel deformation. A significant movement was observed in the 3.5 m wide main roadway. Load cells and closure studs were installed upto 4 m behind the face. The roadway deformation was observed to be 3% (Jethwa, 1981) and the support pressure was observed to be in the range of 0.05-0.20 MPa.

3.13 NATHPA-JHAKRI HEP TUNNELS

The Nathpa-Jhakri hydro power project is located between 77^{o} and 78^{o} longitude and 31^{o} and 32^{o}N latitude in the northern state of Himachal Pradesh (India), on the downstream of Wangtoo bridge and derives its name from the names of two villages in the project vicinity - Nathpa in district Kinnaur and Jhakri in district Shimla (Bhasin et al., 1995). The project was conceived as a run-off-river type hydro power development, harnessing hydroelectric potential of the middle reaches of the river Satluj, one of the principal tributaries of the river Indus in the south western Himalayas. The head race tunnel, with 10.15 m excavated diameter and 27394.5 m long, was constructed to carry a design discharge of 405 m^3/s.

The major rock types of the area are augen gneiss, quartz-biotite schist, amphibolites and some pegmatite lenses at places (Fig. 3.11).

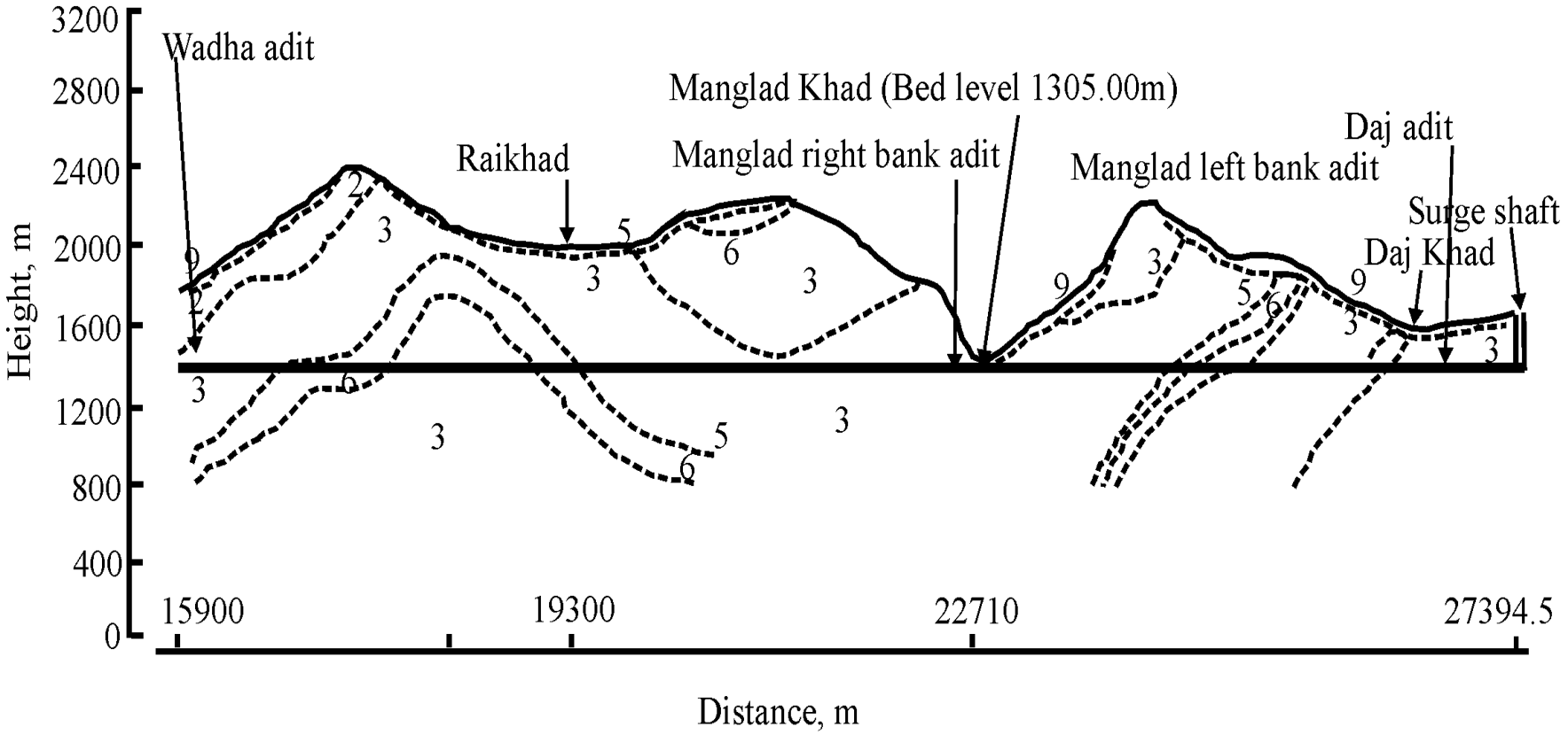

Fig. 3.11 Geological Section along Nathpa-Jhakri Head Race Tunnel (after Kumar, 2002)

Augen gneiss consists of two feldspars, two micas (mainly biotite), gneiss with a porphyro-blastic texture, which at places are mylonitic. The foliations are defined by the micaceous layers, which flow around the augens. The elongation direction of the augens defines a strong stretching lineation. The shape of the augens varies from nearly round to lensoidal at places, showing well drawn out porphyroclast tails. Schistocity of quartz-biotite-schist has a strong dominant character with well defined quartzose and micaceous layers. The layers are tabular to lensoidal. At places some biotite rich lenses are also seen. Strong stretching lineation on the foliation plane is marked. At places, the biotite altering to sericite, indicated by crumpling and high fissility, is also noticed. The amphibolites are massive weakly foliated with a prominent amphibole lineation, which appears to be a primary igneous flow structure. The quartz, feldspar content is very low and the rock is especially a biotite rich amphibolite. The amphibolites occur as narrow linear belts in the outcrop and generally unparallel to the foliation of the country rocks except at places where they are at an angle to the country rocks. Pegmatite occurs both as concordant and discordant bodies and are commonly associated with the gneisses. These are present as tabular laths. Quartz and feldspar exhibit a graphic texture and show two sets of fractures (Kumar, 2002).

There are three sets of joints, two of them are at right angles to each other and the third, oblique to them, is sub-vertical and results in wedge shaped block or rocks. Foliations were observed dipping with 30°-70^{o}, 40°-75^{o}, 15°-55^{o}, and 30°-85^{o} towards North-East in various sections of the tunnel.

The head race tunnel (HRT) traverses through augen gneiss, gneiss, quartz mica schist, biotite schist, sericite schist, amphibolites, granite gneiss, and pegmatite (Fig. 3.10). In-situ stresses were measured using hydro fracturing technique and ratio of horizontal to vertical in-situ stresses (k) was found to be equal to 1.3 (Dwivedi et al., 2014a).

The excavation of tunnel was carried out through seven adits by heading and benching method and using drill & blast technique. The geological section along the head race tunnel from chainage of 15900 m to 27394.5 m (Fig. 3.11) at various locations posed squeezing problems during tunnelling. Large tunnel deformations were observed due to high ground stresses and poor quality of rock mass between chainage 24438.0 m and chainage 24745.0 m (rock cover of 600 m-700 m) where quartz-mica schist was striking sub-parallel to the tunnel.

The type of support varied with the category of rock mass encountered. Steel ribs (300 mm x 140 mm) were installed at a spacing of 1.25 m c/c to support the squeezing sections of the tunnel. Concrete lining of 400 - 600 mm thickness was applied as final lining (Kumar, 2002). Load cells and closure studs were installed up to 5 m behind the advancing face. Tunnel deformation and support pressure were measured and were found to be 3.5% - 6% and 0.26 - 1.02 MPa respectively. To get the required clear space, the tunnel has been over excavated by 300 mm.

3.14 TEHRI HEP TUNNELS

The Tehri project is an irrigation-cum-hydro power project consisting of a 260.5 m high rock fill storage dam with an inclined clay core and is constructed across river Bhaghirathi about 1.5 km downstream of its confluence with its tributary river Bhillangana near Tehri town. An underground powerhouse complex with 2000 MW capacity is constructed on the left bank hill. Four horse-shoe shaped, 13 m wide diversion tunnels have been constructed for diverting the water during the construction of the dam. Two of these tunnels, T3 and T4, carry the water from the right bank of river on to the downstream of the dam site near Bhaintogi Nala. Out of the two right bank diversion tunnels, T3 and T4, T3 is straight and is 1298 m long, while T4 traverses a horizontal curve of 78^{o} after being straight in the first 28 m length. The remaining length of this tunnel is straight and parallel to T3. The other two tunnels, T1 and T2, each 1750m long, off-take the water from the left bank of river Bhillangana and discharge it on the left bank of river Bhaghirathi downstream of the point where right bank diversion tunnels T3 and T4 join the river Bhagirathi. The lower portions of the left bank diversion tunnels are used as tail-race tunnels (Verma et al., 1979). In addition to the four diversion tunnels, four head race tunnels, HRT-1 to HRT-4, are constructed on the left side of river Bhagirathi with the inlet portals about 250 m downstream of the Tehri town (Fig. 3.12).

Rock masses exposed in the vicinity of the Tehri tunnels are the phyllites of Chandpur series. Towards the North and East of the dam site, these are in contact with Shimla slates. At some places, the phyllites are directly in contact with the younger dolomites and quartzites of the Garhwal group. The contact between the Shimla slates and the rock masses of Garhwal group is called the ‘Srinagar thrust’, which is considered to be a counterpart of the ‘Krol thrust’ (art. 3.8, Chhibro-Khodri tunnel).

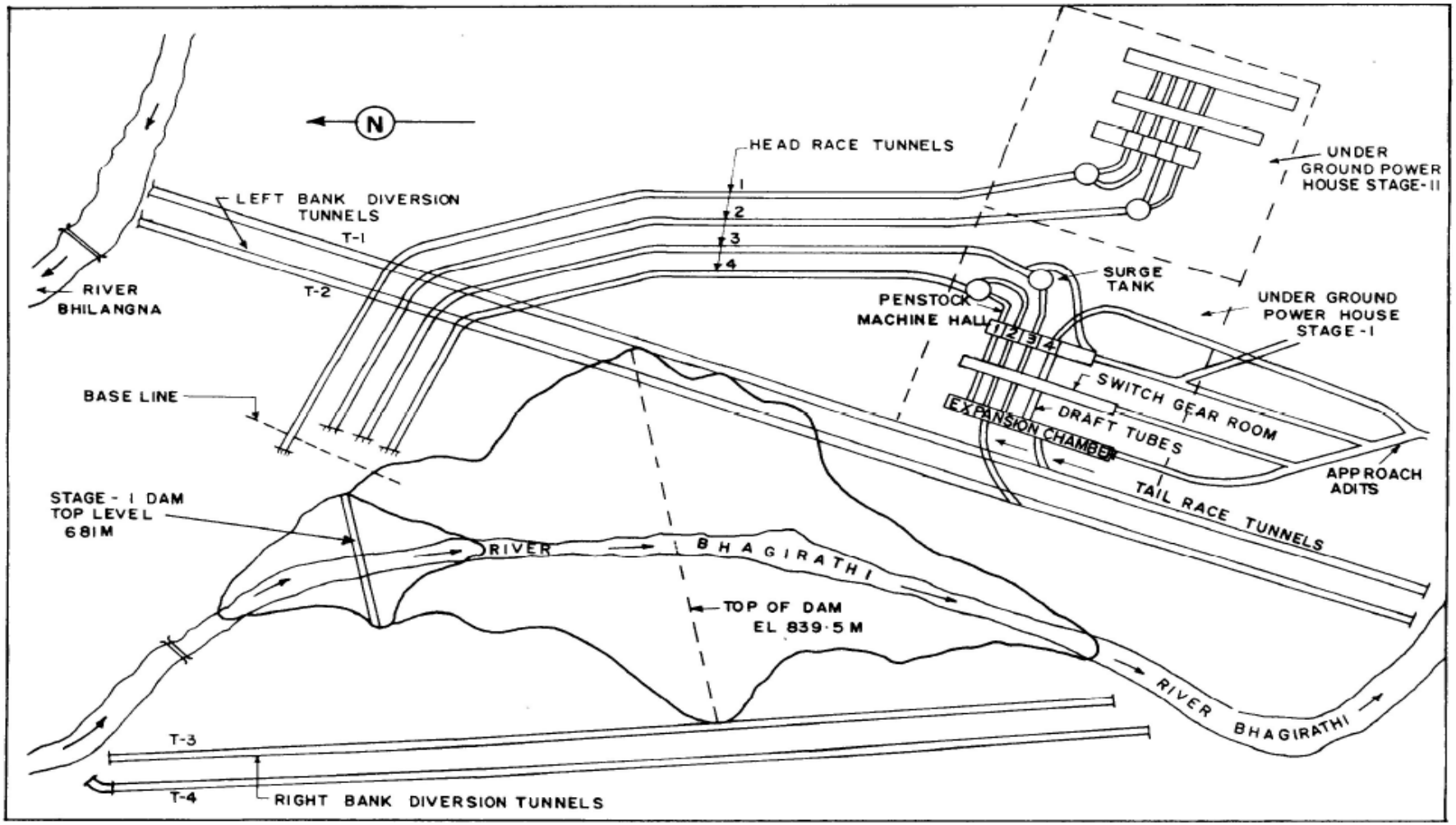

Fig. 3.12 Layout Plan of Tehri Hydro Power Project (after Goel, 1994)

The Srinagar thrust lies at a distance of 5 km NE of the Tehri dam site and has a dip of 50^{o}-60^{o} in the NE direction, where it separates Shimla slates from rock masses of the Garhwal group. There is a change, however, in the direction of the thrust which dips towards SW, where the Chandpur formations are in direct contact with the Garhwal group.

A few local faults like Gadolia tear fault, Deul tear fault, Tehri tear fault, Marh tear fault, and Chamba fault have been discovered within a distance of 2 to 10 km from the dam site. The Chandpur phyllites occurring in the Tehri gorge are banded. These bands are constituted of argillaceous and arenaceous materials. On basis of the argillaceous and the arenaceous materials and the varying magnitude of tectonic disturbances suffered by them, the phyllites are broadly grouped into grade-I, grade-II, and grade-III, which are described in following paragraphs:

Grade-I phyllites is predominantly arenaceous, massive in character and distinctly jointed. The foliation planes are least developed. The thickness of the individual bands varies from a few cm to 1m. This rock type constitutes about 45% of the Tehri gorge. Under microscope, the foliation is not much pronounced. The only effect of metamorphism is the elongation of quartz and muscovite. Except at places where grade-I phyllites are in the contact of grade-II phyllites, no primary supports were required. The *Q* and *RMR* values for this grade of phyllites varied from 6 to 15 and 65 to 70 respectively.

Grade-II phyllites are conspicuously banded due to rapid alterations of arenaceous and argillaceous materials. In physical quality and competence, this unit is considered next to grade-I phyllites. The grade-II phyllites are considerably impregnated with quartz veins, both along and across the foliation planes. The thickness of individual bands varies from a few centimetres to 0.10 m. These constitute about 25% of the total exposures in the area. Steel rib supports without invert struts were used as no side pressure was encountered. The *Q* and *RMR* values for grade-II phyllites varied from 1 to 5 and 30 to 40 respectively.

Grade-III phyllites are mainly composed of the argillaceous component with lesser amount of arenaceous material. It has quartz veins and is traversed by closely spaced foliation planes, cleavages and joints. The rock masses constitute 30% of the total rock exposed in the area and are mostly weathered. It shows the presence of calcite in addition to quartz and sericite layers under the microscope. Side pressure was observed at places requiring full periphery steel rib

supports. The values of *Q* and *RMR* varied for grade-III phyllites from 0.1 to 0.8 and 15 to 25 respectively.

Grade-II phyllites were commonly found in the right bank diversion tunnels. Bands of grade-I and III were also seen occasionally. The grade-II phyllites were highly jointed and have as many as five joint sets. The average strike of foliations was N70^{o}W-S70^{o}E with dip of about 50^{o} due SW i.e., on downstream side. The right bank diversion tunnels were aligned in N6^{o}W-S6^{o}E direction. The tunnels were driven across the strike and were, therefore, favourably oriented. Figure 3.13 shows the predicted geological cross-section along the right bank diversion tunnel. The invert of the inlet portals of these two diversion tunnels were at RL 606 m and 609 m.

The left bank diversion tunnels have been driven mainly through grade-II phyllites. Grade-III phyllites exposed at the outlet end. There were a few bands of grade-I and III phyllites also. Figure 3.14 shows the tentative geological cross - section drawn on the basis of surface exploration.

The head race tunnels (HRTs), the approach adits to the power house cavern and the cavern itself are located in grade I and grade-II phyllites with occasional bands of grade-III phyllites.

Except grade-III phyllites and presence of shear zones at a few locations, the phyllites are considered as a good tunnelling media and no problems were encountered during the construction of tunnels.

As a result of flat jack test carried out in the field, the value of horizontal to vertical in-situ stress (*k*) was observed to be 0.6 Bahuguna et al., (2008).

Tunnel closure observations indicated that bench excavation did not affect the heading. Benching was therefore done after lining the heading. The overall tunnelling experience of the project has shown that the presence of 13 m wide parallel twin tunnels about 50m apart have not created stability problems.

Construction-stage instrumentation was adopted in the tunnels to monitor the behaviour of the surrounding rock masses. Average values of closures and support pressure in various grades of phyllites are presented in Table 3.3.

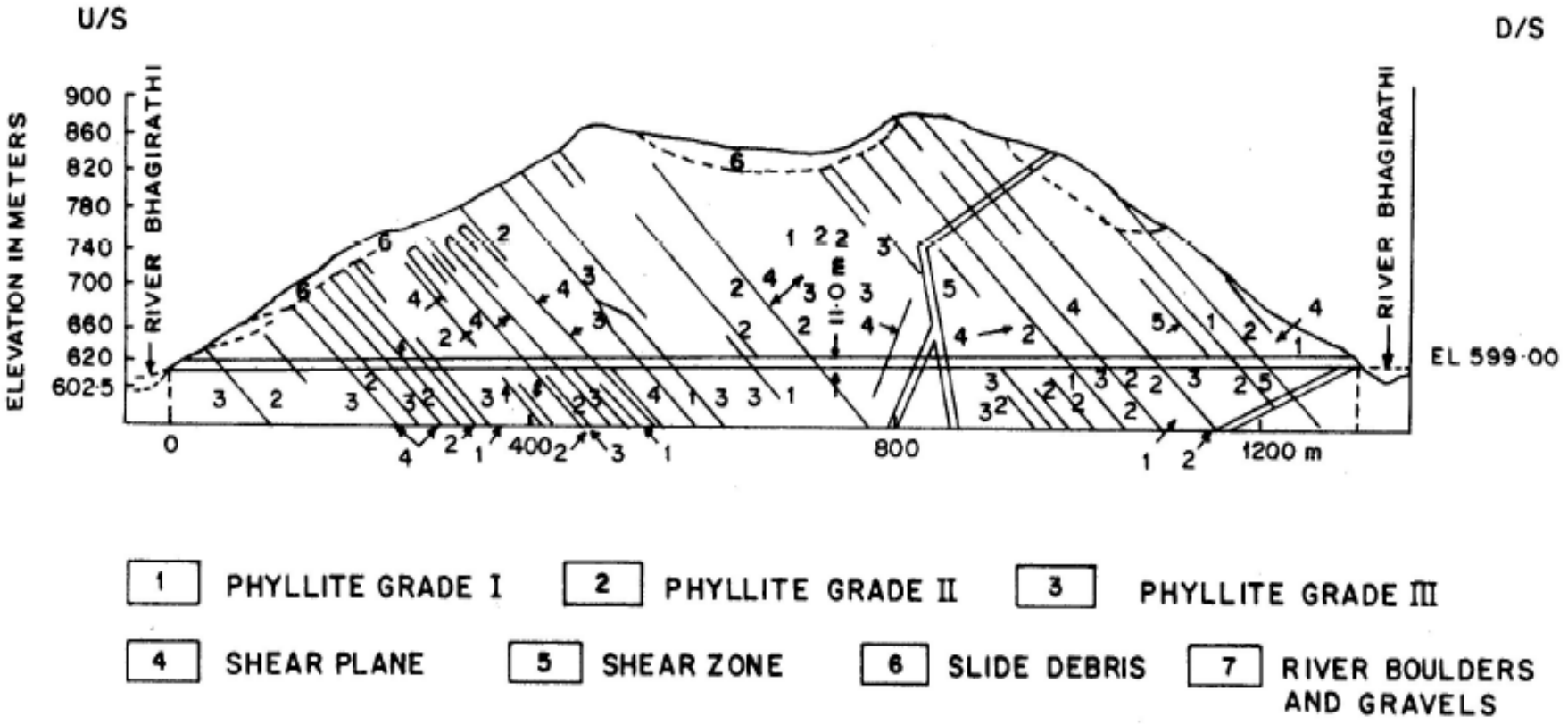

Fig. 3.13 Geological Cross Section along Right Bank Diversion Tunnel of Tehri Hydro Power Project (after Goel, 1994)

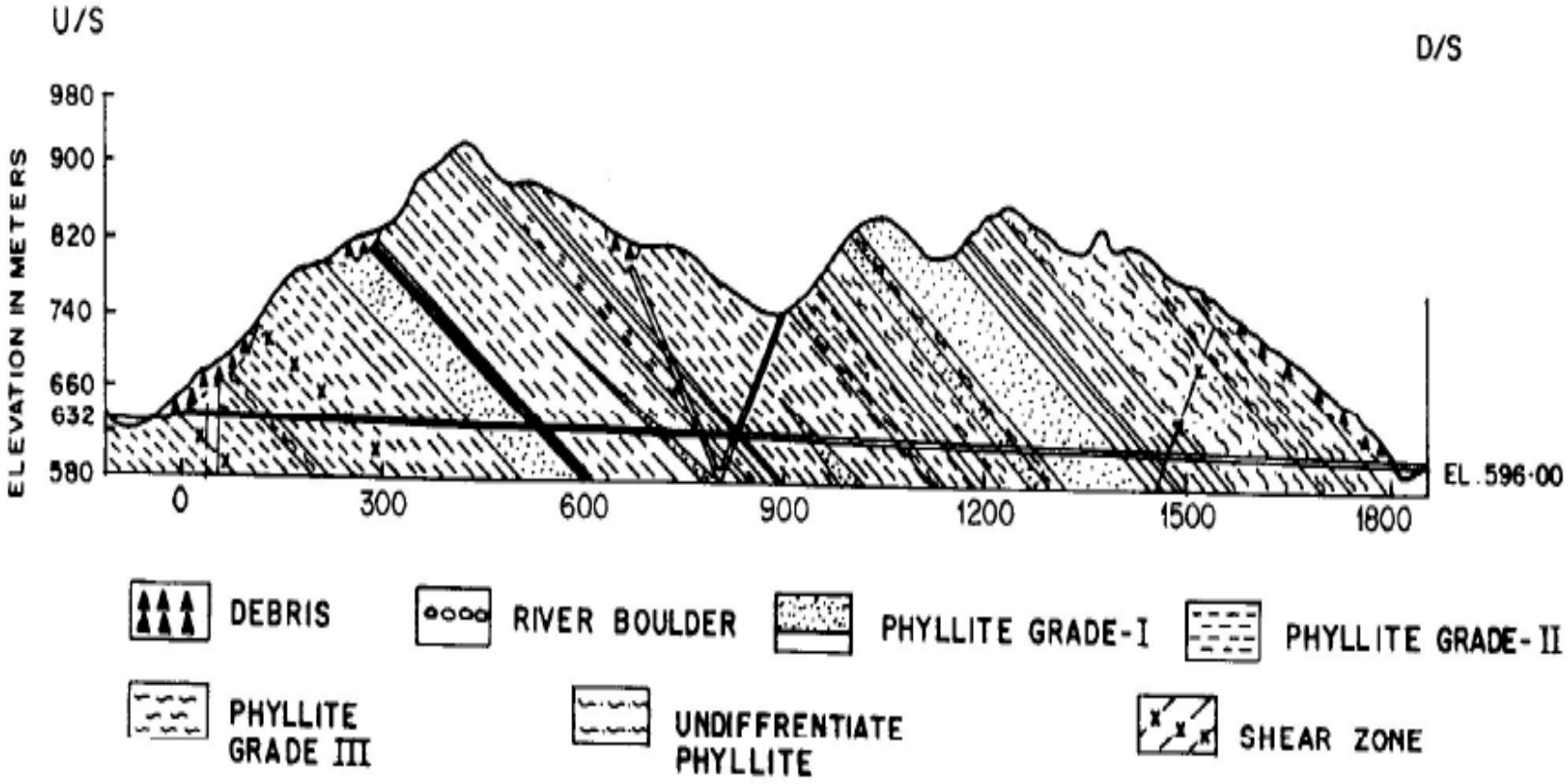

Fig. 3.14 Geological Cross Section along Left Bank Diversion Tunnel of Tehri Hydro Power Project (after Goel, 1994)

Table 3.3 Closures and Support Pressures in Various Grades of Phyllites in Tehri project

Grade of Phyllite	Radial Deformation (%)	Support Pressure (MPa)
Grade-I	0.2	0.046
Grade-II	0.4	0.12-0.2
Grade-III	0.65	0.3-0.4

3.15 LOWER PERIYAR HEP TUNNEL

The project area encountered formations of Archaean age consisting of composite gneisses and intermediate acid charnockites with inclusions of amphibolites. The tunnel passes through a hill located on the left bank of the Periyar river and is aligned in N60^{o}W direction, except in the initial reaches between chainage 0.0 m and 42.5 m, where it is aligned in a N35^{o}E direction and between chainage 42.5 m and 1205.2 m, it is aligned in N8^{o}W direction (Fig. 3.15). At the inlet, the Reduced Level is 229.1 m and at the surge location, it is 18.70 m. The rock cover along the tunnel alignment varies from a minimum of 38.0 m to a maximum of 285 m at chainage of 3200 m in the vicinity of a place called Arrathukadavuthodu. Massive to jointed composite gneisses comprising of charnockites, with lenses of amphibolites and granite-biotite gneisses belonging to the archaean super group, are the main rock types along the tunnel alignment. Drag folds are seen throughout the length of the tunnel.

Pegmatite veins appear along some of the major joint planes. The foliation of the composite gneisses varies from NE-SW to N70^{o}E-S70^{o}W direction with dips of 20^{o} to 50^{o} towards SE direction. In the initial reaches up to chainage of 42.5 m, the strike of the foliation is in NW-SE direction with dips of 70^{o} towards SW. Beyond chainage of 42.5 m and up to the surge shaft, the gently dipping foliation planes make an angle of 30^{o} to 45^{o} with the tunnel direction. Two shear zones, at a chainage of 10500 m and 11410 m, have also been encountered along the alignment. The width of these shear zones varies between 1 m and 2 m, and the gouge consists of crushed and fragmented gneissic rock with clays. *Q* and *RMR* values of the geological formation are given in Table 3.4.

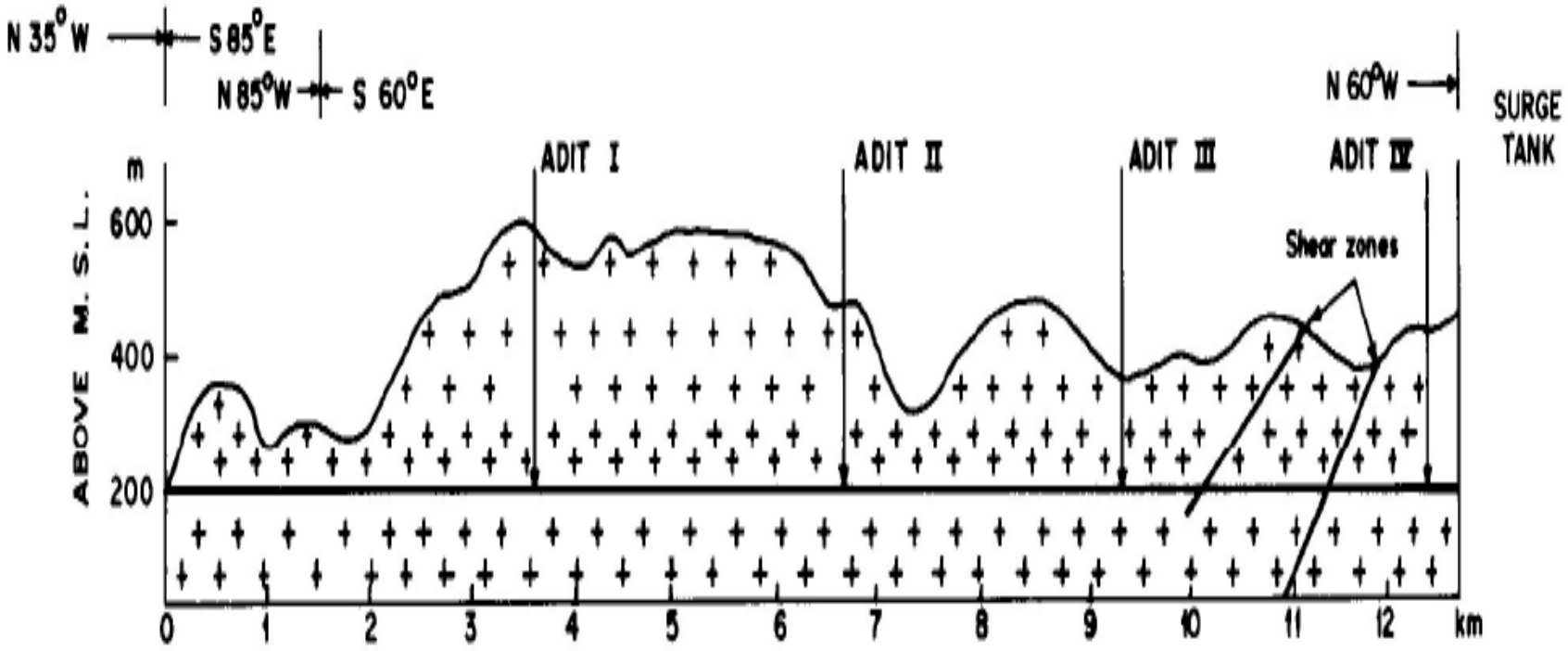

Fig.3.15 Geological Cross Section along Lower Periyar Tunnel (after Jethwa et al., 1987)

Table 3.4 Rock Mass along Head Race Tunnel in Lower Periyar
(after Jethwa et al., 1986)

S. No.	Rock type	Overburden, (m)	Q	RMR
1.	Pegmatite-granite gneiss	38	2	50
2.	Pegmatite-granite gneiss	275	10.7	65
3.	Pegmatite-granite gneiss	51	6	60
4.	Shear zone	250	0.25	31
5.	Other reach	125-225	27	74

Composite granite-pegmatite gneiss is considered a good tunnelling media. Hence, no tunnelling problem was encountered. Rock mass characterisation parameters, *Q* and *RMR* were estimated (Jethwa et al., 1986) for all the five zones in Table 3.4.

3.16 LOKTAK HEP TUNNEL

This project lies 39 km south of Imphal, the capital city of Manipur State in northeast India. It diverts 58.8 m^3/s of water from Loktak lake to supply 16.8 m^3/s for irrigation. The remaining 42 m^3/s of water with a gross head of 312 m is used to generate 105 MW of power from three units. The finished diameter of 6.5 km long head race tunnel is 3.65 m.

Loktak tunnel traverses through lake deposits, terrace deposits and shales with thin bands of sandstones and siltstones. In the first stretch of about 830 m, the tunnel passes through lacustrine deposits. Terrace deposits were encountered in the next stretch of 420 m and the remaining part of the tunnel traverses through splintary shales, sandy shales with variation of slaty and phyllitic types and some sandstones under the rock cover of 300 m. The sandstones were bedded and flaggy in nature, whereas the shales were thinly laminated (Fig.3.16). The general trend of the rock masses was in N-S direction i.e. perpendicular to the tunnel axis.

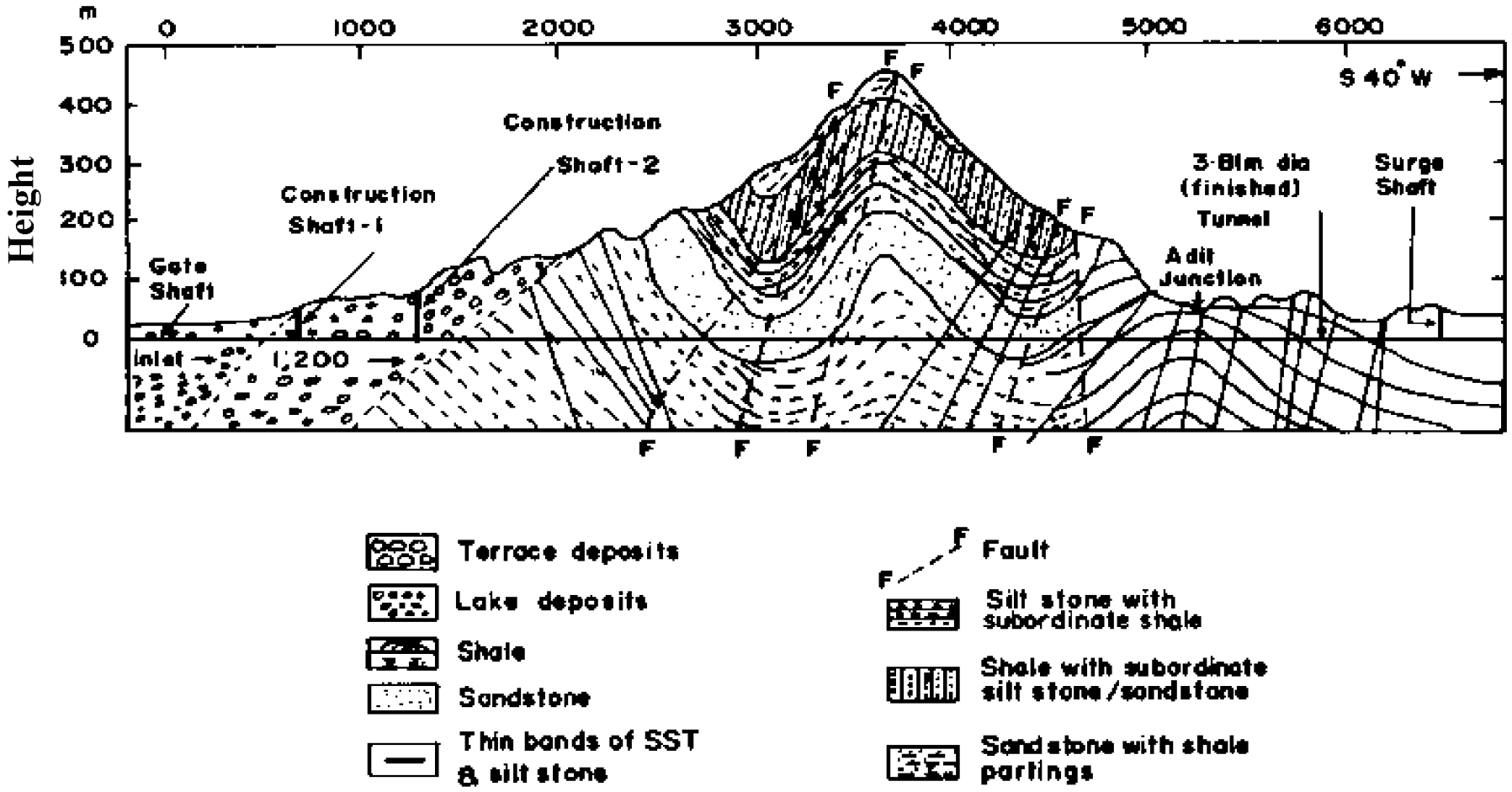

Fig.3.16 Geological Section along Loktak Head Race Tunnel (after Malhotra et al., 1982)

In-situ stresses were measured using flat jack technique and ratio of horizontal to vertical in-situ stresses (*k*) was estimated as 1.0 (Dwivedi et al., 2014a).

The tunnel was excavated by drill & blast method. The Loktak tunnel is the first tunnel in India, where NATM was used in some stretches to tackle the squeezing ground (Malhotra et al., 1982). Serious difficulties were experienced during excavation due to excessive deformation and the high squeezing behaviour of laminated shales. Steel ribs (150 mm x 150 mm) at 1 m c/c spacing were used in conjunction with – i) 4 m long rock bolts which were provided at 1 mc/c spacing, and ii) 150 mm shotcrete to support the tunnel.

Load cells and closure studs were installed up to a distance of 4 m behind the face. Support pressure of 0.4 - 0.6 MPa and large tunnel deformations of about 7% of tunnel diameter were observed. Conventional tunnelling was adopted to go ahead in the squeezing section of the tunnel. The diameter of the excavated tunnel was increased to accommodate the excess deformation.

3.17 FREJUS HIGHWAY TUNNEL

The Frejus highway tunnel links the city of Modane in France to the city of Bardonnechia in Italy through the Alps. The tunnel is 12.57 km long and 10.52 m wide with a two lane horse shoe section. The overburden along most of the tunnel layout is over 1000 m, but with a maximum of 1800 m.

The French side of the tunnel passes through an over thrust of calc-schists. The strike of the plane of schistosity is approximately parallel to the longitudinal axis of the tunnel and its dip varies between 25^{o} and 50^{o}. The calc-schists result from a light metamorphism of marl sand and limy marls with the formation of phyllitous minerals (muscovite, chlorite). This information appears to be relatively homogeneous. A detailed analysis shows some variations, locally more calcareous or more micaceous with some graphic beds. Some variations are equally due to the intensity of tectonic deformations with local sharp bends of the beds.

The calc-schists formation is an anisotropic rock mass as indicated by the seismic velocity. The seismic velocity of a wave propagating orthogonally to the schistosity varies between 1300 m/s and 3000 m/s. Similarly, for a wave propagating parallel to the plane of schistosity, velocities were found to lie between 3500 m/s and 6000 m/s. The values of uniaxial

compressive strength of laboratory samples were less indicative of anisotropy of the rock and the scatter of the measurements (10-130 MPa) is very high. As has often been noted, the anisotropy of the rock mass is much larger than that of the intact rock samples.

5 m long, 28 mm diameter rock bolts were installed in a staggered pattern at spacing of 1 m x 1 m. It was followed by 50 mm thick shotcreting (Panet, 1996). Deformation of 1.1-3.8% was observed in the tunnel.

3.18 KALETEPE HIGHWAY TUNNEL

Bilecik-Istanbul highway carries a heavy traffic and connects Marmara region to Aegean and Mediterranean regions. On the highway, Kaletepe tunnel has been excavated under a hill having a maximum cover of about 300 m. The tunnel has an excavation width of 12.7 m, a wall height of 9.6 m and a length of 2.5 km. The tunnel is located 3 km North of Bilecik city in Turkey. It is driven through the Derbent limestone of Upper Permian age. It is olistotite in the Lower Triassic age Karakaya formation (Can and Ertunc, 2000). This formation includes different sizes of old Derbent limestone olistolites. The spilite and sandstone inclusions are observed at the slope of the hill and the exit of the tunnel cross-section. The size of limestone changes from a few meters to 5-10 km. The strength of limestone can be classified in the range of medium to high strength and it shows a slightly weathered structure. The spilite in the Karakaya formation is gray in colour, of fair strength and highly weathered at some places. The spilite and Derbent limestones are also characterized by faults, which are not regular. The volcanic originated sandstone is gray in colour, and it is also characterized by fair to medium strength, fine-medium layer and moderately weathered. The water level is lower than the tunnel axis. The dip of joints generally varies from 45^o to 90^o. The joint apertures are mostly less than 1 mm. The discontinuities are medium in spacing and blocky and surfaces are undulated-planar and rough. The dip and direction of main discontinuities are 73^o/063, 65^o/319, 70^o/379 and 68^o/113. Uni-axial compressive strength (σ_{ci}), deformation modulus (E_i), Poisson's ratio (v) of intact rock were determined to be in the range, 71-110 MPa, 67-87 GPa, and 0.28-0.32 respectively. *Q*-values of rock mass were observed between 0.016 and 10.82. Upon measurement, Support pressure and tunnel deformation were observed to be 0.08-0.1 MPa and 0.02-0.12% respectively. Installed support system includes – i) 4-5 m long systematic rock bolts at 1.5-2.5 m spacing, ii) 100m - 150 mm thick shotcrete at crown

and 100 mm thick on the side walls light, and iii) steel ribs at 1.5 m spacing, wherever required (Sari and Pasamehmetoglu, 2004).

The properties of the most critical joints of various rock types of different case histories considered for the study are presented in Table 3.5.

Table 3.5 Geo-mechanical Data of Case Histories Considered for Analysis

Name of Project	Rock Type	Dip (°)	Joint Dip Direction (° due N)	Joint Condition	ϕ (°)	Spacing (mm)	α (°)	Tunnel Depth H (m)	σ_{ci} MPa	k or σ_h / σ_v	Ground Condition
Udhampur	Soft sandstone	60-74	240	Clay filled	25	50-55	30	29-37	50	-	Non-squeezing
	Claystone & silty claystone	70	240	Clay filled	24-26	40-42	30	270-313	20	1.2	Squeezing
Salal	Dolomite	40-55	0	Clay filled	23	30-100	25	150	60	-	Non-squeezing
Giri-Bata	Crushed phyllites	60-70	90	Silty-clay	20-22	45-50	0	20-450	14-20	2.0	Squeezing
	Crushed Blaini's slates	60-70	90	Silty-clay	21-26	45	0	400			
Maneri Stage-I	Moderately fractured quartzite	35-47	20	Silty-clay	22	40	30	225		0.3-0.7	Non-squeezing
	Foliated metabasics	35-49	20	Silty-clay	23-25	34-44	30	225-550			Non-squeezing
		35-49	20	Silty-clay	20	45	30	635			Squeezing
	Sheared metabasics	35-49	20	Silty-clay	13-19	55-56	30	250-350			Non-squeezing
		35-49	20	Silty-clay	15-20	30-39	30	450-700	10-21		Squeezing
	Siliceoius phyllites	35-49	20	Silty-clay	20	36-45	30	50-650			Squeezing
	Crushed quartzites	35-49	20	Silty-clay	20	35	30	750			Squeezing

……***Contd.***

Name of Project	Rock Type	Dip (°)	Joint Dip Direction (° due N)	Joint Condition	ϕ (°)	Spacing (mm)	α (°)	Tunnel Depth H (m)	σ_{ci} MPa	k or σ_h / σ_v	Ground Condition
Maneri Stage-II	Greywacke	50-60	45	Clay filled	25	74-210	55	250-325		0.3	Non-squeezing
	Metabasics	40-80	45	Clay filled	24	83-90	55	175-200			
	Metavolcanic	40-80	45	Clay filled	24	85-90	55	415-510	11-24		Squeezing
	Sheared metabasics	50-60	45	Clay filled	24	43-73	55	285-410			
Chhibro-Khodri	Crushed red shales	60	23	Clay filled	21-25	45	46	280-680	8-21	1.0	Squeezing
	Soft & plastic black clays	60	23	Clay filled	21	50	46	280-580			
Tala	Adverse geology occurrences (AGO)	50	40	Clay filled	24	38-48	0	337	10	0.6	Squeezing
Kaligan-daki 'A'	Graphic phyllites (GP)	50-60	45	Clay filled 75%	10	100-155	0	550-620	39	0.5	Squeezing
	Siliceous phyllites (SP)	50	45			84-140	0				
	SP & GP	60	45			600	0	600			
Khimti-1	Gneiss and schist	55-65	35-40	Rough, clay filled	14-27	43-102	34	98-300	26	1.0	Squeezing
Noonidih colliery	Weak coal	9	50	Smooth	19	13-15	0	450	21	0.86	Squeezing
Nathpa-Jhakri	QMS, SQ & A	50-75	35-40	25% clay filled	25	43-76	35-40	400-800	32	1.3	Squeezing
	Gneiss & schistose gneiss	40-75	45	Rough, tight	30-55	4-6	90	1060-1430	42-60	1.0	Rock burst

…..***Contd.***

Name of Project	Rock Type	Dip (°)	Joint Dip Direction (° due N)	Joint Condition	ϕ (°)	Spacing (mm)	α (°)	Tunnel Depth H (m)	σ_{ci} MPa	k or σ_h/σ_v	Ground Condition
Tehri	Phyllites grade-I	50-57	70	Clay filled	24-30	90-133	23	210-300	52-93	0.6	Non-squeezing
	Phyllites grade-II	50-60	70	Clay filled	19-22	68-100	23	220-310	43		
	Phyllites grade-III	50	70	Clay filled	15-19	74-106	23	225-300	40		
Lower Periyar	Pegmetite-granite gneiss	54	70	Rough and tight joint	40	45-50	30	150-197	-	-	Non-squeezing
Loktak	Splintery shales	40-70	90	Silty-clay filled	15	68	40	300	27	1.0	Squeezing
Frejus	Calcschist	25-50	90	Clay filled	20	65-70	0	1000-1800	30-80	-	Squeezing
Kaletepe	Limestone	40-60	319	Silty sand	31	48-62	25	52-215	71-110	-	Non-squeezing

Notation: ***QMS-Quartz mica schist; SQ-Schistose quartzite; A-Amphibolite.***

Chapter 4

PREDICTION OF GROUND CONDITION

4.1 GENERAL

Reliable correlations predicting the condition of ground through which a tunnel or a cavern is to be excavated are like a torch, which throw light on the response of the ground (self-supporting or non-squeezing or squeezing). The ground condition is required to be defined in the contract document which is prepared before the national/ international bids are invited for tunnel construction, so that the contractor gets sufficiently good idea about the geology and the geological conditions and can keep contingency plans ready before he comes across the problems during construction. Also, if the information about ground behaviour is available prior to excavation, the site engineers can plan their strategy with regard to excavation method and the supporting elements for the tunnel for safe and time efficient tunnelling.

On basis of the analysis of data collected from various tunnelling projects in India and abroad (Chapter 3), an attempt has been made in the present study to develop empirical correlations using joint factor (J_f), rock mass quality (Q), rock mass number (N) as a measure of rock mass quality and overburden height or tunnel depth (H) for prediction of ground behaviour.

4.2 SELECTION OF PARAMETERS

Behaviour of the ground is primarily governed by two factors, namely rock mass quality and in situ stress conditions. Rock mass quality is characterised by properties of joints (joint spacing, in-fill material, and joint condition). Further, diameter or the size of tunnel also plays an important role in rock mass characterisation. Large diameter of a tunnel attracts larger values of induced stresses around the tunnel periphery and hence invites large tunnel deformations, which leads to further loosening of rock joints thereby resulting in reduced rock mass strength around the tunnel periphery. On the other hand, in situ stresses are characterised by tectonic activities in the region and the overburden height (tunnel depth). In view of the aforementioned key parameters, following parameters have been selected for development of empirical correlations for prediction of ground condition:

4.2.1 Rock Mass Quality Parameter

Following rock mass quality parameters have been considered for the present study:

i) Joint factor (J_f),

ii) Rock mass quality (Q), and

iii) Rock mass number (N).

All these parameters have already been described in arts. 2.9, 2.11 and 2.12 of chapter - 2.

4.2.2 Diameter of Tunnel (D)

In weak rock masses, diameter of tunnel plays an important role with regard to the ground behaviour because increase in diameter gives rise to increased induced stresses around the tunnel periphery leading to increased plastic deformation. Thus, diameter of excavated profile of tunnels is an important parameter and has been considered for development of the correlations for ground behaviour.

4.2.3 Overburden Height or Tunnel Depth (H)

In situ stress is a function of overburden height. The value of vertical in situ stress increases with increase in overburden height. Induced stresses are directly proportional to the in situ stress. Increased in situ stresses weaken the rock mass around the tunnel periphery by pushing it inwards in to the tunnel. Therefore, H is also an important parameter which should be considered for the study of ground behaviour.

4.3 COLLECTION OF FIELD DATA

There are basically four sets of data, namely – i) those tunnelling cases wherein the ground condition corresponds to self supporting ground condition, ii)) those cases which correspond to tunnels in non-squeezing ground conditions, iii) those tunnels which fall in the category of the squeezing ground condition, and iv) cases where rock bursting phenomenon was observed. The squeezing ground condition has been further classified in to mild squeezing, moderate squeezing and high squeezing.

Different ground conditions are identified on basis of the strain levels observed around the tunnel periphery. In case of self supporting and non-squeezing ground conditions, the associated strain level is less than or equal to 1%. However, if the strain level exceeds 1%, it results in to a squeezing ground condition. Squeezing is 'mild' if the strain level lies between 1% and 3%, and it is 'moderate' if the strain level lies between 3% and 5%. 'High squeezing' condition exists if the strain level exceeds 5%.

The basic data collected in the field at various tunnelling project sites includes information related to : rock type, Rock Mass Quality (Q), Rock Mass Number (N), joint spacing of the most critical joint, its true dip (θ) and apparent dip (θ_A), orientation of tunnel axis with respect to the strike of the most critical joint (α), friction angle of joint (ϕ), Joint frequency, J_n , inclination parameter of joints (n), joint strength parameter (r), joint factor (J_f) , depth of overburden (H) and diameter of tunnel (D). In the analysis, for non-circular tunnels, equivalent diameter, D_e has been consided, which is computed using expression: $D_e = (4A/\pi)^{0.5}$ where A is cross-sectional area of tunnel. Hence, for such cases, $D_e = D$.

An attempt was made during the course of the study to collect maximum possible data from different project sites. In all, data has been collected from 181 tunnel cross sections including – i) 25 tunnel sections in self-supporting ground condition, ii) 54 tunnel sections in non-squeezing ground condition, iii) 85 tunnel sections in squeezing ground condition, and iv) 17 sections in rock burst condition. The data has been arranged systematically and is presented here in Table 4.1 for tunnel sections in self-supporting ground condition, in Table 4.2 for tunnel sections in non-squeezing ground condition, in Table 4.3 for tunnel sections in squeezing ground condition and in Table 4.4 for tunnel sections in rock burst condition.

Table 4.1 Data Collected from Various Tunnel Sections in Self-Supporting Ground Condition

Sl. No.	Name of the Tunnel	Rock Type	Reference	Q	N	Spacing, mm	θ (^{o})	θ_A (^{o})	α (^{o})	ϕ (^{o})	J_n	n	r	J_f	H, m	D, m
	SELF-SUPPORTING															
1.	Lower Periyar Tunnel	PG	Jethwa et al., 1986	7.5	37.5	46	54	50	30	40	13.89	0.09	0.839	184	29.5	7
2.	Lower Periyar Tunnel	PG		13.53	67.65	52	54	50	30	40	12.46	0.09	0.839	165	48	7
3.	Lower Periyar Tunnel	PG		1.35	6.75	35	54	50	30	40	18.12	0.09	0.839	240	54	7
4.	Lower Periyar Tunnel	PG		1.86	4.65	37	54	50	30	40	17.37	0.09	0.839	230	61	7
5.	Tehri Tunnel	P-I	Bahuguna et al., 2008; Goel, 1994	24.2	48.4	121	52	50	23	22	5.31	0.09	0.404	146	295	9.5
6.	Tehri Tunnel	P-I		29.2	59.8	126	52	50	23	22	5.09	0.09	0.404	140	280	9.5
7.	Koyna Tunnel	Basalt	Goel, 1994; Chakraborty et al., 1996 & 2004	29.7	29.7	22	73	70	35	45	15.40	0.11	1.000	140	350	6.5
8.	Koyna Tunnel	Basalt		31.35	78.38	44	70	65	40	45	9.66	0.07	1.000	138	37	10
9.	Koyna Tunnel	Basalt		28.05	28.05	44	69	65	35	45	9.87	0.07	1.000	141	334	7.7
10.	Tandsi Inclines	Ss	Goel, 1994; Sinha et al., 2013	16	40	18	78	74	40	16	15.15	0.33	0.287	160	26	3.8
11.	Tandsi Inclines	Ss		10.6	26.66	17	78	74	40	16	16.38	0.33	0.287	173	20	3.8
12.	Tandsi Inclines	Ss		14.02	14.02	18	78	74	40	16	15.53	0.33	0.287	164	57	3.8
13.	Tandsi Inclines	Ss		6.18	6.18	15	78	74	40	16	18.09	0.33	0.287	191	32	3.8
14.	Kielder Expt. Tunnel	Ms	Ward et al., 1983	10.74	40.27	72	65	65	0	26	5.91	0.07	0.488	173	40	3.3
15.	Kielder Expt. Tunnel	Ms		4.23	12.69	61	65	65	0	26	6.93	0.07	0.488	203	110	3.3

Notation: ***PG-Pegmatite granites (foliated);P-I-Phyllites grade-I; Mb-Metabasics; Ss-Sandstone; LG-Leptite gneiss; LS- Laminated Schist; Ms-Mudstone.***

.....***Contd.***

Sl. No.	Name of the Tunnel	Rock Type	Reference	Q	N	Spacing, mm	θ (^{o})	θ_A (^{o})	α (^{o})	ϕ (^{o})	J_n	n	r	J_f	H, m	D, m
	SELF-SUPPORTING															
16.	Kielder Expt. Tunnel	Ms	Ward et al., 1983	1.7	10.61	53	65	65	0	26	7.96	0.07	0.488	233	120	3.3
17.	Barton's Case History	LG	Goel, 1994; Barton et al., 1974	35	35	92	50	50	0	30	6.96	0.09	0.577	134	140	9
18.	Barton's Case History	Q		4.4	11	88	50	50	0	22	7.34	0.09	0.404	202	80	5.9
19.	Barton's Case History	Q		12	30	105	50	50	0	22	6.14	0.09	0.404	169	15	8
20.	Barton's Case History	LG		50	50	105	65	65	0	25	4.01	0.07	0.466	123	100	12
21.	Barton's Case History	LG		160	400	123	65	65	0	25	3.43	0.07	0.577	85	18	20
22.	Barton's Case History	LG		67.5	67.5	110	50	50	0	30	5.87	0.09	0.577	113	60	12
23.	Barton's Case History	Q		3.7	3.7	85	50	50	0	22	7.53	0.09	0.404	207	65	3.5
24.	Barton's Case History	Q		50	25	85	50	50	0	30	5.87	0.09	0.577	113	300	6.1
25.	Barton's Case History	MG		200	500	70	70	70	0	30	4.89	0.11	0.577	77	30	22

***Notation**: Ms-Mudstone; LG-Leptite gneiss; LS- Laminated schist; Q-Quartzites; MG-Massive gneiss.*

Table 4.2 Data Collected from Various Tunnel Sections in Non-squeezing Ground Condition

Sl. No.	Name of the Tunnel	Rock Type	Reference	Q	N	Spacing, mm	θ (^{o})	θ_A (^{o})	α (^{o})	ϕ (^{o})	J_n	n	r	J_f	H, m	D, m
	NON-SQUEEZING															
1.	Tehri Tunnel	P-II	Goel, 1994; Singh et al., 2007; Bahuguna,et al, 2008	0.78	3.66	88	52	50	23	19	7.99	0.09	0.344	258	205	11
2.	Tehri Tunnel	P-II		4.8	12	98	52	50	23	22	7.24	0.09	0.404	199	200	11
3.	Tehri Tunnel	P-I		6	15	101	52	50	23	22	6.98	0.09	0.404	192	500	11
4.	Tehri tunnel	P-III		0.17	0.425	80	47	45	23	16	7.96	0.09	0.287	308	110	9.5
5.	Tehri tunnel	P-III		0.1	0.5	77	52	50	23	16	8.39	0.09	0.287	325	50	6.5
6.	Tehri tunnel	P-III		0.17	0.85	80	52	50	23	16	7.96	0.09	0.287	308	30	6.5
7.	Tehri tunnel	P-II		0.42	0.42	75	52	50	23	19	8.61	0.09	0.344	278	60	6.5
8.	Tehri tunnel	P-III		0.23	0.575	83	52	50	23	16	7.70	0.09	0.287	298	70	6.5
9.	Tehri tunnel	P-III		0.4	2	89	52	50	23	16	7.23	0.09	0.287	280	40	6.5
10.	Tehri tunnel	P-II		1.7	1.7	80	52	50	23	21	8.05	0.09	0.384	233	100	6.5
11.	Tehri tunnel	P-III		0.23	1.15	83	52	50	23	16	7.70	0.09	0.287	298	25	8
12.	Tehri tunnel	P-II		1.9	1.9	81	52	50	23	21	7.91	0.09	0.384	229	60	11.3
13.	Tehri tunnel	P-III		0.25	0.625	85	52	50	23	15	7.59	0.09	0.286	295	30	9.1
14.	Tehri tunnel	P-III		0.027	0.135	68	52	50	23	15	9.47	0.09	0.286	368	30	9.1
15.	Tehri tunnel	P-III		0.15	0.15	80	52	50	23	15	8.06	0.09	0.286	312	190	9
16.	Tehri tunnel	P-III		0.18	0.9	68	52	50	23	15	9.47	0.09	0.286	368	200	8

Notation: ***Mv-Metavolcanics; P-I, P-II & P-III-Phyllites grade I, II, & III; Mb-Metabasics; Gw-Grewackes; LG-Leptite gneiss; LS-Laminated schist Q-Sheared quartzites.***

….Contd.

Sl. No.	Name of the Tunnel	Rock Type	Reference	Q	N	Spacing, mm	θ (^{o})	θ_A (^{o})	α (^{o})	ϕ (^{o})	J_n	n	r	J_f	H, m	D, m
	NON-SQUEEZING															
17.	Tehri tunnel	P-III	Goel, 1994; Singh et al., 2007	0.017	0.043	65	52	50	23	15	9.86	0.09	0.286	383	100	5.9
18.	Tehri tunnel	P-III		0.067	0.167	74	52	50	23	15	8.7	0.09	0.286	338	100	6.5
19.	Salal Tunnel	Dol	Goel, 1994	1.5	1.5	78	53	50	25	23	9.04	0.09	0.424	237	150	12
20.	Giri Tunnel	BS	Dube, 1979	3	7.5	70	65	65	0	22	6.05	0.07	0.404	214	400	4.2
21.	Maneri Stage I Tunnel	FM	Dube, 1979; Goel, 1994; Singh et al., 2007	4.2	10.5	34	49	45	30	25	20.8	0.22	0.466	203	260	5.8
22.	Maneri Stage I Tunnel	SM		1	5	28	49	45	30	25	25.63	0.22	0.466	250	350	5.8
23.	Maneri Stage I Tunnel	MFQ		5.2	13	41	49	45	30	22	17.42	0.22	0.404	196	500	5.8
24.	Maneri Stage I Tunnel	FM		3.6	9	33	49	45	30	25	21.32	0.22	0.466	208	225	4.8
25.	Maneri Stage I Tunnel	FM		4.8	12	38	49	45	30	23	18.6	0.22	0.424	199	550	4.8
26.	Lower Periyar Tunnel	PG	Jethwa et al., 1986; Goel, 1994	0.48	1.2	31	54	50	30	40	20.69	0.09	0.839	274	38	6.8
27.	Lower Periyar Tunnel	PG		0.08	0.4	26	54	50	30	40	25.07	0.09	0.839	332	26	6.8
28.	Lower Periyar Tunnel	PG		0.055	0.137	25	54	50	30	40	25.98	0.09	0.839	344	55	6.8
29.	Lower Periyar Tunnel	PG		0.04	0.2	24	54	50	30	40	26.80	0.09	0.839	355	48	6.8
30.	Lower Periyar Tunnel	PG		0.08	0.2	26	54	50	30	40	25.07	0.09	0.839	332	61	6.8
31.	Khimti-1 Adit-1 d/s	GS	Shrestha, 2005	0.07	0.325	41	55	50	34	27	15.56	0.09	0.51	339	95	4
32.	Khimti-1 Adit-1 d/s	GS		0.08	0.2	42	55	50	34	27	15.24	0.09	0.51	332	98	4
33.	Khimti-1 Adit-1 d/s	GS		0.06	0.15	41	55	50	34	27	15.70	0.09	0.51	342	112	4

<u>Notation</u>: ***Dol-Dolomites; BS- Blaini's slates; BG-Biotite gneiss; FM-Foliated metabasics; SM-Sheared metabasics; MFQ- Moderately fractured quartzite; PG-Pegmatite granites (foliated); GS-Gneiss and schist.***

*……**Contd.***

Sl. No.	Name of the Tunnel	Rock Type	Reference	Q	N	Spacing, mm	θ (^{o})	θ_A (^{o})	α (^{o})	ϕ (^{o})	J_n	n	r	J_f	H, m	D, m
	NON-SQUEEZING															
34.	Khimti-1 Adit-2 d/s	GS	Shrestha, 2005	0.3	0.75	61	55	50	34	22	10.51	0.09	0.404	289	126	4
35.	Khimti-1 Adit-2 d/s	GS		0.14	0.35	45	55	50	34	27	14.41	0.09	0.51	314	198	4
36.	Khimti-1 Adit-3 u/s	GS		0.2	0.5	59	55	50	34	22	10.98	0.09	0.404	302	130	5
37.	Khimti-1 Adit-3 u/s	GS		0.23	0.58	78	55	50	34	17	8.21	0.09	0.306	298	158	4.1
38.	Mansar Incline	BG	Mohanty and Mohanty, 1996	0.11	0.29	44	66	65	21	23	9.56	0.07	0.424	322	40	3
39.	Kielder Expt. Tunnel	Mud-stone	Ward et al., 1983	0.036	0.225	44	65	65	0	21	9.62	0.07	0.384	358	100	3.3
40.	Barton,s case history	LS	Barton et al., 1974; Goel, 1994	4.3	10.75	59	45	45	0	31	10.91	0.09	0.60	202	400	20.4
41.	Barton,s case history	LS		7.5	18.75	65	45	45	0	31	9.94	0.09	0.60	184	400	20.4
42.	Barton's case history	LG		31.6	15.8	90	50	50	0	30	7.17	0.09	0.577	138	260	19.5
43.	Barton's case history	LG		27.75	13.82	98	65	65	0	25	4.30	0.07	0.466	142	335	23.5
44.	Barton's case history	LS		0.6	1.5	84	60	60	0	24	5.94	0.05	0.445	267	100	9
45.	Barton's case history	Mil		1.3	3.25	58	45	45	0	13	12.25	0.22	0.231	241	60	12.5
46.	Barton's case history	Mil		2.5	2.5	80	50	50	0	21	8	0.09	0.384	220	100	12.5
47.	Barton's case history	Q		5.2	2.6	90	50	50	0	22	7.13	0.09	0.404	196	260	24.7
48.	Barton's case history	LS		0.3	0.75	86	50	50	0	16	7.46	0.09	0.287	289	15	16

Notation: ***GS-Gneiss and schist; BG-Biotite gneiss; LS-Laminated schist; LG-Leptite gneiss; Mil-Milonite; Q-Quartzite.***

…Contd.

Sl. No.	Name of the Tunnel	Rock Type	Reference	*Q*	*N*	Spacing, mm	θ (^{o})	θ_A (^{o})	α (^{o})	ϕ (^{o})	J_n	*n*	*r*	J_f	*H*, m	*D*, m
	NON-SQUEEZING															
49.	Maneri-II	Mv	Goel, 1994	0.67	1.67	85	72	60	55	24	5.85	0.05	0.445	263	70	6.5
50.	Maneri-II	Mv		0.67	1.67	85	72	60	55	24	5.85	0.05	0.445	263	60	6.5
51.	Maneri-II	Mb		0.8	2	87	72	60	55	24	5.72	0.05	0.445	257	90	4.2
52.	Maneri-II	Gw		1.3	3.25	93	72	60	55	24	5.36	0.05	0.445	241	85	6.5
53.	Maneri-II	Mb		1	2.5	90	72	60	55	24	5.56	0.05	0.445	250	107.5	30.5
54.	Maneri-II	Gw		1.5	22.5	95	72	60	55	24	5.27	0.05	0.445	237	400	30.5

Notation: ***Mv-Metavolcanics; Mb-Metabasics; Gw-Greywackes; LS- Laminated schist; Q-Sheared quartzites.***

Table 4.3 Data Collected from Various Tunnel Sections in Squeezing Ground Condition

Sl. No.	Name of the Tunnel	Rock Type	Reference	*Q*	*N*	Spacing, mm	θ (^{o})	θ_A (^{o})	α (^{o})	ϕ (^{o})	J_n	*n*	*r*	J_f	*H*, m	*D*, m
	SQUEEZING															
1.	Chhibro-Khodri	CRS	Jethwa, 1981; Goel, 1994; Choudhari, 2007	0.022	0.11	50	60	50	46	21	12.9	0.09	0.384	373	280	9
2.	Chhibro-Khodri	CRS		0.022	0.11	50	60	50	46	21	12.9	0.09	0.384	373	280	3
3.	Chhibro-Khodri	CRS		0.05	0.5	45	60	50	46	25	14.3	0.09	0.466	348	680	9
4.	Chhibro-Khodri	CRS		0.05	0.375	45	60	50	46	25	14.3	0.09	0.466	341	280	3
5.	Chhibro-Khodri	SPBC		0.026	0.195	45	60	50	46	24	14.7	0.09	0.445	367	680	9
6.	Chhibro-Khodri	SPBC		0.037	0.28	45	60	50	46	24	14.3	0.09	0.445	357	280	3
7.	Chhibro-Khodri	CRS		0.014	0.11	48	60	50	46	21	13.4	0.09	0.384	388	250	2.5
8.	Giri Tunnel	CBS	Dube, 1979; Goel, 1994; Choudhari, 2007	0.029	0.145	45	65	65	0	20	9.3	0.07	0.364	365	200	4.6
9.	Giri Tunnel	CBS		0.04	0.2	48	65	65	0	20	8.9	0.07	0.364	355	414	4.6
10.	Giri Tunnel	CBS		0.094	0.47	48	65	65	0	21	8.8	0.07	0.384	327	465	4.6
11.	Giri Tunnel	CBS		0.12	0.6	50	65	65	0	21	8.5	0.07	0.384	320	240	4.6
12.	Giri Tunnel	CBS		0.38	1.9	55	65	65	0	21	7.69	0.07	0.384	282	465	4.6
13.	Giri Tunnel	CP		0.52	2.6	55	65	65	0	22	7.70	0.07	0.404	272	380	4.6
14.	Giri Tunnel	CP		0.05	0.25	45	65	65	0	21	9.35	0.07	0.384	348	400	4.6
15.	Giri Tunnel	CP		0.03	0.15	41	65	65	0	22	10.29	0.07	0.404	364	400	4.6
16.	Giri Tunnel	CP		0.06	0.3	49	65	65	0	20	8.71	0.07	0.364	342	450	4.6
17.	Giri Tunnel	CP		0.05	0.25	45	65	65	0	21	9.35	0.07	0.384	348	440	4.6

Notation: ***CRS-Crushed red shales; SPBC-Soft & plastic black clays; CBS-Crushed Blaini's slates; CP-Crushed phyllites.*** ***……Contd.***

Sl. No.	Name of the Tunnel	Rock Type	Reference	Q	N	Spacing, mm	θ (^{o})	θ_A (^{o})	α (^{o})	ϕ (^{o})	J_n	n	r	J_f	H, m	D, m
SQUEEZING																
18.	Loktak Tunnel	SS	Choudhari, 2007	0.021	0.105	71	54	50	30	15	9.07	0.09	0.268	376	164	4.8
19.	Loktak Tunnel	SS		0.021	0.105	71	54	50	30	15	9.07	0.09	0.268	376	300	4.8
20.	Maneri Stage I Tunnel	SM	Jethwa, 1981; Goel, 1994	0.31	0.8	31	49	45	30	20	23.06	0.22	0.364	288	350	4.8
21.	Maneri Stage I Tunnel	CQ		0.5	3.75	34	49	45	30	19	20.66	0.22	0.344	273	350	5.8
22.	Maneri Stage I Tunnel	SM		0.3	2.25	31	49	45	30	20	23.14	0.22	0.364	289	700	5.8
23.	Maneri Stage I Tunnel	SP		1.7	8.5	38	49	45	30	20	18.66	0.22	0.364	233	550	5.8
24.	Maneri Stage I Tunnel	FM		4	20	40	49	45	30	20	17.62	0.22	0.364	220	635	5.8
25.	Maneri Stage I Tunnel	SP		4.12	0.62	39	49	45	30	20	18.02	0.22	0.364	225	650	5.8
26.	Maneri Stage II Tunnel	SM	Goel, 1994; Choudhari, 2007	0.1	0.5	69	72	60	55	24	7.23	0.05	0.445	325	250	7
27.	Maneri Stage II Tunnel	Mv		1	5	90	72	60	55	24	5.56	0.05	0.445	250	500	7
28.	Maneri Stage II Tunnel	SM		0.18	0.9	73	72	60	55	24	6.81	0.05	0.445	306	410	7
29.	Maneri Stage II Tunnel	Mv		0.8	4	75	72	60	55	24	6.68	0.05	0.445	300	480	2.5
30.	Maneri Stage II Tunnel	Mv		0.88	4.4	88	72	60	55	24	5.65	0.05	0.445	254	510	7
31.	Maneri Stage II Tunnel	SM		0.3	1.5	56	64	50	55	24	11.57	0.09	0.445	289	410	7
32.	Noonidih Jitpur colliery	WC	Jethwa, 1981	0.59	1.48	13	9	9	0	19	75.32	0.82	0.344	267	450	7

<u>Notation</u>: ***SS-Splintery shales; SM-Sheared metabasics; CQ-Crushed quartzites; SP-Siliceous phyllites; FM-Foliated metabasics; Mv-Metavolcanic.***

……***Contd.***

Sl. No.	Name of the Tunnel	Rock Type	Reference	Q	N	Spacing, mm	θ (^{o})	θ_A (^{o})	α (^{o})	ϕ (^{o})	J_n	n	r	J_f	H, m	D, m
SQUEEZING																
33.	Talal Hydro HRT, Bhutan	AGO	Sripad et al., 2007	0.006	0.045	39	50	50	0	24	16.70	0.09	0.445	417	337	6.8
34.	Talal Hydro HRT, Bhutan			0.007	0.053	39	50	50	0	24	16.50	0.09	0.445	412	337	6.8
35.	Talal Hydro HRT, Bhutan			0.009	0.068	40	50	50	0	24	16.14	0.09	0.445	403	337	6.8
36.	Talal Hydro HRT, Bhutan			0.01	0.075	40	50	50	0	24	16.02	0.09	0.445	400	337	6.8
37.	Talal Hydro HRT, Bhutan			4.3	10.75	79	50	50	0	24	8.09	0.09	0.445	202	400	44.5
38.	Talal Hydro HRT, Bhutan			7.5	18.75	87	50	50	0	24	7.37	0.09	0.445	184	400	44.5
39.	Kaligandaki HRT, Nepal	SP	NEA, 2002; Panthi and Nilsen, 2007	0.015	0.11	147	60	60	0	10	3.41	0.05	0.176	387	600	8.7
40.	Kaligandaki HRT, Nepal	GP		0.019	0.14	150	60	60	0	10	3.34	0.05	0.176	379	600	8.7
41.	Kaligandaki HRT, Nepal	GP		0.025	0.19	153	60	60	0	10	3.26	0.05	0.176	370	575	8.7
42.	Kaligandaki HRT, Nepal	GP		0.008	0.06	140	60	60	0	10	3.58	0.05	0.176	407	620	8.7
43.	Kaligandaki HRT, Nepal	SP		0.016	0.12	147	60	60	0	10	3.39	0.05	0.176	385	620	8.7
44.	Kaligandaki HRT, Nepal	GP		0.023	0.17	152	60	60	0	10	3.28	0.05	0.176	373	580	8.7
45.	Kaligandaki HRT, Nepal	GP		0.01	0.08	142	60	60	0	10	3.52	0.05	0.176	400	620	8.7
46.	Kaligandaki HRT, Nepal	GP		0.001	0.01	120	60	60	0	10	4.18	0.05	0.176	475	575	8.7
47.	Kaligandaki HRT, Nepal	GP		0.02	0.15	151	60	60	0	10	3.32	0.05	0.176	377	575	8.7
48.	Kaligandaki HRT, Nepal	GP		0.009	0.07	141	60	60	0	10	3.55	0.05	0.176	403	620	8.7
49.	Kaligandaki HRT, Nepal	GP		0.2	1.50	188	60	60	0	10	2.66	0.05	0.176	302	550	8.7

<u>Notation</u>: AGO-Adverse geological occurrences; SP-Siliceous phyllites; GP-Graphic phyllites. ……***Contd.***

Sl. No.	Name of the Tunnel	Rock Type	Reference	*Q*	*N*	Spacing, mm	θ (^{o})	θ_A (^{o})	α (^{o})	ϕ (^{o})	J_n	*n*	*r*	J_f	*H*, m	*D*, m
	SQUEEZING															
50.	Kaligandaki HRT, Nepal	GP		0.023	0.17	152	60	60	0	10	3.28	0.05	0.176	373	550	8.7
51.	Kaligandaki HRT, Nepal	GP		0.9	6.75	224	60	60	0	10	2.23	0.05	0.176	253	550	8.7
52.	Kaligandaki HRT, Nepal	GP		0.025	0.19	153	60	60	0	10	3.26	0.05	0.176	370	550	8.7
53.	Kaligandaki HRT, Nepal	GP		0.007	0.05	138	60	60	0	10	3.63	0.05	0.176	412	450	8.7
54.	Kaligandaki HRT, Nepal	GP		0.023	0.17	152	60	60	0	10	3.28	0.05	0.176	373	525	8.7
55.	Kaligandaki HRT, Nepal	GP		0.025	0.19	153	60	60	0	10	3.26	0.05	0.176	370	510	8.7
56.	Kaligandaki HRT, Nepal	GP		0.024	0.18	153	60	60	0	10	3.26	0.05	0.176	370	500	8.7
57.	Kaligandaki HRT, Nepal	GP		0.025	0.19	153	60	60	0	10	3.26	0.05	0.176	370	475	8.7
58.	Kaligandaki HRT, Nepal	GP		0.025	0.19	153	60	60	0	10	3.26	0.05	0.176	370	425	8.7
59.	Kaligandaki HRT, Nepal	GP		0.023	0.17	152	60	60	0	10	3.28	0.05	0.176	373	440	8.7
60.	Kaligandaki HRT, Nepal	GP		0.02	0.15	151	60	60	0	10	3.32	0.05	0.176	377	490	8.7
61.	Kaligandaki HRT, Nepal	GP		0.011	0.08	143	60	60	0	10	3.49	0.05	0.176	397	500	8.7
62.	Frejus Road Tunnel, France	CS	Panet, 1996	0.23	1.73	66	50	50	0	20	9.76	0.09	0.364	298	700	10.52
63.	Frejus Road Tunnel, France	CS		0.23	1.725	66	50	50	0	20	9.76	0.09	0.364	298	850	10.52
64.	Frejus Road Tunnel, France	CS		0.23	1.725	66	50	50	0	20	9.76	0.09	0.364	298	1000	10.52
65.	Frejus Road Tunnel, France	CS		0.23	1.725	66	50	50	0	20	9.76	0.09	0.364	298	1125	10.52
66.	Frejus Road Tunnel, France	CS		0.33	2.475	69	50	50	0	20	9.37	0.09	0.364	286	1250	10.52
67.	Frejus Road Tunnel, France	CS		0.33	2.475	69	50	50	0	20	9.37	0.09	0.364	286	1375	10.52

***Notation**: CS-Calc-schist*

……***Contd.***

Sl. No.	Name of the Tunnel	Rock Type	Reference	Q	N	Spacing, mm	θ (^{o})	θ_A (^{o})	α (^{o})	ϕ (^{o})	J_n	n	r	J_f	H, m	D, m
SQUEEZING																
68.	Khimti-1 Hydro Tunnel, Nepal	GS	Shrestha, 2005; Panthi., 2011	0.01	0.025	62	55	50	34	16	10.33	0.09	0.287	400	100	4.2
69.	Khimti-1 Hydro Tunnel, Nepal	GS		0.005	0.025	95	65	60	34	14	5.27	0.05	0.249	423	100	4.2
70.	Khimti-1 Hydro Tunnel, Nepal	GS		0.008	0.04	76	55	50	34	13	8.46	0.09	0.231	407	111	4.3
71.	Khimti-1 Hydro Tunnel, Nepal	GS		0.013	0.065	103	65	60	34	14	4.87	0.05	0.249	391	138	4
72.	Khimti-1 Hydro Tunnel, Nepal	GS		0.04	0.2	66	55	50	34	17	9.78	0.09	0.306	355	212	4.4
73.	Khimti-1 Hydro Tunnel, Nepal	GS		0.095	0.475	43	55	50	34	27	15.00	0.09	0.51	327	261	4
74.	Khimti-1 Hydro Tunnel, Nepal	GS		0.25	0.625	63	55	50	34	21	10.20	0.09	0.384	295	276	5
75.	Khimti-1 Hydro Tunnel, Nepal	GS		0.28	0.7	65	55	50	34	21	9.95	0.09	0.384	291	276	5
76.	Khimti-1 Hydro Tunnel, Nepal	GS		0.009	0.045	62	55	50	34	16	10.40	0.09	0.287	403	140	4
77.	Khimti-1 Hydro Tunnel, Nepal	GS		0.09	0.45	43	55	50	34	27	15.06	0.09	0.51	328	284	5
78.	Khimti-1 Hydro Tunnel, Nepal	GS		0.09	0.45	43	55	50	34	27	15.06	0.09	0.51	328	300	5
79.	Khimti-1 Hydro Tunnel, Nepal	GS		0.05	0.25	67	55	50	34	17	9.58	0.09	0.306	348	300	5
80.	Khimti-1 Hydro Tunnel, Nepal	GS		0.14	0.35	56	55	50	34	22	11.42	0.09	0.404	314	225	4
81.	Khimti-1 Hydro Tunnel, Nepal	GS		0.07	0.35	69	55	50	34	17	9.28	0.09	0.306	337	218	4
82.	Khimti-1 Hydro Tunnel, Nepal	GS		0.008	0.04	76	55	50	34	13	8.46	0.09	0.231	407	112	4
83.	Khimti-1 Hydro Tunnel, Nepal	GS		0.006	0.03	96	65	60	34	14	5.19	0.05	0.249	417	112	4
84.	Barton's Case History	SG	Barton et al., 1974	0.001	0.021	78	60	60	0	15	6.37	0.05	0.268	475	400	14.6
85.	Barton's Case History			0.39	5.85	89	50	50	0	16	7.26	0.09	0.287	281	400	30.5

<u>Notation</u>: GS-Gneiss and schist; SG-Sheared granites.

Table 4.4 Data Collected from Various Tunnel Sections in Rock Burst Ground Condition

Sl. No.	Name of the Tunnel	Rock Type	Reference	*Q*	*N*	θ (^{o})	θ_A (^{o})	α	ϕ (^{o})	J_n	*n*	*r*	J_f	σ_{ci}, *MPa*	*H*, m	*D*, m
	ROCK BURST															
1.	Nathpa Jhakri	Massive gneiss	Kumar, 2002	4.7	11.8	50	0	90	46	200	0.95	1.04	203	125	1430	11
2.	Nathpa Jhakri	Massive gneiss		4	10.0	50	0	90	52	250	0.95	1.28	206	88	1420	11
3.	Nathpa Jhakri	Massive gneiss		4.5	11.3	55	0	90	46	200	0.95	1.04	203	50	1420	11
4.	Nathpa Jhakri	Massive gneiss		1.8	4.5	60	0	90	48	250	0.95	1.11	237	42	1320	11
5.	Nathpa Jhakri	Massive gneiss		3.5	8.8	50	0	90	45	200	0.95	1.00	211	50	1300	11
6.	Nathpa Jhakri	Massive gneiss		2	5.0	70	0	90	42	200	0.95	0.90	234	60	1300	11
7.	Nathpa Jhakri	Massive gneiss		1.8	4.5	60	0	90	48	250	0.95	1.11	237	55	1300	11
8.	Nathpa Jhakri	Massive gneiss		3.3	8.3	55	0	90	39	166.7	0.95	0.81	217	50	1300	11
9.	Nathpa Jhakri	Massive gneiss		2.2	5.5	60	0	90	49	250	0.95	1.15	230	50	1230	11
10.	Nathpa Jhakri	Massive gneiss		4.7	11.8	70	0	90	46	200	0.95	1.04	203	42	1180	11
11.	Nathpa Jhakri	Massive gneiss		2.0	5.0	60	0	90	50	250	0.95	1.91	221	34	1180	11
12.	Nathpa Jhakri	Massive gneiss		3.4	8.5	50	0	90	51	250	0.95	1.23	213	42	1180	11
13.	Nathpa Jhakri	Massive gneiss		7.5	18.8	65	0	90	49	200	0.95	1.15	184	42	1100	11
14.	Nathpa Jhakri	Massive gneiss		7.0	17.5	70	0	90	55	250	0.95	1.40	187	50	1090	11
15.	Nathpa Jhakri	Massive gneiss		3.8	9.5	60	0	90	40	166.7	0.95	0.84	209	50	1060	11

……***Contd.***

Sl. No.	Name of the Tunnel	Rock Type	Reference	Q	N	θ (^{o})	θ_A (^{o})	α (^{o})	ϕ (^{o})	J_n	n	r	J_f	σ_{ci}, MPa	H, m	D, m
ROCK BURST																
16.	Laerdal Road Tunnel, Norway	Precambrian gneiss	The Engineer, (2006); NFF, 2000	0.8	2.0	70	67	30	35	17.99	0.10	0.700	257	100	1400	11.3
17.	Dulhasti Hydro Tunnel	Quartzite	Vibert et al., 2005; Goel, 1994	51.2	128.1	67	65	22	40	7.16	0.07	0.839	122	95	1000	8.3

4.4 EMPIRICAL CORRELATIONS FOR GROUND CONDITION PREDICTION

This large data presented in Tables 4.1 – 4.4 has been studied and analysed to prepare plots presented in Figs. 4.1 - 4.3 and separate correlations have been developed involving rock mass characteristics represented by Joint Factor (J_f), Rock Mass Quality (Q) and Rock Mass Number (N) for prediction of the ground condition for tunnelling.

Quadrilateral ABCA formed by line boundaries AB and BC in Figs. 4.1- 4.3 accommodates the points representing the 'rock burst' type of ground condition. Line AB is represented by equations,

$J_f = 260$, $Q/D = 0.03$, and $N/D = 0.14$ (4.1 a,b,c)

in Figs. 4.1, 4.2 and 4.3 respectively, whereas the line BC is represented by equations,

$H = 4189\, D^{-1}\, e^{0.0049\, Jf}$, $Q/D = 10^{15} H^{5.28}$ and $H = 1035\, (N/D)^{-0.096}$ (4.2 a,b,c)

in Figs. 4.1, 4.2 and 4.3 respectively. Lines DE and FG represent boundaries between self-supporting / non-squeezing and non-squeezing / squeezing ground conditions respectively in Figs. 4.1-4.3. In Fig. 4.1, lines HI and JI represent boundaries between low squeezing / moderate squeezing and moderate squeezing / high squeezing respectively. The proposed empirical correlations are as follows:

4.4.1 Prediction of Ground Condition using Joint Factor (J_f)

Figure 4.1 shows the plot of Joint Factor (J_f) as an abscissa on arithmetic scale versus product of tunnel depth and tunnel diameter ($H.D$) plotted as an ordinate on logarithmic scale. In this figure, there are basically three sets of points, namely – i) those corresponding to self supporting ground condition, ii)) those corresponding to non-squeezing ground conditions, and iii) those belonging to squeezing ground condition. The squeezing ground condition has been further classified in to mild, moderate and high squeezing. Different ground conditions are identified on basis of the strain levels around the tunnel periphery. In case of self supporting and non-squeezing ground conditions, the associated strain level is less than or equal to 1%. However, if the strain level exceeds 1%, it results in to a squeezing ground condition. Squeezing is 'mild' if the strain level lies between 1% to 3%, it is 'moderate' if the

strain level lies between 3% to 5% , and is a 'high squeezing' condition if the strain level exceeds 5%.

In Fig. 4.1, line DE is the boundary between self-supporting and non-squeezing condition, which is represented by Eq. 4.3.

$$H = 170009 D^{-1} e^{-0.025 J_f} \tag{4.3}$$

From the Eq. 4.3, one can say that -

<u>For self-supporting condition</u>

$$H < 170009 D^{-1} e^{-0.025 J_f} \tag{4.4}$$

Therefore, all points corresponding to self-supporting ground condition are found to lie below line DE.

All points lying between the line DE and the line FG correspond to non-squeezing ground condition and the equation of this line FG is given by –

$$H = 170234 D^{-1} e^{-0.017 J_f} \tag{4.5}$$

From the Eq. 4.5 therefore, one can say that –

<u>For non-squeezing condition</u>

$$H < 170234 D^{-1} e^{-0.017 J_f} \tag{4.6}$$

In other words, if the plot of product (*H.D)* versus joint factor, J_f results in to a point which lies above the FG , then the tunnelling condition would be a squeezing ground condition. Therefore,

<u>For squeezing condition</u>

$$H > 170234 D^{-1} e^{-0.017 J_f} \tag{4.7}$$

In Eq. 4.7, for lower values of the right hand side (RHS) term, severity of the squeezing will increase. Value of RHS term decreases with increase in the values of *D* or / and J_f. This effect

shows that the parameters D and J_f are qualitatively at right place in the correlation. The expression can be deduced to

$$HD > 170234\, e^{-0.017\, Jf}, \tag{4.8}$$

With the help of the above equations, one can predict the ground behaviour at a certain tunnel depth, for known values of J_f and D. For example, a tunnel having 7 m diameter and having joint factor, J_f = 300 will not show squeezing behaviour at a tunnel depth less than 148 m and the ground will show non-squeezing behaviour.

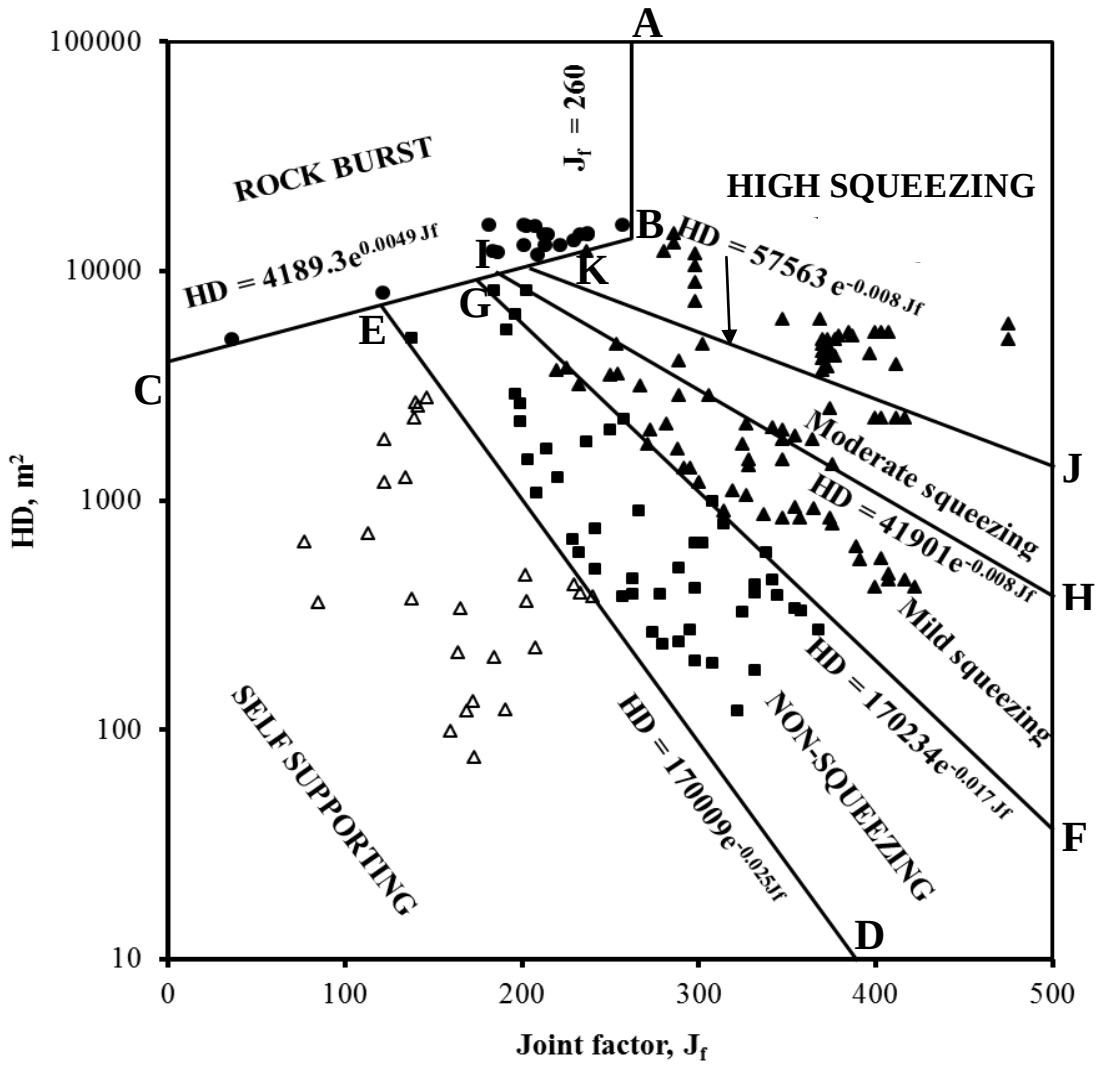

Fig. 4.1 Plot of Product of Tunnel Depth *(H)* and Diameter *(D)* versus Joint Factor, J_f

In Fig. 4.1, the demarcation lines, AB and BC are boundaries containing data of rock burst condition. These lines are represented by Eq. 4.9 and Eq. 4.10 respectively,

$$J_f = 260 \tag{4.9}$$

$$H = 4189.3D^{-1}e^{0.0049J_f} \tag{4.10}$$

From the above equations, one can say that -

For rock-burst condition

$$H > 4189D^{-1}e^{0.0049J_f} \quad \text{and} \quad J_f < 260 \tag{4.11}$$

4.4.2 Prediction of Degree of Squeezing

Degree of squeezing indicates the degree of tunnel deformation due to excessive stresses around the tunnel periphery. The squeezing behaviour has been classified into three categories viz., low or mild squeezing (strain level = 1-2 %), moderate squeezing (strain level = 2-3 %) and high squeezing (strain level >3 %) The demarcation lines HI and JK in Fig. 4.1 imply following inequalities respectively:

For mild Squeezing

$$41901D^{-1}e^{-0.008J_f} > H > 170234D^{-1}e^{-0.017J_f} \tag{4.12}$$

For moderate squeezing

$$57563D^{-1}e^{-0.008J_f} > H > 41901D^{-1}e^{-0.008J_f} \tag{4.13}$$

For high squeezing

$$4189D^{-1}e^{0.0049J_f} > H > 57563D^{-1}e^{-0.008J_f} \qquad (\text{for } J_f > 260) \tag{4.14}$$

4.4.3 Prediction of Ground Condition using Rock Mass Quality (*Q*)

Strength of the rock mass around the tunnel periphery increases with improvement in Rock Mass Quality (*Q*) and decreases with tunnel depth (*H*) and increase diameter of tunnel (*D*). The data presented in Tables 4.1 – 4.4 has been analysed again and used for prediction of ground condition based on values of *Q*. That is why depth of overburden, *H* has been plotted versus (*Q/D*) in Fig. 4.2 for development of the correlation.

For self-supporting ground condition

All points corresponding to tunnelling cases, wherein self supporting ground condition was observed, lie below line DE in Fig. 4.2 whereas Demarcation line DE between non-squeezing and self-supporting ground behaviour in Fig. 4.2 is represented by Eq. 4.15.

$$H = 191\left(\frac{Q}{D}\right)^{0.642} \tag{4.15}$$

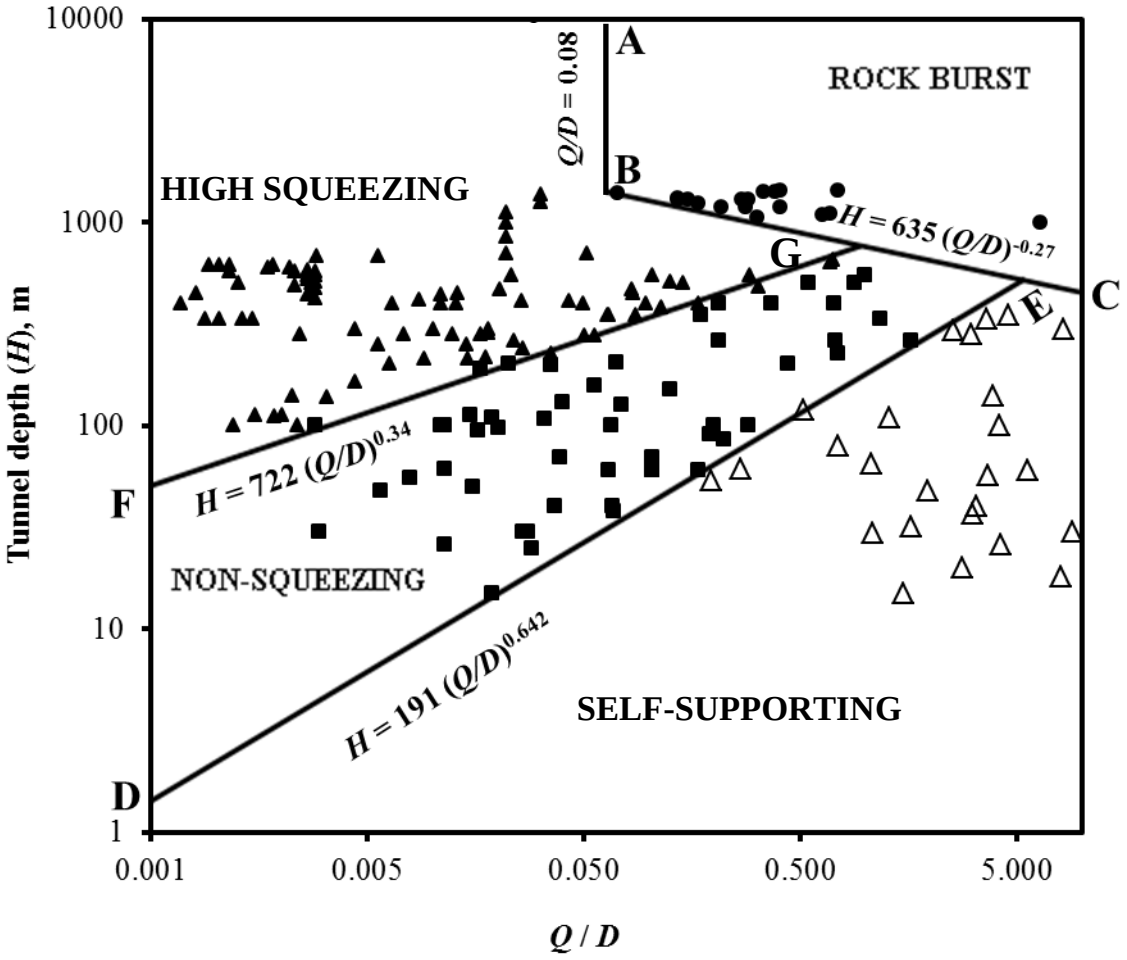

Fig. 4.2 Variation of Tunnel Depth (*H*) versus (*Q/D*)

The Eq. 4.15 implies that for self-supporting condition,

$$H < 191\left(\frac{Q}{D}\right)^{0.642} \tag{4.16}$$

The line FG in Fig. 4.2 is a demarcation between squeezing and non-squeezing ground behaviour and can be represented by Eq. 4.17 as follows:

$$H = 722\left(\frac{Q}{D}\right)^{0.34} \tag{4.17}$$

From Eq. 4.17 therefore, it can be stated that -

For squeezing condition

$$H > 722\left(\frac{Q}{D}\right)^{0.34} \tag{4.18}$$

Obviously,

For non- squeezing condition

$$H < 722\left(\frac{Q}{D}\right)^{0.34} \tag{4.19}$$

In Fig. 4.2, rock burst data has been demarcated by boundary lines AB and BC. These lines are represented by Eqs. 4.20 and 4.21 respectively.

$$Q/D = 0.08 \tag{4.20}$$

$$H = 635\left(\frac{Q}{D}\right)^{-0.27} \tag{4.21}$$

From the Eqs. 4.20 & 4.21, one can state that -

For rock-burst condition

$$H > 635\left(\frac{Q}{D}\right)^{-0.27} \quad \text{and} \quad Q/D > 0.08 \tag{4.22}$$

4.4.4 Prediction of Ground Condition using Rock Mass Number (*N*)

Rock mass strength increases with increase in rock mass number (*N*) as in case of *Q*, and therefore the plot of Fig. 4.3 is similar to the plot given in Fig. 4.2.

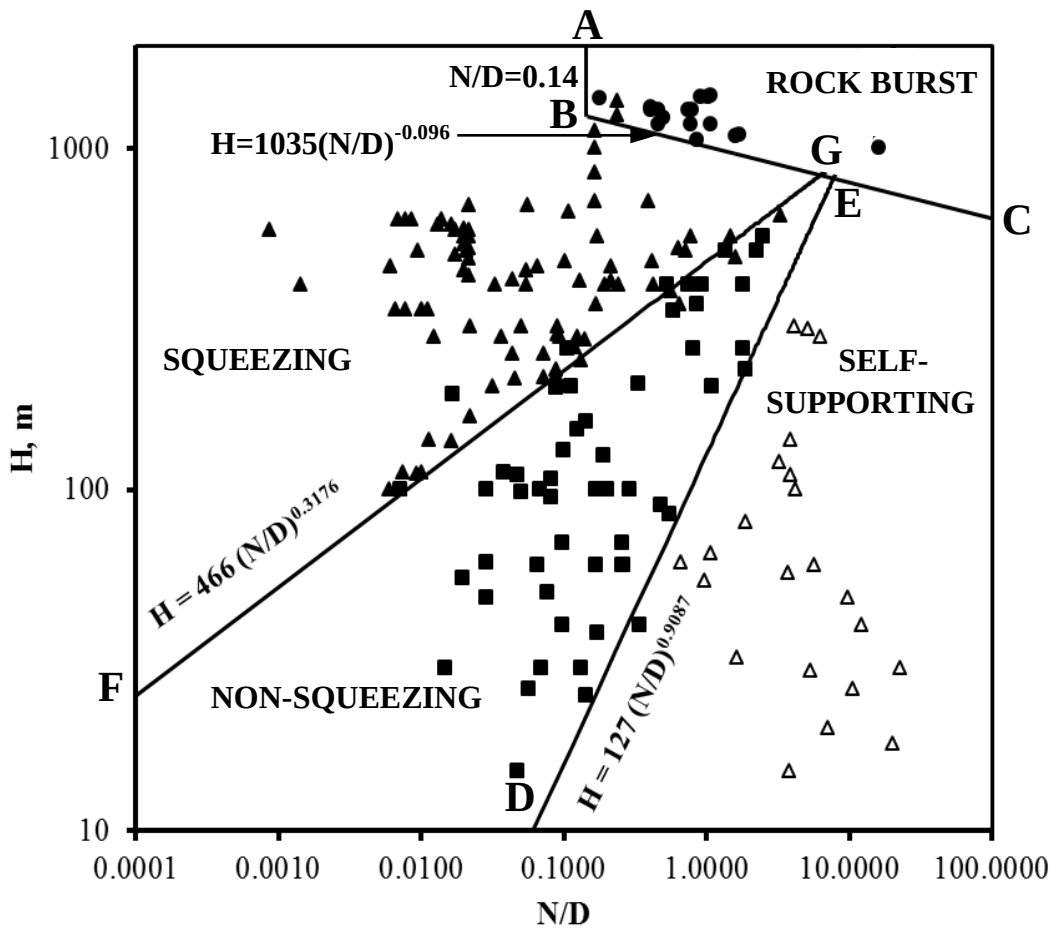

Fig. 4.3 Variation of Tunnel Depth (*H)* versus (*N/D)*

The line FG in Fig. 4.3 is a demarcation between squeezing and non-squeezing ground behaviour and can be represented by following equation:

$$H = 466(N/D)^{0.3176} \tag{4.23}$$

From the Eq. 4.23, one gets,

For squeezing condition

$$H > 466(N/D)^{0.3176} \quad (4.24)$$

For non- squeezing condition

$$H < 466(N/D)^{0.3176} \quad (4.25)$$

Demarcation line DE between non-squeezing and self-supporting ground behaviour in Fig. 4.3 is represented by Eq. 4.26.

$$H = 127(N/D)^{0.9087} \quad (4.26)$$

Therefore,

For self-supporting condition

The Eq. 4.26 implies that for self-supporting condition,

$$H < 127(N/D)^{0.9087} \quad (4.27)$$

The boundary lines (AB & BC) separating the rock burst data from all other data in Fig. 4.3, are represented by Eqs. 4.28 and 4.29 respectively.

$$N/D > 0.14 \quad (4.28)$$

and $$H = 1035(N/D)^{-0.096} \quad (4.29)$$

From the above equations, it is clear that -

For rock-burst condition

$$H > 1035(N/D)^{-0.096} \quad \text{and} \quad N/D > 0.14 \quad (4.30)$$

4.5 CORRELATION BETWEEN JOINT FACTOR AND ROCK MASS NUMBER

Values of joint factor, J_f and the rock mass number, N from all data sets presented in Tables 4.1-4.4 have been plotted in Fig. 4.4 and utilised to develop correlation between Joint Factor and Rock Mass Number. The proposed correlation given by Eq. 4.31 is the best line fit with a correlation coefficient of 0.94.

$$J_f = -37.3\ln(N) + 293 \qquad (R^2 = 0.94) \qquad (4.31)$$

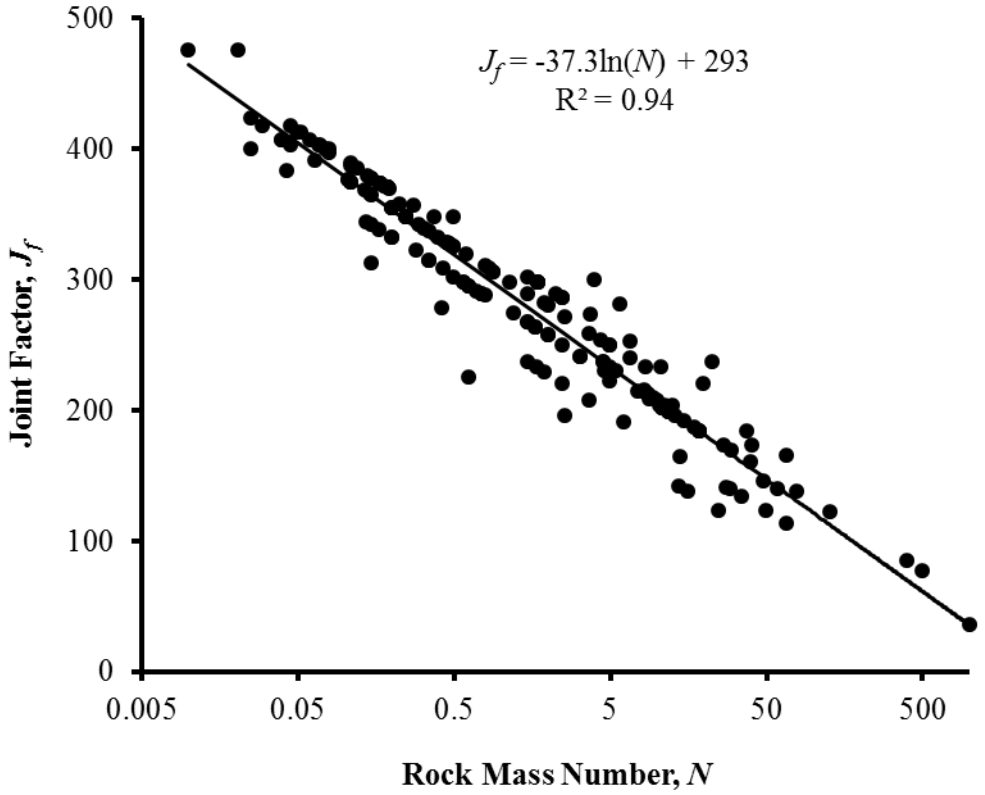

Fig. 4.4 Variation of Joint Factor, J_f versus Rock mass Number, N

4.6 LIMITATIONS OF ABOVE STUDY

Limitations of the study presented in this chapter are:

- The empirical correlations developed in the present study use data of tunnel sections excavated by drill and blast method and therefore predictions will hold good for the tunnels driven using same method of excavation. It is because of the fact that rock mass surrounding the tunnels excavated by machines like tunnel boring machine get less affected as compared to the drill and blast method, which induces numerous cracks into the rock mass.

- In the analysis, for non-circular tunnels, equivalent diameter, D_e has been taken in to consideration, which is computed using expression: $D_e = (4A/\pi)^{0.5}$ where A is cross-sectional area of tunnel.

4.7 CONCLUDING REMARKS

Empirical correlations for prediction of ground condition (self-supporting, non-squeezing, squeezing and rock burst) have been developed using J_f, Q and N separately. In addition to the rock characterising parameters (J_f , Q, N), diameter of tunnels (D) and overburden height or tunnel depth (H) are the other parameters which have been used in the development of correlations.

In addition, an inter-relation between J_f and N has also been developed.

All correlations proposed in the present study are reliable and may be used for prediction of ground conditions.

Chapter 5

PREDICTION OF TUNNEL DEFORMATION

5.1 GENERAL

Tunnel deformation has been a major concern especially in case of squeezing ground conditions. In such grounds, rock mass around the tunnel periphery behaves plastically and time dependent deformation continues, if proper counter measures to install sufficient supports are not taken in time. Excessive deformation loosens the surrounding rock mass and gives rise to an increase plastic zone posing great supporting problems. It is therefore necessary to have prior knowledge of deformation level before the excavation of a tunnel so that the contingency plans of the required support can be kept ready before any problems during construction are encountered. On the other hand, if rock mass around the tunnel periphery behaves elastically, tunnel deformations are within elastic limit (non-squeezing ground condition i.e., strain level < 1 %), and doesn't pose any supporting problems.

Nowadays, New Austrian Tunnelling Method (NATM) is being commonly adopted as a conventional method of tunnelling in which deformation monitoring data plays a key role in the assessment of the quantity and quality of the required support for a particular round of excavation. Predicted values of tunnel deformation using the correlations proposed in this chapter would help in the support design and making preparatory support arrangements during tunnelling in squeezing ground conditions.

5.2 PARAMETERS INFLUENCING TUNNEL DEFORMATIONS

Following parameters have been included for developing the correlations:

i) Size of tunnel or tunnel radius, a,

ii) In-situ stresses (vertical, σ_v and horizontal, σ_h),

iii) Support stiffness, K,

iv) Rock mass characteristics defined by joint factor, J_f, rock mass quality, Q and rock mass number, N and

v) Uniaxial compressive strength of intact rock (σ_{ci}).

The aforementioned parameters have been used in deriving the empirical correlations for prediction of tunnel deformations in tunnel. Parametric analysis has also been carried out to study the influence of each parameter.

5.2.1 Support Stiffness

Data of support stiffness has been collected either from the literature or knowing a particular support system at a given tunnel section, it was calculated as follows:

Steel ribs with back fill (Hoek and Brown, 1982)

$$K = \frac{p.a}{\Delta a} \tag{5.1}$$

where K, p, a and Δa are effective stiffness of steel ribs with backfill, observed support pressure, tunnel radius and the measured radial deformation respectively. If stiffness of steel ribs (K_s) and backfill (K_B) are separately known, then effective support stiffness (K) may be calculated (Hoek and Brown, 1982) as -

$$\frac{1}{K} = \frac{1}{K_s} + \frac{1}{K_B} \tag{5.2}$$

Rock bolts (Hoek and Brown, 1982)

$$\frac{1}{K_b} = \frac{S_c S_l}{r_i}\left[\frac{4l}{3.14 {d_b}^2 E_b} + Q\right] \tag{5.3}$$

where K_b is the stiffness of rock bolt; S_c and S_l are the circumferential and longitudinal spacing of the rock bolt; r_i, the radius of tunnel; d_b, the diameter of rock bolt; E_b, the elastic modulus of bolt material; l, the length of the bolt, and Q defines the load deformation constant for anchor and the bolt head.

Concrete or SFRS lining (Hoek and Brown, 1982)

$$K_c = \left(\frac{E_c}{1+\nu_c}\right)\frac{r_i^2 - (r_i - t_c)^2}{(1-2\nu_c)r_i^2 + (r_i - t_c)^2} \tag{5.4}$$

where K_c , E_c , ν_c and t_c are the stiffness, the modulus of elasticity, the Poisson's ratio and the thickness of concrete or SFRS respectively; r_i is radial distance of the concrete/SFRS lining. Combined support stiffness of rock bolts with shotcrete or concrete,

$$K = K_b + K_c \tag{5.5}$$

5.2.2 In-situ Stresses

In-situ stresses play a major role on development of stresses around the tunnel periphery resulting in tunnel deformation. Vertical in-situ stress has been calculated as following:

$$\sigma_v = \gamma.H \tag{5.6}$$

where σ_v , γ and H are vertical in-situ stress, unit weight of rock (0.027 MN/m^3) and tunnel depth respectively. Magnitude of horizontal in-situ stresses (σ_h) is taken from the literature of case study projects (Dube, 1979; Jethwa 1981; Sripad et al., 2007;Bahuguna et al., 2008; and others).

5.3 DATA COLLECTION

The case histories from hydroelectric projects, viz., Giri Bata (1 tunnel), Chhibro–Khodri (2 adits/ tunnels), Maneri stage-I & II (4 adits/tunnels), Tala (1 tunnel), Kaligandaki (1 tunnel), Khimti-1 (4 adits); and a mine roadway of Noonidih-Jitpur Colliery have been analysed for the present study. Data related to :

i) rock type,
ii) tunnel radius a,
iii) tunnel depth H,
iv) joint properties (dip, spacing, friction angle of joint),
v) angle between tunnel alignment and strike of joints, α,
vi) uniaxial compressive strength of intact rock, σ_{ci},
vii) horizontal in-situ stress, σ_h ,
viii) rock mass characteristics, Q or N ,
ix) observed tunnel deformation, u_{obs} , etc.

of various tunnels have been collected from 63 sections of tunnels/ adits/ mine galleries etc. Joint factor, J_f was calculated using the joint properties as explained on basis of one example in Chapter 3. Data related to rock-joint properties observed at various tunnel sections has been presented in Table 3.5 of chapter 3. Data of rock type, Q, N, H, a, u_{obs}, and J_f with values of its parameters (inclination or orientation parameter, n and joint strength parameter, r as defined in art. 2.9) has been presented in Table 5.1, whereas, values of σ_{ci}, σ_v, and σ_h have been presented in Table 5.2. In addition to this, information of installed support, tunnel advance rate, adjacent geological structure, water pressure and tunnelling method has been provided in Table 5.3.

Table 5.1 Data Collected from Various Case Histories for Prediction of Tunnel Deformation in Squeezing Ground

S. No.	Name of Tunnel	Rock Type	Reference	*Q*	*N*	*a (m)*	*H (m)*	*(u_{obs} mm)*	*K (MPa)*	J_n	*n*	*r*	J_f
1	Maneri Stage-II tunnel	Sheared metabasics	Goel, 1994; Choudhari, 2007	0.1	0.5	3.5	285	100.5	9.79	8	0.05	0.445	360
2	Maneri Stage-II tunnel	Sheared metabasics		0.3	2.25	3.5	410	98	9.79	11.68	0.09	0.445	291
3	Maneri Stage-II tunnel	Metavolcanic		0.88	4.4	3.5	415	76.8	9.79	5.88	0.05	0.445	264
4	Maneri Stage-II tunnel	Metavolcanic		0.8	4	1.25	480	36	9.84	5.88	0.05	0.445	264
5	Maneri Stage-II tunnel	Metavolcanic		1	5	3.5	500	92.5	9.79	5.56	0.05	0.445	250
6	Maneri Stage-II tunnel	Metavolcanic		0.88	4.4	1.25	510	30.2	9.84	5.88	0.05	0.445	264
7	Giri-Bata tunnel	Crushed phyllites	Dube, 1979; Goel, 1994; Choudhari, 2007	0.12	0.6	2.3	240	103.5	3.97	8.5	0.07	0.384	320
8	Giri-Bata tunnel	Crushed phyllites		0.05	0.25	2.3	440	231	3.97	9.43	0.07	0.384	351
9	Giri-Bata tunnel	Crushed phyllites		0.06	0.3	2.3	450	237	3.97	9.43	0.07	0.384	351
10	Giri-Bata tunnel	Crushed phyllites		0.03	0.15	2.3	400	240	3.98	9.43	0.07	0.364	370
11	Giri-Bata tunnel	Crushed phyllites		0.05	0.25	2.3	400	175	3.98	9.43	0.07	0.404	333
12	Giri-Bata tunnel	Crushed phyllites		0.02	0.2	2.3	200	142.5	2.98	9.43	0.07	0.364	370
13	Giri-Bata tunnel	Crushed phyllites		0.03	0.3	2.3	325	201.2	2.98	9.43	0.07	0.384	350
14	Giri-Bata tunnel	Crushed slates		0.512	2.56	2.3	400	15..5	2.98	9.43	0.07	0.488	276
15	Chhibro-Khodri tunnel	Crushed red shales	Jethwa, 1981; Goel, 1994; Choudhari, 2007	0.05	0.375	1.5	280	42	9.8	14.3	0.09	0.466	341
16	Chhibro-Khodri tunnel	Soft & plastic black clays		0.022	0.11	1.5	280	67.5	5.96	12.9	0.09	0.384	373
17	Chhibro-Khodri tunnel	Seamy crushed red shales		0.05	0.5	4.5	680	270	9.9	14.3	0.09	0.445	357
18	Chhibro-Khodri tunnel	Soft & plastic black clays		0.022	0.11	4.5	280	90	48.56	12.9	0.09	0.384	373
19	Maneri Stage-I tunnel	Sheared metabasics	Jethwa, 1981; Goel, 1994	0.3	2.25	2.9	700	140	9.81	23.6	0.22	0.364	295
20	Maneri Stage-I tunnel	Siliceous phyllites		1.7	8.5	2.9	550	77	9.81	19.6	0.22	0.364	245
21	Maneri Stage-I tunnel	Foliated metabasics		4	20	2.9	635	67.5	9.81	15.7	0.22	0.364	196
22	Maneri Stage-I tunnel	Siliceous phyllites		4.12	20.62	2.9	650	60	9.81	15.7	0.22	0.364	196
23	Maneri Stage-I tunnel	Sheared metabasics		0.31	6.2	2.9	450	140	5.1	23.6	0.22	0.364	295

.....Contd.

S. No.	Name of Tunnel	Rock Type	Reference	*Q*	*N*	*a (m)*	*H (m)*	*(u_{obs} mm)*	*K (MPa)*	*J_n*	*n*	*r*	*J_f*
24	Maneri Stage-I tunnel	Crushed quartzite		0.5	10	2.9	750	120	8.1	20.2	0.22	0.344	267
25	Noonidih colliery	Weak coal	Jethwa, 1981	0.59	5.9	3.5	450	105	9.67	71.4	0.82	0.344	253
26	Tala HRT, Bhutan	Adverse geological occurrences (AGO)	Sripad et al., 2007	0.011	0.1	3.4	337	120	8.97	16	0.09	0.445	399
27	Kaligandaki-A HRT	Siliceous and graphic phyllites	----------NEA, 2002; Panthi and Nilsen, 2007----------	0.015	0.075	4.35	600	126	34.52	3.57	0.05	0.18	396
28	Kaligandaki-A HRT	Gaphic phyllites		0.023	0.115	4.35	600	61	90.71	3.33	0.05	0.18	370
29	Kaligandaki-A HRT	Gaphic phyllites		0.025	0.125	4.35	600	100	34.17	3.33	0.05	0.18	370
30	Kaligandaki-A HRT	Gaphic phyllites		0.018	0.09	4.35	600	170	26.20	3.44	0.05	0.18	382
31	Kaligandaki-A HRT	Gaphic phyllites		0.023	0.12	4.35	600	140	28.48	3.33	0.05	0.18	370
32	Kaligandaki-A HRT	Gaphic phyllites		0.02	0.3	4.35	620	213	26.20	6.1	0.09	0.18	377
33	Kaligandaki-A HRT	Gaphic phyllites		0.008	0.16	4.35	620	370	14.67	6.5	0.09	0.18	401
34	Kaligandaki-A HRT	Gaphic phyllites		0.009	0.18	4.35	620	334	14.67	6.5	0.09	0.18	401
35	Kaligandaki-A HRT	Gaphic phyllites		0.01	0.2	4.35	620	27.	26.20	6.5	0.09	0.18	401
36	Kaligandaki-A HRT	Gaphic phyllites		0.009	0.18	4.35	620	356	14.67	3.6	0.05	0.18	400
37	Kaligandaki-A HRT	Siliceous phyllites		0.016	0.32	4.35	620	191	26.20	6.3	0.09	0.18	389
38	Kaligandaki-A HRT	Siliceous phyllites		0.02	0.1	4.35	620	178	26.20	6.1	0.09	0.18	377
39	Kaligandaki-A HRT	Siliceous phyllites		0.025	0.5	4.35	620	109	56.96	6	0.09	0.18	370
40	Kaligandaki-A HRT	Siliceous phyllites		0.023	0.115	4.35	580	161	26.20	6	0.09	0.18	370
41	Kaligandaki-A HRT	Siliceous phyllites	----------	0.025	0.125	4.35	580	74	74.66	6	0.09	0.18	370
42	Kaligandaki-A HRT	Siliceous phyllites		0.001	0.005	4.35	575	260	34.17	7.6	0.09	0.18	469
43	Kaligandaki-A HRT	Siliceous phyllites		0.025	0.125	4.35	550	104	39.87	6	0.09	0.18	370

.....Contd.

S. No.	Name of Tunnel	Rock Type	Refe-rence	*Q*	*N*	*a (m)*	*H (m)*	*(u_{obs} mm)*	*K (MPa)*	*J_n*	*n*	*r*	*J_f*
44	Khimti-1 hydro adit-1 d/s 475	Augen gneiss, STS	--Shrestha, 2005; Panthi, 2011--	0.08	0.42	2	98	15.5	933.0	8.6	0.09	0.287	333
45	Khimti-1 hydro adit-1 d/s 580	STC		0.008	0.07	2.15	111	16	1936.0	8.5	0.09	0.231	409
46	Khimti-1 hydro adit-1 d/s 665	Augen gneiss; schist		0.06	0.42	2	112	6	458.0	9.5	0.09	0.306	345
47	Khimti-1 hydro adit-2 d/s 441	Augen gneiss		0.3	0.55	2	126	5	461.0	8	0.09	0.306	291
48	Khimti-1 hydro adit-2 d/s 601	STS		0.013	0.17	2	138	4	1934.0	4.9	0.05	0.249	393
49	Khimti-1 hydro adit-2 d/s 895	Gneiss, Chlorite Schist		0.14	1.67	2	198	.6	934.0	11.5	0.09	0.404	316
50	Khimti-1 hydro adit-2 u/s 1357	Banded gneiss, CS		0.095	0.44	2	261	3	931.0	14.9	0.09	0.51	325
51	Khimti-1 hydro adit-2 u/s 1730	AG with clay gauge		0.065	0.55	2	95	6	933.0	9.3	0.09	0.306	338
52	Khimti-1 hydro adit-3 u/s 15	Shear bands of AG & S		0.2	1.94	2.5	130	8.5	936.0	12.7	0.09	0.466	303
53	Khimti-1 hydro adit-3 u/s 59	Augen gneiss at crown; schist at wall		0.23	0.63	2.05	158	6.5	650.0	9.2	0.09	0.34	297
54	Khimti-1 hydro adit-3 u/s 200	Augen gneiss		0.25	1.48	2.5	276	19.3	940.0	10.2	0.09	0.38	295
55	Khimti-1 hydro adit-3 u/s 210	Schist		0.28	1.48	2.5	276	9	652.0	10.2	0.09	0.38	295
56	Khimti-1 hydro adit-3 d/s 220	Augen gneiss, SS		0.009	0.09	2	140	16	430.0	10.4	0.09	0.287	403
57	Khimti-1 hydro adit-3 u/s 345	GG, STS		0.05	0.33	2.5	300	4.5	1430.0	9.6	0.09	0.306	349
58	Khimti-1 hydro adit-4 u/s 503	CSS		0.14	1.00	2	225	5	1430.0	11.5	0.09	0.404	316
58	Khimti-1 hydro adit-4 u/s 550	Banded gneiss		0.07	0.94	2	218	3	739.0	14	0.09	0.466	334
60	Khimti-1 hydro adit-4 u/s 852	BGS		0.47	1.41	2	114	5	648.0	11.7	0.09	0.466	279
61	Khimti-1 hydro adit-4 u/s 876	Sheared augen gneiss		0.6	1.72	2	114	5	556.0	6.3	0.05	0.466	270
62	Khimti-1 hydro adit-4 u/s 974	Sheared augen gneiss with clay fill		0.008	0.08	2	112	4	936.0	5.1	0.05	0.249	409
63	Khimti-1 hydro adit-4 u/s 1045			0.008	0.06	2	112	2	651.0	5.1	0.05	0.249	409

<u>Notation:</u> AGO – Weathered biotite schist associated with banded gneiss, amphibolites and quartzites in thin bands; AG- Augen gneiss; STS- Sericite talcose schist; STC- Sheared talcose chlorite; CS- Chlorite schist; S- Schist; SS- Sericite schist; GG- Granitic gneiss; CSS- Chlorite sericite schist; BGS-Banded gneiss with shear planes.

Table 5.2 Values of Horizontal In-situ Stress, σ_h and Uniaxial Compressive Strength, σ_{ci} as Obtained from Case Study Projects

S. No.	Name of Tunnel	Rock Type	σ_{ci} (MPa)	σ_h (MPa)	σ_v (MPa)
1.	Maneri stage-II tunnel	Sheared metabasics	11	2.5	7.7
2.	Maneri stage-II tunnel	Sheared metabasics	11	3.7	11.1
3.	Maneri stage-II tunnel	Metavolcanic	24	3.7	11.2
4.	Maneri stage-II tunnel	Metavolcanic	24	4.3	13.0
5.	Maneri stage-II tunnel	Metavolcanic	24	4.5	13.5
6.	Maneri stage-II tunnel	Metavolcanic	24	4.5	13.8
7.	Giri-Bata tunnel	Crushed phyllites	14	13.0	6.5
8.	Giri-Bata tunnel	Crushed phyllites	14	23.8	11.9
9.	Giri-Bata tunnel	Crushed phyllites	14	24.3	12.2
10.	Giri-Bata tunnel	Crushed phyllites	14	21.6	10.8
11.	Giri-Bata tunnel	Crushed phyllites	14	21.6	10.8
12.	Giri-Bata tunnel	Crushed phyllites	14	10.8	5.4
13.	Giri-Bata tunnel	Crushed phyllites	14	17.6	8.8
14.	Giri-Bata tunnel	Crushed slates	20	21.6	10.8
15.	Chhibro-Khodri tunnel	Crushed red shales	21	7.6	7.6
16.	Chhibro-Khodri tunnel	Soft & plastic black clays	8	7.6	7.6
17.	Chhibro-Khodri tunnel	Seamy crushed red shales	21	18.4	18.4
18.	Chhibro-Khodri tunnel	Soft & plastic black clays	8	7.6	7.6
19.	Maneri stage-I tunnel	Sheared metabasics	10	6.2	18.9
20.	Maneri stage-I tunnel	Siliceous phyllites	10	4.9	14.9
21.	Maneri stage-I tunnel	Foliated metabasics	10	11.8	17.1
22.	Maneri stage-I tunnel	Siliceous phyllites	10	5.8	17.6
23.	Maneri stage-I tunnel	Sheared metabasics	10	4.0	12.2
24.	Maneri stage-I tunnel	Crushed quartzite	21	6.7	20.3
25.	Noonidih Colliery	Weak coal	21	10.4	12.2
26.	Tala HRT, Bhutan	AGO	10	5.5	9.1
27.	Kaligandaki-A HRT	Siliceous and graphic phyllites	39	8.1	16.2
28.	Kaligandaki-A HRT	Graphic phyllites	39	8.1	16.2
29.	Kaligandaki-A HRT	Graphic phyllites	39	8.1	16.2

.....Contd.

S. No.	Name of Tunnel	Rock Type	σ_{ci} (MPa)	σ_h (MPa)	σ_v (MPa)
30.	Kaligandaki-A HRT	Graphic phyllites	39	8.1	16.2
31.	Kaligandaki-A HRT	Graphic phyllites	39	8.1	16.2
32.	Kaligandaki-A HRT	Graphic phyllites	39	8.4	16.7
33.	Kaligandaki-A HRT	Graphic phyllites	39	8.4	16.7
34.	Kaligandaki-A HRT	Graphic phyllites	39	8.4	16.7
35.	Kaligandaki-A HRT	Graphic phyllites	39	8.4	16.7
36.	Kaligandaki-A HRT	Graphic phyllites	39	8.4	16.7
37.	Kaligandaki-A HRT	Siliceous phyllites	39	8.4	16.7
38.	Kaligandaki-A HRT	Siliceous phyllites	39	8.4	16.7
39.	Kaligandaki-A HRT	Siliceous phyllites	39	8.4	16.7
40.	Kaligandaki-A HRT	Siliceous phyllites	39	7.8	15.7
41.	Kaligandaki-A HRT	Siliceous phyllites	39	7.8	15.7
42.	Kaligandaki-A HRT	Siliceous phyllites	39	7.8	15.5
43.	Kaligandaki-A HRT	Siliceous phyllites	39	7.4	14.9
44.	Khimti-1 hydro adit-1 d/s 475	Augen gneiss, STS	26	2.6	2.6
45.	Khimti-1 hydro adit-1 d/s 580	STC	26	3.0	3.0
46.	Khimti-1 hydro adit-1 d/s 665	Augen gneiss; schist	26	3.0	3.0
47.	Khimti-1 hydro adit-2 d/s 441	Augen gneiss	26	3.4	3.4
48.	Khimti-1 hydro adit-2 d/s 601	STS	26	3.7	3.7
49.	Khimti-1 hydro adit-2 d/s 895	Gneiss, Chlorite Schist	26	5.3	5.3
50.	Khimti-1 hydro adit-2 u/s 1357	Banded gneiss, CS	26	7.0	7.0
51.	Khimti-1 hydro adit-2 u/s 1730	AG with clay gauge	26	2.6	2.6
52.	Khimti-1 hydro adit-3 u/s 15	Shear bands of AG & S	26	3.5	3.5
53.	Khimti-1 hydro adit-3 u/s 59	Augen gneiss and schist	26	4.3	4.3
54.	Khimti-1 hydro adit-3 u/s 200	Augen gneiss	26	7.5	7.5
55.	Khimti-1 hydro adit-3 u/s 210	Schist	26	7.5	7.5
56.	Khimti-1 hydro adit-3 d/s 220	Augen gneiss, SS	26	3.8	3.8
57.	Khimti-1 hydro adit-3 u/s 345	GG, STS	26	8.1	8.1
58.	Khimti-1 hydro adit-4 u/s 503	CSS	26	6.1	6.1
59.	Khimti-1 hydro adit-4 u/s 550	Banded gneiss	26	5.9	5.9
60.	Khimti-1 hydro adit-4 u/s 852	BGS	26	3.1	3.1
61.	Khimti-1 hydro adit-4 u/s 876	Sheared augen gneiss	26	3.1	3.1
62.	Khimti-1 hydro adit-4 u/s 974	Sheared augen gneiss	26	3.0	3.0
63.	Khimti-1 hydro adit-4 u/s 1045		26	3.0	3.0

<u>Notation:</u> References of the respective tunnels are as given in Table 5.1.

Table 5.3 Data related to Tunnel Size, Support Systems, Advance Rate, Tunnelling Method and Water Pressure etc. Collected from Various Case Study Projects

S. No.	Name of HEP or Road Tunnels/ Adits (radius)	Types of Support	Advance Rate per Month	Adjacent Geologic Structure	Tunnelling Method	Water Pressure, (MPa)
1	Maneri Stage-I (2.9 m)	Indian Standard Medium weight Beams (ISMB) 150 mm x 150 mm (31.5kg/m) at 0.8-1.0m spacing c.c.	30-38m	Main Central Thrust in North & North-East and Almora Thrust in South of the project area; Presence of fault and folds along tunnel alignment	Heading & bench; D&B	< 0.1
2	Maneri Stage-II (3.5 m)	Steel ribs (250 mm x 250 mm) at 1m spacing c.c.	25-30 m	One Srinagar -thrust and many localised faults passing through the tunnel alignment	Heading & bench; D&B	< 0.1
3	Maneri Stage-II (1.25 m)	Steel ribs (100 mm x 100 mm) at 1.5 m spacing c.c.	28-32 m	One Srinagar-thrust and two faults passing through the tunnel alignment	Full face; D&B	< 0.1
4	Giri-Bata (2.3)	RSJ Steel ribs (150 mm x 150 mm, 31.5kg/m) at 0.50m spacing c.c.	22-30 m	Three thrusts, locally known as Renuka, Krol and Nahan in close proximity of the tunnel; Two faults across the tunnel alignment	Full face; D&B	< 0.1
5	Chhibro-Khodri (4.5 m)	RSJ Steel ribs of 300 mm x 140 mm sections at spacing of 0.25-0.50 m	28m; (5-6 m in intra thrust zone)	Two thrusts (Krol and Nahan) in close proximity of the tunnel; Three faults across the tunnel alignment	Heading & bench; D&B	< 0.1
6	Chhibro-Khodri (1.5 m)	RSJ Steel ribs (150mm x 150mm, 31.5 kg/m) at spacing of 1m	37-49 m; (20 m in intra thrust zone)	-do-	Full face; D&B	< 0.1
7	Noonidih-Jitpur Colliery (3.5 m)	Indian Standard Medium weight Beams (ISMB) 150 mm x 150 mm (31.5 kg/m) at 0.5 m spacing c.c.	34 m	Coal seam sandwiched between shales bands	Heading & bench; D&B	0
8	Tala (3.4 m)	steel ribs (ISMB 200 or SMB 250 at 0.5m spacing c.c.), 5-6m long rock bolts of 25 mm diameter at 2 m spacing; 175mm steel fibre shotcrete (SFRS)	32-40 m	Weathered biotite schist associated with banded gneiss, amphibolites and quartzites in thin bands	Heading & bench; D&B	< 0.1

Contd…

9	Kaligandaki 'A' (4.35 m)	Steel ribs at 1m spacing c.c.; SFRS: 20-25cm.	-------	Main Boundary Thrust (MBT), shear zones	Heading & bench; D&B	0
10	Khimti-1 adit-1 d/s 475; adit-2 d/s 895; adit-2 u/s 1357, 1730; adit-4 u/s 550, 1045 (2 m)	Bolts in pattern 1.0 x 1.2 m. SFRS: 15 cm at crown and 10 cm on wall. Spilling at 0.4 m c.c in crown and 1 m in walls. Spilling length 4 m.	80-90 m	Midland Thrust to the South and Jiri Thrust to the North	Full face; D&B	<0.1
11	Khimti-1 Hydro adit-2 d/s 441, 665 (2 m); adit-3 u/s 15 (2.5 m), 59 (2.05 m), 200, 210 (2.5 m); adit-4 u/s 503, 852, 876 (2 m)	Bolts in pattern 1.0 x 1.5 m. SFRS: 10 cm at crown and 5 cm on wall. Spilling c.c. 0.5 m in crown. Spilling length 4 m.	80-90 m	-do-	Full face; D&B	< 0.1
12	Khimti-1 Hydro adit-1 d/s 580 (2.15 m), 601 (2 m); adit-3 d/s 220 (2 m); adit-3 u/s 345 (2.5 m); adit-4 u/s 974 (2 m)	Bolts in pattern 1 x 1 m; 20 cm thick SFRS. Spilling at 0.3 m c.c. in crown and 0.7 m c.c. in walls. Spilling length 3 m.	80-90 m	-do-	Full face; D&B	< 0.1

<u>Note:</u> References of the respective tunnels are as given in Table 5.1.

5.4 DEVELOPMENT OF EMPIRICAL CORRELATIONS

5.4.1 Correlations using Joint Factor, J_f

Based on the study and analysis of the data presented in art. 5.3 above, an attempt has made to develop dimensionally correct (same dimension of units on both sides of the equations) empirical correlations using non-linear regression analysis. Several trials were conducted to arrive at the dimensionally correct correlations (Eqs. 5.7-5.9) for predicting the tunnel deformation for tunnels excavated in squeezing ground conditions.

The concept of joint factor has been used in the process of this development. Correlation represented by Eq.5.7 has been developed from the plot of $\boldsymbol{u_{obs}/a}$ versus $\boldsymbol{J_f^3.\sigma_v/K}$ which is presented in Fig. 5.1. It can be observed from this plot that the tunnel strain (u_{obs}/a) increases with increase in tunnel depth or with increase in vertical in-situ stress, σ_v . Tunnel strain has been found to increase with reduction in rock mass quality or increase in the value of joint factor, J_f. On the other hand, the tunnel strain decreases with increase in stiffness (K) of the supports. That is why σ_v and J_f are in the numerator and K is in denominator in the expression: $\boldsymbol{J_f^3.\sigma_v/K}$, which has been plotted as an abscissa in Fig. 5.1. Therefore, the observed tunnel strain follows the relation given by Eq. 5.7 with a correlation coefficient of 94 %.

$$\frac{u_p}{a} = \frac{7*10^{-10} J_f{}^3 \sigma_v}{K} + 0.0062 \qquad R^2 = 0.94 \qquad (5.7)$$

where u_p is the predicted radial tunnel deformation (m); a , the tunnel radius (m); J_f , the joint factor (dimensionless); σ_v , the vertical in-situ stress (= γH, H being the tunnel depth) expressed in MPa; and K represents the support stiffness (MPa).

Later, it was realised that the above correlation (Eq. 5.7) becomes insignificant for the case of unsupported tunnels, i.e. when K=0. Due to this reason, another correlation (Eq. 5.8) was developed, which can predict the tunnel strain for the unsupported condition i.e. when K= 0. This correlation has been developed based on the plot of $\boldsymbol{(J_f^3.\sigma_v/(2K+1))}$ plotted as an abscissa versus $\boldsymbol{(u_{obs}/a)}$ plotted as an ordinate and is presented in Fig. 5.2. For the abscissa, the expression in the denominator has been obtained by replacing (K) in Eq. 5.7 with $(K+0.5)$ in the Eq. 5.8. The corresponding correlation which has been proposed with a correlation coefficient of 94 % is given by -

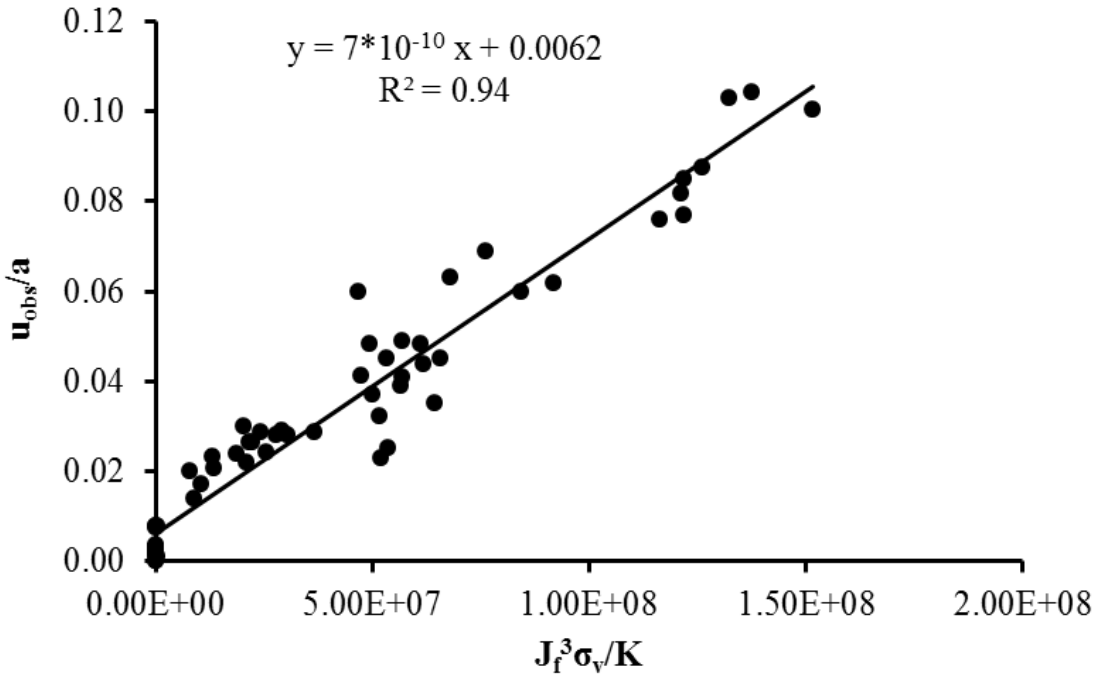

Fig. 5.1 Plot of (u_{obs}/a) versus ($J_f^3\sigma_v/K$) for Squeezing Ground

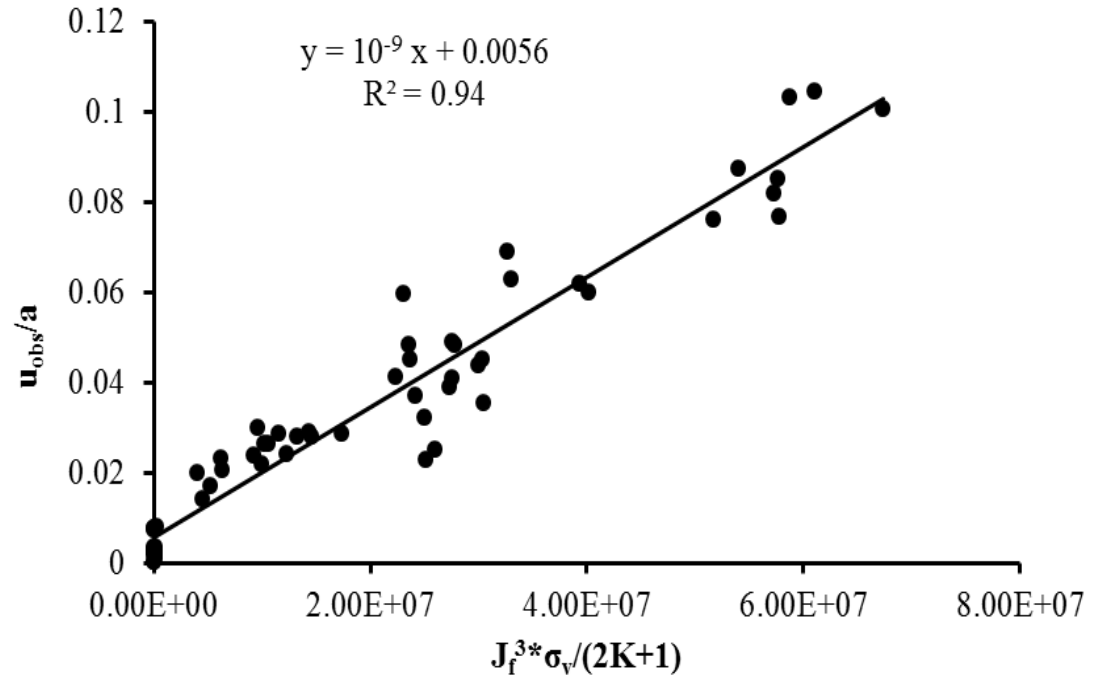

Fig. 5.2 Plot of (u_{obs}/a) versus ($J_f^3\sigma_v/(2K+1)$) for Squeezing Ground

$$\frac{u_p}{a} = \frac{5*10^{-10} J_f{}^3 \sigma_v}{K + 0.5} + 0.0056 \qquad R^2 = 0.94 \qquad (5.8)$$

To study the effect of parameters, namely the horizontal in-situ stress, σ_h and the uniaxial compressive strength of intact rock material, σ_{ci}, correlation represented by Eq. 5.9 has been developed based on the plot of (u_{obs}/a) versus $(J_f^3.\sigma_v/(K+\sigma_{ci}/\sigma_h))$ which is presented in Fig. 5.3. In the expression on X-axis, σ_{ci} has been taken in the denominator and σ_{ci} has been included in such a way so as to give the effect as its presence in the numerator. It is because, tunnel deformation increases with reduction in the value of σ_{ci} and with increase in σ_h value.

$$\frac{u_p}{a} = 10^{-10}\left(-6*10^{-9} J^2 + 9J\right) + 0.0069 \qquad R^2 = 0.94 \qquad (5.9)$$

where σ_{ci} is the uniaxial compressive strength of intact rock, MPa; σ_h, the horizontal in-situ stress, MPa, and

$$J = \frac{\sigma_v J_f{}^3}{K + \frac{\sigma_{ci}}{\sigma_h}} \qquad (5.9a)$$

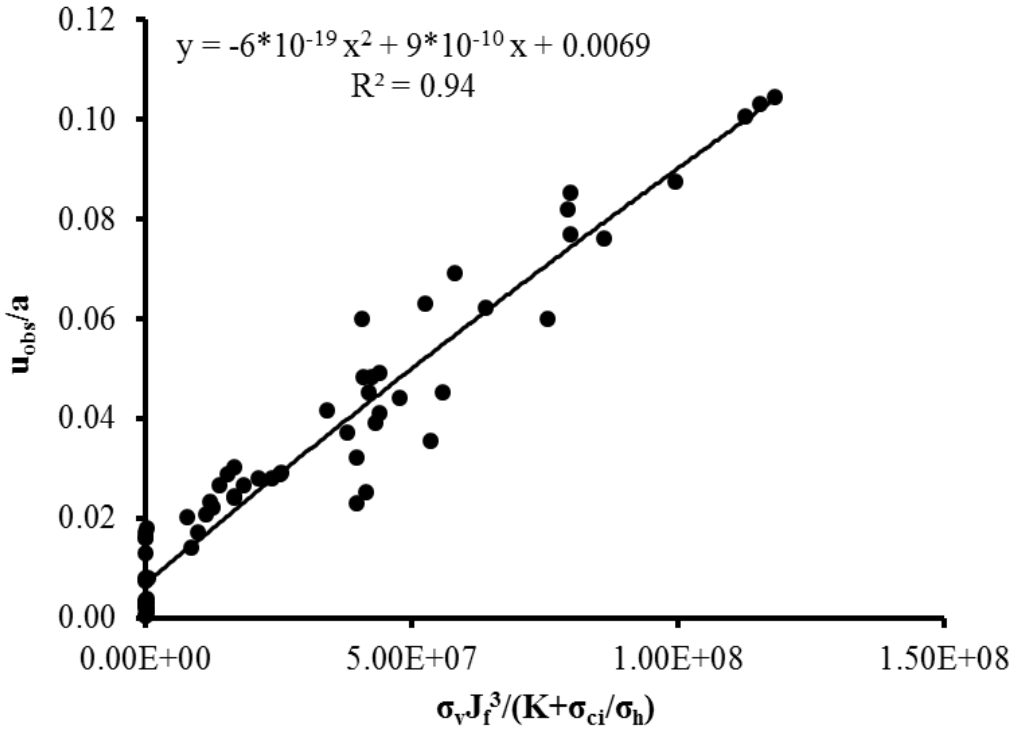

Fig. 5.3 Plot of (u_{obs}/a) versus $(\sigma_v J_f^3/(K+\sigma_{ci}/\sigma_h))$ for Squeezing Ground

Equation 5.10 has been developed based on the plot of **(u_{obs}/a)** versus **($a^{0.1}.J_f^3.\sigma_v/(K+\sigma_{ci}/\sigma_h)$)** which is presented Fig. 5.4 so as to include the effect of tunnel radius (*a*). This parameter has been kept in the numerator in the expression plotted as abscissa because the tunnel deformation increases with increase in tunnel radius.

$$\frac{u_p}{a} = 8*10^{-10} a^{0.1} J + 0.0072 \qquad R^2 = 0.94 \qquad (5.10)$$

After realising the insignificant effect of tunnel radius (art. 5.4.1), the correlation represented by Eq. 5.9 for predicting tunnel deformation has been proposed for use in field as well as in design.

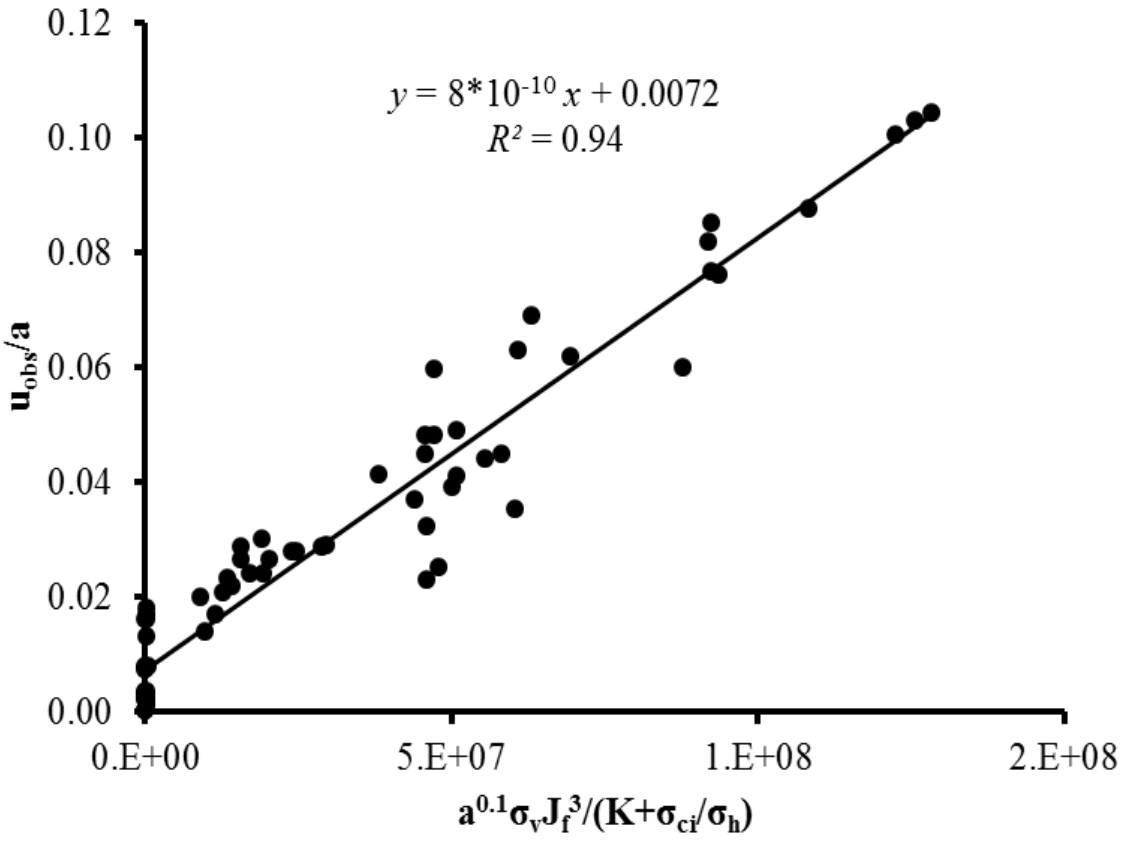

Fig. 5.4 Plot of (u_{obs}/a) versus ($a^{0.1}\sigma_v J_f^3/(K+\sigma_{ci}/\sigma_h)$) for Squeezing Ground

5.4.2 Correlations using Rock Mass Quality, *Q*

Dimensionally correct correlation represented by Eq. 5.11 has been developed by plotting (u_{obs}/a) versus ($\sigma_v / Q^{0.33}.K$) in Fig. 5.5. Unlike the joint factor (J_f), rock mass quality, Q is in denominator here in the expression along the abscissa. This is due to the fact that tunnel deformation increases with deterioration in Q-value or the rock mass quality, whereas tunnel deformation increases with increase in value of J_f. Other parameters have been taken in an appropriate order in the expression plotted as abscissa for the reason similar to the case of Fig. 5.1. The best fit line corresponds to the correlation coefficient of 92 %.

$$\frac{u}{a} = \frac{0.0097\sigma_v}{Q^{0.33}K} + 0.0067 \qquad R^2 = 0.92 \qquad (5.11)$$

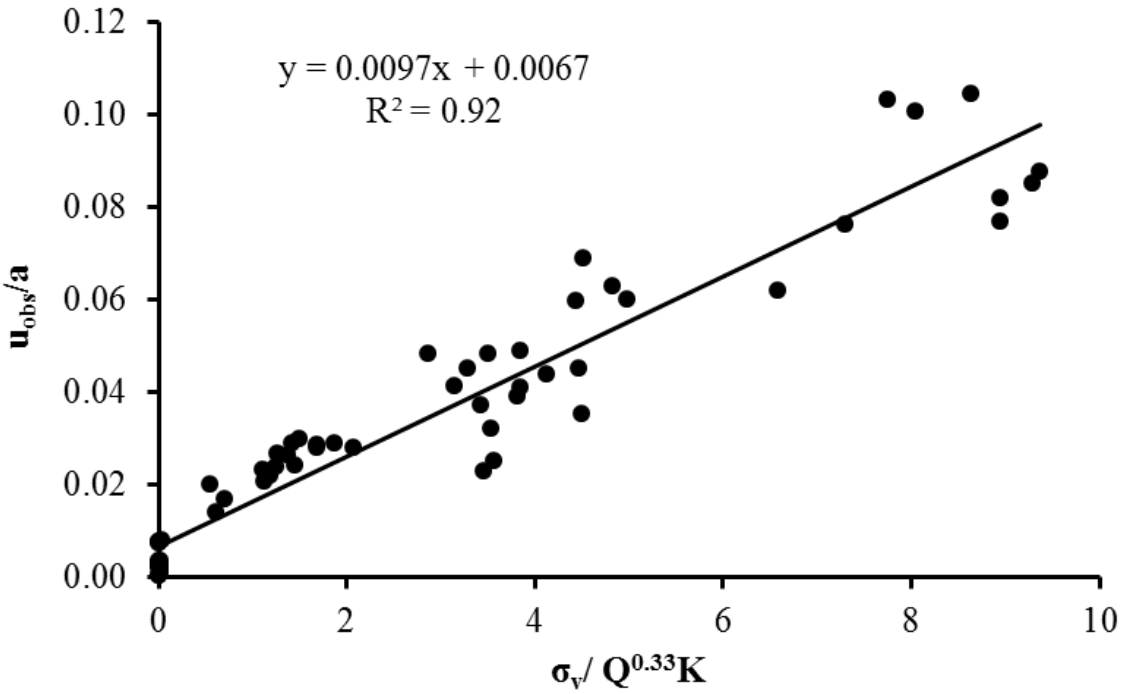

Fig. 5.5 Plot of (u_{obs}/a) versus ($\sigma_v / Q^{0.33}K$) for Squeezing Ground

For the case of an unsupported tunnel, i.e. when $K = 0.$, Eq. 5.12 has been developed with a correlation coefficient of 92 %. It is represented in the plot of (u_{obs}/a) versus (σ_v / $\{Q^{0.2}(K+1)\}$) in Fig. 5.6.

$$\frac{u_p}{a} = \frac{0.0194\sigma_v}{Q^{0.2}(K+1)} + 0.0031 \qquad R^2 = 0.92 \qquad (5.12)$$

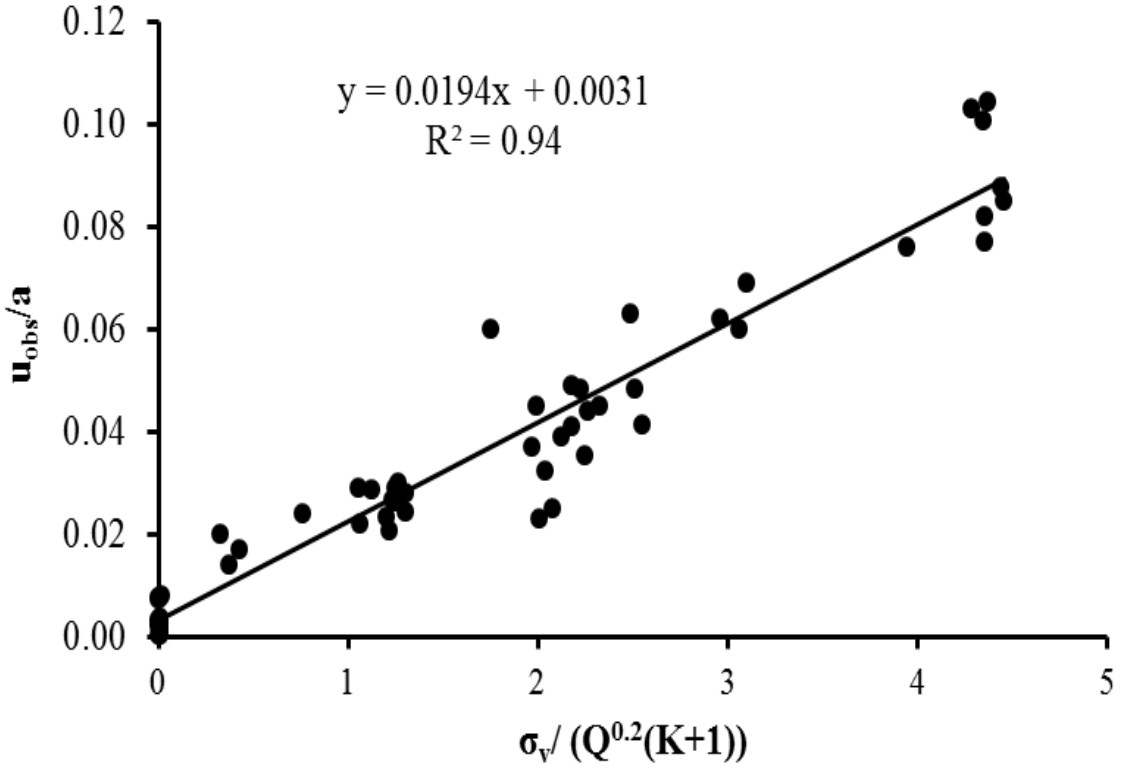

Fig. 5.6 Plot of (u_{obs}/a) versus ($\sigma_v / Q^{0.2} (K+1)$) for Squeezing Ground

Further, correlation given by Eq. 5.13 has been developed to study the influence of σ_{ci} and σ_h. The corresponding variation is shown in Fig. 5.7 which is a plot of (u_{obs}/a) versus $(\sigma_v / \{Q^{0.2}(K+\sigma_{ci}/\sigma_h)\})$ in Fig. 5.7. The best line fit gives a correlation coefficient of 93%.

$$\frac{u_p}{a} = 10^{-4}\left(-2U^3 + 11U^2 + 187U + 61\right) \qquad R^2 = 0.93 \qquad (5.13)$$

where

$$U = \frac{\sigma_v}{Q^{0.2}\left(K + \frac{\sigma_{ci}}{\sigma_h}\right)} \qquad (5.13a)$$

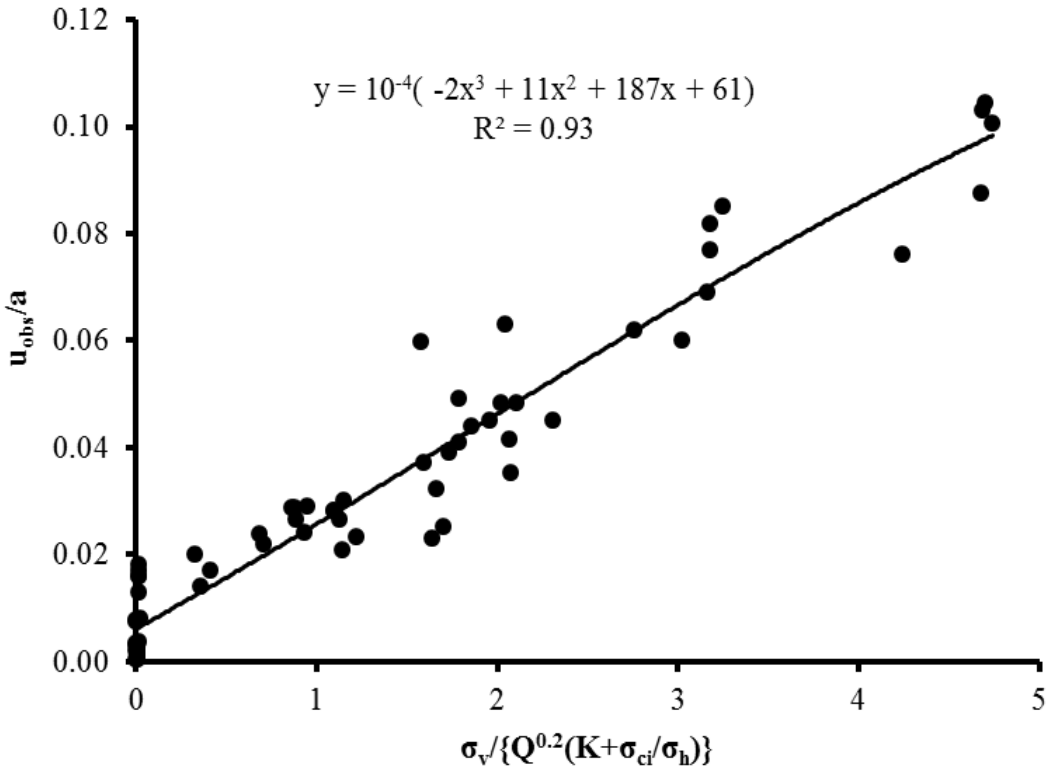

Fig. 5.7 Plot of (u_{obs}/a) versus ($\sigma_v / Q^{0.2}(K+ \sigma_{ci}/ \sigma_h)$) for Squeezing Ground

5.4.3 Correlations using Rock Mass Number, *N*

As it is difficult to obtain the value of stress reduction factor, SRF in the field, it is always convenient to work with rock mass number, N in which case SRF is treated as unity. Dimensionally correct correlation represented by Eq. 5.14 has been developed on basis of the plot of **(u_{obs}/a)** versus **($\sigma_v / (N^{0.33}K)$)** shown in Fig. 5.8. In the expression on the X-axis, *N* has been taken in the denominator in the same way as *Q* in the plots given in Figs. 5.5-5.7. The best line fit gives a correlation coefficient of 93%.

$$\frac{u_p}{a} = \frac{0.0201\sigma_v}{N^{0.33}K} + 0.0065 \qquad R^2 = 0.93 \qquad (5.14)$$

Similarly, correlation given in Eq. 5.15 has been developed to include the significance of the case of unsupported tunnel, i.e. when $K = 0$. The plot of **(u_{obs}/a)** versus **($\sigma_v / \{N^{0.33}(K+1)\}$)** in Fig. 5.9 shows the best line fit with a correlation coefficient of 94%.

$$\frac{u_p}{a} = \frac{0.0447\sigma_v}{N^{0.33}(K+1)} + 0.0057 \qquad R^2 = 0.94 \qquad (5.15)$$

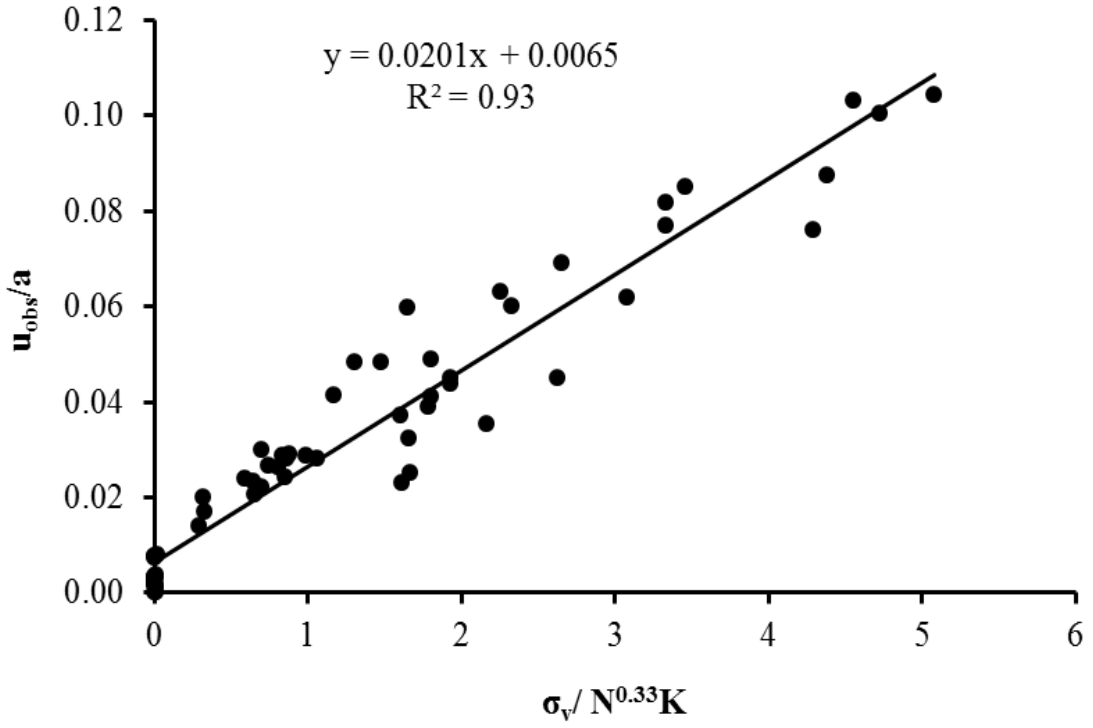

Fig. 5.8 Plot of (u_{obs}/a) versus ($\sigma_v / N^{0.33} K$) for Squeezing Ground

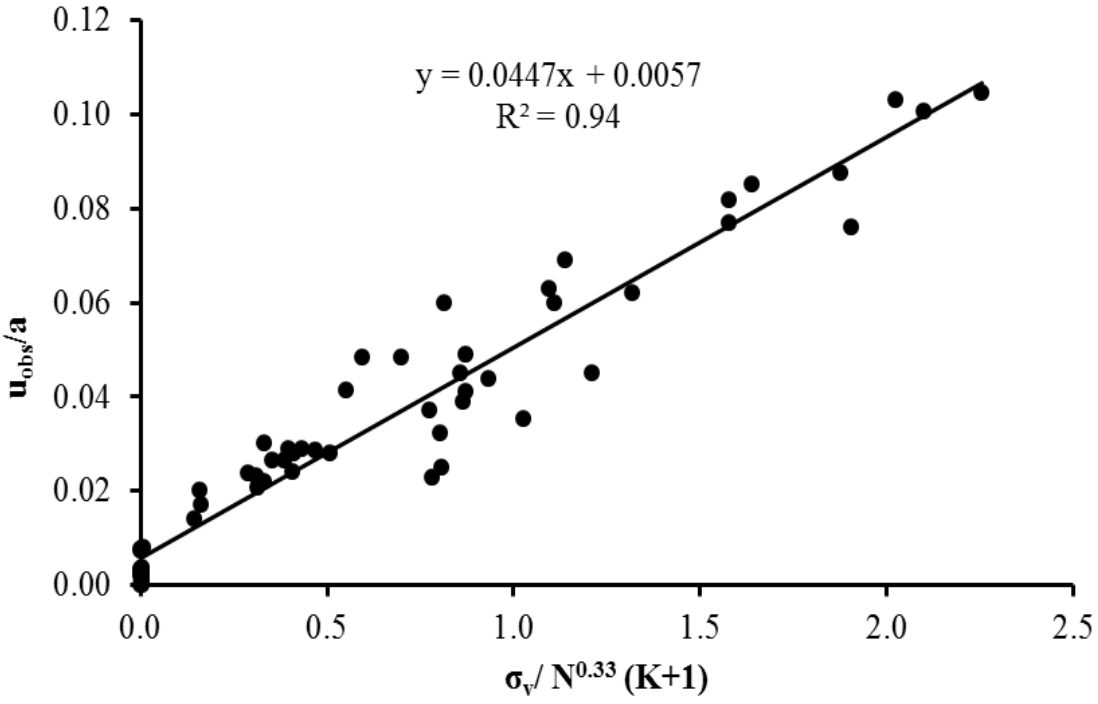

Fig. 5.9 Plot of (u_{obs}/a) versus ($\sigma_v / N^{0.33}(K+1)$) for Squeezing Ground

5.5 COMPARISON OF PREDICTED AND OBSERVED TUNNEL DEFORMATIONS

An attempt has been made here to compare the observed values of tunnel deformations, (u_{obs}/a) in the squeezing ground condition at 63 tunnel sections from various project sites (Table 5.1) with the values of tunnel deformations predicted $(u/a)_p$ on the basis of empirical correlations developed (Eqs. 5.7 – 5.15) in art. 5.4. The values of tunnel deformations thus predicted on basis of correlations given by Eqs. 5.7 to 5.15 are presented in Table 5.4. Observed values of tunnel deformations at various tunnel sections of different project sites are also presented in Column-2 of Table 5.4. The row numbers, 1-63 of Table 5.4 correspond to the row numbers 1-63 of Table 5.1 indicting the correspondence of various tunnel sections at different project sites. Such a comparison of the observed and the predicted values of tunnel deformations is made in Figs. 10 a, b, c & d.

Comparison of the predicted values (Eqs. 5.7-5.15) has also been made with values of tunnel deformation predicted on basis of an empirical correlation (Eq. 5.16) given for the purpose by Goel et. al. (1994)

$$\frac{u_p}{a} = \frac{a^{0.12} H^{0.81}}{10.5 N^{0.27} K^{0.62}} \tag{5.16}$$

The last column of Table 5.4 gives values of tunnel deformations predicted on basis of Eq. 5.16.

An index called as the Coefficient of Accordance (COA) has also been computed for values of deformation predicted on basis of various correlations (Eqs. 5.7-5.16). COA (ψ^2) is defined as follows:

$$\psi^2 = \frac{\Sigma\left((u_{obs}/a) - (u_p/a)\right)^2}{\Sigma\left((u_{obs}/a) - \dfrac{\Sigma(u_p/a)}{n}\right)^2} \tag{5.17}$$

where ψ^2 is COA and n is number of data sets. Lower value of COA indicates a better correlation.

The calculated values of ψ^2 are presented in the last row of Table 5.4. It has been found from Table 5.4 that the value of ψ^2 is the lowest (= 0.054) for the correlation (Eq. 5.9) developed using additional parameters, σ_{ci} and σ_h .

Table 5.4 Comparison of Predicted and Observed Strain Levels at Different Tunnel Sections

S. No.	$(u/a)_{obs}$	$(u/a)_p$ Eq. 5.7	$(u/a)_p$ Eq.5.8	$(u/a)_p$ Eq.5.9	$(u/a)_p$ Eq.5.10	$(u/a)_p$ Eq.5.11	$(u/a)_p$ Eq.5.12	$(u/a)_p$ Eq.5.13	$(u/a)_p$ Eq.5.14	$(u/a)_p$ Eq.5.15	$(u/a)_p$ Eq.5.16
1.	0.0287	0.0277	0.0230	0.0292	0.0303	0.0226	0.0250	0.0229	0.0256	0.0267	0.0316
2.	0.0280	0.0224	0.0189	0.0256	0.0265	0.0226	0.0284	0.0277	0.0231	0.0241	0.0283
3	0.0219	0.0183	0.0156	0.0181	0.0187	0.0181	0.0238	0.0198	0.0199	0.0206	0.0238
4	0.0288	0.0202	0.0171	0.0205	0.0198	0.0201	0.0274	0.0232	0.0225	0.0234	0.0242
5	0.0264	0.0186	0.0158	0.0192	0.0198	0.0198	0.0274	0.0235	0.0221	0.0229	0.0267
6	0.0242	0.0211	0.0179	0.0217	0.0209	0.0205	0.0284	0.0244	0.0230	0.0240	0.0248
7	0.0450	0.0378	0.0294	0.0432	0.0438	0.0373	0.0418	0.0455	0.0442	0.0440	0.0435
8	0.1004	0.0966	0.0729	0.0981	0.1052	0.0811	0.0875	0.0982	0.0992	0.0996	0.0901
9	0.1030	0.0851	0.0644	0.1001	0.1077	0.0783	0.0864	0.0974	0.0958	0.0961	0.0873
10	0.1043	0.0882	0.0667	0.1020	0.1100	0.0865	0.0879	0.0976	0.1061	0.1065	0.0956
11	0.0761	0.0755	0.0573	0.0888	0.0821	0.0742	0.0797	0.0901	0.0906	0.0908	0.0833
12	0.0620	0.0608	0.0449	0.0611	0.0628	0.0677	0.0607	0.0619	0.0668	0.0647	0.0604
13	0.0875	0.0815	0.0597	0.0885	0.0938	0.0933	0.0893	0.0973	0.0924	0.0895	0.0802
14	0.0689	0.0514	0.0382	0.0564	0.0577	0.0487	0.0633	0.0699	0.0585	0.0566	0.0532
15	0.0280	0.0241	0.0202	0.0278	0.0271	0.0262	0.0278	0.0276	0.0271	0.0284	0.0304
16	0.0450	0.0452	0.0360	0.0546	0.0538	0.0482	0.0483	0.0527	0.0579	0.0599	0.0576
17	0.0600	0.0563	0.0458	0.0703	0.0775	0.0530	0.0626	0.0672	0.0520	0.0553	0.0654
18	0.0200	0.0105	0.0096	0.0139	0.0146	0.0121	0.0094	0.0123	0.0125	0.0128	0.0179
19	0.0483	0.0354	0.0291	0.0436	0.0450	0.0335	0.0463	0.0485	0.0351	0.0371	0.0426
20	0.0266	0.0191	0.0162	0.0231	0.0236	0.0188	0.0271	0.0283	0.0208	0.0216	0.0244

.....Contd.

S. No.	u_{obs}/a	u_p/a Eq. 5.7	u_p/a Eq.5.8	u_p/a Eq.5.9	u_p/a Eq.5.10	u_p/a Eq.5.11	u_p/a Eq.5.12	u_p/a Eq.5.13	u_p/a Eq.5.14	u_p/a Eq.5.15	u/a Eq.5.16
21	0.0233	0.0136	0.0119	0.0176	0.0180	0.0173	0.0264	0.0302	0.0189	0.0195	0.0218
22	0.0207	0.0138	0.0120	0.0170	0.0174	0.0174	0.0268	0.0287	0.0191	0.0197	0.0220
23	0.0483	0.0424	0.0334	0.0424	0.0438	0.0394	0.0519	0.0468	0.0318	0.0323	0.0339
24	0.0414	0.0343	0.0280	0.0367	0.0377	0.0360	0.0527	0.0477	0.0291	0.0303	0.0339
25	0.0300	0.0179	0.0153	0.0217	0.0225	0.0209	0.0276	0.0289	0.0199	0.0206	0.0237
26	0.0400	0.0444	0.0361	0.0527	0.0556	0.0484	0.0467	0.0479	0.0488	0.0516	0.0588
27	0.0290	0.0232	0.0200	0.0293	0.0309	0.0244	0.0236	0.0248	0.0234	0.0250	0.0453
28	0.0140	0.0111	0.0101	0.0145	0.0152	0.0128	0.0104	0.0130	0.0118	0.0121	0.0222
29	0.0230	0.0368	0.0307	0.0413	0.0441	0.0389	0.0421	0.0388	0.0379	0.0407	0.0639
30	0.0400	0.0396	0.0330	0.0443	0.0474	0.0422	0.0444	0.0409	0.0412	0.0443	0.0694
31	0.0322	0.0367	0.0306	0.0412	0.0439	0.0397	0.0427	0.0394	0.0387	0.0416	0.0645
32	0.0490	0.0399	0.0332	0.0448	0.0479	0.0425	0.0453	0.0419	0.0416	0.0447	0.0519
33	0.0851	0.0788	0.0633	0.0736	0.0812	0.0926	0.0896	0.0717	0.0742	0.0789	0.0881
34	0.0768	0.0789	0.0633	0.0736	0.0812	0.0895	0.0877	0.0702	0.0717	0.0762	0.0854
35	0.0630	0.0465	0.0386	0.0519	0.0559	0.0515	0.0515	0.0473	0.0506	0.0546	0.0578
36	0.0818	0.0783	0.0629	0.0731	0.0807	0.0895	0.0877	0.0702	0.0717	0.0762	0.0854
37	0.0439	0.0429	0.0356	0.0481	0.0516	0.0450	0.0470	0.0434	0.0441	0.0475	0.0508
38	0.0409	0.0399	0.0332	0.0448	0.0479	0.0425	0.0453	0.0419	0.0416	0.0447	0.0698
39	0.0251	0.0379	0.0316	0.0427	0.0456	0.0399	0.0434	0.0402	0.0390	0.0419	0.0452
40	0.0370	0.0357	0.0298	0.0399	0.0424	0.0386	0.0414	0.0379	0.0377	0.0404	0.0635
41	0.0170	0.0121	0.0109	0.0157	0.0164	0.0136	0.0115	0.0140	0.0126	0.0131	0.0238

.....Contd.

S. No.	u_{obs}/a	u_p/a Eq. 5.7	u_p/a Eq.5.8	u_p/a Eq.5.9	u_p/a Eq.5.10	u_p/a Eq.5.11	u_p/a Eq.5.12	u_p/a Eq.5.13	u_p/a Eq.5.14	u_p/a Eq.5.15	u_p/a Eq.5.16
42	0.0598	0.0663	0.0287	0.0422	0.0451	0.0951	0.0372	0.0375	0.0762	0.0421	0.0914
43	0.0239	0.0342	0.0149	0.0216	0.0227	0.0362	0.0178	0.0194	0.0353	0.0187	0.0336
44	0.0078	0.0058	0.0057	0.0069	0.0073	0.0072	0.0032	0.0062	0.0062	0.0058	0.0008
45	0.0074	0.0058	0.0057	0.0069	0.0073	0.0072	0.0032	0.0062	0.0062	0.0058	0.0009
46	0.0030	0.0059	0.0057	0.0070	0.0074	0.0073	0.0033	0.0063	0.0063	0.0059	0.0013
47	0.0003	0.0058	0.0057	0.0070	0.0074	0.0072	0.0033	0.0063	0.0063	0.0059	0.0014
48	0.0020	0.0058	0.0057	0.0069	0.0073	0.0072	0.0032	0.0062	0.0062	0.0058	0.0008
49	0.0030	0.0058	0.0057	0.0070	0.0074	0.0072	0.0033	0.0063	0.0062	0.0058	0.0009
50	0.0015	0.0059	0.0057	0.0070	0.0074	0.0073	0.0033	0.0063	0.0063	0.0059	0.0017
51	0.0030	0.0058	0.0057	0.0069	0.0073	0.0072	0.0032	0.0062	0.0062	0.0058	0.0007
52	0.0034	0.0058	0.0057	0.0069	0.0073	0.0072	0.0032	0.0062	0.0062	0.0058	0.0007
53	0.0032	0.0058	0.0057	0.0070	0.0073	0.0072	0.0033	0.0063	0.0063	0.0059	0.0013
54	0.0078	0.0058	0.0057	0.0070	0.0074	0.0072	0.0033	0.0063	0.0062	0.0059	0.0013
55	0.0036	0.0059	0.0057	0.0071	0.0075	0.0073	0.0034	0.0064	0.0063	0.0059	0.0016
56	0.0080	0.0060	0.0059	0.0073	0.0077	0.0075	0.0035	0.0065	0.0065	0.0061	0.0025
57	0.0018	0.0058	0.0057	0.0070	0.0074	0.0072	0.0033	0.0063	0.0063	0.0059	0.0016
58	0.0025	0.0058	0.0057	0.0069	0.0073	0.0072	0.0032	0.0062	0.0062	0.0058	0.0009
59	0.0015	0.0059	0.0057	0.0071	0.0075	0.0073	0.0034	0.0064	0.0063	0.0059	0.0014
60	0.0003	0.0058	0.0057	0.0069	0.0073	0.0072	0.0032	0.0062	0.0062	0.0058	0.0008
61	0.0025	0.0058	0.0057	0.0069	0.0073	0.0072	0.0032	0.0062	0.0062	0.0058	0.0008
62	0.0020	0.0058	0.0057	0.0070	0.0074	0.0072	0.0033	0.0063	0.0062	0.0059	0.0013
63	0.0010	0.0059	0.0058	0.0071	0.0075	0.0073	0.0033	0.0063	0.0063	0.0060	0.0018
ψ2		**0.061**	**0.234**	**0.054**	**0.062**	**0.109**	**0.060**	**0.056**	**0.064**	**0.060**	**0.176**

Figure 5.10a gives comparison of values of tunnel deformation predicted on basis of Eqs. 5.7, 5.8, 5.9 and 5.10 with those obtained from correlation given by Eq. 5.16 (Goel et al. ,1994). Similarly, Fig. 5.10b shows the comparison of values of tunnel deformation predicted on basis of Eqs. 5.11, 5.12 and 5.13 with those predicted from correlation Eq. 5.16 (Goel et al. ,1994). Also, the predictions based on Eqs. 5.14 and 5.15 are compared with those of Eq. 5.16 in Fig. 5.10c. Finally, Fig. 5.10d gives the comparison of all the predictions of tunnel deformation based on all the empirical correlations developed (Eqs. 5.7-5.15) with those by Eq. 5.16 (Goel et. al., 1994).

It can also be seen in the Fig. 5.10 (a-d) that the values of tunnel strain predicted by Eq. 5.9 are closest to AB line (1:1 line) as compared to the values predicted by other respective correlations**. This indicates that the correlation (Eq. 5.9) with least COA value 0.054 fits best with the observed values and is the best among all the correlations.** Moreover, correlation given Eq. 5.13 which was developed on basis of Q-values, σ_{ci} and σ_h and having COA value equal to 0.056 is the second best after Eq. 5.9.

For unsupported tunnel sections, support stiffness, K is equal to zero. In this respect, the correlations defined by Eqs. 5.7, 5.11, 5.14 & 5.16 do not offer any significant value of deformation of unsupported tunnel, when $K = 0$ is substituted. On the other hand, Eqs. 5.8, 5.9, 5.10, 5.12, 5.13 and 5.15 predict realistic values of deformations of unsupported tunnels, if support stiffness, $K = 0$ is substituted.

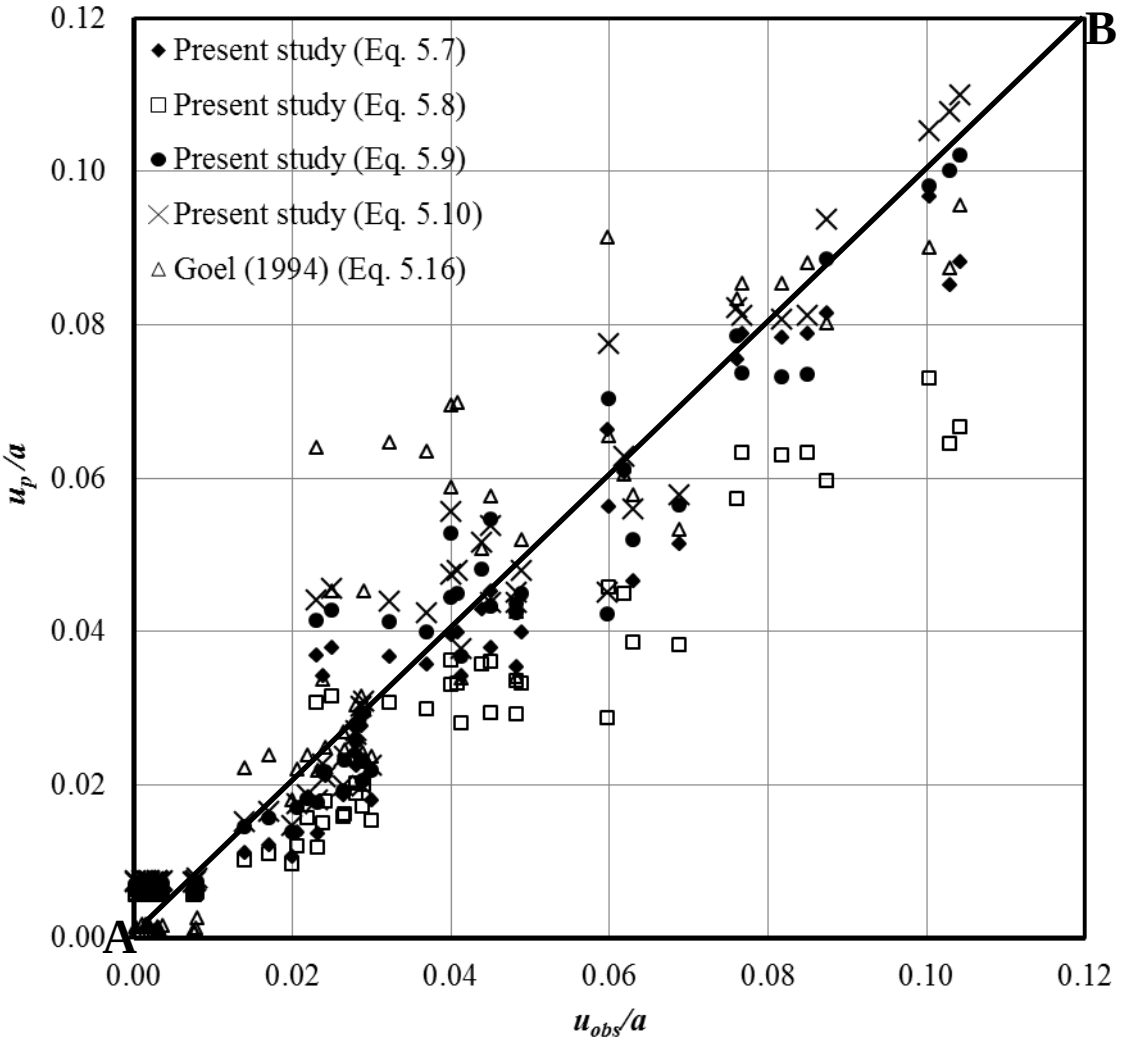

Fig. 5.10a Comparison of Predicted Values of Tunnel Strain with Goel (1994)

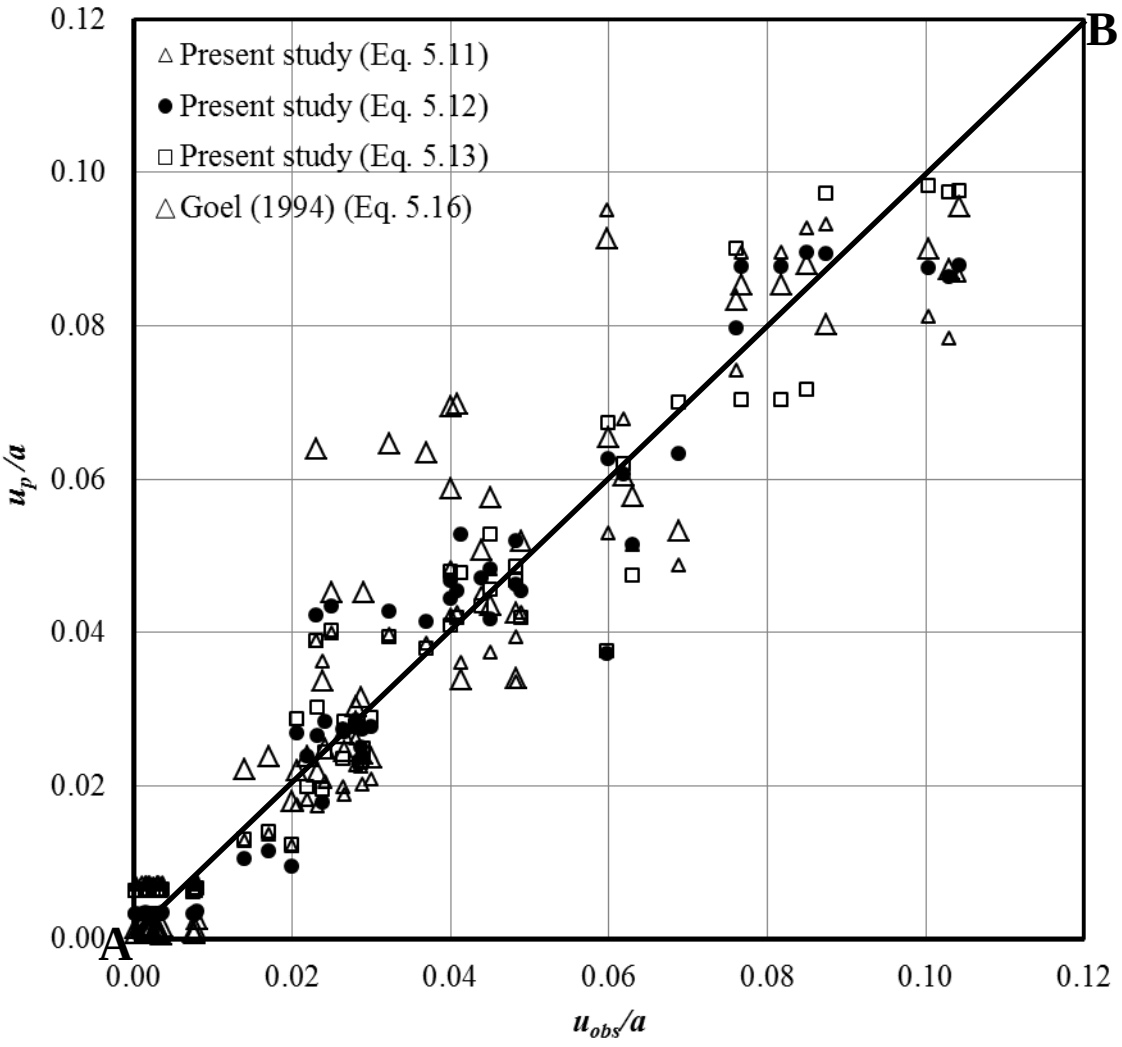

Fig. 5.10b Comparison of Predicted Values of Tunnel Strain with Goel (1994)

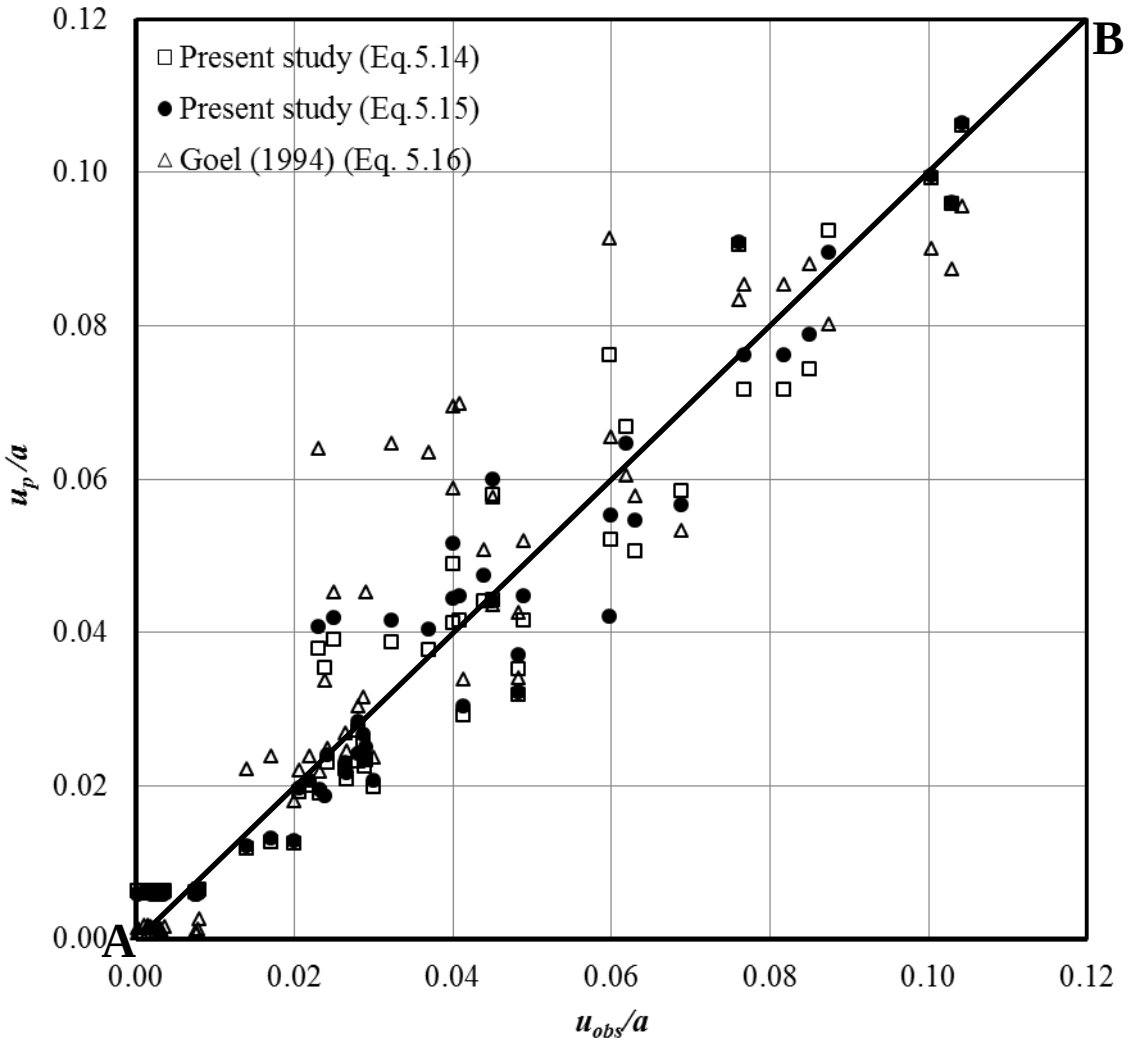

Fig. 5.10c Comparison of Predicted Values of Tunnel Strain with Goel (1994)

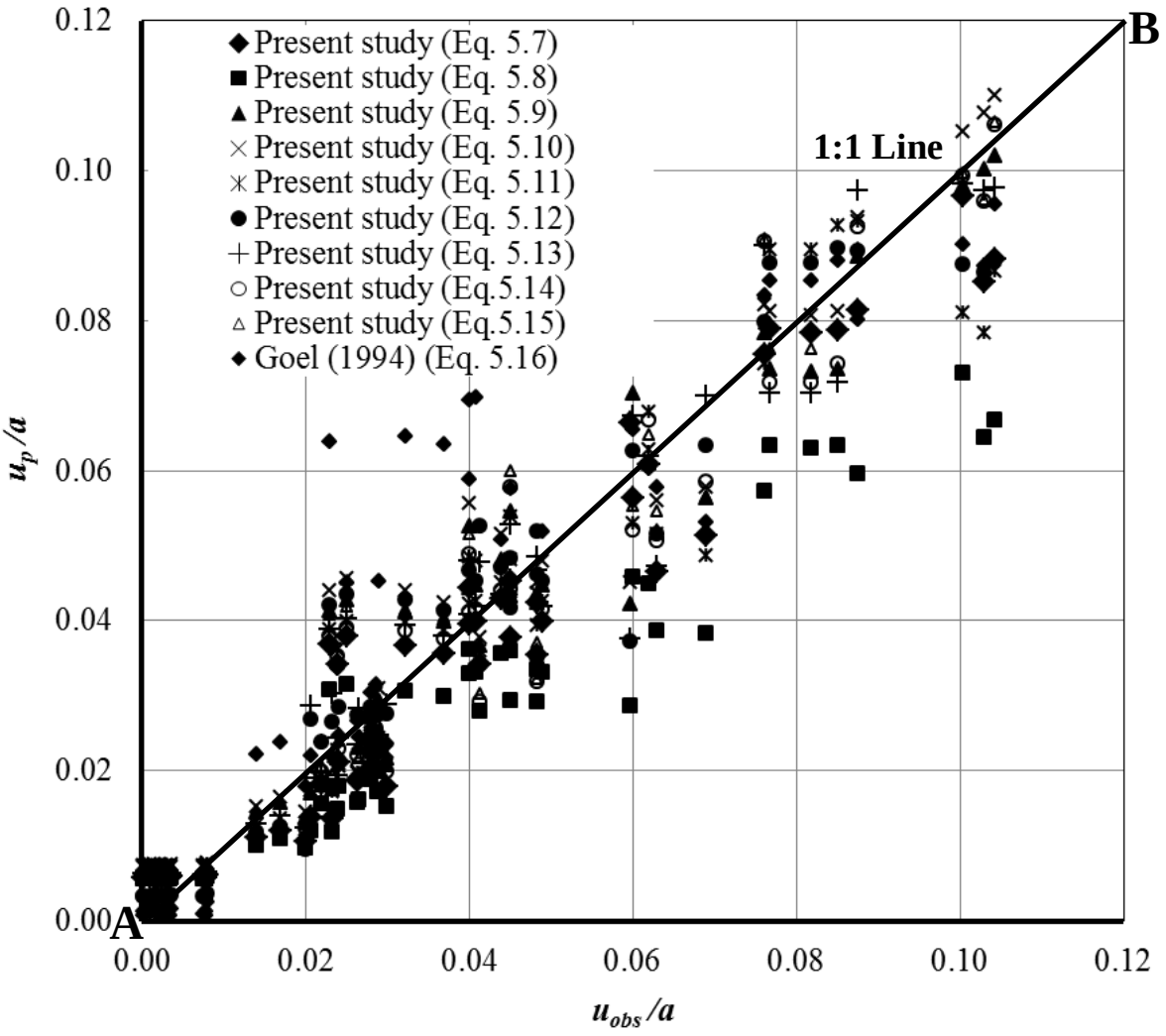

Fig. 5.10d Comparison of Predicted Values of Tunnel Strain with Goel (1994)

5.6 PARAMETRIC STUDY

It may be seen that Eqs. 5.9 & 5.10 are providing normalized tunnel deformation (u_p/a) or the tunnel strain. Equation 5.10 has been developed to study the effect of tunnel radius on the tunnel strain. Correlation developed vide Eq. 5.9 has been proposed in the present study after realizing insignificant effect of tunnel radius (see art. 5.4.1) and therefore, the **following parametric study has been carried out using Eq. 5.9 so as to investigate the influence of other parameters:**

5.6.1 Effect of Tunnel Depth, *H*

Using Eq. 5.9, values of tunnel strain in percent have been plotted in Fig. 5.11 versus the tunnel depth, considering constant values of K = 10MPa, and σ_{ci} = 30 MPa. The plot shows variation of tunnel strain in percent, (u_p /$_a$) x100) with tunnel depth. It can be seen that the tunnel strain increases with increase in tunnel depth for all values of J_f (= 250, 300, 350). It is due to the fact that increase in tunnel depth gives rise to in-situ stresses (vertical and horizontal) leading to larger deformation (Dwivedi et al., 2014b). The slope of the curves increases with increase in the value of J_f. It indicates that tunnel strain increases at a faster rate with tunnel depth for the rock masses having higher values of J_f.

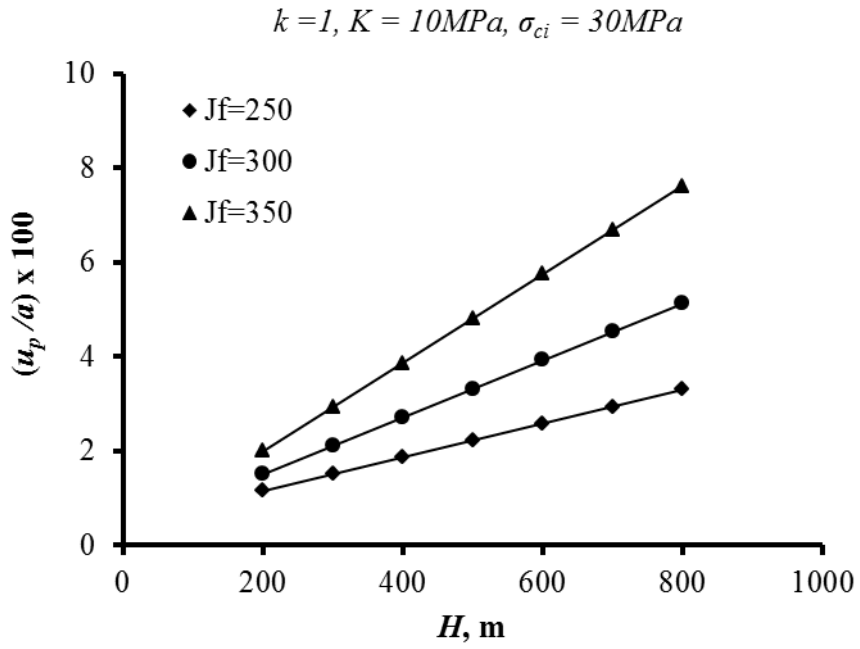

Fig. 5.11 Variation of Tunnel Strain with Tunnel Depth, *H*

5.6.2 Effect of Rock Mass Quality defined by Joint Factor, J_f

A plot of tunnel strain (%) versus joint factor (J_f) for a given support stiffness K= 10MPa and σ_{ci} value of 30MPa has been shown in Fig. 5.12 for three different values of tunnel depth. This plot is prepared using the values of tunnel strain obtained from Eq. 5.9. The plot indicates that the tunnel strain increases with increase in the values of joint factor for tunnel depths of 250 m, 450 m and 650 m. It means that tunnel deformations would be large in weak rock masses. Increase in slope of the curves for higher tunnel depth indicates that the tunnel strain increases at a faster rate at higher depth as compare to that at shallow depths.

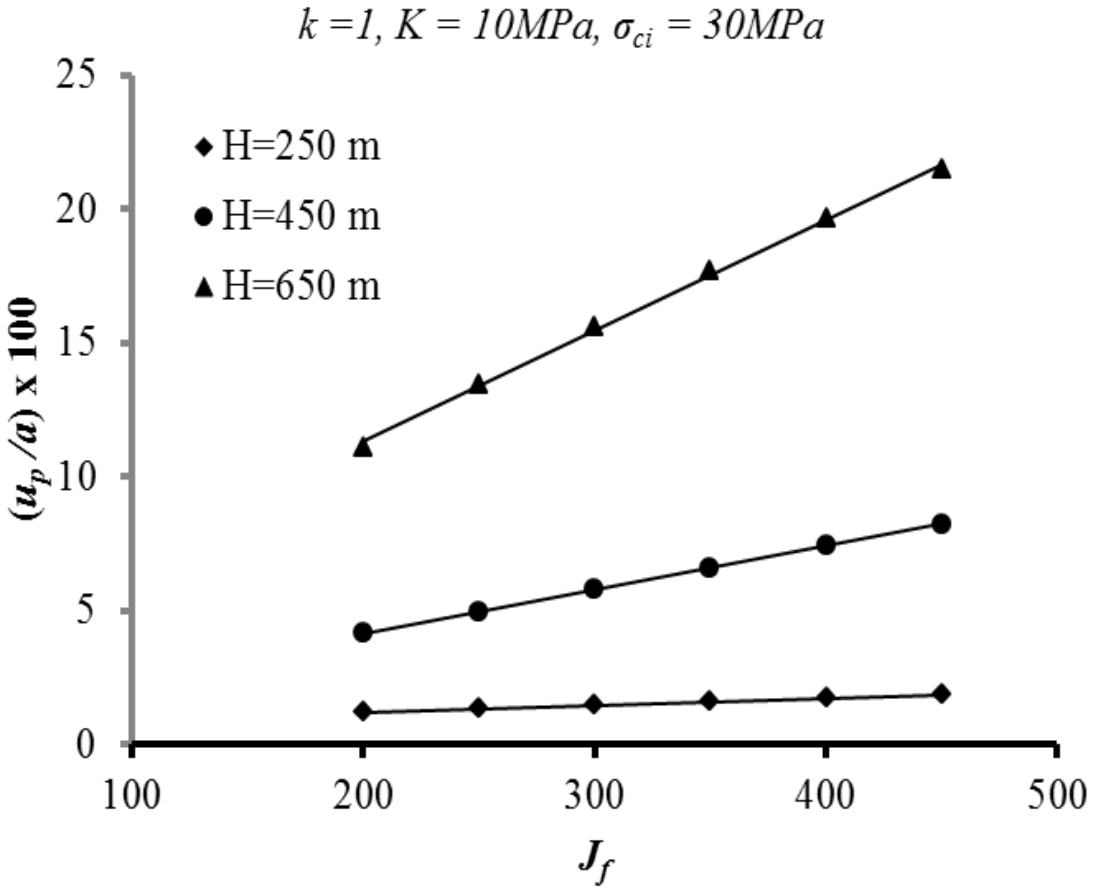

Fig. 5.12 Variation of Tunnel Strain with Joint Factor, J_f

5.6.3 Effect of Support Stiffness, *K*

Variation of Tunnel strain has also been plotted in Fig. 5.13with support stiffness using Eq. 5.9 for a tunnel depth of 400m and σ_{ci} value of 30 MPa. The plot suggests that tunnel strain decreases with increase in support stiffness which is obvious. The reduction is faster for weaker rock masses (having large J_f values). For instance, tunnel strain decreases from 1.29% at *K*=100 MPa to 0.90% at *K*=300 MPa corresponding to J_f = 400. The reduction is 0.39% whereas on the other hand, this decrease is from 0.77% at *K*=100 to 0.72% at *K*=300 for J_f = 200 i.e. reduction by about 0.05% only. This suggests that timely installation of adequate support in case of weaker rock masses (exhibiting squeezing conditions) can effectively control the excessive undesirable tunnel deformations.

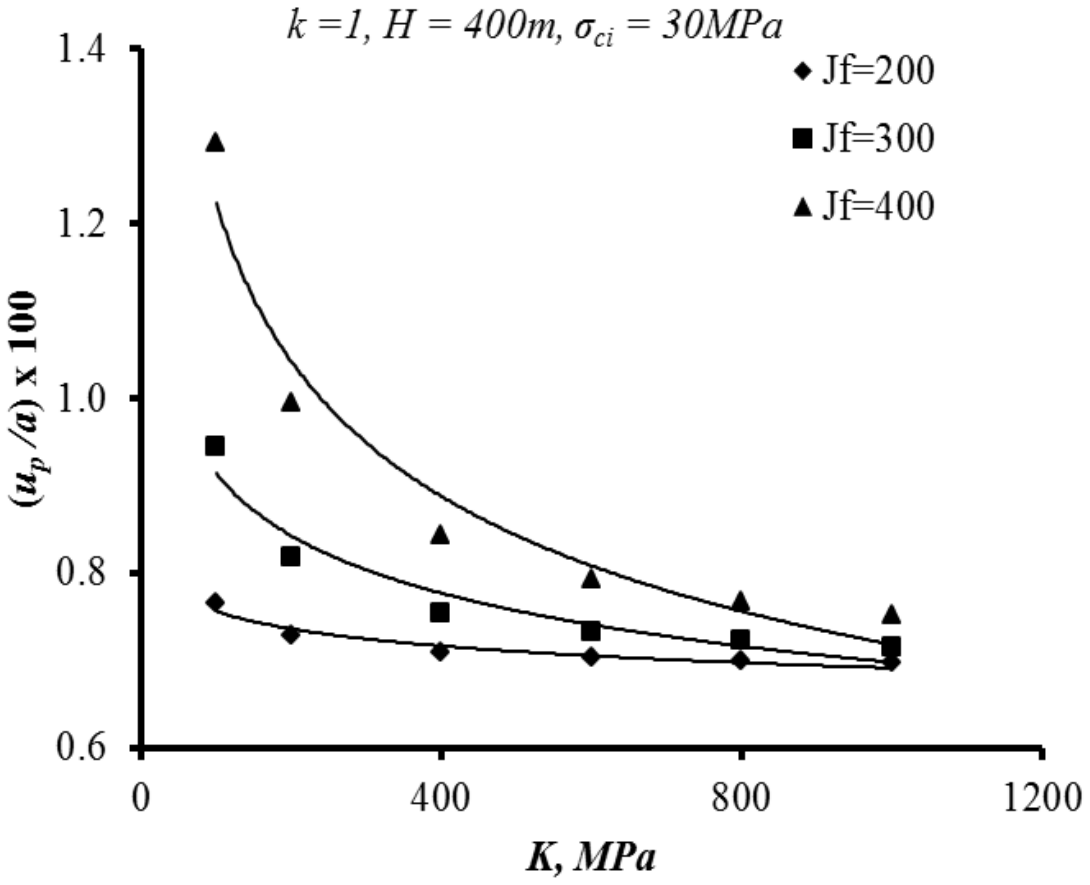

Fig. 5.13 Variation of Tunnel Strain with Support Stiffness, *K*

5.6.4 Effect of Uniaxial Compressive Strength of Intact Rock, σ_{ci}

Figure 5.14 has been plotted to study the influence of uniaxial compressive strength (UCS) of intact rock using Eq. 5.9. The effect of UCS has been studied for three different values of tunnel depth (H=200 m, 400 m, 600 m) keeping values of support stiffness, K =10 MPa and J_f =300 as constant. The best fit equations with correlation factor of '0.99' have also been determined. Plot for H = 600 m, gives the highest slope. In addition to this, on reduction of σ_{ci} value from 30MPa to 10MPa, it has been found that tunnel strain increases by 0.4% and 0.26% respectively at depths, H = 400 m and 200 m. It indicates that tunnel strain increases at faster rate with reduction in σ_{ci} and with increase in tunnel depth, i.e. at higher depths, σ_{ci} plays a role in the development of tunnel strain in squeezing ground conditions.

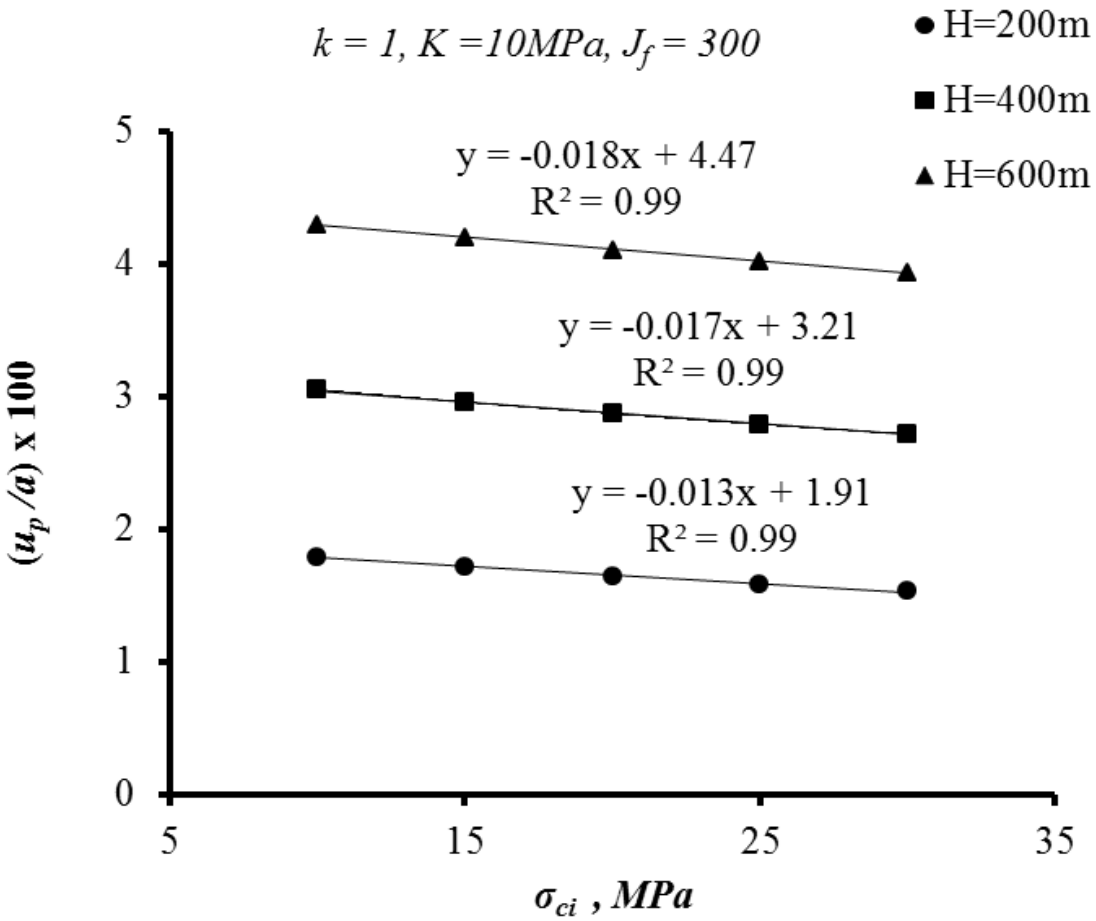

Fig. 5.14 Variation of Tunnel Strain with Uniaxial Compressive Strength, σ_{ci}

5.6.5 Effect of Tunnel Radius, *a*

Figure 5.15 shows variation of tunnel strain versus tunnel radius and this plot has been prepared using Eq.5.10. It can be seen that for a tunnel depth, H = 200 m, tunnel strain increases by 0.04% only when tunnel radius increases from 2.0 m to 8.0 m. The tunnel strain increases by 0.1% only corresponding to a tunnel depth, H = 400 m and 600m for the same increase in tunnel size. However, for the same tunnel size, tunnel strain increases significantly when the tunnel depth also increases. For example, in case of tunnel of 2.0 m radius, tunnel strain increases from 1% to 1.6% as depth of tunnel increases from 200 m to 600 m, whereas, when the tunnel size increases from 2.0 m to 8.0 m, tunnel strain increases from 1.04% to 1.7% for the same increase in depth of tunnel.

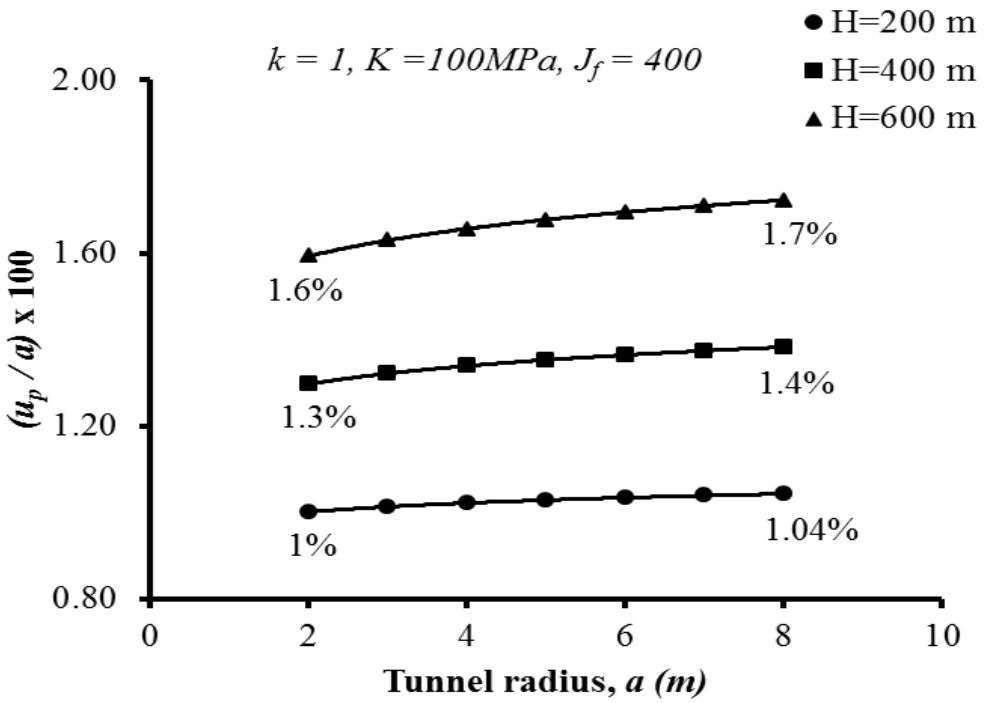

Fig. 5.15 Variation of tunnel Strain with Tunnel Radius, *a*

The reason for the above observation may be that increase in radius leads directly to increased induced stresses around the tunnel opening which results in reduced rock mass quality, which in turn may be due to development of additional cracks and shearing of the joints etc. The effect of weakened rock mass has already been taken care by evaluation of rock mass quality (J_f , Q or N) and these parameters have already been included in correlations. ***Hence,***

correlation represented by Eq. 5.9 is suggested for the purpose of estimating tunnel strain in the field or during design.

5.7 CORRELATIONS FOR NON-SQUEEZING GROUND

The case histories from hydroelectric projects, viz., Giri–Bata (1 tunnel), Chhibro–Khodri (2 adits/ tunnels), Maneri stage-I & II (4 adits/ tunnels), Kaligandaki (1 tunnel), Khimti-1 (4 adits); have been analysed for the present study. Data of rock type, rock mass characteristics (*Q, N*), tunnel depth (*H*), tunnel radius (*a*), observed tunnel deformation (u_{obs}) in non-squeezing grounds, horizontal in-situ stress (σ_h), uniaxial compressive strength of intact rock (σ_{ci}), joint properties (dip, spacing, friction angle), angle between tunnel alignment and strike of joints (α) has been collected. Data from 35 sections of tunnels / adits has been analysed for development of different correlations for non-squeezing ground condition. Joint factor (J_f) has been calculated using joint properties as shown by one example in chapter 3. Data of rock-joint properties of tunnels and value of σ_{ci} have been listed in Table 3.5 of chapter 3. Data of rock type, *Q, N, H, a,* u_{obs}, J_f with values of its parameters (*n and r*) has been presented in Table 5.5 for all the 35 sections of tunnels at various project sites whereas, values of σ_v, and σ_h observed at these project sites are presented in Table 5.6.

Data from 35 tunnel sections listed in Table 5.5 was collected to develop dimensionally correct empirical correlations for prediction of tunnel deformation in non-squeezing ground conditions.

Table 5.5 Data Collected from Various Tunnel Sections for Prediction of Tunnel Deformation in Non-squeezing Ground Conditions

Sl. No.	Name of Tunnel	Rock Type	Reference	Q	N	a (m)	H (m)	u_{obsd} (m)	K (MPa)	J_n	n	r	J_f
1.	Tehri tunnel	Phyllite Grade-I	Goel (1994); Bahuguna et al. (2008)	24.2	48.4	4.75	295	0.006	4.61	4.3	0.065	0.466	142
2.	Tehri tunnel	Phyllite Grade-I		29.9	59.8	4.75	280	0.0045	4.61	7.1	0.09	0.577	136
3.	Tehri tunnel	Phyllite Grade-I		26	52	4.75	210	0.0027	9.44	4.3	0.065	0.466	142
4.	Tehri tunnel	Phyllite Grade-III		0.9	4.5	4.75	225	0.01	9.44	6	0.09	0.268	249
5.	Tehri tunnel	Phyllite Grade-III		0.9	4.5	4.75	240	0.011	9.44	6	0.09	0.268	249
6.	Tehri tunnel	Phyllite Grade-I		18.14	36.28	4.75	265	0.0041	9.44	6.6	0.09	0.466	157
7.	Tehri tunnel	Phyllite Grade-II		3.96	19.8	4.75	310	0.0075	9.44	7.2	0.09	0.404	198
8.	Tehri tunnel	Phyllite Grade-II		1	6	4.75	275	0.0116	9.44	7.6	0.09	0.344	245
9.	Tehri tunnel	Phyllite Grade-II		4.2	21	4.75	300	0.007	9.44	7.1	0.09	0.404	195
10.	Tehri tunnel	Phyllite Grade-II		4.45	22.25	4.75	225	0.0037	9.55	6.4	0.09	0.364	195
11.	Tehri tunnel	Phyllite Grade-III		0.15	0.75	4.75	225	0.0235	9.55	8.2	0.09	0.287	318
12.	Tehri tunnel	Phyllite Grade-II		2.23	11.15	4.75	295	0.0082	9.55	7.6	0.09	0.384	220
13.	Tehri tunnel	Phyllite Grade-I		14	49	6	225	0.0025	9.39	6.4	0.09	0.445	160
14.	Tehri tunnel	Phyllite Grade-II		2.38	8.33	6	200	0.0065	9.39	8	0.09	0.404	220
15.	Tehri tunnel	Phyllite Grade-II		1.9	3.8	6	300	0.0141	9.51	8	0.09	0.384	232
16.	Tehri tunnel	Phyllite Grade-III		0.36	2.7	4.75	295	0.0175	9.44	8.7	0.09	0.344	281
17.	Tehri tunnel	Phyllite Grade-III		0.36	2.7	4.75	300	0.0185	9.44	8.7	0.09	0.344	281

…..Contd.

Sl. No.	Name of Tunnel	Rock Type	Reference	*Q*	*N*	*a* (m)	*H* (m)	u_{obsd} (m)	*K* (MPa)	J_n	*n*	*r*	J_f
18.	Maneri-II tunnel	Mv / Mb (Foliated)	Goel (1994)	0.62	3.1	3.5	200	0.007	9.79	5.9	0.05	0.445	265
19.	Maneri-II tunnel	Metabasics		0.55	2.75	3.5	250	0.0109	9.58	6	0.05	0.445	270
20.	Maneri-II tunnel	Greywackes		2.75	5.5	3.5	250	0.0067	9.79	5	0.05	0.466	215
21.	Maneri-II tunnel	Metabasics		1.02	2.04	3.5	175	0.0085	9.58	5.6	0.05	0.445	252
22.	Maneri-II tunnel	Greywackes		2.7	13.5	3.5	300	0.007	9.58	8.7	0.09	0.445	217
23.	Maneri-II tunnel	Greywackes		3	15	3.5	325	0.0058	9.58	4.8	0.05	0.445	216
24.	Maneri-II tunnel	Greywackes		3	15	3.5	305	0.0062	9.58	4.8	0.05	0.445	216
25.	Lower Periyar tunnel	PGF		5.5	5.5	3.4	197	0.0053	9.28	14.3	0.09	0.839	190
26.	Lower Periyar tunnel	PGF		7	7	3.4	150	0.0035	8.6	12.9	0.09	0.839	171
27.	Maneri-I tunnel	Sheared metabasics	Jethwa (1981); Jethwa et al. (1982); Goel (1994)	0.8	4	2.9	250	0.0073	9.69	12.9	0.22	0.466	253
28.	Maneri-I tunnel	MFQ		3.6	9	2.9	225	0.002	9.81	17.7	0.22	0.404	199
29.	Maneri-I tunnel	Foliated metabasics		4.7	23.5	2.9	275	0.0045	9.32	18.6	0.22	0.424	199
30.	Maneri-I tunnel	Foliated metabasics		4.24	14.84	2.9	225	0.0044	9.75	20.8	0.22	0.466	203
31.	Maneri-I tunnel	Sheared metabasics		1.3	9.75	2.9	350	0.0096	9.81	12.6	0.22	0.231	248
32.	Maneri-I tunnel	Foliated metabasics		4	20	2.9	225	0.003	9.75	20.8	0.22	0.466	203
33.	Maneri-I tunnel	Foliated metabasics		5.5	27.5	2.9	250	0.0027	9.8	19.6	0.22	0.466	191
34.	Maneri-I tunnel	Foliated metabasics		4.24	21.2	2.9	250	0.0037	9.75	20.8	0.22	0.466	203
35.	Maneri stage-I	Foliated metabasics		6.8	17	2.9	225	0.002	9.81	16	0.22	0.466	171

Notation: ***Mv/Mb-Metavolcanics/Metabasics; PGF-Pegmatite granite foliated; MFQ-Moderately fractured quartzite.***

Table 5.6 Value of In-situ Stresses at Different Tunnel Sections of Case Study Projects

Sl. No.	Name of Tunnel	Rock Type	σ_h (MPa)	σ_v (MPa)
1.	Tehri tunnel	Phyllite Grade I	4.8	8.0
2.	Tehri tunnel	Phyllite Grade I	4.5	7.6
3.	Tehri tunnel	Phyllite Grade I	3.4	5.7
4.	Tehri tunnel	Phyllite Grade III	3.6	6.1
5.	Tehri tunnel	Phyllite Grade III	3.9	6.5
6.	Tehri tunnel	Phyllite Grade I	4.3	7.2
7.	Tehri tunnel	Phyllite Grade II	5.0	8.4
8.	Tehri tunnel	Phyllite Grade II	4.5	7.4
9.	Tehri tunnel	Phyllite Grade II	4.9	8.1
10.	Tehri tunnel	Phyllite Grade II	3.6	6.1
11.	Tehri tunnel	Phyllite Grade III	3.6	6.1
12.	Tehri tunnel	Phyllite Grade II	4.8	8.0
13.	Tehri tunnel	Phyllite Grade I	3.6	6.1
14.	Tehri tunnel	Phyllite Grade II	3.2	5.4
15.	Tehri tunnel	Phyllite Grade II	4.9	8.1
16.	Tehri tunnel	Phyllite Grade III	4.8	8.0
17.	Tehri tunnel	Phyllite Grade III	4.9	8.1
18.	Maneri Stage-II tunnel	Metavolcanics/Metabasics (Foliated)	1.8	5.4
19.	Maneri Stage-II tunnel	Metabasics	2.2	6.8
20.	Maneri Stage-II tunnel	Greywackes	2.2	6.8
21.	Maneri Stage-II tunnel	Metabasics	1.6	4.7
22.	Maneri Stage-II tunnel	Greywackes	2.7	8.1
23.	Maneri Stage-II tunnel	Greywackes	2.9	8.8
24.	Maneri Stage-II tunnel	Greywackes	2.7	8.2
25.	Lower Periyar	Pegmatite granite (foliated)	-	5.3
26.	Lower Periyar	Pegmatite granite (foliated)	-	4.1
27.	Maneri Stage-I tunnel	Sheared metabasics	2.2	6.8
28.	Maneri Stage-I tunnel	Moderately fractured quartzites	2.0	6.1
29.	Maneri Stage-I tunnel	Foliated metabasics	2.5	7.4
30.	Maneri Stage-I tunnel	Foliated metabasics	2.0	6.1

…..Contd.

Sl. No.	Name of Tunnel	Rock type	σ_h (MPa)	σ_v (MPa)
31.	Maneri Stage-I tunnel	Sheared metabasics	3.1	9.5
32.	Maneri Stage-I tunnel	Foliated metabasics	2.0	6.1
33.	Maneri Stage-I tunnel	Foliated metabasics	2.2	6.8
34.	Maneri Stage-I tunnel	Foliated metabasics	2.2	6.8
35.	Maneri Stage-I tunnel	Foliated metabasics	2.0	6.1

Notation: ***References of the respective tunnels are as given in Table 5.5.***

5.7.1 Correlations using Joint Factor, J_f

Observed values of tunnel deformation, (u_{obs}/a) are plotted versus ($J_f^3.\sigma_v/K$) in Fig. 5.16 and regression analysis has been carried out to develop Eq. 5.18 which is a dimensionally balanced correlation. The parameters used in the plot have been appropriately kept in numerator and denominator as per their influence on tunnel deformation. The influence of parameters on tunnel deformation has already been discussed in art. 5.4.1. Equation 5.18 is given by -

$$\frac{u_p}{a} = \frac{2*10^{-10} J_f{}^3 \sigma_v}{K} + 0.0001 \qquad R^2 = 0.92 \qquad (5.18)$$

where u_p is the predicted value of tunnel deformation which has been expressed as a function of J_f, σ_v and support stiffness, K. The corresponding value of correlation coefficient is 92%.

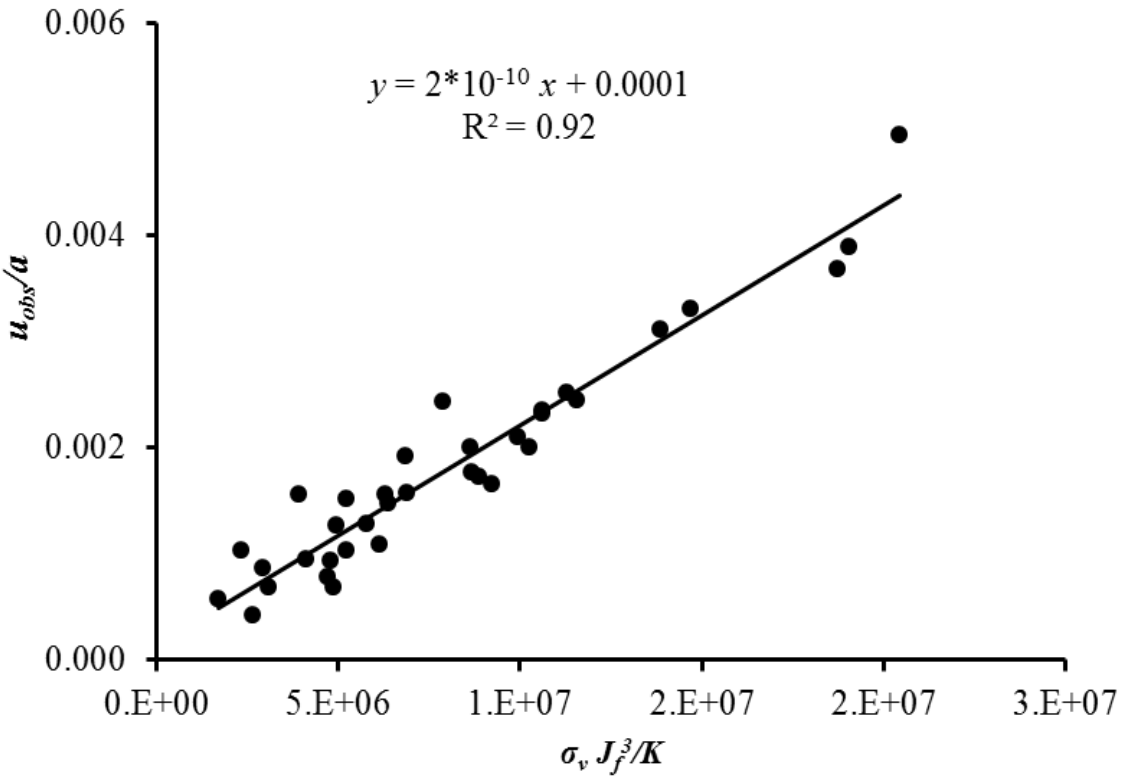

Fig. 5.16 Plot of (u_{obs}/a) versus ($\sigma_v J_f^3/K$) for Non-squeezing Ground

Equation 5.18 cannot be used for the case of unsupported tunnels. Therefore, further analysis has been carried out to modify Eq. 5.18 to Eq. 5.19 which was developed by plotting the observed tunnel deformation, (u_{obs}/a) versus ($J_f^3.\sigma_v/(K+6)$) in Fig. 5.17. This equation can also predict the tunnel deformation for unsupported tunnels (K = 0) excavated in non-squeezing ground.

$$\frac{u_p}{a} = \frac{3*10^{-10} J_f{}^3 \sigma_v}{K+6} + 0.0003 \qquad R^2 = 0.92 \qquad (5.19)$$

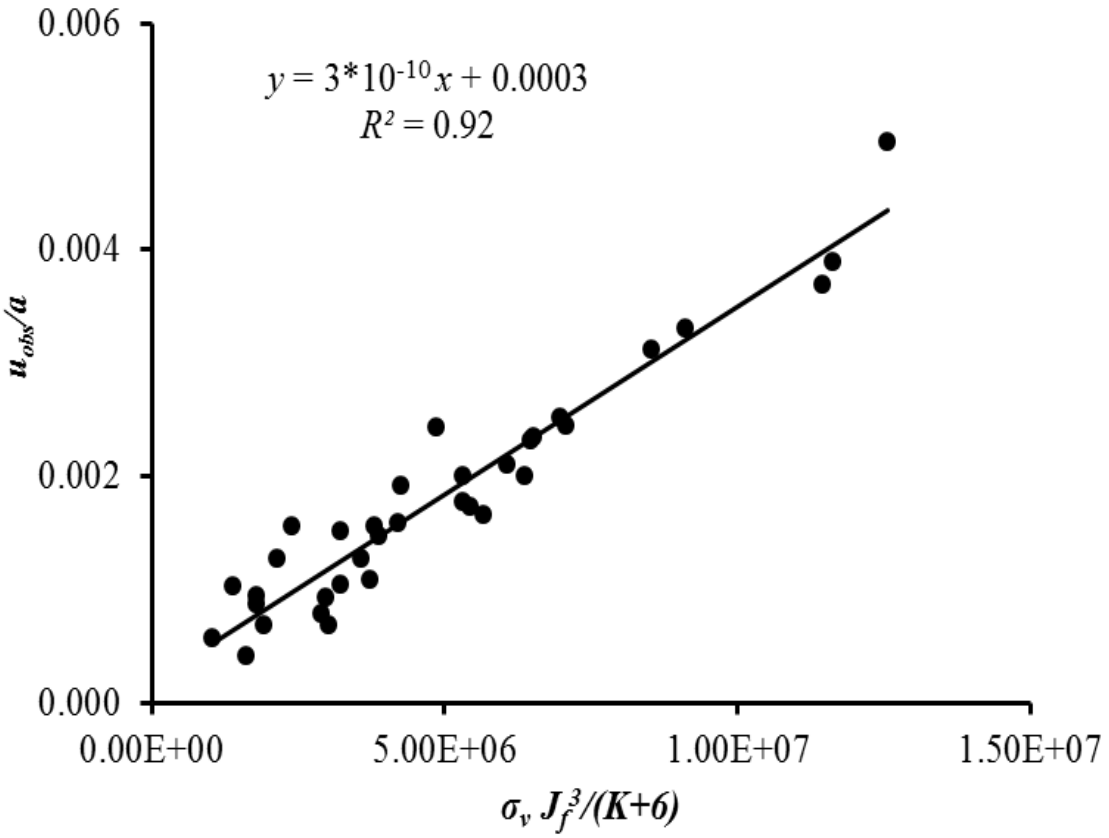

Fig. 5.17 Plot of (u_{obs}/a) versus ($\sigma_v J_f^3/(K+6)$) for Non-squeezing Ground

5.7.2 Correlations using Rock Mass Quality, *Q*

Dimensionally correct correlation represented by Eq. 5.20 has been developed based on a plot of (u_{obs}/a) versus $\sigma_v / (Q^{0.5}K)$ which is presented in Fig. 5.18.

$$\frac{u_p}{a} = \frac{0.0027\sigma_v}{Q^{0.5}K} + 0.0004 \qquad R^2 = 0.91 \qquad (5.20)$$

The best line fit represented by Eq. 5.20 has a correlation coefficient of 91%.

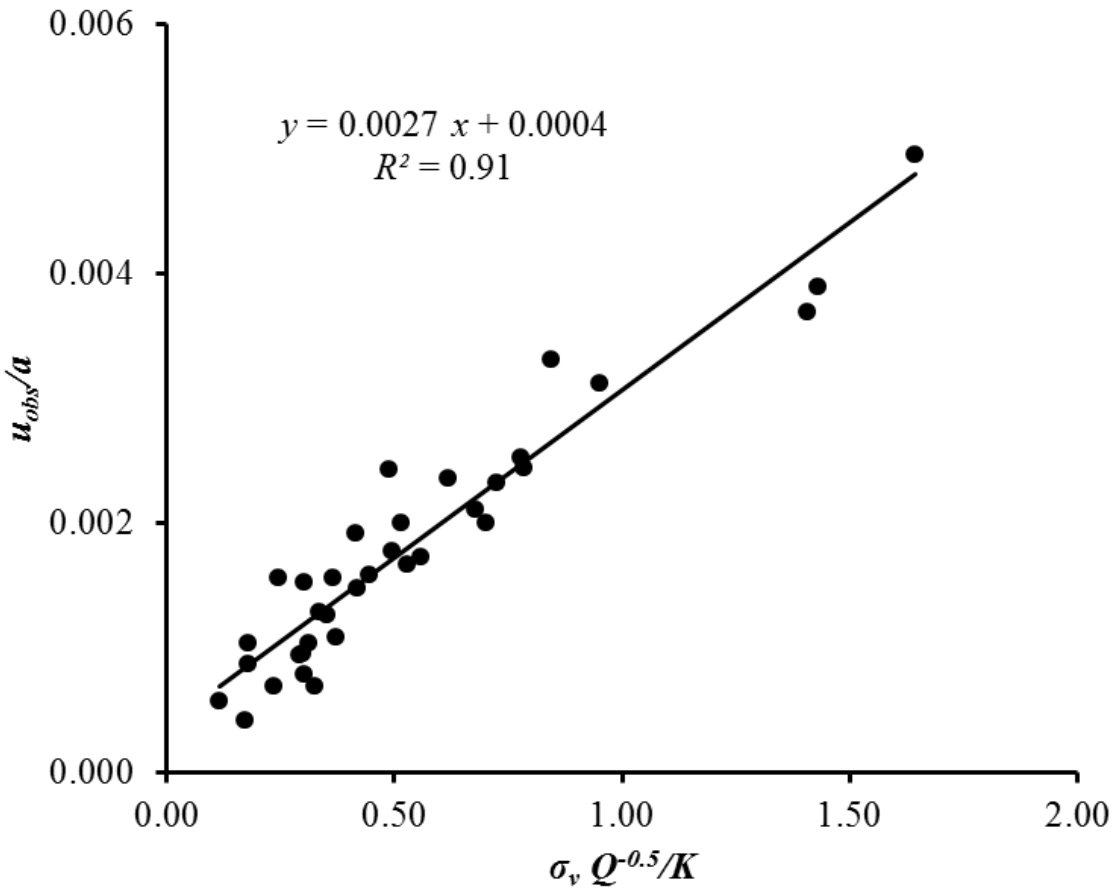

Fig. 5.18 Plot of (u_{obs}/a) versus ($\sigma_v Q^{-0.5}/K$) for Non-squeezing Ground

Again for the case of unsupported tunnels, correlation represented by Eq. 5.21 has been developed on basis of the plot of (u_{obs}/a) versus ($\sigma_v / \{ Q^{0.5}(K+7)\}$) which is depicted in Fig. 5.19. This equation can predict the tunnel deformation of unsupported tunnels in non-squeezing ground condition.

$$\frac{u_p}{a} = \frac{0.0046\sigma_v}{Q^{0.5}(K+7)} + 0.0004 \qquad R^2 = 0.91 \qquad (5.21)$$

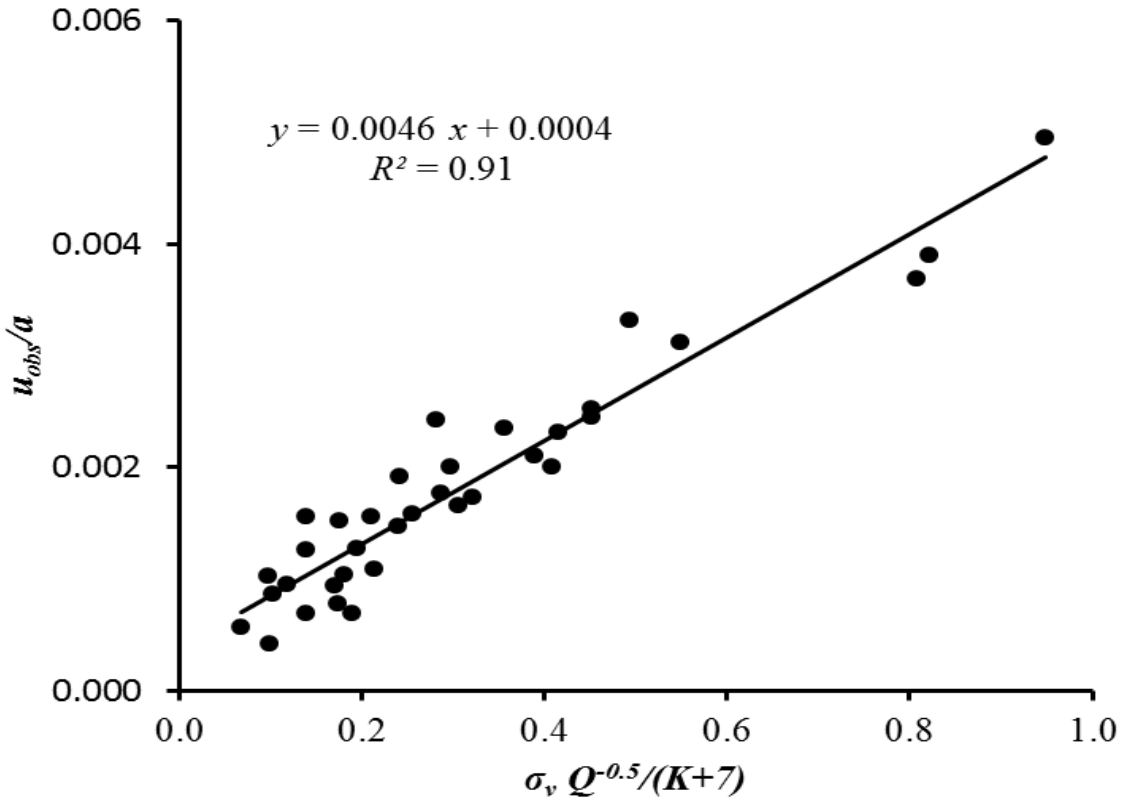

Fig. 5.19 Plot of (u_{obs} /a) versus ($\sigma_v\, Q^{-0.5}$ / (K+7)) for Non-squeezing Ground

5.7.3 Correlations using Rock Mass Number, *N*

Figure 5.20 shows the plot of the observed tunnel deformation values, (u_{obs} /a) as a function of $(\sigma_v/(N^{0.5}K))$. The best line fit of this data has been represented by dimensionally correct correlation expressed by Eq. 5.22 which has a correlation coefficient of 88%.

$$\frac{u_p}{a} = \frac{0.007\sigma_v}{N^{05}K} - 0.00002 \qquad R^2 = 0.88 \qquad (5.22)$$

Further, correlation represented by Eq. 5.23 has been proposed on basis of the plot of (u_{obs} /a) versus $[\sigma_v\ /\{\ N^{0.5}\ (K+7\ )\ \}]$ as shown in Fig. 5.21. It can be employed to predict the deformation of unsupported tunnels in non-squeezing ground condition. The corresponding correlation coefficient is 90%.

$$\frac{u_p}{a} = \frac{0.0121\sigma_v}{N^{0.5}(K+7)} + 0.00002 \qquad R^2 = 0.90 \qquad (5.23)$$

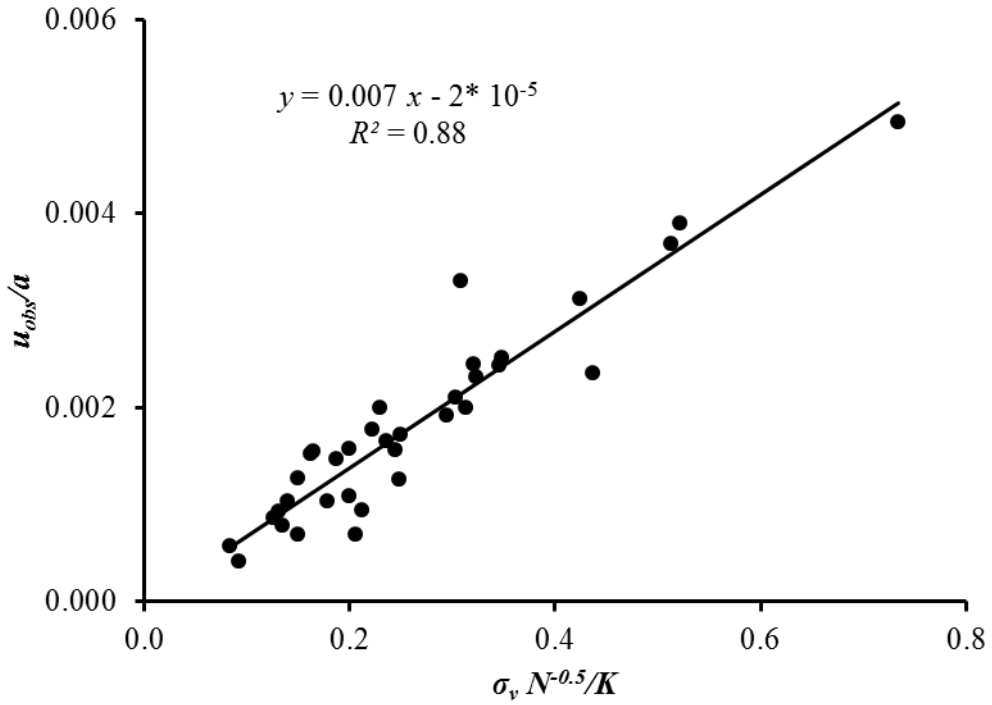

Fig. 5.20 Plot of (u_{obs} /a) versus (σ_v / $N^{0.5}$ K) for Non-squeezing Ground

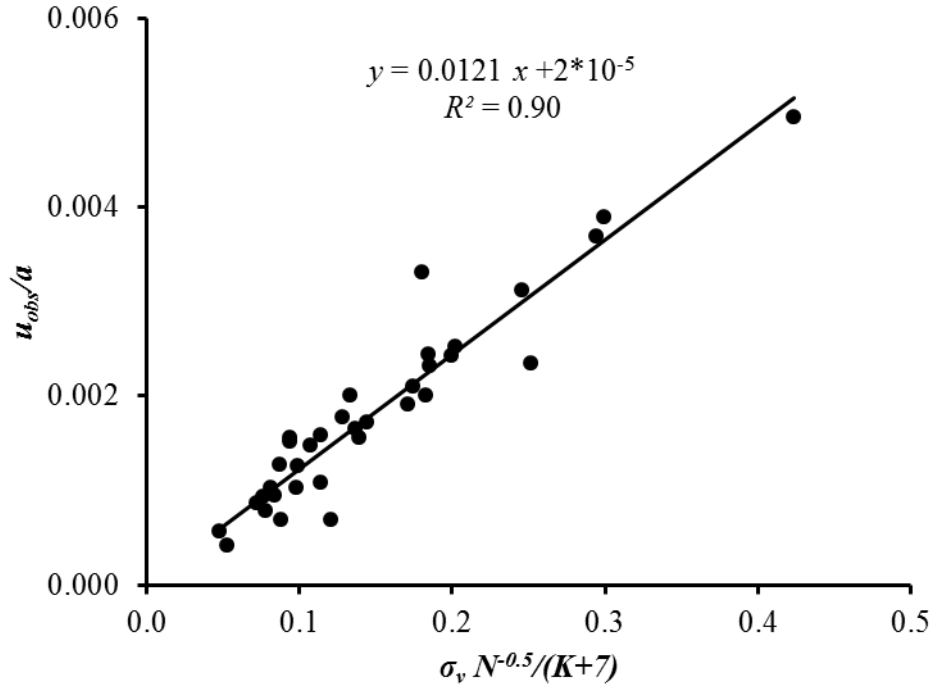

Fig. 5.21 Plot of (u_{obs} /a) versus (σ_v $N^{-0.5}$ /(K+7)) for Non-squeezing Ground

All the parameters used in Eqs. 5.18-5.23 have already been defined in Eqs. 5.9-5.15. Considering the Joint Factor (J_f) as a measure of rock mass quality, the proposed correlations fit with correlation factor of 0.92 (Eqs. 5.18-5.19). On the other hand, using Q as rock mass quality parameter, the correlations developed fit with correlation coefficient of 0.91, and those correlations developed on basis of rock mass number, N and represented by Eqs. 5.22 & 5.23 fit with a correlation coefficient of 0.88 and 0.90 respectively. Correlations represented by Eqs. 5.18, 5.20 & 5.22 don't exhibit any significance as regards prediction of deformation of unsupported tunnels in non-squeezing ground conditions is concerned, whereas other correlations (Eqs. 5.19, 5.21 & 5.23) have meaningful significance, when the support stiffness, $K = 0$ is substituted.

Goel (1994) suggested following empirical correlation (Eq. 5.24) for prediction of tunnel deformation in non-squeezing ground conditions using rock mass number, N,

$$\frac{u_p}{a} = \frac{H^{0.61}}{28N^{0.406}K^{0.35}} \tag{5.24}$$

5.8 COMPARISON OF PREDICTED AND OBSERVED TUNNEL DEFORMATIONS

For the available data of 35 tunnel sections excavated in non-squeezing ground conditions, especially the data related to the geometry of tunnels and the rock mass characteristics which have been presented in Table 5.5, attempt was made to predict the values of tunnel strain, ($\boldsymbol{u_p/a}$) using correlations (Eqs. 5.18 - 5.23) developed in art. 5.7. Values of tunnel deformation have also been predicted using the correlation (Eq. 5.24) developed by Goel (1994). A comparison of the predicted values of tunnel deformation has been presented in Table 5.7 with the observed values of deformations in non-squeezing ground conditions.

Table 5.7 Comparison of Predicted and Observed Strain Levels for Tunnels in Non-squeezing Ground Condition

S. No.	u_{obs}/a	u_p/a Eq. 5.18	u_p/a Eq. 5.19	u_p/a Eq. 5.20	u_p/a Eq. 5.21	u_p/a Eq.5.22	u_p/a Eq.5.23	u_p/a Eq. 5.24
1.	0.0013	0.0011	0.0009	0.0013	0.0010	0.0018	0.0012	0.0014
2.	0.0009	0.0009	0.0008	0.0012	0.0009	0.0015	0.0010	0.0012
3.	0.0006	0.0004	0.0006	0.0007	0.0007	0.0006	0.0006	0.0009
4.	0.0021	0.0021	0.0021	0.0022	0.0022	0.0021	0.0021	0.0024
5.	0.0023	0.0022	0.0022	0.0024	0.0023	0.0023	0.0023	0.0025
6.	0.0009	0.0007	0.0008	0.0009	0.0009	0.0009	0.0009	0.0011
7.	0.0016	0.0015	0.0016	0.0016	0.0016	0.0014	0.0014	0.0016
8.	0.0024	0.0024	0.0024	0.0025	0.0025	0.0023	0.0023	0.0024
9.	0.0015	0.0014	0.0015	0.0015	0.0015	0.0013	0.0013	0.0015
10.	0.0007	0.0007	0.0009	0.0010	0.0010	0.0011	0.0011	0.0014
11.	0.0008	0.0010	0.0012	0.0012	0.0012	0.0010	0.0010	0.0013
12.	0.0049	0.0042	0.0041	0.0048	0.0048	0.0052	0.0051	0.0050
13.	0.0017	0.0019	0.0019	0.0019	0.0019	0.0018	0.0018	0.0017
14.	0.0004	0.0006	0.0008	0.0009	0.0009	0.0007	0.0007	0.0004
15.	0.0011	0.0013	0.0014	0.0014	0.0014	0.0014	0.0014	0.0011
16.	0.0024	0.0022	0.0023	0.0021	0.0020	0.0031	0.0031	0.0024
17.	0.0037	0.0038	0.0037	0.0042	0.0041	0.0036	0.0036	0.0037
18.	0.0039	0.0039	0.0038	0.0043	0.0042	0.0037	0.0036	0.0039
19.	0.0020	0.0022	0.0022	0.0023	0.0023	0.0022	0.0022	0.0020
20.	0.0031	0.0029	0.0029	0.0030	0.0029	0.0030	0.0030	0.0031
21.	0.0019	0.0015	0.0016	0.0015	0.0015	0.0021	0.0021	0.0019
22.	0.0024	0.0017	0.0018	0.0017	0.0017	0.0024	0.0024	0.0024
23.	0.0020	0.0018	0.0019	0.0018	0.0018	0.0016	0.0016	0.0020
24.	0.0017	0.0019	0.0020	0.0018	0.0018	0.0017	0.0017	0.0017
25.	0.0018	0.0018	0.0019	0.0017	0.0017	0.0016	0.0016	0.0018
26.	0.0016	0.0009	0.0010	0.0011	0.0010	0.0017	0.0017	0.0016
27.	0.0010	0.0006	0.0007	0.0009	0.0009	0.0013	0.0012	0.0010
28.	0.0025	0.0024	0.0024	0.0025	0.0025	0.0025	0.0025	0.0025
29.	0.0007	0.0011	0.0012	0.0013	0.0013	0.0015	0.0015	0.0007
30.	0.0016	0.0014	0.0014	0.0014	0.0014	0.0012	0.0012	0.0016
31.	0.0015	0.0011	0.0013	0.0012	0.0012	0.0012	0.0012	0.0015
32.	0.0033	0.0030	0.0030	0.0027	0.0027	0.0022	0.0022	0.0033
33.	0.0010	0.0011	0.0013	0.0012	0.0012	0.0010	0.0010	0.0010
34.	0.0009	0.0011	0.0012	0.0012	0.0012	0.0009	0.0009	0.0009
35.	0.0013	0.0013	0.0014	0.0013	0.0013	0.0011	0.0011	0.0013
Ψ^2		**0.084**	**0.089**	**0.094**	**0.091**	**0.116**	**0.100**	**0.177**

Note: ***Serial numbers and references of cases are same as in Table 5.5.***

The comparison of the observed values of tunnel deformation with the predicted values has also been presented in the form of plots of predicted values ***(u_p /a)*** versus the observed values (***u_{obs} /a***) in Figs. 5.22 a,b,c & d.

Figure 5.22a shows the comparison of values of tunnel deformation predicted on basis of Eqs. 5.18 and 5.19 with the observed values. Values of tunnel deformation predicted on basis of Eq. 5.24 (Goel et al., 1994) have also been plotted in the same figure. Similarly, values predicted on basis of Eqs. 5.20, 5.21 and 5.24 are presented in Fig. 5.22b, those predicted using Eqs. 5.22, 5.23 and 5.24 are presented in Fig. 5.22c. Figure 5.22d shows comparison of all the predictions (Eqs. 5.18-5.24) with the observed values.

The correlation, which predicts values of tunnel strain closest to the line AB (1:1) in the Figs. 5.22 (a-d) fits best with the observed values. Coefficient of accordance ***(ψ^2)*** has been found to be the lowest i.e., 0.084 and 0.089 for correlations given by Eqs. 5.18 and 5.19 respectively (Table 5.7). These equations make use of joint factor indicting the rock mass quality. Further, the correlations given by Eqs. 5.20 and 5.21 which use *Q* values as rock mass quality parameter ashow the second best fit with COA values of 0.094 and 0.091 respectively. Correlations using rock mass number, *N* (Eqs. 5.22-5.23) fit with COA values of 0.116 and 0.100 respectively. On the other hand, values predicted by Eq. 5.24 fit with a COA value of 0.177. Correlation represented by Eq. 5.19 showing the second best fit having a little larger COA of 0.089 as compared to that of Eq. 5.18 (COA = 0.084). **Equation 5.19 has therefore been proposed for use in the field and also for design when it comes to prediction of strain in tunnels excavated in non-squeezing ground condition, particularly because it is also applicable for unsupported tunnels, in which case support stiffness, *K* = 0.**

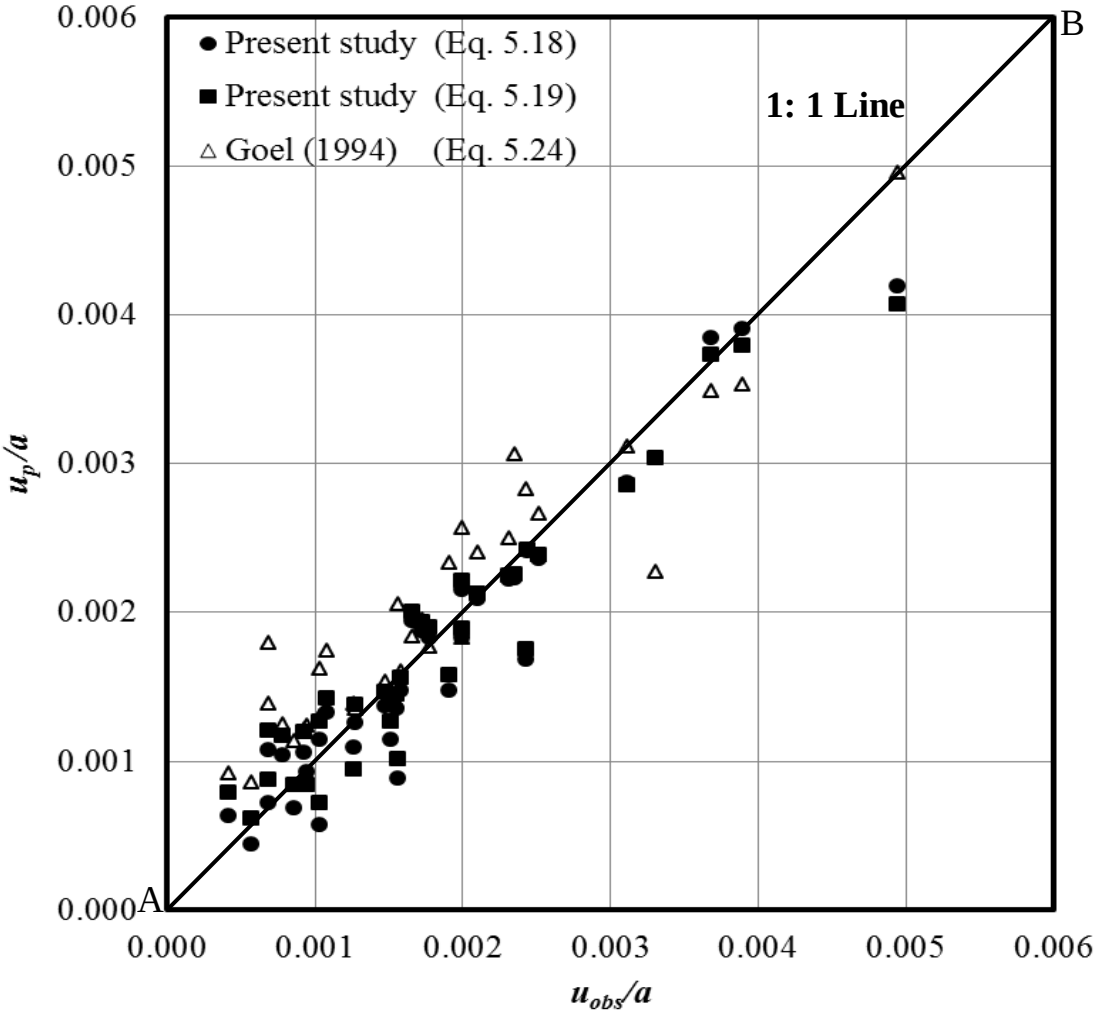

Fig. 5.22a Comparison of Predicted Values of Tunnel Strain with Goel (1994)

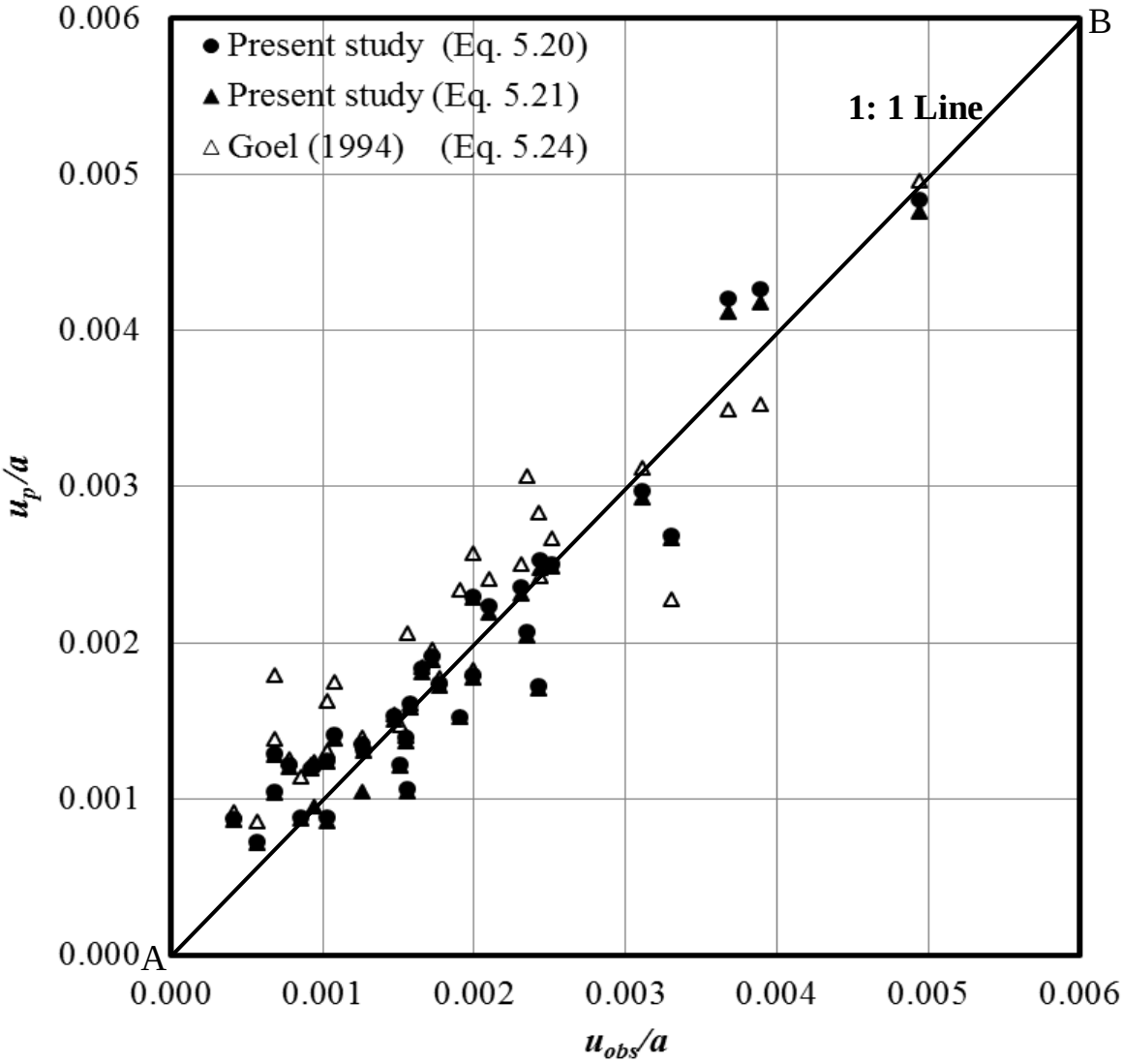

Fig. 5.22b Comparison of Predicted Values of Tunnel Strain with Goel (1994)

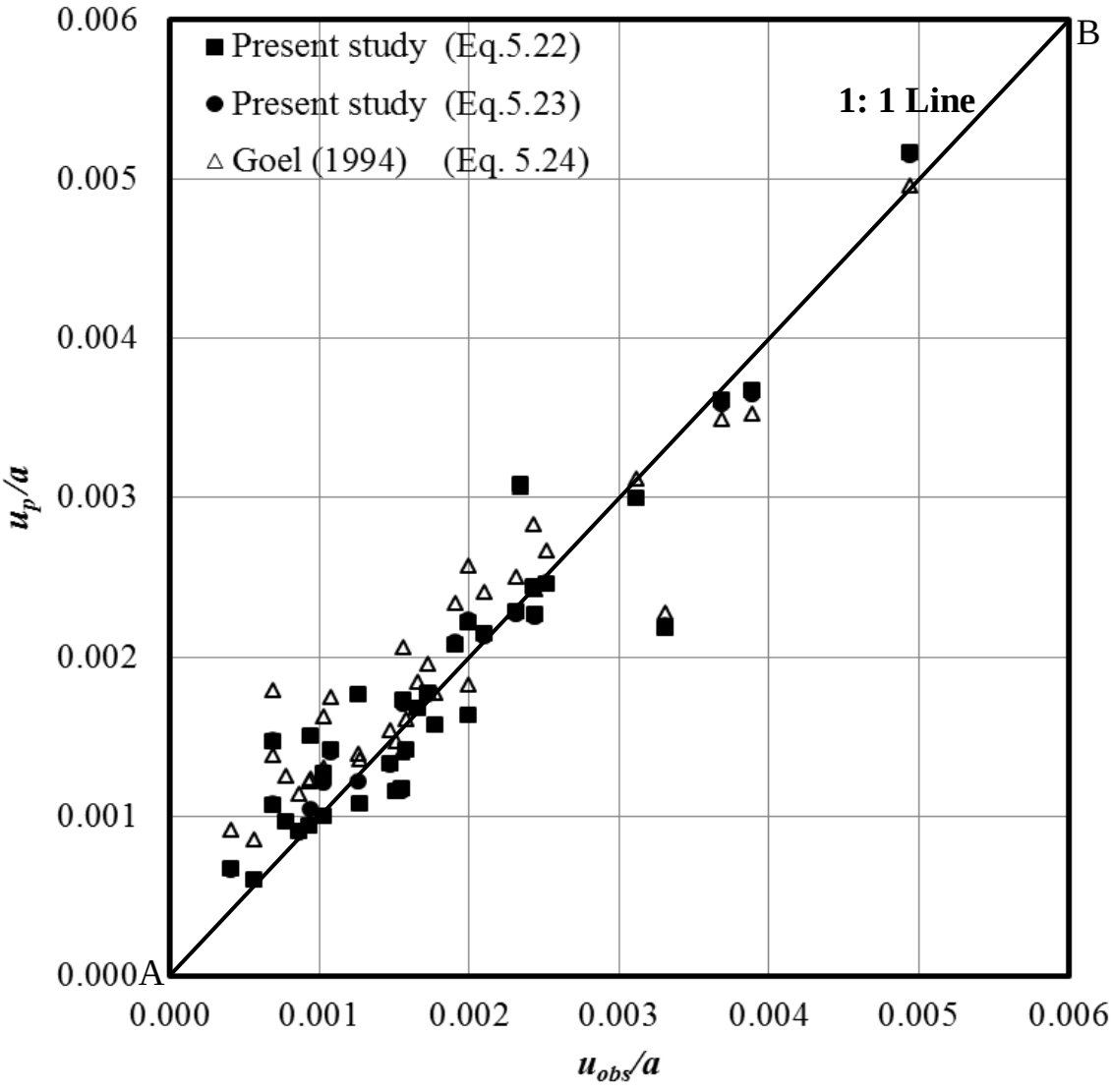

Fig. 5.22c Comparison of Predicted Values of Tunnel Strain with Goel (1994)

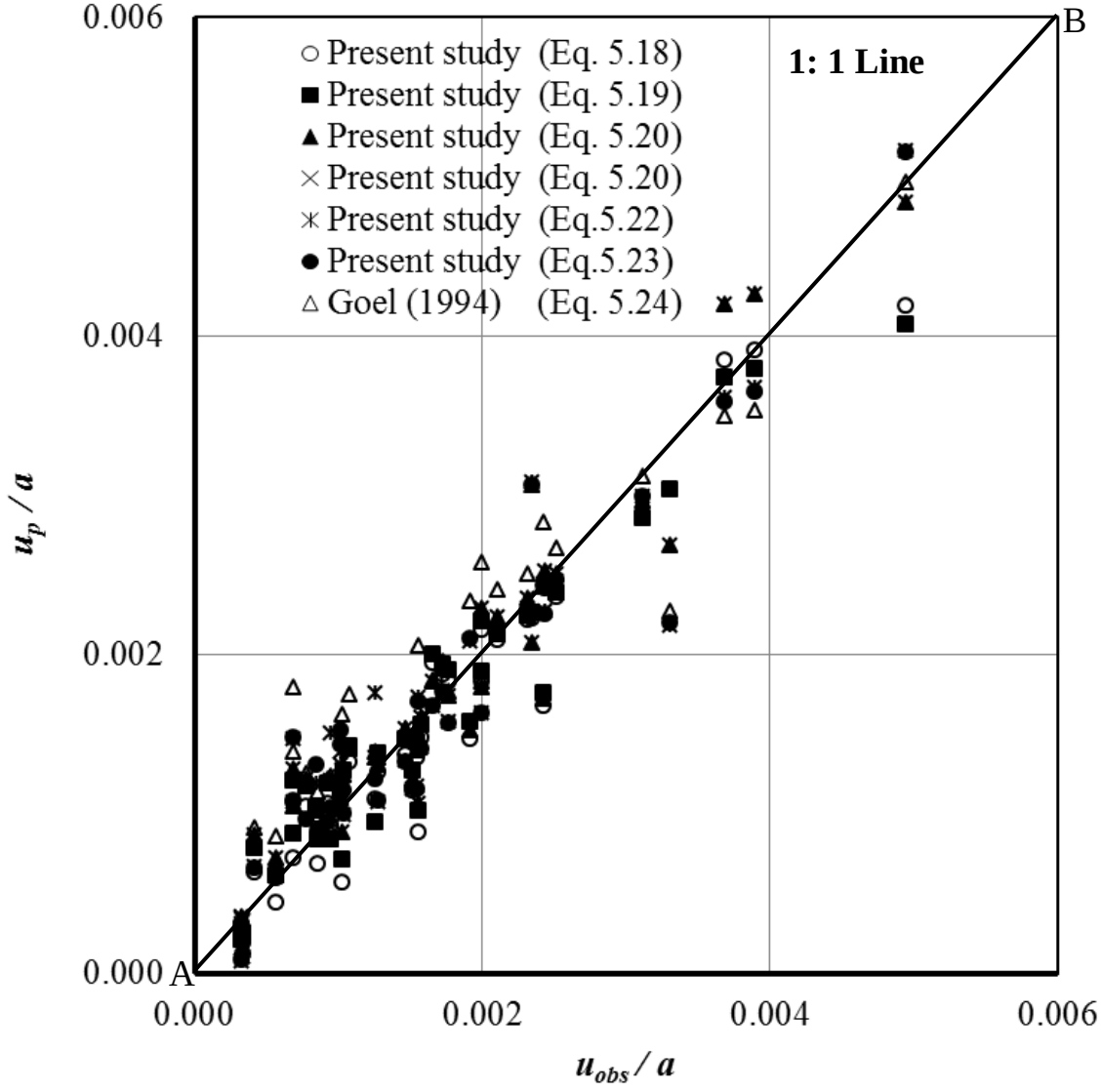

Fig. 5.22d Comparison of Predicted Values of Tunnel Strain with Goel (1994)

5.9 PARAMETRIC STUDY

This study was undertaken to study the influence of various parameters like tunnel depth, *H*; rock mass quality, *Q* and support stiffness. Using correlation represented by Eq. 5.19, variation in values of tunnel strain has been plotted with respect to tunnel depth, *H* in Fig. 5.23; with respect to tunnel radius, *a* in Fig. 5.24; versus rock mass quality defined by joint factor, J_f in Fig. 5.25 ; and versus support stiffness, *K* in Figs. 5.26.

5.9.1 Effect of Tunnel Depth, *H*

Figure 5.23, which has been plotted for three different values of joint factor (J_f) shows that tunnel strain increases with increase in tunnel depth. The rate of increase is higher for higher values of J_f as indicated by the slopes of the curves in the Fig. 5.23. For example, tunnel strain increases by 0.03%, 0.05% and 0.11% for J_f = 150, J_f = 200 and J_f = 250 respectively for the overburden depth from 50 m to 300 m. Increase in height invites large induced stresses at the periphery of the tunnel leading to larger deformation.

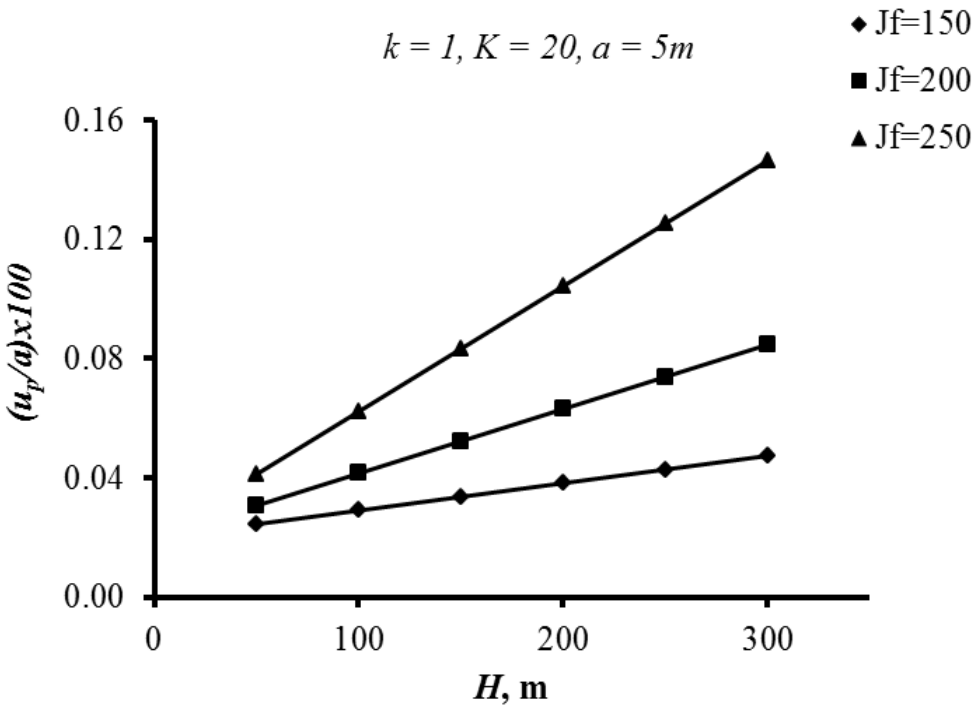

Fig. 5.23 Variation of Tunnel Strain with Tunnel Depth

5.9.2 Effect of Tunnel Radius, *a*

The predicted values of tunnel strain have been found to be independent of the tunnel radius, which can be seen in Fig. 5.24 which has been plotted for J_f = 150, 200 and 250.

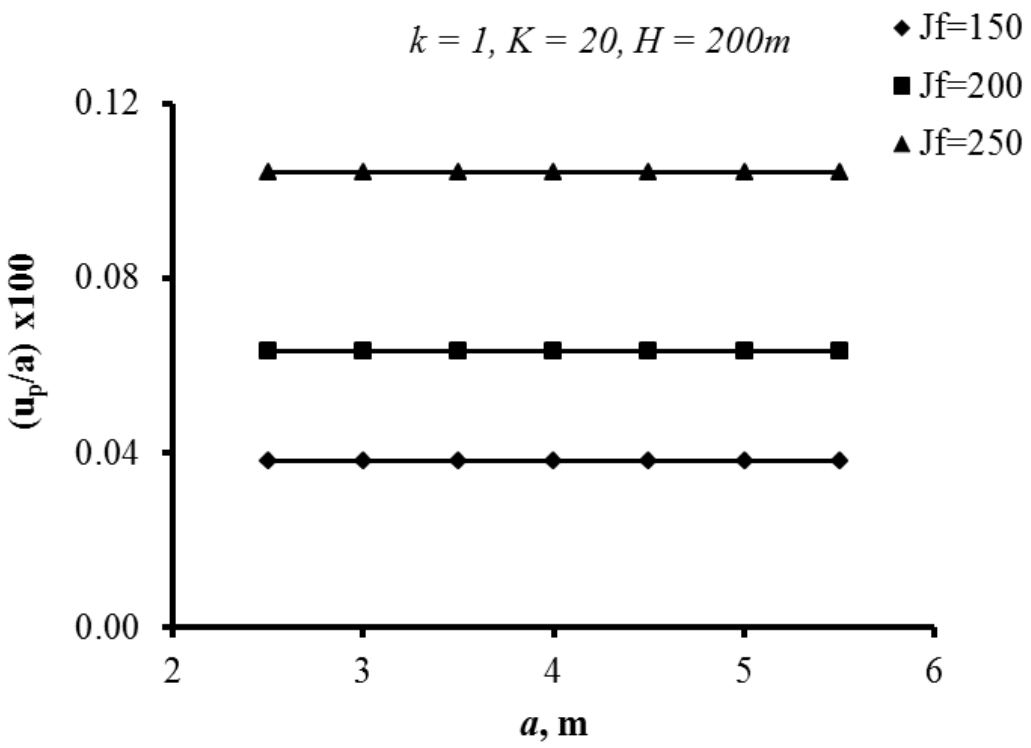

Fig. 5.24 Variation of Tunnel Strain with Tunnel Radius

5.9.3 Effect of Rock Mass Quality defined by Joint Factor, J_f

Figure 5.25 depicts the variation in tunnel strain with increase in values of joint factor (which corresponds to decrease in rock mass quality). It can be seen that tunnel strain increases with increase in values of joint factor and follows the second degree of polynomial trend. The rate of increase is faster for higher tunnel depths. For example, tunnel strain increases by 0.04%, 0.07% and 0.12% corresponding to tunnel depth of 100 m, 200 m and 300m respectively. It may be due to the fact that quality of rock mass around the tunnel deteriorates at a faster rate with increase in tunnel depth because of larger values of in-situ stresses at higher depths.

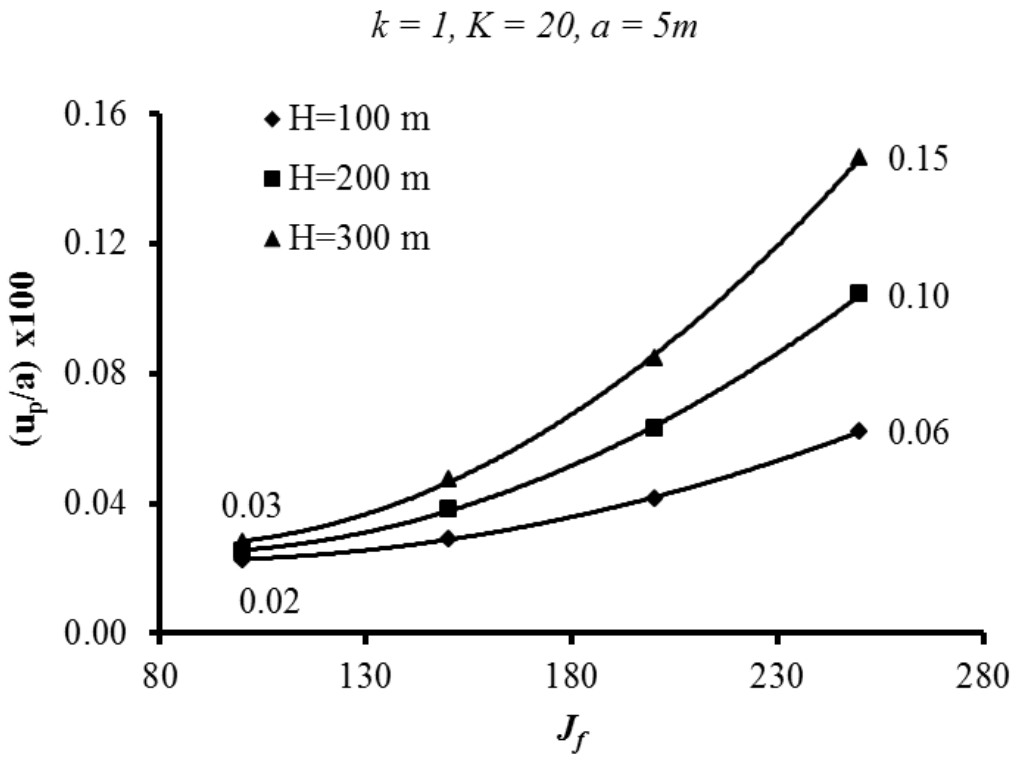

Fig. 5.25 Variation of tunnel Strain with Joint Factor, J_f

5.9.4 Effect of Support Stiffness, *K*

Plot of tunnel strain with variation in support stiffness is presented in Fig. 5.26 for different values of joint factor and the plot shows that tunnel strain reduces with increase in support stiffness. Slopes of the curves indicate a faster decrease in tunnel strain values with increase in support stiffness for all the values of the joint factor or the rock mass quality. Tunnel strain has been found to increase with increase in value of J_f for the same stiffness of the support, especially for the values of *K* less than 175 MPa (Fig. 5.26).

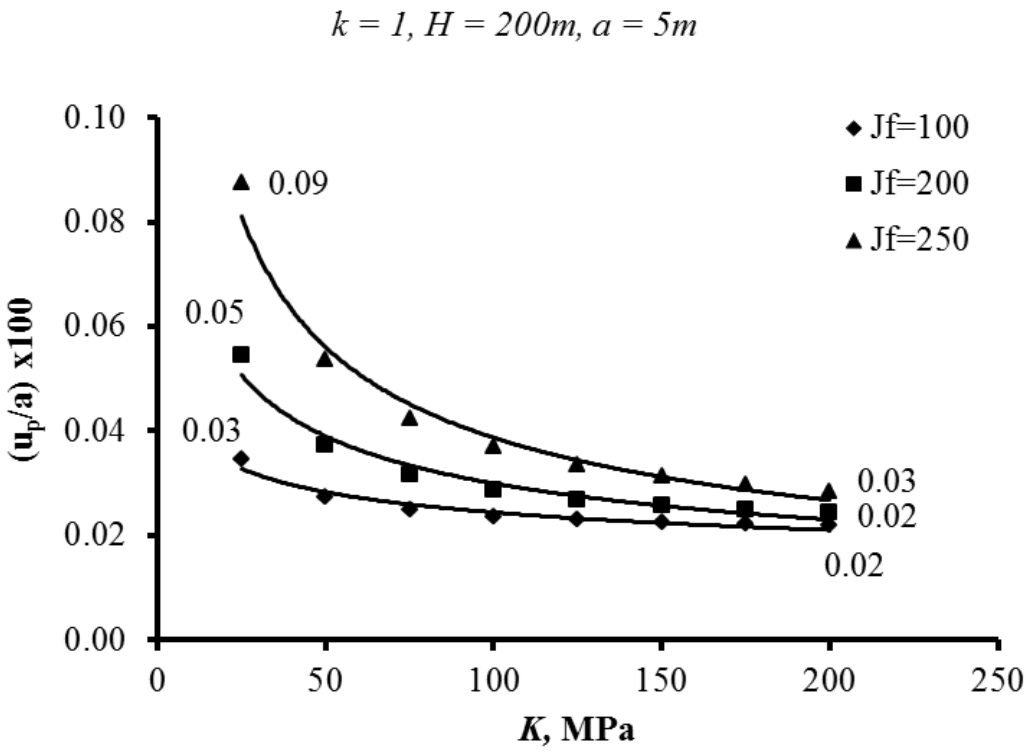

Fig. 5.26 Variation of Tunnel Strain with Support Stiffness, *K*

5.10 LIMITATIONS OF PRESENT STUDY

The present study has following limitations.

- The proposed correlations (Eq. 5.7 - 5.15) for squeezing ground conditions are valid for tunnels excavated by drill and blast method in squeezing ground conditions (where convergence is larger than 1% of the opening size).
- The developed correlations (Eq. 5.26-5.31) for non-squeezing ground conditions are valid for tunnels excavated in non-squeezing ground conditions (where convergence is smaller than 1% of opening size).
- Influence of the method of construction, rate of advance of tunnelling and the timing of second lining have not been considered in the analysis.

5.11 CONCLUDING REMARKS

- Among all the empirical correlations proposed in this chapter and the existing correlation proposed by Goel (1994), the correlation involving joint factor, J_f give predictions with best fit with the observed values for both squeezing and the non-squeezing ground conditions. This may be due to the fact that, the concept of joint factor, J_f developed by Ramamurthy and co-workers (Arora, 1987; Ramamurthy, 1993 & 2004; Ramamurthy and Arora, 1994, Roy, 1993; Singh, 1997; Singh et al., 2002) has been derived through extensive experimental studies in the laboratory. Moreover, this concept involves very few parameters (only three) which can be easily assessed in the field and hence used for development of the correlations as it accounts for anisotropy of rock mass strength.
- Equation 5.9 may be used for the purpose of estimating tunnel strain in the field or during design for tunnels in squeezing ground conditions.
- Similarly, Eq. 5.19 may be used for use in the field and also for design when it comes to prediction of strain in tunnels excavated in non-squeezing ground condition.

Chapter 6

PREDICTION OF SUPPORT PRESSURE

6.1 GENERAL

Himalayan region is full of geological surprises when it comes to the underground construction activities due to fragile nature and frequently changing geology (Singh and Goel, 2006). The region is tectonically highly active and squeezing of rock mass around underground structures has been a major problem faced by Geologists and Engineers (Panthi and Nilsen, 2007) during the construction of many hydro electric projects. It is because of this reason that this region has been a study centre for many research workers. The underground excavations have to be made structurally stable by installing appropriate support systems with appropriate stiffness at appropriate times. As the rock mass surrounding the excavation continues to deform even after installation of the supporting system, it exerts large pressure on it. Therefore, it is essential to have a proper knowledge of the support pressures exerted and attempt has been made here in this chapter to make reliable prediction of support pressures on basis of data collected from various case studies from the lower Himalayas.

This study involves development of empirical correlations for assessment of support pressure in tunnels, which are excavated in squeezing and non-squeezing ground conditions. The concept of 'joint factor (J_f), a measure of rock mass quality, allowable deformation, depth and radius of tunnel are the governing parameters, which have been considered for the study. The values of support pressure predicted by these correlations have been compared with the results obtained via already existing approaches, which are based on rock mass quality (Q) and rock mass number (N).

Stability is the major concern for underground constructions in weak rock masses due to the presence of discontinuities and high in situ stress conditions. High in-situ stress or anisotropic stress condition causes rock bursting, squeezing or other stress induced stability problems (Selmer-Olsen & Broch, 1977). Stress induced stability problems in weak rock masses are characterized by squeezing. Thus, a combination of weak rock mass with high in situ stress multiplies the squeezing problem. According to Barla (1995), squeezing around the tunnel opening may terminate by end of construction period or it may prolong for considerable

amount of time. According to Kovári (1998), squeezing is the phenomenon of large deformations that develops during tunnelling through weak rocks and if an attempt is made to arrest these deformations with the help of a lining or a support system, rock pressure builds up and may reach values beyond the structurally manageable range. The only feasible solution in highly squeezing ground is a flexible tunnel support system in combination with a certain amount of over-excavation in order to accommodate the deformations (Cantieni and Anagnostou, 2009).

Squeezing conditions may vary over short distances due to rock heterogeneity and variations in rock mass properties. Thus, in case of unreliable predictions of support pressure at the design stage, tunnel construction in squeezing ground becomes a herculean task claiming high cost and delay in time. However, if the support pressure can be reliably predicted using the governing parameters which can be easily assessed in the field, and accordingly appropriate stabilisation measures are implemented, then a good tunnelling rate can be achieved (Barla et al., 2011).

6.2 SELECTION OF PARAMETERS

Following parameters have been considered for development of dimensionally correct empirical correlations for prediction of support pressure in squeezing and non-squeezing ground conditions:

i) Size of tunnel or tunnel radius, a
ii) In situ stresses (vertical, σ_v and horizontal, σ_h)
iii) Support stiffness, K
iv) Uni-axial compressive strength of intact rock (σ_{ci})
v) Rock mass characteristics defined by joint factor, J_f, rock mass quality, Q and rock mass number, N and
vi) Tunnel deformation, d.

In case of a flexible support system, rock mass and support system continue to deform together after installation of the support system and hence support pressure decreases. Therefore, radial deformation of tunnel (%) has been considered as one of the governing parameters. This parameter has been determined as follows with the help of collected data of radius and radial deformation of tunnel:

$$d = \frac{u}{a} * 100\,\% \qquad (6.1)$$

where d represents the radial tunnel deformation (%), u, the radial tunnel deformation (m), and a is the radius of the tunnel (m).

6.3 CORRELATION FOR SUPPORT PRESSURE IN SQUEEZING GROUND

It's a general understanding that the support pressure should increase with increase in in-situ stresses and it should decrease with increase in the value of allowable tunnel deformation. Also, the competent rock mass will exert small support pressure and hence a low value of J_f will result in a lower value of support pressure. Using this analogy, an attempt has been made here to study and analyse the data of 53 tunnel sections of 10 different projects in India and other countries. This data for the squeezing ground condition has been presented in Tables 6.1 a,b. The data was analysed using non-linear regression analysis. Several trials were conducted to arrive at the dimensionally correct correlation between the observed support pressure and the joint factor. This correlation is given by Eq. 6.2 which has a correlation coefficient of 92% and the corresponding plot is presented in Fig. 6.1. In Fig.6.1, ratio ($\boldsymbol{10P_{obs}/\sigma_v}$) has been plotted against $\boldsymbol{[J_f{}^3\sigma_h{}^{0.1}/\{10^7\sigma_{ci}{}^{0.1}(d^{0.2}+J_f/1434)\}]}$.

$$P_s = 9.23 * 10^{-3}\sigma_v \left(\frac{J_f{}^3\sigma_h{}^{0.1}}{10^7\sigma_{ci}{}^{0.1}\left(d^{0.2} + \frac{J_f}{1434}\right)} \right)^{1.7} \qquad (R^2=0.92) \qquad (6.2)$$

where

P_s = predicted support pressure, MPa,

J_f = joint factor,

σ_v = vertical in situ stress ($0.027H$), MPa,

σ_{ci} = uniaxial compressive strength of intact rock, MPa

σ_h = horizontal in situ stress, MPa, and

d = radial tunnel deformation (%).

Table 6.1a Data Collected from Various Case Studies for Development of Correlations to Predict Support Pressure in Squeezing Ground Condition

Sl. No.	Name of Tunnel	Rock Type	Reference	*Q*	J_r	J_n	*N*	*a, m*	*H, m*	*d=u/a (%)*	J_n	*n*	*r*	J_f
1.	Chhibro-Khodri adit	Crushed red shales	Jethwa, 1981; Goel, 1994; Choudhari, 2007	0.05	1.5	12	0.375	1.5	280	2.8	14.3	0.09	0.445	357
2.	Chhibro-Khodri HRT	Crushed red shales		0.024	1.2	4	0.5	4.5	680	6	12.9	0.09	0.384	373
3	Chhibro-Khodri adit	Soft & plastic black clays		0.022	1.2	4	0.11	1.5	280	4.5	12.9	0.09	0.384	373
4.	Chhibro-Khodri HRT	Soft & plastic black clays		0.022	1.2	4	0.11	4.5	580	2	12.9	0.09	0.384	373
5.	Giri-Bata HRT	Blaini's slates	Dube, 1979; Goel, 1994; Choudhari, 2007	0.36	1	6	2.55	2.3	380	7.6	7.69	0.07	0.384	286
6	Giri-Bata HRT	Crushed phyllites		0.12	1	4	0.6	2.3	240	5.5	8.45	0.07	0.364	332
7.	Loktak HRT	MFSS		0.015	0.5	6	0.173	2.4	300	7	9.45	0.09	0.268	392
8.	Maneri stage-I HRT	Sheared metabasics	Jethwa, 1981	0.16	1.2	9	3.75	2.9	450	7.3	18.1	0.22	0.268	307
9.	Maneri stage-II HRT	Metavolcanic	Goel, 1994; Choudhari, 2007	0.8	1.2	4	4	1.25	480	2.5	5.75	0.05	0.445	258
10.	Maneri stage-II HRT	Sheared metabasics		0.18	1.2	9	0.9	3.5	410	3	6.85	0.05	0.445	308
11.	Noonidih colliery MG	Weak coal	Jethwa, 1981	0.59	1	6	5.9	3.5	450	3	71.4	0.82	0.344	253
12.	Tala hydro HRT	AGO (Adverse geological occurrences): Completely sheared, highly weathered biotite schist associated with banded gneiss, amphibolites and quartzites in thin bands	Sripad et al., 2007	0.007	1	15	0.07	3.4	337	2.1	16.91	0.09	0.445	422
13.	Tala HRT, Bhutan			0.011	1	15	0.11	3.4	337	3.8	16	0.09	0.445	399
14.	Tala HRT, Bhutan			0.006	1	15	0.06	3.4	337	3.1	16.48	0.09	0.445	411
15.	Tala HRT, Bhutan			0.006	1	15	0.06	3.4	337	2.2	16.48	0.09	0.445	411
16.	Tala HRT, Bhutan			0.08	1	15	0.8	3.4	337	2.2	13.39	0.09	0.445	334
17.	Kaligandaki 'A' HRT	Graphic phyllites	NEA, 2002; Panthi and Nilsen, 2007	0.029	1	15	0.125	4.35	550	2.3	3.29	0.05	0.18	365
18.	Kaligandaki'A' HRT	Graphic phyllites		0.023	1	15	0.115	4.35	600	1.4	3.33	0.05	0.18	370
19.	Kaligandaki'A' HRT	Graphic phyllites		0.03	1	15	0.15	4.35	600	2.9	3.23	0.05	0.18	359
20.	Kaligandaki 'A' HRT	Graphic phyllites		0.018	1	15	0.09	4.35	600	3.9	3.42	0.05	0.18	380
21.	Kaligandaki 'A' HRT	Graphic phyllites		0.023	1	15	0.12	4.35	600	3.2	3.33	0.05	0.18	370
22.	Kaligandaki 'A'HRT	Graphic phyllites		0.02	1	15	0.3	4.35	620	4.9	3.36	0.05	0.18	373
23.	Kaligandaki 'A' HRT	Graphic phyllites		0.008	1	15	0.16	4.35	620	8.5	6.4	0.09	0.18	401

…..Contd.

Sl. No.	Name of Tunnel	Rock Type	Reference	*Q*	J_r	J_n'	*N*	*a, m*	*H, m*	*d=u/a (%)*	J_n	*n*	*r*	J_f
24.	Kaligandaki 'A' HRT	Graphic phyllites		0.009	1	15	0.18	4.35	620	7.7	3.6	0.05	0.18	400
25.	Kaligandaki 'A' HRT	Graphic phyllites	NEA, 2002; Panthi and Nilsen, 2007	0.009	1	15	0.18	4.35	620	8.2	3.6	0.05	0.18	400
26.	Kaligandaki 'A' HRT	Siliceous phyllites		0.016	1	15	0.32	4.35	620	4.4	6.3	0.09	0.18	389
27.	Kaligandaki 'A' HRT	Graphic phyllites		0.02	1	15	0.1	4.35	620	4.1	3.36	0.05	0.18	373
28.	Kaligandaki 'A' HRT	Graphic phyllites		0.025	1	15	0.5	4.35	620	2.5	5.95	0.09	0.18	367
29.	Kaligandaki 'A' HRT	Graphic phyllites		0.023	1	15	0.115	4.35	580	3.7	3.33	0.05	0.18	370
30.	Kaligandaki 'A' HRT	Graphic phyllites		0.025	1	15	0.125	4.35	580	1.7	5.95	0.09	0.18	367
31.	Kaligandaki 'A' HRT	Graphic phyllites		0.025	1	15	0.125	4.35	550	2.4	5.95	0.09	0.18	367
32.	Kaligandaki 'A' HRT	Graphic phyllites		0.007	1	15	0.035	4.35	575	6.0	6.4	0.09	0.18	401
33.	Nathpa Jhakri-HRT	Quartz mica schist; Schistose quartzites and amphibolites	Kumar, 2002	0.417	1.5	9	8.333	5.5	700	3.5	6.1	0.05	0.47	260
34.	Nathpa Jhakri-HRT			0.333	1.5	9	1.665	5.5	700	3.5	8.77	0.05	0.47	273
35.	Nathpa Jhakri-HRT			0.333	1.5	9	1.665	5.5	750	3.5	7.7	0.06	0.47	274
36.	Nathpa Jhakri-HRT			0.25	1.5	9	1.25	5.5	600	3.5	10.99	0.08	0.47	292
37.	Nathpa Jhakri-HRT			0.056	1.5	9	0.556	5.5	850	5.0	8.06	0.05	0.47	343
38.	Nathpa Jhakri-HRT			0.033	1.5	9	0.167	5.5	600	3.0	8.77	0.05	0.47	373
39.	Nathpa Jhakri-HRT			0.001	1.5	9	0.019	5.5	300	6.0	11.63	0.05	0.47	495
40.	Nathpa Jhakri-HRT			0.003	1.5	9	0.052	5.5	400	6.0	10.64	0.06	0.47	453
41.	Nathpa Jhakri-HRT			0.194	1.5	9	0.97	5.5	800	3.5	7.2	0.05	0.47	306
42.	Udhampur rail tunnel (T1)	Claystone, Silty claystone	CIMFR, 2007	0.0625	1.5	12	0.313	3.25	300	3.0	9.5	0.06	0.47	340
43.	Udhampur rail tunnel (T1)			0.0938	1.5	12	0.469	3.25	312	1.5	9.1	0.06	0.47	327
44.	Udhampur rail tunnel (T1)			0.0833	2	12	0.417	3.25	280	1.5	9.7	0.06	0.49	331
45.	Udhampur rail tunnel (T1)			0.125	2	12	0.625	3.25	270	2.2	9.3	0.06	0.49	318
46.	Udhampur rail tunnel (T1)			0.0625	2	12	0.625	3.25	285	2.5	9.5	0.06	0.47	340
47.	Udhampur rail tunnel (T1)			0.0313	1.5	12	0.313	3.25	280	2.6	9.3	0.06	0.45	348
48.	Udhampur rail tunnel (T1)			0.0417	2	12	0.417	3.25	280	2.4	9.3	0.06	0.45	348

…..Contd.

Sl. No.	Name of Tunnel	Rock Type	Reference	*Q*	J_r	J_n'	*N*	*a, m*	*H, m*	*d=u/a (%)*	J_n	*n*	*r*	J_f
49.	Chenani-Nashri escape tunnel	Siltstone, Silty claystone	Facibeni et al., 2011	2.287	3.5	12	5.718	3	727	1.7	5.15	0.05	0.47	221
50.	Chenani-Nashri escape tunnel			2.426	2.5	12	6.065	3	736	1.3	5.09	0.05	0.47	218
51.	Chenani-Nashri escape tunnel	Siltstone, Silty claystone	GEODATA/ LIN, 2011a	2.903	3.5	12	7.258	3	733	1.6	4.88	0.05	0.47	209
52.	Chenani-Nashri escape tunnel			1.65	3.5	12	4.125	3	690	1.6	5.34	0.05	0.47	229
53.	Chenani-Nashri main tunnel	Siltstone		1.517	3.5	12	3.793	6.5	577	1.8	5.34	0.05	0.45	240

Notation: ***HRT' Head race tunnel; MG- Mine gallery; MFSS- Moderately fractured splintery shales with clay coatings; J_n'- Joint set number.***

Table 6.1b Values of Parameters, σ_{ci} , σ_h and σ_v at Various Tunnel Sections Listed in Table 6.1a

Sl. No.	σ_{ci} (MPa)	σ_h (MPa)	σ_v (MPa)	**Sl. No.**	σ_{ci} (MPa)	σ_h (MPa)	σ_v (MPa)	**Sl. No.**	σ_{ci} (MPa)	σ_h (MPa)	σ_v (MPa)
1.	21	7.6	7.6	**19.**	39	7.4	16.2	**37.**	32	29.8	23.0
2.	21	18.4	18.4	**20.**	39	8.1	16.2	**38.**	32	21.1	16.2
3.	8	7.6	7.6	**21.**	39	8.1	16.2	**39.**	32	10.5	8.1
4.	8	15.7	15.7	**22.**	39	8.1	16.7	**40.**	32	14.0	10.8
5.	20	20.5	10.3	**23.**	39	8.1	16.7	**41.**	32	28.1	21.6
6.	14	13.0	6.5	**24.**	39	8.4	16.7	**42.**	20	9.7	8.1
7.	27	8.1	8.1	**25.**	39	8.4	16.7	**43.**	20	10.1	8.4
8.	10	3.6	12.2	**26.**	39	8.4	16.7	**44.**	20	9.1	7.6
9.	24	3.9	13.0	**27.**	39	8.4	16.7	**45.**	20	8.7	7.3
10.	11	3.3	11.1	**28.**	39	8.4	16.7	**46.**	20	9.2	7.7
11.	21	10.4	12.2	**29.**	39	8.4	15.7	**47.**	20	9.1	7.6
12.	10	4.5	9.1	**30.**	39	8.4	15.7	**48.**	20	9.1	7.6
13.	10	4.5	9.1	**31.**	39	7.8	14.9	**49.**	35	23.6	19.6
14.	10	4.5	9.1	**32.**	39	7.8	15.5	**50.**	35	23.8	19.9
15.	10	4.5	9.1	**33.**	32	7.4	18.9	**51.**	35	23.7	19.8
16.	10	4.5	9.1	**34.**	32	7.8	18.9	**52.**	35	22.4	18.6
17.	39	7.6	14.9	**35.**	32	24.6	20.3	**53.**	40	18.7	15.6
18.	39	18.4	16.2	**36.**	32	24.6	16.2				

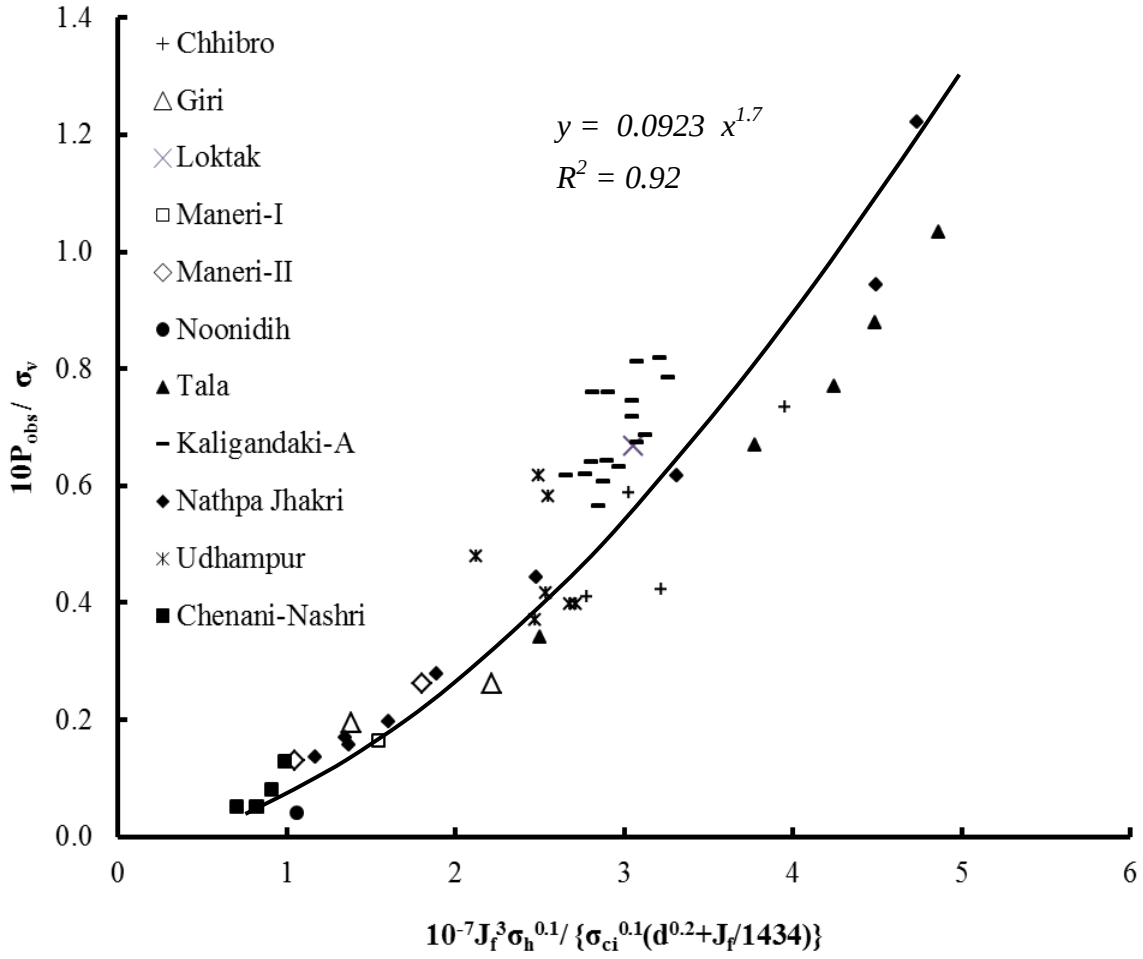

Fig. 6.1 Plot of $[10P_{obs}/\sigma_v]$ Versus $[10^{-7}J_f^3\sigma_h^{0.1}/\{\sigma_{ci}^{0.1}(d^{0.2}+J_f/1434)\}]$ for Squeezing Grounds

6.4 EMPIRICAL CORRELATIONS AVAILABLE IN LITERATURE

For comparing the support pressure predicted on basis of proposed equation (Eq. 6.2), attempt has been made to predict the values of support pressure on basis of other correlations already available in the literature. The other correlations available in the literature are :

6.4.1 Grimstad and Barton (1993) Correlation using Rock Mass Quality, *Q*

Grimstad and Barton (1993) suggested an empirical approach for estimation of roof support pressure in tunnels using rock mass quality, *Q* (Eq. 6.3). Accordingly, the support pressure is independent of the span or the diameter of tunnel and is given by –

$$P_u = \frac{0.2\sqrt{J_n}}{3J_r} Q^{-1/3} \tag{6.3}$$

where P_u is the tunnel support pressure, MPa; J_n , the joint set number; J_r , the joint roughness number; and Q is the rock quality index.

6.4.2 Goel (1994) Correlation using Rock Mass Number, *N*

Due to difficulty in assessment of the stress reduction factor (*SRF*), which is required for obtaining the *Q* value, Goel (1994) proposed another expression based on rock mass number, *N*. Goel (1994) realised the influence of size (diameter or span) of tunnel on support pressure and hence suggested the following empirical correlation to predict the support pressure for tunnels excavated in squeezing grounds:

$$P_N = \left(\frac{f}{30}\right) 10^{\frac{H^{0.6} a^{0.1}}{50N^{0.33}}} \tag{6.4}$$

where P_N represents the tunnel support pressure in squeezing ground condition in MPa; f , the correction factor for tunnel closure (Fig. 2.7 in Chap. 2); H , the depth of tunnel (m); a , the radius of tunnel (m) , and *N*, is the rock mass number.

6.4.3 Bhasin and Grimstad (1996) correlation using Rock Mass Quality, *Q*

Based on - i) the cases studies of Scandinavian tunnels, ii) the data of Singh et al. (1992), and iii) studies conducted by Goel et al. (1995), Bhasin and Grimstad (1996) suggested a new correlation for poor quality brecciated rock mass (Eq. 6.5). In this correlation, size of tunnel was taken into consideration as follows:

$$P_b = \frac{0.04}{J_r} .D.Q^{-1/3} \tag{6.5}$$

where P_b defines the ultimate tunnel support pressure, MPa; D is the diameter or span of the tunnel (m); J_r is the joint roughness number, and Q is the rock quality index.

6.5 COMPARISON OF PREDICTED AND OBSERVED SUPPORT PRESSURE

An index called Coefficient of Accordance (COA) has been computed for values of support pressure estimated from correlations given by Grimstad and Barton (1993), Goel (1994),

Bhasin and Grimstad (1996) and author's Eq. 6.2 presented in art. 6.3. Values of COA are presented in Table 6.2 (col. for comparison of the various approaches. COA (ψ^2) is defined as follows:

$$\psi^2 = \frac{\sum(P_{obs} - P_{est})^2}{\sum\left(P_{obs} - \frac{\sum P_{obs}}{n}\right)^2} \tag{6.6}$$

where ψ^2 is COA, P_{obs} is the observed support pressure (col. 4 of Table 6.2), P_{est} is estimated support pressure (col. 5 for support pressure, P_N using Eq. 6.4; col. 8 for support pressure, *Pu* using Eq. 6.3 ; col. 10 for support pressure, P_b using Eq. 6.5; and col. 12 for support pressure, P_s using Eq. 6.2) and *n* is number of data sets. Lower value of COA indicates a better correlation. **Study of Table 6.2 suggests that predicted values of support pressure estimated from the correlation given by Eq. 6.2 gives the least Coefficient of Accordance of 0.08 as compared to values of support pressure predicted by using other correlations. It can therefore be concluded that the proposed correlation (Eq. 6.2) is definitely an improvement over the other correlations.**

In addition to the above method of comparison (Table 6.2), estimated values of support pressure have also been plotted in Fig. 6.2 with the observed values of support pressure for the sake of comparison. The plot also shows a line AB with 1:1 gradient. If predictions by a given approach are better, the points should lie close to 1:1 line. It can be seen that the predictions made by the proposed approach lie closer to the line AB as compared to the other approaches.

Table 6.2 Coefficient of Accordance for Values of Support Pressure Estimated from Various Approaches

Sl. No.	Name of Tunnel	Rock Type	P_{obs}, MPa	P_N, MPa	$(P_{obs}-P_N)^2$	$(P_{obs}-\Sigma P_{obs}/n)^2$	P_u, MPa	$(P_{obs}-P_u)^2$	P_b, MPa	$(P_{obs}-P_b)^2$	P_s, MPa	$(P_{obs}-P_s)^2$
1.	Chhibro-Khodri adit	Crushed red shales	0.31	0.26	0.00	0.21	1.25	0.89	0.22	0.01	0.40	0.01
2.	Chhibro-Khodri HRT	Crushed red shales	1.08	1.02	0.00	0.10	1.16	0.01	1.04	0.00	1.11	0.00
3.	Chhibro-Khodri adit	Soft & plastic black clays	0.32	0.39	0.00	0.18	1.19	0.76	0.36	0.00	0.51	0.04
4.	Chhibro-Khodri HRT	Soft & plastic black clays	1.15	7.98	46.63	0.18	1.19	0.00	1.07	0.01	1.50	0.12
5.	Giri-Bata HRT	Blaini's slates	0.20	0.22	0.00	0.25	0.69	0.24	0.26	0.00	0.16	0.00
6.	Giri-Bata HRT	Crushed phyllites	0.17	0.14	0.00	0.28	0.81	0.41	0.37	0.04	0.23	0.00
7.	Loktak HRT	MFSS	0.54	0.81	0.07	0.02	3.97	11.78	1.56	1.03	0.50	0.00
8.	Maneri Stage-I HRT	Sheared metabasics	0.20	0.21	0.00	0.23	0.92	0.52	0.36	0.02	0.23	0.00
9.	Maneri Stage-II HRT	Metavolcanic	0.17	0.14	0.00	0.26	0.36	0.04	0.09	0.01	0.13	0.00
10.	Maneri Stage-II HRT	Sheared metabasics	0.29	0.25	0.00	0.15	0.89	0.35	0.41	0.02	0.28	0.00
11.	Noonidih Colliery MG	Weak coal	0.15	0.10	0.00	0.27	0.58	0.19	0.33	0.03	0.12	0.00
12.	Tala Hydro HRT	AGO (Adverse geological occurrences): Completely sheared, highly weathered biotite schist associated with banded gneiss, amphibolites and quartzites in thin bands	0.94	3.05	4.47	0.08	4.05	9.67	1.42	0.23	1.24	0.09
13.	Tala HRT, Bhutan		0.61	0.86	0.06	0.00	3.48	8.25	1.22	0.38	0.80	0.04
14.	Tala HRT, Bhutan		0.70	2.52	3.33	0.01	4.26	12.69	1.50	0.64	0.98	0.08
15.	Tala HRT, Bhutan		0.80	3.53	7.47	0.04	4.26	11.99	1.50	0.49	1.08	0.08
16.	Tala HRT, Bhutan		0.31	0.29	0.00	0.08	1.80	2.21	0.63	0.10	0.40	0.01
17.	Kaligandaki 'A' HRT	Graphic phyllites	0.90	1.60	0.50	0.10	2.52	2.63	1.13	0.05	0.83	0.01
18.	Kaligandaki'A' HRT	Graphic phyllites	1.27	3.37	4.41	0.51	2.72	2.11	1.22	0.00	1.11	0.02
19.	Kaligandaki'A' HRT	Graphic phyllites	1.00	1.50	0.25	0.22	2.49	2.23	1.12	0.01	0.79	0.04
20.	Kaligandaki 'A' HRT	Graphic phyllites	1.02	1.80	0.61	0.27	2.96	3.73	1.33	0.09	0.95	0.01
21.	Kaligandaki 'A' HRT	Graphic phyllites	0.92	1.75	0.70	0.19	2.72	3.27	1.22	0.09	0.88	0.00
22.	Kaligandaki 'A'HRT	Graphic phyllites	1.27	1.54	0.07	0.66	2.85	2.51	1.28	0.00	0.90	0.14
23.	Kaligandaki 'A' HRT	Graphic phyllites	1.25	7.65	41.05	0.68	3.87	6.89	1.74	0.24	1.03	0.05
24.	Kaligandaki 'A' HRT	Graphic phyllites	1.13	5.36	17.94	0.54	3.72	6.75	1.67	0.30	1.05	0.01

…….Contd.....

Sl. No.	Name of Tunnel	Rock Type	P_{obs}, MPa	P_N, MPa	$(P_{obs}-P_N)^2$	$(P_{obs} - \Sigma P_{obs}/n)^2$	P_u, MPa	$(P_{obs}-P_u)^2$	P_b, MPa	$(P_{obs}-P_b)^2$	P_s, MPa	$(P_{obs}-P_s)^2$
25.	Kaligandaki 'A' HRT	Graphic phyllites	1.20	5.88	21.85	0.70	3.72	6.37	1.67	0.22	1.03	0.03
26.	Kaligandaki 'A' HRT	Siliceous phyllites	1.15	0.83	0.10	0.66	3.07	3.70	1.38	0.05	1.07	0.01
27.	Kaligandaki 'A' HRT	Graphic phyllites	1.07	1.54	0.22	0.58	2.85	3.17	1.28	0.04	0.89	0.03
28..	Kaligandaki 'A' HRT	Graphic phyllites	1.27	2.26	0.97	0.98	2.65	1.90	1.19	0.01	0.95	0.10
29.	Kaligandaki 'A' HRT	Graphic phyllites	0.97	1.29	0.10	0.52	2.72	3.08	1.22	0.06	0.82	0.02
30.	Kaligandaki 'A' HRT	Graphic phyllites	1.27	2.61	1.79	1.09	2.65	1.90	1.19	0.01	0.98	0.09
31.	Kaligandaki 'A' HRT	Graphic phyllites	0.95	1.81	0.73	0.57	2.65	2.88	1.19	0.06	0.84	0.01
32.	Kaligandaki 'A' HRT	Graphic phyllites	1.27	3.55	5.21	1.20	4.05	7.72	1.82	0.30	1.04	0.05
33.	Nathpa Jhakri-HRT	Quartz mica schist; Schistose quartzites and amphibolites	0.26	0.10	0.03	0.01	0.54	0.08	0.39	0.02	0.23	0.00
34.	Nathpa Jhakri-HRT		0.32	0.26	0.00	0.03	0.58	0.07	0.42	0.01	0.29	0.00
35.	Nathpa Jhakri-HRT		0.32	0.29	0.00	0.04	0.58	0.07	0.42	0.01	0.32	0.00
36.	Nathpa Jhakri-HRT		0.32	0.26	0.00	0.04	0.63	0.10	0.47	0.02	0.33	0.00
37.	Nathpa Jhakri-HRT		1.02	1.01	0.00	0.82	1.05	0.00	0.77	0.06	0.99	0.00
38.	Nathpa Jhakri-HRT		1.00	3.24	5.04	0.83	1.25	0.06	0.91	0.01	1.14	0.02
39.	Nathpa Jhakri-HRT		0.99	4.81	14.59	0.86	4.00	9.06	2.93	3.78	1.05	0.00
40.	Nathpa Jhakri-HRT		1.02	4.37	11.23	0.82	2.77	3.07	2.03	1.03	1.28	0.07
41.	Nathpa Jhakri-HRT		0.60	0.52	0.01	0.34	0.69	0.01	0.51	0.01	0.59	0.00
42.	Udhampur rail tunnel (T1)	Claystone, Silty claystone	0.30	0.32	0.00	0.05	1.16	0.75	0.44	0.02	0.35	0.00
43.	Udhampur rail tunnel (T1)		0.52	0.46	0.00	0.20	1.02	0.25	0.38	0.02	0.37	0.02
44.	Udhampur rail tunnel (T1)		0.44	0.44	0.00	0.15	0.79	0.12	0.30	0.02	0.34	0.01
45.	Udhampur rail tunnel (T1)		0.35	0.26	0.01	0.09	0.69	0.12	0.26	0.01	0.24	0.01
46.	Udhampur rail tunnel (T1)		0.32	0.25	0.01	0.08	0.87	0.31	0.33	0.00	0.35	0.00
47.	Udhampur rail tunnel (T1)		0.30	0.34	0.00	0.07	0.88	0.34	0.33	0.00	0.37	0.01
48.	Udhampur rail tunnel (T1)		0.30	0.32	0.00	0.08	1.00	0.49	0.37	0.01	0.38	0.01
49.	Chenani-Nashri escape tunnel	Siltstone, Silty claystone	0.10	0.28	0.03	0.01	0.15	0.00	0.05	0.00	0.13	0.00
50.	Chenani-Nashri escape tunnel		0.10	0.30	0.04	0.01	0.15	0.00	0.05	0.00	0.13	0.00

…..Contd.

Sl. No.	Name of Tunnel	Rock Type	P_{obs}, MPa	P_N, MPa	$(P_{obs}-P_N)^2$	$(P_{obs} - \Sigma P_{obs}/n)^2$	P_u, MPa	$(P_{obs}-P_u)^2$	P_b, MPa	$(P_{obs}-P_b)^2$	P_s, MPa	$(P_{obs}-P_s)^2$
51.	Chenani-Nashri escape tunnel	Siltstone, Silty claystone	0.10	0.26	0.02	0.01	0.14	0.00	0.05	0.00	0.10	0.00
52.	Chenani-Nashri escape tunnel		0.15	0.32	0.03	0.02	0.17	0.00	0.06	0.01	0.15	0.00
53.	Chenani-Nashri main tunnel	Siltstone	0.20	0.29	0.01	0.04	0.17	0.00	0.13	0.00	0.14	0.00
					For P_N		**For P_u**		**For P_b**		**For P_s**	
				$\Sigma((P_{obs}-P_{est})^2$	93.26		135.72		9.6		1.25	
				$\Sigma\{(P_{obs} - \Sigma P_{obs}/n)^2\}$		14.93						
				Coefficient of accordance (Ψ^2) = $\Sigma((P_{obs}-P_{est})^2 / \Sigma\{(P_{obs} - \Sigma P_{obs}/n)^2\}$		6.25	9.01		0.64		0.08

<u>Notation:</u> ***HRT' Head race tunnel; MG- Mine gallery; MFSS- Moderately fractured splintery shales with clay coatings; P_N, P_u, P_b and P_s are estimated support pressures using approaches given by Goel (1994), Grimstad and Barton (1993), Bhasin and Grimstad (1996) and authors respectively, P_{est}-estimated support pressure.***

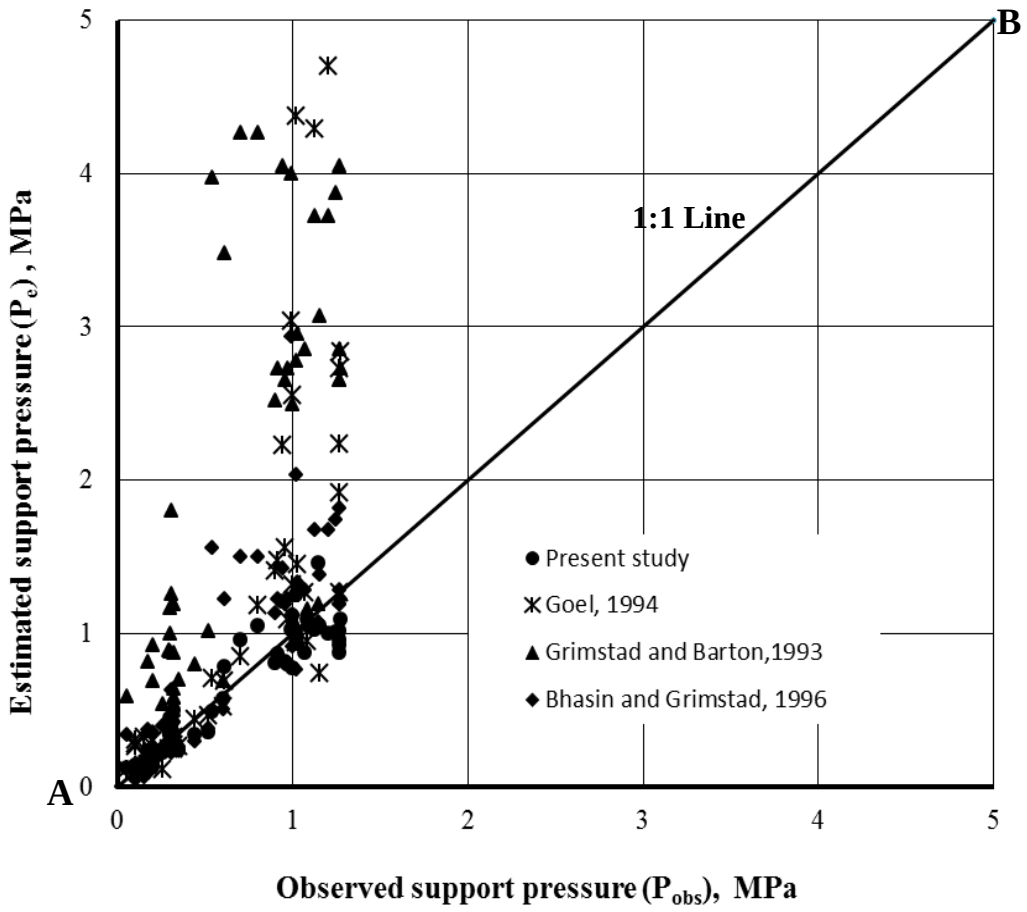

Fig. 6.2 Comparison of Predicted Values of Support Pressure by Various Correlations with Observed Values

Equation 6.3 proposed by Grimstad and Barton (1993) does not involve parameters like diameter or span of tunnel and the magnitude of tunnel deformation, which are important parameters especially in squeezing grounds. These parameters are less important for estimation of support pressure in elastic or non-squeezing ground conditions. Due to this reason, support pressures estimated from Eq. 6.3 (Grimstad and Barton, 1993) and presented in col. 8 of Table 6.2 and support pressures estimated from Eq. 6.5 (Bhasin and Grimstad, 1996) and presented in col. 10 of Table 6.2, do not hold good correlation with values of observed support pressure. Hence corresponding values of COA are 9.01 and 0.64 respectively (Table 6.2) and the corresponding points lie far away from the line AB in Fig. 6.2. Equation 6.4 proposed by Goel (1994) uses closure correction to consider the effect of tunnel deformation (Fig. 2.6 in Chapter 2). The values of correction factors depend upon in-situ stresses, diameter or span of the tunnel and rock mass quality and hence will vary with these parameters, whereas values of correction factors as suggested in Fig. 2.7 of Chapter 2 are constant with respect to the aforesaid parameters. May be due to this reason, the values of

support pressure using Eq. 6.4 show low degree of correlation with observed support pressures as the estimated support pressure values have high COA of 6.25 (Table 6.2) and lie very far away from line AB in Fig. 6.2. Moreover, all the above approaches (art. 6.4) suffer from the drawback of not being dimensionally correct. On the other hand, the proposed correlation (Eq. 6.2) involves both the parameters as discussed above and shows a very good accordance with the observed support pressures, as the predicted values of support pressure give very low COA i.e. 0.08 (Table 6.2) and the corresponding points lie very close to the AB line in Fig. 6.2.

The proposed correlation (Eq.6.2) for prediction of support pressure in tunnels excavated in squeezing grounds involves tunnel size (diameter or span) as one of the parameters which significantly affects the behaviour of tunnels (Goel et al., 1996; Bhasin et al., 2006). Tunnel deformation is another parameter which plays a very important role in the mobilisation of support pressure. The predicted values on comparison with observed support pressures give a very low Coefficient of Accordance (Table 6.2 & Fig. 6.2) and a good correlation coefficient of 0.92. This may be attributed to involvement of horizontal in situ stress and uniaxial compressive strength of intact rock as additional influencing parameters in Eq. 6.2. On the other hand, Eq. 6.3 does not involve the above stated four parameters and therefore the predictions using Eq. 6.3 is not reliable for squeezing grounds and hence the values of predicted support pressure fit with values of observed support pressure with a poor Coefficient of Accordance (Table 6.2 & Fig. 6.2). Approach suggested by Bhasin and Grimstad (1996) is a modification of the approach suggested by Grimstad and Barton (1993) in which tunnel size was introduced as a new parameter (Eq. 6.5). However, Eq. 6.5 doesn't involve tunnel deformation, σ_h and σ_{ci} as parameters and the values of predicted support pressure using this approach were found to fit with observed values of support pressure with COA of 0.64 (Fig. 6.3) i.e. the prediction is much better than that given by Eq. 6.3. Equation 6.4 uses both tunnel size and tunnel deformation as parameters by introducing a correction factor, f and the predicted values fit with very low accordance with the observed values of support pressure (Fig.6.2 and Table 6.2).

The dimensionally correct correlation represented by Eq. 6.2 and involving joint factor (J_f) exhibits significance for zero value of tunnel deformation and it predicts support pressure, when the supports are installed without any delay on substituting tunnel deformation, $d = 0$.

6.6 PARAMETRIC STUDY

Variation in values of support pressure predicted by the dimensionally correct empirical correlation developed in the present study (Eq. 6.2) with various influencing parameters has been studied by carrying out following parametric study:

6.6.1 Influence of Tunnel Depth, *H*

An attention was made to consider 3 values of J_f, namely 300, 350 and 400 and values of support pressure were predicted on basis of Eq. 6.2 for different values of *H* and this variation has been potted in Fig. 6.3. Figure 6.3 shows that support pressure increases with increase in depth of overburden rock mass for the values of J_f between 300 and 400. The slope of the curve increases with value of J_f . For example, slope (*dy* /*dx*) of the curves for J_f = 300, 350 and 400 are $2.2*10^{-4}$ *x*, $3.3*10^{-4}$ *x* and $5.5*10^{-4}$ *x* respectively, where *x* denotes the values on x-axis i.e. tunnel depth (Fig. 6.3). Slope of the curve for J_f = 400 is the highest indicating that tunnel attracts higher support pressure at faster rate with tunnel depth in the presence of weaker rock mass.

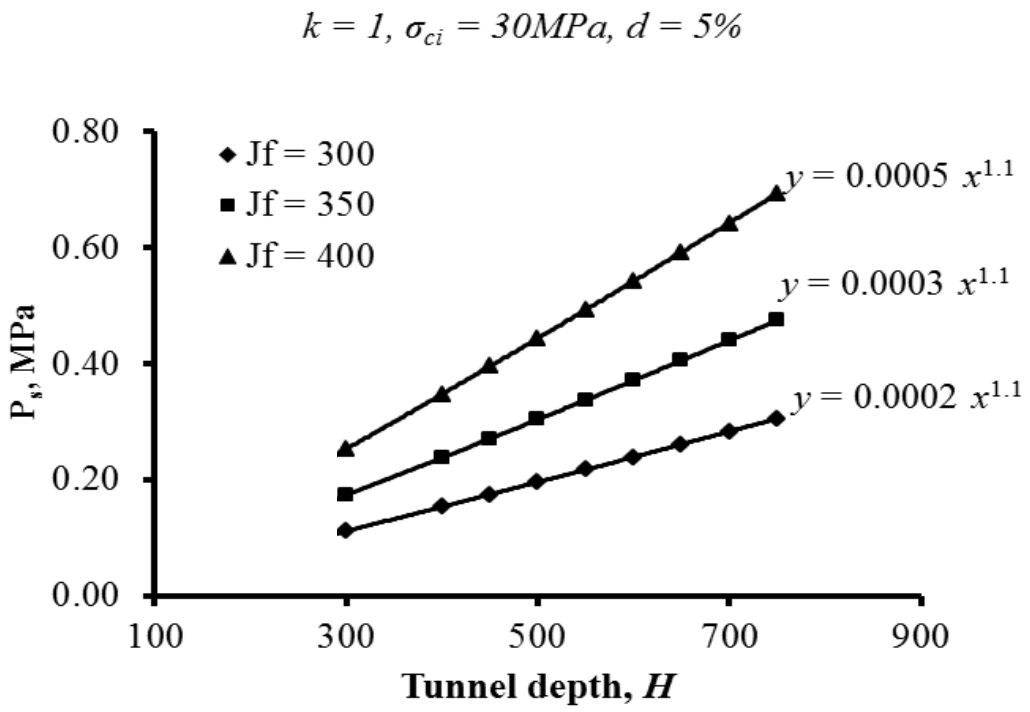

Fig. 6.3 Variation of Tunnel Support Pressure with Tunnel Depth

6.6.2 Influence of Tunnel Radius, *a*

The influence of the size of tunnel on support pressure has been studied in the form of variation of support pressure with radius of the tunnel and has been plotted in Fig. 6.4. which suggests that support pressure increases only marginally with increase in tunnel radius. However, support pressures increase for tunnels excavated at large depth.

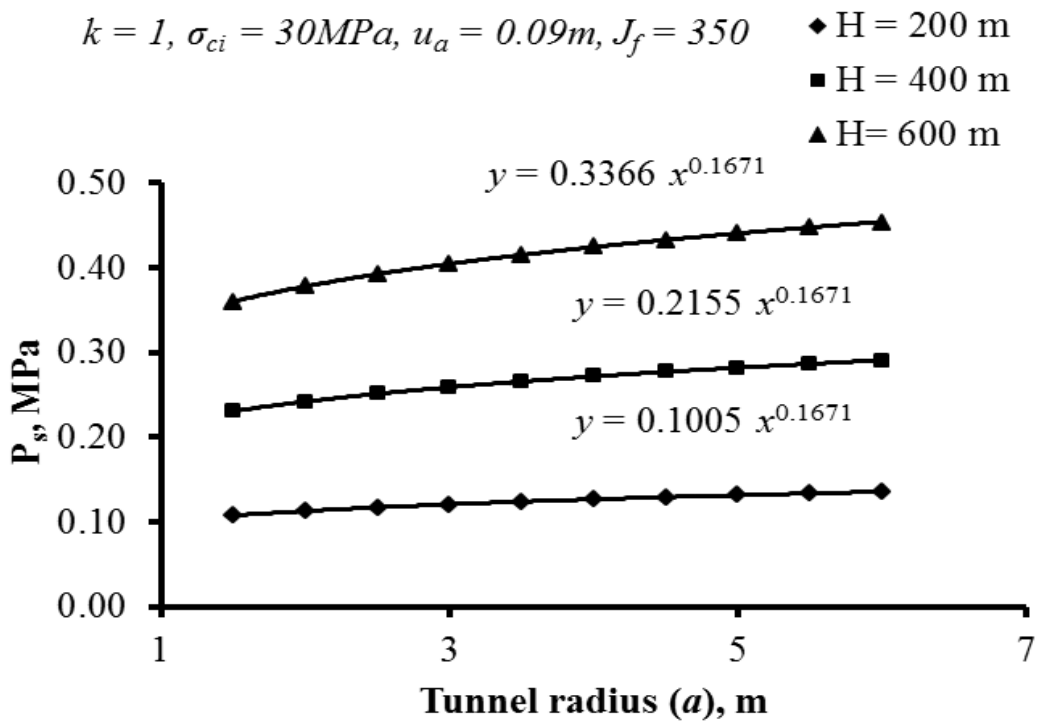

Fig. 6.4 Variation of Tunnel Support Pressure with Tunnel Radius

6.6.3 Influence of Joint Factor, J_f

Figure 6.5 shows the effect of joint factor, J_f on tunnel support pressure. It is clear that tunnel support pressure increases significantly with increase in joint factor, J_f. In other words, tunnel support pressure is highly influenced with quality of rock mass and it increases exponentially, if the rock mass quality deteriorates, i.e., for high values of joint factor. In addition to this, support pressure increases for tunnels having larger radius. This effect can be clearly seen in Fig. 6.5, where curve for 8 m radius tunnel has a steeper slope as compared to that for tunnel having radius of 4 m.

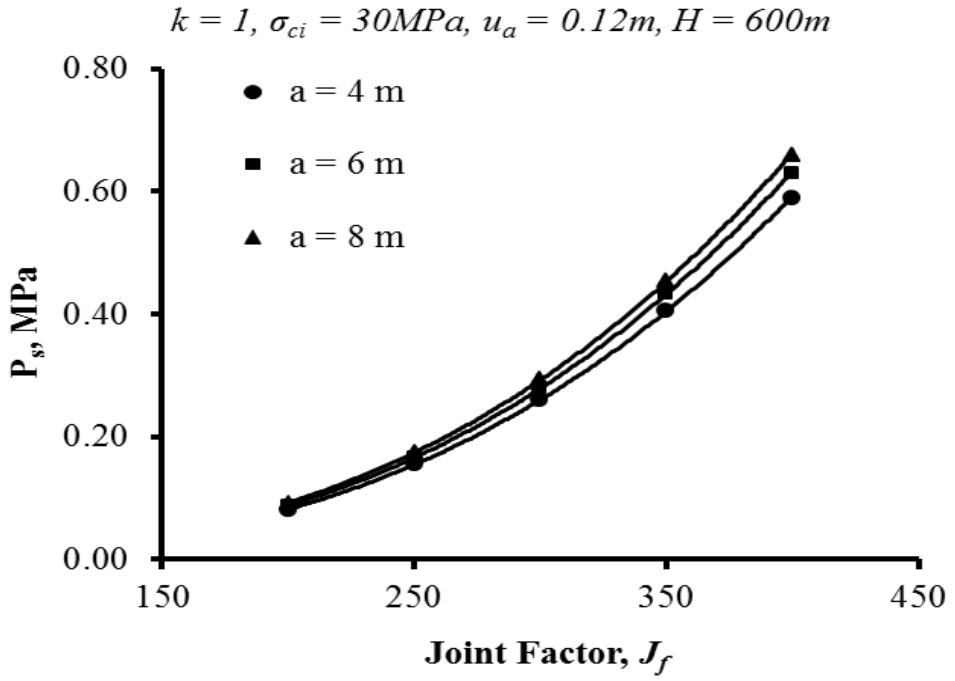

Fig. 6.5 Variation of tunnel Support Pressure with Joint Factor

6.6.4 Influence of Tunnel Closure, *d*

Values of tunnel support pressure have been plotted with the values of allowed tunnel deformation in Fig. 6.6. The plot suggests that support pressure decreases on increasing allowable limit of tunnel deformation. This is because induced stresses around a tunnel opening are released when tunnel deformation is allowed leading to reduced support pressure.

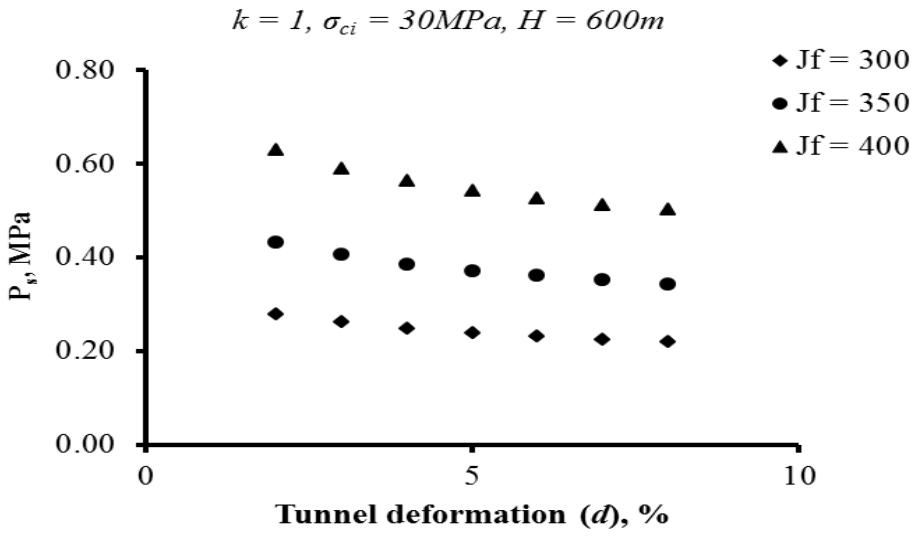

Fig. 6.6 Variation of tunnel Support Pressure with Tunnel Deformation

6.6.5 Influence of Horizontal In-situ Stress, σ_h

Plot in Fig. 6.7 indicates that for a given value of J_f, support pressure is marginally affected due to increasing horizontal in-situ stress. However, tunnel support pressure increases with horizontal in-situ stress for higher J_f values. The severity increases with reduction in the quality of rock mass or an increase in J_f value.

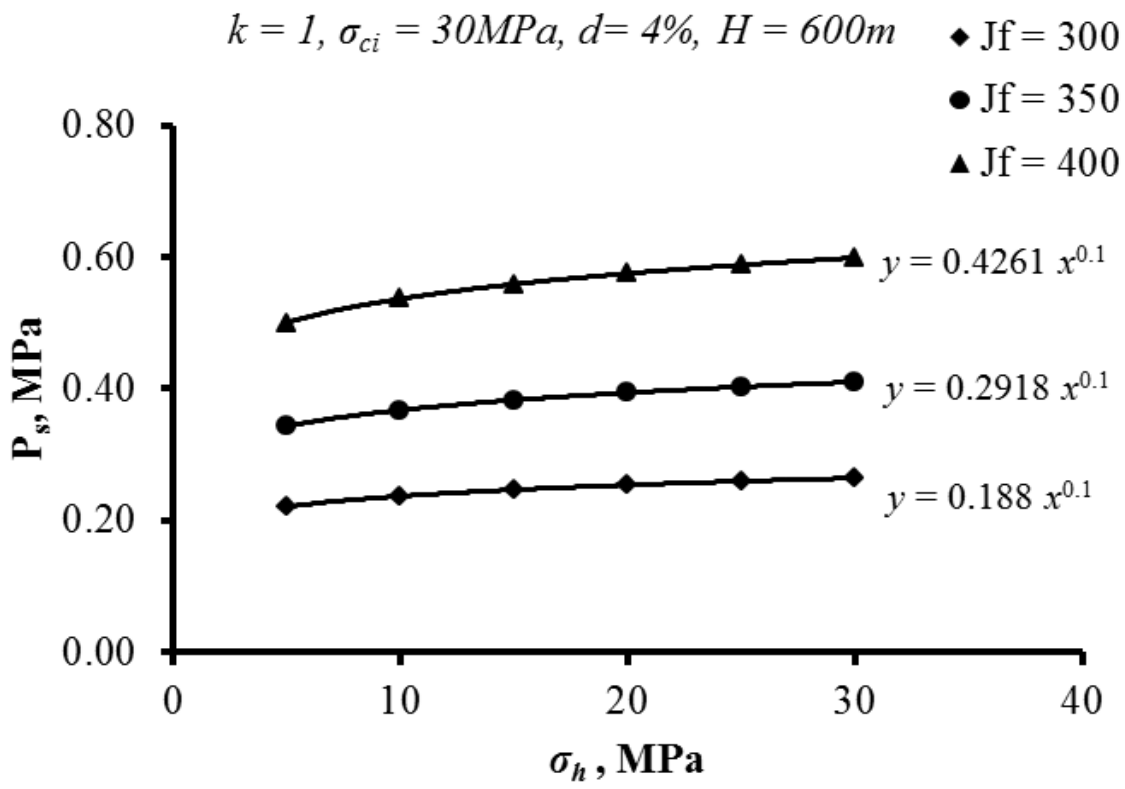

Fig. 6.7 Variation of Tunnel Support Pressure with σ_h

6.6.6 Influence of Uniaxial Compressive Strength, σ_{ci}

Figure 6.8 shows the variation of tunnel support pressure with uniaxial compressive strength of intact rock. The plot indicates that tunnel support pressure decreases only marginally with increase in σ_{ci} values. The variation is plotted for three different values of J_f . All the curves show that support pressure is unaffected beyond σ_{ci} = 40 MPa. It can therefore be inferred that for rock masses exhibiting, J_f < < 250, the influence of σ_{ci} – values on tunnel support pressure will be absent.

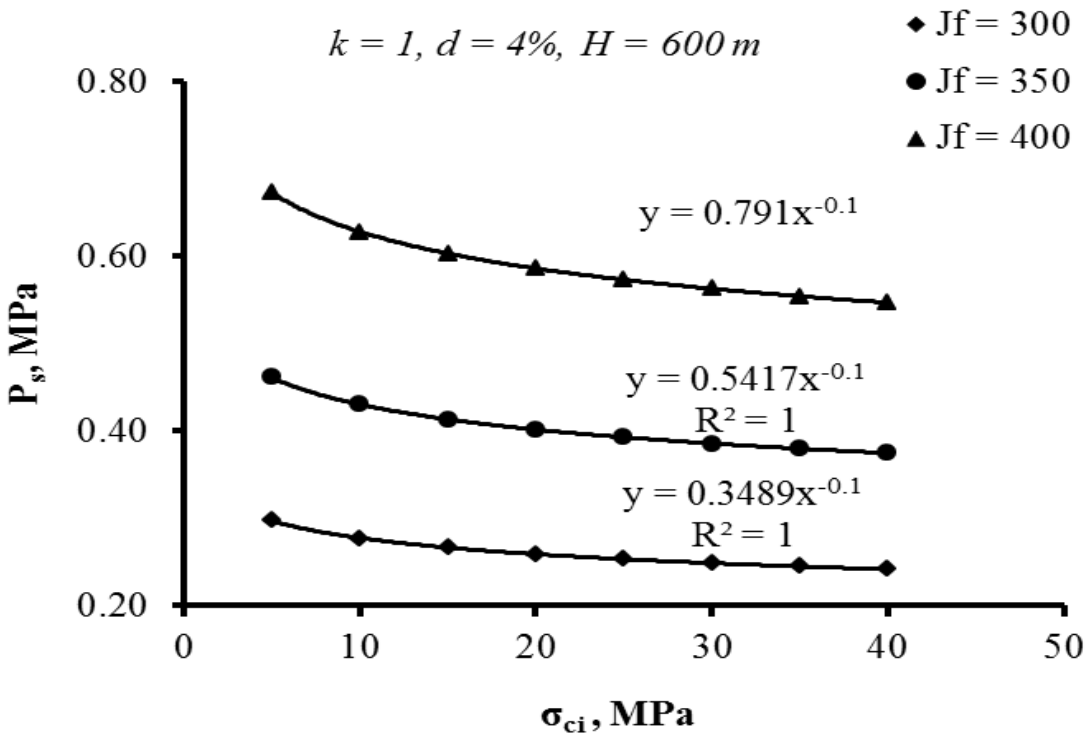

Fig. 6.8 Variation of Tunnel Support Pressure with σ_{ci}

6.7 CORRELATIONS FOR NON-SQUEEZING GROUND

When deformation of an unsupported tunnel doesn't exceed 1% of its diameter, the condition is said to be non-squeezing or elastic. This condition is prevalent when a tunnel of small diameter is excavated in the good quality rock mass exposed to low in situ stress field. In such cases, rock mass around the tunnel boundary is capable of mobilising the required strength to resist the support pressure and hence the required quantity of support is less in such a case. Attempt has also been made to develop an empirical correlation for prediction of support pressure for tunnels excavated in non-squeezing ground condition.

The data of 35 tunnel sections from 10 different tunnelling projects has been used in this analysis. This data is presented in Table 6.3 which includes apart from the rock type at the location of different tunnel sections under consideration, data related to geometry and the rock mass characteristics at that location. The data was analysed using non-linear regression analysis. Several trials were conducted to arrive at the dimensionally correct correlation between the observed support pressure and the joint factor.

This correlation is given by Eq. 6.7 which has a correlation coefficient of 93 % and the corresponding plot is presented in Fig. 6.9. In Fig.6.9, ratio ($100P_{obs}/\sigma_v$) has been plotted against $[J_f^3/(10^4 d^{0.2})]$.

$$P_e = 10^{-6}\sigma_v\left(\frac{7*10^{-4}J_f^{\ 3}}{d^{0.2}} + 4058\right) \qquad (R^2 = 0.93) \qquad (6.7)$$

where

P_e = ultimate support pressure in non-squeezing ground, MPa,

J_f = Joint Factor,

σ_v = vertical in situ stress (0.027H), MPa, and

d = radial tunnel deformation (%).

Values of uniaxial compressive strength of intact rock have not been taken into consideration in development of correlation given by Eq. 6.7 as it has no significant effect on support pressure in non- squeezing ground condition.

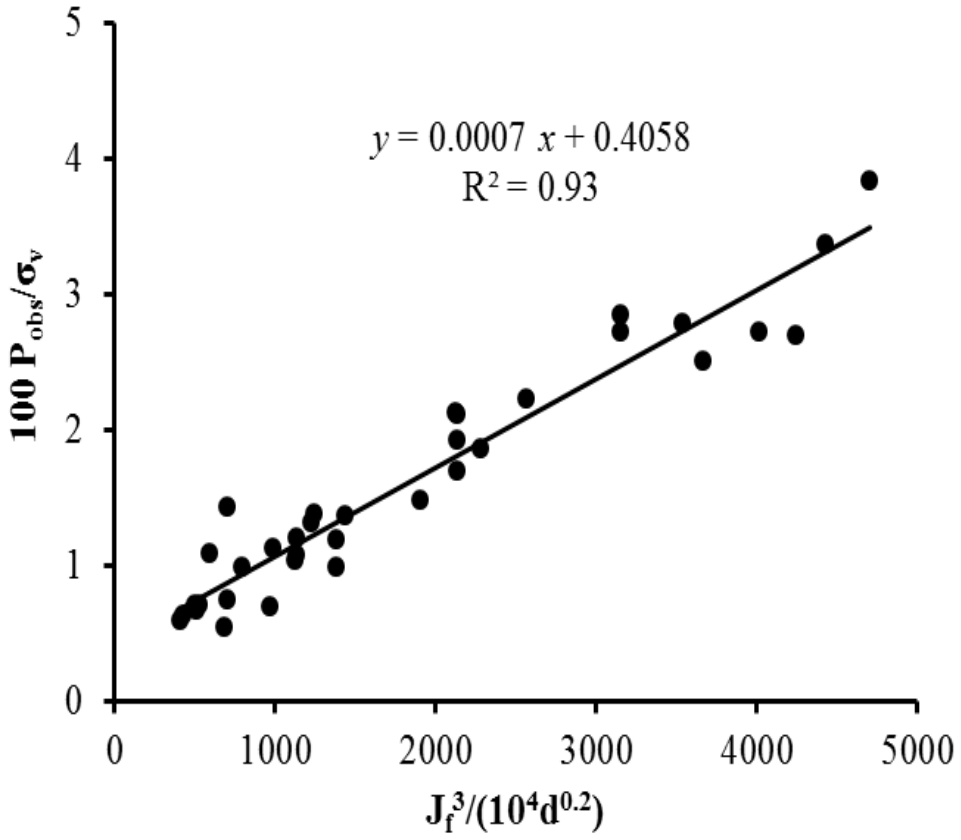

Fig. 6.9 Plot of (100 P_{obs}/σ_v) and $[J_f^3/(10^4 d^{0.2})]$ for Non-squeezing Ground

Table 6.3 Data Considered for Development of Correlation to Predict Tunnel Support Pressure in Non-squeezing Ground Condition

Sl. No.	Name of Tunnel	Rock Type	Reference	Q	J_n	J_r	N	*a* (m)	*H* (m)	*d* (%)	p_{obsd} (MPa)	J_n*	*n*	*r*	J_f
1.	Maneri stage-I	Moderately fractured quartzite	Dube, 1979; Goel, 1994; Singh et al., 2007	3.6	6	1.5	9	2.9	225	0.06	0.06	17.7	0.22	0.404	199
2.	Maneri stage-I	Foliated metabasics		4.5	6	1.5	12.8	2.9	550	0.16	0.08	15.7	0.22	0.425	168
3.	Maneri stage-I	Sheared metabasics		0.8	9	1	4.95	2.9	250	0.25	0.13	12.9	0.22	0.231	253
4.	Maneri stage-I	Foliated metabasics		4.7	6	1.5	11.8	2.9	275	0.16	0.08	18.6	0.22	0.425	199
5.	Maneri stage-I	Sheared metabasics		1.3	4	1	3.25	2.9	350	0.33	0.14	12.6	0.22	0.231	248
6.	Maneri stage-I	Foliated metabasics		5.5	4	1.5	13.8	2.9	250	0.09	0.07	19.6	0.22	0.466	191
7.	Khara	Argilaceous conglomerates	Goel, 1994	0.4	9	1.5	2	3	150	0.75	0.11	8.67	0.06	0.466	310
8.	Khara	Argilaceous conglomerates		0.4	9	1.5	2	3	200	0.42	0.15	8.67	0.06	0.466	310
9.	Lakhwar	Tightly jointed basic rock		8.5	9	1.5	21.3	3	250	0.2	0.05	6.21	0.09	0.445	155
10.	Lakhwar	Tightly jointed basic rock		8.5	6	1.5	21.3	7	250	0.4	0.05	7.21	0.09	0.445	180
11.	Maneri Stage-II	Metabasics	Jethwa, 1981; Goel, 1994	0.57	9	1.5	2.5	3.5	200	0.4	0.1	5.95	0.05	0.443	267
12.	Maneri Stage-II	Metabasics		0.84	9	1.5	4.2	3.5	175	0.3	0.08	5.7	0.05	0.445	256
13.	Maneri Stage-II	Greywakes		2.75	9	1.5	7	3.5	250	0.19	0.08	5	0.05	0.466	215
14.	Maneri Stage-II	Metabasics		1.02	9	1.5	2.55	3.5	175	0.24	0.1	5.6	0.05	0.445	252
15.	Maneri Stage-II	Metabasics		0.62	9	1.5	1.55	3.5	200	0.2	0.12	5.9	0.05	0.445	265
16.	Maneri Stage-II	Greywakes		3	9	1.5	7.5	3.5	325	0.17	0.12	4.8	0.05	0.445	216
17.	Salal	Highly jointed dolomites		1.1	6	1.5	3.5	6	150	0.03	0.11	10.4	0.09	0.425	271
18.	Tehri	Phyllites Grade-I	Goel, 1994; Singh et al., 2007	6	6	1.5	15	6	300	0.2	0.06	6.99	0.09	0.404	192
19.	Tehri	Phyllites Grade-II with banded structure of argillaceous material		0.8	6	1.5	3.5	6	220	0.38	0.13	9.45	0.09	0.404	260

…..Contd.

Sl. No.	Name of Tunnel	Rock Type	Reference	Q	J_n	J_r	N	a (m)	H (m)	d (%)	p_{obsd} (MPa)	J_n*	n	r	J_f
20.	Tehri	Phyllites grade-I		18.14	4	1.5	18.4	4.75	265	0.2	0.05	6.6	0.09	0.466	157
21.	Tehri	Phyllites grade-II		3.96	6	1.5	3.96	4.75	310	0.16	0.1	7.22	0.09	0.404	199
22.	Tehri	Phyllites grade-II		4.45	6	1.5	4.45	4.75	225	0.08	0.08	6.4	0.09	0.364	195
23.	Tehri	Phyllites grade-I		29.9	3	2	29.9	4.75	280	0.09	0.05	7.1	0.09	0.577	136
24.	Tehri	Phyllites grade-I	Jethwa et al., 1987; Goel, 1994	26	4	2	26	4.75	210	0.06	0.04	4.3	0.065	0.466	142
25.	Tehri	Phyllites grade-I		24	4	2	24	4.75	295	0.13	0.05	4.3	0.065	0.466	142
26.	Lower Periyar	PGG		5.5	6	1.5	5.5	3.4	197	0.16	0.06	14.3	0.09	0.839	190
27.	Lower Periyar	PGG		7	6	1.5	7	3.4	150	0.1	0.04	12.9	0.09	0.839	171
28.	Upper Krishna	TSC	Singh et al., 1992; Goel, 1994	15	4	1.5	37.5	6.5	52	0.08	0.02	6.79	0.09	0.466	162
29.	Upper Krishna	TSC		15	4	1.5	75	6.5	34	0.18	0.01	6.79	0.09	0.466	162
30.	Kaletepe tunnel, Turkey (Section II)	Limestone	Sari and Pasameh meto, 2004	1.52	9	1.5	9.1	6.35	52	0.03	0.04	13.5	0.09	0.60	250
31.	Kaletepe tunnel, Turkey (Section III)	Limestone		10.8	9	1.5	64.78	6.35	215	0.05	0.08	10.3	0.09	0.60	190
32.	Udhampur railway tunnel No.3 Ch.13267 m	Soft sandstone	Goel et al., 2004; CIMFR, 2007	0.56	6	1.5	1.4	3.5	33	0.02	0.024	7.52	0.06	0.466	269
33.	Udhampur railway tunnel No.3 Ch.13235.5 m	Soft sandstone		0.5	6	1.5	1.25	3.5	33	0.02	0.03	7.63	0.06	0.466	273
34.	Udhampur railway tunnel No.3 Ch13177.5 m	Soft sandstone		0.67	6	1.5	1.675	3.5	37	0.03	0.025	7.35	0.06	0.466	263
35.	Udhampur railway tunnel No.3 Ch12831 m	Soft sandstone		0.62	6	1.5	1.55	3.5	29	0.01	0.03	7.44	0.06	0.466	266

Notation: ***J_n* is joint frequency, a parameter of Joint factor; PGG-Pegmatite granite gneiss (foliated); TSC-Thinly bedded shales with calcite bands.***

6.8 EMPIRICAL CORRELATIONS AVAILABLE IN LITERATURE

Correlations represented by Eqs 6.3 and 6.5 which were suggested by Grimstad & Barton (1993) and Bhasin & Grimstad (1996) respectively are valid for non-squeezing ground conditions also. Based on rock mass number, *N*, Goel (1994) presented a correlation (Eq. 6.8) for prediction of support pressure in non-squeezing ground condition.

$$P_e = \frac{0.07 H^{-0.1} a^{-0.1}}{N^{0.33}} + 0.022 \qquad (6.8)$$

6.9 COMPARISON OF EMPIRICAL CORRELATIONS

For the sake of comparison, values of tunnel support pressure have been predicted using by Eq. 6.7 (art. 6.7 above), Eq. 6.3 (Grimstad and Barton, 1993), and Eq. 6.8 (Goel, 1994). These values have been presented in Table 6.4 along with the observed values of support pressure for all the 35 tunnel cross sections (Table 6.3). The predicted values of support pressure have also been plotted against the observed values in Fig. 6.10.

It can be seen that support pressures predicted by the empirical correlation involving joint factor, J_f as a measure of rock mass quality and represented by Eq. 6.7 fits with the observed support pressures with the coefficient of accordance COA value of 0.14 i.e. the lowest. Support pressures predicted by using correlations of Grimstad and Barton (1993) and Goel (1994) fit with COA values of 1.64 and 1.03 respectively. **Hence, it can be inferred that the proposed correlation given by Eq. 6.7, which uses joint factor, J_f is a further modification of the empirical correlation given by Eqs. 6.3 and 6.8 and is recommended for use in prediction of support pressure for non-squeezing ground conditions.**

Table 6.4 Comparison of Predicted and Observed Values for Non-squeezing Condition

Sl. No.	P_{obs}	P_e , using J_f, Eq. 6.7		P_e , using Q Eq. 6.3		P_e, using N Eq.6.8	
1.	0.06	0.08	Coefficient of accordance (COA) ψ^2 = 0.14	0.07	Coefficient of accordance (COA) ψ^2 = 1.64	0.04	Coefficient of accordance (COA) ψ^2 = 1.03
2	0.08	0.13		0.07		0.04	
3	0.13	0.13		0.22		0.06	
4	0.08	0.09		0.06		0.04	
5	0.14	0.16		0.12		0.07	
6	0.07	0.08		0.05		0.03	
7	0.11	0.11		0.18		0.08	
8	0.15	0.16		0.18		0.08	
9	0.05	0.05		0.07		0.03	
10	0.10	0.11		0.16		0.08	
11	0.08	0.09		0.14		0.06	
12	0.08	0.09		0.10		0.05	
13	0.10	0.09		0.13		0.08	
14	0.12	0.12		0.16		0.09	
15	0.12	0.12		0.09		0.05	
16	0.11	0.13		0.11		0.07	
17	0.06	0.09		0.06		0.04	
18	0.13	0.11		0.12		0.07	
19	0.05	0.06		0.03		0.03	
20	0.10	0.10		0.07		0.07	
21	0.08	0.08		0.07		0.06	
22	0.05	0.05		0.02		0.02	
23	0.04	0.04		0.02		0.03	
24	0.05	0.06		0.02		0.03	
25	0.06	0.06		0.06		0.05	
26	0.04	0.04		0.06		0.05	
27	0.02	0.01		0.04		0.02	
28	0.01	0.01		0.04		0.01	
29	0.05	0.06		0.05		0.03	
30	0.04	0.04		0.12		0.04	
31	0.08	0.07		0.06		0.01	
32	0.02	0.03		0.13		0.08	
33	0.03	0.03		0.14		0.08	
34	0.03	0.03		0.12		0.07	
35	0.03	0.03		0.13		0.07	

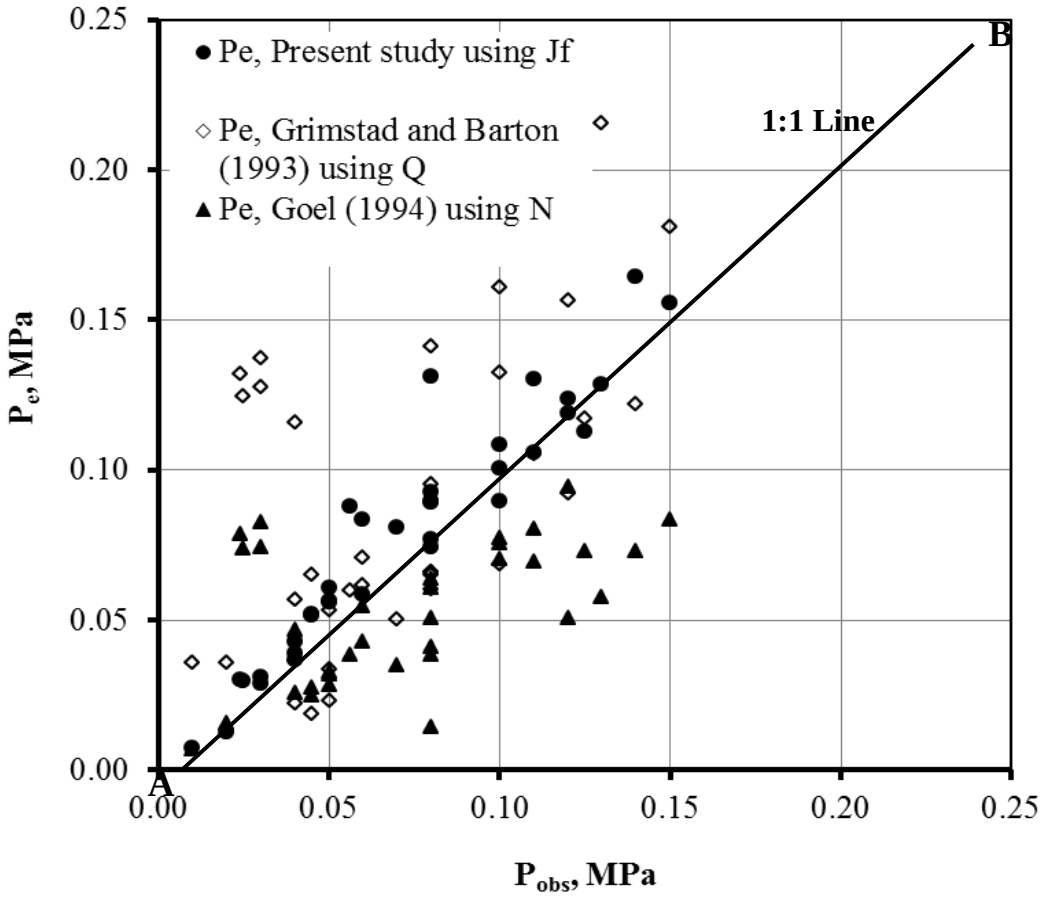

Fig. 6.10 Comparative Plot of Predicted Versus Observed Support Pressures in Non-squeezing Ground Condition

6.10 PARAMETRIC STUDY

Parametric study was carried out for tunnels in non-squeezing ground condition using the proposed equation (Eq. 6.7) exactly on the same lines as it was done for the squeezing ground condition.

6.10.1 Influence of Tunnel Depth, *H*

Figure 6.11 shows the variation of tunnel support pressure with change in tunnel depth and suggests that tunnel support pressure increases linearly with tunnel depth. It is due to the fact that vertical in-situ stress increases with tunnel depth (overburden height) leading to increased induced stresses around the tunnel opening. The high induced stresses led to an increase the tunnel support pressure.

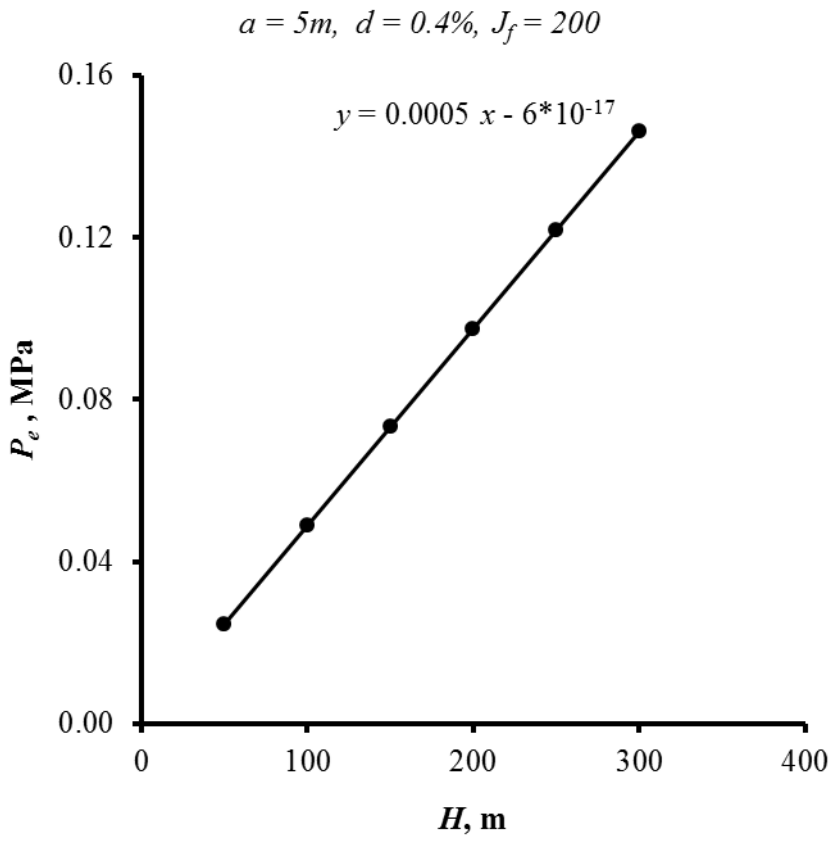

Fig. 6.11 Variation of Tunnel Support Pressure with Tunnel Depth in Non-squeezing Ground Condition

6.10.2 Influence of Joint Factor, J_f

Tunnel support pressure has been found to increase with degradation in the quality of rock mass. This effect is evidenced by the plot shown in Fig 6.12. The plot shows steep increase in values of tunnel support pressure with increase in values of joint factor, J_f or with deterioration in rock mass quality.

6.10.3 Influence of Tunnel Deformation, *d (%)*

Tunnel support pressure drastically decreases with increase in allowable tunnel deformation. It is evidenced from exponentially decreasing trend of the curve plotted for tunnel support pressure versus allowed tunnel deformation in Fig. 6.13. For instance, support pressure decreases by about 78% from 0.49 MPa at d = 0.1% to 0.11 MPa at d = 0.6%.

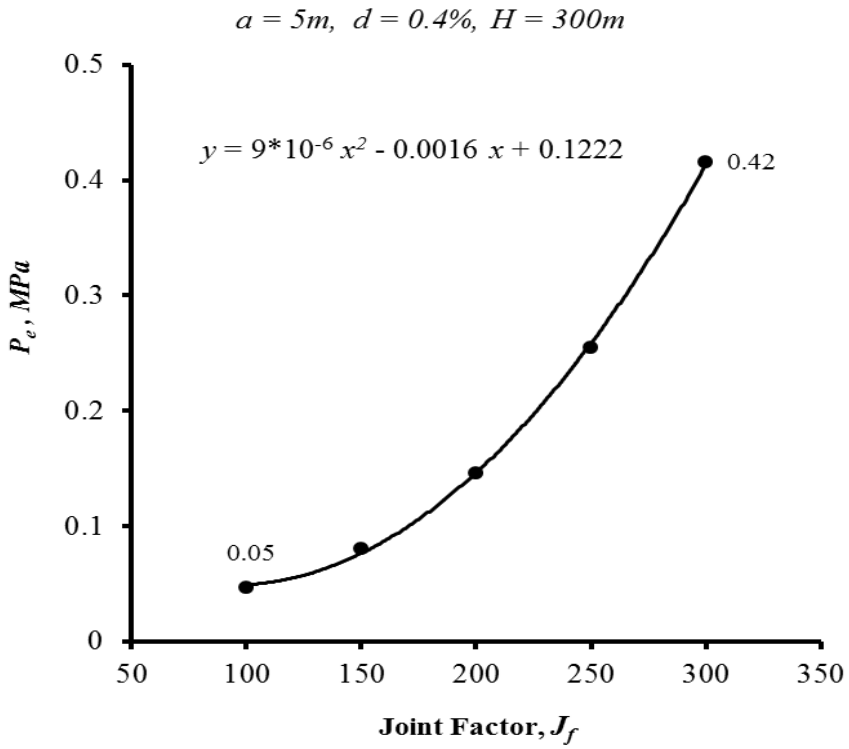

Fig. 6.12 Variation of Tunnel Support Pressure with J_f– Values in Non-squeezing Ground Condition

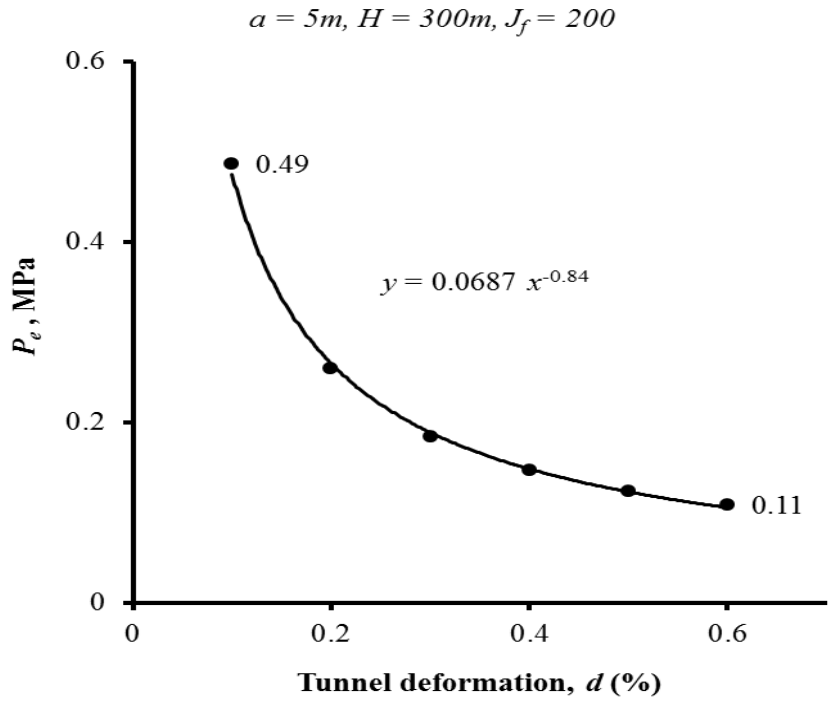

Fig. 6.13 Variation of tunnel support pressure with allowed tunnel deformation in Non-squeezing Ground Condition

6.10.4 Influence of Tunnel Size

Figure 6.14 which shows variation of support pressure with tunnel size, indicates that when the tunnel is excavated in elastic or non-squeezing ground conditions, tunnel support pressure is independent of the tunnel size,

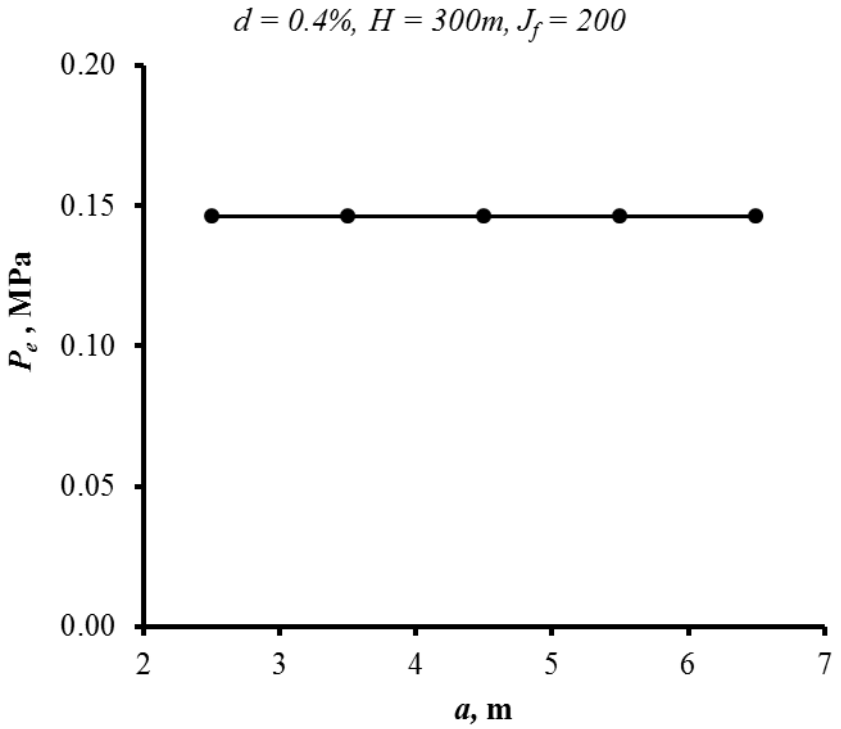

Fig. 6.14 Variation of tunnel support pressure with tunnel radius in Non-squeezing Ground Condition

6.11 LIMITATIONS OF THE STUDY

The limitations of the present study are same as given in the art. 5.10 of Chapter 5.

6.12 CONCLUDING REMARKS

- In the present study, the proposed correlations represented by Eq. 6.2 and Eq. 6.7 are suggested to be used for prediction of support pressure in squeezing and non-squeezing ground conditions respectively.
- Support pressure increases with increase in tunnel depth and joint factor for both squeezing and non-squeezing ground conditions.

- No significant effect of tunnel size was observed on support pressure in squeezing ground condition. Similarly, in non-squeezing condition, the influence of the tunnel size is absent.

- The support pressure decreases at faster rate for σ_c < 20 MPa as compared to the higher values of σ_c in squeezing ground condition.

Chapter 7

VALIDATION OF PROPOSED CORRELATIONS

7.1 GENERAL

In Chapters 4, 5 and 6, empirical correlations have been developed for assessing ground conditions (squeezing / non-squeezing), tunnel deformation and support pressure with tunnel geometry, rock mass quality, in-situ stresses and support stiffness as input data. A data base comprising of about 14 tunnelling projects in squeezing and 10 tunnelling projects in non-squeezing ground conditions was used in developing these correlations. In this chapter, an independent ongoing project has been considered in which tunnel deformations have been monitored and documented and this data has been used to validate the earlier developed correlations for assessing the ground conditions and tunnel deformations. In addition, numerical modelling has also been done using Phase^2 software (Rocscience Inc., Toranto, Canada) for the prediction of ground condition and tunnel deformation

7.2 CHENANI-NASHRI NATIONAL HIGHWAY TUNNELS

Independent project considered here in this chapter is an ongoing project of Chenani-Nashri highway tunnel in the state of Jammu & Kashmir in India. The new highway link project envisaged by the Govt. of India linking Udhampur and Banihal on National Highway-1A (NH-1A) in the state of Jammu & Kashmir, India is one of the most important Indian projects planned to connect the Kashmir valley with the rest of the Indian transportation network (Fig. 7.1). Government of India has entrusted the National Highway Authority of India (NHAI) with the responsibility of four laning of Chenani to Nashri Section of NH-1A between km 89.00 to km 130.00. Apart from other engineering structures, this project includes the construction of 9.2 km long bi-directional traffic main tunnel with a parallel escape tunnel. The tunnel will reduce the existing route of highway from 41 km to 9.2 km only. In addition to this, the traffic diverted towards the tunnel would also be saved of the heavy snow on the highway route near Patnitop during

peak winter seasons. NHAI through the international bidding process has awarded the road tunnel project to IL&FS Transportation Networks Limited (ITNL) as the developer.

Fig. 7.1 Location of Chenani-Nashri Tunnelling Project

For tunnel excavation works, M/s Leighton Contractors (India) Pvt Ltd. (LIN) has been engaged on Engineering, Procurement and Construction (EPC) basis, who have in turn engaged M/s Geodata, Italy as their design and supervision consultant.

For proof checking of designs and technical suggestions during the construction of tunnels, CNTL engaged CSIR-CIMFR Regional Centre, Roorkee. The author is also a team member in CSIR-CIMFR's work. The scope of CIMFR's team work includes: i) Review of the geological and geotechnical data during investigation and construction stages, and ii) Checking of the layout and design of all tunnelling works and recommendations for final design with the progress of work.

The construction of tunnels has been planned to be completed in five years. The main and the escape tunnels are being excavated from both the ends i.e. South end towards Chenani and the North end towards Nashri. The tunnel construction was started in August 2011 and shall be completed by July 2016. The tunnel passes through Murree formations of the Himalayas, which are influenced by the regional and the local faults and shear zones as well. Design and construction of tunnels through such a complex and varying geology with a rock cover of more than 1000 m is a difficult and challenging task. The tunnels have been designed using the conventional concept (NATM) of tunnelling.

7.3 SALIENT FEATURES OF TUNNELS

The cross-sectional area of horse-shoe shaped escape and main tunnels are 34.96 m^2 and 140.03 m^2 respectively (Fig. 7.2 & Fig. 7.3). The two tunnels, having a pillar width of 33.5 m, are interconnected at regular intervals to provide cross passages. Two types of cross passages have been provided, viz. pedestrian and the vehicular emergency exits at a distance of 300 m and 1200 m centre to centre respectively. The typical section of pedestrian cross passage has been designed considering the same size of the Escape Tunnel (ET) section, whereas vehicular cross passages are larger in cross-section having the dimensions of 7.50 m (H) x 4.50 m (V).

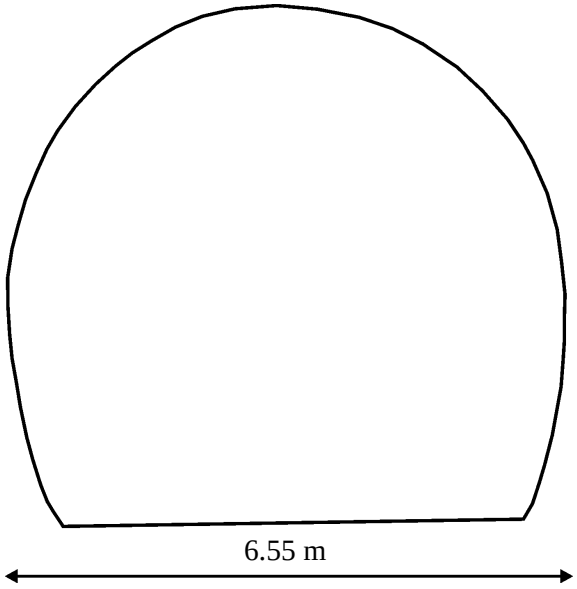

Fig. 7.2 Section of Escape Tunnel

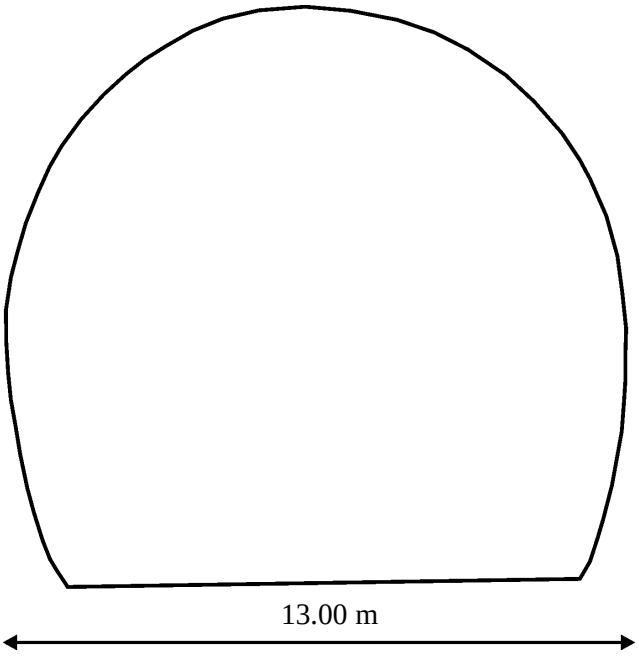

Fig. 7.3 Section of Main Tunnel

The tunnels have an up-gradient of 0.5% from Chenani village and downward gradient of 1.0% towards Nashri village from the centre. Maximum road level will be 1252.40 m at Tunnel Metre (TM) 4445 m from South end. Tunnel excavation is being carried out by heading and benching method for the main tunnel and the vehicular cross passage using drill and blast method, whereas full face excavation is being adopted for the escape tunnel and the pedestrian cross passages. The tunnel is supported by a primary lining (shotcrete and rockbolts in combination) and completed with a cast-in-place concrete final lining. A water proofing membrane paired with geotextile protective will be installed all around the tunnel section (except at the invert) for the complete length of the tubes (Facibeni et al., 2011).

7.4 GEOLOGY OF THE PROJECT AREA

The project area lies in Western Himalayan region in a sector of collisional belt known as sub-Himalayas. This tectonic domain is bounded towards the south by the Himalayan Frontal Thrust (HFT) or the Main Frontal Thrust (MFT) and by the Main Boundary Thrust (MBT) towards the North (Fig. 7.4). These main thrusts as well as most of the belts and units of this NW region of Himalaya orogen show a regional strike of NWSE to WNW-ESE with moderate to steep dips either towards the north or the south. The rock masses along the Chenani-Nashri tunnel project belong to the Lower Murree formation. This sedimentary succession is classified as the "Lower Tertiary Sediments" of the "Murree Structural Belt" and are bounded on the south by the MFT and on the north by a complex of thrusts, which are regionally referred to as the MBT. The Murree formation is characterised by a sequence of argillaceous and arenaceous rocks which includes a sequence of inter-bedded sandstone, siltstone and claystone beds with thickness ranging from a few metres up to 10 m (Goel et al., 2012).

Rock mass of the area has three sets of joints, i.e., bedding planes dipping at 30^{o}-45^{o} towards N 90^{o}-110^{o}, second joint set dipping at 50^{o}-75^{o} towards N 250^{o}-300^{o} and the third joint set dipping at 50^{o}-80^{o} towards N 200^{o}-255^{o}. The strike of the joints makes an angle of about 8^{o}-33^{o} with the tunnel axis. The bands of sandstone, siltstone, and claystone of varying thicknesses are frequently encountered during the tunnel excavation. There is no fixed pattern of the bands of these rocks.

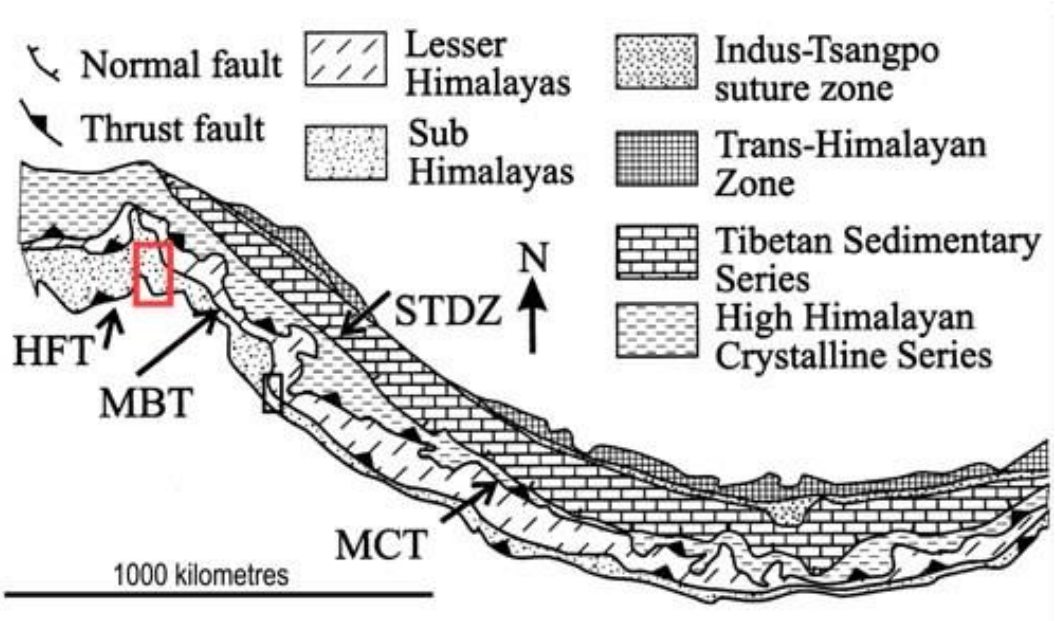

Fig. 7.4 Himalayan Orogenic Belt showing Potential Himalayan Source Rocks for the Sediments *(The study area is marked by a rectangle)*
(after Geodata/LIN, 2011b)

In fact, the bands of mixed rocks, for example, intermixed siltstone and sandstone and intermix siltstone and claystone are also encountered frequently (Fig. 7.5 a, b). The uniaxial compressive strengths of freshly obtained rock samples of sandstone, siltstone and claystone are 50-100 MPa, 30-50 MPa and 20-35 MPa respectively. Squeezing problem has been encountered in siltstone, claystone and intermixed rock sections. The intermixed rocks have a uniaxial compressive strength of 40-50 MPa.

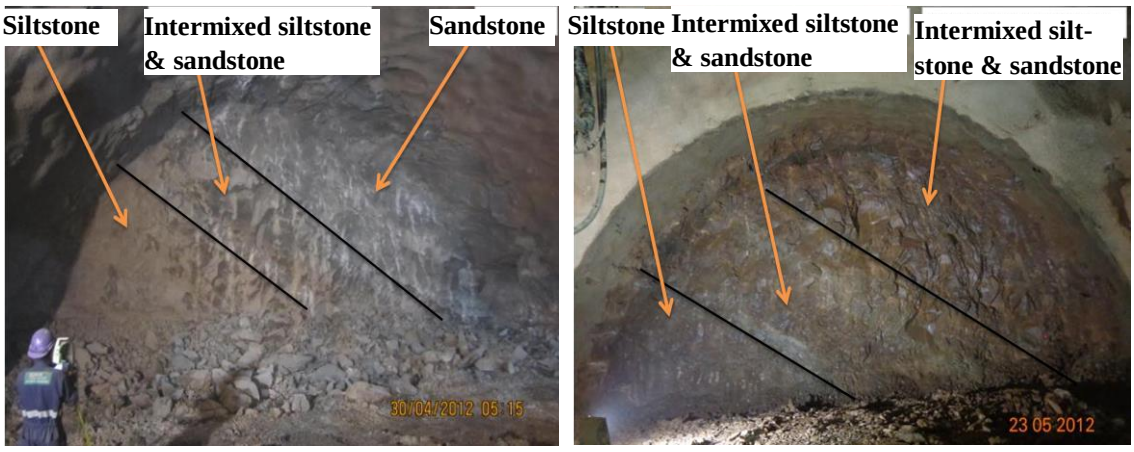

(a) **(b)**

Fig. 7.5 View from Main tunnel, South End showing Bands of Various Rocks of Murree Formations

7.5 TUNNELLING PROBLEMS AND INSTALLED SUPPORTS

Major portion of alignment of the main tunnel and the escape tunnel traverses through weak rock types inter-bedded with sandstone, siltstone and claystone and display squeezing behaviour. But, some stretches of tunnels, which traverse through comparatively better rock quality, show non-squeezing behaviour. Shotcrete of 0.1-0.25 m thickness and 28 mm diameter rock bolts, at a spacing of 1.5-2.5 m x 1.5-2.5 m c/c, were installed as a support system. Rock bolts of 3 m and 6 m length were installed in escape and the main tunnels respectively. The geo-mechanical details of the tunnel faces at various sections are presented in **Appendix- I and Appendix - II**.

7.6 MONITORING OF RESPONSE OF TUNNELS

The Chenani-Nashri tunnels are being constructed following the conventional method of tunnelling (NATM) in which monitoring is an important aspect for optimum design of supports and thus safety during the construction of tunnels. Systematic tunnel monitoring by fixing bireflex targets for tunnel deformation / convergence is being carried out in tunnels for better understanding of rock mass-tunnel support interaction. The convergence targets are fixed at a regular interval of 50 m or as and when required on the basis of the ground condition / geology. The observed deformation readings are analysed and if required, the support capacity is revised on the basis of the analysis of data. A dual limit action plan adopted for remedial measures is as follows:

i) **Attention limit**: It is expressed in percentage of the predicted deformation. On exceeding this level/limit of convergence, the frequency of readings is increased in order to obtain the rate of deformation. This trigger limit is set to study the deformation trends more closely and take counter measures, if the deformations continue with the same rate to the alarm limit. The attention limit, in general, is 80% of the alarm limit.

ii) **Alarm limit**: It is the complete maximum expected deformation level as per the design. Appropriate action should be taken to strengthen the deforming zone before tunnel deformation crosses the alarm limit. Otherwise, excessive deformation will attract very high support pressure, which sometimes becomes almost impossible to control and the deformed section requires replacement.

Convergence attention and alarm limits as determined for Chenani-Nashri escape and main tunnels, for the sections included for the study, are 48 mm and 60 mm respectively.

At one tunnel section, five bireflex target points (T1, T2, T3, T4 and T5) are fixed to measure the tunnel deformations (Fig. 7.6). Deformations along X, Y and Z co-ordinates are recorded at each target point (Fig. 7.7) at regular interval. The readings are analysed to obtain the deformation of individual target points and the chord convergence between various target points. Figure 7.8 shows the deformations at various target points and Figure 7.9 shows the plot of convergence of various chords joining different pairs of target points.

To determine the total deformation of tunnel, average of total deformation at various measuring target points is computed. Total deformation at a measuring target point is given by-

$$u_{aobs} = \frac{\left(x_1^{\,2} + z_1^{\,2}\right)^{0.5} + \left(x_2^{\,2} + z_2^{\,2}\right)^{0.5} + \left(x_3^{\,2} + z_3^{\,2}\right)^{0.5} + \left(x_4^{\,2} + z_4^{\,2}\right)^{0.5} + \left(x_5^{\,2} + z_5^{\,2}\right)^{0.5}}{5} \qquad (7.1)$$

Tunnel strain is expressed as $(\boldsymbol{u_{obs}/a})$ x 100 %, where

u_{obs} = total deformation of the tunnel at a respective cross section,

$x_1, x_2 \ldots x_5$ = horizontal component of tunnel deformation at T1, T2,…T5 target points respectively,

$z_1, z_2 \ldots z_5$ = vertical components of tunnel deformation at T1, T2,…T5 target points respectively.

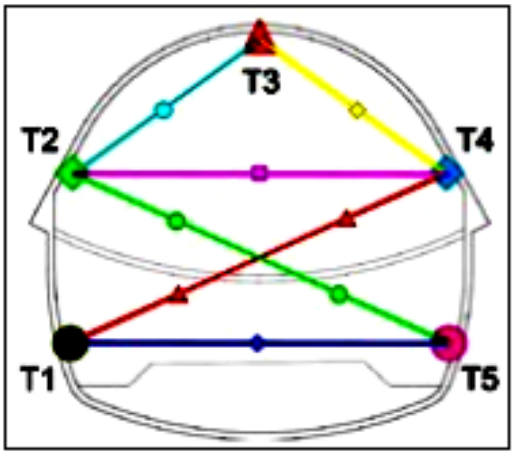

Fig. 7.6 Array of Five Target Points at One Location to Measure Tunnel Convergence

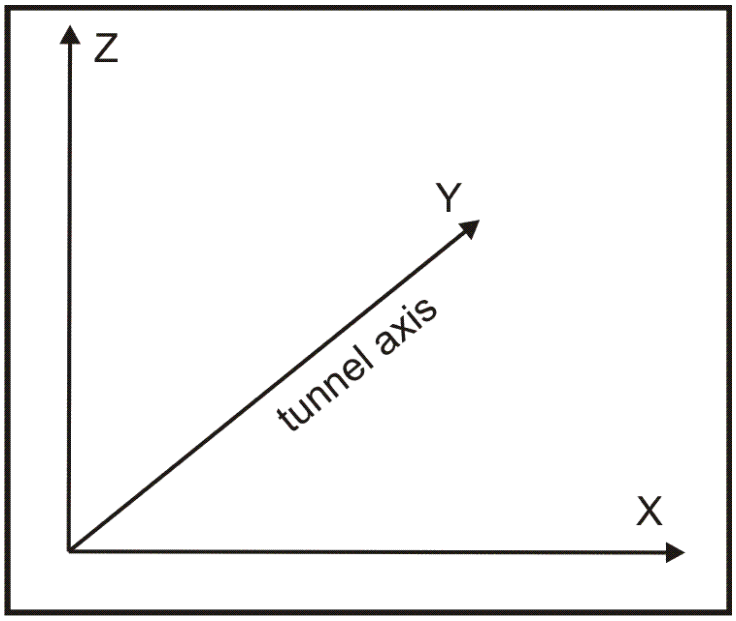

Fig. 7.7 Directions of X, Y and Z Co-ordinates of Readings

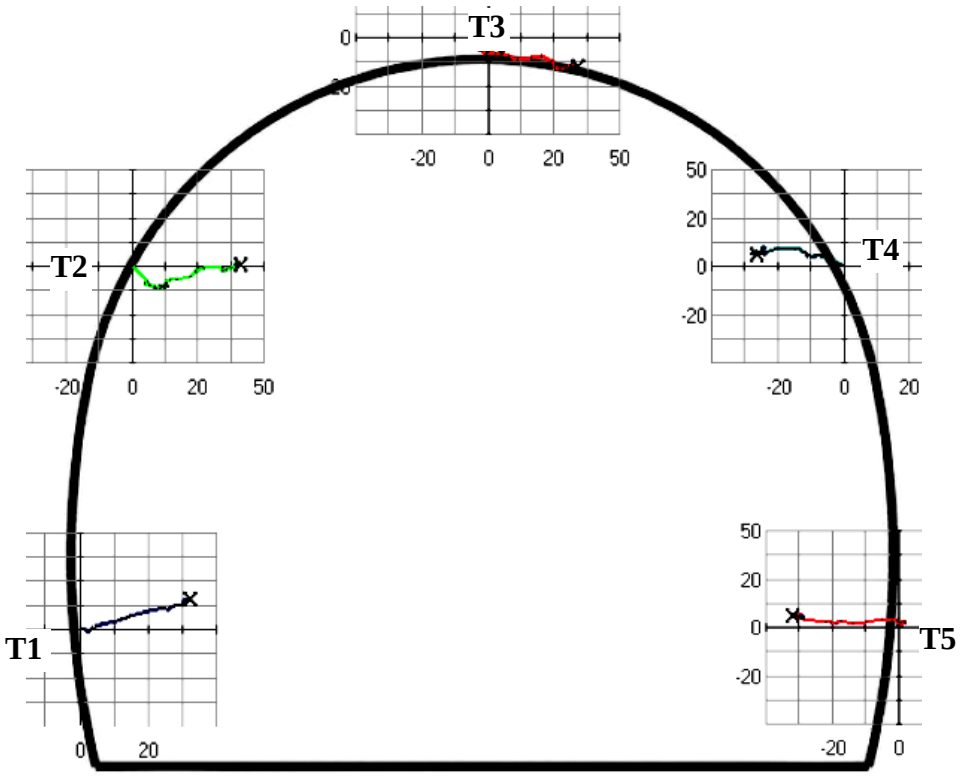

Fig. 7.8 Deformation (mm) at Various Points Around Tunnel Periphery

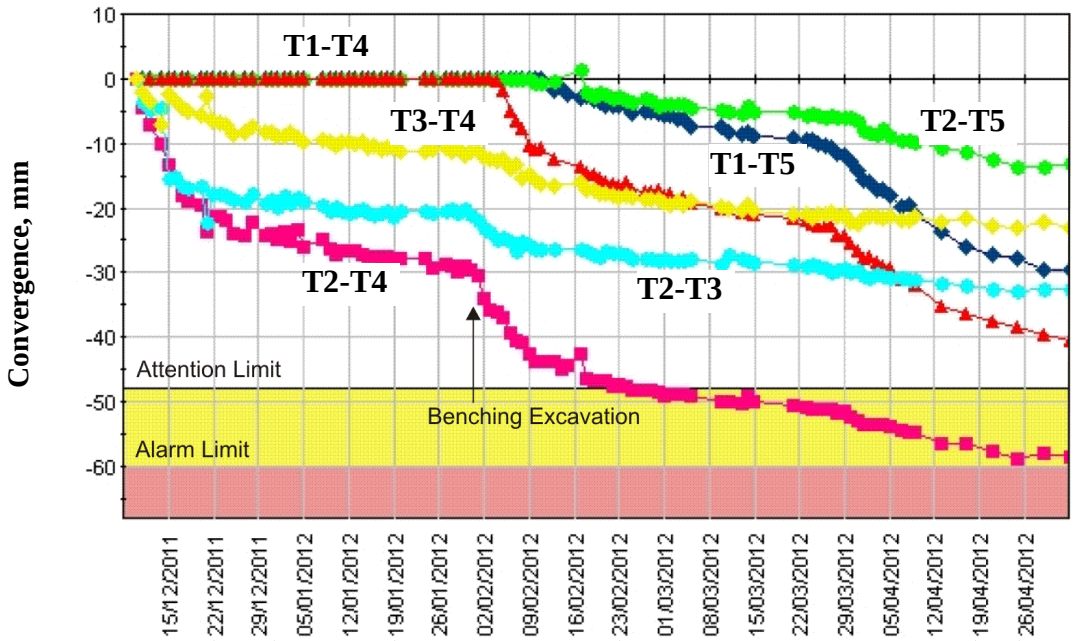

Fig. 7.9 Variation of Convergence with Time at a Section of Main Tunnel

In Fig. 7.9, date wise chord (T1-T4, T2-T5, T2-T4, T3-T4, T2-T3 and T1-T5) conversions have been plotted. Maximum convergence was recorded on Chord, T2-T4. The deformation has crossed the attention limit of 48 mm and is also touching the alarm limit of 60 mm. It indicates immediate requirement of counter measures in form of additional supports.

7.7 NUMERICAL MODELLING

Phase^2 numerical code has been used for modelling the deformation process at various tunnel sections. It is a 2D elasto-plastic finite element stress analysis program for underground or surface excavations in rock or soil. It can be used for support design, slope stability analysis, ground water seepage and for the probabilistic analysis.

Joint networks can be easily created and quickly analysed while modelling tunnels or caverns in weak or jointed rock. Progressive failure, support interaction and a variety of other problems can also be addressed.

A wide range of support modelling options is available in this numerical code. In support design, liner elements can be applied in the modelling of shotcrete, concrete and steel set systems. Liner design tools include support capacity plots which allow the determination of the safety factor of reinforced liners. End anchored, fully bonded, cable bolts, split sets and grouted tie back type of rock bolts can be used in the analysis.

Phase^2 offers various failure criteria, viz., Mohr-Coulomb, Drucker Prager, Hoek-Brown and Generalised Hoek-Brown for analysis of tunnels. In the present study, Generalised Hoek-Brown failure criterion has been used.

Powerful new analysis features for modelling jointed rock allows the user to automatically generate discrete joint or fracture networks according to a variety of statistical models.

7.7.1 Numerical Analysis of Tunnel Sections

The tunnel sections were analysed the using plane strain theory with Gaussian Elimination solver. Box shaped model boundary having width of 30 times the tunnel radius has been considered for analysis. External boundaries of the models were fixed to simulate the in-situ stress conditions at infinity in the rock mass. Field stresses were applied as per the actual conditions in the field. Material properties were set as per the values listed in Table 7.1. Rock mass was intermixed with one or two rock types, viz., intermixed sandstone with siltstone, intermixed siltstone with claystone and intermixed sandstone with siltstone and claystone. Properties of joints (normal stiffness, K_n and shear stiffness, K_s) were assigned as per the values listed in Table 7.2.

Generalised Hoek-Brown failure criterion (Hoek et al., 2002) has been used for studying the tunnel behaviour. This is a non-linear empirical failure criterion which determines the strength of rock in terms of major and minor effective principal stresses. The criterion is expressed as follows:

$$\sigma_1' = \sigma_3' + \sigma_{ci}\left(m_b \frac{\sigma_3}{\sigma_{ci}} + s\right)^a \qquad (7.2)$$

where σ_1' and σ_3' are the axial (major) and confining (minor) effective principal stresses respectively. σ_{ci} is the uniaxial compressive strength (UCS) of the intact rock material, m_b is a reduced value (for the rock mass) of the material constant m_i (for the intact rock), s and a are constants depending upon the characteristics of the rock mass. *Phase*^{2} numerical code automatically computes the values of m_b, s and a using m_i and GSI values. Values of m_i for various rock types are selected from the list provided in the numerical code.

Table 7.1 Material Properties of Different Rock Types Encountered (after Geodata, 2011)

S. No.	Rock type	σ_{ci}, MPa	E_i, MPa	GSI	m_i
1.	Sandstone	50-65	15000	50-65	15
2.	Siltstone	45-50	10000	40-50	7
3.	Claystone	20-35	5000	25-40	6
4.	Intermixed sandstone and siltstone	55-60	12500	55-60	11
5.	Intermixed siltstone and claystone	40-50	7500	45-50	6.5
6.	Intermixed sandstone, siltstone and claystone	40-45	11660	45-50	10

Table 7.2 Values of Rock Joint Stiffness (after Geodata, 2011)

Sl. No.	Joint boundaries	K_n, MPa/m	K_s, MPa/m
1.	Joints between sandstone and siltstone	100000	10000
2.	Joints between siltstone and claystone	68750	57292
3.	Joints between sandstone and claystone	68750	57292
4.	Joints within sandstone	100000	10000
5.	Joints within siltstone	68750	57292
6.	Joints within claystone	68750	57292

The tunnel and the surrounding rock mass were discretized with 6 noded triangular elements (Fig.7.10). In fact, the tunnel section starts deforming immediately after the excavation takes place. Therefore in order to consider this effect, the model was allowed to deform in ten stages initially (Fig.7.11). A uniform distributed load (an internal pressure corresponding to the support pressure) was applied to the tunnel in stage-1 (Fig.7.12).

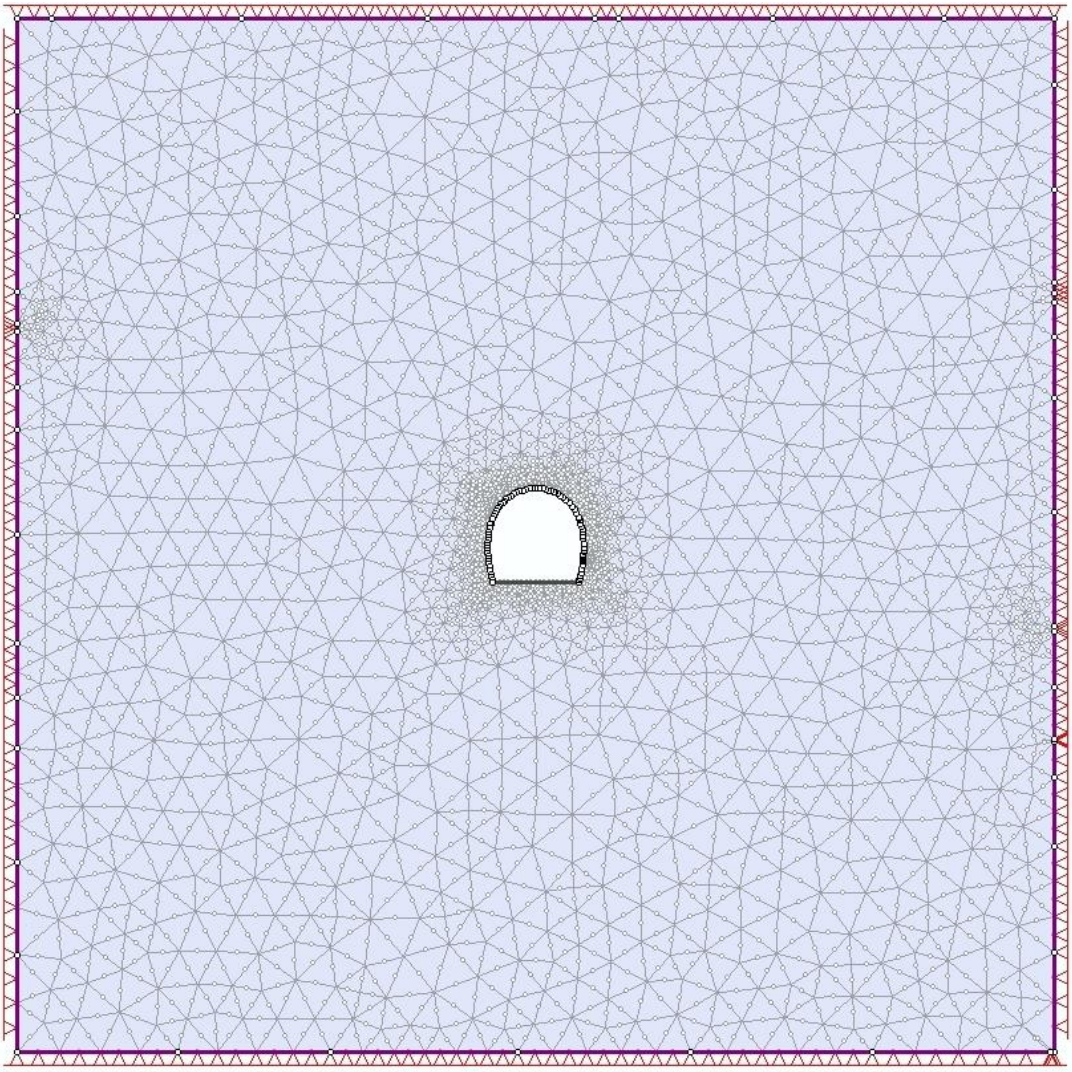

Fig.7.10 Model of Horse-Shoe Shaped Escape Tunnel Section

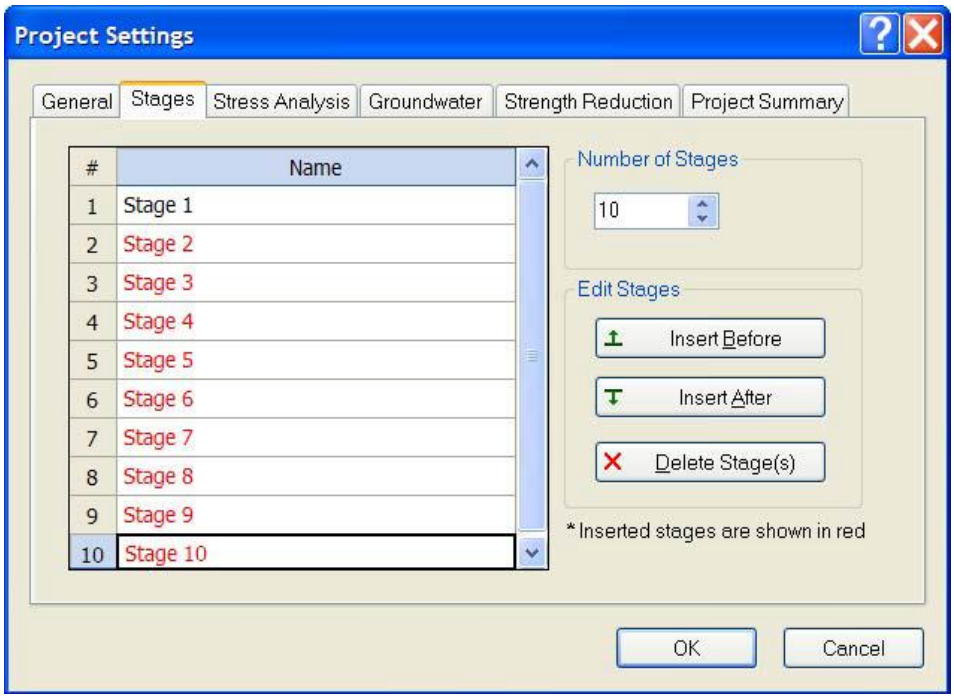

Fig.7.11 Model Staging in the Phase^2 Menu "Project Setting"

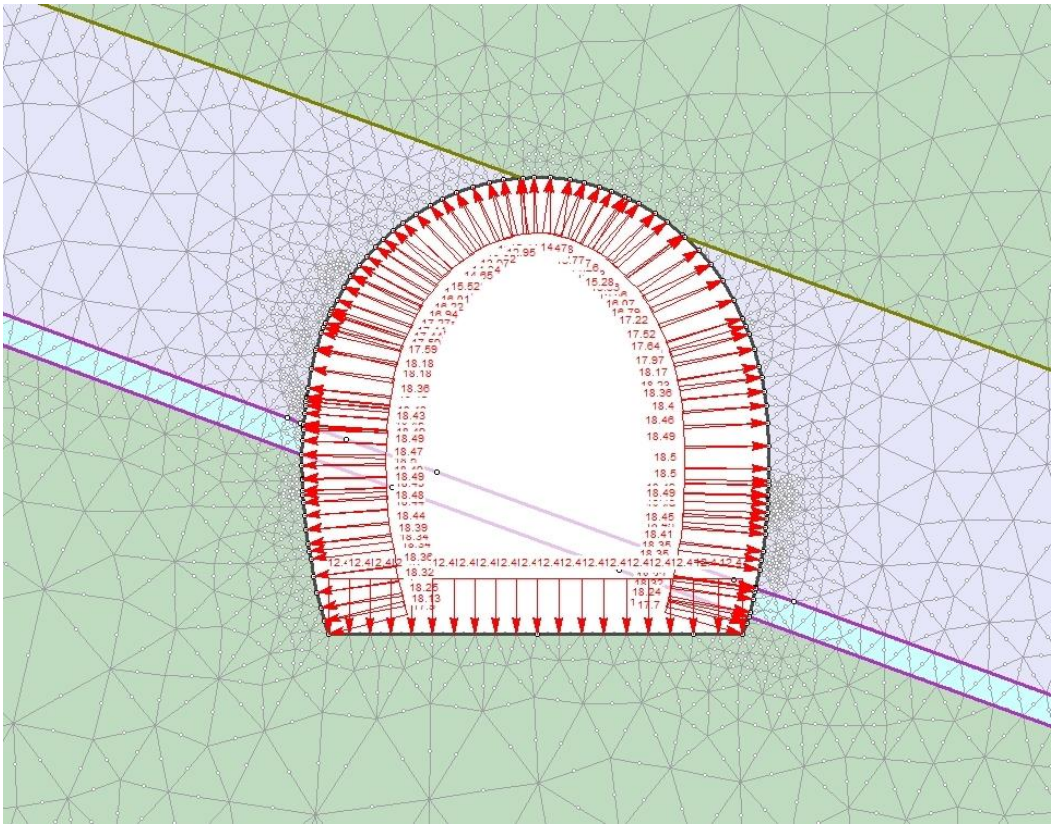

Fig.7.12 Uniformly Distributed Internal Pressure in the Model at the First Stage

Vertical in-situ stresses were calculated using the height of overburden ($\sigma_v = \gamma H$) and horizontal in-situ stresses were computed as $k.\ \sigma_v$ where $k = \sigma_h / \sigma_v$. (k = 1.2 for Chenani-Nashri tunnels).

Uniformly distributed load reduced by certain factor (1 to 0 from stage 1 to stage 10) is applied in successive stages (Fig. 7.13). In the 1st stage, the magnitude and direction of the load is equal and opposite to the in situ stresses thus forming a balance between the stresses in the rock and the pressure inside the tunnel. This effect simulates the condition of in situ stresses before excavation. Since the pressure is equal and opposite of the in situ stress, no deformation should occur in the 1st stage. However, in successive stages i.e. from stage-2 onwards, the internal load is reduced by a load factor which gradually reduces the magnitude of the pressure (Fig. 7.13). As a result, tunnel deformation will increase as the pressure is gradually reduced to zero. Load Factor = 1 means the magnitude of distributed load inside is the same as the field stress while a Load Factor = 0 means no load acts on the internal periphery at that stage. The model is analysed and deformation of rock mass which occurs before installation of the support system is computed. For this, an empirical relationship developed by Vlachopoulos and Diederichs was used (Hoek et al., 2008). To use the Vlachopoulos and Diederichs method, values of radius of plastic zone and the maximum tunnel wall displacement far from the tunnel face are required from the finite-element analysis. Both of these values are computed from a plane strain analysis with zero internal pressure inside the excavation. In the model, the results from stage-10 were used since there is zero internal pressure at this stage. Radius of the plastic zone (r_p) was determined by measuring the distance of the farthest yielded element from the centre of the tunnel section (Fig.7.14).

Value of maximum radial deformation (u_{max}) is picked up from the computed model of a tunnel section choosing menu option of "total displacement" in Phase^2 window. Now, for the known data, i.e. tunnel radius, a = 3 m; radius of the plastic zone, r_p = 6.8 m; distance of the face from support, X = 2 m; and maximum radial tunnel deformation, u_{max} = 0.040 m, ratio of distance from tunnel face to tunnel radius, X/a and ratio, r_p/a were computed. Then, using these ratios, ratio of radial deformation, u_a to maximum radial deformation, u_{max}, was determined from the plot given in Fig. 7.15. This was approximately equal to 0.52.

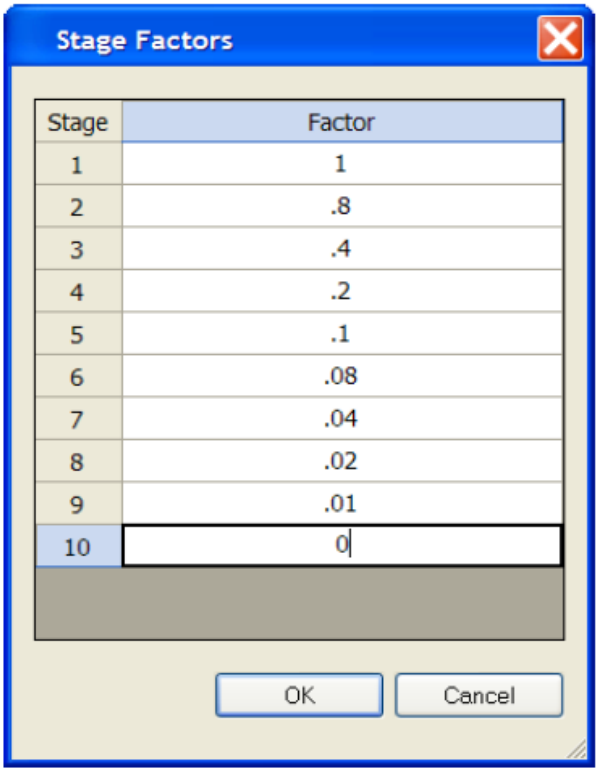

Fig.7.13 Load Factors Assigned to Different Excavation Stages in Model

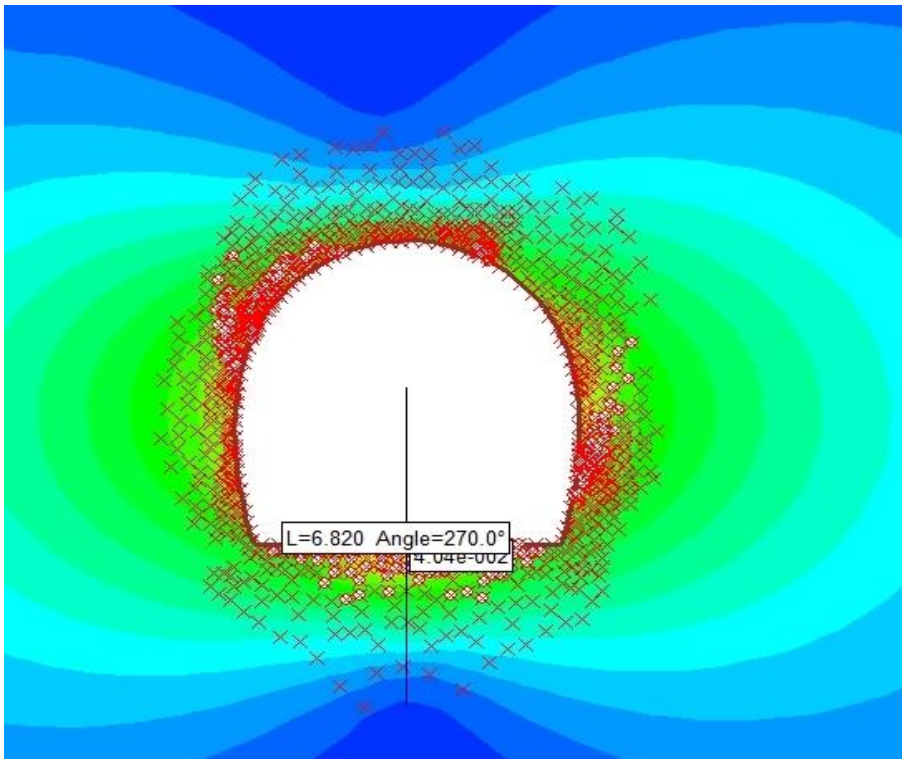

Fig.7.14 Assessment of Radius of Plastic Zone

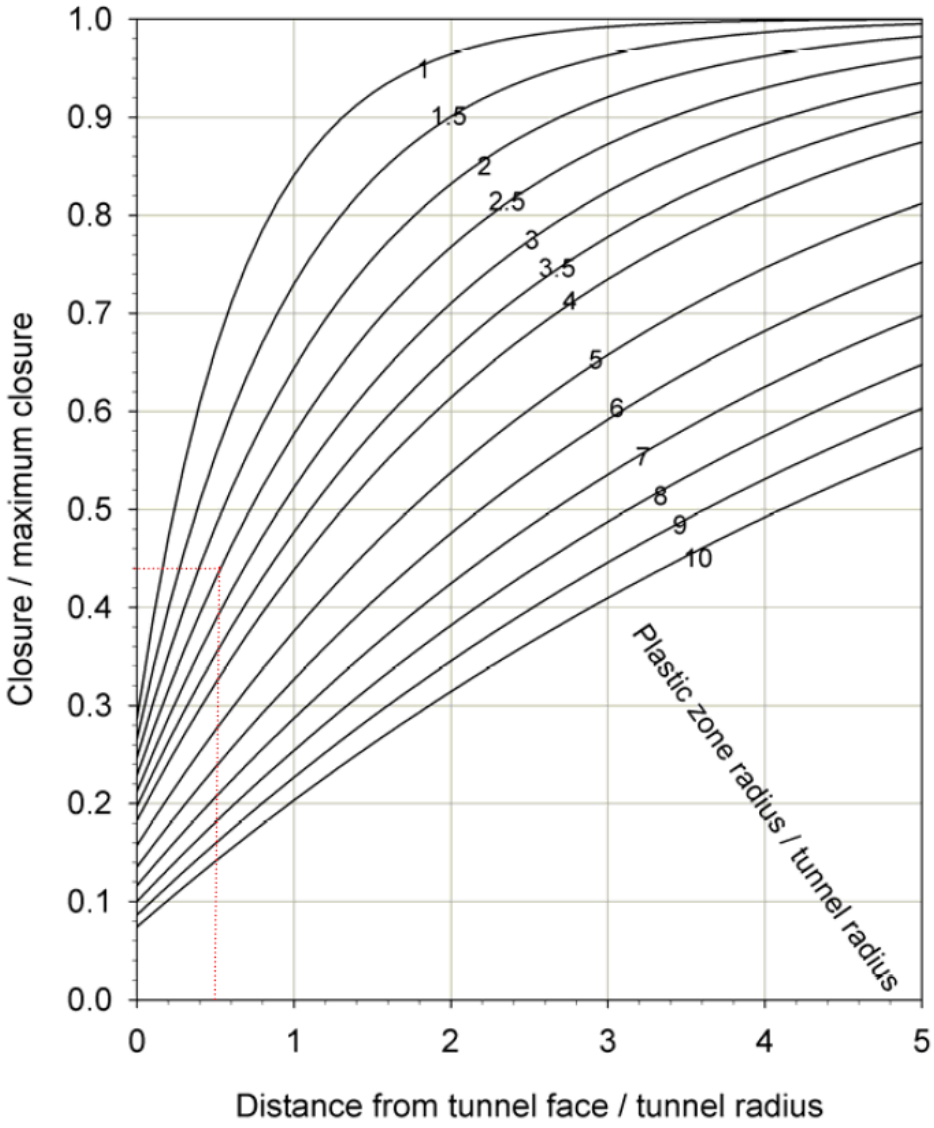

Fig.7.15 Values of Tunnel Deformation before Support Installation
(Tutorial Manual, 2011)

Thus, the radial tunnel deformation = (0.52)*(0.040) = 0.021 m. It meant that the tunnel roof deformed by 0.021 m (21 mm) before the support was installed.

Now, in the next step, internal pressure that yields a displacement of 0.021 m at the bottom of the tunnel was determined. The location, which was used to determine u_{max}, was maintained as the location of maximum displacement which can change depending on the magnitude of the internal pressure. To determine the internal pressure that yields a displacement 0.021 m at the bottom, a graph of displacement versus excavation stage for

a point at the bottom of the excavation was plotted (Fig.7.16). From this plot, it can be seen that in stage 6, the wall displacement at the floor of the tunnel was 0.021m. This represents an internal pressure load factor of 0.08 (Fig.7.13) which was defined in the model for the field stress vector distributed load.

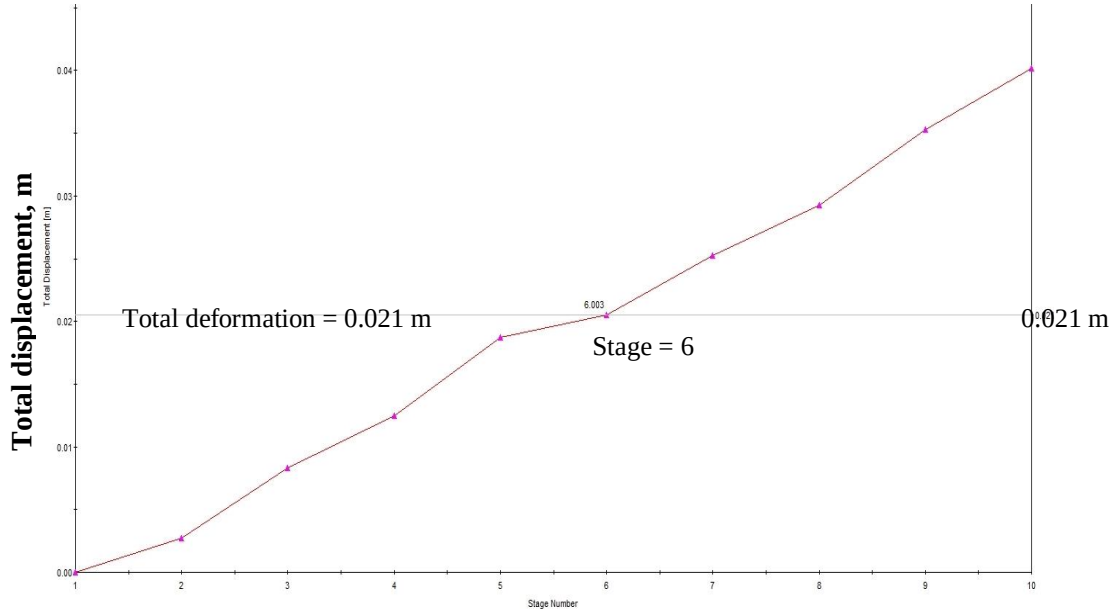

Fig.7.16 Variation of Tunnel Deformation with Excavation Stages

Thus, the tunnel relaxes up to the stage 6. The stages 2-5 and 7-9 were deleted from the model and the supports were installed at the stage 10 (Fig.7.17). Now there are three stages, i.e., initial stage (stage-1), tunnel relaxation stage (stage-6) and support installation stage (stage-10). In the present study, SN rock bolts of 25-28 mm diameter were installed and 100-250 mm thick shotcrete was applied as per the actual supports installed in the field (Fig. 7.17).

In the numerically modelled tunnel sections, the average total tunnel strain (u_{nm}/a) was assessed by averaging the total strain at five target points (T1, T2, T3, T4 & T5), where the strains were actually measured in the field (Fig. 7.18). These numerically obtained values of average total tunnel strain are presented in Tables 7.3-7.5 along with the values of actually observed average total tunnel strain in the field.

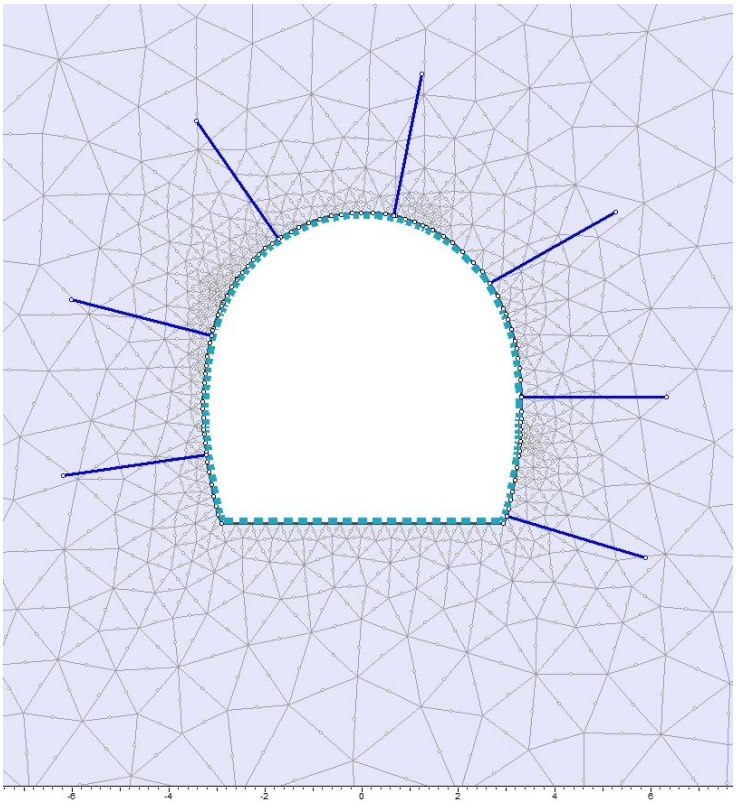

Fig.7.17 Support System Installed in Tunnel Section

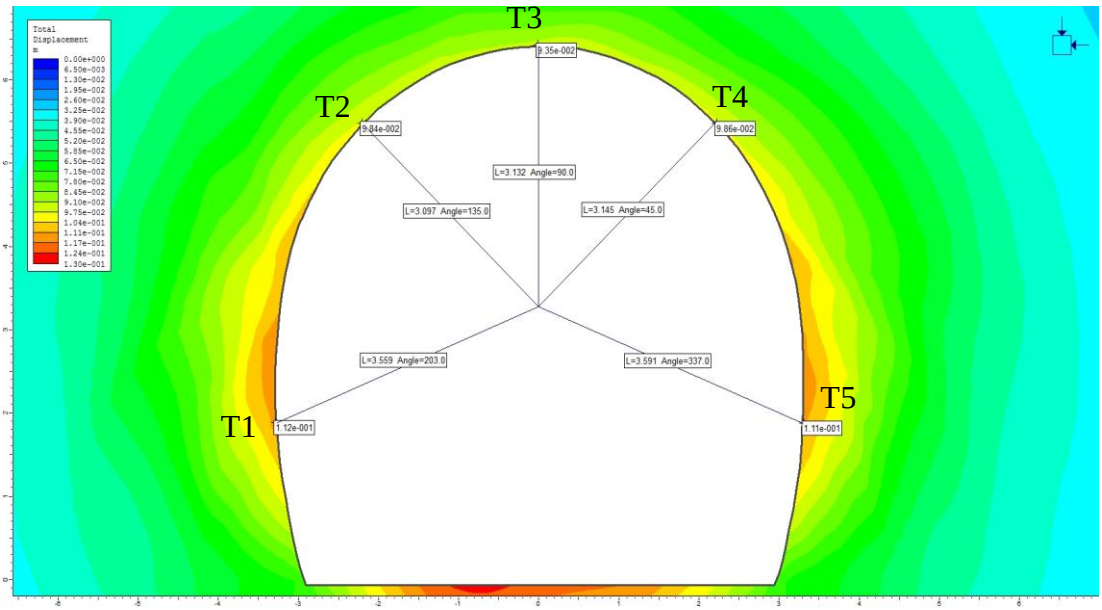

Fig.7.18 Total Strain Measured at Five Target Points at a Tunnel Section

7.8 VALIDATION OF RECOMMENDED CORRELATIONS

Various geo-mechanical parameters of rock mass observed at various tunnel sections of Chenani-Nashri Highway Tunnel are presented on the geo-mapping sheets attached as **Appendix -I and II**. Details include type and quality of rock mass (*Q, RMR, GSI*), rock cover, information of joint sets, rock pull per blast and average uni-axial compressive strength of intact rock.

7.8.1 Prediction of Ground Condition

For prediction of ground condition at different sections of Chenani-Nashri National Highway Tunnel in the state of Jammu & Kashmir, use is made of the empirical correlations which were recommended in this study (Chapter 4) for prediction of different ground conditions for tunnelling. These correlations were developed on basis of three different parameters defining the rock mass characteristics:

i) **Joint factor, J_f** : (Eq. 4.4 for self supporting, Eq. 4.6 non-squeezing, Eq. 4.7 for squeezing ground conditions (Eqs. 4.12, 4.13 and 4.14 for mild, moderate and high squeezing respectively) , and Eq. 4.11 for rock bursting condition)
ii) **Barton's rock mass quality, *Q*:** (Eq. 4.16 for self supporting, Eq. 4.19 for non-squeezing, Eq. 4.18 for squeezing and Eq. 4.22 for rock bursting condition)
iii) **Rock Mass Number, *N*:** (Eq. 4.27 for self supporting, Eq. 4.25 for non-squeezing, Eq. 4.24 for squeezing and Eq. 4.30 for rock bursting condition)

i) Chenani-Nashri Tunnel Sections in Squeezing Ground Condition

The geometrical details and rock mass characteristics observed at different tunnel sections of Chenani-Nashri Escape Tunnel are presented in columns 1-9 of Table 7.3a along with the chainages of these tunnel sections. The tunnel depth, *H* at respective chainages is stated in Column 10. The values of H_1 , which defines the right hand side term ($=170234D^{-1}e^{-0.017J_f}$) of Eq. 4.7, are presented in column 11. The values of H_2 , which defines the right hand side term ($=41901D^{-1}e^{-0.008J_f}$ **)** of Eq. 4.12, are presented in column 12. Similary, the values of H_3 , which defines the right hand side term ($=57563D^{-1}e^{-0.008J_f}$ **)** of Eq. 4.13, are presented in column 13. In columns 14 and 15,

values of average total strain developed in the tunnel before and after the installation of the support system and obtained on basis of numerical modelling are mentioned. Finally, observed values of average total strain mobilised in the tunnel are presented in column 16 of Table 7.3a.

On comparison, it can be seen in Table 7.3a that H *i*s larger than H_1 at all chainages indicating that tunnel stretch between chainage 385 m to chainage 2178 m is experiencing a squeezing ground condition. Table 7.3b shows the application of different criteria to decide upon the degree of squeezing on basis of permissible strain levels (art. 4.4.2 of Chapter 4). It can be seen that tunnel stretch between Chainage -385 m to chainage 1122 m and at chainage 1514 m is experiencing mild squeezing; tunnel stretch between Chainage 1685 m to chainage 1743 m is experiencing moderate squeezing; and tunnel stretch between Chainage 1960 m to chainage 2178 m is experiencing high squeezing.

In addition to this, numerical modelling has been carried out for four Escape Tunnel sections (ETSP chainage 385 m, 707 m, 1122 m, and 2178 m) and strain levels have been computed for both the unsupported tunnel case (ε % = 100*u_{nm} /a)' and the supported tunnel case (ε % = 100*u_{nm}/a). Values of these strain levels are presented in columns 14 and 15 of Table 7.3a. It can be seen on comparison that strains of supported tunnel sections obtained from numerical modelling are in good agreement with the respective observed tunnel strains (column 16). Therefore, it would not be wrong to infer that the strains of unsupported tunnel sections obtained via numerical modelling are realistic.

Now, it can be observed in Table 7.3a that the values of average total tunnel strain, ε at respective tunnel sections (ETSP chainage: 385 m, 707 m, 1122m, and 2178 m) are in excess of 1%, which satisfies the squeezing ground condition. Further, in column 16 of Table 7.3a, observed strain values of supported tunnel sections – ETSP: 690 m, 850 m, 1514 m, 1685 m, 1743 m and 1960 m exceed 1% which also means that strain levels at respective unsupported tunnel sections would be certainly larger than 1% indicating squeezing behaviour of the ground.

Further, at sections, ETSP 1384 m and at ETSP 2066 m, observed strain level equals 1% when the tunnel is supported and therefore it is obvious that the total tunnel strain at these sections would exceed 1% in unsupported condition and will be categorised under the squeezing ground condition. Table 7.3b shows the criteria for different degree of squeezing. For example, tunnel sections at ETSP 385 m, 690 m, 707 m, 850 m and 1122 m satisfy the condition : $H_2 > H > H_1$ condition for mild squeezing condition. Strain level, as computed by numerical modeling, at tunnel sections :ETSP 385 m, 707 m and 1122 m is in the range of 1% - 3% which supports the mild squeezing condition at the respective tunnel sections.

Tunnel sections at ETSP 1685 m and 1743 m satisfy $H > H_1$ and $H_3 > H > H_2$ conditions showing a moderate squeezing condition (Table 7.3b). On the other hand, tunnel sections: ETSP 1384 m, 1960 m, 2066 m and 2178 m satisfy $H > H_1$ and $H > H_3$ conditions and exhibit high squeezing ground conditions.

The Strain level in an unsupported condition at tunnel section: ETSP 2178 m is 5.4% as obtained by numerical modelling and exceeds strain level of 5% (Tables 7.3a, b) and supports the case of high squeezing at this tunnel section.

Table 7.3a Validation of Squeezing Ground Condition

Column →	*2*	*3*	*4*	*5*	*6*	*7*	*8*	*9*	*10*	*11*	*12*	*13*	*14*	*15*	*16*
Chainage	θ_A	S_d (mm)	J_n	n	ϕ	r	J_f	D (m)	H (m)	H_1 (m)	H_2 (m)	H_3 (m)	$(u_{nm}/a)'$ *100	(u_{nm}/a) *100	(u_{obs}/a) *100
ETSP 385 m	58	188	5.3	0.05	15	0.27	367	6.67	178	50	334	458	1.6	1.1	0.8
ETSP 690 m	59	177	5.7	0.05	17	0.31	348	6.67	294	69	388	533	-	-	1.1
ETSP 707 m	62	214	4.7	0.06	15	0.27	293	6.67	315	175	603	828	1.2	0.9	0.6
ETSP 850 m	61	185	5.4	0.06	17	0.31	319	6.67	359	113	490	673	-	-	1.1
ETSP 1122 m	63	217	4.6	0.06	17	0.31	246	6.67	458	390	878	1206	1.2	0.8	0.8
ETSP 1384 m	58	186	5.4	0.05	15	0.27	366	6.67	495	51	336	462	-	-	1.0
ETSP 1514 m	58	188	5.3	0.05	19	0.34	286	6.67	493	197	638	876	-	-	1.1
ETSP 1685 m	58	188	5.3	0.05	17	0.31	322	6.67	505	107	478	657	-	-	1.1
ETSP 1743 m	58	188	5.3	0.05	17	0.31	322	6.67	514	107	478	657	-	-	1.4
ETSP 1960 m	58	188	5.3	0.05	15	0.27	367	6.67	538	50	334	458	-	-	1.1
ETSP 2066 m	59	193	5.2	0.05	15	0.27	364	6.67	566	52	342	469	-	-	1.0
ETSP 2178 m	58	172	5.8	0.05	15	0.27	406	6.67	575	26	244	335	5.4	1.8	1.4

Notation: ***ETSP - Escape tunnel south portal end; S_d - spacing of joint in the loading direction; ϕ - angle of friction of joint; $(u_{nm}/a)'$ - strain of unsupported tunnel; H_1 -*** $170234D^{-1}e^{-0.017J_f}$ ***(Eq. 4.7 for squeezing condition); H_2 -*** $41901D^{-1}e^{-0.008J_f}$ ***(Eq. 4.12 for mild squeezing condition); H_3 -*** $57563D^{-1}e^{-0.008J_f}$ ***(Eq. 4.13 for moderate squeezing condition); u_{obs} - observed total deformation of supported tunnel; (u_{nm}/a) - strain after installation of supports (from numerical modelling); For squeezing ground – $H > H_1$; For mild squeezing – $H_2 > H > H_1$; For moderate squeezing - $H_3 > H > H_2$; For high squeezing – $H > H_1$ and $H > H_3$.***

Table 7.3b Validation of Squeezing Ground Condition

Chainage	H (m)	H_1 (m)	H_2 (m)	H_3 (m)	Satisfying Condition		Ground Condition
					Correlation	Strain of Unsupported Tunnel, ε (%)	
ETSP 385 m	178	50	334	458	$H_2>H>H_1$	3% > ε >1%	Mild squeezing
ETSP 690 m	294	69	388	533	$H_2>H>H_1$	N. A.	Mild squeezing
ETSP 707 m	315	175	603	828	$H_2>H>H_1$	3% > ε >1%	Mild squeezing
ETSP 850 m	359	113	490	673	$H_2>H>H_1$	N. A.	Mild squeezing
ETSP 1122 m	458	390	878	1206	$H_2>H>H_1$	3% > ε >1%	Mild squeezing
ETSP 1384 m	495	51	336	462	$H>H_1; H>H_3$	N. A.	High squeezing
ETSP 1514 m	493	197	638	876	$H_2>H>H_1$	N. A.	Mild squeezing
ETSP 1685 m	505	107	478	657	$H>H_1; H_3>H>H_2$	N. A.	Moderate squeezing
ETSP 1743 m	514	107	478	657	$H>H_1; H_3>H>H_2$	N. A.	Moderate squeezing
ETSP 1960 m	538	50	334	458	$H>H_1; H>H_3$	N. A.	High squeezing
ETSP 2066 m	566	52	342	469	$H>H_1; H>H_3$	N. A.	High squeezing
ETSP 2178 m	575	26	244	335	$H>H_1; H>H_3$	ε >5%	High squeezing

Notation: ***N. A. – Data is not available;*** ε ***(%) =*** $(u_{nm}/a)'$ ****100 for unsupported tunnel.***

ii) Chenani-Nashri Tunnel Sections in Non-squeezing Ground Condition

The exercise carried out for the case of squeezing ground condition through Tables 7.3a,b has been repeated for the case of tunnel sections in non-squeezing ground condition also. Accordingly, Tables 7.4a,b are presented for tunnel sections at ESTP: 1566 m, 2225 m, 2435 m, 2486 m, 2600 m, 2649 m, and 2803 m. Column 10 in Table 7.4a gives values of tunnel depth, H. Column 12 gives the value of H_1 and column 11 gives the value of H_4 computed from Eq. 4.6 for the non-squeezing ground condition. In Table 7.4b, strain level criterion has been included for the non-squeezing ground condition.

Values of average total tunnel strain, obtained from numerical modelling for supported and unsupported tunnel sections (except for sections: ETSP 2486 m, 2907 m and 3107 m), have been presented in columns 13 and 14 of Table 7.4a along with the observed strain levels at respective supported tunnel sections which are given in column 16. It can be seen that the values of strain levels at unsupported tunnel sections (column 13) are less than 1%, which satisfies the non-squeezing ground condition.

Table 7.4b states the satisfying condition required for non-squeezing ground in column 6. Tunnel depth, H (column 10) has been found to be less than value of H_1 (column 12) and it is larger than the value of H_4 or ($170009D^{-1}e^{-0.025J_f}$) as seen in column 11 of Table 7.4b. It shows that the tunnel sections reported in the Tables 7.4a,b exhibit non-squeezing ground condition.

Thus, it can be inferred from the study of Tables 7.3a,b and 7.4a,b that the empirical correlations developed for prediction of ground conditions (Squeezing and non-squeezing) are valid and hence can be used both in the field as well as in the design office with confidence.

Table 7.4a Validation of Non-squeezing Ground Condition

Column→	2	3	4	5	6	7	8	9	10	11	12	13	14	15
Chainage	Θ_A	S_d (mm)	J_n	n	ϕ	r	J_f	D_e (m)	H (m)	H_4 (m)	H_1 (m)	$(u_{nm}/a)'$ *100	(u_{nm}/a) *100	(u_{obs}/a) *100
ETSP 1566	58	223	4.5	0.05	20	0.36	225	6.67	495	93	559	0.3	0.2	0.1
ETSP 2225	59	231	4.3	0.05	21	0.38	212	6.67	588	128	699	0.4	0.2	0.2
ETSP 2435	63	218	4.6	0.06	19	0.34	213	6.67	623	123	678	0.3	0.2	0.1
ETSP 2486	59	231	4.3	0.05	21	0.38	212	6.67	626	128	699	-	-	0.1
ETSP 2600	63	221	4.5	0.06	20	0.36	194	6.67	652	202	950	0.3	0.2	0.1
ETSP 2649	59	212	4.7	0.05	23	0.42	209	6.67	656	138	734	0.4	0.2	0.1
ETSP 2803	63	221	4.5	0.06	19	0.34	205	6.67	672	153	788	0.3	0.2	0.2
ETSP 2856	63	240	4.2	0.06	19	0.34	194	6.67	676	199	942	0.3	0.2	0.1
ETSP 2907	63	218	4.6	0.06	21	0.38	191	6.67	668	213	985	-	-	0.1
ETSP 3107	57	219	4.6	0.06	23	0.42	191	6.67	645	217	1000	-	-	0.2

Notation: ***De - equivalent diameter (4*cross-sectional area/π)*** $^{0.5}$***;*** ***$a = D_e / 2$;***

H_1 - right hand term of the inequality expressed for squeezing ground condition by Eq. 4.7;

H_4 - $170009D^{-1}e^{-0.025J_f}$ ***(self-supporting ground condition expressed by extreme left hand side term in Eq. 4.4);***

For non-squeezing condition – $H_1 > H > H_4$. (Eq. 4.6)

Table 7.4b Validation of Non-Squeezing Ground Condition

Column→	1	2	3	4	5	6	7
Chainage	***D* (m)**	***H* (m)**	***H*$_4$ (m)**	***H*$_1$ *(m)***	***(u*$_{nm}$ */a)' *100***	**Satisfying Condition**	**Strain of Unsupported Tunnel**
ETSP 1566	6.67	495	93	559	0.3	$H_4<H<H_1$	ε < 1%
ETSP 2225	6.67	588	128	699	0.4	$H_4<H<H_1$	ε < 1%
ETSP 2435	6.67	623	123	678	0.3	$H_4<H<H_1$	ε < 1%
ETSP 2486	6.67	626	128	699	-	$H_4<H<H_1$	-
ETSP 2600	6.67	652	202	950	0.3	$H_4<H<H_1$	ε < 1%
ETSP 2649	6.67	656	138	734	0.4	$H_4<H<H_1$	ε < 1%
ETSP 2803	6.67	672	153	788	0.3	$H_4<H<H_1$	ε < 1%
ETSP 2856	6.67	676	199	942	0.3	$H_4<H<H_1$	ε < 1%
ETSP 2907	6.67	668	213	985	-	$H_4<H<H_1$	-
ETSP 3107	6.67	645	217	1000	-	$H_4<H<H_1$	-

Notation: ***H*$_1$ *- right hand term of the inequality expressed for squeezing ground condition by Eq.7.2;***
H*$_4$ -** $170009D^{-1}e^{-0.025J_f}$ **(*self-supporting ground condition expressed by extreme left hand side term in Eq.7.3);
For non-squeezing condition – H*$_4$ *< H < H*$_1$*.

7.8.2 Prediction of Tunnel Deformation in Squeezing Ground Condition

Following correlation (Eq.7.3) has been recommended in the present study represented which in fact is the same as Eq.5.9 in Chapter 5 for estimation of tunnel deformation in squeezing ground conditions:

$$\frac{u_p}{a} = 10^{-10}\left(-6*10^{-9}J^2 + 9J\right) + 0.0069 \qquad \text{(Eq. 5.9 from Chap. 5)} \qquad (7.3)$$

where u_p is the predicted radial tunnel deformation; a, the tunnel radius; J_f, the joint factor; σ_v and σ_h, the in-situ vertical (γH) and horizontal stresses; γ, the unit weight of rock mass (0.027 MN/m^3); H, the tunnel depth; K, the support stiffness; σ_{ci}, the uni-axial compressive strength of intact rock; and

$$J = \frac{\sigma_v J_f^{\,3}}{K + \frac{\sigma_{ci}}{\sigma_h}} \qquad (7.3a)$$

Four sections of escape tunnel (ETSP:385 m, 707 m, 1122 m & 2178 m) and four sections of main tunnel (MTSP: 721 m, 837 m, 919 m & 1009 m) of Chenani-Nashri Highway Tunnel Project have been **numerically analysed** and average total tunnel strain has been obtained and presented in columns of Table 7.5. Data of **observed values** of average total tunnel strain level, *$(u_{obs}/a)*100$* at various tunnel sections of supported escape and main tunnels have been tabulated in Table 7.5 and compared with the values of average total tunnel strain level, *$(u_p/a)*100$* **predicted** on basis of the recommended correlation (Eq. 7.3 above). It can be seen that the predicted values of tunnel strain are reasonably in good agreement with the respective values observed in the field. The values of tunnel strain predicted by the recommended correlation (Eq. 7.3) and the values obtained via numerical modelling have been plotted with the respective observed values in Fig. 7.19. The tunnel strain values predicted by the recommended correlation have a coefficient of accordance (COA) of 0.13 and are close to the 1:1 line (AB) in the Fig. 7.19, showing good agreement with the observed values. The tunnel strain values computed via numerical modelling have coefficient of accordance of 0.34 and do not give a very good agreement.

Table 7.5 Validation of Correlation for Estimation of Tunnel Deformation in Squeezing Ground Condition

Chainage	Θ (^{o})	α (^{o})	Θ_A (^{o})	S_d (mm)	J_n	β (^{o})	n	ϕ (^{o})	r	J_f	$H>H_1$		K (MPa)	σ_v (MPa)	σ_h (MPa)	σ_{ci} (MPa)	Supported Tunnel Strain		
											H (m)	H_1 (m)					(u_{obs}/a) *100	(u_p/a) *100 Eq.7.4	(u_{nm}/a) *100
ETSP 334	60	20	58	191	5.2	32	0.05	15	0.27	366	195	51	250	5.3	7.9	40	0.8	0.8	-
ETSP 385	60	23	58	188	5.3	32	0.05	15	0.27	367	178	50	250	4.8	7.2	48	0.8	0.8	1.1
ETSP 535	60	8	60	198	5.0	30	0.05	18	0.33	290	238	184	250	6.4	9.6	40	0.6	0.7	-
ETSP 690	65	38	59	177	5.7	31	0.05	17	0.31	348	294	69	167	7.9	11.9	40	1.1	0.9	-
ETSP 707	65	28	62	214	4.7	28	0.06	15	0.27	293	315	175	334	8.5	12.8	40	0.7	0.7	0.9
ETSP 800	60	20	58	191	5.2	32	0.05	17	0.31	321	346	109	167	9.3	14.0	40	0.9	0.9	-
ETSP 850	65	33	61	185	5.4	29	0.06	17	0.31	319	359	113	169	9.7	14.5	40	1.1	0.9	-
ETSP 1069	60	8	60	238	4.2	30	0.05	18	0.33	242	427	417	250	11.5	17.3	40	0.6	0.7	-
ETSP 1122	65	26	63	217	4.6	27	0.06	17	0.31	246	458	390	436	12.4	18.5	50	0.8	0.7	0.8
ETSP 1384	60	25	58	186	5.4	32	0.05	15	0.27	366	495	51	167	13.4	20.0	40	1.0	1.0	-
ETSP 1514	60	23	58	188	5.3	32	0.05	19	0.34	286	493	197	167	13.3	20.0	40	1.1	0.9	-
ETSP 1685	60	23	58	188	5.3	32	0.05	17	0.31	322	505	107	167	13.6	13.6	40	1.1	0.9	-
ETSP 1960	60	23	58	188	5.3	32	0.05	15	0.27	367	538	50	167	14.5	14.5	40	1.1	1.1	-
ETSP 2066	60	18	59	193	5.2	31	0.05	15	0.27	364	566	52	167	15.3	15.3	40	1.0	1.1	-

…Contd.

Chainage	Θ (^{o})	α (^{o})	Θ_A (^{o})	S_d (mm)	J_n	β (^{o})	n	ϕ (^{o})	r	J_f	$H>H_1$		K (MPa)	σ_v MPa	σ_h MPa	σ_{ci} MPa	Supported Tunnel Strain		
											H (m)	H_1 (m)					(u_{obs}/a) *100	(u_p/a) *100 Eq.7.4	(u_{nm}/a) *100
ETSP 2119	65	28	62	257	3.9	28	0.06	15	0.27	244	568	403	250	15.3	15.3	40	0.7	0.8	-
ETSP 2178	60	20	58	172	5.8	32	0.05	15	0.27	406	575	26	250	15.5	15.5	45	1.4	1.1	1.8
ETSP 3220	60	18	59	231	4.3	31	0.05	19	0.34	236	621	462	250	16.8	16.8	40	0.5	0.8	-
MTSP 721	60	8	60	238	4.2	30	0.05	19	0.34	228	294	264	207	7.9	11.9	40	0.4	0.7	0.6
MTSP 771	65	28	62	235	4.2	28	0.06	17	0.31	234	320	239	207	8.6	13.0	40	0.4	0.7	-
MTSP 823	65	23	63	221	4.5	27	0.06	18	0.33	217	342	319	207	9.2	13.9	40	0.5	0.7	-
MTSP 837	60	28	57	183	5.5	33	0.06	15	0.27	362	347	27	207	9.4	14.1	50	1.0	0.9	0.9
MTSP 874	65	28	62	235	4.2	28	0.06	18	0.33	220	360	303	207	9.7	14.6	40	0.5	0.7	-
MTSP 892	60	33	55	194	5.2	35	0.06	21	0.38	219	365	308	207	9.9	14.8	40	0.5	0.7	-
MTSP 919	60	28	57	219	4.6	33	0.06	21	0.38	211	374	353	207	10.1	15.1	35	0.6	0.7	0.9
MTSP 948	60	28	57	164	6.1	33	0.06	15	0.27	403	379	13	207	10.2	15.3	35	0.9	1.0	-
MTSP 980	65	28	62	257	3.9	28	0.06	17	0.31	214	404	335	207	10.9	16.4	40	0.5	0.7	-
MTSP 1009	65	23	63	221	4.5	27	0.06	19	0.34	205	413	391	207	11.2	16.7	40	0.7	0.7	0.8

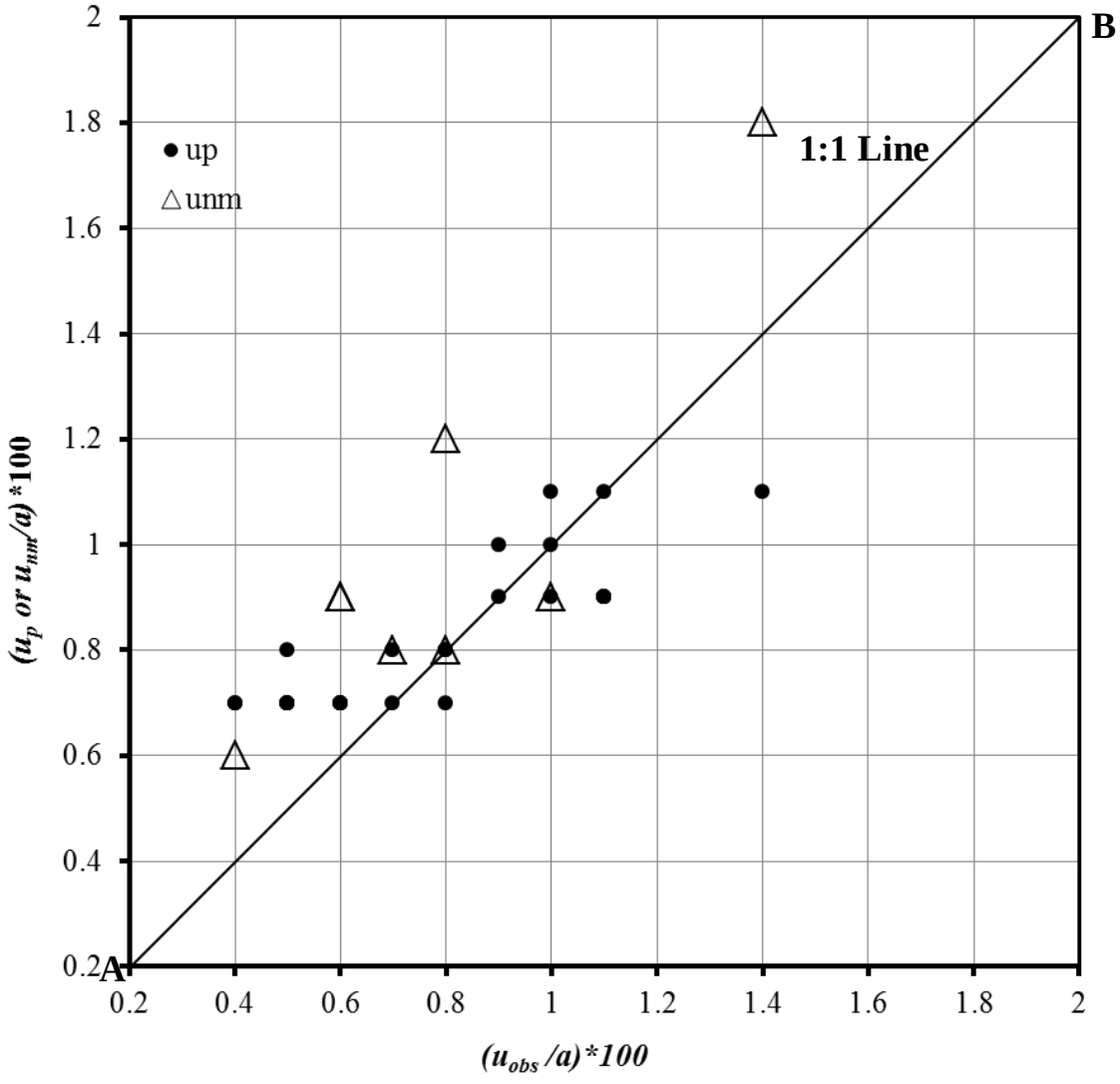

Fig.7.19 Predicted Tunnel Strain versus Observed Tunnel Strain in Squeezing Ground

7.8.3 Prediction of Tunnel Deformation in Non-squeezing Ground Condition

Eleven supported sections of escape tunnel of Chenani-Nashri Highway Tunnel Project have been numerically analysed to obtain average total tunnel strain, $100*u_{nm}/a$. These values are listed in the last column of Table 7.6. For these tunnel sections, tunnel strain values have also been obtained via the recommended correlation (Eq. 5.19) for non-squeezing ground condition and reproduced here as Eq. 7.4. These strain levels are also presented in Table 7.6.

$$\frac{u_p}{a} = \frac{3*10^{-10} J_f{}^3 \sigma_v}{K+6} + 0.0003 \qquad \text{(Eq. 5.19 from Chap.5)} \qquad (7.4)$$

Table 7.6 also gives values of H_1 , the depth for satisfying the squeezing ground condition and H_4 , the depth for satisfying the self supporting ground condition. It can be seen that values of H, the tunnel depth lie between the values of H_1 and H_4 , which suggests that the ground condition at the location of all the tunnel sections under consideration is non-squeezing in nature. It can be observed in Table 7.6 that tunnel strain values predicted on basis of correlation (Eq. 7.4) are very close to the values of strain levels observed in the field. Values of tunnel strain obtained from numerical modelling also show a non-squeezing behaviour of the ground. Thus the recommended correlation (Eq. 7.4 or Eq. 5.19) can be treated as valid for estimation of tunnel strain in non-squeezing ground conditions. It can as well be observed in Table 7.6 that the values of tunnel strain predicted on basis of correlation (Eq. 7.4 or Eq. 5.19) are closer to the observed values at many tunnel sections than the corresponding values obtained via numerical modelling.

Table 7.6 Validation of Correlation for Estimation of Tunnel Deformation in Non-squeezing Ground Condition

Chainage	Θ (^{o})	α (^{o})	Θ_A (^{o})	S_d (mm)	J_n	β (^{o})	n	ϕ (^{o})	r	J_f	$H_4<H<H_1$			K (MPa)	Supported Tunnel Strain		
											H (m)	H_1 (m)	H_4 (m)		(u_{obs}/a) *100	(u_p/a) *100 Eq.7.4	(u_{nm}/a) *100
ETSP 1566	60	25	58	223	4.5	32	0.05	20	36	225	495	559	93	169	0.1	0.1	0.2
ETSP 2225	60	18	59	231	4.3	31	0.05	21	0.38	212	588	699	128	181	0.2	0.1	0.2
ETSP 2435	65	25	63	218	4.6	27	0.06	19	0.34	213	623	678	123	167	0.1	0.1	0.2
ETSP 2486	60	18	59	231	4.3	31	0.05	21	0.38	212	626	699	128	167	0.1	0.1	-
ETSP 2600	65	23	63	221	4.5	27	0.06	20	0.36	194	652	950	202	167	0.1	0.1	0.2
ETSP 2649	60	18	59	212	4.7	31	0.05	23	0.42	209	656	734	138	167	0.1	0.1	0.2
ETSP 2803	65	23	63	221	4.5	27	0.06	19	0.34	205	672	788	153	167	0.2	0.1	0.2
ETSP 2856	65	25	63	240	4.2	27	0.06	19	0.34	194	676	942	199	167	0.1	0.1	0.2
ETSP 2907	65	25	63	218	4.6	27	0.06	21	0.38	191	668	985	213	167	0.1	0.1	-
ETSP 3107	60	28	57	219	4.6	33	0.06	23	0.42	191	645	1000	217	167	0.2	0.1	-
ETSP 3167	65	25	63	240	4.2	27	0.06	19	0.34	194	628	942	199	167	0.2	0.1	-

Notation: ***H_1 - squeezing ground condition; H_4 - self-supporting ground condition.***

Chapter 8

SUMMARY AND CONCLUSION

8.1 SUMMARY OF WORK DONE

Squeezing ground condition in tunnelling has been creating the problems of supporting and hence stability of tunnels. The problem of supporting may affect the long term stability of tunnel, if adequate supports are not provided in time. After going through the relevant literature in detail, following gaps were identified:

i) The available analytical, empirical, and numerical approaches can reliably predict tunnel deformation response and the support pressure for non-squeezing conditions which is in good agreement with the field observed behaviour. However, this is not true for the squeezing ground conditions. For instance, in Khimti hydroelectric tunnels (Nepal), the predicted values of support pressure and tunnel deformation by various available approaches were found to be in good agreement with the respective values observed in the field for non-squeezing grounds but not for squeezing grounds (Shrestha, 2005).

ii) The available approaches are valid only for circular shape of tunnels and hydrostatic in-situ stress conditions.

iii) In addition, the approaches involve number of parameters to be determined in the laboratory.

In view of the above observations, an attempt has been made in this study to develop empirical correlations considering the parameters which can be easily assessed for prediction of ground condition, tunnel deformation and tunnel support pressure. Even though the present study lays more emphasis on the squeezing ground condition, non-squeezing ground condition has also been taken for study. In the present study, following major objectives were set forth:

- Study of large no. of tunnel case histories,
- Collection of required data, viz., diameter and depth of tunnel, in situ stresses, rock mass quality parameters (joint properties, uniaxial compressive strength and rock mass number, etc.), observed radial tunnel deformation (closure), support pressure and details of supports installed in tunnels,
- Development of empirical correlations for prediction of different ground conditions,
- Development of empirical correlations for prediction of tunnel deformation and support pressure for non-squeezing and squeezing ground conditions.

Data of 366 tunnel sections from 24 tunnelling projects located in India and abroad was collected for the present study. The correlations developed use joint factor J_f, rock mass quality, Q and rock mass number, N as a measure of rock mass quality for prediction of the ground condition. Dimensionally correct empirical correlations have been developed for prediction of tunnel deformation/strain and support pressure for non-squeezing and squeezing ground conditions.

The correlations developed for prediction of ground condition and tunnel deformation have been validated by on basis of the field data collected from an independent and an important Chenani-Nashri national Highway Project presently being executed in the state of Jammu & Kashmir. The data of this project was not used in earlier in the development of various empirical correlations.

8.2 CONCLUSIONS

8.2.1 Proposed Correlations

On the basis of the data collected from various project sites, empirical correlations have been developed for prediction of ground condition, tunnel deformation and the support pressure for squeezing and non-squeezing ground conditions for use in the field and also in the design office. The proposed correlations are:

i) Prediction of Ground Condition

<u>Correlations based on Joint Factor</u>, Jf

Self-supporting ground condition : $H < 170009 D^{-1} e^{-0.025 J_f}$

Non-squeezing ground condition : $H < 170234 D^{-1} e^{-0.017 J_f}$

Squeezing ground condition : $H > 170234 D^{-1} e^{-0.017 J_f}$

Mild-squeezing ground condition : $41901 D^{-1} e^{-0.008 J_f} > H > 170234 D^{-1} e^{-0.017 J_f}$

Moderate squeezing ground : $57563 D^{-1} e^{-0.008 J_f} > H > 41901 D^{-1} e^{-0.008 J_f}$

High-squeezing ground : $4189 D^{-1} e^{0.0049 J_f} > H > 57563 D^{-1} e^{-0.008 J_f}$

Condition for rock bursting : $H > 4189 D^{-1} e^{0.0049 J_f}$ and $J_f < 260$

<u>Correlations based on rock mass quality</u>, Q

Self-supporting ground condition : $H < 191 \left(\frac{Q}{D} \right)^{0.642}$

Non-squeezing ground condition : $H < 722 \left(\frac{Q}{D} \right)^{0.34}$

Squeezing ground condition : $H > 722 \left(\frac{Q}{D} \right)^{0.34}$

Condition for rock bursting : $H > 635 \left(\frac{Q}{D} \right)^{-0.27}$ and $Q/D = 0.08$

<u>Correlations based on rock mass number</u> , N

Condition for self-supporting ground : $H < 127 (N/D)^{0.9087}$

Condition for non-squeezing ground : $H < 466 (N/D)^{0.3176}$

Condition for squeezing ground : $H > 466 (N/D)^{0.3176}$

Condition for rock burst ground : $H > 1035 (N/D)^{-0.096}$ and $N/D > 0.14$

ii) Prediction of Tunnel Deformation

Following dimensionally correct correlations have been recommended for prediction of tunnel deformation in non-squeezing and squeezing ground conditions:

For non-squeezing ground: $$\frac{u_p}{a} = \frac{3*10^{-10} J_f{}^3 \sigma_v}{K+6} + 0.0003 \qquad (R^2 = 0.92)$$

For squeezing ground: $$\frac{u_p}{a} = 10^{-10}\left(-6*10^{-9} J^2 + 9J\right) + 0.0069 \qquad (R^2 = 0.94)$$

iii) Prediction of Tunnel Support Pressure

Following dimensionally correct correlations have been recommended for prediction of tunnel support pressure in non-squeezing and squeezing ground conditions:

For non-squeezing ground: $$P_e = 10^{-6}\sigma_v\left(\frac{7*10^{-4} J_f{}^3}{d^{0.2}} + 4058\right) \qquad (R^2 = 0.93)$$

For squeezing ground: $$P_s = 9.23*10^{-3}\sigma_v\left(\frac{J_f{}^3 \sigma_h{}^{0.1}}{10^7 \sigma_{ci}{}^{0.1}\left(d^{0.2} + \frac{J_f}{1434}\right)}\right)^{1.7} \qquad (R^2 = 0.92)$$

In above correlations, u_p defines the predicted radial tunnel deformation (m); a, the tunnel radius (m); J_f, the joint factor (dimensionless); σ_v, the vertical in situ stress = γH = 0.027H (MPa); σ_h, the horizontal in situ stress (MPa); K, the support stiffness (MPa); and σ_{ci}, the uni-axial compressive strength of intact rock (MPa). The parameters J, U and d involved in the above correlations are defined as -

$$J = \frac{\sigma_v J_f{}^3}{K + \frac{\sigma_{ci}}{\sigma_h}}, \qquad \text{and} \qquad d = \frac{u}{a}*100\,\%$$

where

P_s is the predicted support pressure (MPa) and d is the % radial tunnel deformation.

8.2.2 Parametric Study

Parametric study was also carried out for the correlations recommended for prediction of tunnel deformation and support pressure. It was observed that there is no influence of tunnel radius (size) on either the tunnel strain or the tunnel support pressure when tunnels are excavated in non-squeezing ground condition.

Similarly, tunnel size was also found to have no influence on tunnel support pressure in squeezing ground condition.

Uniaxial compressive strength of intact rock (σ_{ci}) has been found to have a significant bearing for tunnels in weak rocks (σ_{ci} < 20 MPa) particularly in squeezing ground condition at higher tunnel depth.

8.3 SCOPE FOR FURTHER INVESTIGATION

In the present study, the influence of following parameters has not been investigated:

i) Tunnel shape,
ii) Stand-up time of unsupported tunnels,
iii) Active span i.e. safe distance of the face of advance from the nearest support installed, and
iv) Rate of advance of tunnelling.

All these parameters can have a significant bearing on the tunnel response and therefore it is suggested that work in this direction must be carried out and their effect on the tunnel deformation and support pressure be investigated, especially in the squeezing ground condition.

REFERENCES

1. Ahmad F., Masoud R., 2009. Analytical approach for the design of active grouted rock bolts in tunnel stability based on convergence-confinement method. Tunnelling and Underground Space Technology 24 (4), 263-275.

2. Arora V.K., 1987. Strength and deformation behaviour of jointed rocks. Ph.D. Thesis, IIT Delhi, India.

3. Attewell P.B., Sandford M.R., 1974. Intrinsic shear strength of a brittle anisotropic rock-I: Experimental and mechanical interpretation. Int. J. Rock Mech. Min. Sci. & Geomech. Abstr. 11 (11), 423-430.

4. Aydan O., Akagi T., Kawamoto T., 1993. The squeezing potential of rocks around tunnels: theory and prediction. Rock Mech. Rock Engng. 26 (2), 125-143.

5. Aydan O., Akagi T., Kawamoto T., 1996. The squeezing potential of rocks around tunnels: theory and prediction with examples taken from Japan. Rock Mech. Rock Engng. 29 (3), 137-163.

6. Bahuguna H., Khanduri H.C., Dangwal D.P., Gajbhiye P. K., Charaborty I., 2008. Geotechnical investigations in the planning of powerhouse complex of Tehri dam project (stage-I) India. Proc. World Tunnel Cong. Underground Facilities for Better Environment and Safety, 19-25 Sept., New Delhi, India.

7. Barla G., 1995. Squeezing Rocks in Tunnels, ISRM News Journal 2 (3 & 4), 44-49.

8. Barla G., 2001. Tunnelling under squeezing rock conditions. A lecture note available on website: www.polito.it, 17/03/03, 96 p.

9. Barla G., Barla M., Bonini M., 2004. Characterisation of Italian clay shales for tunnel design. Int. J. Rock Mech. Min. Sci. 41, 221-227.

10. Barla G., Bonini M., Debernardi D., 2010a. Time dependent deformations in squeezing tunnels. International Journal of Geoengineering Case Histories,

Retrieved from website http://casehistories.geoengineer.org, 2(1), 40-65. doi: 10.4417/IJGCH-02-01-03.

11. Barla G., Bonini M., Semeraro M., 2010 b. Performance monitoring and analysis of a yield-control support system in squeezing rock. Proc. Eurock 2010, Lausanne, June 15-18, 459-462.

12. Barla G., Bonini M., Semeraro M., 2011. Analysis of the behaviour of a yield-control support system in squeezing rock Tunnelling and Underground Space Technology 26, 146–154.

13. Barla G., Debernardi D., Sterpi D., 2012. Time dependent modelling of tunnels in squeezing conditions. Int. J. Geomech. 12 (6), 697-710.

14. Barton N., Lien R., Lunde J., 1974. Engineering classification of rock masses for the design of tunnel support. Rock Mech. Rock Engg. 6 (4), 189-236.

15. Bhasin R., Barton N., Grimstad E., Chryssanthakis P., 1995. Engineering geological characterization of low strength anisotropic rocks in the Himalayan region for assessment of tunnel support. Engineering Geology 40, 169–193.

16. Bhasin R., Grimstad E., 1996. Use of stress-strength relationship in the assessment of tunnel stability. Tunnelling and Underground Space Technology 11 (1), 93-98.

17. Bhasin R., Magnussen A.W., Grimstad E., 2006. The effect of tunnel size on stability problems in rock masses. Tunnelling and Underground Space Technology 21 (3-4), 405.

18. Bhasin R.K., Barton N., Grimstad E., Chryssanthakis P., Shende F.P., 1996. Comparison of predicted and measured performance of a large cavern in the Himalayas. Int. J. Rock Mech. Min. Sci & Geomech. Abstr. 33, 607–626.

19. Bieniawski Z.T., 1976. Rock mass classification in rock engineering. Proc. Symp. Exploration for Rock Engineering, Z. T. Bieniawski, ed., 1, 97-106. Cape Town: Balkema.

20. Bieniawski Z.T., 1984. Rock mechanics design in mining and tunnelling. A.A. Balkema Publishers, Rotterdam, 272 p.

21. Bieniawski Z.T., 1989. Engineering Rock Mass Classification, John Wiley & Sons, New York, 251 p.

22. Brown E.T., 1970a. Strength of models of rock with intermittent joints. J. Soil Mech. & Found. and Proc. ASCE, 96 (SM6), 1935-1949.

23. Brown E.T., 1970b. Modes of failure in jointed rock masses. Proc. 2nd Cong. of ISRM, Belgrade, 2, 293-298.

24. Brown E.T., Bray J.W., Ladanyi B., Hoek E., 1983. Ground response curves for rock tunnels. J. Geotech. Eng. ASCE 109, 15-39.

25. Brown E.T., Trollope D.H., 1970. Strength of a model of jointed rock. J. Soil Mech. & Found. and Proc. ASCE, 96 (SM6), 1935-1949.

26. Can T., Ertunc A., 2000. Bilecik-Osmaneli karayolu tunellerinin on_tasariminda ampirik ve analitik yaklasimlar. The 5th National Rock Mechanics Symposium. Turkish National Rock Mechanics Society (TUKMD), Isparta, Turkey, 45– 56.

27. Cantieni L., Anagnostou G., 2009. The interaction between yielding supports and squeezing ground. Tunnelling and Underground Space Technology 24, 309–322.

28. Cantieni L., Anagnostou G., Hug R., 2011. Interpretation of core extrusion measurements when tunnelling through squeezing grounds. Rock Mech. Rock Engg. 44, 641–670.

29. Carranza-Torres C., 2003. Dimensionless graphical representation of the exact elastoplastic solution of a circular tunnel in a Mohr-Coulomb material subject to uniform far field stresses. Rock Mech. Rock Eng. 36 (3), 237-253.

30. Carranza-Torres C., Fairhurst C., 2000. Application of the convergence confinement method of tunnel design to rock masses that satisfy the Hoek-Brown failure criteria. Tunnelling and underground space Technology 15 (2), 187-213.

31. Chakraborty A.K., Murthy V.M.S.R., Jethwa J.L., 1996. Blasting Problems in Underground Constructions through Deccan Trap Formation: Some Experiences at Koyna Hydro-Electric Project, Stage IV. Tunnelling and Underground Space Technology 11 (3), 311-324.

32. Chakraborty A.K., Raina A.K., Ramulu M., Choudhury P.B., Haldhar A., Shahoo P., Bandopadhyay C., 2004. Development of rational models for tunnel blast prediction based on a parametric study. Geotechnical and Geological Engineering, 22, 477-496.

33. Chern J.C., Yu C.W., Shiao F.Y., 1998. Tunnelling in squeezing ground and support estimation. Proc. Regional Symp. Sedimentary Rock Engg., Taipei, 192-202.

34. Choudhari J.B., 2007. Closure of Underground Opening in Jointed Rocks. Ph. D. Thesis, Dept. of Civil Engg., IIT Roorkee, Roorkee, India.

35. CIMFR, 2007. Instrumentation, evaluation and design of support system in tunnels of Udhampur-Katra rail link project. Internal report, Central Institute of Mining and Fuel Research, Dhanbad, India, GC/MT/R/2/2006-07.

36. CIMFR, 2012. Design of Chenani-Nashri highway tunnel of NHAI in the state of J & K. Internal report, Central Institute of Mining and Fuel Research, Dhanbad, India, CNP/R/2926/2011-12, 80p.

37. Corbetta F., Bernaud D., Minh D.N., 1991. Contribution to the convergence-confinement method by the principle of similitude (in French). Rev. Fr. Geotech., 54, 5-11.

38. Daemen J.J.K., 1975. Tunnel support loading caused by rock failure. Ph.D. Thesis, University of Minnesota, Minneapolis, USA, 434p.

39. Daemen J.J.K., 1977. Problems in tunnel support mechanics. Proc. 12th U.S. Symp. on Rock Mechanics. Underground Space 1, 163-172.

40. Daemen J.J.K., 1983. Slip zones for discontinuities parallel to circular tunnels or shafts. Int. J. Rock Mech. Min. Sci. & Geomech. Abstr. 20 (3), 135-148.

41. Daemen J.J.K., Fairhurst C., 1969. Rational design of tunnel supports. 2nd Symp. Rapid Excavation, California, U.S.A.

42. Daemen J.J.K., Fairhurst C., 1970. Influence of failed rock properties on tunnel stability. Proc. 12th U. S. Symp. Rock Mech., Rolla, Missouri, New York, 855-875.

43. Detourney E., Fairhurst C., 1987. Two-dimensional elasto-plastic analysis of a long cyllindrical cavity under non-hydrostatic loading, Int. J. Rock Mech. Min. Sci., 24 (4), 197-211.

44. Dube A.K., 1979. Geo-mechanical evaluation of tunnel stability under failing rock conditions in a Himalayan tunnel. Ph.D. Thesis, Dept Civil Engg, University of Roorkee, India, 212p.

45. Dube A.K., Singh B., Singh Bhawani, 1986a. Study of squeezing pressure phenomenon in a tunnel-I. Tunnelling and Underground Space Technology 1 (1), 35-39.

46. Dube A.K., Singh B., Singh Bhawani, 1986b. Study of squeezing pressure phenomenon in a tunnel-II. Tunnelling and Underground Space Technology, 1 (1), 41-48.

47. Duncan J.M., Chang C.Y., 1970. Non-linear analysis of stress and strain in soils. J Soil Mech. Found Engg., ASCE, 96 SM 5, 623-653.

48. Dwivedi R.D., Goel R.K., Singh M., Viladkar M.N., 2012. State-of-the-art of tunnelling through squeezing grounds. Journal of Rock Mech. Tunlg. Tech. 18 (2), 117-140.

49. Dwivedi R.D., Singh M., Viladkar M.N., Goel R.K., 2013. Prediction of tunnel deformation in squeezing grounds. Engineering Geolog. 161, 55-64.

50. Dwivedi R.D., Singh M., Viladkar M.N., Goel R.K., 2014a. Estimation of support pressure during tunnelling through squeezing grounds. Engineering Geology, 168, 9-22.

51. Dwivedi R.D., Singh M., Viladkar M.N., Goel R.K., 2014b. Parametric analysis of an empirical correlation predicting deformation of squeezing tunnels. Proc. IPRM-2014, 6-8 Feb, NIRM Bengaluru 255-260.

52. Egger P., 2000. Design and construction aspects of deep tunnels (with particular emphasis on strain softening rocks). Tunnelling and Underground Space Technology 15 (4), 403-408.

53. Einstein N.H., Hirschfield R.C., 1973. Model studies on mechanics of jointed rock. J. Soil Mech. & Found Div., Proc. ASCE 90, 229-248.

54. Eisenstein Z., Branco P., 1991. Convergence - confinement method in shallow tunnels. Tunnelling and Underground Space Technology 6 (3), 343-346.

55. Facibeni L., Palomba M., Carrieri G., Russo G., Guvenc A.H., 2011. Critical aspects in the design of the Chenani-Nashri tunnel. Proc. 3rd Indian Rock Conference-INDOROCK 2011, ISRMTT Roorkee Chapter Roorkee, Oct. 13-15, Roorkee, India.

56. Fairhurst C., 1976. The application of mechanics of rock engineering. Proc. Symp. on Exploration for Rock Engineering, Johannesburg.

57. Federica S., Vincent L., 2010. Analysis of the evolution of road tunnels equilibrium conditions with a convergence-confinement approach. Rock Mech. Rock Engng, 43 (2), 201-218.

58. Fenner R., 1938. Untersuchungen Zur Erkenntnis Des, Gebirgsdruckes. Gluckauf, 32:681-695, 33:705-715.

59. Fritz P., 1982. Modelling rheological behaviour of rock. Proc. 4th Int. Conf. Numerical Methods in Geomechanics, Edmonton, June.

60. Fritz P., 1984. An analytical solution for axisymmetric tunnel problems in elasto-viscoplastic media. Int. J. Numerical and Analytical Methods in Geomechanics 8, 325-342.

61. Gansser A., 1964. Geology of the Himalayas. Interscience Publishers, 289p.

62. GEODATA, 2011. Rehabilitation, Strengthening and four laning of Chenani to Nashri section of NH-1A including 9 km long tunnel (2 lanes) with parallel escape tunnel in the state of Jammu & Kashmir. Base line geological report submitted to ITNL, India, I1007-GDE-ENG-RPT-GE-0003 Rev B.

63. Geodata/LIN, 2011a. Chenani-Nashri Tunnel: Tunnel Works, Main Tunnel Design Report, Doc. No. I1007-GDE-ENG-C-RPT-3001(D), 31 July 2001, 252p.

64. Geodata/LIN, 2011b. Chenani-Nashri Tunnel: Tunnel Works, Escape Tunnel Design Report, Doc. No. I1007-GDE-ENG-C-RPT-3002(D), 31 July, 231p.

65. Gioda G., Cividini A., 1996. Numerical methods for analysis of tunnel performance in squeezing rocks. Rock Mech. Rock Engng 29 (4), 171-193.

66. Goel R.K, Swarup A., Dwivedi R.D., Mishra S., 2004. Case history of a railway tunnel. Proc. Need for Accelerated Underground Construction Issues & Challenges (Tunnelling Asia' 2004), Dec 14-17, New Delhi, India.

67. Goel R.K., 1994. Correlations for predicting support pressures and closures in tunnels, Ph.D. Thesis, University of Nagpur, India, 310p.

68. Goel R.K., Dwivedi R.D., Viswanathan G., Rathore J.S., 2012. Challenges of design and construction of a highway tunnel through mixed geology in Himalayas. Proc. 7th Asian Rock Mechanics Symposium, Oct 15-19, Seoul, Korea.

69. Goel R.K., Jethwa J.L., 1991. Prediction of support pressure using RMR. Proc. Geotech. Conf., Surat, India, 203-205.

70. Goel R.K., Jethwa J.L., Dhar B.B., 1996. Effect of tunnel size on support pressure, Technical note, Int. J. Rock Mech. Min. Sci. Geomech. Abstr. 33(7), 749-755.

71. Goel R.K., Jethwa J.L., Paithankar A.G., 1995. Indian experiences with Q and RMR systems. Tunnelling and Underground Space Technology, 10 (1), 97-109.

72. Goel R.K., Jethwa J.L., Singh B., 1988. Case history of Maneri- Uttarkashi power tunnel. Proc. 2nd Int. Conf. on Case Histories in Geotechnical Engineering, St. Louis, June 1-5.

73. Goguel J., 1947. Repartition des Contraintes autour d'un tunnel cyllindrique', annales des Pouits et chaussees, 117 e Annee, 157-183.

74. González-Nicieza C., Álvarez-Vigil A.E., Menéndez-Díaz A., González-Palacio C., 2008. Influence of the depth and shape of a tunnel in the application of the convergence‑confinement method. Tunnelling and Underground Space Technology 23 (1), 25-37.

75. Grimstad E., Barton N., 1993. Updating the Q-System for NMT. Proc. Int. Symp. Sprayed Concrete - modern use of wet mix sprayed concrete for underground support, Fagernes. 46-66. Oslo: Norwegian Concrete Association.

76. Grimstad E., Bhasin R., 1999. Rock support in hard rock tunnels under high stress. Norwegian Geotechnical Institute, 205, 10.

77. Gutierrez M., Xia C.C., 2009. Squeezing potentials of tunnels in clays and clayshales from normalized undrained shear strength, unconfined compressive strength and seismic velocity. Proc. Geotechnical Aspects of Underground Construction in Soft Ground, H.W. Huang & G.B. Liu, eds., London, 537-541.

78. Hoek E., 2000. Big tunnels in bad rock (The thirty-sixth Karl Terzaghi Lecture). The paper presented at the ASCE 2000 Civil Engineering Conference and Exposition, Seatle, Oct.18-21, also in ASCE Journal of Geotechnical and Geo-environmental Engineering, Sept. 2001, 127 (9), 726-740.

79. Hoek E., Brown E.T., 1982. Underground excavations in Rock. Pub: The Institution of Mining and Metallurgy, London, 527p.

80. Hoek E., Carranza-Torres C., Diederichs M.S., Corkum B., 2008. Integration of geotechnical and structural design in tunnelling. Proceedings University of Minnesota 56th Annual Geotechnical Engineering Conference. Minneapolis, 29 February, 1-53.

81. Hoek E., Carranza-Torres C.T., Corkum B.T., 2002. Hoek-Brown failure criterion: 2002 edition. In Hammah, Bawden, Curran & Telesnicki, eds., Proc. 5th North American Rock Mech. Symp. Toronto, 7-10 July. University of Toronto Press 267-274.

82. Hoek E., Marinos P., 2000. Predicting tunnel squeezing problem in weak heterogeneous rock masses. Tunnels and Tunnelling International 32 (11), 45-51 & 32 (12), 34-36.

83. Indraratna B., 1990. Laboratory simulation of joints and their influence on rock mass behaviour. Rock Joints, Rotterdam, 235-242.

84. Indraratna B., Kaiser P.K., 1990. Design for grouted rock bolts based on the convergence control method. Int. J Rock Mech. Min. Sci. 27 (4), 269-281.

85. Jaeger J.C., Cook N.G.W., 1976. Fundamentals of rock mechanics, Chapman and Hall, London, 585p.

86. Jain M.S., Andotra B.S., Sondhi S.N., 1975. Note on geological features of the Chhibro-Khodri tunnel and occurences of Subathu shales. Unpubl. Rep. of Geological Survey of India.

87. Jain M.S., Jaitly G.S., Sondhi S.N., Rajagopalan G., 1976. Geotechnical note on the alternative alignments between Heena and Tiloth adits, Memo. XIV Meeting, Board of Consultants, Maneri Stage I Project.

88. Jethwa J.L., 1981. Evaluation of rock pressures in tunnels through squeezing ground in lower Himalayas. Ph. D. Thesis, University of Roorkee, Roorkee, India.

89. Jethwa J.L., Dube A.K., Singh B., Bagchi S., 1979. Estimation of Rock Pressure and Support Requirements for Unexcavated Portions of Loktak Hydel Tunnel. C.M.R.S. Report No. AC/16/78, April.

90. Jethwa J.L., Dube A.K., Singh B., Mithal R.S., 1982. Evaluation of methods for tunnel support design in squeezing rock conditions. Proc. 4th Int. Congr. Int. Assoc. Engg. Geol., Delhi, 5, 125-134.

91. Jethwa J.L., Goel R.K., 1992. Recent experiences with *Q* and *RMR* systems. Proc. 6th National Conf. on Rock Mech., Bangalore, India, October, 143-154.

92. Jethwa J.L., Goel R.K., Ram B., Verman M.K., Singh B., 1986. Rock mechanics instrumentation of lower Periyar tunnel, Kerala, India. CMRS Report, March, 16 p.

93. Jethwa J.L., Goel R.K., Ram B., Verman M.K., Singh B., 1987. Rock Mechanics Instrumentation of Lower Periyar Tunnel, Kerala, India. CMRS Report, March, 16 p.

94. Jethwa J.L., Singh B., Singh Bhawani, Mithal R.S., 1980. Influence of geology on tunnelling conditions and deformational behaviour of supports in the faulted Zones - a case history of Chhibro-Khodri tunnel in India. Eng. Geol. 16 (3/4), 291-318.

95. Jiang Y., Yoneda H., Tanabashi Y., 2001. Theoretical estimation of loosening pressure on tunnels in soft rocks. Tunn. Undergr. Sp. Tech. 16, 99-105.

96. Kaiser P.K., 1980. Effect of stress history on the deformation behaviour of underground openings. Proc. 13th Canadian Rock Mech. Symp. Underground Rock Engineering, The Canadian Institute of Min. and Metallurgy, Montreal, Canada, 133-140.

97. Kaiser P.K., 1981. A new concept to evaluate tunnel performance - influence of excavation procedure. Rock Mech. from Research to Application, Proc. 22nd US Sym on Rock Mech, Massachusetts Institute of Technology, Cambridge, 264-271.

98. Khushlani M., 2013. Run of River Project in Bhutan: Tala Hydroelectric Project. Retrieved from www.unouniverse.com/pages/water/Dams/Tala_Project.htm.

99. Kimura F., Okabayashi N., Kawamoto T., 1987. Tunnelling through squeezing rock in two large fault zones of the Enasan Tunnel II, Rock Mech. Rock Engng., 20 (3), 151-166.

100. Kobayashi S., Tamura T., Nishimura N., 1981. Stress and deformations around tunnel face in soft rock. Proc. Int. Symp. Weak Rock, Tokyo, 21-24 Sept., 813-818.

101. Kontogianni V., Psimoulis P., Stiros S., 2006. What is the contribution of time-dependent deformation in tunnel convergence? Engg Geo. 82, 264-267.

102. Kovari K., 1982. Rock mass behaviour and its mathematical modelling. Numerical Methods in Geomechanics, NATO Advanced Study Institutes Series, 92, 145-163.

103. Kovari K., 1998. Tunnelling in squeezing rock. Tunnel, 5, May, 12-31.

104. Kovari K., Staus J., 1996. Basic considerations on tunnelling in squeezing ground. Rock Mech. Rock Engng. 29 (4), 203-210.

105. Kulatilake P.S.H.W., Wang S., Stephansson O., 1993. Effect of finite size joints on the deformability of jointed rock in three dimensions. Int. J. Rock Mech. Min. Sci. & Geomech. Abstr. 30 (5), 479-501.

106. Kumar N., 2002. Rock mass characterization and evaluation of supports for tunnels in Himalaya. PhD Thesis, Dept Civil Engg, IIT Roorkee, India, 295p.

107. Labasse H., 1949. Les pressions de terrians autour des puits. Revue Universelle des Mine. 92 e Annee, 5, 78-88.

108. Ladanyi B., Archambalut G., 1972. Evaluation of shear strength of jointed rock mass. Proc. 24th Int. Geol. Cong., Montreal, Section 13D, 249-270.

109. Lama R.D., 1974. The uniaxial compressive strength of jointed rock. Prof L Muller Festschrift, Inst Soil Mech & Rock Mech, Univ Karlsruhe, 67-77.

110. Lee C.F., Lo K.Y., 1976. Analysis of rock squeeze problem by the recoverable strain energy. Proc. 3rd Symp. Engineering Application of Solid Mechanics, Toronto, Canada.

111. Lee Youn-Kyou, Pietruszczak S., 2008. A new numerical procedure for elasto-plastic analysis of a circular opening excavated in a strain-softening rock mass. Tunnelling and Underground Space Technology 23, 588-599.

112. Lian-Chong L., Chun-An T., Tian-Hui M.A., Xing-Dong Z., 2008. Research on the closure and creep mechanism of circular tunnels. Journal of Coal science & Engineering 14 (2), 195-199.

113. Londe P., 1988. Discussion on paper 20431 by R. Ucar entitled "Determination of shear failure envelope in rock masses. J. Geotech. Engng. Div., ASCE 114 (3), 374-376.

114. Lu J., 1986. Elasto-plastic analysis of rock masses surrounding circular opening considering strain hardening. Proc. Int. Symp. Large Rock Caverns, Helsinki, August 2, 1329-1335.

115. Lunardi P., 1980. Application de la mecanique des roches aux tunnels autoroutiers. Example des tunnels du Frejus (cote Italie) et du Gran Sasso. Revue Franc. Geotechn. 12, 5-43.

116. Malan D.F., Basson F.R.P., 1998. Ultra-deep mining: The increased potential for squeezing conditions. The Journal of South African Institute of Mining and Metallurgy, Nov-Dec., 353-363.

117. Malhotra V.K., Tyagi G.D., Sharma K.S., 1982. NATM for Tunnel Boring at Loktak H. E. Project, Proc. Symp. Tunnelling, 52nd Session of the Central Board of Irrigation & Power, New Delhi, India, June, 35-58.

118. Mclamore R., Gray K.E., 1967. The mechanical behaviour of anisotropic sedimentary rocks. Trans. Am. Soc. Mech. Engrs. Ser. B 89: 62-79.

119. Mehrotra V.K., 1992. Estimation of engineering parameters of rock mass. PhD Thesis, Dept Civil Engg, University of Roorkee, India, 267p.

120. Mohanty A.K., Mohanty S., 1996. Structural patterns in the Sausar Group around Mansar, Nagpur district, Maharashtra. Journal of the Geological Society of India, 48, 559-565.

121. Muller L., 1978. Removing misconceptions on the New Austrian Tunnelling Method. Tunnels and Tunnelling, World news, 14th October, 29-32.

122. Myer L.R., Brekke T.L., Dare C.T., Dill R.B., Korbin G.E., 1981. An investigation of stand-up time of tunnels in squeezing ground. Proc. Conf. Rapid Excavation and Tunnelling (RETC): Tunnelling Excavation and Productivity (TEAM), 2, 1415-1433.

123. Nepal Electricity Authority (NEA), 2002. Project completion report. Geology and Geotechnical. Kaligandaki 'A" hydroelectric project, Syanga, Nepal, Vol. IV-A and V-C.

124. Norwegian Tunnelling Society (NFF), 2000. The world's longest road tunnel. Retrieved from the website: http://www.tunnel.no/article.php?id=64.

125. Oda M., 1982. Fabric tensor for discontinuous geological materials. Soil Mech. Foundat. 22, 96-108.

126. Oreste P., 2009. The Convergence-confinement Method: Roles and limits in modern geomechanical tunnel design. American Journal of Applied Sciences 6 (4), 757-771.

127. Oreste P.P., Peila D., 1996. Radial passive rock bolting in tunnelling design with a new convergence-confinement model. Int. J. Rock Mech. Min. Sci. & Geomech. Abstr. 33 (5), 443-454.

128. Palmstrom A., 1995. RMi-a rock mass characterization system for rock engineering purposes. Ph D Thesis, Oslo University, Norway, 400p.

129. Pan Y.W., Dong J.J., 1991a. Time dependent tunnel convergence-I: Formulation of the model. Int. J. Rock Mech. Min. Sci. & Geomech. Abstr. 28(6), 469-475.

130. Pan Y.W., Dong J.J., 1991b. Time dependent tunnel convergence-II: Formulation of the model. Int. J. Rock Mech. Min. Sci. & Geomech. Abstr. 28 (6), 477-488.

131. Panet M., 1975. Stability analysis of tunnel driven in a rock mass taking into account the post-failure behaviour. Rock Mechanics 8 (4), 209-223.

132. Panet M., 1996. Two case histories of tunnels through squeezing rocks. Rock Mech Rock Engng. 29 (3), 155-164.

133. Panet M., Guenot A., 1982. Analysis of convergence behind the face of a tunnel. Tunnelling, 82, The Institution of Mining and Metallurgy, 197-204.

134. Panthi K.K., 2011. Effectiveness of Post-injection Grouting in Controlling Leakage: A Case Study. Hydro Nepal: Journal of water, Energy and Environment 8, 14-18.

135. Panthi K.K., Nilsen B., 2007. Uncertainty analysis of tunnel squeezing for two tunnel cases from Nepal Himalaya. Int. J. Rock Mech. Min. Sci. 44, 67-76.

136. Park K.H., Kim Y.J., 2006. Analytical solution for a circular opening in an elastic-brittle-plastic rock. Int. J. Rock Mech. Min. Sci. 43, 616-622.

137. Park K.H., Tontavanich B., Lee J.G., 2008. A simple procedure for ground response curve of circular tunnel in elastic-strain softening rock masses. Tunnelling and Underground Space Technology 23, 151-159.

138. Rabcewicz L.V., 1964. The New Austrian Tunnelling method. Water Power, London, 16 (11-12) & 17 (1), 453-457.

139. Ramamurthy T., 1993. Strength and modulus response of anisotropic rocks. In: Comprehensive Rock Engg, Pergamon Press, UK 1, 313-329.

140. Ramamurthy T., 2004. A geo-engineering classification of rocks and rock masses. Int J Rock Mech Min Sci. 41, 89-101.

141. Ramamurthy T., Arora V.K., 1994. Strength prediction for jointed rocks in confined and unconfined states, Int. J. Rock. Mech. Min. Sci. 31 (1), 9-22.

142. Rao K.S., 1984. Strength and deformation behaviour of sandstones. PhD Thesis, IIT Delhi, India.

143. Rose D., 1982. Revising Terzaghi's tunnel rock load coefficients. Proc. 23rd U.S. Sym. Rock Mech., AIME, New York, 953-960.

144. Roy N., 1993. Engineering behaviour of rock masses through study of jointed models. PhD Thesis, IIT Delhi, India.

145. Russo G., 2008. A simplified rational approach for the preliminary assessment of the excavation behaviour in rock tunneling, Tunnels et Ouvrages Souterrains N.207, May-June 2008, Downloaded in July 2011, source: http://www.webalice.it/ giordandue/.

146. Russo G., 2009. A new rational method for calculating the GSI, Tunnel. Underground Space Tech., 24, 103-111.

147. Russo G., Grasso P., 2007. On the classification of rock mass excavation behaviour in tunnelling. Proc. 11th Congress of International Society of Rock Mechanics ISRM, Lisbon.

148. Saari K., 1982. Analysis of plastic deformation (squeezing) of layers intersecting tunnels and shafts in rock. Ph.D. Thesis, University of California, Berkeley, 183p.

149. Saini G.S., Dube A.K., 1990. Tunnelling under squeezing conditions: a case history-Maneri Bhali stage-II project, India. Proc. Int. Conf. Tunnel Construction'90, 3-4 April, IMM, London, 119-124.

150. Saini G.S., Dube, A.K., 1989. Severe tunnelling problem in young Himalayan rocks for deep underground openings. In: Rock at Great Depth, Maury & Fourmaintraux, eds., Balkema, Rotterdam, ISBN 9061919754, 677-685.

151. Sakurai S., 1997. Lessons learned from field measurements in tunneling. Tunnelling and Underground Space Technology 12 (4), 453-460.

152. Sari D., Pasamehmetoglu A.G., 2004. Proposed support design, Kaletepe tunnel, Turkey. Engg. Geo. 72 (3), 201-216.

153. Schubert W., 1996. Dealing with squeezing conditions in Alpine tunnels. Rock Mech. Rock Engng. 29 (3), 145-153.

154. Scussel D., Chandra S., 2013. A new approach to obtain tunnel support pressure for polyaxial state of stress. Tunnelling and Underground Space Technology 36, 80-88.

155. Scussel D., Chandra S., 2014. New approach to the design of tunnels in squeezing ground. Int. J. Geomech. 14 (1), 110–117.

156. Selmer-Olsen R., Broch E., 1977. General design procedure for underground openings in Norway. Proc. Int. Symp. ROCKSTORE - 77, Stockholm, 219-226.

157. Shalabi F.I., 2005. FE analysis of time-dependent behaviour of tunnelling in squeezing ground using two different creep models. Tunnelling and Underground Space Technology 20 (3), 271-279.

158. Sharan S.K., 2003. Elastic-brittle-plastic analysis of circular openings in Hoek-Brown media. Int. J. Rock Mech. Min. Sci. 40, 817-824.

159. Sharma K.G., Ramamurthy T., Ailawadi O.P., 1985a. Elasto-palstic finite element analysis of rock slopes. Proc. 5th Int. Conf. Numerical Methods in Geomechanics, Nagoya, Japan, 981-987.

160. Sharma K.G., Sharma M.K., 1986. Finite element analysis of tunnels in anisotropic rock medium. Indian Geotechnical Journal 16 (3), 225-243.

161. Sharma K.G., Vardarajan A., Srivastava R.K., 1985b. Elasto-viscoplastic finite element analyses of tunnels. Proc. 5th Int. Conf. Numerical Methods in Geomechanics, Nagoya, Japan, 1141-1148 BN-90-6191-582-1.

162. Sharma V.M., 1985. Prediction of closure and rock loads for tunnels in squeezing grounds. PhD Thesis, Indian Institute of Technology, Delhi, India, 254p.

163. Shome S.K., Andotra B.S., Jain M.S., 1973. Review of failure patterns in the stage II tunnels of Yamuna hydroelectric scheme, Dehradun District. Proc. Symp. Rock Mech. and Tunnelling Problems, Kurukshetra University 1, 70-79.

164. Shrestha G.L., 2005. Stress Induced Problems in Himalayan Tunnels with Special Reference to Squeezing. Ph. D. Thesis, Deptt. of Geology and Mineral Resources, Faculty of Engineering Science and Technology, Norwegian University of Science and Technology (NTNU), Trondheim, Norway, 195P.

165. Singh B., Goel R.K., 2006. Tunnelling in weak rocks. Ed: John, Elsevier Ltd, The Boulevard, Langford, Kidlington, Oxford (UK).

166. Singh B., Goel R.K., 2011. Engineering Rock Mass Classifications: Tunnelling, Foundations and Landslides, BH Elsevier, USA, p.365.

167. Singh B., Goel R.K., Jethwa J.L., Dube A.K., 1997. Support pressure assessment in arched underground openings through poor rock masses. Engineering Geology 48, 59-81.

168. Singh B., Jethwa J.L., Dube A.K., 1995. A classification system for support pressure in tunnels and caverns. J. Rock Mech. & Tunn. Tech., ISRMTT, India 1 (1), 13-24.

169. Singh B., Jethwa J.L., Dube A.K., Singh B., 1992. Correlation between observed support pressure and rock mass quality. Tunn. Undergr. Sp. Tech. 7 (1), 59-74.

170. Singh M., 1997. Engineering behaviour of jointed model materials. Ph.D. Thesis, Indian Institute of Technology, New Delhi, India, 334p.

171. Singh M., Rao K.S., 2005. Empirical methods to estimate the strength of jointed rock masses. Engng. Geol. 77, 127-137.

172. Singh M., Rao K.S., Ramamurthy T., 2002. Strength and deformational behaviour of a jointed rock mass. Rock Mech. Rock Engng. 35 (1), 45-64.

173. Singh M., Rao K.S., Ramamurthy T., 2004. Engineering behaviour of jointed rock mass. Indian Geotechnical Journal 34 (2), 2004.

174. Singh M., Singh B., Choudhari J., 2007. Critical strain and squeezing of rock mass in tunnels. Tunn. Undergr. Sp. Tech. 22 (3), 343-350.

175. Singh T.N., Singh V.K., 1999. Effect of confined and unconfined stress on jointed rocks. Indian Journal of Engineering & Materials Sciences 6, 198-205.

176. Sinha R.K., Jawed M., Sengupta S., 2013. Influence of anisotropic stress conditions on design of development workings in bord and pillar mining. ISRM (India) Journal 2 (1), 16-24.

177. Sitharam T.G., Latha G.M., 2002. Simulation of excavations in jointed rock masses using a practical equivalent continuum approach. Int. J. Rock Mech. Min. sci. 39, 515-525.

178. Sitharam T.G., Maji V.B., Verma A.K., 2005. Equilibrium continuum analysis of jointed rock mass. Proc. 40th US Symp. Rock Mech. (USRMS): Rock Mechanics for Energy, Mineral and Infrastructure Development in the Northern regions, Anchorage, Alaska, June 25-29.

179. Sitharam T.G., Sridevi J., Shimizu N., 2001. Practical equivalent continuum characterization of jointed rock masses. Int. J. Rock Mech. Min. sci. 38, 437-448.

180. Sridevi J., Sitharam T.G., 2000. Analysis of strength and moduli of jointed rocks. Geotech. Geol. Engg. 18, 3-21.

181. Sripad S.K., Raju G.D., Singh R., Khazanchi R.N., 2007. Instrumentation of underground excavations at Tala hydroelectric project in Bhutan. Proc. Int. Workshop on Experiences and Construction of Tala Hydroelectric Project Bhutan, Rajbal Singh and A.K. Sthapak, eds., 14-15 June, New Delhi, India 269-282.

182. Steiner W., 1996. Tunnelling in squeezing rocks: case histories. Rok Mech. Rock Engng. 29 (4), 211-246.

183. Sterpi D., Gioda G., 2009. Visco-plastic behaviour around advancing tunnels in squeezing rock. Rock Mech. Rock Engng. 42, 319-339.

184. Stille H., Holmberg M., Nord G., 1989. Support of weak rock with grouted bolts and Shotcrete, Int. J. of Rock Mech. & Min. Sci. 26 (1), 99-113.

185. Sulem J., Panet M., Guenot A., 1987a. Closure analysis in deep tunnels. Int. J. Rock Mech. Min. Sci. Geomech. Abst. 24 (3), 145-154.

186. Sulem J., Panet M., Guenot A., 1987b. Closure analysis in deep tunnels. Int. J. Rock Mech. Min. Sci. & Geomech. Abst. 24 (3), 155-164.

187. Sunuwar S.C., 2007. Rock squeezing problem in tunnels of Nepal and its prediction. Journal of Nepal Geological Society, 36.

188. Sunuwar S.C., Shrestha G., O'Neill B., 2000. Rock squeezing and rock bursts problems in the Himalayas. Journal of Nepal Geological Society 22: 227-236.

189. Takano A., Kitahara S., Kurosawa H., Ueno M., 1981. The tunnelling by NATM in heavy squeezing pressure zone and the study on the ground arch around tunnel as to construction records of Nabetachiyama tunnel. Proc. Int. Symp. Weak Rock, Tokyo, 21-24 Sept., 939-944.

190. Terzaghi K., 1946. Rock defects and load on tunnel supports. In: Introduction to Rock Tunnelling with Steel Supports. R.V. Proctor and T.L. White, eds.,The Commercial Shearing and Stamping Co., Youngstown, Ohio, USA, 17-99.

191. The Engineer, 2006. Laerdal Tunnel. Retrieved from a website: http://www.engineering.com/ Library/ArticlesPage/tabid/85/ArticleID/60/Laerdal-Tunnel.aspx.

192. Tiwari R.P., Rao K.S., 2004. Physical modelling of a rock mass under a true triaxial stress state. Int. J. Rock Mech. Min. Sci. 41 (SUPPL 1), 2-14.

193. Tripathy P.K., Kapadia H., Kumar S., 2000. Use of alkali free accelerators in Tala hydroelectric project. Proc. Tunnelling Asia '2000', S.P. Kaushish, T. Ramamurthy, eds., 26-29 Sep., New Delhi, India, 292-295.

194. Tutorial Manual, 2011. Tunnel lining design. Phase^2 v.7.0, 24, 31p.

195. Unal E., 1983. Design guidelines and roof control standards for coal mine roofs. Ph.D. Thesis, The Pennsylvania State University, Also In: Rock Mechanics in mining and Tunnelling by Z.T. Bieniawski, ed., A.A. Balkema Publishers, 113p.

196. Varshney R.S., 1988. Tunnelling in squeezing rocks. Proc. Int. Symp. Tunnelling for water resources and power project. Jan 19-23. New Delhi, India 34-47.

197. Verma A.K., Singh T.N., 2010. Modelling of a jointed rock mass under triaxial condition. International Journal of Arabian Geosciences 14 (1), 181-192.

198. Verma B.K., Tyagi V.K., 1979. Scheme of diversion arrangements including structural design of tunnels and portals of Tehri dam project. Proc. Workshop Tehri Dam Project, U.O.R., Roorkee, India.

199. Verman M.K., 1993. Rock mass –tunnel support interaction analysis. PhD Thesis, Dept Civil Engg, University of Roorkee, India, 258p.

200. Vibert C., Gupta S.C., Felix Y., Binquet J., Robert F., 2005. Dul Hasti hydroelectric project (India): Experience gained from back analysis of the excavation of the headrace tunnel. Proc. of Geoloine 2005, 23-25 May, Lyon, France.

201. Viladkar M.N., Verman M., Singh B., Jethwa J.L., 2008a. Rock mass-tunnel support interaction analysis: Part I- Ground response curves. J. Rock Mech. Tun. Tech. 14 (2), 103-125.

202. Viladkar M.N., Verman M., Singh B., Jethwa J.L., 2008b. Rock mass –tunnel support interaction analysis: Part II-Support reaction curves. J. Rock Mech. Tun. Tech. 14 (2), 127-145.

203. Vutukuri V.S., Hossaini S.M.F., Foroughi M.A., 1995. A study of the effect of roughness and inclination of weakness planes on the strength properties of rock and coal, Proc. Mechanics of Jointed and Faulted Rock, Rossmonith, ed., 151-155.

204. Walker P.F., 1971. The shearing behaviour of block jointed rock model. Ph.D. Thesis, Queens Univ, Belfast.

205. Wang Y., 1996. Ground response of circular tunnel in poorly consolidated rock. Journal of Geotechnical Engineering 122 (9), 703-708.

206. Ward W.H., (1978). Ground supports for tunnels in weak rocks. Geo-technique 28 (2), 133-171.

207. Ward W.H., Tedd P., Berry N.S.M., 1983. The Kielder experimental tunnel: final results. Geotechnique 33 (3), 275-291.

208. Whittaker B.N., Hassani F.P., Bonsall C.J., White M.J., 1983. Investigations into the development of rock yield zones around mining tunnels. Proc. Int. Sym. on Field Measurements in Geomechanics, Zurich, September, 2, 1257-1266.

209. Wickham G.E., Tiedmann H.R. and Skinner E.H., 1972. Support determinations based on geologic predictions. Proc. 1st North American rapid excavation and tunnelling conference, Chicago, Am. Inst. Min. Met. and Pet. Engr. Inc., New York, 1, 43-64.

210. Wickham G.E., Tiedmann H.R., Skinner E.H., 1974. Ground support prediction model-RSR concept. Proc. North American rapid excavation and tunnelling conference, San Francisco, California, 1, 691-708.

211. Winkel B.V., Gerstle K.H., Ko H.Y., 1972. Analysis of time-dependent deformations of openings in salt media. Int. J. Rock Mech. Min. Sci. 9, 249-260.

212. Wood A.M., 1972. Tunnels for roads and motorways. J. Engg. Geol. 5, 117-126.

213. Yaji R.K., 1984. Shear strength and deformation response of jointed rocks. Ph.D. Thesis, IIT Delhi, India.

214. Zhu Weishen, Shcai Li, Shuchen Li, Weizhong C., Lee C.F., 2003. Systematic numerical simulation of rock tunnel stability considering different rock conditions and construction effects. Tunnelling and Underground Space Technology 18, 531-536.

215. Zurick D., 2006. The natural environment. In: Illustrated Atlas of the Himalaya. The university press of Kentucky, USA, 209 p.

ANNEXURE-1

GEOTECHNICAL MAPPING OF CHENANI-NASHRI TUNNEL SECTIONS (SQUEEZING GROUND BEHAVIOUR)

Chenani-Nashri Escape Tunnel Face Mapping Sheet Date/Time: 25-11-2011/ 12:00 am			
Previous Face Chainage	331.5m	Elevation at the front	1230m
Present Face Chainage (ETSP)	334m	Overburden [m]	195m
Total Pull	2.5m	Excavation method	Drill & blast
Unsupported length	2.5m	Excavation approach	NATM
Bolting distance from the face	2.5m	GSI	41

TUNNEL EXCAVATION FACE GEOTECHNICAL DESCRIPTION

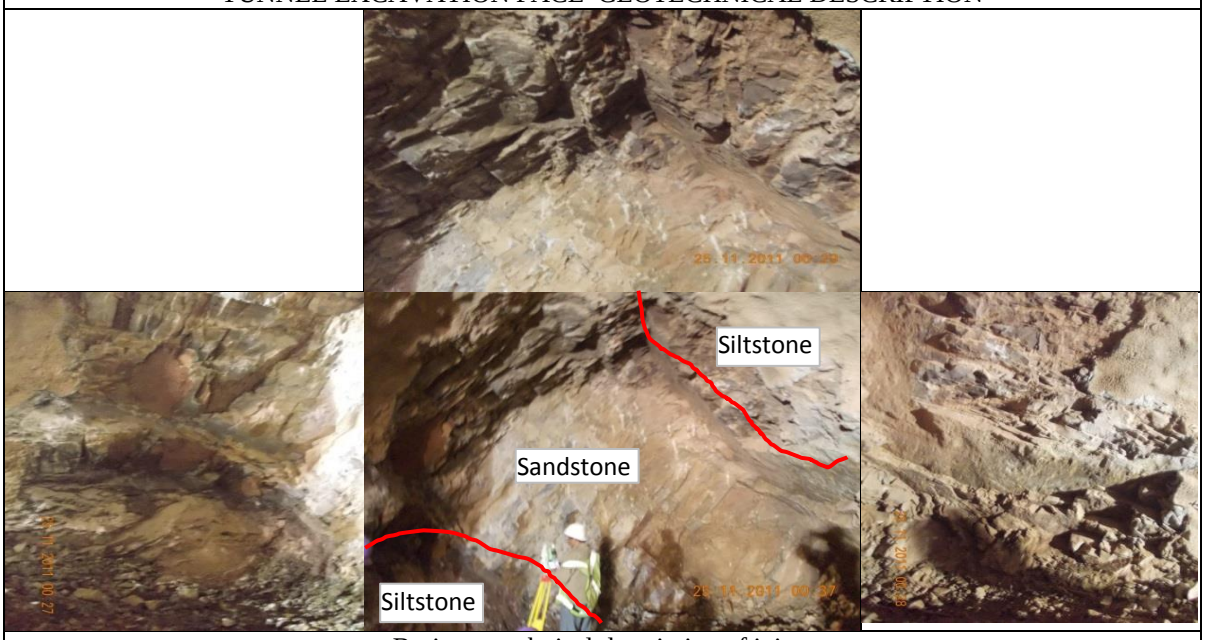

Basic geotechnical description of joints

Joint	Dip -dip/dir	Spacing	Persistence (m)	roughness	Conditions	Aperture	Filling	Seepage
Bedding joint	$40^o/90^o$	1m	1-3,3-10	Rough-Slightly Rough	Fresh to slightly wthd.	1-2mm	Clay filling	Dry
JS2	$60^o/250\text{-}260^o$	10cm	do	do	do	1-5	Clay filling	do
JS3	$65\text{-}75^o/215^o$	15cm	3-5m	do	do	do	clay filling	do
UCS	40MPa	J_v=21	RQD = 115-3.3J_v = 45.7					

Classification parameters		Value	Rating	Q Parameter	Rating	
Strength of intact rock		40MPa	7	RQD (%)	45	RQD/J_n
RQD		45%	8	J_n	12	3.75
Spacing of discontinuities		60mm-2m	10	J_r	0.5	J_r/J_a
Condition of discontinuities	Persistence	1-3m, 3-10m	3	J_a	3	0.17
	Opening	1-5mm (avg)	3	J_w	1	J_w/SRF
	Roughness	Rough to Slightly rough	4	SRF	5	0.2
	Infilling	Soft Clay	2			
		Slightly weathered	5			
Ground water		Dry to slightly damp	14			
Adjust for Joint Orient.		Fair	-5			
		RMR	51	Q-value	0.13	

Chenani-Nashri Escape Tunnel Face Mapping Sheet Date/Time: 05-12-2011/ 11:15 am			
Previous Face Chainage	382.5m	Elevation at the front	1230m
Present Face Chainage (ETSP)	385m	Overburden [m]	178m
Total Pull	2.5m	Excavation method	Drill & blast
Unsupported length	2.5m	Excavation approach	NATM
Bolting distance from the face	2.5m	GSI	42

TUNNEL EXCAVATION FACE GEOTECHNICAL DESCRIPTION

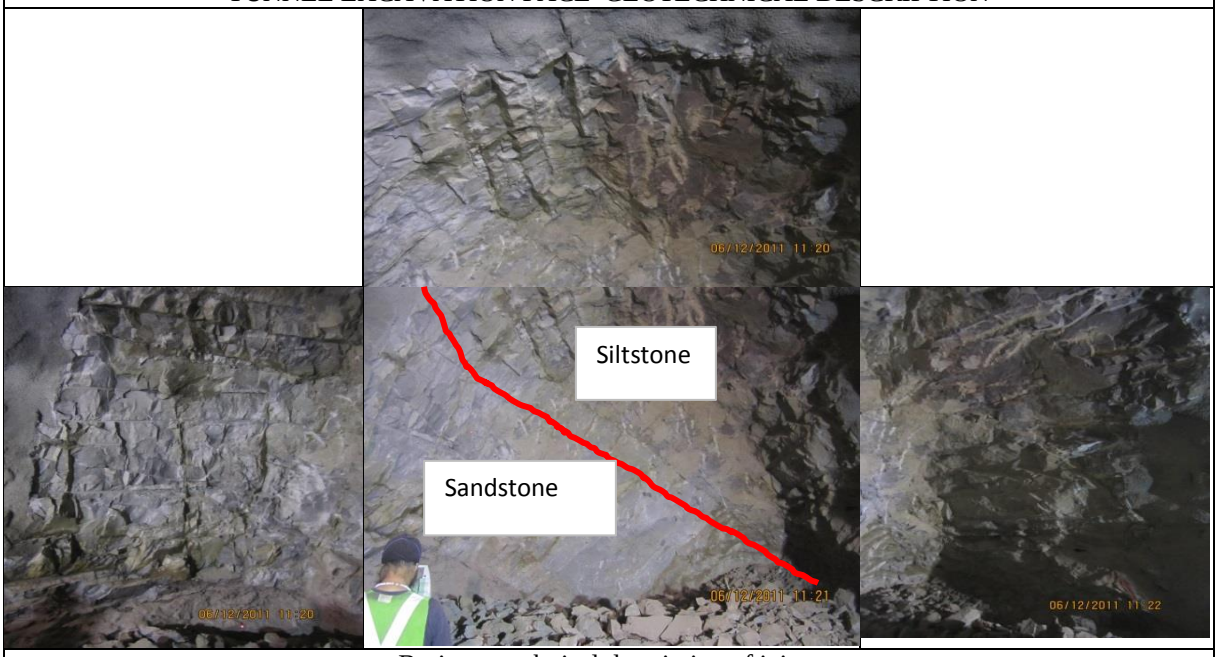

Basic geotechnical description of joints

Joint	Dip -dip/dir	Spacing	Persistence (m)	Roughness	Conditions	Aperture	Filling	Seepage
Bedding joint	$40^o/95^o$	1m	1-3,3-10	R-Slightly Rough	Fresh- Slight weathered	1-2mm	Clay filling	Dry
JS2	$60^o/250\text{-}270^o$	10cm	do	do	do	1-5	Clay filling	do
JS3	$75^o/200^o$	20cm	3-5m	do	do	do	Clay filling	do
UCS	48MPa	Jv=15	RQD = 115-3.3Jv = 65.5					

Classification parameters		Value	Rating	Q Parameter	Rating	
Strength of intact rock		55MPa	7	RQD(%)	65	RQD/J_n
RQD		62%	13	J_n	12	5.42
Spacing of discontinuities		60-1.5m	11	J_r	0.5	J_r/J_a
Condition of discontinuities	Persistence	1-3m, 3-10m	2	J_a	3	0.17
	Opening	0.1-1mm (avg)	4	J_w	1	J_w/SRF
	Roughness	Rough to Slightly Rough	4	SRF	5	0.2
	Infilling	Clay (1-5mm)	2			
		Fresh to Slightly Wthd.	5			
Ground water		Dry	15			
Adjust for Joint Orient.		Fair	-5			
		RMR	58	Q-value	0.18	

Chenani-Nashri Escape Tunnel Face Mapping Sheet Date/Time: 02-01-2012/ 12:00 pm			
Previous Face Chainage	533m	Elevation at the front	1230m
Present Face Chainage (ETSP)	535m	Overburden [m]	238m
Total Pull	2m	Excavation method	Drill & blast
Unsupported length	2m	Excavation approach	NATM
Bolting distance from the face	2m	GSI	44

TUNNEL EXCAVATION FACE GEOTECHNICAL DESCRIPTION

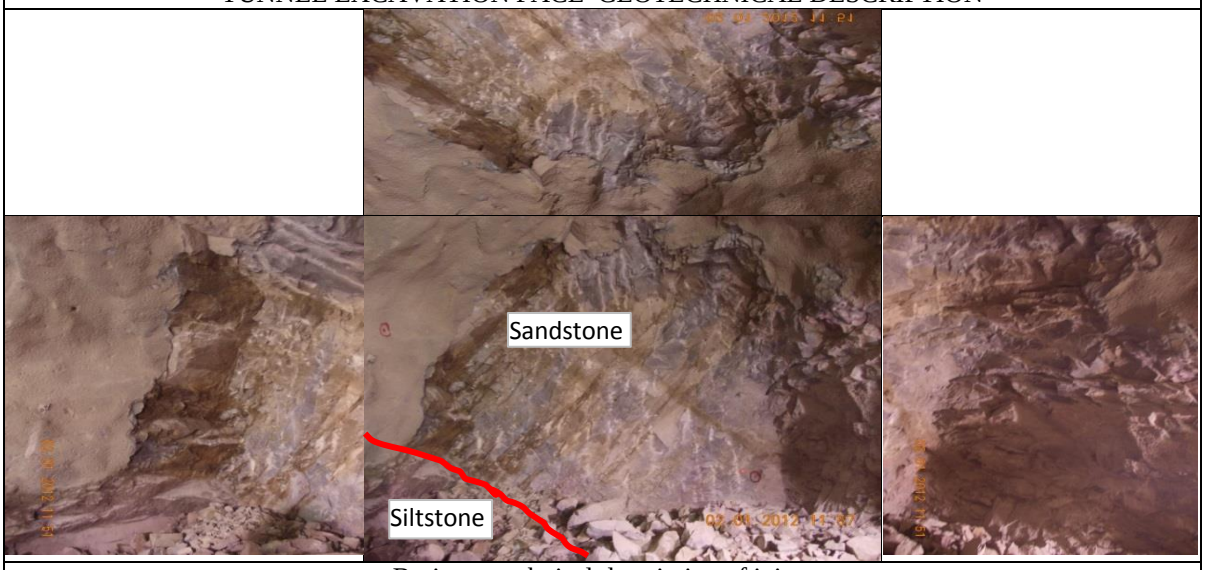

Basic geotechnical description of joints

Joint	Dip -dip/dir	Spacing	Persistence (m)	roughness	Conditions	Aperture	Filling	Seepage
Bedding joint	$35^o/95^o$	1m	1-3,3-10	R-Slightly Rough	Fresh-Slight weathered	1-2mm	Clay filling	Dry
JS2	$60^o/270^o$	10cm	do	do	do	1-5mm	Clay filling	do
JS3	$65^o/200^o$	15cm	3-5m	do	do	do	Clay filling	do
UCS	40MPa	Jv=20	RQD = 115-3.3Jv = 49					

Classification parameters		Value	Rating	Q Parameter	Rating	
Strength of intact rock		40MPa	7	RQD (%)	49	RQD/J_n
RQD		49%	8	J_n	12	4.08
Spacing of discontinuities		60mm-2m	12	J_r	0.7	J_r/J_a
Condition of discontinuities	Persistence	1-3m, 3-10m	2	J_a	3	0.23
	Opening	0.1-1mm (avg)	4	J_w	1	Jw/SRF
	Roughness	Rough to Slightly rough	4	SRF	5	0.2
	Infilling	Clay (1-5mm)	2			
		Fresh to Slightly wthd.	5			
Ground water		Dry	15			
Adjust for Joint Orient.		Fair	-5			
		RMR	54	Q-value	0.19	

Chenani-Nashri Escape Tunnel Face Mapping Sheet Date/Time: 31-01-2012/ 105:30 pm			
Previous Face Chainage	687.5m	Elevation at the front	1230m
Present Face Chainage (ETSP)	690m	Overburden [m]	294m
Total Pull	2.5m	Excavation method	Drill & blast
Unsupported length	2.5m	Excavation approach	NATM
Bolting distance from the face	2m	GSI	43

TUNNEL EXCAVATION FACE GEOTECHNICAL DESCRIPTION

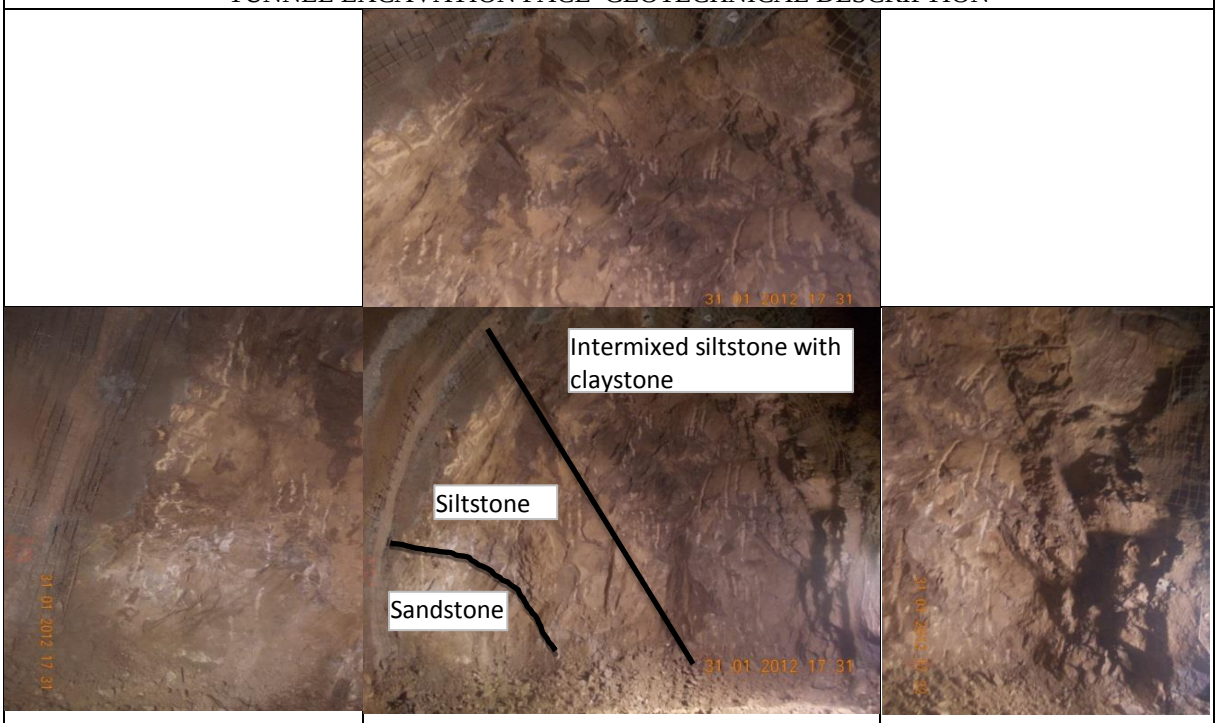

Basic geotechnical description of joints

Joint	Dip -dip/dir	Spacing	Persistence (m)	Roughness	Conditions	Aperture	Filling	Seepage
Bedding joint	$35^o/95^o$	1m	1-3,3-10	Rough-Slight Rough	Fresh-Slightly weathered	1-2mm	Clay filling	Dry
JS2	$65^o/240^o$	10cm	do	do	do	1-5	Clay filling	do
JS3	$65^o/200^o$	15cm	3-5m	do	do	do	Clay filling	do
UCS	40MPa	Jv=20	RQD = 115-3.3Jv = 49					

Classification parameters		Value	Rating	Q Parameter	Rating	
Strength of intact rock		40MPa	7	RQD (%)	49	RQD/J_n
RQD		49%	8	J_n	12	4.08
Spacing of discontinuities		60mm-2m	11	J_r	0.8	J_r/J_a
Condition of discontinuities	Persistence	1-3m, 3-10m	2	J_a	4	0.2
	Opening	0.1-5mm (avg)	3	J_w	1	Jw/SRF
	Roughness	Slightly rough to smooth	2	SRF	5	0.2
	Infilling	Clay (1-5mm)	2			
		Slight to moderate wthd.	4			
Ground water		Dry to damp	12			
Adjust for Joint Orient.		Fair	-5			
		RMR	46	Q-value	0.16	

Chenani-Nashri Escape Tunnel Face Mapping Sheet Date/Time: 02-02-2012/ 02:40pm			
Previous Face Chainage	705.5m	Elevation at the front	1230m
Present Face Chainage (ETSP)	707m	Overburden [m]	315m
Total Pull	1.5m	Excavation method	Drill & blast
Unsupported length	1.5m	Excavation approach	NATM
Bolting distance from the face	1.5m	GSI	48

TUNNEL EXCAVATION FACE GEOTECHNICAL DESCRIPTION

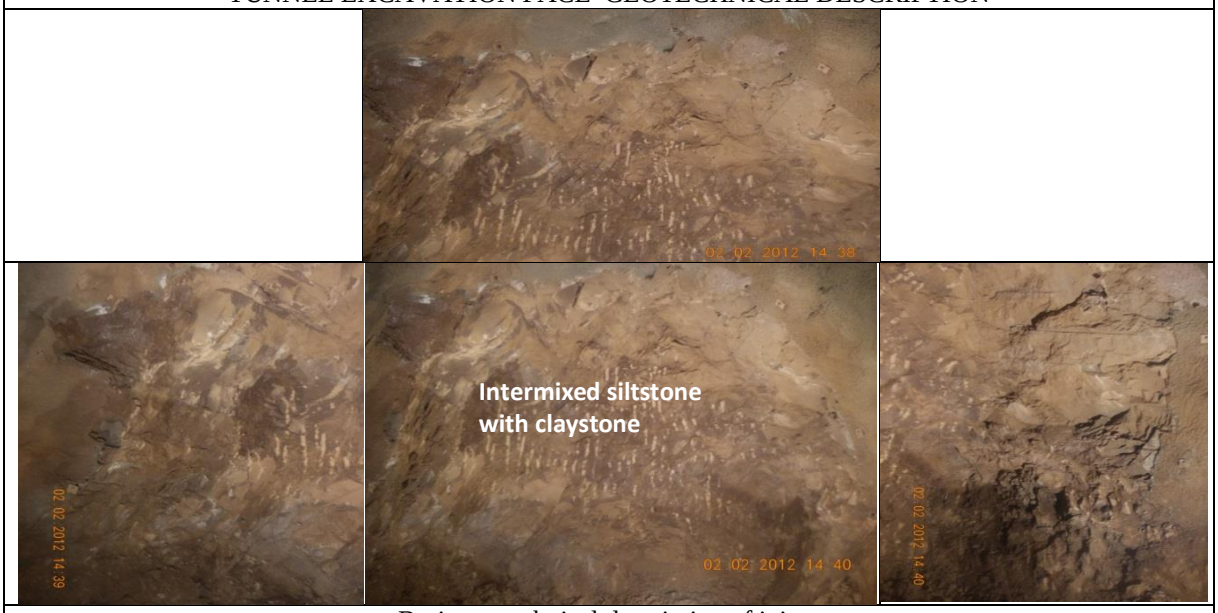

Basic geotechnical description of joints

Joint	Dip -dip/dir	Spacing	Persistence (m)	roughness	Conditions	Aperture	Filling	Seepage
Bedding joint	$35^o/95^o$	35cm	1-3,3-10	Rough-Slight Rough	Fresh-Slightly weathered	0.1-5mm	Clay filling	Dry to damp
JS2	$60^o/250^o$	10cm	do	do	do	do	do	do
JS3	$65^o/200^o$	13cm	3-7	do	do	do	do	do
UCS	40MPa	Jv=22	RQD = 115-3.3Jv = 42					

Classification parameters		Value	Rating	Q Parameter	Rating	
Strength of intact rock		40MPa	4	RQD (%)	42	RQD/J_n
RQD		42%	8	J_n	12	3.5
Spacing of discontinuities		60mm-1.5m	10	J_r	0.5	J_r/J_a
Condition of discontinuities	Persistence	1-3m, 3-7m	3	J_a	3	0.17
	Opening	0.1-5mm (avg)	3	J_w	1	Jw/SRF
	Roughness	Slightly rough to smooth	2	SRF	5	0.2
	Infilling	Clay (>5mm)	0			
		Slight to moderate wthd.	4			
Ground water		Dry to damp	12			
Adjust for Joint Orient.		Fair	-5			
		RMR	41	Q-value	0.12	

Chenani-Nashri Escape Tunnel Face Mapping Sheet Date/Time: 23-02-2012/ 10:30 am			
Previous Face Chainage	797.5m	Elevation at the front	1230m
Present Face Chainage (ETSP)	800m	Overburden [m]	346m
Total Pull	2.5m	Excavation method	Drill & blast
Unsupported length	2.5m	Excavation approach	NATM
Bolting distance from the face	2.5m	GSI	40

TUNNEL EXCAVATION FACE GEOTECHNICAL DESCRIPTION

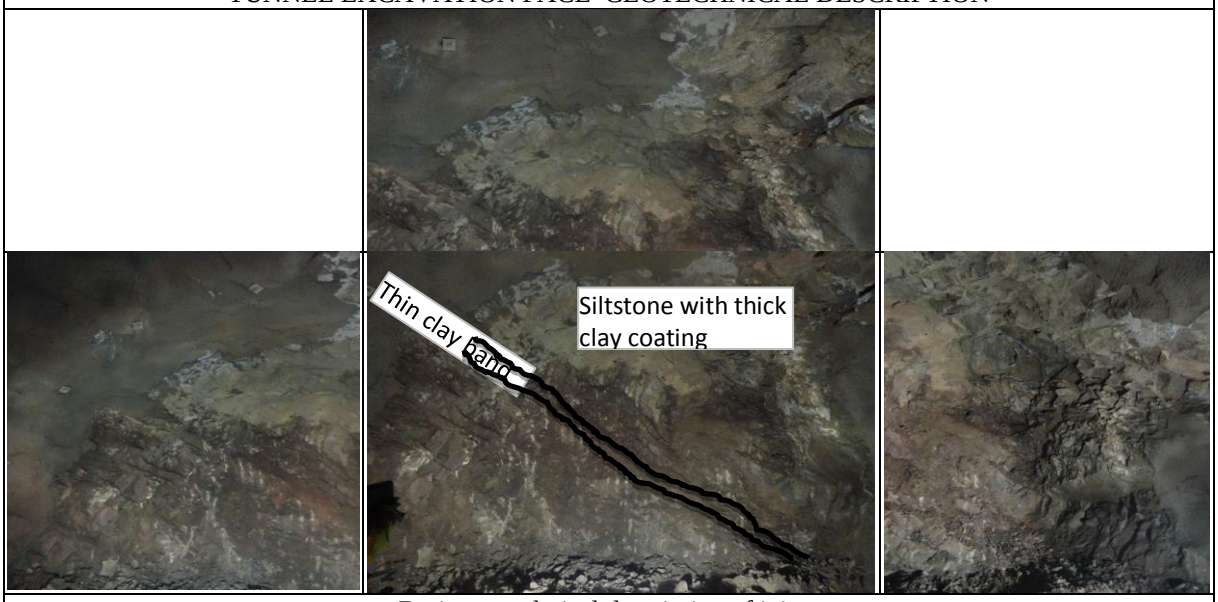

Basic geotechnical description of joints

Joint	Dip -dip/dir	Spacing	Persistence (m)	Roughness	Conditions	Aperture	Filling	Seepage
Bedding joint	$35^o/95^o$	1m	1-3,3-10	Rough-Slightly smooth	Fresh to slightly wthd.	1-2mm	Clay filling	Dry
JS2	$60^o/256\text{-}260^o$	10cm	do	do	do	do	do	do
JS3	$65^o/200^o$	15cm	3-7m	do	do	do	do	do
UCS	40MPa	Jv=20	RQD = 115-3.3Jv = 49					

Classification parameters		Value	Rating	Q Parameter	Rating	
Strength of intact rock		40MPa	4	RQD (%)	49	RQD/J_n
RQD		49%	8	J_n	12	4.08
Spacing of discontinuities		200-600mm	10	J_r	0.8	J_r/J_a
Condition of discontinuities	Persistence	1-3m, 3-10m	3	J_a	4	0.2
	Opening	0.1-1mm (avg)	3	J_w	1	Jw/SRF
	Roughness	Slightly rough to smooth	2	SRF	5	0.2
	Infilling	Silty Clay	2			
		Slightly wthd.	5			
Ground water		Dry	15			
Adjust for Joint Orient.		Fair	-5			
		RMR	47	Q-value	0.16	

Chenani-Nashri Escape Tunnel Face Mapping Sheet Date/Time: 03-03-2012/ 02:20 am			
Previous Face Chainage	846m	Elevation at the front	1230m
Present Face Chainage (ETSP)	850m	Overburden [m]	358m
Total Pull	4m	Excavation method	Drill & blast
Unsupported length	4m	Excavation approach	NATM
Bolting distance from the face	2m	GSI	40

TUNNEL EXCAVATION FACE GEOTECHNICAL DESCRIPTION

Basic geotechnical description of joints

Joint	Dip -dip/dir	Spacing	Persistence (m)	Roughness	Conditions	Aperture	Filling	Seepage
Bedding joint	$35^o/95^o$	18cm	1-3,3-10	Slightly Rough	Slightly weathered	0.1-5mm	Clay filling	Dry
JS2	$65^o/245^o$	90cm	do	do	do	do	Soft clay	do
JS3	$65^o/200^o$	18cm	3-7m	do	do	do	Clay filling	do
UCS	40MPa	Jv=22	RQD = 115-3.3Jv = 42.4					

Classification parameters		Value	Rating	Q Parameter	Rating	
Strength of intact rock		40MPa	4	RQD (%)	42	RQD/J_n
RQD		42%	8	J_n	12	3.5
Spacing of discontinuities		200mm-2m	12	J_r	0.8	J_r/J_a
Condition of discontinuities	Persistence	1-3m, 1-7m	3	J_a	4	0.2
	Opening	0.1-5mm (avg)	3	J_w	1	Jw/SRF
	Roughness	Slightly Rough	3	SRF	10	0.1
	Infilling	Clay	2			
		Slightly weathered	5			
Ground water		Dry	15			
Adjust for Joint Orient.		Fair	-5			
		RMR	50	Q-value	0.07	

Chenani-Nashri Escape Tunnel Face Mapping Sheet Date/Time: 13-04-2012/ 9:30 pm			
Previous Face Chainage	1066.5	Elevation at the front	1230m
Present Face Chainage (ETSP)	1069m	Overburden [m]	426.5m
Total Pull	2.5m	Excavation method	Drill & blast
Unsupported length	2.5m	Excavation approach	NATM
Bolting distance from the face	2.5m	GSI	45

TUNNEL EXCAVATION FACE GEOTECHNICAL DESCRIPTION

Basic geotechnical description of joints

Joint	Dip -dip/dir	Spacing	Persistence (m)	Roughness	Conditions	Aperture	Filling	Seepage
Bedding joint	35^o/95-110^o	15cm	1-3,3-8	Slightly rough	Slightly weathered	0.1-5mm	Clay filling	Dry to damp
JS2	60^o/270^o	12cm	do	do	do	1-5	Soft clay	do
JS3	65^o/200^o	20cm	3-7m	do	do	do	Clay filling	do
UCS	40MPa	Jv=21	RQD = 115-3.3Jv = 45.7					

Classification parameters		Value	Rating	Q Parameter	Rating	
Strength of intact rock		40MPa	4	RQD (%)	45	RQD/J_n
RQD		45%	8	J_n	12	3.75
Spacing of discontinuities		120-350mm	10	J_r	0.9	J_r/J_a
Condition of discontinuities	Persistence	1-3m, 3-8m	2	J_a	4	0.225
	Opening	0.1-5mm (avg)	3	J_w	1	Jw/SRF
	Roughness	Rough to Slightly rough	4	SRF	5	0.2
	Infilling	Clay	2			
		Slightly weathered	5			
Ground water		Dry to damp	12			
Adjust for Joint Orient.		Fair	-5			
		RMR	45	Q-value	0.17	

Chenani-Nashri Escape Tunnel Face Mapping Sheet Date/Time: 21-04-2012/ 049:45 am			
Previous Face Chainage	1120.5	Elevation at the front	1230m
Present Face Chainage (ETSP)	1122m	Overburden [m]	458m
Total Pull	1.5m	Excavation method	Drill & blast
Unsupported length	1.5m	Excavation approach	NATM
Bolting distance from the face	1.5m	GSI	50

TUNNEL EXCAVATION FACE GEOTECHNICAL DESCRIPTION

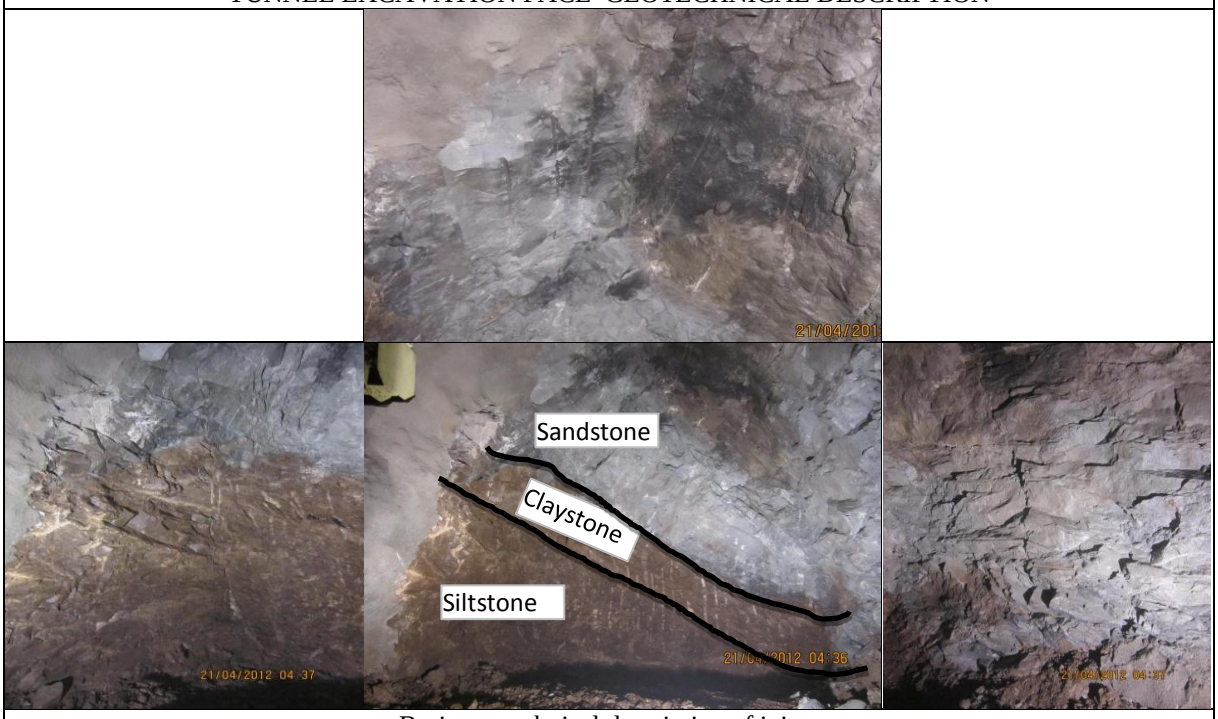

Basic geotechnical description of joints

Joint	Dip -dip/dir	Spacing	Persistence (m)	Roughness	Conditions	Aperture	Filling	Seepage
Bedding joint	35^o/95-110^o	20cm	1-3,3-8	Slightly rough	Slightly weathered	0.1-5mm	Clay filling	Dry to damp
JS2	65^o/270^o	15cm	do	do	do	do	Soft clay	do
JS3	65^o/250-255^o	10cm	3-7m	do	do	do	Clay filling	do
UCS	50MPa	Jv=23	RQD = 115-3.3Jv = 39.1					

Classification parameters		Value	Rating	Q Parameter	Rating	
Strength of intact rock		50MPa	4	RQD (%)	39	RQD/J_n
RQD		39%	8	J_n	12	3.25
Spacing of discontinuities		600mm-2m	11	J_r	0.8	J_r/J_a
Condition of discontinuities	Persistence	1-3m, 3-8m	2	J_a	4	0.2
	Opening	0.1-5mm (avg)	3	J_w	1	Jw/SRF
	Roughness	Slightly rough	3	SRF	10	0.1
	Infilling	Clay	2			
		Slightly weathered	5			
Ground water		Dry to damp	13			
Adjust for Joint Orient.		Fair	-5			
		RMR	46	Q-value	0.07	

Chenani-Nashri Escape Tunnel Face Mapping Sheet Date/Time: 19-06-2012/ 3:30 pm			
Previous Face Chainage	1381.5m	Elevation at the front	1243.7m
Present Face Chainage (ETSP)	1384m	Overburden [m]	495m
Total Pull	2.5m	Excavation method	Drill & blast
Unsupported length	2.5m	Excavation approach	NATM
Bolting distance from the face	2.5m	GSI	45

TUNNEL EXCAVATION FACE GEOTECHNICAL DESCRIPTION

Basic geotechnical description of joints

Joint	Dip -dip/dir	Spacing	Persistence (m)	Roughness	Conditions	Aperture	Filling	Seepage
Bedding joint	35^o/90-110^o	20-60cm	1-3	Slightly Rough	Slightly weathered	0.1-1mm	Silty clay	Dry
JS2	60^o/253^o	10cm	3-10	do	do	do	Silty clay	do
JS3	65^o/210^o	60cm	3-7	do	do	do	Silty clay	do
UCS	40MPa	Jv=21	RQD = 115-3.3Jv = 45.7					

Classification parameters		Value	Rating	Q Parameter	Rating	
Strength of intact rock		40MPa	4	RQD (%)	45	RQD/J_n
RQD		45%	8	J_n	12	3.76
Spacing of discontinuities		100mm-600mm	9	J_r	0.5	J_r/J_a
Condition of discontinuities	Persistence	1-3m	3	J_a	3	0.17
	Opening	1-3mm	3	J_w	1	Jw/SRF
	Roughness	Slightly rough to smooth	3	SRF	5	0.2
	Infilling	Silty clay	2			
		Fresh- Slightly weathered	5			
Ground water		Dry to damp	15			
Adjust for Joint Orient.		Fair /Ufavo	-7			
		RMR	45	Q-value	0.13	

Chenani-Nashri Escape Tunnel Face Mapping Sheet Date/Time: 04-07-2012/ 7:00 am			
Previous Face Chainage	1511.5	Elevation at the front	1230m
Present Face Chainage (ETSP)	1514m	Overburden [m]	493m
Total Pull	2.5m	Excavation method	Drill & blast
Unsupported length	2.5m	Excavation approach	NATM
Bolting distance from the face	2.5m	GSI	40

TUNNEL EXCAVATION FACE GEOTECHNICAL DESCRIPTION

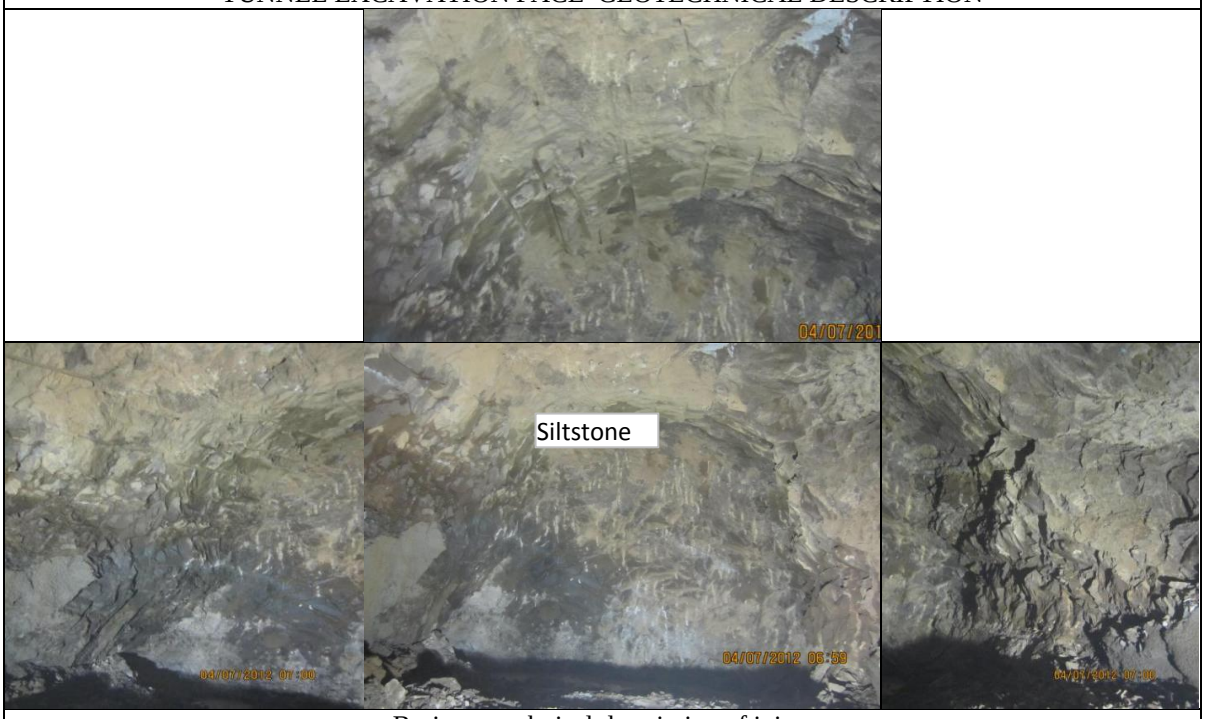

Basic geotechnical description of joints

Joint	Dip -dip/dir	Spacing	Persistence (m)	Roughness	Conditions	Aperture	Filling	Seepage
Bedding joint	35/95-110	15cm	1-3,3-8	Slightly rough	Slightly weathered	0.1-1mm	Clay filling	Dry
JS2	$60^o/255^o$	10cm	do	do	do	do	Clay filling	do
JS3	$65^o/200^o$	25cm	3-7m	do	do	do	Clay filling	do
UCS	40MPa	Jv=21	RQD = 115-3.3Jv = 45.7					

Classification parameters		Value	Rating	Q Parameter	Rating	
Strength of intact rock		40MPa	4	RQD (%)	45	RQD/J_n
RQD		45%	8	J_n	12	3.75
Spacing of discontinuities		100mm-250mm	9	J_r	1	J_r/J_a
Condition of discontinuities	Persistence	1-3m, 3-8m	3	J_a	4	0.25
	Opening	0.1-1.5mm (avg)	3	J_w	1	Jw/SRF
	Roughness	Rough to Slightly rough	4	SRF	7	0.14
	Infilling	Clay	2			
		Fresh to slightly wthd.	5			
Ground water		Dry	15			
Adjust for Joint Orient.		Fair	-5			
		RMR	48	Q-value	0.13	

Chenani-Nashri Escape Tunnel Face Mapping Sheet Date/Time: 25-07-2012			
Previous Face Chainage	1682.5m	Elevation at the front	1243.7m
Present Face Chainage (ETSP)	1685m	Overburden [m]	505m
Total Pull	2.5m	Excavation method	Drill & blast
Unsupported length	2.5m	Excavation approach	NATM
Bolting distance from the face	2.5m	GSI	40

TUNNEL EXCAVATION FACE GEOTECHNICAL DESCRIPTION

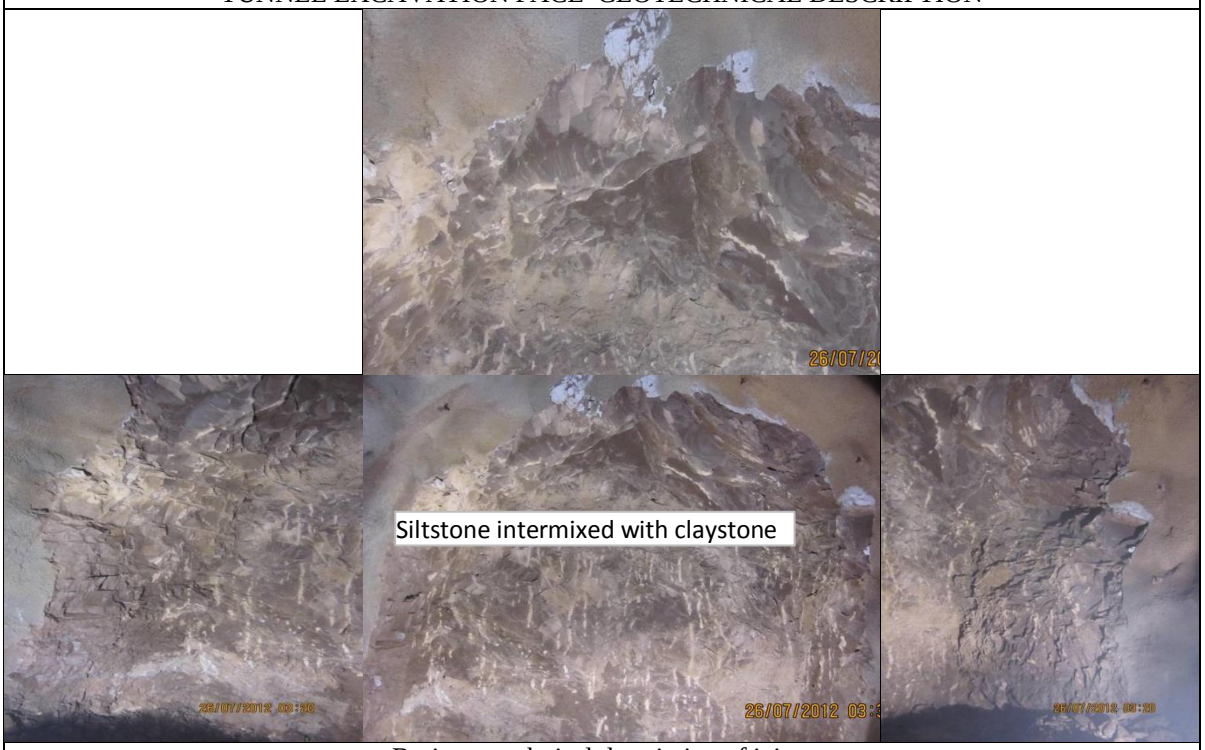

Basic geotechnical description of joints

Joint	Dip -dip/dir	Spacing	Persistence (m)	Roughness	Conditions	Aperture	Filling	Seepage
Bedding joint	35^o/95-110^o	20-60cm	1-10	Slightly rough	Slightly weathered	0.1-3mm	Clay filling	Dry
JS2	60^o/255^o	10cm	do	do	do	0.1-1mm	Clay filling	do
JS3	60^o/210^o	60cm	3-7m	do	do	do	Clay filling	do
UCS	40MPa	Jv=21	RQD = 115-3.3Jv = 45.7					

Classification parameters		Value	Rating	Q Parameter	Rating	
Strength of intact rock		40MPa	4	RQD (%)	45	RQD/J_n
RQD		45%	8	J_n	12	3.76
Spacing of discontinuities		100mm-600mm	9	J_r	0.8	J_r/J_a
Condition of discontinuities	Persistence	1-10m	3	J_a	4	0.2
	Opening	0.1-3mm (avg)	3	J_w	1	Jw/SRF
	Roughness	Slightly Rough	3	SRF	10	0.1
	Infilling	Clay	3			
		Fresh to slightly wthd.	5			
Ground water		Dry	15			
Adjust for Joint Orient.		Fair	-5			
		RMR	48	Q-value	0.13	

Chenani-Nashri Escape Tunnel Face Mapping Sheet Date/Time: 01-08-2012			
Previous Face Chainage	1740.5m	Elevation at the front	1243m
Present Face Chainage (ETSP)	1743m	Overburden [m]	514m
Total Pull	2.5m	Excavation method	Drill & blast
Unsupported length	2.5m	Excavation approach	NATM
Bolting distance from the face	2.5m	GSI	40

TUNNEL EXCAVATION FACE GEOTECHNICAL DESCRIPTION

Basic geotechnical description of joints

Joint	Dip -dip/dir	Spacing	Persistence (m)	Roughness	Conditions	Aperture	Filling	Seepage
Bedding joint	35^o/95-110^o	15cm	1-10	Rough-Slight rough	Fresh-slightly weathered	0.1-3mm	Clay filling	Dry
JS2	60^o/255^o	10cm	do	do	do	0.1-1mm	Clay filling	do
JS3	60^o/210^o	25cm	3-7m	do	do	do	Clay filling	do
UCS	40MPa	Jv=20	RQD = 115-3.3Jv = 49					

Classification parameters		Value	Rating	Q Parameter	Rating	
Strength of intact rock		40MPa	4	RQD (%)	49	RQD/J_n
RQD		49%	8	J_n	12	4.08
Spacing of discontinuities		100-250mm	9	J_r	0.8	J_r/J_a
Condition of discontinuities	Persistence	1-3m, 3-8m	3	J_a	4	0.2
	Opening	0.1-1.5mm (avg)	3	J_w	1	Jw/SRF
	Roughness	Slightly rough- smooth	3	SRF	10	0.1
	Infilling	Clay	2			
		Fresh to slightly wthd.	5			
Ground water		Dry	15			
Adjust for Joint Orient.		Fair/Unfav	-7			
		RMR	45	Q-value	0.08	

Chenani-Nashri Escape Tunnel Face Mapping Sheet Date/Time: 03-09-2012			
Previous Face Chainage	1957.5m	Elevation at the front	1243.7m
Present Face Chainage (ETSP)	1960m	Overburden [m]	538m
Total Pull	2.5m	Excavation method	Drill & blast
Unsupported length	2.5m	Excavation approach	NATM
Bolting distance from the face	2.5m	GSI	40

TUNNEL EXCAVATION FACE GEOTECHNICAL DESCRIPTION

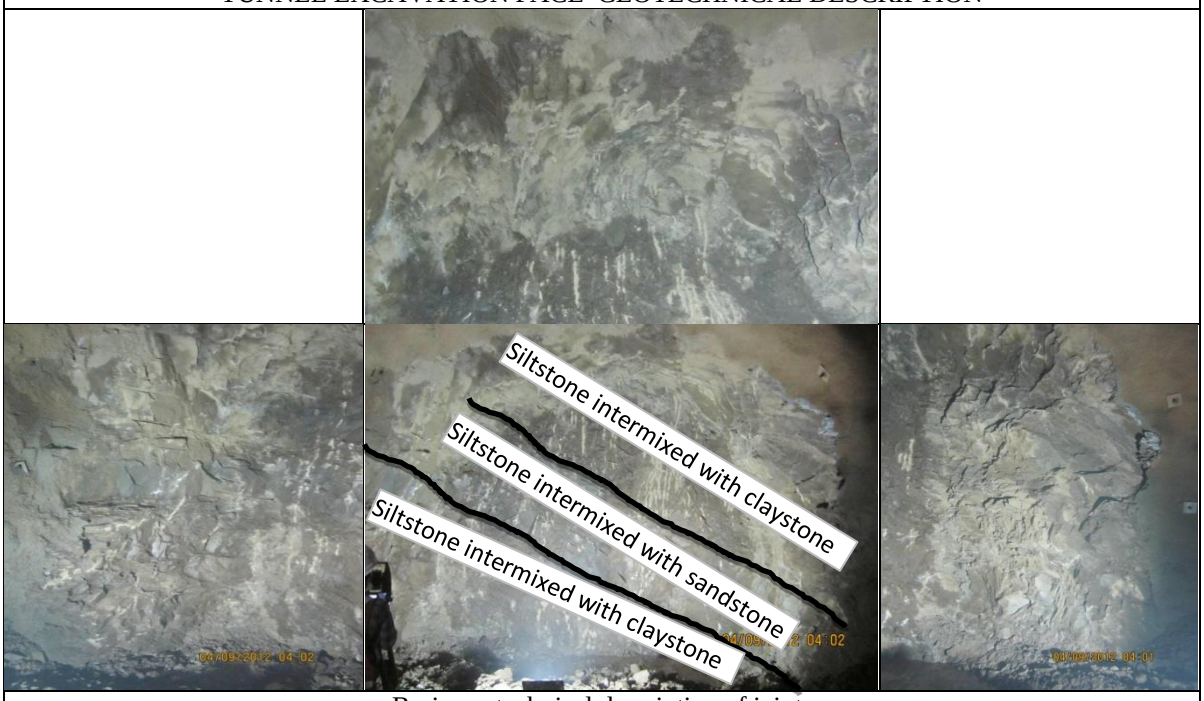

Basic geotechnical description of joints

Joint	Dip -dip/dir	Spacing	Persistence (m)	Roughness	Conditions	Aperture	Filling	Seepage
Bedding joint	30-40°/90-100°	20-60cm	1-10	R-Slightly rough	Fresh-slightly weathered	0.1-3mm	Clay filling	Dry
JS2	60°/250-260°	10cm	do	do	do	0.1-1mm	Clay filling	do
JS3	65°/200°	60cm	3-7m	do	do	do	Clay filling	do
UCS	40MPa	Jv=21	RQD = 115-3.3Jv = 45.7					

Classification parameters		Value	Rating	Q Parameter	Rating	
Strength of intact rock		40MPa	4	RQD (%)	46	RQD/J_n
RQD		46%	8	J_n	12	3.83
Spacing of discontinuities		200mm-600mm	10	J_r	0.5	J_r/J_a
Condition of discontinuities	Persistence	1-10m, 3-7m	3	J_a	3	0.17
	Opening	0.1-2mm (avg)	3	J_w	1	Jw/SRF
	Roughness	Slightly rough to smooth	4	SRF	10	0.1
	Infilling	Clay	2			
		Fresh- slightly weathered	5			
Ground water		Dry	15			
Adjust for Joint Orient.		Fair/Unfav	-7			
		RMR	47	Q-value	0.06	

Chenani-Nashri Escape Tunnel Face Mapping Sheet Date/Time: 23-09-2012			
Previous Face Chainage	2063.5m	Elevation at the front	1243.7m
Present Face Chainage (ETSP)	2066m	Overburden [m]	566m
Total Pull	2.5m	Excavation method	Drill & blast
Unsupported length	2.5m	Excavation approach	NATM
Bolting distance from the face	2.5m	GSI	40

TUNNEL EXCAVATION FACE GEOTECHNICAL DESCRIPTION

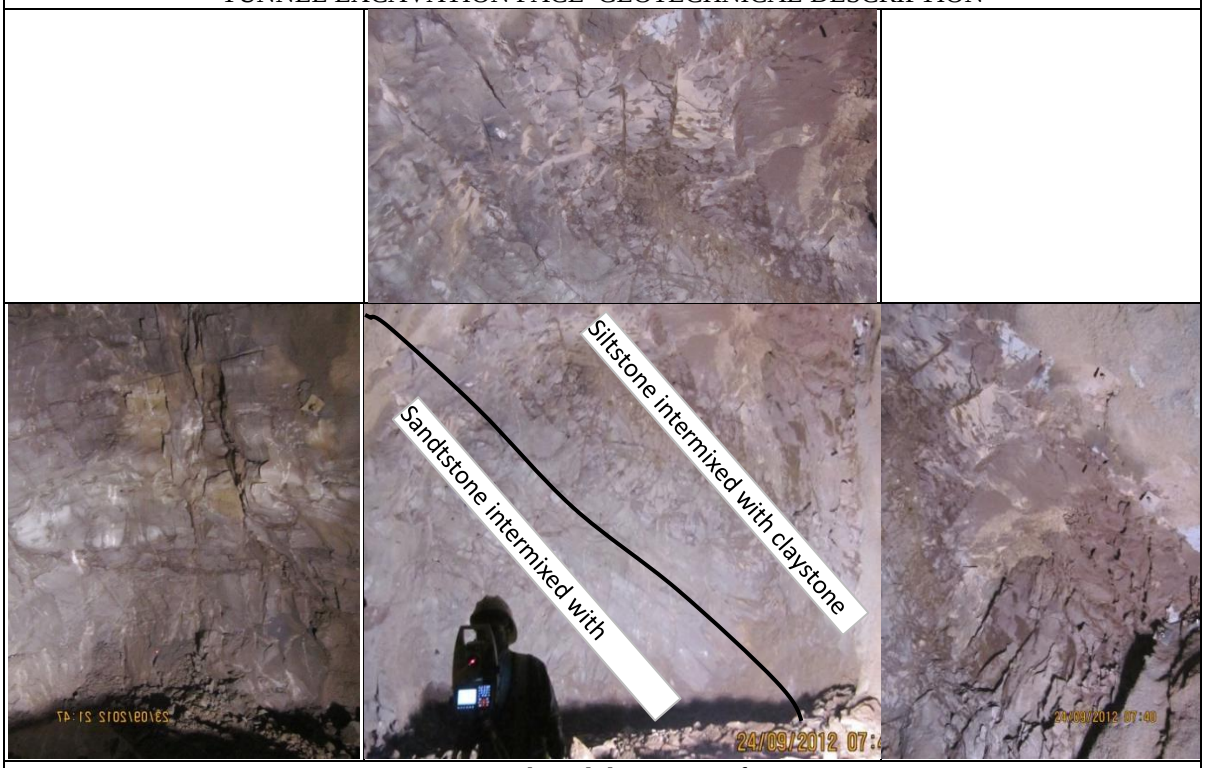

Basic geotechnical description of joints

Joint	Dip -dip/dir	Spacing	Persistence (m)	Roughness	Conditions	Aperture	Filling	Seepage
Bedding joint	$35^o/95^o$	20-60cm	1-10	R-Slightly rough	Fresh-Slight weathered	0.1-3mm	clay filling	Dry
JS2	$60^o/260^o$	10cm	do	do	do	0.1-1mm	clay filling	do
JS3	$55\text{-}65^o/210^o$	60cm	3-7m	do	do	do	clay filling	do
UCS	40MPa	Jv=19	RQD = 115-3.3Jv = 52.3					

Classification parameters		Value	Rating	Q Parameter	Rating	
Strength of intact rock		40MPa	4	RQD (%)	52	RQD/J_n
RQD		52%	13	J_n	12	4.33
Spacing of discontinuities		200mm-600mm	9	J_r	0.5	J_r/J_a
Condition of discontinuities	Persistence	1-3m, 3-7m	3	J_a	3	0.17
	Opening	0.1-3mm (avg)	3	J_w	1	Jw/SRF
	Roughness	Rough to slightly Rough	3	SRF	5	0.2
	Infilling	Clay	2			
		Fresh to slightly wthd.	5			
Ground water		Dry	15			
Adjust for Joint Orient.		Fair	-5			
		RMR	52	Q-value	0.14	

Chenani-Nashri Escape Tunnel Face Mapping Sheet Date/Time: 25-09-2012			
Previous Face Chainage	2116.5m	Elevation at the front	1243.7m
Present Face Chainage (ETSP)	2119m	Overburden [m]	568m
Total Pull	2.5m	Excavation method	Drill & blast
Unsupported length	2.5m	Excavation approach	NATM
Bolting distance from the face	2.5m	GSI	45

TUNNEL EXCAVATION FACE GEOTECHNICAL DESCRIPTION

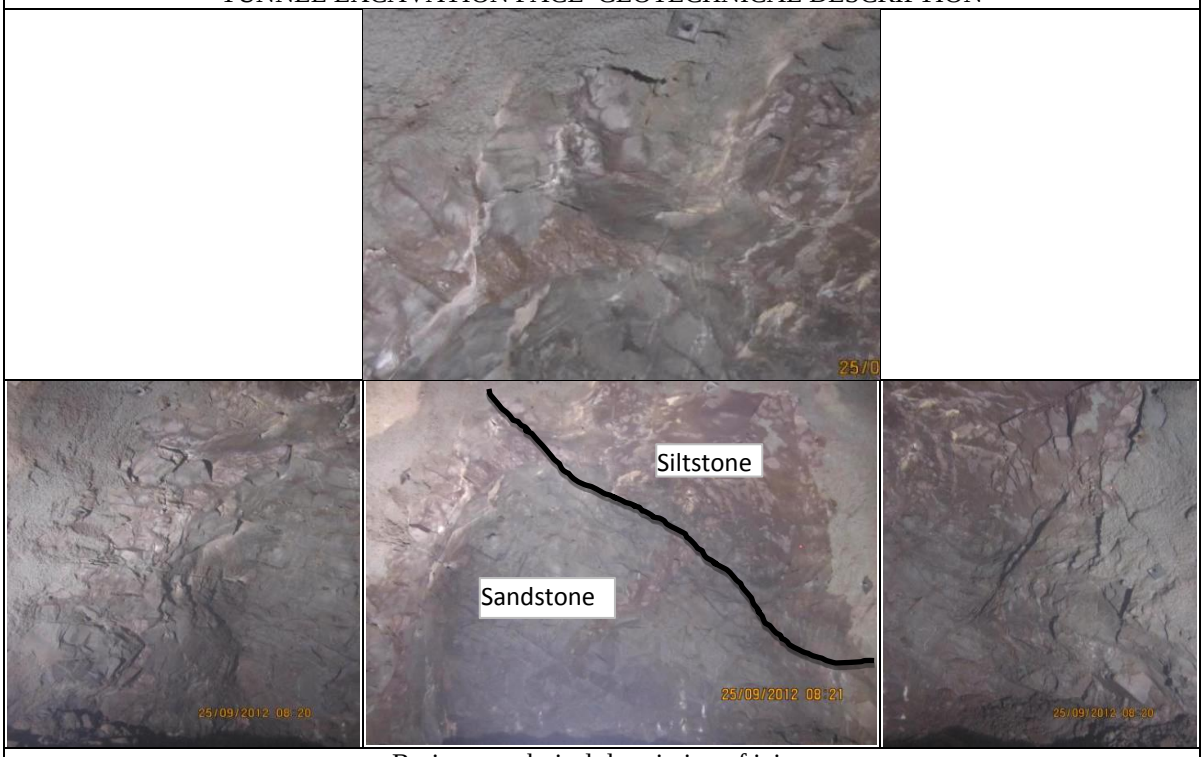

Basic geotechnical description of joints

Joint	Dip -dip/dir	Spacing	Persistence (m)	Roughness	Conditions	Aperture	Filling	Seepage
Bedding joint	40-45°/115°	20cm	1-6	R-Slightly Rough	Slightly wthd.	0.1-1.5mm	Clay filling	Dry
JS2	65°/250°	12cm	do	do	do	do	Clay filling	do
JS3	70°/200-220°	20cm	3-5m	do	do	do	Clay filling	do
UCS	40MPa	Jv=19	RQD = 115-3.3Jv = 52.3					

Classification parameters		Value	Rating	Q Parameter	Rating	
Strength of intact rock		40MPa	4	RQD (%)	52	RQD/J_n
RQD		52%	9	J_n	12	4.36
Spacing of discontinuities		200-600mm	10	J_r	0.5	J_r/J_a
Condition of discontinuities	Persistence	1-6m	3	J_a	3	0.17
	Opening	0.1-1.5mm (avg)	4	J_w	1	Jw/SRF
	Roughness	Rough to Slightly rough	4	SRF	5	0.2
	Infilling	Clay	2			
		Fresh to slightly wthd.	5			
Ground water		Dry	15			
Adjust for Joint Orient.		Fair	-5			
		RMR	51	Q-value	0.15	

Chenani-Nashri Escape Tunnel Face Mapping Sheet Date/Time: 03-10-2012/10:00 pm			
Previous Face Chainage	2176m	Elevation at the front	1230m
Present Face Chainage (ETSP)	2178m	Overburden [m]	575m
Total Pull	2m	Excavation method	Drill & blast
Unsupported length	2m	Excavation approach	NATM
Bolting distance from the face	2m	GSI	46

TUNNEL EXCAVATION FACE GEOTECHNICAL DESCRIPTION

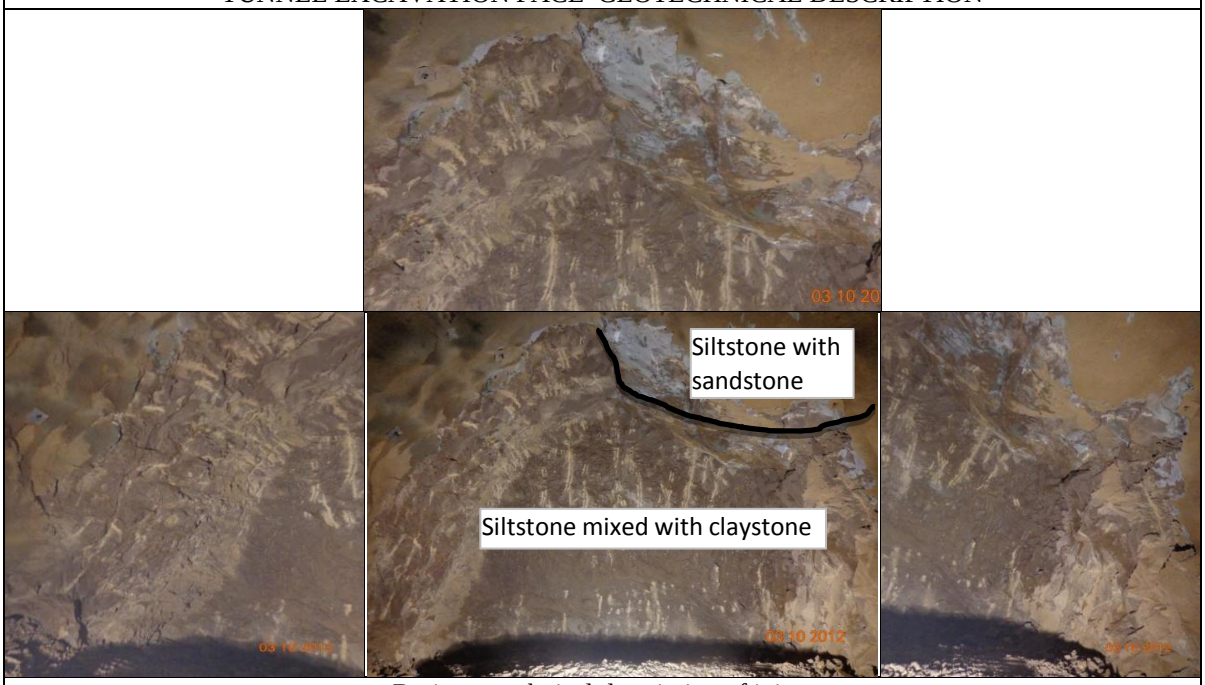

Basic geotechnical description of joints

Joint	Dip -dip/dir	Spacing	Persistence (m)	Roughness	Conditions	Aperture	Filling	Seepage
Bedding joint	40-45°/115°	15cm	1-6	R-Slightly Rough	Slightly wthd.	0.1-1.5mm	Clay filling	Dry
JS2	55-65°/258°	9cm	do	do	do	do	Clay filling	do
JS3	70°/200-220°	20cm	3-7m	do	do	do	Clay filling	do
UCS	45MPa	Jv=21	RQD = 115-3.3Jv = 45.7					

Classification parameters		Value	Rating	Q Parameter	Rating	
Strength of intact rock		45MPa	4	RQD (%)	46	RQD/J_n
RQD		46%	8	J_n	12	3.83
Spacing of discontinuities		90-200mm	8	J_r	0.5	J_r/J_a
Condition of discontinuities	Persistence	1-6m; 3-7m	3	J_a	3	0.17
	Opening	0.1-1.5mm (avg)	4	J_w	1	Jw/SRF
	Roughness	Slightly rough-smooth	3	SRF	10	0.1
	Infilling	Clay	2			
		Slightly weathered	5			
Ground water		Dry	10			
Adjust for Joint Orient.		Fair	-5			
		RMR	42	Q-value	0.06	

Chenani-Nashri Escape Tunnel Face Mapping Sheet Date/Time: 23-03-2013			
Previous Face Chainage	3217.5m	Elevation at the front	1230m
Present Face Chainage (ETSP)	3220m	Overburden [m]	621m
Total Pull	2.5m	Excavation method	Drill & blast
Unsupported length	2.5m	Excavation approach	NATM
Bolting distance from the face	2.5m	GSI	50

TUNNEL EXCAVATION FACE GEOTECHNICAL DESCRIPTION

Basic geotechnical description of joints

Joint	Dip -dip/dir	Spacing	Persistence (m)	Roughness	Conditions	Aperture	Filling	Seepage
Bedding joint	40-45°/115°	20-60cm	1-10	R-Slightly rough	Slightly weathered	0.1-1mm	Silty clay	Dry
JS2	60°/250-270°	12cm	do	do	do	0.1-5mm	Silty clay	do
JS3	60-70°/215°	60cm	3-7	do	do	do	Silty clay	do
UCS	40MPa	Jv=20	RQD = 115-3.3Jv = 49					

Classification parameters		Value	Rating	Q Parameter	Rating	
Strength of intact rock		40MPa	4	RQD (%)	49	RQD/J_n
RQD		49%	8	J_n	12	4.08
Spacing of discontinuities		200-600mm	9	J_r	1	J_r/J_a
Condition of discontinuities	Persistence	1-10m	3	J_a	4	0.25
	Opening	0.1-5mm (avg)	3	J_w	1	Jw/SRF
	Roughness	Rough to slightly Rough	3	SRF	5	0.2
	Infilling	Silty clay	3			
		Slightly weathered	5			
Ground water		Dry	15			
Adjust for Joint Orient.		Fair/ Unfav	-7			
		RMR	46	Q-value	0.2	

Chenani-Nashri Main Tunnel Face Mapping Sheet Date/Time: 27-04-2012/ 07:45 pm			
Previous Face chainage	718.5m	Elevation at the front	1243.7m
Present Face chain age (MTSP)	721m	Overburden [m]	294m
Total Pull	2.5m	Excavation method	Drill & blast
Unsupported length	2.5m	Excavation approach	NATM
Bolting distance from the face	2.5m	GSI	48

TUNNEL EXCAVATION FACE GEOTECHNICAL DESCRIPTION

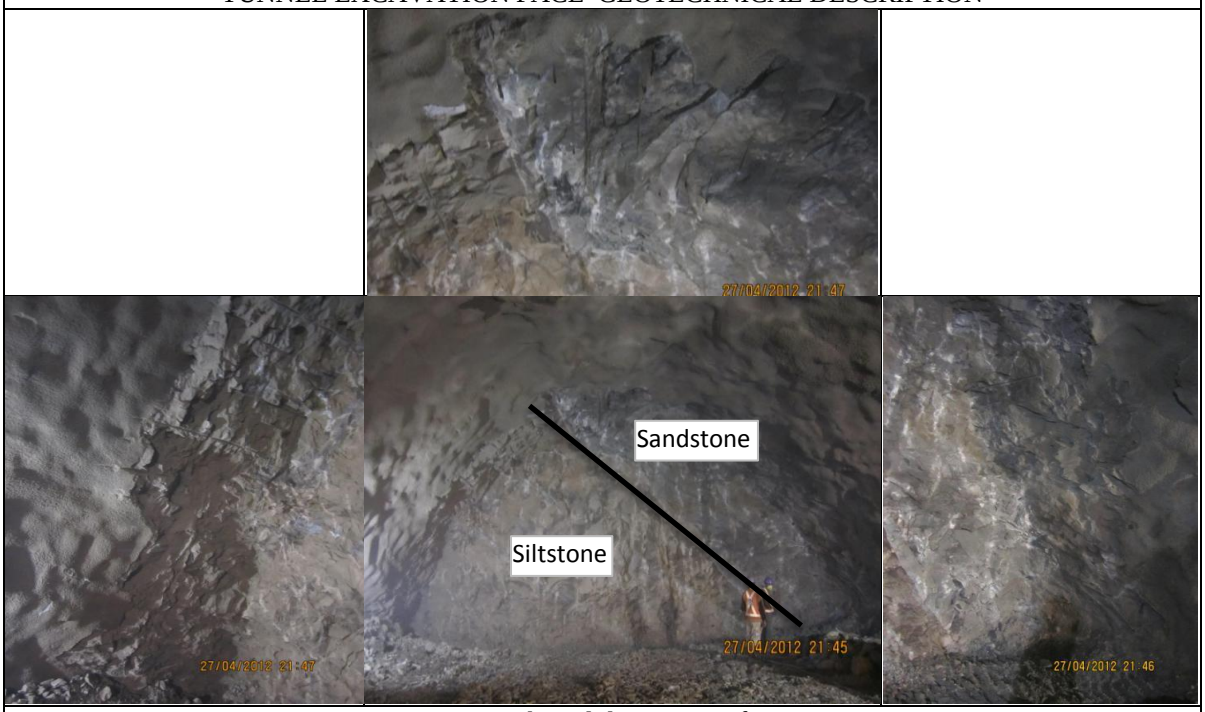

Basic geotechnical description of joints

Joint	Dip -dip/dir	Spacing	Persistence (m)	Roughness	Conditions	Aperture	Filling	Seepage
Bedding joint	$35^o/95^o$	50cm	1-3; 10-15	Slightly Rough	Fresh to slightly wthd.	0.1-5mm	Silty clay	Dry to slightly damp
JS2	$60^o/270^o$	12cm	1-3; 3-10	do	do	do	Silty clay	do
JS3	$50^o/200^o$	15cm	1-12m	do	do	do	Silty clay	do
UCS	40	Jv=18	RQD = 115-3.3Jv = 55.6					

Classification parameters		Value	Rating	Q Parameter	Rating	
Strength of intact rock		40 MPa	4	RQD (%)	55	RQD/J_n
RQD		55%	9	J_n	12	4.58
Spacing of discontinuities		120mm-600mm	10	J_r	1	J_r/J_a
Condition of discontinuities	Persistence	3-15m	3	J_a	4	0.25
	Opening	0.1-5mm (avg)	4	J_w	1	Jw/SRF
	Roughness	Rough to slightly Rough	4	SRF	5	0.2
	Infilling	Silty clay	2			
		Slightly wthd.	5			
Ground water		Dry	15			
Adjust for Joint Orient.		Fair	-5			
		RMR	51	Q-value	0.23	

Chenani-Nashri Main Tunnel Face Mapping Sheet Date/Time: 07-05-2012/ 1:00 pm			
Previous Face chainage	768.5m	Elevation at the front	1230m
Present Face chain age (MTSP)	771m	Overburden [m]	320m
Total Pull	2.5m	Excavation method	Drill & blast
Unsupported length	2.5m	Excavation approach	NATM
Bolting distance from the face	2.5m	GSI	45

TUNNEL EXCAVATION FACE GEOTECHNICAL DESCRIPTION

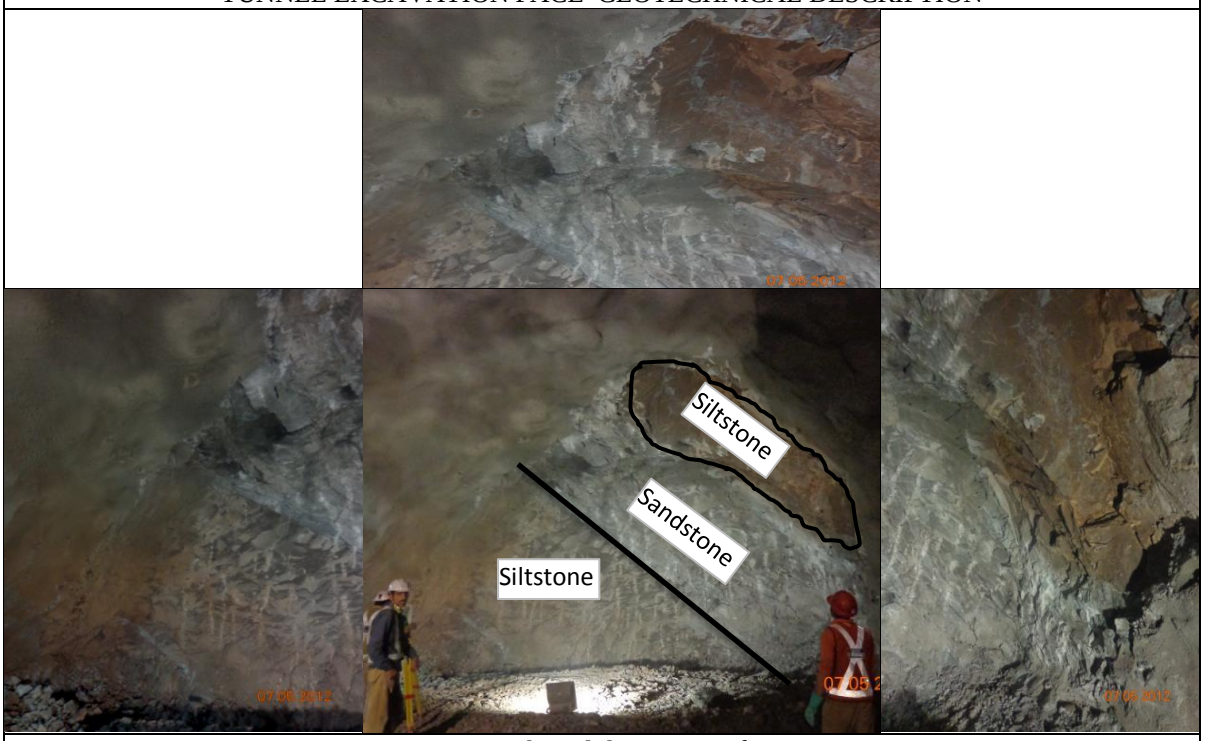

Basic geotechnical description of joints

Joint	Dip -dip/dir	Spacing	Persistence (m)	Roughness	Conditions	Aperture	Filling	Seepage
Bedding joint	$35^o/95^o$	50cm	1-3; 10-15	Slightly Rough	Fresh to slightly wthd.	0.1-5mm	Silty clay	Dry to slightly damp
JS2	$65^o/250^o$	11cm	1-3; 3-10	do	do	do	Silty clay	do
JS3	$50^o/200^o$	15cm	1-12m	do	do	do	Silty clay	do
UCS	40	Jv=23	RQD = 115-3.3Jv = 39.1					

Classification parameters		Value	Rating	Q Parameter	Rating	
Strength of intact rock		40 MPa	4	RQD (%)	39	RQD/J_n
RQD		39%	9	J_n	12	3.25
Spacing of discontinuities		110mm-500mm	10	J_r	0.8	J_r/J_a
Condition of discontinuities	Persistence	3-15m	3	J_a	4	0.2
	Opening	0.1-5mm (avg)	4	J_w	1	Jw/SRF
	Roughness	Slightly Rough	3	SRF	5	0.2
	Infilling	Silty clay	2			
		Slightly wthd.	5			
Ground water		Dry	15			
Adjust for Joint Orient.		Fair	-5			
		RMR	49	Q-value	0.13	

Chenani-Nashri Main Tunnel Face Mapping Sheet Date/Time: 18-05-2012/ 02:30 pm			
Previous Face chainage	820.5m	Elevation at the front	1230m
Present Face chain age (MTSP)	823m	Overburden [m]	342m
Total Pull	2.5m	Excavation method	Drill & blast
Unsupported length	2.5m	Excavation approach	NATM
Bolting distance from the face	2.5m	GSI	45

TUNNEL EXCAVATION FACE GEOTECHNICAL DESCRIPTION

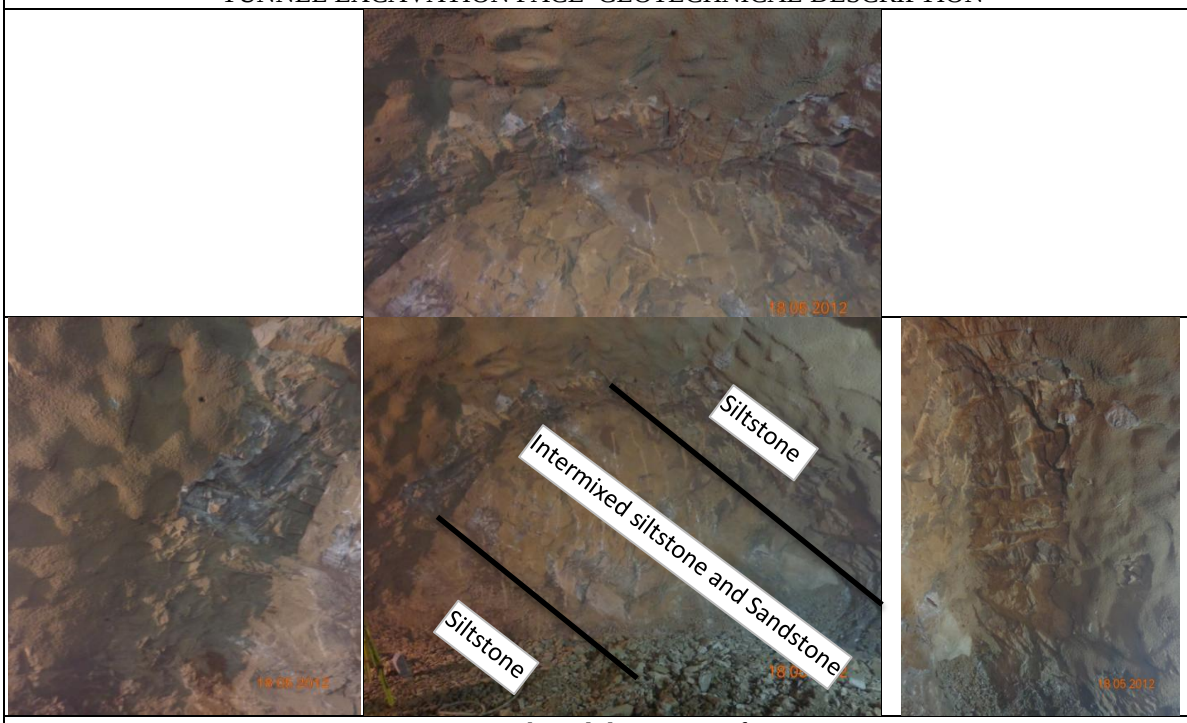

Basic geotechnical description of joints

Joint	Dip -dip/dir	Spacing	Persistence (m)	Roughness	Conditions	Aperture	Filling	Seepage
Bedding joint	$35^o/95^o$	45cm	1-3; 10-15	Slightly Rough	Fresh to slightly wthd.	0.1-5mm	Silty clay	Dry to slightly damp
JS2	$65^o/255^o$	10cm	1-3; 3-10	do	do	do	Silty clay	do
JS3	$50^o/200^o$	20cm	1-12m	do	do	do	Silty clay	do
UCS	40	Jv=18	RQD = 115-3.3Jv = 55.6					

Classification parameters		Value	Rating	Q Parameter	Rating	
Strength of intact rock		40 MPa	4	RQD (%)	55	RQD/J_n
RQD		55%	9	J_n	12	4.58
Spacing of discontinuities		100mm-450mm	9	J_r	1	J_r/J_a
Condition of discontinuities	Persistence	3-15m	3	J_a	4	0.25
	Opening	0.1-5mm (avg)	4	J_w	1	Jw/SRF
	Roughness	Slightly Rough	3	SRF	5	0.2
	Infilling	Silty clay	2			
		Slightly wthd.	5			
Ground water		Dry	15			
Adjust for Joint Orient.		Fair	-5			
		RMR	49	Q-value	0.23	

Chenani-Nashri Main Tunnel Face Mapping Sheet Date/Time: 23-05-2012/ 10:15 am			
Previous Face chainage	834.5m	Elevation at the front	1230m
Present Face chain age (MTSP)	837m	Overburden [m]	347m
Total Pull	2.5m	Excavation method	Drill & blast
Unsupported length	2.5m	Excavation approach	NATM
Bolting distance from the face	2.5m	GSI	50

TUNNEL EXCAVATION FACE GEOTECHNICAL DESCRIPTION

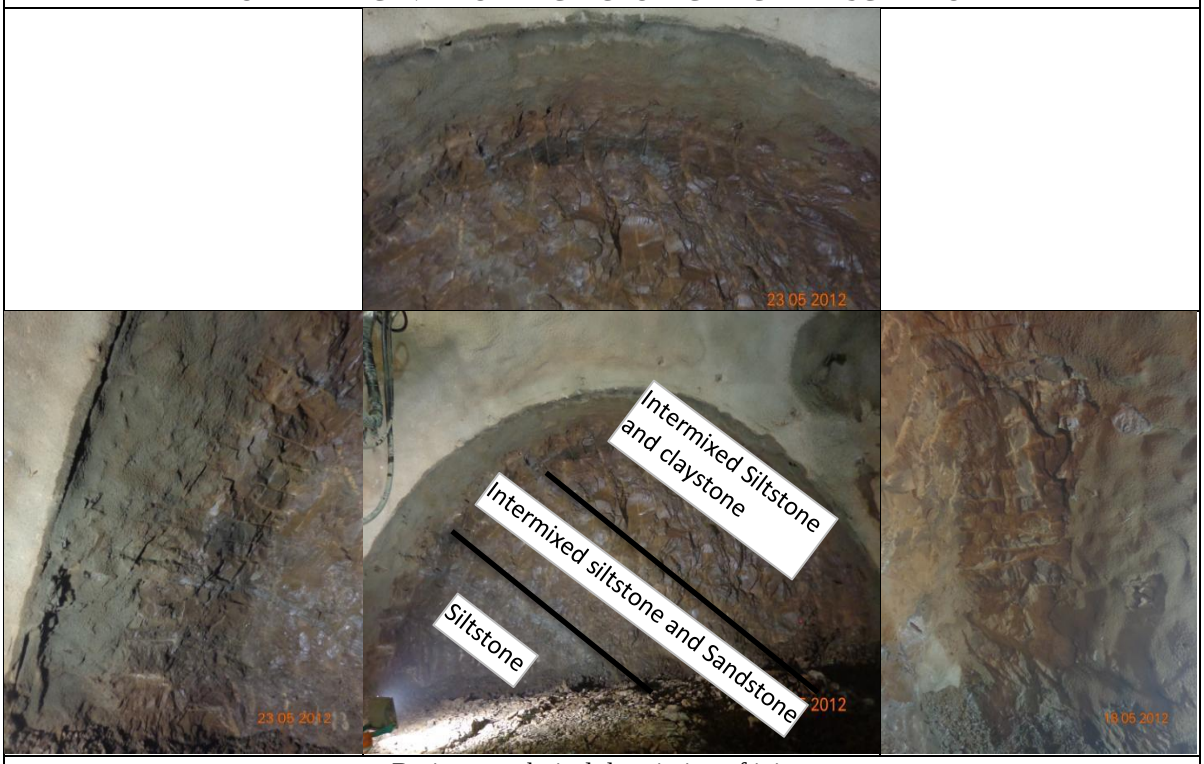

Basic geotechnical description of joints

Joint	Dip -dip/dir	Spacing	Persistence (m)	Roughness	Conditions	Aperture	Filling	Seepage
Bedding joint	$35^o/95^o$	45cm	1-3; 10-15	Slightly Rough	Fresh to slightly wthd.	0.1-5mm	Silty clay	Dry to slightly damp
JS2	$60^o/250^o$	10cm	1-3; 3-10	do	do	do	Silty clay	do
JS3	$50^o/200^o$	20cm	1-12m	do	do	do	Silty clay	do
UCS	50	Jv=18	RQD = 115-3.3Jv = 55.6					

Classification parameters		Value	Rating	Q Parameter	Rating	
Strength of intact rock		50 MPa	4	RQD (%)	55	RQD/J_n
RQD		55%	9	J_n	12	4.58
Spacing of discontinuities		100mm-450mm	9	J_r	0.5	J_r/J_a
Condition of discontinuities	Persistence	3-15m	2	J_a	3	0.17
	Opening	0.1-5mm (avg)	4	J_w	1	Jw/SRF
	Roughness	Slightly Rough	2	SRF	7	0.14
	Infilling	Silty clay	2			
		Slightly wthd.	5			
Ground water		Dry	15			
Adjust for Joint Orient.		Fair	-5			
		RMR	47	Q-value	0.11	

Chenani-Nashri Main Tunnel Face Mapping Sheet Date/Time: 23-05-2012/ 10:15 am			
Previous Face chainage	834.5m	Elevation at the front	1230m
Present Face chain age (MTSP)	837m	Overburden [m]	347m
Total Pull	2.5m	Excavation method	Drill & blast
Unsupported length	2.5m	Excavation approach	NATM
Bolting distance from the face	2.5m	GSI	50

TUNNEL EXCAVATION FACE GEOTECHNICAL DESCRIPTION

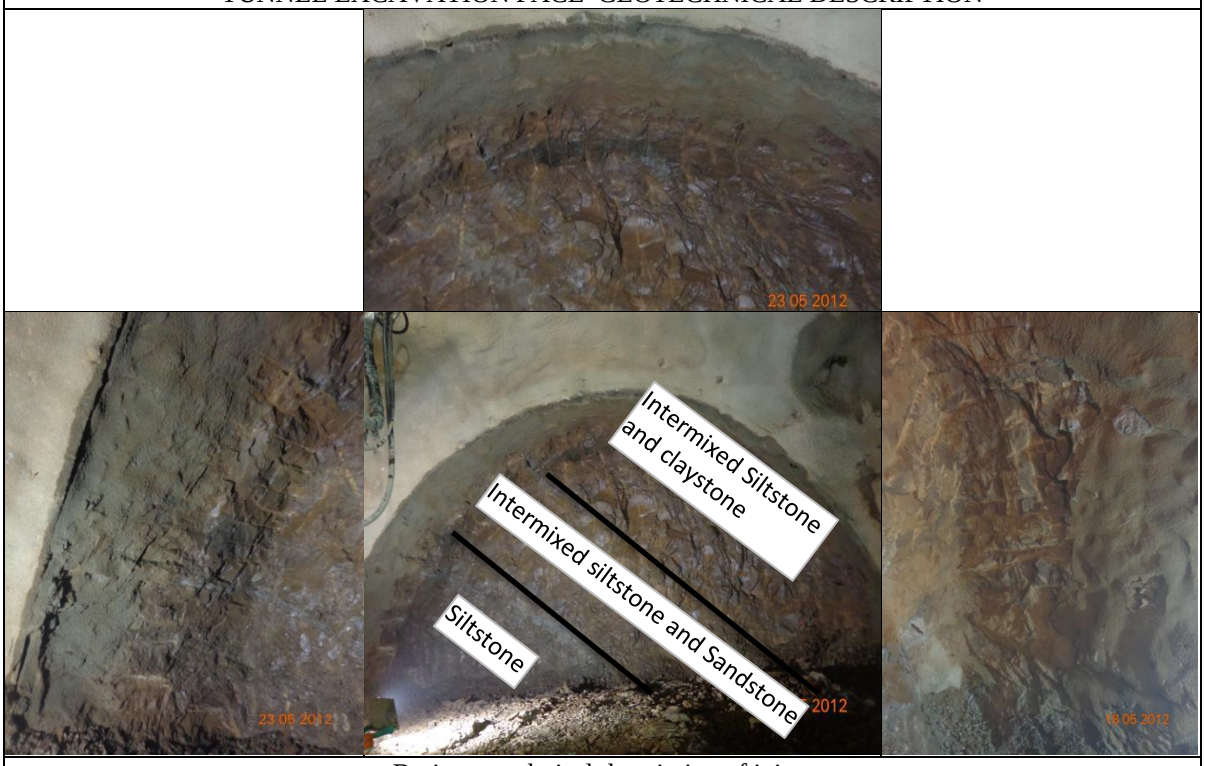

Basic geotechnical description of joints

Joint	Dip -dip/dir	Spacing	Persistence (m)	Roughness	Conditions	Aperture	Filling	Seepage
Bedding joint	$35^o/95^o$	6-20cm	1-3	Slightly Rough	Slightly wthd.	0.1-1mm	Clay	Dry
JS2	$60\text{-}70^o/250^o$	6-12cm	3-10	do	do	do	Clay	do
JS3	$60\text{-}70^o/200^o$	60cm	do	do	do	do	Clay	do
UCS	40	Jv=22	RQD = 115-3.3Jv = 42.4					

Classification parameters		Value	Rating	Q Parameter	Rating	
Strength of intact rock		40 MPa	4	RQD (%)	42	RQD/J_n
RQD		42%	8	J_n	12	3.5
Spacing of discontinuities		60-600mm	9	J_r	1	J_r/J_a
Condition of discontinuities	Persistence	1-10m	3	J_a	4	0.25
	Opening	0.1-1mm (avg)	3	J_w	1	Jw/SRF
	Roughness	Slightly Rough	3	SRF	5	0.2
	Infilling	Silty clay	2			
		Slightly wthd.	5			
Ground water		Dry	12			
Adjust for Joint Orient.		Fair/Unfav	-7			
		RMR	42	Q-value	0.18	

Chenani-Nashri Main Tunnel Face Mapping Sheet Date/Time: 24-06-2012			
Previous Face chainage	889.5m	Elevation at the front	1243.7m
Present Face chain age (MTSP)	892m	Overburden [m]	365m
Total Pull	2.5m	Excavation method	Drill & blast
Unsupported length	2.5m	Excavation approach	NATM
Bolting distance from the face	2.5m	GSI	40

TUNNEL EXCAVATION FACE GEOTECHNICAL DESCRIPTION

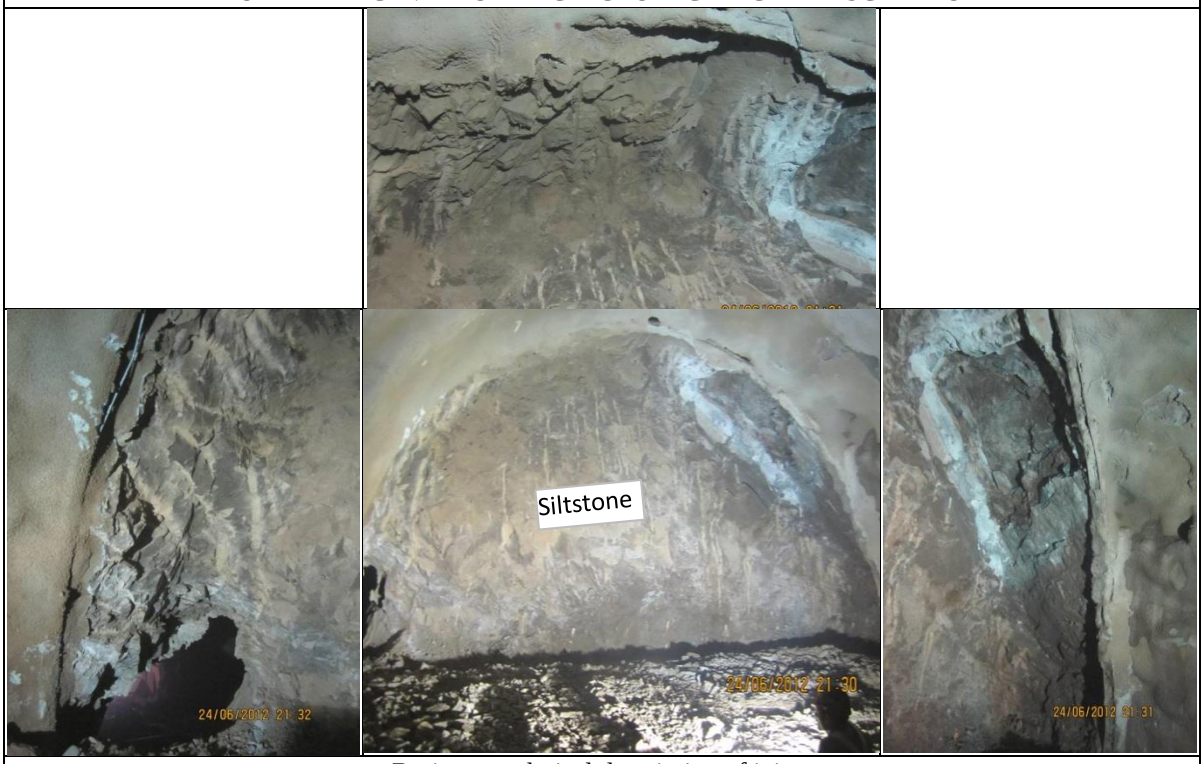

Basic geotechnical description of joints

Joint	Dip -dip/dir	Spacing	Persistence (m)	Roughness	Conditions	Aperture	Filling	Seepage
Bedding joint	35-40°/95°	6-20cm	1-3	Slightly Rough	Slightly wthd.	0.1-1mm	Clay	Dry
JS2	60°/240-250°	10-12cm	3-10	do	do	do	Clay	do
JS3	60-70°/210°	60cm	do	do	do	do	Clay	do
UCS	40	Jv=21	RQD = 115-3.3Jv = 45.7					

Classification parameters		Value	Rating	Q Parameter	Rating	
Strength of intact rock		40 MPa	4	RQD (%)	45	RQD/J_n
RQD		45%	8	J_n	9	5
Spacing of discontinuities		60-600mm	9	J_r	0.8	J_r/J_a
Condition of discontinuities	Persistence	1-10m	3	J_a	3	0.26
	Opening	0.1-1mm (avg)	3	J_w	1	Jw/SRF
	Roughness	Slightly Rough	3	SRF	5	0.2
	Infilling	Silty clay	2			
		Slightly wthd.	5			
Ground water		Dry	15			
Adjust for Joint Orient.		Fair/Unfav	-7			
		RMR	45	Q-value	0.27	

Chenani-Nashri Main Tunnel Face Mapping Sheet Date/Time: 01-07-2012			
Previous Face chainage	916.5m	Elevation at the front	1243.7m
Present Face chain age (MTSP)	919m	Overburden [m]	374m
Total Pull	2.5m	Excavation method	Drill & blast
Unsupported length	2.5m	Excavation approach	NATM
Bolting distance from the face	2.5m	GSI	40

TUNNEL EXCAVATION FACE GEOTECHNICAL DESCRIPTION

Basic geotechnical description of joints

Joint	Dip -dip/dir	Spacing	Persistence (m)	Roughness	Conditions	Aperture	Filling	Seepage
Bedding joint	35-40°/95°	6-20cm	1-3	Slightly Rough	Slightly wthd.	0.1-1mm	Clay	Dry
JS2	60°/240-260°	10-14cm	3-10	do	do	do	Clay	do
JS3	60-70°/200°	60cm	do	do	do	do	Clay	do
UCS	35	Jv=21	RQD = 115-3.3Jv = 45.7					

Classification parameters		Value	Rating	Q Parameter	Rating	
Strength of intact rock		35 MPa	4	RQD (%)	45	RQD/J_n
RQD		45%	8	J_n	9	5
Spacing of discontinuities		60-600mm	9	J_r	0.8	J_r/J_a
Condition of discontinuities	Persistence	1-10m	3	J_a	3	0.27
	Opening	0.1-1mm (avg)	4	J_w	1	Jw/SRF
	Roughness	Slightly Rough	3	SRF	10	0.1
	Infilling	Silty clay	2			
		Slightly wthd.	5			
Ground water		Dry	15			
Adjust for Joint Orient.		Fair/Unfav	-7			
		RMR	46	Q-value	0.13	

Chenani-Nashri Main Tunnel Face Mapping Sheet Date/Time: 08-07-2012			
Previous Face chainage	945.5m	Elevation at the front	1243.7m
Present Face chain age (MTSP)	948m	Overburden [m]	385m
Total Pull	2.5m	Excavation method	Drill & blast
Unsupported length	2.5m	Excavation approach	NATM
Bolting distance from the face	2.5m	GSI	35-45

TUNNEL EXCAVATION FACE GEOTECHNICAL DESCRIPTION

Basic geotechnical description of joints

Joint	Dip -dip/dir	Spacing	Persistence (m)	Roughness	Conditions	Aperture	Filling	Seepage
Bedding joint	35-40°/90°	6-20cm	1-3	Slightly Rough	Slightly wthd.	0.1-1mm	Clay	Dry
JS2	60°/240-260°	9cm	3-10	do	do	do	Clay	do
JS3	60-70°/210°	60cm	do	do	do	do	Clay	do
UCS	35	Jv=20	RQD = 115-3.3Jv = 49					

Classification parameters		Value	Rating	Q Parameter	Rating	
Strength of intact rock		35 MPa	4	RQD (%)	49	RQD/J_n
RQD		49%	8	J_n	9	5.4
Spacing of discontinuities		60-600mm	9	J_r	0.5	J_r/J_a
Condition of discontinuities	Persistence	1-10m	3	J_a	3	0.17
	Opening	0.1-1mm (avg)	3	J_w	1	Jw/SRF
	Roughness	Slightly Rough	3	SRF	7	0.14
	Infilling	Silty clay	2			
		Slightly wthd.	5			
Ground water		Dry	15			
Adjust for Joint Orient.		Fair/Unfav	-7			
		RMR	45	Q-value	0.13	

Chenani-Nashri Main Tunnel Face Mapping Sheet Date/Time: 16-07-2012/ 09:30 am			
Previous Face chainage	977.5m	Elevation at the front	1230m
Present Face chain age (MTSP)	980m	Overburden [m]	404m
Total Pull	2.5m	Excavation method	Drill & blast
Unsupported length	2.5m	Excavation approach	NATM
Bolting distance from the face	2.5m	GSI	40

TUNNEL EXCAVATION FACE GEOTECHNICAL DESCRIPTION

Basic geotechnical description of joints

Joint	Dip -dip/dir	Spacing	Persistence (m)	Roughness	Conditions	Aperture	Filling	Seepage
Bedding joint	$35^o/95^o$	30cm	1-3; 10-15	R-Slightly Rough	Fresh-Slight wthd.	0.1-5mm	Silty clay	Dry
JS2	$60\text{-}70^o/250^o$	12cm	3-10; 3-10	do	do	do	Silty clay	do
JS3	$60\text{-}70^o/200^o$	18cm	1-12	do	do	do	Silty clay	do
UCS	40	Jv=21	RQD = 115-3.3Jv = 45.7					

Classification parameters		Value	Rating	Q Parameter	Rating	
Strength of intact rock		40 MPa	4	RQD (%)	45	RQD/J_n
RQD		45%	8	J_n	12	3.75
Spacing of discontinuities		60-600mm	9	J_r	0.8	J_r/J_a
Condition of discontinuities	Persistence	1-15m	2	J_a	4	0.2
	Opening	0.1-1mm (avg)	3	J_w	1	Jw/SRF
	Roughness	Rough-Slightly Rough	4	SRF	5	0.2
	Infilling	Silty clay	2			
		Fresh-Slightly wthd.	5			
Ground water		Dry	15			
Adjust for Joint Orient.		Fair	-5			
		RMR	47	Q-value	0.15	

Chenani-Nashri Main Tunnel Face Mapping Sheet Date/Time: 27-07-2012			
Previous Face chainage	1006.5m	Elevation at the front	1243.7m
Present Face chain age (MTSP)	1009m	Overburden [m]	413m
Total Pull	2.5m	Excavation method	Drill & blast
Unsupported length	2.5m	Excavation approach	NATM
Bolting distance from the face	2.5m	GSI	38

TUNNEL EXCAVATION FACE GEOTECHNICAL DESCRIPTION

Basic geotechnical description of joints

Joint	Dip -dip/dir	Spacing	Persistence (m)	Roughness	Conditions	Aperture	Filling	Seepage
Bedding joint	35-40°/95°	6-20cm	1-3	Slightly Rough	Slightly wthd.	0.1-1mm	Clay	Dry
JS2	60-70°/255°	10cm	3-10	do	do	do	Clay	do
JS3	60-70°/210°	60cm	do	do	do	do	Clay	do
UCS	45	Jv=20	RQD = 115-3.3Jv = 49					

Classification parameters		Value	Rating	Q Parameter	Rating	
Strength of intact rock		45 MPa	4	RQD (%)	49	RQD/J_n
RQD		49%	8	J_n	9	5.4
Spacing of discontinuities		60-600mm	9	J_r	1	J_r/J_a
Condition of discontinuities	Persistence	1-10m	3	J_a	4	0.25
	Opening	0.1-1mm (avg)	3	J_w	1	Jw/SRF
	Roughness	Slightly Rough	3	SRF	5	0.2
	Infilling	Silty clay	2			
		Slightly wthd.	5			
Ground water		Dry	122			
Adjust for Joint Orient.		Fair/Unfav	-7			
		RMR	45	Q-value	0.27	

ANNEXURE-2

GEOTECHNICAL MAPPING OF CHENANI-NASHRI TUNNEL SECTIONS (NON-SQUEEZING GROUND BEHAVIOUR)

Chenani-Nashri Escape Tunnel Face Mapping Sheet Date/Time: 12-07-2012			
Previous Face Chainage	1564m	Elevation at the front	1243.7m
Present Face Chainage (ETSP)	1566m	Overburden [m]	495m
Total Pull	2m	Excavation method	Drill & blast
Unsupported length	2m	Excavation approach	NATM
Bolting distance from the face	2m	GSI	65

TUNNEL EXCAVATION FACE GEOTECHNICAL DESCRIPTION

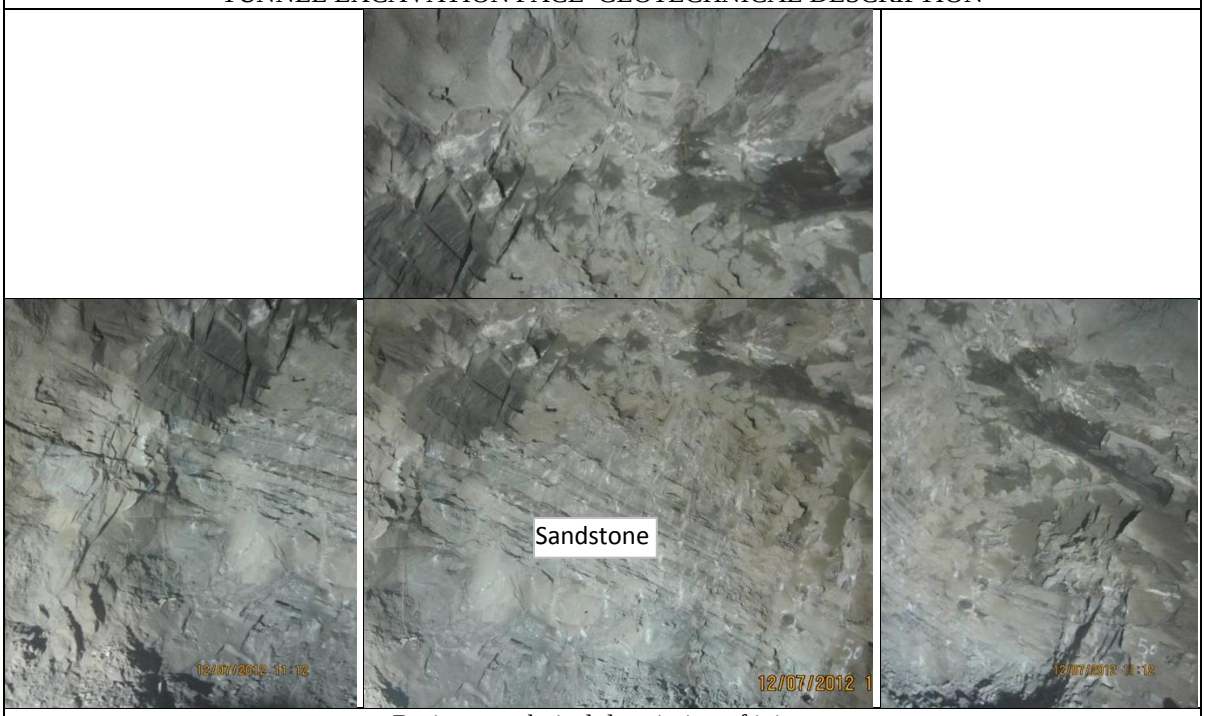

Basic geotechnical description of joints

Joint	Dip -dip/dir	Spacing	pers. (m)	Roughness	Conditions	Aperture	Filling	Seepage
Bedding joint	$30^o/115^o$	60cm	1-3	Rough	Fresh	0.1-1mm	Silt	Dry
JS2	$60^o/250\text{-}255^o$	12cm	3-10	do	do	0.1-5mm	Silt	do
JS3	$55^o/215^o$	100cm	3-7	do	do	do	Silt	do
UCS	65MPa	Jv=21	RQD = 115-3.3Jv = 45.7					

Classification parameters		Value	Rating	Q Parameter	Rating	
Strength of intact rock		65MPa	5	RQD (%)	45	RQD/J_n
RQD		45%	8	J_n	9	5
Spacing of discontinuities		120-1000mm	12	J_r	0.8	J_r/J_a
Condition of discontinuities	Persistence	1-10m	4	J_a	3	0.27
	Opening	0.1-1mm (avg)	4	J_w	1	Jw/SRF
	Roughness	Rough	6	SRF	2	0.5
	Infilling	silt	4			
		Fresh	6			
Ground water		Dry	15			
Adjust for Joint Orient.		Fair	-5			
		RMR	57	Q-value	0.67	

Chenani-Nashri Escape Tunnel Face Mapping Sheet Date/Time: 12-07-2012			
Previous Face Chainage	2223m	Elevation at the front	1243.7m
Present Face Chainage (ETSP)	2225m	Overburden [m]	588m
Total Pull	2m	Excavation method	Drill & blast
Unsupported length	2m	Excavation approach	NATM
Bolting distance from the face	2m	GSI	60

TUNNEL EXCAVATION FACE GEOTECHNICAL DESCRIPTION

Basic geotechnical description of joints

Joint	Dip -dip/dir	Spacing	pers. (m)	Roughness	Conditions	Aperture	Filling	Seepage
Bedding joint	45-55°/100°	20-60cm	1-10	R-Slightly Rough	Fresh-Slight wthd.	0.1-1mm	Clay	Dry
JS2	60°/260°	12cm	do	do	do	0.1-1mm	Clay	do
JS3	60-70°/215°	60cm	3-7m	do	do	do	Clay	do
UCS	60MPa	Jv=21	RQD = 115-3.3Jv = 45.7					

Classification parameters		Value	Rating	Q Parameter	Rating	
Strength of intact rock		60 MPa	5	RQD (%)	45	RQD/J_n
RQD		45%	8	J_n	9	5.11
Spacing of discontinuities		100-600mm	10	J_r	0.8	J_r/J_a
Condition of discontinuities	Persistence	1-10m	3	J_a	3	0.27
	Opening	0.1-1mm (avg)	3	J_w	1	Jw/SRF
	Roughness	Slightly Rough-smooth	4	SRF	2.5	0.4
	Infilling	clay	3			
		Slightly wthd.	4			
Ground water		Dry	15			
Adjust for Joint Orient.		Fair/ Unfav	-5			
		RMR	50	Q-value	0.55	

Chenani-Nashri Escape Tunnel Face Mapping Sheet Date/Time: 21-11-2012			
Previous Face Chainage	2432.5m	Elevation at the front	1230m
Present Face Chainage (ETSP)	2435m	Overburden [m]	623m
Total Pull	2.5m	Excavation method	Drill & blast
Unsupported length	2.5m	Excavation approach	NATM
Bolting distance from the face	2.5m	GSI	60

TUNNEL EXCAVATION FACE GEOTECHNICAL DESCRIPTION

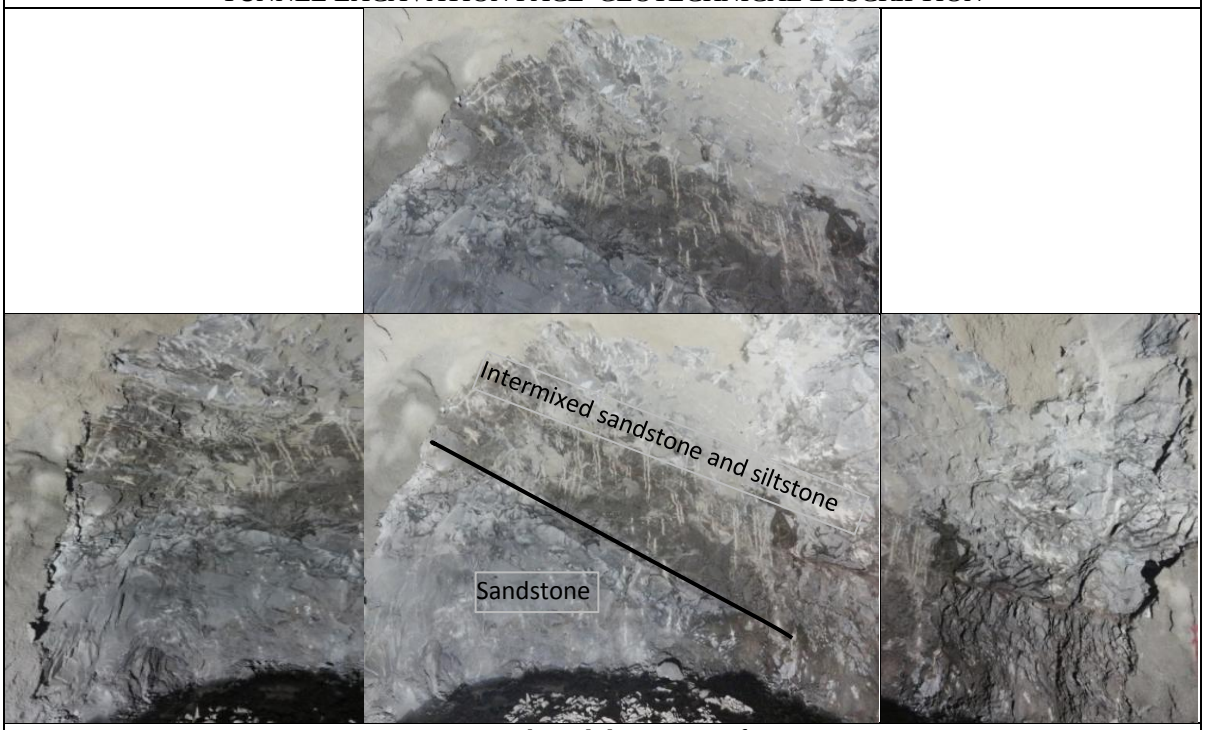

Basic geotechnical description of joints

Joint	Dip -dip/dir	Spacing	pers. (m)	Roughness	Conditions	Aperture	Filling	Seepage
Bedding joint	45^o/95-115^o	5m	1-10	R-Slightly Rough	Fresh-Slight wthd.	0.1-1mm	Silty clay	Dry
JS2	60^o/253^o	10cm	do	do	do	do	Silty clay	do
JS3	60-70^o/215^o	100cm	3-7m	do	do	do	Silty clay	do
UCS	60MPa	Jv=21	RQD = 115-3.3Jv = 45.7					

Classification parameters		Value	Rating	Q Parameter	Rating	
Strength of intact rock		60MPa	5	RQD (%)	45	RQD/J_n
RQD		45%	8	J_n	12	3.75
Spacing of discontinuities		100-5000mm	15	J_r	1	J_r/J_a
Condition of discontinuities	Persistence	1-10m	3	J_a	4	0.25
	Opening	0.1-1mm (avg)	4	J_w	1	Jw/SRF
	Roughness	Slightly Rough	4	SRF	2.5	0.4
	Infilling	Silty clay	3			
		Fresh to slightly wthd.	5			
Ground water		Dry	15			
Adjust for Joint Orient.		Fair/ Unfav	-5			
		RMR	57	Q-value	0.38	

Chenani-Nashri Escape Tunnel Face Mapping Sheet Date/Time: 03-12-2012/ 04:30 pm			
Previous Face Chainage	2483.5m	Elevation at the front	1230m
Present Face Chainage (ETSP)	2486m	Overburden [m]	626m
Total Pull	2.5m	Excavation method	Drill & blast
Unsupported length	2.5m	Excavation approach	NATM
Bolting distance from the face	2.5m	GSI	62

TUNNEL EXCAVATION FACE GEOTECHNICAL DESCRIPTION

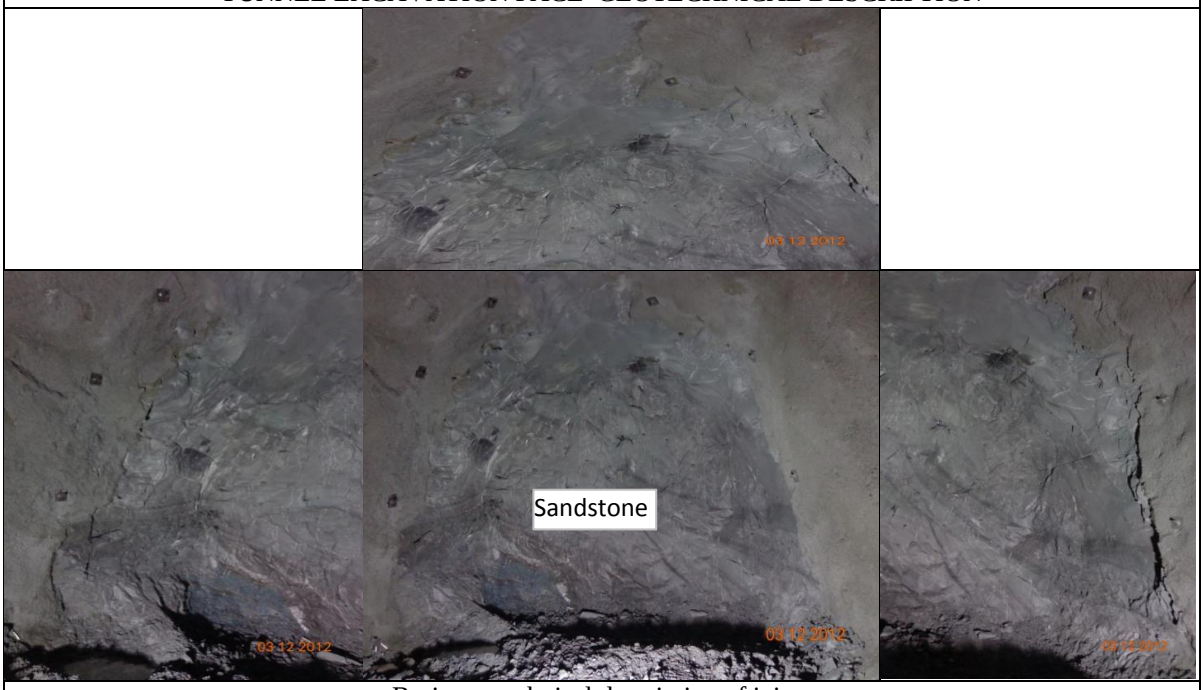

Basic geotechnical description of joints

Joint	Dip -dip/dir	Spacing	pers. (m)	Roughness	Conditions	Aperture	Filling	Seepage
Bedding joint	$45^o/115^o$	500cm	1-3	Slightly Rough	Slightly wthd.	0.1-1mm	Silty clay	Dry
JS2	$60^o/250\text{-}255^o$	10-14cm	3-10	do	do	do	Silty clay	do
JS3	$60\text{-}70^o/215^o$	30cm	3-7m	do	do	do	Silty clay	do
UCS	65MPa	Jv=15	RQD = 115-3.3Jv = 65.5					

Classification parameters		Value	Rating	Q Parameter	Rating	
Strength of intact rock		65 MPa	7	RQD (%)	65.5	RQD/J_n
RQD		65.5%	11	J_n	12	5.45
Spacing of discontinuities		100-5000mm	15	J_r	0.8	J_r/J_a
Condition of discontinuities	Persistence	1-10m	3	J_a	3	0.27
	Opening	0.1-1mm (avg)	4	J_w	1	Jw/SRF
	Roughness	Slightly Rough	4	SRF	2	0.5
	Infilling	clay	2			
		Fresh to slightly wthd.	6			
Ground water		Dry	15			
Adjust for Joint Orient.		Fair	-5			
		RMR	62	Q-value	0.72	

Chenani-Nashri Escape Tunnel Face Mapping Sheet Date/Time: 18-12-2012/ 05:00 pm			
Previous Face Chainage	2597.5m	Elevation at the front	1230m
Present Face Chainage (ETSP)	2600m	Overburden [m]	652m
Total Pull	2.5m	Excavation method	Drill & blast
Unsupported length	2.5m	Excavation approach	NATM
Bolting distance from the face	2.5m	GSI	60

TUNNEL EXCAVATION FACE GEOTECHNICAL DESCRIPTION

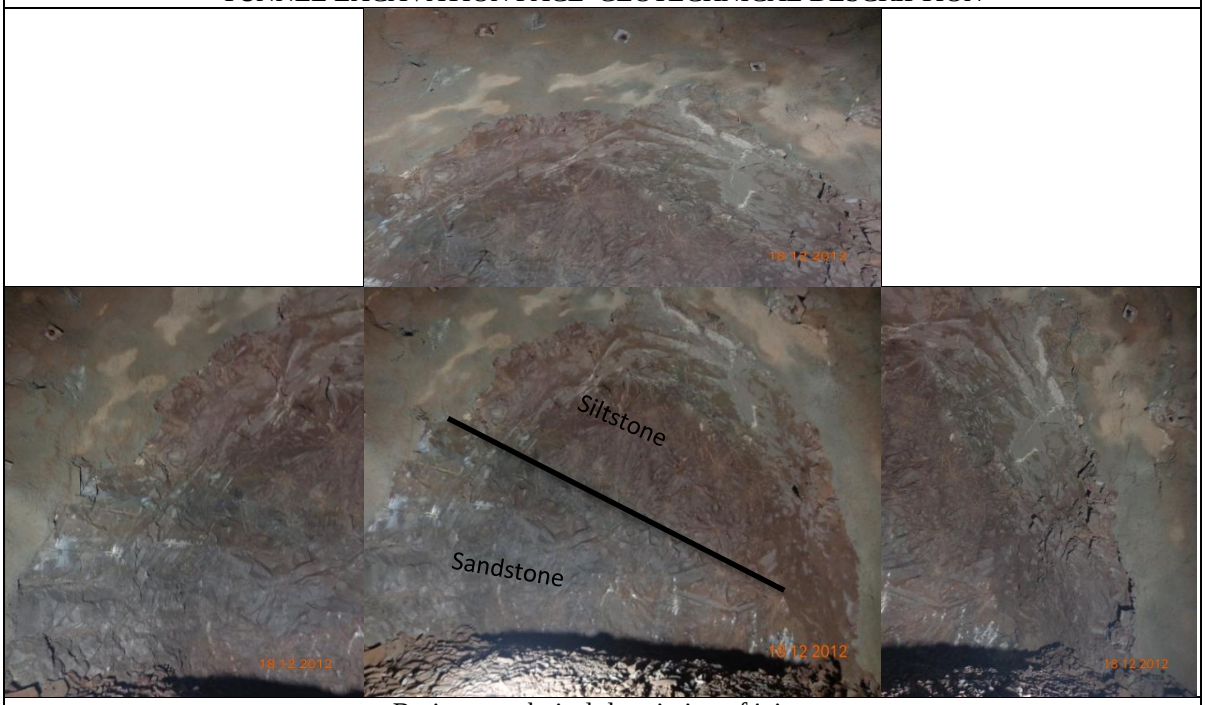

Basic geotechnical description of joints

Joint	Dip -dip/dir	Spacing	pers. (m)	Roughness	Conditions	Aperture	Filling	Seepage
Bedding joint	40-45°/115°	500cm	1-6	Slightly Rough	Slightly wthd.	0.1-1mm	Silt	Dry
JS2	65°/255°	10cm	do	do	do	do	Silt	do
JS3	70°/210°	400cm	3-6	do	do	do	Silt	do
UCS	60MPa	Jv=22	RQD = 115-3.3Jv = 42.4					

Classification parameters		Value	Rating	Q Parameter	Rating	
Strength of intact rock		60 MPa	5	RQD (%)	42.4	RQD/J_n
RQD		42.4%	8	J_n	12	3.53
Spacing of discontinuities		100-5000mm	15	J_r	0.8	J_r/J_a
Condition of discontinuities	Persistence	1-10m	3	J_a	3	0.27
	Opening	0.1-1mm (avg)	2	J_w	1	Jw/SRF
	Roughness	Slightly Rough	4	SRF	2.5	0.4
	Infilling	Silt	4			
		Fresh to slightly wthd.	5			
Ground water		Dry	15			
Adjust for Joint Orient.		Fair	-5			
		RMR	56	Q-value	0.38	

Chenani-Nashri Escape Tunnel Face Mapping Sheet Date/Time: 23-12-2012			
Previous Face Chainage	2646.5m	Elevation at the front	1230m
Present Face Chainage (ETSP)	2649m	Overburden [m]	656m
Total Pull	2.5m	Excavation method	Drill & blast
Unsupported length	2.5m	Excavation approach	NATM
Bolting distance from the face	2.5m	GSI	50-60

TUNNEL EXCAVATION FACE GEOTECHNICAL DESCRIPTION

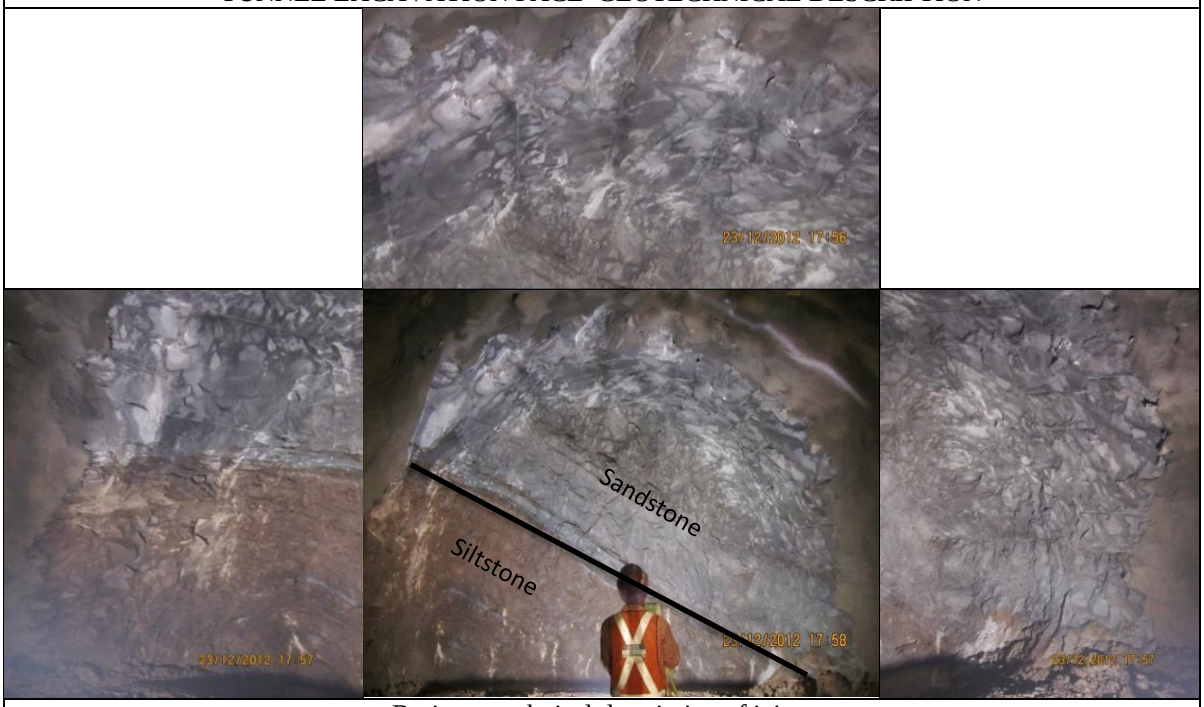

Basic geotechnical description of joints

Joint	Dip -dip/dir	Spacing	Pers. (m)	Roughness	Conditions	Aperture	Filling	Seepage
Bedding joint	45^o/95-115^o	20-60cm	1-10	Rough	Fresh-Slight wthd.	0.1-1mm	Silt	Dry
JS2	60^o/250-270^o	10-12cm	do	do	do	do	Silt	do
JS3	70^o/210^o	>60cm	3-7	do	do	do	Silt	do
UCS	60MPa	Jv=20	RQD = 115-3.3Jv = 49					

Classification parameters		Value	Rating	Q Parameter	Rating	
Strength of intact rock		60 MPa	7	RQD (%)	49	RQD/J_n
RQD		49%	8	J_n	12	4.08
Spacing of discontinuities		200-5000mm	15	J_r	1	J_r/J_a
Condition of discontinuities	Persistence	1-10m	3	J_a	3	0.33
	Opening	0.1-1mm (avg)	3	J_w	1	Jw/SRF
	Roughness	Rough	5	SRF	2.5	0.4
	Infilling	Silt	4			
		Fresh to slightly wthd.	5			
Ground water		Dry	15			
Adjust for Joint Orient.		Fair	-5			
		RMR	60	Q-value	0.54	

Chenani-Nashri Escape Tunnel Face Mapping Sheet Date/Time: 21-01-2013 / 01:00 pm			
Previous Face Chainage	2853.5m	Elevation at the front	1230m
Present Face Chainage (ETSP)	2856m	Overburden [m]	676m
Total Pull	2.5m	Excavation method	Drill & blast
Unsupported length	2.5m	Excavation approach	NATM
Bolting distance from the face	2.5m	GSI	60

TUNNEL EXCAVATION FACE GEOTECHNICAL DESCRIPTION

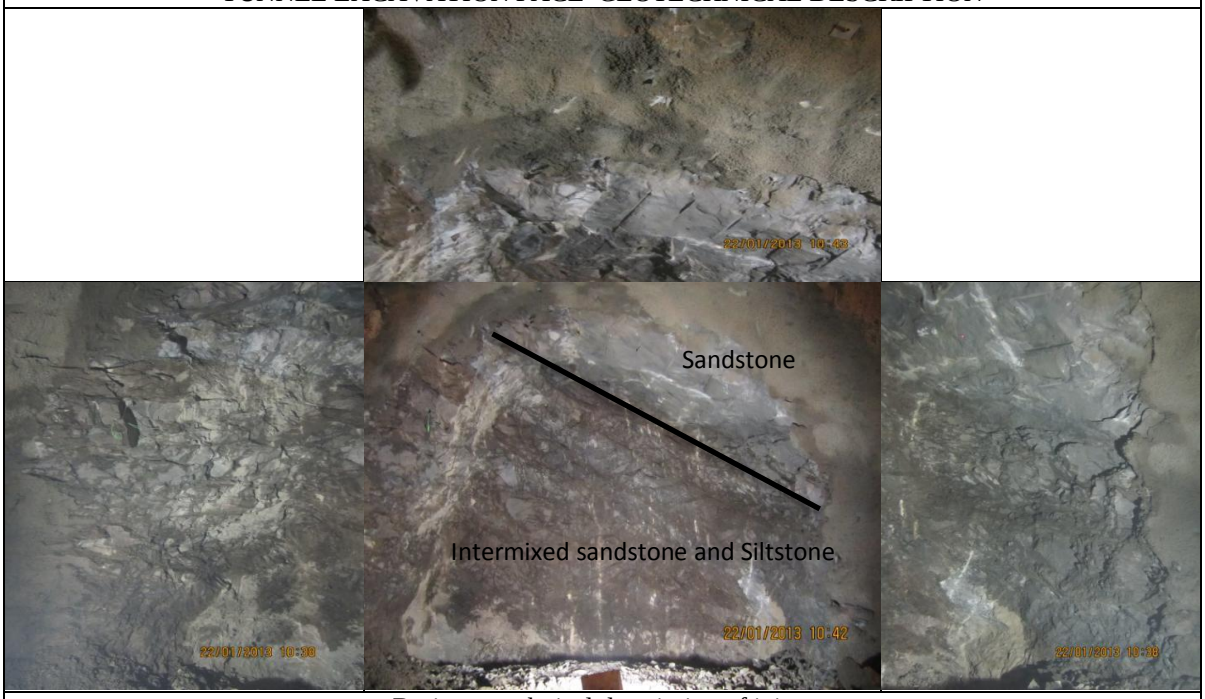

Basic geotechnical description of joints

Joint	Dip -dip/dir	Spacing	Pers. (m)	Roughness	Conditions	Aperture	Filling	Seepage
Bedding joint	$45^o/115^o$	500cm	1-6	Slightly Rough	Slight wthd.	0.1-1mm	Silt	Dry
JS2	$65^o/250\text{-}255^o$	10-12cm	3-6	do	do	do	Silt	do
JS3	$70^o/200\text{-}220^o$	100cm	3-5	do	do	do	Silt	do
UCS	60MPa	Jv=21	RQD = 115-3.3Jv = 45.7					

Classification parameters		Value	Rating	Q Parameter	Rating	
Strength of intact rock		60 MPa	7	RQD (%)	45.7	RQD/J_n
RQD		45.7%	8	J_n	12	3.8
Spacing of discontinuities		100-5000mm	15	J_r	1	J_r/J_a
Condition of discontinuities	Persistence	1-6m	2	J_a	4	0.25
	Opening	0.1-1mm (avg)	3	J_w	2	Jw/SRF
	Roughness	Slightly rough	4	SRF	2.5	0.8
	Infilling	Silt	4			
		Fresh to slightly wthd.	5			
Ground water		Dry	15			
Adjust for Joint Orient.		Fair	-5			
		RMR	58	Q-value	0.76	

Chenani-Nashri Escape Tunnel Face Mapping Sheet Date/Time: 21-01-2013/ 01:00 pm			
Previous Face Chainage	2853.5m	Elevation at the front	1230m
Present Face Chainage (ETSP)	2856m	Overburden [m]	676m
Total Pull	2.5m	Excavation method	Drill & blast
Unsupported length	2.5m	Excavation approach	NATM
Bolting distance from the face	2.5m	GSI	50

TUNNEL EXCAVATION FACE GEOTECHNICAL DESCRIPTION

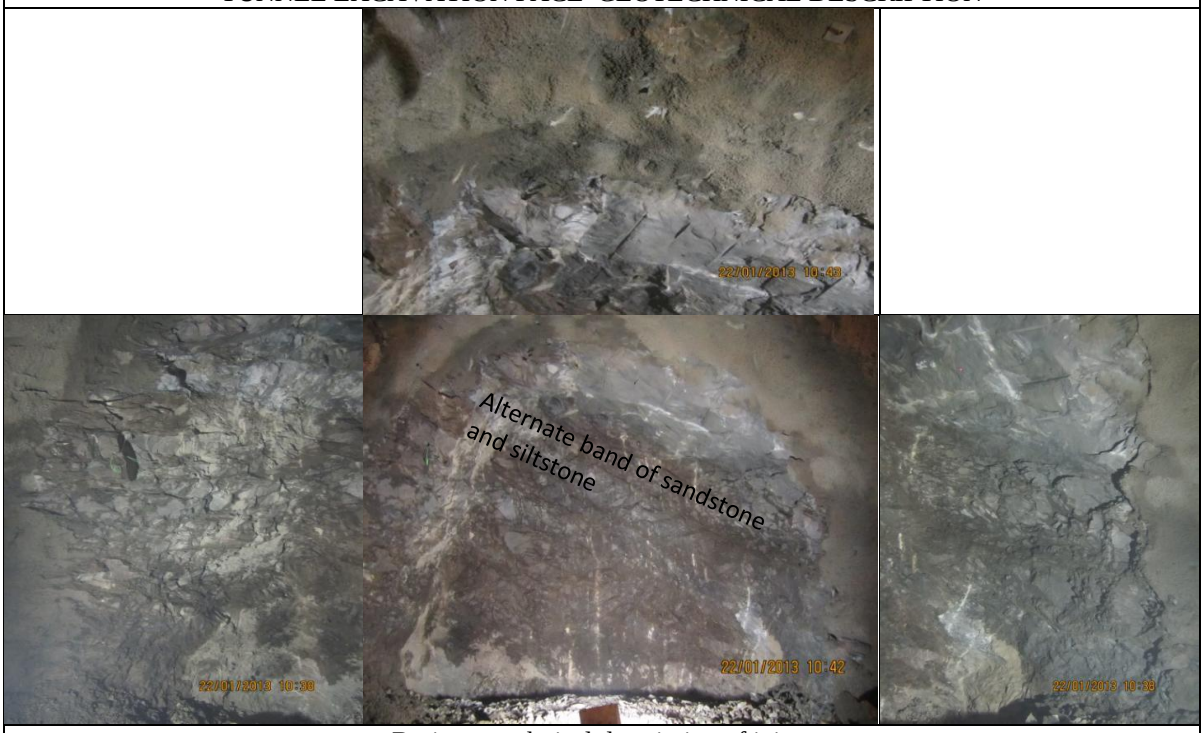

Basic geotechnical description of joints

Joint	Dip -dip/dir	Spacing	pers. (m)	Roughness	Conditions	Aperture	Filling	Seepage
Bedding joint	45^o/110-120^o	5m	1-6	Slightly Rough	Slightly wthd.	0.1-1mm	Silty clay	Dry
JS2	65^o/250-255^o	10-12cm	3-6	do	do	do	Silty clay	do
JS3	60^o/200-220^o	26cm	3-5	do	do	do	Silty clay	do
UCS	60	Jv=21	RQD = 115-3.3Jv = 45.7					

Classification parameters		Value	Rating	Q Parameter	Rating	
Strength of intact rock		60 MPa	6	RQD (%)	47.7	RQD/J_n
RQD		45.7%	8	J_n	12	3.8
Spacing of discontinuities		100-500mm	10	J_r	1	J_r/J_a
Condition of discontinuities	Persistence	1-6m	2	J_a	4	0.25
	Opening	0.1-1mm (avg)	3	J_w	2	Jw/SRF
	Roughness	Slightly Rough	3	SRF	2.5	0.8
	Infilling	Silty clay	3			
		Fresh to slightly wthd.	5			
Ground water		Dry	15			
Adjust for Joint Orient.		Fair/ Unfav	-5			
		RMR	50	Q-value	0.38	

Chenani-Nashri Escape Tunnel Face Mapping Sheet Date/Time: 30-01-2013 / 01:00 pm			
Previous Face Chainage	2904.5m	Elevation at the front	1230m
Present Face Chainage (ETSP)	2907m	Overburden [m]	668m
Total Pull	2.5m	Excavation method	Drill & blast
Unsupported length	2.5m	Excavation approach	NATM
Bolting distance from the face	2.5m	GSI	65

TUNNEL EXCAVATION FACE GEOTECHNICAL DESCRIPTION

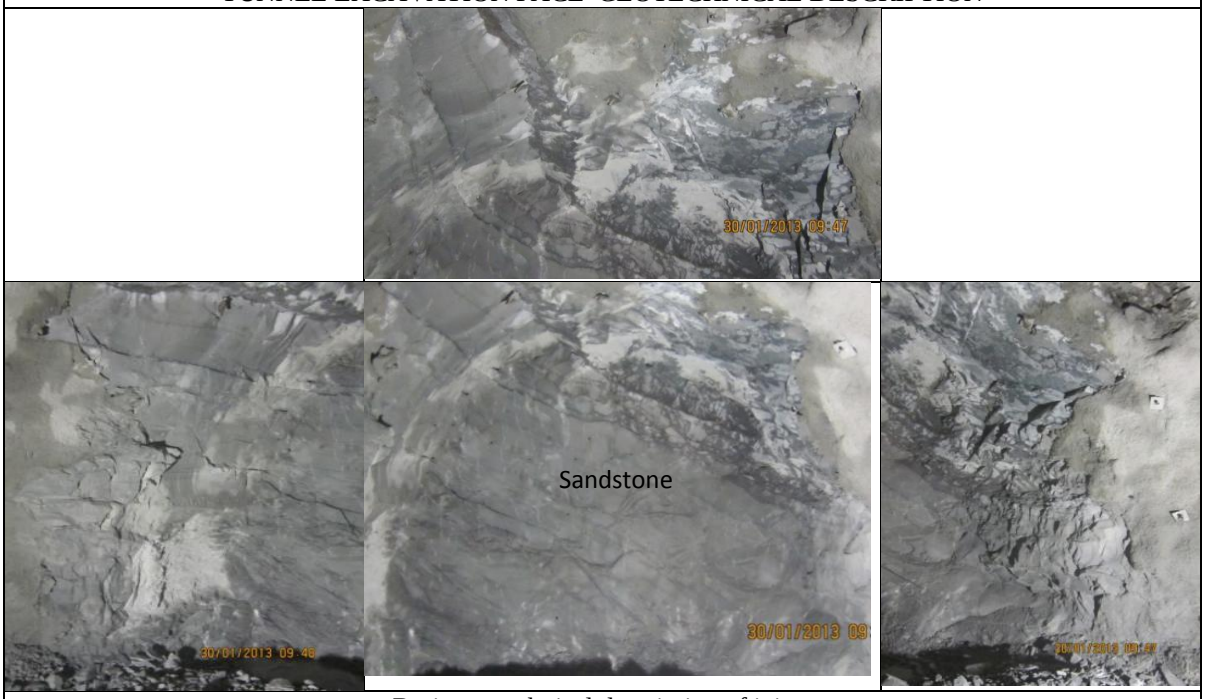

Basic geotechnical description of joints

Joint	Dip -dip/dir	Spacing	Pers. (m)	Roughness	Conditions	Aperture	Filling	Seepage
Bedding joint	40-45°/105°	500cm	1-10	Rough	Fresh	0.1-1mm	Silty clay	Dry
JS2	65°/250-255°	10cm	do	do	do	do	Silty clay	do
JS3	60-70°/215°	400cm	3-6	do	do	do	Silty clay	do
UCS	60MPa	Jv=16	RQD = 115-3.3Jv = 62.2					

Classification parameters		Value	Rating	Q Parameter	Rating	
Strength of intact rock		65MPa	6	RQD (%)	62.2	RQD/J_n
RQD		62.2%	11	J_n	9	6.91
Spacing of discontinuities		100-5000mm	15	J_r	0.8	J_r/J_a
Condition of discontinuities	Persistence	1-10m	3	J_a	3	0.27
	Opening	0.1-1mm (avg)	3	J_w	1	Jw/SRF
	Roughness	Rough	5	SRF	2.5	0.4
	Infilling	Silty clay	3			
		Fresh	6			
Ground water		Dry	15			
Adjust for Joint Orient.		Fair	-5			
		RMR	62	Q-value	0.74	

Chenani-Nashri Escape Tunnel Face Mapping Sheet Date/Time: 03-04-2013 / 01:00 pm			
Previous Face Chainage	3104.5m	Elevation at the front	1230m
Present Face Chainage (ETSP)	3107m	Overburden [m]	645m
Total Pull	2.5m	Excavation method	Drill & blast
Unsupported length	2.5m	Excavation approach	NATM
Bolting distance from the face	2.5m	GSI	60

TUNNEL EXCAVATION FACE GEOTECHNICAL DESCRIPTION

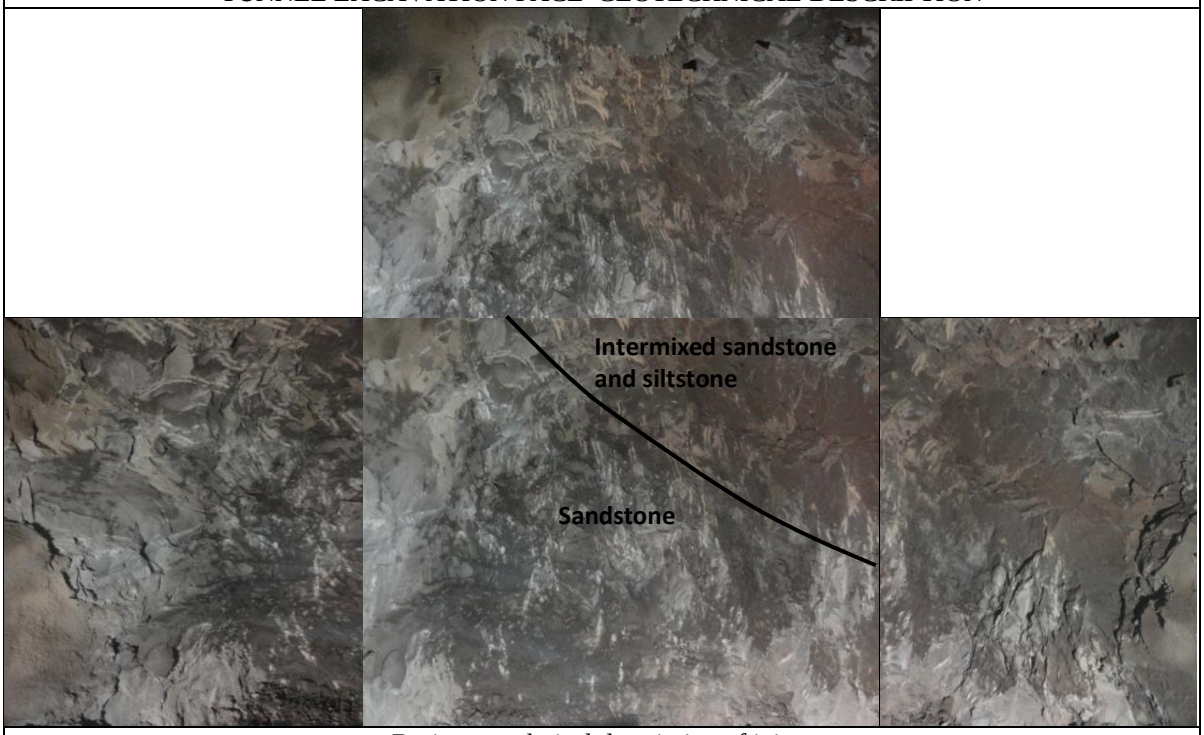

Basic geotechnical description of joints

Joint	Dip -dip/dir	Spacing	Pers. (m)	Roughness	Conditions	Aperture	Filling	Seepage
Bedding joint	40-45°/105°	500cm	1-10	Rough-silght rough	Fresh	0.1-1mm	Silty clay	Dry
JS2	60°/240-260°	10-14cm	do	do	do	do	Silty clay	do
JS3	65°/200-230°	400cm	3-6	do	do	do	Silty clay	do
UCS	60MPa	Jv=20	RQD = 115-3.3Jv = 49					

Classification parameters		Value	Rating	Q Parameter	Rating	
Strength of intact rock		60MPa	7	RQD (%)	49	RQD/J_n
RQD		49%	8	J_n	12	4.08
Spacing of discontinuities		100-5000mm	15	J_r	1	J_r/J_a
Condition of discontinuities	Persistence	1-10m	3	J_a	3	0.33
	Opening	0.1-1mm (avg)	3	J_w	1	Jw/SRF
	Roughness	Rough-Slight rough	3	SRF	2.5	0.4
	Infilling	Silty clay	4			
		Fresh	5			
Ground water		Dry	15			
Adjust for Joint Orient.		Fair	-5			
		RMR	58	Q-value	0.54	

Chenani-Nashri Escape Tunnel Face Mapping Sheet Date/Time: 16-03-2013			
Previous Face Chainage	3164.5m	Elevation at the front	1230m
Present Face Chainage (ETSP)	3167m	Overburden [m]	628m
Total Pull	2.5m	Excavation method	Drill & blast
Unsupported length	2.5m	Excavation approach	NATM
Bolting distance from the face	2.5m	GSI	50

TUNNEL EXCAVATION FACE GEOTECHNICAL DESCRIPTION

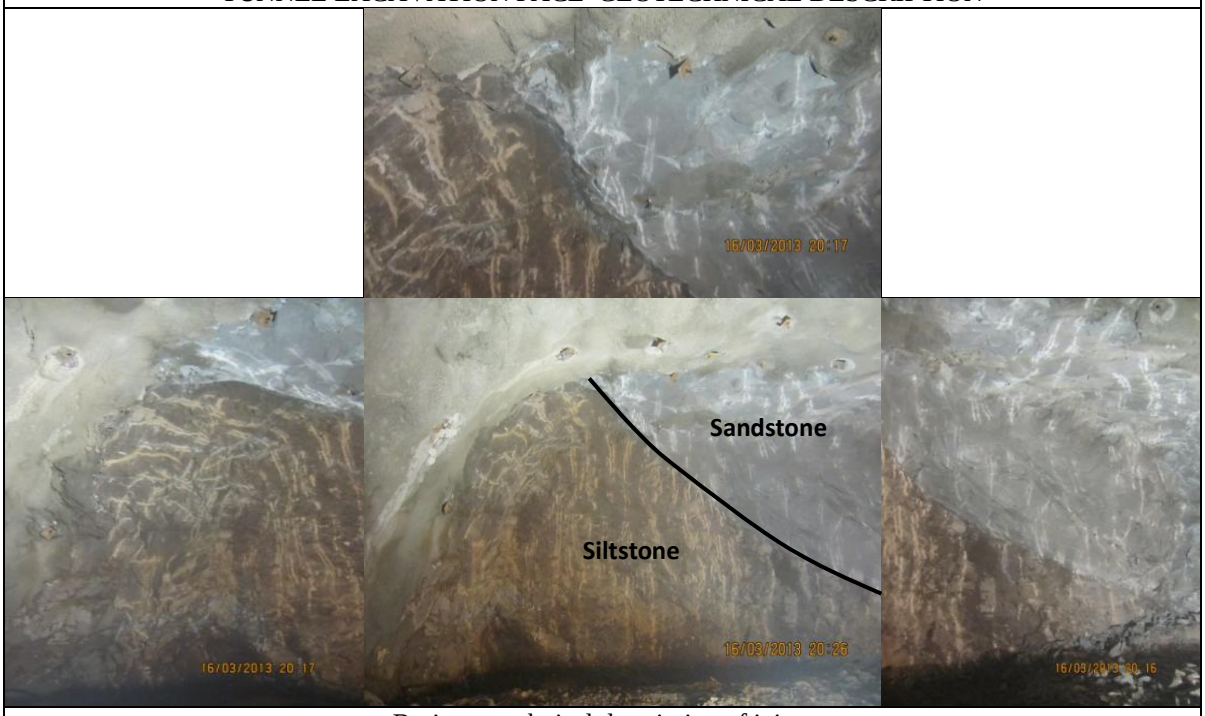

Basic geotechnical description of joints

Joint	Dip -dip/dir	Spacing	Pers. (m)	Roughness	Conditions	Aperture	Filling	Seepage
Bedding joint	40-45°/105°	20-60cm	1-10	Rough-silght rough	Fresh-Slight weathered	0.1-1mm	Silty clay	Dry
JS2	65°/250-255°	10-12cm	do	do	do	do	Silty clay	do
JS3	65°/200-230°	>60cm	3-6	do	do	do	Silty clay	do
UCS	60MPa	Jv=20	RQD = 115-3.3Jv = 49					

Classification parameters		Value	Rating	Q Parameter	Rating	
Strength of intact rock		60MPa	6	RQD (%)	49	RQD/J_n
RQD		49%	8	J_n	12	4.08
Spacing of discontinuities		100-600mm	9	J_r	1	J_r/J_a
Condition of discontinuities	Persistence	1-10m	3	J_a	4	0.25
	Opening	0.1-1mm (avg)	3	J_w	1	Jw/SRF
	Roughness	Rough-Slight rough	3	SRF	2.5	0.4
	Infilling	Silty clay	3			
		Fresh	5			
Ground water		Dry	15			
Adjust for Joint Orient.		Fair/ Unfav	-7			
		RMR	48	Q-value	0.41	

Chenani-Nashri Main Tunnel Face Mapping Sheet Date/Time: 23-03-2013			
Previous Face Chainage	2138.5m	Elevation at the front	1230m
Present Face Chainage (MTSP)	2141m	Overburden [m]	566m
Total Pull	2.5m	Excavation method	Drill & blast
Unsupported length	2.5m	Excavation approach	NATM
Bolting distance from the face	2.5m	GSI	45

TUNNEL EXCAVATION FACE GEOTECHNICAL DESCRIPTION

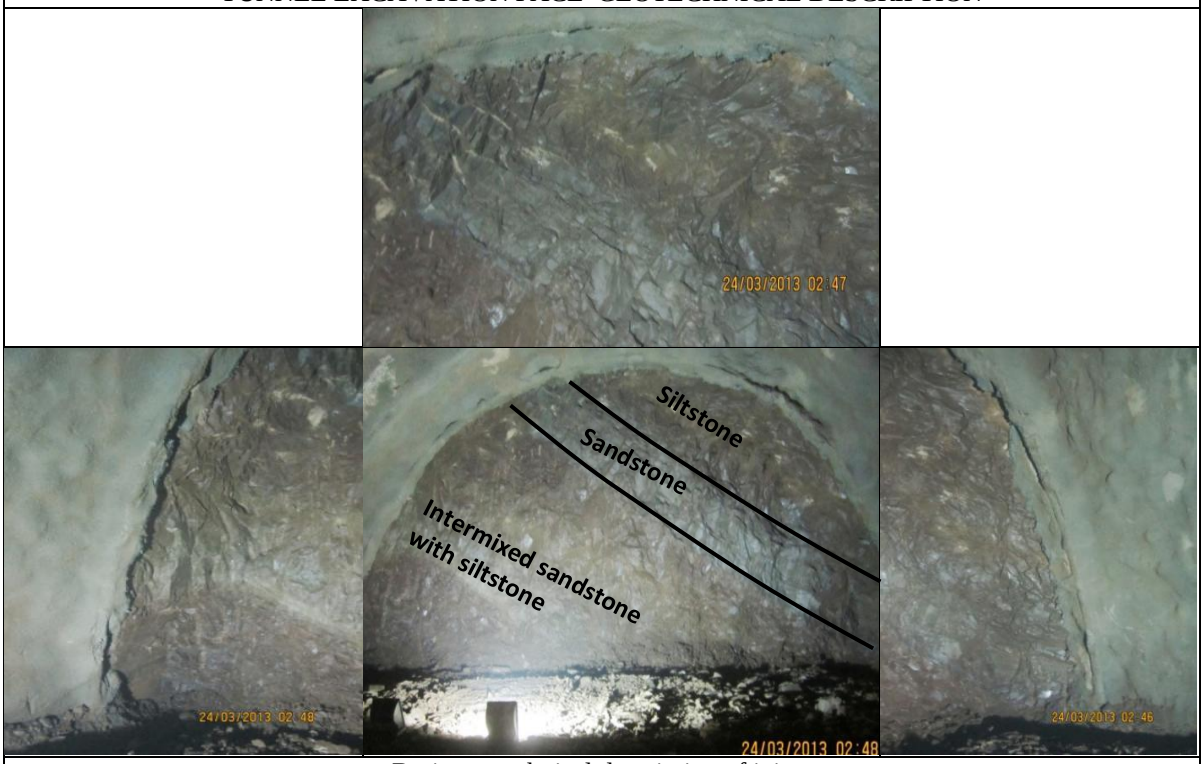

Basic geotechnical description of joints

Joint	Dip -dip/dir	Spacing	Pers. (m)	Roughness	Conditions	Aperture	Filling	Seepage
Bedding joint	35-40°/105°	20cm	1-3	Silght rough	Fresh-Slight weathered	0.1-1mm	Silty clay	Dry
JS2	60-70°/255°	10-12cm	3-6	do	do	do	Silty clay	do
JS3	65°/200-230°	>60cm	3-6	do	do	do	Silty clay	do
UCS	50MPa	Jv=20	RQD = 115-3.3Jv = 49					

Classification parameters		Value	Rating	Q Parameter	Rating	
Strength of intact rock		50MPa	5	RQD (%)	49	RQD/J_n
RQD		49%	8	J_n	12	4.08
Spacing of discontinuities		100-600mm	9	J_r	0.8	J_r/J_a
Condition of discontinuities	Persistence	1-10m	3	J_a	3	0.27
	Opening	0.1-1mm (avg)	3	J_w	1	Jw/SRF
	Roughness	Rough-Slight rough	3	SRF	2.5	0.4
	Infilling	Silty clay	3			
		Fresh	5			
Ground water		Dry	15			
Adjust for Joint Orient.		Fair/ Unfav	-7			
		RMR	47	Q-value	0.44	

Chenani-Nashri Main Tunnel Face Mapping Sheet Date/Time: 13-04-2013 / 6:00 pm			
Previous Face Chainage	2189.5m	Elevation at the front	1230m
Present Face Chainage (MTSP)	2192m	Overburden [m]	574m
Total Pull	2.5m	Excavation method	Drill & blast
Unsupported length	2.5m	Excavation approach	NATM
Bolting distance from the face	2.5m	GSI	60

TUNNEL EXCAVATION FACE GEOTECHNICAL DESCRIPTION

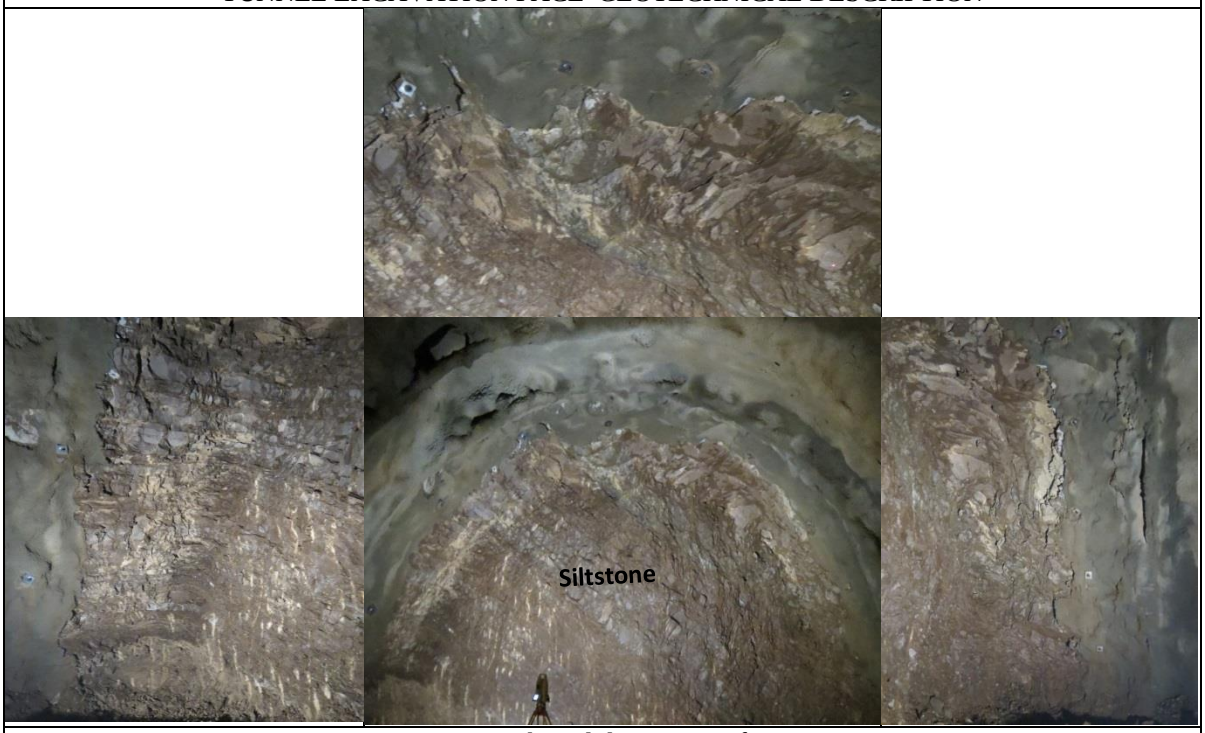

Basic geotechnical description of joints

Joint	Dip -dip/dir	Spacing	Pers. (m)	Roughness	Conditions	Aperture	Filling	Seepage
Bedding joint	$35^o/105^o$	500cm	3-6	R-Silghtly rough	Fresh-Slight weathered	0.1-0.5mm	Silty clay	Dry
JS2	$60^o/260^o$	10-14cm	3-6	do	do	do	Silty	do
JS3	$75^o/210^o$	400m	3-6	do	do	do	Silty	do
UCS	60MPa	Jv=21	RQD = 115-3.3Jv = 45.7					

Classification parameters		Value	Rating	Q Parameter	Rating	
Strength of intact rock		60MPa	7	RQD (%)	45.7	RQD/J_n
RQD		45.7%	8	J_n	12	3.81
Spacing of discontinuities		100-5000mm	15	J_r	0.8	J_r/J_a
Condition of discontinuities	Persistence	3-6m	2	J_a	3	0.27
	Opening	0.1-0.5mm (avg)	4	J_w	1	Jw/SRF
	Roughness	Rough-Slight rough	4	SRF	2.5	0.4
	Infilling	Silt	4			
		Fresh-Slightly weathered	5			
Ground water		Dry	15			
Adjust for Joint Orient.		Fair	-5			
		RMR	59	Q-value	0.41	

BRIEF CURRICULUM VITAE

Er. R. D. Dwivedi did B. E. (Mining Engineering) from Visvesvaraya Regional College of Engineering (now VNIT), Nagpur in 1993 and M. Tech. (Mining Engineering) from Institute of Technology (now IIT), Banaras Hindu University (Varanasi) in 1996. He joined Central Institute of Mining and Fuel Research (erstwhile CMRI) as Scientist-B in 1996. Currently he is working as Principal Scientist in CIMFR Regional Centre, Roorkee. His main areas of work are rock testing and tunnelling & underground space technology.

More than 17 years of experience as scientist, he worked on more than 30 tunnelling/mining projects and he also disseminated his knowledge and imparted trainings to the site personal engaged in tunnelling. He has also used his expertise to develop facilities for defence purposes.
He has been engaged in testing of rocks in the temperature range from -50^{o}C to 200^{o}C for defence and civil utility projects.

He received two best paper awards; one by Indian Geotechnical Society in the year 2003 and other by ISRMTT in the year 2013.

He has published 56 research papers in International/National journals and conferences. He has also reviewed papers for some international journals; notable amongst these are *International Journal of Rock Mechanics and Mining Sciences, Rock mechanics and Rock Engineering* and *Tunnelling, and Underground Space Technology.*

Organized a course on "Underground Engineering" during 15-17 Feb., 2010 for geologists and engineers engaged in tunneling and related projects in India and Bhutan. He is a faculty of *Academy of Scientific & Innovative Research (AcSIR).*

LIST OF PAPERS PUBLISHED FROM THE RESEARCH WORK

International Journal

1. Dwivedi R.D., Singh M., Viladkar M.N., Goel R.K. 2014. Estimation of support pressure during tunnelling through squeezing grounds. **Engineering Geology**, 168, 9-22.

2. Dwivedi R.D., Singh M., Viladkar M.N., Goel R.K. 2013. Prediction of tunnel deformation in squeezing grounds. **Engineering Geology**, 161, 55-64.

National Journal

3. Dwivedi R.D., Goel R.K., Singh M., Viladkar M.N., 2012. State of art of tunnelling through squeezing grounds. **Journal of Rock Mech. Tunlg. Tech.**, 18 (2), 117-140.

(The paper was selected for "Best paper award" by ISRMTT for the year 2012)

Conference

4. Dwivedi, R.D., Singh, M., Viladkar, M.N., Goel, R.K., 2014. Parametric analysis of an empirical correlation predicting deformation of squeezing tunnels. **Proc.** A National Seminar "Innovative Practices in Rock Mechanics (IPRM-2014)", Eds: Sripad R.N., Naithani A.K., Balasubramaniam V.R., 6-8 Feb, NIRM Bengaluru, 255-260.

5. Dwivedi, R.D., Goel, R.K., Singh, M., Viladkar, M.N., Sinha, A. 2013. Empirical approach to estimate tunnel deformation in squeezing grounds. **Proc.** 12th Int. Conf. of Underground Construction Prague 2013, 22-24 April, Prague, Czech Republic, 160p.

6. Dwivedi, R.D., Singh, M., Viladkar, M.N., Goel, R.K., 2012. Closure behaviour of tunnels in squeezing conditions. **Proc.** 28th NCCE & National Seminar on Role of infrastructure for sustainable development; 12-14 Oct, IE Local Chapter Roorkee; 464-475.

7. Dwivedi, R.D., Singh, M., Viladkar, M.N., Goel, R.K., 2009. Tunnel support design for squeezing conditions-a review. **Proc.** of 2nd Indian Rock Conference, INDOROCK, New Delhi, India, 261-272.